

**Prediction of Drawdown and Groundwater Inflow Rates over the Life of the
Sakatti Project**

**Prepared
for
Sakatti Project**

**Prepared
by
Itasca Denver, Inc.
143 Union Boulevard, Suite 525
Lakewood, Colorado**

#4064

March 2023



TABLE OF CONTENTS

	<u>Page</u>
TABLE OF CONTENTS	ii
LIST OF FIGURES.....	v
LIST OF TABLES.....	viii
LIST OF APPENDICES	ix
LIST OF ABBREVIATIONS.....	x
EXECUTIVE SUMMARY	xii
1.0 INTRODUCTION	1
1.1 DISCUSSION OF TERMINOLOGY	2
2.0 CONCEPTUAL HYDROGEOLOGIC MODEL	3
2.1 HYDROLOGIC STUDY AREA	3
2.2 KEY COMPONENTS OF THE CONCEPTUAL HYDROGEOLOGIC MODEL.....	4
3.0 KEY HYDROGEOLOGIC DATA.....	9
3.1 GEOLOGIC SETTING.....	9
3.1.1 Geologic Units.....	10
3.1.1.1 The Mire	11
3.1.1.2 Glacial and Fluvial Sediments	12
3.1.1.3 Fractured Bedrock.....	13
3.1.1.4 Unfractured Bedrock	14
3.1.2 Geologic Structures	14
3.1.3 Hydraulic Testing at the Project Site	15
3.1.3.1 Summary of Hydraulic Testing.....	15
3.1.3.2 Summary of Hydraulic Test Results	15
3.1.4 Summary of Hydrogeology Setting	18
3.2 METEOROLOGIC DATA.....	20
3.2.1 Precipitation	20
3.2.2 Pan Evaporation	21
3.2.3 Snow Depth and Snowmelt.....	21
3.2.4 Recharge from Snowmelt and Precipitation.....	22
3.2.5 Future Climate	24
3.3 SURFACE WATER.....	27
3.4 GROUNDWATER	28
3.4.1 Monitoring Network.....	28
3.4.2 Measured Groundwater Levels.....	29

TABLE OF CONTENTS (continued)

	<u>Page</u>
3.5 PROPOSED MINING AT THE SAKATTI PROJECT	31
4.0 GROUNDWATER FLOW MODEL.....	34
4.1 GROUNDWATER FLOW MODEL CODE	34
4.2 GROUNDWATER FLOW MODEL GRID	34
4.3 SIMULATED HYDROGEOLOGIC UNITS	35
4.4 SIMULATED MODEL BOUNDARY CONDITIONS.....	37
4.4.1 Simulation of Constant Heads.....	37
4.4.2 Variable-Flux Boundary	38
4.4.3 No-Flow Boundary Conditions	38
4.5 SIMULATED RECHARGE TO THE GROUNDWATER SYSTEM	38
4.6 GROUNDWATER FLOW MODEL CALIBRATION	39
4.7 STEADY-STATE MODEL CALIBRATION	40
4.7.1 Steady-State Model Targets.....	41
4.7.2 Steady-State Model Calibration	41
4.8 TRANSIENT MODEL CALIBRATION.....	42
4.8.1 Transient Model Targets	42
4.8.2 Transient Model Calibration.....	43
5.0 PREDICTIVE GROUNDWATER FLOW MODEL.....	46
5.1 PREDICTIVE GROUNDWATER FLOW MODEL SETUP	46
5.1.1 Simulated Boundary Conditions.....	46
5.1.2 Simulated Mining Operation.....	46
5.1.3 Predictive Model Simulations for Environmental Assessment	48
5.2 PREDICTIVE RESULTS DURING MINING FOR THE ENVIRONMENTAL ASSESSMENT	49
5.2.1 Predicted Groundwater Inflow Rates	49
5.2.2 Predicted Drawdown.....	51
5.2.3 Predicted Baseflow to the Kitinen River	56
5.3 PREDICTIVE RESULTS WITH ADDITIONAL MITIGATION FOR THE ENVIRONMENTAL ASSESSMENT.....	56
5.3.1 Predicted Groundwater Inflow Rates	57
5.3.2 Predicted Drawdown.....	59
5.3.3 Predicted Baseflow to the Kitinen River	62
5.4 PREDICTIVE RESULTS OF GROUNDWATER RECOVERY AFTER MINING.....	62

TABLE OF CONTENTS
(continued)

	<u>Page</u>
5.4.1 Predicted Groundwater Recovery for Mine Plan with the NE Deposit.....	63
5.4.2 Predicted Groundwater Recovery for Mine Plan without the NE Deposit	65
6.0 SUMMARY OF KEY MODEL UNCERTAINTIES	69
7.0 CONCLUSIONS	74
8.0 REFERENCES	78
FIGURES	
TABLES	
APPENDICES	

LIST OF FIGURES

Figure 2-1	Hydrologic Study Area of the Sakatti Project
Figure 2-2	Viiankiaapa Mire Area within the Hydrologic Study Area
Figure 2-3	Conceptual Hydrogeologic Model
Figure 2-4	Conceptual Hydrogeologic Model of the Mire
Figure 3-1	Surficial Deposits within the Hydrologic Study Area
Figure 3-2	Geologic Map of Bedrock Units within the Hydrologic Study Area
Figure 3-3	North-South Cross Section of Geologic Units across the Mining Area
Figure 3-4	Local and Regional-Scale Faults in the Hydrologic Study Area
Figure 3-5	Extent of the Geologic Block Models within the Hydrologic Study Area
Figure 3-6	Estimated Thickness of the Peat Layer at the Project Site
Figure 3-7	Measured Hydraulic Conductivities from Packer Tests
Figure 3-8	Measured Hydraulic Conductivities from Packer Testing by Rock Type
Figure 3-9	Measured Hydraulic Conductivities from Pumping, Spinner Log, and Falling Head Tests versus Packer Tests
Figure 3-10	Measured Hydraulic Conductivities from Packer Tests at Elevation Ranges of 135 to 0 mamsl and 0 to -100 mamsl
Figure 3-11	Measured Hydraulic Conductivities from Packer Tests at Elevation Ranges of -100 to -200 mamsl and -200 to -300 mamsl
Figure 3-12	Measured Hydraulic Conductivities from Packer Tests at Elevation Ranges of -300 to -400 mamsl and -400 to -500 mamsl
Figure 3-13	Measured Hydraulic Conductivities of Faults from Packer Tests
Figure 3-14	Meteorological Monitoring Locations Used by the Project Site
Figure 3-15	Measured Annual and Monthly Precipitation at the Sodankylä Tähtelä Station
Figure 3-16	Measured Pan Evaporation Rate at the Sodankylä Tähtelä Station
Figure 3-17	Measured and Calculated Snow Water-Equivalent Depths
Figure 3-18	<i>MIKE SHE</i> and Hydrologic Study Area Boundaries
Figure 3-19	Estimated Recharge Rates from the <i>MIKE SHE</i> Model
Figure 3-20	Future Temperature and Precipitation in Finland under Various Greenhouse Gas Scenarios

Figure 3-21	Future Average Monthly Temperature and Precipitation for the Greenhouse Gas Case RCP4.5 for 2070 to 2099
Figure 3-22	Estimated Future Annual Precipitation and Recharge Rates
Figure 3-23	Future Applied Recharge Rates as a Percentage of Annual Precipitation
Figure 3-24	Surface-Water Bodies in the Hydrologic Study Area
Figure 3-25	Measured River Stages and Discharge Rates from Dams along the Kitinen River
Figure 3-26	Measured and Calculated Streamflow Discharge Rates from the Mine Area
Figure 3-27	Monitoring Locations in the Hydrologic Study Area
Figure 3-28	Monitoring Locations by Hydrogeologic Unit in the Hydrologic Study Area
Figure 3-29	Measured Groundwater Levels across the Project Site
Figure 3-30	Future Spatial and Vertical Extent of Decline and Mine Workings
Figure 3-31	Surface Locations of Future Mine Infrastructure
Figure 3-32	Backfilling Plans and Estimated Hydraulic Conductivities
Figure 4-1	Plan View of Simulated Hydrogeologic Units in Model Layer 1
Figure 4-2	West-East Cross Section of Simulated Hydrogeologic Units in the Mine Area
Figure 4-3	Simulated Hydraulic Conductivities in Groundwater Flow Model versus Measured Hydraulic Conductivities from Packer Tests
Figure 4-4	Values of Hydraulic Conductivity Used in the 2022 Sakatti Mine Groundwater Flow Model
Figure 4-5	Simulated Spatial Extents of the More and Less Permeable Bedrock Units
Figure 4-6	Simulated Spatial Extents of the Fractured Bedrock Units
Figure 4-7	Simulated Boundary Conditions in the Groundwater Flow Model
Figure 4-8	Simulated Recharge Rates in the Groundwater Flow Model Based on the <i>MIKE SHE</i> Model
Figure 4-9	Simulated Spatial Extent of Recharge Zones in the Groundwater Flow Model
Figure 4-10	Simulated Steady-State Groundwater Levels within the Hydrologic Study Area
Figure 4-11	Simulated Depth to Groundwater under Steady-State Conditions
Figure 4-12	Simulated Areas of Discharge and Recharge under Steady-State Conditions
Figure 4-13	Quality Line of Steady-State Model Calibration
Figure 4-14	Temporal Quality Lines of Transient Model Calibration
Figure 4-15	Simulated Annual Recharge Rates as a Percentage of Precipitation

Figure 4-16	Calibrated Water Budget for the Groundwater Flow Model
Figure 4-17	Calibrated Groundwater Outflow Rate to Key Streams and Lakes
Figure 5-1	Simulated Future Recharge Rates
Figure 5-2	Predicted Groundwater Inflow for the 65% and 80% Success in Grouting Scenarios
Figure 5-3	Predicted Drawdown over the LOM at Key Locations around the Mine Area for the 65% and 80% Success in Grouting Scenarios
Figure 5-4	Monitoring Location Drawdown for Selected Years over the Life of Mine
Figure 5-5	Predicted Drawdown at the End of Mining for the 65% and 80% Success in Grouting Scenarios
Figure 5-6	Comparison of Measured versus Simulated Seasonal Groundwater-Level Changes
Figure 5-7	Predictions of Seasonal Groundwater-Level Changes for the 80% Success in Grouting with the NE Deposit Scenario
Figure 5-8	Predicted Baseflow to the Kitinen River for the 65% and 80% Success in Grouting with the NE Deposit Scenarios
Figure 5-9	Predicted Groundwater Inflow for the 65% and 80% Success in Grouting without the NE Deposit Scenarios
Figure 5-10	Predicted Drawdown over the LOM at Key Locations around the Mine Area for the 65% and 80% Success in Grouting without the NE Deposit Scenarios
Figure 5-11	Predicted Drawdown at the End of Mining for the 65% and 80% Success in Grouting without the NE Deposit Scenarios
Figure 5-12	Predictions of Seasonal Groundwater-Level Changes for the 80% Success in Grouting without the NE Deposit Scenario
Figure 5-13	Predicted Baseflow to the Kitinen River for the 65% and 80% Success in Grouting without the NE Deposit Scenarios
Figure 5-14	Predicted Groundwater Recovery after Mining at Key Locations around the Mine Area for the 65% and 80% Success in Grouting Scenarios
Figure 5-15	Predicted Groundwater Recovery after Mining at Key Locations around the Mine Area for the 65% and 80% Success in Grouting without the NE Deposit Scenarios
Figure 6-1	Levels of Hydrogeologic Effort at Different Project Stages
Figure 6-2	Evolution of a Groundwater Flow Model

LIST OF TABLES

Table 3-1	Summary of Measured Hydraulic Conductivity Values of the Primary Hydrogeologic Units within the Hydrologic Study Area
Table 3-2	Summary of Measured Hydraulic Conductivity Values from Packer Tests
Table 3-3	Summary of Measured Hydraulic Conductivity Values from Falling Head Tests
Table 3-4	Summary of Measured Hydraulic Conductivity Values from Pump Tests
Table 3-5	Summary of Measured Hydraulic Conductivity Values from Air-Lift Tests
Table 3-6	Measured Hydraulic Conductivity Values at Fault Structures
Table 3-7	Measured Annual Precipitation Data at the Sodankylä Tähtelä Station
Table 3-8	Average Monthly and Daily Precipitation Rates at the Sodankylä Tähtelä Station
Table 3-9	Measured Annual Pan Evaporation Data at the Sodankylä Tähtelä Station
Table 3-10	Estimated Future Recharge Rates to Hydrogeologic Units for the Climate Case RCP4.5
Table 3-11	Summary of Details on Groundwater Monitoring Network at the Project Site
Table 4-1	Simulated Hydraulic Properties of the Hydrogeologic Units in the Sakatti Mine Groundwater Flow Model
Table 4-2	Simulated Recharge Rates for the Hydrogeologic Units in the Groundwater Flow Model
Table 4-3	Monitoring Locations Used in the Steady-State Groundwater Flow Model Calibration
Table 4-4	Calculated Statistics of the Steady-State Groundwater Flow Model Calibration
Table 4-5	Monitoring Locations Used in the Transient Groundwater Flow Model Calibration
Table 4-6	Summary of Calculated Statistics of the Transient Groundwater Flow Model Calibration
Table 5-1	Summary of Simulated Model Scenarios
Table 5-2	Summary of Predicted Groundwater Inflow Rates and Cumulative Volumes for Model Scenarios with the NE Deposit
Table 5-3	Summary of Predicted Groundwater Inflow Rates and Cumulative Volumes for Model Scenarios without the NE Deposit
Table 6-1	Summary of Key Model Parameters and Uncertainties

LIST OF APPENDICES

- A Measured versus Simulated Hydrographs of the Transient Groundwater Flow Model Calibration
- B Predictive Results for Sensitivity Model Scenarios

LIST OF ABBREVIATIONS

%	percent
3-D	three-dimensional
°C	degrees Celsius
AASM Oy	AA Sakatti Mining Oy
ET	evapotranspiration
HSA	hydrologic study area
<i>K</i>	hydraulic conductivity
km	kilometers
km ²	square kilometers
LAI	leaf area index
LOM	life of mine
m	meters
mm	millimeters
m/s	meters per second
m ³ /day	cubic meters per day
m ³ /s	cubic meters per second
m ³ /hr	cubic meters per hour
mm/day	millimeters per day
mm/yr	millimeters per year
mm/month	millimeters per month
mamsl	meters above mean sea level
MAE	mean absolute error
mbgs	meters below ground surface
ME	mean error
NE	northeast
OL	overland flow
r ²	coefficient of determination

RMSE	root mean square error
RQD	rock quality designation
S_s	specific storage
S_y	Specific yield
SZ	saturated zone
TBM	tunnel bore machine
UZ	unsaturated zone
VWP	vibrating-wire piezometer

EXECUTIVE SUMMARY

BACKGROUND AND OBJECTIVES

The Sakatti Project is a proposed copper-nickel-platinum group element mine located in the northern part of Finland, approximately 16 kilometers (km) northeast of Sodankylä in the Finnish Lapland. Anglo American's subsidiary AA Sakatti Mining Oy (AASM Oy), who owns and will operate the proposed Sakatti Project Site (referred to hereafter as the "Project Site"), tasked Itasca Denver, Inc. (Itasca) with the following objectives:

1. Review available hydrogeologic data that have been collected at the Project Site;
2. Review and update the conceptual hydrogeologic model based on the recently collected hydrogeologic data, including groundwater levels, geologic data, and mine plan data;
3. Develop a groundwater flow model that is representative of the conceptual hydrogeologic model and focuses on the mining operation;
4. Calibrate the groundwater flow model to seasonal changes in groundwater levels;
5. Predict the future groundwater inflow rates to the Mine Workings and potential drawdown in the groundwater system using different scenarios;
6. Conduct a robust sensitivity analysis of the key model parameters within the groundwater flow model;
7. Provide an assessment of the overall groundwater flow model uncertainty;
8. Assess the effect of climate change on the future groundwater conditions; and
9. Provide guidance and recommendations on the future dewatering and groundwater monitoring at the Project Site.

CONCEPTUAL HYDROGEOLOGIC MODEL

A hydrologic study area (HSA) was defined for the project. The HSA is much larger than the proposed mining area to minimize potential hydraulic stresses at the HSA boundaries. A key area within the HSA is the Viiankiaapa Mire (the Mire). The Mire is a part of the national Mire Conservation Programme and is part of the European Union's Natura 2000 network. The Mire consists of Natura-

EXECUTIVE SUMMARY (continued)

protected aapa mires and other protected habitats and has several protected plant species. The proposed underground mining is located directly east of the Kitinen River in the corner of the Mire and partly beneath the Mire in the HSA.

The groundwater system and primary hydrogeology within the HSA can be described by the following:

1. A Shallow Groundwater System in the shallow alluvial and fluvial deposits,
2. A Fractured Bedrock in the Shallow Groundwater System in the upper portion of the bedrock consisting of preglacial weathered bedrock and fractured bedrock, and
3. A Deep Groundwater System in the Unfractured Bedrock in the lower portion of the bedrock underneath the Fractured Bedrock that has not been weathered.

The conceptual hydrogeologic model is a description of the major components that affect the Shallow and Deep Groundwater Systems, interactions between the Shallow and Deep Groundwater Systems, the future groundwater inflows into the Mine Workings, and the potential drawdown associated with underground mining within the HSA. The following are the key components of the conceptual hydrogeologic model of the HSA and Project Site:

1. **Precipitation and Evapotranspiration** – Precipitation at the Project Site varies throughout the year. Precipitation occurs as rain during the summer/autumn months and snow in the winter months. During the winter months, snow accumulates on the ground surface, resulting in snowpack of varying depths each winter. The groundwater system is recharged by the spring snowmelt and the summer/autumn rainfall events.

Evapotranspiration, which occurs primarily in the summer, is approximately 300 millimeters per year.
2. **Snowmelt and Spring Thaw** – As the ambient temperature warms in the spring, the snowpack begins to melt, with approximately 50 percent (%) of yearly surface-water runoff occurring during the spring snowmelt. It is during this snowmelt that recharge to the Shallow Groundwater System (peat, glacial and fluvial, and Fractured Bedrock) occurs.

EXECUTIVE SUMMARY (continued)

3. **Recharge from Snowmelt and Precipitation** – The HSA is characterized by long winters and accumulations of snow. Recharge to groundwater, especially in areas dominated by alluvial sediments and shallow aquifers, primarily occurs due to snowmelt during the spring thaw. Recharge is greatest in the late spring or early summer after the snowpack has melted and then again during the summer/autumn months during periods of higher rainfall. Recharge to the groundwater system varies depending on the hydrogeologic conditions and geologic setting.
4. **Future Climate** – Numerous studies have been conducted on the future climate of Finland. Studies indicate that there are likely to be increasing temperatures and precipitation in the HSA. Due to the projections in temperature changes, it is likely that the precipitation type (rain or snow) and snowmelt timing may change. Changes to these variables are likely to affect seasonal changes in groundwater levels and recharge to the groundwater system.
5. **The Mire** – The Mire is described as aapa mires and raised bogs, rich fens, petrifying springs, bog woodland, and western taiga and is the key environmentally sensitive area within the HSA, with many types of vegetation and animals that are assigned with threatened status. The peat is a saturated hydrogeologic unit within the Mire that stores a significant amount of water that is used by the Mire ecosystem. Water within the peat is partially perched, with a leaky base of compacted peat with low hydraulic conductivity (K) values that separates the peat from the underlying glacial and fluvial sediments. This low- K -value zone is not present everywhere in the peat, which results in localized hydraulic connection between the peat and the glacial and fluvial sediments. Surface-water runoff occurs across the Mire during the snowmelt, with areas of the Mire retaining water during the summer months due to the lakes, strings, and flark features.
6. **Groundwater Levels and Groundwater Quality** – Measured groundwater levels within the Shallow Groundwater System hydrogeologic units show seasonal changes in groundwater levels due to seasonal recharge. Similar measured groundwater-level responses occur within the Fractured Bedrock. Measured groundwater levels in the bedrock show less seasonal response, which indicates limited hydraulic connection between the overlying Shallow Groundwater System and the Deep Groundwater System.

Groundwater in the Fractured Bedrock unit communicates with groundwater in the overlying glacial and fluvial sediments, as evidenced by similar water chemistry. The available data suggest that the Unfractured Bedrock has a distinct groundwater chemistry with higher dissolved solids concentrations and contrasting characteristics from the water chemistry found in the glacial/fluvial sediments and Fractured Bedrock. These water-chemistry data suggest limited hydrologic interchange between the Unfractured Bedrock of the Deep Groundwater System and the Shallow Groundwater System hydrogeologic units.

EXECUTIVE SUMMARY (continued)

7. **Surface Water** – Surface-water runoff over the ground surface above the underground mining zone occurs primarily during the spring melt season, when over 50% of the yearly runoff occurs. Surface water drains across the ground surface above the underground mining zone through a series of channels and drainages. Surface-water runoff in channels results in recharging along channel areas (i.e., losing streams) and discharging of surface water to the primary rivers. The primary rivers within the HSA are the Kitinen, Kelujoki, Hiivanahaara, and Ylijoki Rivers. The Kitinen River flows through the center of the HSA and is regulated by hydroelectric dams. The other two primary rivers drain the eastern and southern sides of the HSA and eventually flow into the Kitinen River at the southern boundary of the HSA.
8. **Geologic Setting** – The hydrogeologic setting of the Project Site can be characterized by Shallow and Deep Groundwater Systems with distinct hydrogeologic units. The Shallow Groundwater System is primarily sediment deposits of fluvial and glacial origins and underlain by the Fractured Bedrock. Below the Fractured Bedrock, within the Deep Groundwater system, is an Unfractured Bedrock that is primarily mafic and ultramafic volcanic bedrock.

The fluvial and glacial sediment deposits have moderate to high K values ($> 1 \times 10^{-6}$ meters per second [m/s]). The Fractured Bedrock has higher K values than the underlying Unfractured Bedrock, which has low K values, with a median measured K value of 1×10^{-8} m/s. Groundwater flow is primarily limited to localized fractures within the Unfractured Bedrock.
9. **Local and Regional Geologic Faults** – The Project Site comprises the following primary faults in the vicinity of the Mine Workings: the Basal Thrust, East, East-West, SENW1 and SENW2, East-West Central, and Hanging Wall Shear Faults. In addition, there are regional faults. The primary fault that is encountered by the underground mining zone is the Basal Thrust. Measured K -value data from hydraulic testing indicate that the Basal Thrust has increased K values compared to the surrounding bedrock, while other faults have similar K values to the Unfractured Bedrock.
10. **Mine, Decline, and Underground Working Development** – Exploration drilling before 2017 at the Project Site has resulted in open boreholes that intercept the mineralized area and may have hydraulic connection with groundwater in the overlying hydrogeologic units during the operational stage. AASM Oy is in the process of sealing the boreholes that could potentially be intercepted by the underground mining operation. According to current plans by AASM Oy, all boreholes within the underground mine footprint and within a 50-meter (m) buffer zone from the underground mine footprint will be sealed during the construction phase.

EXECUTIVE SUMMARY

(continued)

Four Declines will be developed from the ground surface in the Kuusivaara area to the primary Mine Workings that are located in the Deep Groundwater System underneath the Mire. The Mine Workings will be within the Deep Groundwater System. The construction of the Declines and underground workings is likely to affect the groundwater system in the Deep Groundwater System and, depending on the hydraulic properties of the bedrock and structures, there may be localized hydraulic connection between the Deep and Shallow Groundwater Systems.

Groundwater inflow will occur at the Mine Workings depending on the hydraulic parameters of the geologic setting and geologic structures. In places where large groundwater inflow is occurring that could affect the operation or induce large drawdown of groundwater levels, AASM Oy plans to use mitigation methods such as grouting water-bearing faults.

Due to the emplacement of the underground workings in the low-*K*-value bedrock in the Deep Groundwater System, the potential effect of the mining on the Shallow Groundwater System and water table is likely to be limited.

GROUNDWATER FLOW MODEL

The groundwater flow model used in this study was constructed using the finite-element code *MINEDW* (Itasca 2012), which solves three-dimensional (3-D) groundwater flow problems using the finite-element method. The following are the key components of the groundwater flow model:

1. The groundwater flow model boundaries were selected to follow natural hydrologic divides and flow paths, such as ground-surface divides and surface-water rivers.
2. The groundwater flow model simulates surface-water rivers at the boundaries with constant heads and regional groundwater flow with a variable-flux boundary.
3. Recharge was applied to the groundwater system based on data from a *MIKE SHE* model for the till, sorted sediments, and peat hydrogeologic units.
4. The hydrogeologic units were based on the geologic models that were provided by AASM Oy. Hydraulic parameters of the hydrogeologic units were defined based on the groundwater flow model calibration and the field data collected at the Project Site.

The groundwater flow model was calibrated to measured steady-state groundwater levels and measured transient groundwater-level data within the groundwater systems from June 2012

EXECUTIVE SUMMARY

(continued)

through June 2021. A groundwater flow model calibration is the process of varying model input parameters over measured or likely ranges of values in a systematic way until a satisfactory match between simulated and measured data is obtained. Statistical measures (mean error, mean absolute error, root mean square error, normalized root mean square error, and coefficient of determination) were used to evaluate the groundwater flow model calibration. The following is a summary of the groundwater flow model calibration:

1. The simulated steady-state groundwater-level contours follow the ground-surface topography within the HSA. Simulated steady-state groundwater levels indicate that groundwater drains toward the primary rivers that are within the HSA. The simulated steady-state groundwater levels closely agree with measured values at the Project Site.
2. The mean error (ME), mean absolute error (MAE), and root mean square error (RMSE) for the steady-state groundwater flow model calibration are 0.1 m, 0.6 m, and 0.8 m, respectively. Overall, the simulated steady-state groundwater levels are well calibrated to the measured groundwater levels. Calculated model statistics of ME, MAE, and RMSE are within normal ranges of well-calibrated values as defined by various references (Anderson and Woessner 1992; ESI 2017; Spitz and Moreno 1996). Definition of these statistical terms is presented in the main text. The mass balance error for the entire steady-state groundwater flow model is less than 0.001%, which is much lower than the maximum global mass balance acceptance level of 0.5% recommended by Reilly and Harbaugh (2004).
3. An examination of measured versus simulated groundwater level transient hydrographs from June 2012 through June 2021 shows that the simulated groundwater levels in monitoring wells are well calibrated (Hill 1998) to the measured groundwater levels with respect to seasonal changes in groundwater levels and groundwater-level magnitude.
4. The transient groundwater flow model is well calibrated to trends and magnitudes of the measured groundwater levels near the future Mine Workings, along the Declines, and within the Mire.
5. Across the HSA, the transient groundwater flow model is well calibrated to trends and magnitudes of measured groundwater levels within the Shallow and Deep Groundwater System, Fractured Bedrock, and Unfractured Bedrock.
6. Overall, the simulated transient groundwater levels are well calibrated to the measured groundwater levels. Calculated transient model statistics of ME, MAE, RMSE, and the coefficient of determination (r^2) are within normal ranges of a well-calibrated groundwater flow model as defined by various references (Anderson and Woessner 1992; ESI 2017; Spitz

EXECUTIVE SUMMARY (continued)

and Moreno 1996) and within the assumed measurement error of ± 1.0 m. The ME, MAE, and RMSE are typically less than 1.0 m and r^2 is typically greater than 0.95 over the entire transient calibration time period.

PREDICTIVE MODEL SIMULATIONS AND SENSITIVITY ANALYSIS

The calibrated groundwater flow model was used to provide predictions of future groundwater inflow rates into the proposed Mine Workings and potential drawdown in the groundwater system.

The following are the conclusions from the 80% Success in Grouting predictive model simulation:

1. The predicted peak groundwater inflow rate to the Mine Workings occurs by mid-Year 2, which is in the later stage of the construction phase. At this point in time, the Declines are almost completely constructed and the underground mine development has started. The peak groundwater inflow rate is approximately 118 cubic meters per hour (m^3/hr) (approximately 2,830 cubic meters per day [m^3/day]). After reaching a peak groundwater inflow rate, the groundwater inflow rate gradually decreases to a range between 100 m^3/hr and 110 m^3/hr (2,400 to 2,640 m^3/day) over the life of the mine.
2. Predicted drawdown in the Shallow Groundwater System along the Declines is predicted to be larger than at other locations due to the presence of the permeable Basal Thrust. Due to the higher permeability of the Basal Thrust, depressurization propagates from the Unfractured Bedrock in the Deep Groundwater System to the Shallow Groundwater System, resulting in drawdown in the water table. Peak drawdown values along the Declines are approximately 0.93 and 0.75 m in the winter and summer seasons, respectively, in Year 22 of mining.
3. Peak drawdown over the primary mining area is approximately 0.6 m at the end of mining, or Year 22.
4. The largest drawdown is associated with the shallow Decline and portal area, where the Mine Workings are shallower than 150 meters below ground surface [mbgs]). Along this section of the Declines, drawdown at the end of mining is less than 2.8 m.
5. Predicted drawdown varies seasonally due to the simulated seasonal recharge from snowmelt. Seasonal peak drawdown rates are predicted to occur prior to snowmelt in the spring.
6. Predicted drawdown at the end of mining of 0.6 m or less is within the seasonal variation of 0.5 to 2 m in measured groundwater levels over the primary mining area.

EXECUTIVE SUMMARY (continued)

7. Predicted drawdown at the end of mining of 2.8 m or less is within the seasonal variation of 1 to 20 m in measured groundwater levels in the Kuusivaara area.
8. It is predicted that the groundwater discharge to the Kitinen River may decrease by up to 20 m³/hr, which equates to approximately 4% to 6% of total simulated groundwater discharge to the Kitinen River. The total decrease in simulated discharge is a negligible change (approximately a 0.01% change) in the total measured river flow rate (SYKE 2022). The predicted decrease in the groundwater discharge to the Kitinen River does not incorporate the planned discharge of treated mine water to the Kitinen River. It is likely that if treated water from the groundwater inflow from the Mine Workings and other site water is discharged to the Kitinen River, the amount of the treated water from the Mine Workings would be greater than the predicted reduction of the groundwater discharge to the Kitinen River.
9. Groundwater levels within the Shallow Groundwater System begin to recover after mining ends. Within 5 years after the mine closure, groundwater levels within the Shallow Groundwater System have recovered to within 0.1 m of the pre-mining condition. The Shallow Groundwater System is predicted to recover to less than 0.01 m of the pre-mining condition 75 years after mining ends.
10. Due to the low *K* values of the Unfractured Bedrock, deeper monitoring locations require a longer time to recover than shallower monitoring locations. By 400 years after mining, all monitoring locations within the Unfractured Bedrock have drawdown less than 1 m.

The following are the conclusions from the 65% Success in Grouting predictive simulations:

1. The predicted peak groundwater inflow rate to the Mine Workings occurs by mid-Year 2, which is in the later stage of the construction phase. At this point in time, the Declines are almost completely constructed, and the underground mine development has started. The peak groundwater inflow rate is approximately 122 m³/hr (approximately 2,930 m³/day). After reaching a peak groundwater inflow rate, the groundwater inflow rate gradually decreases to a range between 107 m³/hr and 118 m³/hr (2,570 to 2,830 m³/day) over the life of the mine.
2. Predicted drawdown in the Shallow Groundwater System along the Declines is predicted to be larger than at other locations due to the presence of the permeable Basal Thrust. Due to the higher permeability of the Basal Thrust, depressurization propagates from the Unfractured Bedrock in the Deep Groundwater System to the Shallow Groundwater System, resulting in drawdown in the water table. Peak drawdown values along the Declines are

EXECUTIVE SUMMARY (continued)

approximately 1.0 and 0.8 m in the winter and summer seasons, respectively, in Year 22 of mining.

3. Peak drawdown over the primary mining area is approximately 0.6 m at the end of mining, or Year 22.
4. The largest drawdown is associated with the shallow Decline and portal area, where the Mine Workings are shallower than 150 mbgs. Along this section of the Declines, drawdown at the end of mining is less than 4.0 m.
5. Predicted drawdown varies seasonally due to the simulated seasonal recharge from snowmelt. Seasonal peak drawdown rates are predicted to occur prior to snowmelt in the spring.
6. Predicted drawdown at the end of mining of 0.6 m or less is within the seasonal variation of 0.5 to 2 m in measured groundwater levels over the primary mining area.
7. Predicted drawdown at the end of mining of 4.0 m or less is within the seasonal variation of 1 to 20 m in measured groundwater levels within the Kuusivaara area.
8. It is predicted that the groundwater discharge to the Kitinen River may decrease by up to 20 m³/hr, which equates to approximately 4% to 6% of total groundwater discharge to the Kitinen River. The total decrease in discharge is a negligible change (approximately a 0.01% change) in the total river flow rate (SYKE 2022). The predicted decrease in the groundwater discharge to the Kitinen River does not incorporate the planned discharge of treated mine water to the Kitinen River. It is likely that, if treated water from the groundwater inflow from the Mine Workings and other site water is discharged to the Kitinen River, the amount of the treated water from the Mine Workings would be greater than the predicted reduction of the baseflow of the Kitinen River.
9. Groundwater levels within the Shallow Groundwater System begin to recover after mining ends. Within 10 years after the mine closure, groundwater levels within the Shallow Groundwater System have recovered to within 0.1 m of the pre-mining condition. The Shallow Groundwater System is predicted to recover to less than 0.01 m of the pre-mining condition 75 years after mining ends.
10. Due to the low *K* values of the Unfractured Bedrock, deeper monitoring locations require a longer time to recover than shallower monitoring locations. By 400 years after mining, all monitoring locations within the Unfractured Bedrock have drawdown less than 2.5 m.

The following are conclusions regarding the potential effects on the model predictions of future groundwater inflow and drawdown with the removal of the NE deposit from the mine plan:

EXECUTIVE SUMMARY (continued)

1. There is a long-term reduction in groundwater inflow as compared to the model scenarios with the NE deposit described above. After Year 6 of mining, groundwater inflows reduce to 95 to 100 m³/hr and 100 to 105 m³/hr for the 80% and 65% Success in Grouting without the NE Deposit Scenarios, respectively. This is a reduction of approximately 5 to 10 m³/hr for each model scenario.
2. The peak drawdown over the primary mining area is reduced to approximately 0.2 m. This is a reduction of up to 0.4 m from the mine plan including the NE deposit.
3. Predicted drawdown of 0.2 m or less at the end of mining is less than the seasonal variation of 0.5 to 2 m in measured groundwater levels over the primary mining area.
4. There are limited to no effects on the predicted reduction in the baseflow to the Kitinen River.
5. There are limited to no effects on the predicted groundwater recovery with the removal of the NE deposit from the mine plan. This is because for the Shallow and Deep Groundwater Systems, the predicted drawdown from mining occurs over the main deposit and along the Decline, which remains unchanged between the two mining plans. Consequently, the groundwater recovery times remain unchanged between the mining plans with and without the NE deposit.

Sensitivity analyses were conducted to assess the effect of the key mining parameters and climate on the predicted groundwater conditions. The results from the sensitivity analyses indicate the following:

1. Potential climate change has the following effects on the groundwater flow model predictions:
 - a. There are negligible differences in the predicted groundwater inflow rates into the Mine Workings. This is because the Mine Workings are not directly connected to the Shallow Groundwater System. The predicted groundwater inflow rates into the Mine Workings are related to the removal of groundwater storage in the Unfractured Bedrock.
 - b. The predicted drawdown is highly sensitive to annual precipitation and recharge rates. In drier years, the predicted drawdown rate is increased. In wetter years, the predicted drawdown rate is decreased.

EXECUTIVE SUMMARY (continued)

- c. Predicted long-term drawdown trends indicate that there is increased drawdown in a varying climate in monitoring locations that are near sorted sediments and tills, as the future predicted recharge rates are declining in these hydrogeologic units.
 - d. Long-term trends indicate decreased or similar drawdown in monitoring locations that are within or near peat, as the future predicted recharge rates are increasing in this hydrogeologic unit.
- 2. An increase in grout efficiency is likely to decrease the groundwater inflow rates and drawdown along permeable fault structures. As such, successful implementation of grouting to reduce groundwater inflows from water-bearing structures is crucial.
 - 3. A reduction in K values of the backfill has negligible effect on the overall results, as the K value of the backfill is more permeable than the surrounding bedrock.

KEY ASSUMPTIONS AND UNCERTAINTIES ASSOCIATED WITH THE GROUNDWATER FLOW MODEL

The following is a summary of the key assumptions in the groundwater flow model and the uncertainties:

- 1. Site-specific hydraulic parameters were available over the primary area of the proposed Mine Workings. The following is a summary of the assumptions in the conceptual and numerical models:
 - a. The bedrock along the Decline and Kitinen River area was assigned to be more permeable than the bedrock in the mining area based on K -value data. However, there are less measured K -value data in this area when compared to the extensive K -value dataset in the mining area.
 - b. Packer-testing data indicate that faults in the proposed mining area have similar K values to the bedrock around the faults because the fractures are generally filled and are characterized as mylonitic faults.
 - c. The peat is simulated as one hydrogeologic unit with no spatial variation in K values. Studies of the peat indicate that there is a distribution of K values within the peat, with a lower K value at the base of the peat. This low- K -value zone can impede water seepage to underlying units and separate the peat from the underlying glacial and fluvial sediments in many areas. A reduction in peat K values with depth may limit hydraulic connection with the underlying hydrogeologic units. A discussion of the peat conceptual model is provided in the main text of this report.

EXECUTIVE SUMMARY (continued)

- d. The K values of all Unfractured Bedrock and faults were assumed to decrease with depth based on measured K -value data.
2. The groundwater flow model is well calibrated to the available transient groundwater-level data. The groundwater flow model is calibrated primarily to monitoring locations within the fluvial and glacial deposits, Fractured Bedrock, and shallow Unfractured Bedrock. There are less available data about groundwater levels in the Deep Groundwater System (greater than 200 mbgs) than those of the shallower hydrogeologic units.
3. Recharge to the Shallow Groundwater System is a key component of the water balance and results in fluctuations of the groundwater levels seasonally. A *MIKE SHE* model was used to estimate the recharge to the Shallow Groundwater System.
 - a. It is likely that recharge varies at a smaller spatial scale than assumed for the three hydrogeologic units (i.e., sorted sediments, till, and peat) due to the complexity of the hydrogeologic units and climate. There are extensive monitoring data available in the Mine Workings area; however, less data are available to measure/estimate the variation in recharge rates across the HSA and boundaries of the HSA.
 - b. No data are available on future recharge rates for the HSA. Average recharge rates and estimates of recharge for a future climate were used in the groundwater flow model predictions. The estimated recharge rates are sensitive to the assigned meteorological parameters.
4. The predicted drawdown does not consider the effects of dense vegetation, the suction effect of roots, and the large storage of the shallow surficial composed materials. These effects will reduce the predicted drawdown of the groundwater table.
5. The peat drawdown is predicted based on the assumption that the peat is hydraulically connected to the Shallow Groundwater System and behaves as porous media. Based on the available data, it is reasonable to assume that the peat unit within the Mire system in many areas has low- K -value zones and is only partially hydraulically connected to the Shallow Groundwater System. Consequently, the predicted drawdown from the groundwater flow model is likely to be higher than the actual field-observed drawdown in the peat.
6. The predicted drawdown does not consider the increased recharge that will occur as the result of lowering of the water table induced by the mining operation. The increased recharge will reduce the predicted drawdown of the groundwater table.

1.0 INTRODUCTION

The Sakatti Project is a proposed copper-nickel-platinum group element mine located in the northern part of Finland, approximately 16 kilometers (km) northeast of Sodankylä in the Finnish Lapland. Anglo American's subsidiary AA Sakatti Mining Oy (AASM Oy), who owns and will operate the Sakatti Project, requested that Itasca Denver, Inc. (Itasca) review the available hydrogeologic data that have been collected at the Sakatti Project (referred to hereafter as the "Project Site"), review and update the conceptual hydrogeologic model, develop and calibrate a groundwater flow model that focuses on the future mining operation, and provide predictions of future groundwater conditions over the life of the mine (LOM). The following are the primary objectives of this study and are presented in this report:

1. Review available hydrogeologic data that have been collected at the Project Site;
2. Review and update the conceptual hydrogeologic model based on the recently collected hydrogeologic data, including groundwater levels, geologic data, and mine plan data;
3. Develop a groundwater flow model that is representative of the conceptual hydrogeologic model and focuses on the mining operation;
4. Calibrate the groundwater flow model to seasonal changes in groundwater levels;
5. Predict the future groundwater inflow rates to the Mine Workings and potential drawdown in the groundwater system using different sensitivity scenarios;
6. Conduct a robust sensitivity analysis of the key model parameters within the groundwater flow model;
7. Provide an assessment of the overall groundwater flow model uncertainty;
8. Assess the effect of climate change on the future groundwater conditions; and
9. Provide guidance and recommendations on the future dewatering and groundwater monitoring at the Project Site.

The purpose of this report is to provide a summary of the completed work described above.

1.1 DISCUSSION OF TERMINOLOGY

For brevity, the following terminology is used throughout the report:

1. AASM Oy – This refers to hydrogeologists, scientists, and engineers at the Sakatti Project.
2. The Project Site – This refers to the Sakatti Project entity, including the main and satellite ore deposits, Mine Workings, and surface infrastructure.
3. Mine Workings – This refers to the proposed underground workings around the ore bodies and stopes.
4. Declines – This refers to the underground workings that are constructed by the tunnel bore machine in the construction phase of mining.
5. Groundwater inflow – This refers to seepage into the Mine Workings.
6. Fractured Bedrock – This refers to the upper portion of the bedrock that has been weathered and fractured due to metamorphic processes, faulting, tectonic stresses, and preglacial weathering.
7. Unfractured Bedrock – This refers to the lower portion of the bedrock underneath the Fractured Bedrock that has not been weathered or fractured.
8. Deep Groundwater System – This refers to the groundwater system in the local pores or localized fractured network of the Deep Bedrock.
9. Shallow Groundwater System – This refers to the groundwater system in the shallow alluvial, glacial, and fluvial deposits and Fractured Bedrock.
10. The Mire – This refers to the Viiankiaapa Mire.

2.0 CONCEPTUAL HYDROGEOLOGIC MODEL

2.1 HYDROLOGIC STUDY AREA

Figure 2-1 shows the hydrologic study area (HSA) that was defined for this study. The HSA is much larger than the planned mining zone to minimize the propagation of hydraulic stresses from mine dewatering to the HSA boundaries. The boundaries of the HSA were chosen to align with surface-water bodies (western, southern, and eastern boundaries), topographic divides (northern), and flow path lines for groundwater (northern, northwestern, and northeastern) for ease of boundary condition assignment under pre-mining, transient, and future groundwater conditions. The HSA is much larger than in previous studies (Stantec 2020) to include all available hydrogeologic data into the conceptual and numerical models. The following are the key advantages of the larger HSA domain:

1. The entire Viiankiaapa area (the Mire) is located within the HSA;
2. All Mine Workings (i.e., underground workings and stopes) and the Declines are included within the HSA;
3. The HSA boundary is a significant distance away from potential mining-induced hydraulic stresses to minimize any potential boundary effects on model predictions.

The area of the HSA is approximately 235 square kilometers (km²). Ground-surface elevations within the HSA range from 180 to 300 meters above mean sea level (mamsl). The ground-surface elevation grades from higher elevations at the northern boundary to lower ground-surface elevations at the southern boundary. Ground-surface elevations near the primary area of the Mine Workings range from 185 to 188 mamsl.

The Project Site is located directly east of the Kitinen River, the largest upper branch of the Kemijoki River (Figure 2-1; the Kemijoki River is approximately 60 km south of the HSA and is not shown). The Project Site will have two primary Mine Workings areas, a main deposit and a northeast (NE) deposit. The locations of the deposits are shown in the inset in Figure 2-1. The main deposit is approximately

0.45 km², and the center of the main deposit is located 600 meters (m) east of the Kitinen River. The NE deposit is approximately 0.07 km², and the center of the NE deposit is 1,400 m east of the Kitinen River. The two deposits will be accessed from the ground surface by four Declines that extend southwest from the main deposit for 2 km then an additional 3 km south (red line in Figure 2-1). The four Declines will have portals at the ground surface in the Kuusivaara area. The Kuusivaara area is approximately 10 km northeast of Sodankylä.

Figure 2-2 shows the location of the Viiankiaapa Mire (referred to herein as “the Mire”) and Natura 2000 area within the HSA. The Mire covers approximately 66 km² of the HSA. The Mire is located on the eastern half of the HSA. The Mire can be described by “aapa mires and raised bogs, rich fens, petrifying springs, bog woodland and western taiga” according to the Finnish government (National Parks 2022). The Mire area is the key environmentally sensitive area within the HSA, with many types of vegetation and animals that are assigned with threatened status (National Parks 2022). The Mire is a part of the national Mire Conservation Programme and is part of the European Union’s Natura 2000 network. The proposed underground mining at the Project Site is located directly east of the Kitinen River in the corner of the Mire and partly beneath the Mire in the HSA. The main and NE deposits of the Project Site are located at depth beneath the Mire. The shallowest levels of main and NE deposits are approximately 255 and 80 meters below ground surface (mbgs) underneath the Mire, respectively.

2.2 KEY COMPONENTS OF THE CONCEPTUAL HYDROGEOLOGIC MODEL

Figure 2-3 presents the main components of the conceptual hydrogeologic model along a northwest-facing isometric view of the ore deposit. Figure 2-4 shows the conceptual hydrogeologic model of the Mire system. The conceptual hydrogeologic model is a schematic presentation of the major components that affect the Shallow and Deep Groundwater Systems, interactions between the Shallow and Deep Groundwater Systems, the future groundwater inflows into the Mine Workings, and the potential drawdown associated with underground mining. Numbers that are

shown in Figure 2-3 (such as #1 to #14) are presented below as part of the primary components of the conceptual hydrogeologic model, which are as follows:

1. **Precipitation and Evapotranspiration** – Precipitation at the Project Site varies throughout the year (#1 in Figure 2-3). Precipitation occurs as rain during the summer/autumn months and snow in the winter months. During the winter months, snow accumulates on the ground surface, resulting in snowpack of varying depths each winter. The groundwater system is recharged by spring snowmelt and summer/autumn rainfall events.

Evapotranspiration (ET), which occurs primarily in the summer, is approximately 300 millimeters (mm) per year (#1).

2. **Snowmelt and Spring Thaw** – As the ambient temperature warms in the spring, the snowpack begins to melt, with approximately 50 percent (%) of yearly surface-water runoff occurring during the spring snowmelt (#1). It is during this snowmelt that recharge to the Shallow Groundwater System (peat, glacial and fluvial, and Fractured Bedrock) occurs.
3. **Recharge from Snowmelt and Precipitation** – The HSA region is characterized by long winters and accumulations of snow (#1). Recharge to groundwater, especially in areas dominated by alluvial sediments and shallow aquifers, primarily occurs due to snowmelt during the spring thaw. Recharge is greatest in the late spring or early summer after the snowpack has melted and then again during the summer/autumn months during periods of higher rainfall. Recharge to the groundwater system varies depending on the hydrogeologic condition and geologic setting.
4. **Future Climate** – Numerous studies have been conducted on the future climate of the Project Site. Studies indicate that there are likely to be increasing temperatures and precipitation in the HSA. Due to the projections in temperature changes, it is likely that the precipitation type (rain or snow) and snowmelt timing may change. Changes to these variables are likely to affect seasonal changes in groundwater levels and recharge to the groundwater system.
5. **The Mire** – The Mire is described as aapa mires and raised bogs, rich fens, petrifying springs, bog woodland, and western taiga and is the key environmentally sensitive area within the HSA, with many types of vegetation and animals that are assigned with threatened status. Figures 2-4a and 2-4b show a conceptual illustration of the hydrogeologic units, vegetation, and groundwater system and flow paths through the Mire area. The peat within the Mire is a saturated hydrogeologic unit that stores a significant amount of water that is used by the Mire ecosystem and vegetation. The peat has a variable thickness where the thickness of the peat unit increases with the increasing degree of decomposition. Water in the peat is partially perched, with a leaky base of compacted peat with low hydraulic conductivity (K) values that separates the peat from the underlying glacial and fluvial sediments (Korkka-Niemi et al. 2017; Salonen et al. 2016; Turtiainen 2020). This low- K -value zone is not present

everywhere in the peat and may be absent in mire/peat margins, which results in localized hydraulic connection between the peat and the glacial and fluvial sediments, as evidenced by similar water chemistry. Groundwater flow within the peat is primarily horizontal in the uppermost part of the peat due to the larger horizontal K values. There is a limited vertical groundwater flow component within the peat due to decreasing K values with depth.

The GTK peat survey (1965, unpublished) revealed that the degree of decomposition of the peat increases as the peat thickness increases and the degree of peat decomposition varies mainly between Von Post's classes H2–H8 in Viiankiaapa. The K values of peat have been observed to decrease as Von Post's decomposition rate increases (Morris et al. 2021; Päivänen 1973). The thickness and K values of the decomposed peat at Viiankiaapa can be described as follows:

- a. The weakly decomposed (H2–4) peat has a median thickness of 1 m and a maximum thickness of 4.5 m,
- b. The medium decomposed (H5–6) peat has a median thickness of 0.5 m and a maximum thickness of 2.4 m, and
- c. The well-decomposed (H7–8) peat has a median thickness of 0.3 m and a maximum thickness of 2.0 m (GTK 1965, unpublished).
- d. Generally, the increase in the degree of peat decomposition is steady, but also sharp or alternating changes exist in places. Based on in-situ measurements and the K -value calculations by Päivänen (1973), the K values can vary from 3×10^{-6} to 2×10^{-5} meters per second (m/s) for weakly decomposed peat, 1×10^{-6} to 2×10^{-5} m/s for medium decomposed peat, and 1×10^{-7} to 3×10^{-6} m/s for well-decomposed peat.

Surface-water runoff occurs across the Mire during the snowmelt, with areas of the Mire retaining water during the summer months due to the lakes, strings, and flark features. The suction of the roots is likely to prevent the drawdown of the groundwater levels of the peat layer as the result of the underdrain induced by mining.

Figure 2-4b presents representative hydrographs of groundwater levels within the Mire and beneath the Mire. Within the mine area, the peat has a thickness that ranges from less than 0.5 m to 7 m. Measured porewater pressures within the Mire at monitoring wells installed into the peat show increasing trends in groundwater levels during the winter months as snow depth increases and an ice gap forms on top of the well (i.e., snow depth increases porewater pressure on the peat, resulting in seemingly increasing porewater levels). Measured groundwater levels beneath the peat unit, at GA303 and GA403 (Figure 2-4b), do not have similar responses to pressure increases from snow depth. A comparison of the responses (groundwater and porewater pressure fluctuations) to increased snow depth (GA103 versus GA303/GA403) provides evidence that the peat and underlying sediments may not be hydraulically connected in all areas.

6. **Groundwater Levels and Groundwater Quality** – Measured groundwater levels within the Shallow Groundwater System hydrogeologic units show seasonal changes in groundwater levels due to seasonal recharge (#7). Measured groundwater levels in the Unfractured Bedrock show less seasonal response, which indicates limited hydraulic connection between the overlying Shallow Groundwater System and the Deep Groundwater System.

Groundwater in the Fractured Bedrock unit communicates with groundwater in the overlying glacial and fluvial sediments, as evidenced by similar water chemistry (#9). The available data suggest that the Unfractured Bedrock has a distinct groundwater chemistry with higher dissolved solids concentrations and contrasting characteristics from the water chemistry found in the glacial/fluvial sediments and Fractured Bedrock. These water-chemistry data suggest limited hydrologic interchange between the Unfractured Bedrock and the Shallow Groundwater System hydrogeologic units.

7. **Surface Water** – Surface-water runoff over the ground surface above the underground mining zone occurs primarily during the spring melt season, when over 50% of the yearly runoff occurs (#3). Surface water drains across the ground surface above the underground mining zone through a series of channels and drainages. Surface-water runoff through these channels within the HSA contributes to recharge in shallow sediments and discharge of water to the primary rivers. The primary rivers within the HSA are the Kitinen, Kelujoki, Hiivanahaara, and Ylijoki Rivers.

The Kitinen River flows through the center of the HSA and is regulated by hydroelectric dams (#4 and #5). The other two primary rivers drain the eastern and southern sides of the HSA and eventually flow into the Kitinen River at the southern boundary of the HSA.

8. **Geologic Setting** – The hydrogeologic setting of the Project Site can be characterized by Shallow and Deep Groundwater Systems with distinct hydrogeologic units. The Shallow Groundwater System (#8) is primarily sediment deposits of fluvial and glacial origins and underlain by the Fractured Bedrock unit (#10). Below the Fractured Bedrock unit (#10) is Unfractured Bedrock in the Deep Groundwater System that is primarily mafic and ultramafic volcanic bedrock (#11).

The fluvial and glacial sediment deposits have moderate to high K values ($> 1 \times 10^{-6}$ m/s). The Fractured Bedrock has higher K values than the underlying Unfractured Bedrock, which has low K values, with a median measured K value of 1×10^{-8} m/s. Groundwater flow is primarily limited to localized fractures within the Unfractured Bedrock.

The K values of the geologic units control the groundwater flow and the potential connection between the Shallow and Deep Groundwater Systems.

9. **Local and Regional Geologic Faults** – The Project Site comprises the following primary faults that intersect the main ore body area: the Basal Thrust (#13), East, East-West, SENW1 and SENW2, East-West Central, and Hanging Wall Shear Faults (#12). In addition, there are regional faults. The most significant fault across the Decline and mining area is the Basal

Thrust. Measured K -value data from hydraulic testing indicate that the Basal Thrust has increased K values compared to the surrounding Unfractured Bedrock, while other faults have similar K values to the bedrock.

Local and regional geologic faults could be water conductive or could be barriers to groundwater flow (#12 and #13); either of these conditions would influence the groundwater inflow rates, drawdown, and groundwater recovery.

10. **Mine, Decline, and Underground Working Development** – Exploration drilling before 2017 at the Project Site has resulted in open boreholes that intercept the mineralized area and may have hydraulic connection with water in the overlying hydrogeologic units during the operational stage. AASM Oy is in the process of sealing the boreholes that could potentially be intercepted by the underground mining operation. A majority of these boreholes will be sealed during the construction phase (#14).

Four Declines will be developed from the ground surface in the Kuusivaara area to the primary Mine Workings that are located in the Deep Groundwater System underneath the Mire. The Mine Workings will be within the Deep Groundwater System. The construction of the Declines and Mine Workings is likely to affect the groundwater system in the Deep Groundwater System and, depending on the hydraulic properties of the Unfractured Bedrock and faults, there may be connection between the Deep and Shallow Groundwater Systems. Groundwater inflow will occur at the Mine Workings depending on the hydraulic parameters of the geologic setting and faults. In places where high groundwater inflow is occurring that could affect the operation or induce a large groundwater drawdown, AASM Oy plans to use mitigation methods such as grouting water-bearing faults.

3.0 KEY HYDROGEOLOGIC DATA

The following sections provide an overview of the key hydrogeologic data that were used to support the development of the conceptual hydrogeologic model described in Section 2.0 and to support the development and calibration of a regional groundwater flow model that is described in Section 4.0. The following are the key data used in the development of the conceptual and numerical groundwater flow models and discussed below:

1. Geologic models, including geologic units and faults;
2. Hydraulic data from packer testing;
3. Climate data, including precipitation, ET, and future estimates of climate change; and
4. Proposed mine plans.

3.1 GEOLOGIC SETTING

Figure 3-1 and Figure 3-2 show the surficial geologic maps of the shallow deposits and bedrock in the HSA. The surficial geology map is a compilation of 1:20,000, 1:50,000, and 1:200,000 scale maps from the Geological Survey of Finland (2022). Figure 3-3 shows a north-south cross section of the geologic units in the mining area and the extent of the Mine Workings. Geologic data from the cross section are from geologic block models provided by AASM Oy. A discussion of the available geologic models is provided below. The geology of the Project Site consists of the peat overlying glacial and fluvial sediments. Beneath the glacial and fluvial sediments is Paleoproterozoic bedrock of the Central Lapland Greenstone Belt (Eilu et al. 2012; Pulkkinen 1983; Tyrväinen 1983). The upper portion of the bedrock is mainly preglacially weathered (Hall et al. 2015) and fractured from repeated periods of metamorphic processes, faulting, tectonic stresses, and glacial advancement. The weathered unit is preserved due to relatively weak glacial erosion. The upper portion of the bedrock is referred to herein as the Fractured Bedrock. Below the Fractured Bedrock is referred to as the Unfractured Bedrock. The ore deposit is located at a contact zone between the Lower Sodankylä Group and the Upper Savukoski Group geologic units (Luukas 2017). The Sodankylä Group

consists mainly of mica schists, metasiltsstones, and quartzites, with locally abundant metavolcanic and occasional dolomitic rocks. The overlying Savukoski Group comprises ultramafic volcanic rocks and schists. The ore deposit is hosted by ultramafic volcanics, ultramafic cumulates consisting of peridotites and dunites, mafic volcanics, and volcanic tuffs.

Figure 3-4 shows the primary geologic faults in the HSA based on data from AASM Oy, the Geological Survey of Finland (2022), and Luukas (2017). The primary faults in the HSA are shown in pink, while regionally mapped faults are shown in green (Geological Survey of Finland 2022) and yellow and black (Luukas 2017). Regional mapped faults from the Geological Survey of Finland (2022) and Luukas (2017) are based on airborne geophysical data interpretations. Mapped faults between the different data sources have some degree of overlap, and there is coincidence between the most detailed three-dimensional (3-D) model faults and semi-regional faults mapped in 2017. This coincidence has been confirmed by drilling. The bedrock within the HSA has been subjected to two primary structural events (Luukas 2017). The first north-south compression was caused by uplift and thrusting from the north and the development of shear zones directly below and above ore deposits. The second event resulted in the development of southeast-northwest trending faults that deformed the earlier faults. As shown in Figure 3-4, the Mine Workings intercept with several faults. The primary faults at the Project Site are included in the numerical and conceptual models.

3.1.1 Geologic Units

Figure 3-5 shows the extent of three geologic block models provided by AASM Oy. Geologic models were used directly in the groundwater flow model. The following is a summary of these geologic block models:

1. **Shallow System Geologic Model:** The shallow system geologic model covers the Project Site and the Mire area. The shallow system geologic model includes detailed representation of the shallow system geologic unit of the tills, sands, sediments, and peat and a representation of the Fractured Bedrock unit. Details of the shallow system are presented in Åberg et al. (2021).

2. **2021 Tunnel Bore Machine and Deposit Model:** The tunnel bore machine (TBM) line and deposit model is the latest iteration of geologic data that have been compiled by AASM Oy in 2021. The geologic model provides detailed information of the local faults and geologic units in the mine deposit area and along the TBM line.
3. **Kuusivaara Model:** The Kuusivaara model is a shallow system geologic model that provides detailed representation of the shallow geologic units of the Kuusivaara area. Details of the model are presented in Puumalainen (2021).

The geology of the Project Site can be divided into four main stratigraphic units:

1. The Mire,
2. Glacial and fluvial sediments that underlie the Mire,
3. Fractured Bedrock, and
4. Unfractured Bedrock.

Provided below is a summary of the primary stratigraphic units within the HSA.

3.1.1.1 The Mire

The Mire began as a post-glacial lake starting with the end of the last major glacial advance in Finland (Salonen et al. 2016). As discussed above, the Mire is a Natura 2000 protected area consisting of a wetland peat environment with sensitive and threatened plant and animal species. The Mire contains water bodies and patterned bogs with string and flark patterns (Korkka-Niemi et al. 2017). Figure 3-1 shows the mapped areas of peat within the HSA.

Figure 3-6 shows a map of the peat thickness within the HSA that is based on Åberg et al. (2021). Geological coring (Lappalainen and Pajunen 1982) indicates that the peat is up to 7.8 m thick with an average thickness of 2.3 m. Other Mire studies (Korkka-Niemi et al. 2017) estimated the average peat thickness at approximately 1.9 m. The shallow system geologic model contains the most up-to-date mapping of peat thickness, which is included in the conceptual and numerical models.

The peat becomes more compact with depth and, consequently, has decreasing K values with depth (i.e., limited connection between the peat and underlying units). The decreasing K values with depth result in perched water zones within areas of the Mire. Golder (2015) estimated the K values of the peat to have a range from 1.0×10^{-7} to 2.4×10^{-4} meters per second (m/s) with an average of 1.0×10^{-5} m/s. Additional K -value measurements of the peat ranged from approximately 9.8×10^{-6} to 1.0×10^{-5} m/s (Korkka-Niemi et al. 2017; Korkka-Niemi and Turtiainen 2020). Table 3-1 provides a summary of the measured K -value data for hydrogeologic units within the HSA.

Because the peat unit is considered a partially perched unit (Figure 2-4) that is separated from the underlying glacial and fluvial sediments and rock mass, the predicted drawdown from the groundwater flow model should be considered as drawdown in the glacial and fluvial sediments and rock mass below the peat unit. The drawdown in the peat unit could be significantly smaller than the drawdown in the glacial and fluvial sediments and rock mass due to a limited connection between the peat and underlying units. This statement is supported by the peat conceptual model, as discussed in Section 2.0.

3.1.1.2 Glacial and Fluvial Sediments

The glacial and fluvial hydrogeologic units of the Shallow Groundwater System comprise tills, sands, and gravels (Åberg et al. 2017; Åberg et al. 2021). There are three major till deposits, an upper till, a middle till, and a lower till (Åberg et al. 2020; Salonen et al. 2016). The most continuous sorted sediments above the upper till are top deposits originating from fluvial outwash sediments formed as part of a typical river morphology. Top deposits consist of fluvial sands and gravels, fine-grained flood plain deposits, and aeolian sands. Figure 3-1 shows the locations of the mapped gravel deposits within the HSA. The till deposits are intermixed with sand and gravel zones that generally have limited extents (Åberg et al. 2021; Salonen et al. 2014; Salonen et al. 2016). As shown in Figure 3-1, the gravel areas dominate along the Kitinen River, while tills typically represent areas of higher ground-surface elevations.

The lower till contains a mixture of moderate- and low- K -value units with a compacted lower K value than other till deposits (Åberg et al. 2020). As such, the lower till has the potential to isolate the overlying glacial and fluvial sediments from the underlying bedrock. However, the lower till is not continuous across the HSA. The shallow glacial and fluvial deposits that are located in the main and NE deposit areas are primarily the upper and lower tills and sorted sediments.

Hydraulic testing by Golder (2015) measured a range of K values for the fluvial and glacial deposits from 38 test holes. The K values range from 5.0×10^{-8} to 4.0×10^{-3} m/s with a mean value around 3.0×10^{-6} m/s (Golder 2015).

3.1.1.3 Fractured Bedrock

The Fractured Bedrock that lies beneath the fluvial and glacial deposits was formed from preglacial weathering (Hall et al. 2015) metamorphic processes, faulting, tectonic stresses, and glacial advancement (Helmens et al. 2000; Hättestrand and Stroeven 2002; Helmens et al. 2007; Hall et al. 2015; Sarala et al. 2015). The Fractured Bedrock comprises variable thicknesses of upper bedrock (top), reaching a maximum thickness of 150 to 200 m in places. Figure 3-3 along a north-south cross section through the Project Site shows the estimated Fractured Bedrock thickness. Table 3-1 provides a summary of the measured K values of the Fractured Bedrock. The thickness of the Fractured Bedrock is highly variable across the HSA. The proposed Mine Workings are located below the Fractured Bedrock by 20 to 200 m in the NE deposit and main deposit areas.

Previous studies (AASM Oy 2021; SRK 2019,) have shown that the Fractured Bedrock has K values that are considerably higher than the Unfractured Bedrock. The estimated average K value for the upper 50 m of the Fractured Bedrock is approximately 5.0×10^{-5} m/s with a range of K values from 1.0×10^{-7} m/s to 1.0×10^{-4} m/s. The lower section of the Fractured Bedrock has an average K value of 5.0×10^{-6} (AASM Oy 2021).

3.1.1.4 Unfractured Bedrock

Beneath the Fractured Bedrock is a mixture of mafic and ultramafic volcanic rocks that host the ore deposit. The rock mass of the Unfractured Bedrock is generally characterized as unfractured/unaltered bedrock. The Unfractured Bedrock typically has low K values. The K values of all Unfractured Bedrock data range from 1.0×10^{-12} to 3.4×10^{-5} m/s with a mean value around 1.0×10^{-8} m/s (AASM Oy 2021; SRK 2019). Unfractured bedrock K values that are not associated with localized fractures (discussed below) range from 1.0×10^{-12} to 1.0×10^{-7} m/s.

There are localized fractures within the rock mass of the Unfractured Bedrock. These fractures are small and localized as compared to the Fractured Bedrock, which has large-scale fracturing and weathering. Localized fractures within the Unfractured Bedrock have higher K values that are at a maximum of two orders of magnitude larger than the surrounding rock mass. In comparison to the measured K values of the Unfractured Bedrock, the measured K values of the localized fractures range from 1.0×10^{-8} to 3.4×10^{-5} m/s and are not continuous (as shown in spatial maps of measured K values in Section 3.1.3). Spatial distributions of K values within the Unfractured Bedrock are discussed below in Section 3.1.3. Table 3-1 provides a summary of the measured K values of the Unfractured Bedrock (AASM Oy 2021).

3.1.2 Geologic Structures

As shown in Figure 3-4, there are many interpreted faults from geophysical data within the HSA. The primary faults in the Project Site area have been characterized, while some regional faults outside of the Project Site area have unknown hydrogeologic characteristics. As shown in Figure 3-4, there is overlap in geologic structures between the regional faults and the local faults interpreted from several sources (AASM Oy 2021; GTK 2022; Luukas 2017). The geological fault model encompasses the known faults that will intercept the proposed Mine Workings and have been characterized, which include the Basal Thrust, East, East-West, SENW1 and SENW2, East-West Central, and Hanging Wall Shear Faults. These seven primary faults have both regional and local characteristics and

present the latest interpretation of faults at the Project Site, which is based on extensive drilling and geotechnical studies. Faults occur within both the Fractured and Unfractured Bedrock units but do not intercept the overlying glacial and fluvial sediments (Figure 3-3). Packer-testing data indicate that, at some intercepts of faults, there are increased K values (discussed below). However, the increased K values are typically localized and discontinuous. The estimated K values of the characterized faults within the 3-D geologic models range from 4.3×10^{-11} m/s to 1.3×10^{-7} m/s (AASM Oy 2021). Packer-testing data that were directly collected from the faults indicate that there is no distinct increase in K values at fault structures. Table 3-1 provides a summary of the measured K values of the faults.

The lowermost shear zone is a set of thrust faults and is referred to as the Basal Thrust. The Basal Thrust is a broken rock zone with extensive gravel-like fault breccia zones. The Basal Thrust zone has been known for difficult drilling, with deep exploration holes at the Project Site typically terminating. The Basal Thrust has estimated K values ranging from 5.9×10^{-7} to 9.6×10^{-7} m/s, which are higher than other faults and the Unfractured Bedrock.

3.1.3 Hydraulic Testing at the Project Site

3.1.3.1 Summary of Hydraulic Testing

AASM Oy has conducted an extensive field-testing program with multiple hydraulic testing methods to obtain K values of specific lithology types and geological faults. The methods included packer testing, pumping tests, falling head tests, spinner logging, and air-lift testing. Provided below is a summary of the hydraulic testing and an overview of the measured K values in the vicinity of the Project Site.

3.1.3.2 Summary of Hydraulic Test Results

Figure 3-7 shows the measured K values of all packer tests from 2016–2021 by depth (281 successful tests from 57 boreholes). The figure also shows the delineation of packer-testing data where, based

on rock quality designation (RQD) value distribution within packer interval, bedrock fractures were intercepted (orange) and Unfractured Bedrock (purple) (AASM Oy 2021). To delineate between bedrock fractures and Unfractured Bedrock, a criterion of a RQD <25% class within packer interval was used to indicate bedrock fractures. Due to heterogeneity of fracturing, not all of these occurrences are associated with fault descriptions of the site geologic model. An approximate division between elevated and background K values in the packer data was placed at 1.0×10^{-8} m/s in the bedrock and at 1.0×10^{-7} m/s in the upper part above -100 mamsl. In addition to all measured K -value data, the estimated geometric means and 75th percentile of the bedrock and fractures are shown as well as representative trend lines separately for both the background values and the low-RQD-indicating intervals. A summary of the packer-testing data is provided in Table 3-2. The packer-testing data in Figure 3-7 indicate that the K values of the bedrock decrease with depth. The upper bedrock is more permeable than the deeper bedrock. The measured K values in the upper bedrock, from -100 to 100 mamsl, range from 1.0×10^{-9} to 1.0×10^{-7} m/s. The lower bedrock, beneath -100 mamsl, has background K values that range from 1.0×10^{-11} to 1.0×10^{-7} m/s, with most measured values below 1.0×10^{-8} m/s. Where packer testing intercepted fractures within the bedrock, the measured K values of these localized intervals are higher than the measured K values in the bedrock that does not intercept fractures. The K values of packer testing for intervals containing fractures range from 1.0×10^{-8} to 1.0×10^{-4} m/s. In general, where fractures are intercepted, the K values are typically one to two orders of magnitude larger than the surrounding bedrock. Similar to the measured K values of the rock mass, the measured K values of the fault intervals intercepted by the Fractured Bedrock also show a large degree of variability. In addition, localized bedrock fractures also suggest a decreasing K value trend with depth.

Figure 3-8 shows the measured K -value data from all acceptable packer tests, with 281 measurements from 2016–2021 that are categorized by rock type. As shown in Figure 3-8, packer-test data do not indicate any trend based on the rock type. Though the ranges of measured K values in some lithological intervals (e.g., in scapolite-mica rock or dolomite) are greater than those in other rock types, the mean K values for all rock types are similar. All rock types show a similar trend of

decreasing K values with depth. Figure 3-9 shows the measured K -value data of the packer tests in conjunction with falling head tests (Figure 3-9a), pumping tests (Figure 3-9b), and spinner log tests, with 25 measurements (Figure 3-9c). In addition to the packer testing, all other hydraulic testing at the Project Site indicates similar K values to those from the packer testing. Most spinner log tests were conducted on the upper part of the Unfractured Bedrock and at fracture intercepts. A summary of estimated K values from falling head tests (three measurements), pumping tests (19 measurements), and air-lift tests (nine measurements) is provided in Tables 3-3, 3-4, and 3-5, respectively.

Figures 3-10, 3-11, and 3-12 show spatial plots of the interpolated measured K values from the packer tests. The purpose of these spatial plots is to show spatial trends in K values at specified depth intervals. Interpolated K values on each plot are shown with a kriged surface and a color range. Locations of measured packer-testing data that were used to support the kriged surfaces are shown by green symbols. Based on the spatial plots of 2016–2021 packer-testing data of 281 measurements, the following can be concluded:

1. The Unfractured Bedrock, below 0 mamsl, typically has low K values ranging from 1.0×10^{-11} to 1.0×10^{-7} m/s.
2. Measured K values of the Unfractured Bedrock decrease with depth.
3. At some locations, the measured K values are higher along faults at the Project Site or at fault convergence. However, the higher K values are localized and discontinuous.
4. Measured K -value data indicate that there are increased bedrock K values closer to the Kitinen River and along the Declines. The potential reasons for increased K values are as follows:
 - a. Increased K values along the Declines may be related to the Basal Thrust Fault.
 - b. Increased K values near the Kitinen River may be due to the presence of the river channel.

Figure 3-13 shows the measured K values from packer-testing data at faults of the geological model (from 2016–2019) or fault intercepts from 2020–2021 (31 measurements). Table 3-6 provides a

summary of the measured K values along the fault structures. As shown in the figure and table, there are no distinct or continuous trends of increased K values at geologic model faults in comparison with the measured K values of the Unfractured Bedrock, suggesting that the K values of the faults are similar to the Unfractured Bedrock. However, as described above, there are elevated K values that are discontinuous associated with low-RQD occurrences at packer intervals.

3.1.4 Summary of Hydrogeology Setting

The hydrogeologic setting of the Project Site can be characterized by a Shallow and a Deep Groundwater System with distinct hydrogeologic units. The Shallow Groundwater System is primarily fluvial and glacial sediment deposits underlain by the Fractured Bedrock. Below the Fractured Bedrock, the Deep Groundwater System is an Unfractured Bedrock that is primarily mafic and ultramafic volcanics. The following is a summary of the key geologic setting components at the Project Site from shallow to deep:

1. The fluvial and glacial deposits have the following characteristics:
 - a. The primary units within the Shallow Groundwater System are sands, gravels, tills, and a peat layer.
 - b. The fluvial and glacial deposits have moderate to high K values ranging from 5.0×10^{-8} to 4.3×10^{-3} m/s.
 - c. Due to the heterogeneity of sediment units and, therefore, compartmentalization, the Shallow Groundwater System across the Project Site is not hydraulically connected.
 - d. The thickness of the Shallow Groundwater System varies between 5 and 50 m with a median thickness of 13 m.
2. The Fractured Bedrock has the following characteristics:
 - a. The Fractured Bedrock has higher K values (ranging from 1.0×10^{-7} to 1.0×10^{-5} m/s) than the underlying Unfractured Bedrock (ranging from 1.0×10^{-11} to 1.0×10^{-7} m/s) due to multiple periods of weathering and fracturing.
 - b. Groundwater in the Fractured Bedrock unit is hydraulically connected with groundwater in the overlying glacial and fluvial sediments based on groundwater levels and water chemistry (discussed below).

- c. The thickness of the Fractured Bedrock ranges from 0 to 200 m and is highly variable in thickness. Median thickness of very poor rock quality is on the order of 10 m, though thicknesses exceeding 100 m are found occasionally, partly associated with bedrock interception of fault zones. In the area where there is no Fractured Bedrock, there is a direct contact between the overburden and the Unfractured Bedrock. Contact between the Unfractured Bedrock and Fractured Bedrock can be sharp or gradational.
3. The Unfractured Bedrock has the following characteristics:
 - a. The Unfractured Bedrock has low K values ranging from 1.0×10^{-11} to 1.0×10^{-7} m/s.
 - b. Groundwater movement in the Unfractured Bedrock is primarily limited to local fractures.
 - c. The K -value data of the Unfractured Bedrock show a decreasing trend with depth.
 - d. There are no trends in the K values with respect to geologic unit within the Unfractured Bedrock.

The following is a summary of the geologic faults at the Project Site:

1. 3-D modeled faults at the Project Site include the Basal Thrust, East, East-West, SENW1 and SENW2, East-West Central, and Hanging Wall Shear Faults. In addition, there are regional faults presented as surface lines (GTK 2022; Luukas 2017).
2. Hydraulic testing during drilling indicates that faults that intersect the Project Site have limited hydraulic connectivity, are isolated from overlying formations, and have low storage.
3. The K values of faults intersecting the ore body are highly variable. Spatial distribution of K -value data indicates that most K values along the faults are similar to the K values of the Unfractured Bedrock ranging from 1.0×10^{-11} to 1.0×10^{-7} m/s. However, in isolated areas, the measured K values are higher than the measured K values of the Unfractured Bedrock.
4. The K -value data indicate increased K values were encountered at localized segments of some fractures. However, these increased K values are not continuous. At these locations, the measured K values can be up to one to two orders of magnitude larger than the K values of the Unfractured Bedrock. However, there are no large-scale trends of increasing K values along seven modeled faults in the geologic model.
5. The Basal Thrust is the most significant structure that has been identified at the Project Site. The Basal Thrust is associated with broken ground, and its thickness varies considerably across the Project Site (approximately 5 to 30 m in the Decline area). Hydraulic testing indicates that the Basal Thrust has moderate to slightly elevated K values and significant groundwater storage. The Basal Thrust is expected to be intercepted during construction of

the Declines but not during mining. The main ore body is above the Basal Thrust. AASM Oy plans to not mine near the Basal Thrust with a minimum offset distance of 50 m from the Mine Workings to the Basal Thrust.

6. In addition to the local and regional structures at the Project Site, regional geologic mapping indicates the presence of other large-scale faults within the HSA. The hydrogeologic characteristics of these regional faults are unknown. However, these regional structures do not intercept the Mine Workings. Though limited data are available on faults outside of the Project Site, data from the Project Site indicate that these faults are not likely to be hydraulically connected to faults within the Project Site because Project Site faults have limited connection and continuity and have low-*K*-value characteristics.

3.2 METEOROLOGIC DATA

Figure 3-14 shows a map of the meteorological and hydrological data collection locations for the Project Site. These meteorological sites include measurement locations for precipitation, evaporation, frost, discharge, soil moisture, snow depth, and water content. The primary data collection sites are 20 km south of the HSA at Sodankylä Tähtelä and within the HSA around the Mire and Project Site. Data from these monitoring sites are used by AASM Oy to understand the climatic condition and potential trends in climate across the HSA. Data from these sites are discussed below.

3.2.1 Precipitation

Figure 3-15a shows measured annual precipitation data between 1959 and 2020 for the Sodankylä Tähtelä station and a trend line of the measured annual precipitation. Table 3-7 provides a summary of the measured annual precipitation rates. Annual measured precipitation rates range from 390 to 785 mm with an average of 518 mm between 1959 and 2020. A trend line of the measured precipitation data indicates that measured annual precipitation rates have been increasing since 1959. The average precipitation rates for the last 10 and 20 years are approximately 553 mm and 548 mm, respectively. Precipitation within the HSA is in the form of snow over the winter season and rain during the summer season. Snow during the winter results in an increasing snowpack depth until spring.

Figure 3-15b shows the average monthly precipitation rate for the entire measured precipitation dataset (1959 through 2020), the last 20 years (2001 through 2020), and the last 10 years (2011 through 2020). Table 3-8 provides a summary of the average total monthly and daily precipitation rates for each month for the entire dataset, the last 20 years, and the last 10 years. The monthly average precipitation rate ranges from approximately 20 to 82 millimeters per month (mm/month). Daily precipitation rates for each month range from 1 to 2.7 millimeters per day (mm/day). Peak monthly and daily precipitation rates are in the summer months (May through October). Average monthly precipitation rates show increasing trends over the last 20 and 10 years of precipitation data.

3.2.2 Pan Evaporation

Figure 3-16 shows the measured pan evaporation rate at the Sodankylä Tähtelä station. Table 3-9 provides a summary of the measured annual evaporation data. Data from 2012 through 2015 are not used in the analysis, as pan evaporation data are incomplete. Pan evaporation rates range from 260 to 510 millimeters per year (mm/yr) with an average of 349 mm/yr from 1958 through 2011. A trend line of the measured pan evaporation rate shows that the pan evaporation rate has trended downward since 1957. The average pan evaporation rate from 2000 to 2011 is approximately 329 mm/yr. A recent study by Moroizumi et al. (2014) indicates that as pan evaporation decreases, there is relatively increasing actual ET. This is due to increases in soil moisture (i.e., increasing precipitation; Figure 3-15). Pan evaporation is usually larger than the potential evaporation (Brutsaert 1982). Pan evaporation data are used to estimate the potential ET (i.e., the amount of water consumed from evaporation and plant transpiration). SRK (2019) estimated the total annual average ET to be approximately 269 mm. ET primarily occurs from March through October.

3.2.3 Snow Depth and Snowmelt

Within the HSA, from approximately late October through early April, precipitation primarily falls as snow. It is during this time period that snow accumulates on the ground surface, resulting in

increasing snow depth. Beginning in April, as the ambient temperature warms, the snowpack begins to melt. Approximately 50% of yearly surface-water runoff occurs during the spring snowmelt. It is during this snowmelt time period that recharge to the Shallow Groundwater System (peat, glacial and fluvial, and Fractured Bedrock) occurs.

Figure 3-17 shows the measured and simulated snow water equivalents for two measurement locations, Viiankiaapa and Sodankylä Tähtelä. Simulated snow water equivalents are from a SYKE model provided by AASM Oy. Snow water equivalent measurements are periodically available over the winter seasons. Snow water equivalent data are available since 2019 and 2013 for the Viiankiaapa and Sodankylä Tähtelä measurement locations, respectively. Snow water equivalent measurements were used to calibrate a snow water equivalent in the SYKE model that was used for the Project Site. The calibrated snow water equivalent values are shown in Figure 3-17 with solid lines. In general, snow begins to accumulate in late October and quickly melts in April. Since 2013, measured peak snow water equivalents have ranged from 120 to 260 mm. The calibrated snow water equivalent measurements fit the measured snow water equivalent data well. Observed snow water equivalent data were used in a *MIKE SHE* model as observation points to compare the observed snow water equivalent to the simulated snow water equivalent and to estimate potential recharge rates to the groundwater system.

3.2.4 Recharge from Snowmelt and Precipitation

The HSA region is characterized by long winters and accumulations of snow. Recharge to groundwater, especially in areas dominated by alluvial sediments and shallow aquifers, primarily occurs during the snowmelt. Recharge occurs during the spring melt of snowpack and again during the summer/autumn months during periods of higher rainfall.

For the Project Site, a *MIKE SHE* model has been constructed by using the meteorological variables to estimate potential recharge to the groundwater system seasonally. Figure 3-18 shows the HSA

boundary, which is also the boundary of the groundwater flow model discussed in Section 4.0, and the boundary of the *MIKE SHE* model. The following is a summary of the *MIKE SHE* model:

1. The *MIKE SHE* model area covers the entire main deposit and NE deposit areas and parts of the Mire area. The *MIKE SHE* model domain was delineated based on sub-catchment areas with the ArcMap Hydrogeology tool. The *MIKE SHE* model domain is smaller than the HSA and groundwater flow model developed in this study.
2. The primary climate input variables of the *MIKE SHE* model include precipitation, temperatures, potential evaporation, and leaf area index (LAI). Snowmelt was simulated with the snowmelt module. LAI and potential evaporation were based on MODIS satellite data (2022). LAI and potential evaporation were used to calculate actual ET in the *MIKE SHE* model.
3. Overland flow (OL), unsaturated zone (UZ), and saturated zone (SZ) modules were used to estimate groundwater recharge. OL was calculated with diffusive wave approximation of the Saint-Venant equations, and UZ was calculated with Richard's equation (DHI 2017). SZ was calculated with the 3-D Darcy's equation with the PCG groundwater solver based on a preconditioned conjugate gradient solution technique (DHI 2017).
4. The simulated hydrogeologic units were based on the simplified shallow system geologic model that consisted of seven layers. The following hydrogeologic units were assigned in the model: a peat unit, sorted sediments unit (top deposits, middle and lower sorted, lowest sands and gravels), and till unit (upper till and lower till). A simplified Fractured Bedrock layer was simulated at the base of the *MIKE SHE* model with a constant thickness of 10 m.
5. A uniform K value was defined for the hydrogeologic units.
6. Boundary conditions of the *MIKE SHE* model were defined as follows: the Kitinen River was presented as a constant head, and other areas were no-flow boundaries.
7. The K values in the sorted sediments, tills, and Fractured Bedrock units were calibrated to groundwater-head observations in the SZ module of the *MIKE SHE* model.
8. The *MIKE SHE* model was used to provide predictions of recharge to the shallow system hydrogeologic units used in the groundwater flow model described in Section 4.0.

Figure 3-19 shows the estimated daily recharge (negative values) and discharge rates (positive values) from June 2012 through June 2021 from the *MIKE SHE* model developed by AASM Oy and Stantec. Positive rates are discharge from the groundwater system to the surface-water system, and negative rates are recharge rates to the groundwater system. Recharge rates are summarized for

the three distinct hydrogeologic units in the Shallow Groundwater System: the sorted sediments, till, and peat. The following is a summary of the estimated recharge rates from the *MIKE SHE* model:

1. **Peat:** The estimated daily discharge and recharge rates range from 0 to 8 mm and 0 to 25 mm, respectively. The average recharge rate for the peat hydrogeologic units is approximately 12% of the measured annual precipitation rate.
2. **Sorted Sediments:** The estimated daily discharge and recharge rates range from 0 to 10 mm and 0 to 40 mm, respectively. The average recharge rate for the sorted sediments hydrogeologic unit is approximately 46% of the measured annual precipitation rate.
3. **Till:** The estimated daily discharge and recharge rates range from 0 to 12 mm and 0 to 29 mm, respectively. The average recharge rate for the till hydrogeologic units is approximately 30% of the measured annual precipitation rate.

Estimated recharge rates to the groundwater system from the *MIKE SHE* model are used directly in the groundwater flow model, as discussed in Section 4.0.

3.2.5 Future Climate

Multiple papers and studies have been conducted to understand the potential impacts of a varying climate on groundwater levels and meteorological variables in Finland (Luoma et al. 2013; Mikkonen et al. 2015; Okkonen et al. 2010; Ruosteenoja et al. 2016). Climate projections for Finland show a likelihood of increasing temperatures and precipitation through the year 2100. These changes to temperature may affect how precipitation falls (i.e., snow versus rain) and when accumulated snow melts (Ruosteenoja et al. 2016).

Figure 3-20 shows the mean annual temperature and the mean annual precipitation rates for four climate scenarios (Ruosteenoja et al. 2016). The primary climate scenario that is evaluated in this study is the representation concentration pathway 4.5 (RCP4.5) case. Based on projections for the RCP4.5 case, from 2020 to 2090, the mean annual temperature and precipitation rate in Finland are predicted to increase by 2.5 degrees Celsius (°C) and 11%, respectively.

Figure 3-21 shows the predicted changes to the monthly precipitation and temperature from 2070 to 2099 for the RCP4.5 case. The following is an overview of potential long-term changes for the RCP4.5 case:

1. The projected temperature changes due to climate changes are most prominent in winter. The temperature in the winter is estimated to increase by 1 to 8 °C from the current temperature, whereas the summer temperature is estimated to change by 1 to 4 °C from its current temperature. The 90% certainty range is plus or minus 3 °C.
2. Precipitation rates are expected to increase from 5% to 20%, with the largest increases in precipitation occurring during the winter months. The 90% certainty range is plus or minus 15% to 20%.

The potential impacts of estimated temperature and precipitation changes on the groundwater system within the HSA are unknown. Based on the predicted temperature and precipitation increases, the following may occur:

1. Increasing temperatures in the winter may decrease snowpack.
2. Increasing temperatures may increase the rain to snow ratios.
3. Increasing temperatures may result in earlier snowpack melt times.
4. Increasing temperatures in the summer months may increase the overall ET rates. Increases in ET may also reduce surface-water runoff because the amount of the ET increases is higher than the amount of the precipitation increases.
5. Increasing precipitation, especially in the form of rainfall, could lead to flooding during periods of heavy rain and increased recharge in the summer months.
6. Increasing rainfall in the summer months and winter months may result in more surface-water runoff during rainfall events.

The AASM Oy-developed *MIKE SHE* model described in Section 3.2.4 was used to estimate the future recharge rates into the groundwater system for the RCP4.5 climate case. Data for the RCP4.5 climate case are from Copernicus Climate Store (2022). Potential evaporation was calculated with the Romanenko method based on the RPC 4.5 case temperature and monthly average of relative humidity from 1990–2020 (FMI open data, Sodankylä Tähtelä station). Estimated potential

evaporation was fitted to satellite evaporation data and was used in the *MIKE SHE* model for the period between 2012 and 2021. Figure 3-22 shows the future estimated annual precipitation rates and future annual recharge rates for the till, sorted sediments, and peat. Data are only shown through 2100, which is the sufficient time period of mining operation at the Project Site and groundwater recovery. Table 3-10 provides a summary of the future predicted recharge rates. The following is a summary of the potential changes to climate based on the *MIKE SHE* model results for the RCP4.5 case:

1. Precipitation rates range from 365 to 730 mm/yr. Precipitation rates are relatively constant from 2020 through 2030. However, after 2040, annual precipitation rates show more variability.
2. Long-term trends in precipitation indicate a slight increase in the annual precipitation. The trend line in the figure shows a slight increase in precipitation rate over the time period from 2020 to 2100.
3. Recharge rates for the sorted sediments range from approximately 100 to 375 mm annually. There is a slight decrease in the recharge rate to the sorted sediments through time. It is likely that decreases in recharge to the sorted sediments are due to decreases in snow depth and spring thaw recharge and an increase in ET.
4. Recharge rates for the till range from approximately 55 to 235 mm annually. There is a slight decrease in the recharge rate to the till through time. It is likely that decreases in recharge to the till are due to the decreases in snow depth and spring thaw recharge and an increase in ET.
5. Recharge rates for the peat range from approximately 20 to 165 mm annually. There is an increase in the recharge rate to the peat through time. The reason for increasing recharge in the peat is due to decreased surface-water runoff resulting in increased recharge into the peat. Based on the *MIKE SHE* model from AASM Oy, the overall balance of water (recharge and discharge) from the peat is still a net gaining water from precipitation.

Figure 3-23 shows the estimated recharge rates as a function of the total precipitation rate through time for the till, sorted sediments, and peat. The average recharge rate during the current time period (2012 through 2021) is also shown with a dashed line, while the trend of the estimated recharge rates is shown with a solid line. Recharge rates for the till, sorted sediments, and peat range from 13% to 37%, 27% to 58%, and 1% to 38% of the mean annual precipitation, respectively. Trend

lines of the future recharge rates versus the average recharge rate of the current time period indicate that future recharge rates are expected to increase for the peat and decrease for the till and sorted sediments, as discussed above. The estimated change to the average recharge rates for the till, sorted sediments, and peat from 2020 to 2100 is approximately -3%, -7%, and 3%, respectively. The estimated increase of ET from the *MIKE SHE* model was relatively higher than the estimated increase of precipitation, which leads to the predicted decrease in recharge rate to groundwater from precipitation in the future.

3.3 SURFACE WATER

Figure 3-24 shows the primary rivers and streams and springs that are located within the HSA and general surface-water flow directions. The primary rivers are the Kitinen, Hiivanahaara, Ylijoki, and Kelujoki Rivers. The Kitinen River flows through the center of the HSA and along the southwestern boundary. The Hiivanahaara and Ylijoki Rivers flow along the eastern HSA boundary, and the Kelujoki River flows along the southern boundary. All surface water within the HSA eventually drains to the Kitinen River. The following is a summary of surface-water drainage within the HSA:

1. In general, surface water within the HSA drains toward the Kitinen River through a series of channels, streams, or primary rivers.
2. There is a surface-water divide in the Mire area. The surface-water divide is east of the Project Site. The surface-water divide results in surface water from the Mire flowing west across the Project Site toward the Kitinen River and east toward the Ylijoki River.
3. The Kelujoki River flows west along the southern boundary of the HSA into the Kitinen River.
4. In addition to surface-water runoff that reaches the Kitinen River, there are lowland areas that surface water drains to instead of flowing to the Kitinen River. It is in these lowland areas that water seeps into the ground and recharges the permeable sand/gravels.
5. Groundwater discharge occurs as seepage, individual springs, and a series of springs mapped in 2006–2021 (Salonen et al. 2016). Figure 3-24 shows the locations of 88 springs that have been identified by AASM Oy within the HSA. Because of their shallow locations, the effects of springs on the groundwater inflow to the Mine Workings are considered to be minor in comparison to the volume of recharge from precipitation. Consequently, the springs are not included in the model calibration or sensitivity analysis presented in this report.

6. Large areas of the Mire remain inundated with water during the summer months long after the thaw because of the micro-relief of the Mire, which traps runoff in pools (flarks) isolated by shallow, vegetated peat ridges (strings).

The Kitinen River is a hydroelectric dam-controlled river that has been regulated since the late 1970s. Within the HSA, there are hydroelectric dams located upgradient (Matarakoski) and downgradient (Kelukoski) of the Project Site. The upstream stage and the downstream discharge are measured at both locations. Figure 3-25 shows the measured stage upgradient of each dam and the discharge downstream of the dam. The upstream and downstream locations have relatively constant water levels at 187.8 and 180.9 mamsl, respectively. Discharge from the hydroelectric dams varies seasonally due to snowmelt surface-water runoff. Discharge from the dams ranges from 0 to 700 cubic meters per second (m^3/s) at the upstream and downstream locations (SYKE 2022).

In addition to the primary rivers, there are many streams and creeks that have seasonal surface-water flow that migrates to the primary rivers. These include streams such as the Kärvälslammen purku-uoma, Ruosteoja, Tiukuoja, and Sakattioja. Stream discharge data at these locations are only available for 2021. Figure 3-26 shows the measured discharge rates for the Kärvälslammen purku-uoma, Ruosteoja, and Tiukuoja streams for 2021. Discharge rates from streams that drain the Mire area have measured streamflow rates that range from 0 to $0.6 \text{ m}^3/\text{s}$. High streamflow primarily occurs during the spring melt time period and during heavy rainstorms (e.g., October 2021).

3.4 GROUNDWATER

3.4.1 Monitoring Network

Figure 3-27 shows the monitoring locations that have been installed across the Project Site over the winter fields seasons. In total, AASM Oy has installed 111 groundwater monitoring locations at the Project Site. Table 3-11 provides summary details on the monitoring locations, including locations, construction details, and monitored hydrogeologic units. At the Project Site, 106 monitoring wells and five vibrating-wire piezometers (VWPs) have been installed. The groundwater levels are

measured manually and with data loggers in 82 observation wells and manual measurement in 12 observation wells (2021). The groundwater monitoring was initiated in 2012 with 21 observation wells, and the monitoring has been extended between 2016 and 2021. The installed monitoring network is focused on the Kuusivaara area (i.e., proposed location of infrastructure and the Declines) and the mine area. Additional monitoring locations have been installed north of the Project Site, outside of the Mire, and along the Kitinen River.

Figure 3-28 shows the monitoring locations categorized by hydrogeologic units across the HSA. Of the monitoring locations at the Project Site, AASM Oy has installed four, 42, 42, and 23 monitoring locations within the peat, shallow fluvial and glacial sediments, shallow bedrock, and deep bedrock, respectively. The purpose of the groundwater monitoring network is to measure the seasonal variation of groundwater-level response in the various hydrogeologic units.

3.4.2 Measured Groundwater Levels

Figure 3-29 shows a spatial map of monitoring locations around the Project Site with hydrographs of measured groundwater levels at selected monitoring locations that are representative of measured groundwater levels in the shallow monitoring locations (Figure 3-29a), fractured and shallow bedrock (Figure 3-29b), and the Kuusivaara area (Figure 3-29c). The following can be observed regarding the groundwater levels across the Project Site:

1. Groundwater levels in the Shallow Groundwater System range from 182 to 188 mamsl across the Project Site. Groundwater levels are higher farther away from the Kitinen River. As such, groundwater from the western part of the Mire flows toward the Kitinen River during the spring snowmelt thaw.
2. Groundwater levels in the Shallow Groundwater System have a seasonal trend that corresponds to the snowmelt. Seasonal rise in groundwater levels is 0.5 to 2 m. Groundwater levels have a much larger seasonal water-level response near the Kitinen River as compared to the Mire area.
3. Groundwater hydrographs in the Fractured Bedrock also have seasonal groundwater levels that correspond to the snowmelt. Seasonal rise in groundwater levels is 0.5 to 2 m. Piezometers in the shallow bedrock have similar or slightly lower groundwater levels than

the shallow sediment system. The deep bedrock system groundwater levels have strongly attenuated seasonal patterns, as illustrated in representative groundwater levels at 17HYD013.

4. Monitoring wells (i.e., 18HYD030 and 18HYD033) in the shallow sediment near the Kuusivaara area show variation in the rise of groundwater levels due to snowmelt, as illustrated in representative groundwater levels in Appendix A.
5. Monitoring wells in the Fractured Bedrock in the Kuusivaara area show responses to seasonal snowmelt up to 20 m, as illustrated in representative groundwater levels at 19KUU017. There are larger seasonal changes in groundwater levels in the Kuusivaara area as compared to the mine area. The larger seasonal changes in the Kuusivaara area are a result of the topographic effects and the thin layer of sediments and low-*K*-value bedrock.
6. Because of the snowpack on the peat surface and ice caps in GA101, GA102, and GA103 monitoring wells, porewater levels rise during the winter months and decrease in the spring months. Porewater levels in these wells typically are rising from October to April and declining from April through May. Porewater-level rises within the peat range from 0.2 to 0.5 m.

It was concluded that the measured pressure increases are not accurately representing the actual porewater levels in these monitoring wells. The unseasonal variation of the measured porewater levels in these monitoring wells contradicts the actual seasonal variation of groundwater levels outside of the peat areas.

7. Monitored groundwater levels in the bedrock, as illustrated in representative groundwater levels at 17HYD013, have shown limited response during drilling, aquifer testing, and the spring snowmelt. This suggests a limited connection between the groundwater in the fresh bedrock and groundwater in the overlying units.
8. The responses of groundwater levels in the peat indicate responses to increases in snow depth. Transmission of the pressure responses from the peat to monitoring wells in other sediment types indicates that the groundwater conditions in the peat are partially separated from the other groundwater systems.

AASM Oy installed multi-level VWP's at the Project Site. Due to technical difficulties in installation, measured pressure data have high uncertainty (i.e., groundwater levels are continuously rising/falling or indicate artesian conditions), and as such, the VWP data are not presented.

Many studies have been conducted to understand the groundwater chemistry of the peat, shallow system geologic units, and the bedrock (Bigler 2019; Korkka-Niemi et al. 2017; Lahtinen 2017; Suonperä 2016; Turtiainen 2020). The following is a summary of those studies:

1. The upper three hydrostratigraphic units, the peat, the glacial and fluvial sediments, and the Fractured Bedrock, have a similar groundwater chemistry, suggesting that these three units have similar sources of water, mainly from recharge.
2. Water quality in the Fractured Bedrock is dominated by calcium-magnesium bicarbonate and is similar to the water quality in the overlying glacial and fluvial sediments.
3. Water quality in the Unfractured Bedrock have distinctly higher concentrations of dissolved solids, high in chloride and sulfate, and contains elevated metals derived from the mineralized zones. Water quality in the Unfractured Bedrock is very distinct from that in the overlying Fractured Bedrock, suggesting limited hydrologic interaction between the two zones of the bedrock.
4. Groundwater flow in the Deep Bedrock is not understood at a detailed level due to the compartmentalization and diverse nature of groundwater flow in crystallized rock environments. Korkka-Niemi et al. (2020) conducted age dating of the Unfractured Bedrock groundwater. Age dating indicates groundwater within the Unfractured Bedrock is at least 32,000 years before present. Older-aged groundwater indicates that the Unfractured Bedrock is not recharged by the Shallow Groundwater System. The recharge source for the Unfractured Bedrock is not well understood.

3.5 PROPOSED MINING AT THE SAKATTI PROJECT

Figure 3-30a shows the spatial extent of the primary mining areas and the Declines and an isometric view of the proposed Mine Workings. Figure 3-30b shows a timelapse of the progression of the Declines and Mine Workings. The Mine Workings will be connected to the ground surface by four Declines from the Kuusivaara area. The following is a summary of the proposed Mine Workings:

1. **Declines:** Construction of the Declines is proposed to begin in Year 1. The elevations of the Declines/ramp range from 190 mamsl (at the portal in the Kuusivaara area) to -610 mamsl around the Mine Workings.
2. **Mine Workings:** The fully developed underground mine will have underground workings ranging from 112 mamsl to approximately -935 mamsl.

3. **Main Deposit Stope Area:** Stoping is proposed to begin in Year 2 at -390 mamsl, and stoping ends in Year 22. The stoping elevations range from approximately -935 mamsl to -65 mamsl.
4. **NE Deposit Stope Area:** The NE deposit area will begin with a ramp in Year 7 at -380 mamsl. Stoping will begin in approximately Year 10 at -95 mamsl. Stoping will be finished in Year 20. Stoping elevations will range from -170 mamsl to 112 mamsl.

The proposed Mine Workings will have a length of approximately 420 km, and approximately 11 million cubic meters of stopes will be backfilled.

Groundwater inflows to the Mine Workings will be collected at two pumping locations. The lower pump station will be at an elevation of -635 mamsl and will collect more saline groundwater inflow from production activities below a mine elevation of -420 mamsl. A second pump station will be located at an elevation of -435 mamsl to collect and transport less saline groundwater inflow coming from Mine Workings above -420 mamsl. Each pumping station will have two pumps and one pipeline to the surface. This will be a total of four pumps and two pipelines for the Mine Workings. Both pumping stations will pump water to the mine dewatering pond on the surface. If the water quality of the mine water is suitable, the water is pumped into internal water circulation. Mine water as a part of discharge water will eventually be discharged into the Kitinen River after treatment. Figure 3-31 shows the surface locations of the mine and dewatering infrastructure.

To reduce groundwater inflow into the Mine Workings and potential drawdown in the Shallow Groundwater System, AASM Oy's primary mitigation strategy is grouting the water-bearing faults that are intercepted by the Mine Workings. In addition, the mitigation plans include grouting the upper Declines until 150 mbgs. Potential water-bearing faults include the Basal Thrust, East, East-West, SENW1 and SENW2, East-West Central, and Hanging Wall Shear Faults.

Figure 3-32 shows a schematic of the backfilling conceptual designs. According to preliminary mining plans, stopes will be backfilled with paste or paste aggregate fill. The stopes will be backfilled in two stages. In the first stage, the so-called plug is made for the bottom of the stope. The bottom of the stope is backfilled and allowed to harden about 2 m above the barricade that is built in the lower

part of the stope. When the backfilling of the first stage has reached a sufficient hardness, the rest of the stope is backfilled and allowed to harden again. The backfilling of the stopes will likely reduce the amount of groundwater inflow that may occur directly from the stopes. Depending on how the backfill cures within a stope, it is likely to cause shrinking of the backfill. Shrinking of the backfill during curing will likely result in preferential pathways for groundwater flow around the exterior of the backfilled area. The potential K values of the backfill materials were previously estimated to range from 2×10^{-8} to 1×10^{-7} m/s. This range of potential backfill K values is used in the groundwater flow model to estimate the potential effects of backfill on the model predictions.

Due to the construction of underground workings (tunnels, stopes, and Declines) into the Unfractured Bedrock, it is expected that there will be groundwater inflow into the underground workings. Groundwater inflow is expected to be limited due to the low K values of the Unfractured Bedrock and AASM Oy's mitigation plan of grouting water-bearing faults.

Exploration surface drilling at the Project Site resulted in open boreholes that intercept the mineralized area. The open boreholes may have hydraulic connection to water in the overlying glacial and fluvial sediments during the LOM. Boreholes that may pose a risk for underground mining will be sealed through an ongoing program by AASM Oy during the construction phase. In the conceptual and numerical models, the sealed boreholes are assumed to have the same K value as the Unfractured Bedrock; therefore, they are treated as Unfractured Bedrock.

4.0 GROUNDWATER FLOW MODEL

4.1 GROUNDWATER FLOW MODEL CODE

The groundwater flow model used in this study was constructed using the finite-element code *MINEDW* (Itasca 2012), which solves 3-D groundwater flow problems using the finite-element method. *MINEDW* has several attributes that were specifically developed to address conditions that are often encountered in mine dewatering. This modeling code has been used and verified at more than 75 mine dewatering projects, both open pit and underground, throughout the world and is commercially available. *MINEDW* has been applied in diverse hydrogeologic and climatic conditions on projects from Botswana, North America to Siberia. The *MINEDW* code has also been extensively tested by the Sandia National Lab and approved for permitting use in Nevada (NDEP 2018a). The groundwater flow modeling code has been used worldwide in environmental impact assessments and permitting.

4.2 GROUNDWATER FLOW MODEL GRID

Figure 4-1 shows the finite-element grid for the groundwater flow model. The finite-element grid contains 1,351,533 nodes and 2,666,619 elements. The model grid has a higher density of nodal discretization in the vicinity of the Mine Workings areas. The model grid was finely discretized in these areas to allow for better representation of the geometry of the Mine Workings and hydrogeologic units. In the groundwater flow model, the model grid size was approximately 8 m, 20 m, and 1 km within the Declines, in the main and NE deposit areas, and in the regional zone, respectively. Figure 4-2 shows a west–east model cross section through the primary Mine Workings. The location of the cross section is presented in Figure 4-1. The finite-element grid was vertically discretized in adequate resolution so that it would incorporate the important hydrogeologic features of the area. Between 34 and 75 vertical layers were used to represent the various hydrostratigraphic units in the vicinity of the Mine Workings. Increasing quantities of layers were

used as the Declines progress deeper and over the mine area. For regional grids that are outside of the mine area, there are 28 vertical layers.

4.3 SIMULATED HYDROGEOLOGIC UNITS

Figure 4-1 shows the hydrogeologic units simulated in the uppermost layer of the model, which comprises various glacial and fluvial deposits. Figure 4-2 shows a cross section of the simulated hydrogeologic units in the Mine Workings elevations range. Below the Mine Workings elevation range, the bedrock is simulated as the “Less Permeable Bedrock” hydrogeologic unit. The simulated hydrogeologic units were based on the geologic models that were provided by AASM Oy. The following hydrogeologic units were simulated in the groundwater flow model:

1. Peat
2. Fluvial Deposits: Top deposits, sands, and gravels
3. Glacial Deposits: Upper, middle, and lower till
4. Weathered Deposits: Clay and grus
5. Fractured Bedrock
6. Unfractured Bedrock
7. Faults and Basal Thrust Fault

Figure 4-3 shows the calibrated K values used in the groundwater flow model compared with packer-testing data, and Figure 4-4 shows the simulated K values compared with the observed global ranges of K values from Freeze and Cherry (1979). Table 4-1 provides a summary of the calibrated hydraulic parameters of the hydrogeologic units. The simulated hydrogeologic units were derived with the following considerations and assumptions:

1. The K values and anisotropy of the Shallow Groundwater System were calibrated to seasonal groundwater-level changes in response to snowmelt and groundwater system discharge to the surface-water streams. The following is a summary of the distribution of simulated K values within the groundwater flow model:

- a. Hydrogeologic units were simulated directly based on their distribution within the shallow system geologic model.
 - b. Regional hydrogeologic units were extended to the model boundaries. Data from regional surficial geology maps (Geological Survey of Finland 2022) were used to inform the assignment of regional surficial geologic units.
 - c. Hydrogeologic units were subdivided for the top deposits and peats spatially to provide a better match between the measured and simulated groundwater levels. The top deposits and peats were subdivided to represent the Kuusivaara and the Mire areas (Figure 4-1).
 - d. The K values of the sorted sediments encompassing top deposits are lower than the Freeze and Cherry (1979) range because the sorted sediments at the Project Site consist of multiple different sorted sediments, fluvial/glaciofluvial sediments, braid plain deposits, aeolian sands, and fine-grained flood plain sediments (Åberg et al. 2021).
2. Based on packer-testing data and spatial analysis of packer-testing results, the Unfractured Bedrock was subdivided into a more permeable bedrock along the Decline area and a less permeable bedrock in the Mine Workings areas. Figure 4-5 shows the spatial extent of the more and less permeable bedrock areas. In general, the more permeable bedrock along the Declines is simulated as two times more permeable than the less permeable bedrock (Figure 4-3). The K values of the more and less permeable bedrock zones are simulated to decrease with depth based on the packer-testing data (Figure 4-3). The anisotropy between the horizontal to vertical K values of the Unfractured Bedrock is assigned to be 10 based on the groundwater flow model calibration.
3. The Fractured Bedrock was subdivided into three hydrogeologic units. Figure 4-6 shows the spatial extent of three Fractured Bedrock zones. The three hydrogeologic zones were in the Kuusivaara area, along the Kitinen River, and in the main area. The three extents were based on the groundwater flow model calibration to seasonal fluctuation in groundwater levels.
4. Figure 4-3 shows the assigned K values of the Basal Thrust Fault. The upper K value of the Basal Thrust Fault was assigned based on the measured K value of the pump tests. Similar to the simulated K values along the depth for the Unfractured Bedrock, the Basal Thrust K values were assumed to decrease with depth.
5. The K values of faults within the Project Site are simulated to be equal to the Unfractured Bedrock K values. Spatial analysis of packer-testing data and measurements of K values at faults indicate no trends of increasing K values at faults.
6. Calibrated K values are within the ranges of the measured K -value data, literature values, and global ranges of K values.
7. Regional faults were not included in the groundwater flow model, as no data are available on the hydraulic properties.

4.4 SIMULATED MODEL BOUNDARY CONDITIONS

The groundwater flow model boundaries were selected to follow natural hydrologic divides and flow paths. The boundaries of the numerical groundwater flow model are the same as those of the HSA described in Section 2.0. The boundaries were chosen to limit the effect of the amount of groundwater and surface-water flow that naturally enters and exits the HSA on the predicted inflow and drawdown in the mining area. In addition, the locations of the boundaries were selected to minimize the potential for interactions between the boundaries and the mine dewatering stresses. The same HSA boundary conditions were used for all steady-state, transient, and predictive model simulations.

Topographic data were used to define the ground-surface elevations in the groundwater flow model. The bottom elevation of the groundwater flow model domain is approximately -2,700 mamsl.

Provided below is a summary of the model boundary conditions that were simulated for the HSA.

4.4.1 Simulation of Constant Heads

As described above, the eastern, western, and southern boundaries were defined by surface-water rivers. At each of these boundaries, constant heads are used in the first model layer to represent the river. In addition to the rivers, multiple large surface-water bodies are located within the HSA. Figure 4-7 shows the simulated constant-head boundaries that were used in the groundwater flow model at the rivers and lakes. The elevations of the constant-head boundaries were assigned based on the ground-surface elevation. The constant-head elevations were simulated as constant through time with no seasonal variations in elevation.

4.4.2 Variable-Flux Boundary

Simulated variable-flux boundary locations are shown in Figure 4-7. A variable-flux boundary is used in the transient and predictive model simulations to simulate the groundwater interaction between the simulated groundwater flow model domain boundaries and the regional groundwater system (i.e., beyond the groundwater flow model domain). All nodes along the outer boundary of the groundwater flow model except those with assigned constant-head boundary conditions were assigned with a variable-flux boundary condition. The variable-flux boundary condition is a special feature of *MINEDW* that simulates an essentially infinite aquifer of the same hydraulic properties as those assigned to elements at the groundwater flow model boundaries. This boundary condition allows groundwater flow into and out of the model domain boundary based on the groundwater level and hydraulic properties of the simulated hydrogeologic units.

4.4.3 No-Flow Boundary Conditions

The bottom of the groundwater flow model is at an elevation of approximately -2,700 mamsl, where it is reasonable to assume that there will be no significant amount of groundwater flow across the bottom of the groundwater flow model. Therefore, the nodes on the bottom of the groundwater flow model were assigned as no-flow boundary conditions during all simulations.

4.5 SIMULATED RECHARGE TO THE GROUNDWATER SYSTEM

Figure 4-8 shows the average monthly recharge rates from June 2012 through June 2021 for the hydrogeologic units in the Shallow Groundwater System. Table 4-2 provides the simulated recharge rates for the hydrogeologic units in the groundwater flow model. Figure 4-9 shows the locations of the applied recharge rates for the till, sorted sediments, and peat. The following is a summary of the simulated recharge rates under steady-state and transient conditions:

1. No recharge was applied at the constant-head boundaries.

2. Recharge rates in steady-state model were based on the average recharge rates from the *MIKE SHE* model (Figure 4-8). Average recharge rates were varied spatially within the till in some areas to provide a better match between the simulated and measured groundwater levels.
3. There are subdivided recharge zones within the till as shown by the blue areas.
4. The simulated steady-state recharge rates from the high till, low till, sorted sediments, and peat are 0.18, 0.1, 0.73, and 0.2 mm/day, respectively.
5. Under transient conditions, the recharge rates from the *MIKE SHE* model shown in Figure 4-8 were directly simulated in the groundwater flow model (negative values only from *MIKE SHE* model). Recharge rates were simulated at a monthly time scale.

4.6 GROUNDWATER FLOW MODEL CALIBRATION

Groundwater flow model calibration is the process of varying uncertain model input parameters over likely ranges of values until a satisfactory match between simulated and measured data is obtained (Spitz and Moreno 1996). In this study, K , anisotropy in K , specific yield (S_y), specific storage (S_s), and the distribution and rate of pre-mining recharge were adjusted within the ranges of measured values to achieve a satisfactory groundwater flow model calibration. The model was calibrated to measured pre-mining groundwater levels and groundwater-level responses to snowmelt.

Statistical parameter analyses provide a metric by which a groundwater flow model performance can be evaluated quantitatively (ASTM 2008; Barnett et al. 2012; BLM 2008; NDEP 2018b). Several common statistical measures for comparing observed hydraulic heads with simulated hydraulic heads were used to assess the calibration of the steady-state and transient groundwater flow models: root mean square error (RMSE), mean absolute error (MAE), mean error (ME), and the coefficient of determination (r^2). Because these statistic parameters are well known and are defined elsewhere (e.g., Anderson and Woessner 1992; Davis 1986), their definitions are not repeated in this report. For perfect calibrations, the RMSE, MAE, and ME tend to 0, whereas r^2 tends to 1. The square of the correlation coefficient, r^2 , which is also called the coefficient of determination, is a more sensitive indicator of the linear relationship between variables. The closer the r^2 is to 1.0, the

better the fit between the observed and modeled data. A well calibrated model can be defined by a minimization of calibrated model statistics (Hill 1998).

The quality of a groundwater flow model calibration and the acceptable statistics as measured by the statistical parameters described above depends on several factors (Spitz and Moreno 1996), including the following:

1. The size and discretization of the model domain;
2. The degree of natural heterogeneity or complexity of boundary conditions;
3. The location, number, and accuracy of measured groundwater elevations;
4. The range in measured groundwater elevations over the model domain; and
5. The purpose for which the groundwater flow model was developed.

These factors should be given due consideration when evaluating the calibration of this (or any) model. For an example, the normalized RMSE is a measure of the spread of residuals (differences between simulated and measured values); if the RMSE is small—typically less than 10% to 15%—compared to the overall range in groundwater levels then a “good” calibration is generally indicated (ESI 2017); the remaining error statistic values are considered to be a negligible part of the overall model response (Anderson and Woessner 1992).

4.7 STEADY-STATE MODEL CALIBRATION

Steady-state simulations are used to estimate groundwater-level distributions and groundwater fluxes during periods when the hydrologic system is at (or very near) equilibrium conditions. Under steady-state conditions, hydrologic inflows to the model domain are equal to the outflows without a net change in storage. Steady-state simulations serve as the starting point (i.e., initial groundwater level and flux conditions) for transient simulations. The transient simulations are required to simulate the time-varying stresses and/or physical changes (such as mining and pumping) to the groundwater system.

4.7.1 Steady-State Model Targets

As discussed in Section 3.4.2, there is an extensive number of monitoring wells located within the HSA. Table 4-3 provides a summary of the monitoring locations that were used in the steady-state model calibration. As groundwater-level data indicate, groundwater levels vary seasonally due to snowmelt. As such, the steady-state groundwater level for the monitoring locations was assumed to be the measured groundwater level prior to the onset of snowmelt. Table 4-3 provides a summary of the measured pre-mining groundwater levels at each of the monitoring locations used in the steady-state model calibration.

4.7.2 Steady-State Model Calibration

The simulated groundwater-level contours derived from the calibrated steady-state model are shown in Figure 4-10. The groundwater levels follow the ground-surface topography within the HSA. Simulated groundwater levels indicate that groundwater drains toward the primary rivers that are within the HSA, the Kitinen, Ylijoki, Hiivanahaara, and Kelujoki Rivers. The simulated groundwater levels are consistent with observations at the Project Site.

Figure 4-11 shows the simulated depth to groundwater in the steady-state calibration. Within the HSA, most simulated groundwater levels are within 1 m of the ground surface. In areas where the ground-surface elevation is higher, the depth to groundwater is deeper.

Figure 4-12 shows the simulated areas of discharge and recharge. Areas of discharge are defined as areas where the groundwater level is at the ground surface and water is discharging to ET or surface-water runoff. In areas of recharge, the groundwater level is typically below the ground surface and water is infiltrating into the hydrogeologic units. Within the HSA, most areas of discharge are along channels and drainages, while areas of recharge are at higher elevations. The simulated areas of recharge and discharge are consistent with the *MIKE SHE* model and site observations.

Figure 4-13 shows the simulated versus measured groundwater level quality line plot. Table 4-3 provides a summary of the measured and simulated groundwater levels and calculated model statistics. The statistical measures discussed in Section 4.1 were used to further evaluate the steady-state calibration of the groundwater flow model. The ME, MAE, and RMSE for the steady-state model are 0.1 m, 0.6 m, and 0.8 m, respectively. Table 4-4 provides a summary of the steady-state groundwater flow model calibration statistics. Overall, the simulated steady-state groundwater levels are well calibrated to the measured groundwater levels. Calculated model statistics are within normal ranges of a well-calibrated groundwater flow model. (Anderson and Woessner 1992; Barnett et al. 2012; Hill 1998; NDEP 2018b; Spitz and Moreno 1996). In addition, the calculated model statistics of ME, MAE, and RMSE are near zero, while the r^2 value of the model is near 1, all indicating a well-calibrated model. In addition, the ME, MAE, and RMSE are less than the assumed measurement error of ± 1.0 m.

The mass balance error for the entire model at the end of the steady-state simulation is less than 0.001%, which is less than the 0.5% maximum global mass balance error threshold recommended by Reilly and Harbaugh (2004).

4.8 TRANSIENT MODEL CALIBRATION

4.8.1 Transient Model Targets

The primary purpose of the transient model calibration is to simulate the groundwater responses to the seasonal recharge rates that were estimated in the *MIKE SHE* model from June 2012 through June 2021. The groundwater flow model was calibrated to the measured seasonal changes in groundwater levels at monitoring locations within the HSA. Monitoring locations within the HSA that were used in the transient groundwater flow model calibration consist of locations with data loggers and manual measurements and represent continuous monitoring. Because some monitoring wells were only monitored outside of the calibration period, only a subset of the total monitoring locations that are within the monitoring period was used in the model calibration. The subset

includes monitoring locations in all hydrogeologic units and long-term measured groundwater levels that are representative of the seasonal changes in groundwater levels. Table 4-5 provides a summary of the monitoring locations that were used in the transient model calibration. In total, 98 monitoring locations were used in the transient model calibration. Based on Itasca's experience, the overall number of monitoring locations is adequate and extensive compared to other projects at similar stages.

4.8.2 Transient Model Calibration

Appendix A provides a summary of the measured and simulated groundwater level hydrographs from the transient groundwater flow model calibration. As shown in the hydrographs, the groundwater flow model is well calibrated to the seasonal changes in groundwater levels within the HSA. The following is a summary of the transient groundwater flow model calibration:

1. The model is well calibrated to the measured groundwater levels near the mine area, along the Declines, and within the Mire.
2. Across the HSA, the groundwater flow model is well calibrated to measured groundwater levels within the Shallow Groundwater System, Fractured Bedrock, and Unfractured Bedrock.
3. In the Kuusivaara area, the groundwater flow model is well calibrated to the measured groundwater levels, including both areas that have small (less than 1 m) and areas that have large seasonal changes in groundwater levels (greater than 10 m).

Table 4-6 shows the calculated transient model statistics at points in time over the transient groundwater flow model calibration. The points in time are every 6 months, including both summer and winter data points. Calculated statistics are shown for the ME, MAE, RMSE, normalized RMSE, and r^2 for each point in time. Figure 4-14 shows temporal quality line plots of measured versus simulated groundwater levels at each point in time. Based on these data, the following can be concluded regarding the model calibration:

1. Based on the calculated model statistics, the transient groundwater flow model is well calibrated throughout the entire time period of the transient model calibration.
2. Calculated model statistics are within literature ranges of a well-calibrated model (Anderson and Woessner 1992; Hall 1998; Spitz and Moreno 1996).
3. Quality lines show that there is no bias or trends in model error through time between measured and simulated groundwater levels.
4. The ME, MAE, and RMSE are typically less than 1.0 m.
5. The transient groundwater flow model is well calibrated to groundwater levels for both the summer and winter months.

Figure 4-15 shows the simulated recharge rates as a percentage of precipitation for the till, sorted sediments, and peat for each year and the average simulated recharge rate. The simulated recharge rates are based on the recharge rates from *MIKE SHE* (negative values on Figure 3-19). Recharge rates for the hydrogeologic units vary from 3% to 60% of the precipitation depending on the measured precipitation rate. The average recharge rate for the till, sorted sediments, and peat hydrogeologic units is approximately 30%, 46%, and 12% of the measured annual precipitation rate, respectively. Average recharge values are similar to the methods used in Åberg et al. (2019).

Figure 4-16 shows the simulated water budget for the groundwater flow model domain. Positive values are inflow to groundwater system while negative values are outflow from groundwater system. The following observations can be made regarding the simulated water budget:

1. Water-budget components within the groundwater flow model vary seasonally depending on the amount of applied recharge.
2. The applied recharge rate varies from 0 to 20,000 cubic meters per hour (m^3/hr). The applied recharge rate is highest during the snowmelt season.
3. Surface-water runoff varies from 1,000 to 11,000 m^3/hr .
4. The baseflow to rivers varies from 350 to 650 m^3/hr . The baseflow rate is the discharge rate from the groundwater system to the surface-water system.
5. Groundwater outflow from the model domain varies from 50 to 100 m^3/hr . Groundwater outflow occurs along the variable-flux boundary.

Figure 4-17 shows the simulated water budget for key surface-water bodies. This plot shows the delineation of the calculated baseflow to rivers water-budget components. The outflow in Figure 4-17 does not include surface-water runoff through channels into rivers; it only shows groundwater outflow to the rivers and lake boundaries (constant-head boundaries). The simulated negative value indicates water is leaving the groundwater system. The following can be concluded regarding the groundwater outflow into streams and lakes:

1. Groundwater outflow to lakes ranges from approximately 2 to 25 m³/hr.
2. Groundwater outflow to the Kitinen River ranges from approximately 225 to 510 m³/hr.
3. Groundwater outflow to the Kelujoki, Hiivanahaara, and Ylijoki Rivers ranges from approximately 105 to 150 m³/hr.

5.0 PREDICTIVE GROUNDWATER FLOW MODEL

After the groundwater flow model was well calibrated to the seasonal changes in groundwater levels, the groundwater flow model was used to provide predictions of future groundwater inflows to the proposed Mine Workings and the potential drawdown in the groundwater system. This section of the report focuses on the predictive model simulations and the results.

5.1 PREDICTIVE GROUNDWATER FLOW MODEL SETUP

5.1.1 Simulated Boundary Conditions

As described above in Section 4.0, the following boundary conditions were used in the steady-state and transient models and were continued in the predictive groundwater flow model simulations:

1. Constant heads were assigned at the ground-surface elevations for the Kitinen River, Kelujoki, Hiivanahaara, and Ylijoki Rivers, and lakes within the HSA. It was assumed that the constant head elevations are unchanged over the LOM. Though there is seasonal variation in the water levels of these surface-water bodies, the effect of the seasonal variation on the predicted inflow to the Mine Workings and the groundwater-level drawdown is negligible.
2. The outer model boundary was treated as a variable flux that allows for interaction with the regional groundwater system as shown on Figure 4-7. The variable-flux boundary assumes an infinite aquifer to supply water to the model domain.

Figure 5-1 shows the future simulated daily recharge rates for the till, sorted sediments, and peat hydrogeologic units for each month. An average monthly recharge rate was estimated based on the monthly recharge rates from June 2012 through June 2021. The average monthly recharge rate is repeated annually over the entire model simulation. The effects of potential climate change on the simulated recharge rates were estimated in separate model sensitivity simulations.

5.1.2 Simulated Mining Operation

AASM Oy provided detailed LOM plans in the form of a .dxf file and a detailed LOM schedule in *DESWIK* format. The following is a summary of the simulated LOM mine operations:

1. Year 0 through Year 2: Four Declines are constructed from the Kuusivaara area to the main deposit. The initial Mine Working developments are constructed.
2. Year 3 through Year 8: Stoping begins and the Mine Workings are developed at deeper elevations below -400 mamsl. During this time period, stoping occurs at the deepest elevations.
3. Year 9 through Year 10: A ramp to the NE deposit is developed and stoping begins at elevations above -150 mamsl.
4. Year 11 through Year 22: Stoping continues at shallower elevations in the main deposit from -400 to -70 mamsl and in the NE deposit from -170 to 112 mamsl.

The following is a summary of the simulated boundary conditions for the predictive model simulations:

1. The Mine Workings are simulated as drain nodes based on the mining schedule provided in *DESWIK* and the elevations provided in the .dxf files. It is assumed that all Mine Workings with the exclusion of stopes remain open over the LOM based on the elevation of the tunnels, groundwater level, and the hydraulic properties of the in-situ bedrock.
2. Though backfill will be placed in all stoped areas, the effect of a completely sealed backfill on the groundwater inflow is not considered in the 80% and 65% Success in Grouting Scenarios for the following reasons:
 - a. As the paste backfill cures, it is likely that the backfill shrinks and results in preferential flow paths around the perimeter of the backfill. As such, stopes will likely drain freely over the LOM.
 - b. A review of *K* values from different sites and material mixing suggests a range from 2×10^{-8} to 1×10^{-7} m/s (Figure 3-32). Because the *K* value of 1×10^{-7} m/s in the backfill is higher than the *K* value of the Unfractured Bedrock (2×10^{-9} to 1×10^{-7} m/s), it may not impede the groundwater inflow rate from the Unfractured Bedrock.
3. Based on AASM Oy's mitigation plans, the Mine Workings that intercept known water-bearing faults will be grouted and along the Declines to 150 mbgs. The following assumptions were made when simulating the grouting:
 - a. The grout will be used to mitigate the potential water bearing in the Basal Thrust, East, East-West, SENW1 and SENW2, East-West Central, and Hanging Wall Shear faults.
 - b. The simulation assumed that grouting of the Mine Workings that intercept known water-bearing faults is successful at reducing groundwater inflow into the Mine Workings. As such, selected drain nodes of the presumed mining zone and Mine

Workings are included in areas where grout is to be placed based on the grout efficiency. The effects of the grout efficiency on the model predictions are estimated in a sensitivity analysis.

Based on the LOM plans, the mine life is approximately 22 years. Due to the uncertainty in the mining start date, model predictions are presented as years after mining begins.

For the simulation of backfill scenarios, the lower K value of the in-situ rock mass in the stope is changed to the higher K value of the backfill in the groundwater flow model. Changes in K values will introduce additional groundwater flow as the result of numerical artifacts in the predicted groundwater inflow rate. Such a numerical artifact in predicted groundwater inflow rate, though very small, was adjusted proportionally based on the predicted inflow rate to the mining zone and the Mine Workings without any backfilling materials. The predicted groundwater inflow rate without backfilling materials is considered to be higher than that in any backfilling scenarios.

5.1.3 Predictive Model Simulations for Environmental Assessment

Based on the above description of the predictive model setup and assumptions, the following is a summary of the predictive model scenarios for the environmental assessment:

1. **80% Success in Grouting Scenario:** The 80% Success in Grouting Scenario assumes 80% effectiveness in grouting along fault structures and to a depth of 150 mbgs along the Declines, moderate- K -value backfill material (5.0×10^{-8} m/s), and free-draining stopes throughout the LOM. To simulate an 80% grouting efficiency, selected drain nodes (20% of nodes) are left open to drain in areas of grouting.
2. **65% Success in Grouting Scenario:** The 65% Success in Grouting Scenario assumes 65% effectiveness in grouting along fault structures and to a depth of 150 mbgs along the Declines, high- K -value backfill material (1.0×10^{-7} m/s), and free-draining stopes throughout the LOM. To simulate a 65% grouting efficiency, selected drain nodes (35% of nodes) are left open to drain in areas of grouting.

Table 5-1 provides a summary of the two model scenarios and simulated model parameters. Based on the Sakatti and Itasca team's mining and hydrogeology experience and the available technical

knowledge, the 80% Success in Grouting Scenario is considered to be the most likely scenario that can be achieved in the operation.

In addition to the two scenarios described above, one additional model scenario was simulated without mining to estimate future groundwater conditions based on average recharge to estimate the seasonal changes to the groundwater system as the result of recharge variation alone. The purpose of this model simulation was to have a baseline model of groundwater system variations so that comparison can be made with the mining scenarios to estimate net effects of mining on the groundwater system.

Additional sensitivity scenarios were conducted on key mining-simulated and climate parameters. The predictive model setup and results of these scenarios are provided in Appendix B.

5.2 PREDICTIVE RESULTS DURING MINING FOR THE ENVIRONMENTAL ASSESSMENT

5.2.1 Predicted Groundwater Inflow Rates

Figure 5-2 shows the predicted groundwater inflow rates for the 80% and 65% Success in Grouting Scenarios. Table 5-2 provides a summary of the predicted groundwater inflow rates and cumulative volumes for the 80% and 65% Success in Grouting Scenarios over time. The following observations can be made regarding the future groundwater inflow rates for the 80% Success in Grouting Scenario:

1. The groundwater inflow rates begin to increase in Year 1 of mining as the four Declines are constructed. By mid-Year 2, the groundwater inflow rates reach a peak groundwater inflow rate of 118 m³/hr (2,830 cubic meters per day [m³/day]) due to the presence of the permeable Basal Thrust. Peak groundwater inflow rates occur after the construction of the Declines and the shallow Mine Workings.
2. After reaching a peak groundwater inflow rate, the groundwater inflow rate decreases to approximately 100 m³/hr (2,400 m³/day) by Year 6 as mining is progressing in lower elevations that have lower bedrock *K* values. The groundwater inflow rate does not increase due to mining at the lower elevations due to the low *K* values of the bedrock.

3. Groundwater inflow rates remain relatively constant around 100 m³/hr (2,400 m³/day) through Year 10, at which point groundwater inflow rates begin to rise. Groundwater inflow rates begin to rise during Year 10 as the shallowest Mine Workings of the main deposit and the NE deposit are developed. Groundwater inflow rates increase to 110 m³/hr after Year 10 (2,640 m³/day) and remain relatively constant throughout the rest of the LOM.
4. The predicted groundwater inflow rate (100 to 120 m³/hr) is similar to the overall recharge rate for the Mine Workings area (approximately 1 km²), which ranges seasonally from 0 to 100 m³/hr (Figures 4-16 and 4-17).
5. The total cumulative volume of water extracted from the underground workings over the LOM is approximately 20 million m³.

The following observations can be made regarding the future groundwater inflow rates for the 65% Success in Grouting Scenario (Figure 5-2 and Table 5-2):

1. The groundwater inflow rates begin to increase in Year 1 of mining as the four Declines are constructed. By mid-Year 2, the groundwater inflow rates reach a peak groundwater inflow rate of 122 m³/hr (2,930 m³/day) due to the presence of the permeable Basal Thrust. Peak groundwater inflow rates occur after the construction of the Declines and the shallow Mine Workings.
2. After reaching a peak groundwater inflow rate, the groundwater inflow rate decreases to approximately 107 m³/hr (2,570 m³/day) by Year 6 as mining is progressing in lower elevations that have lower bedrock *K* values. The groundwater inflow rate does not increase due to mining at the lower elevations due to the low *K* values of the bedrock.
3. Groundwater inflow rates remain relatively constant around 107 m³/hr (2,540 m³/day) through Year 10, at which point groundwater inflow rates begin to rise. Groundwater inflow rates begin to rise during Year 10 as the shallowest Mine Workings of the main deposit and the NE deposit are developed. Groundwater inflow rates increase to 118 m³/hr after Year 10 (2,830 m³/day) and remain relatively constant throughout the rest of the LOM.
4. The predicted groundwater inflow rate (107 to 122 m³/hr) is similar to the overall recharge rate for the Mine Workings area (approximately 1 km²), which ranges seasonally from 0 to 100 m³/hr (Figures 4-16 and 4-17).
5. The total cumulative volume of water extracted from the underground workings over the LOM is approximately 21 million m³.

The predicted groundwater inflow rates for the 65% Success in Grouting Scenario follow the same pattern and timing over the LOM as the 80% Success in Grouting Scenario but with groundwater inflow rates that are 5% to 8% higher than in the 80% Success in Grouting Scenario.

5.2.2 Predicted Drawdown

Figure 5-3a and Figure 5-3b show drawdown hydrographs of 11 different hypothetical monitoring locations across the Project Site for the 80% and 65% Success in Grouting Scenarios, respectively. The locations of these hypothetical monitoring locations are also shown in Figure 5-3a and Figure 5-3b. It is assumed that the hypothetical monitoring locations are screened within the Shallow Groundwater System (from 0 to 10 mbgs). For each hypothetical monitoring location, the predicted drawdown is shown over the LOM. The predicted drawdown associated with mining was estimated by comparing the model-predicted drawdown in the 80% and 65% Success in Grouting Scenarios with the No-Mining Scenario. The following can be observed regarding the predicted drawdown across the Project Site for the 80% Success in Grouting Scenario (Figure 5-3a):

1. Predicted drawdown varies seasonally due to the simulated seasonal recharge from snowmelt. Seasonal peak drawdown rates are predicted to occur prior to snowmelt in the spring. Seasonal variations in drawdown range from 0.01 to 0.4 m.
2. Larger seasonal variations in drawdown occur at Monitoring Location 1 due to smaller thickness of shallow sediments and the effects of recharge on lower *K*-value bedrock.
3. Drawdown begins to occur at Monitoring Locations 1 through 5 as the Declines are constructed during the initial part of mining development (Year 1 through Year 2).
4. Drawdowns at Monitoring Locations 3, 4, and 5 are larger than at other locations due to the presence of the permeable Basal Thrust along the Declines. Peak drawdown rates along the Declines are approximately 0.93 and 0.75 m in the winter and summer seasons, respectively.
5. Drawdown at monitoring locations over the main deposit area slowly increases through time as underground mining progresses. Peak drawdown over the primary mining area is approximately 0.6 m in Year 22.
6. There is increased drawdown at Monitoring Locations 8, 9, and 10 in Year 10 as the shallow Mine Workings are developed at the main and NE deposits.

7. Predicted drawdown of 0.6 m or less at the end of mining is within the seasonal variation of 0.5 to 2 m in measured groundwater levels over the primary mining area.

The following can be observed regarding the predicted drawdown across the Project Site for the 65% Success in Grouting Scenario (Figure 5-3b):

1. Predicted drawdown patterns and timing are the same as in the 80% Success in Grouting Scenario with variations in the overall drawdown magnitude.
2. Seasonal variations in drawdown range from 0.01 to 0.8 m at the hypothetical monitoring locations.
3. Drawdowns at Monitoring Locations 1, 3, 4, and 5 are larger than at other locations due to the presence of the permeable Basal Thrust along the Declines and the shallow Declines. Peak drawdown rates along the Declines are approximately 1.0 and 0.8 m in the winter and summer seasons, respectively.
4. Drawdown at monitoring locations over the main deposit area slowly increases through time as underground mining progresses. Peak drawdown over the primary mining area is approximately 0.6 m in Year 22.
5. Predicted drawdown of 0.6 m or less at the end of mining is within the seasonal variation of 0.5 to 2 m in measured groundwater levels over the primary mining area.

Figure 5-4 shows a plot of monthly drawdown at 5-year intervals over the LOM (Year 5, 10, 15, and 22 after mining begins) at two monitoring locations (Monitoring Locations 4 and 8) for the 80% and 65% Success in Grouting Scenarios. The following can be observed regarding the simulated seasonal drawdown at the monitoring locations:

1. Simulated drawdown decreases during the spring melt time period from May to July.
2. After the summer months, simulated drawdown increases over time throughout the rest of the year until the next year's spring melt.
3. Over the LOM (Year 5 to Year 22), the seasonal difference between the peak and minimum drawdown in a calendar year increases (up to 0.2 m).

Figure 5-5a and Figure 5-5b show the predicted drawdown contours associated with mining within the HSA at the end of mining in Year 22 for the 80% and 65% Success in Grouting Scenarios,

respectively. The predicted drawdown is greater in the NE deposit area, along the Declines, and in the area of the shallow Declines. The peak drawdown at the end of mining is centered around the shallow Decline and portal area. The peak drawdown at the end of mining is 2.8 m and 4.0 m for the 80% and 65% Success in Grouting Scenarios, respectively. The predicted peak drawdowns of 2.8 and 4.0 m or less at the end of mining for the 80% and 65% Success in Grouting Scenarios, respectively, are within the seasonal variation of 1 to 20 m in measured groundwater levels in the Kuusivaara area.

It is likely that, as drawdown begins to occur within the Shallow Groundwater System, recharge to the groundwater system will increase. This increased recharge is not simulated in the groundwater flow model. An increase in recharge to the groundwater system would result in less drawdown in the Shallow Groundwater System than is currently predicted by the groundwater flow model.

Figure 5-5a and Figure 5-5b show predicted drawdown within the footprint of the Mire area. This drawdown is predicted based on the assumption that the peat is hydraulically connected to the Shallow Groundwater System and behaves as porous media. Based on the available data, it is reasonable to assume that the peat within the Mire system has low- K -value zones and, therefore, is only partially hydraulically connected to the Shallow Groundwater System. Consequently, the predicted drawdown from the groundwater flow model is likely to be higher than the actual field-observed drawdown in the peat based on Itasca's experience at other mines with similar overburden hydrogeologic settings.

Figure 5-6 shows a comparison of the measured and simulated change in groundwater levels from the average groundwater level during the groundwater flow model calibration time period. Data are shown for six monitoring locations located within the Mire. Also shown in Figure 5-6 are the minimum and maximum change in groundwater levels from the average measured groundwater level. The following approach was used to define groundwater-level changes:

1. The measured maximum and minimum groundwater-level changes are defined by the difference between the maximum/minimum measured groundwater level and the average measured groundwater levels over the period presented in the figure.
2. The difference between the minimum and maximum is the measured range of natural variation of groundwater levels. The range of natural variation in groundwater levels is dependent on the quantity of precipitation.
3. The simulated change in calibrated groundwater levels is the simulated groundwater level through time minus the average simulated water levels over the period presented in the figure.

Based on Figure 5-6, the following can be observed regarding the seasonal changes in measured and simulated groundwater levels:

1. Measured seasonal groundwater-level variations have the following ranges:
 - a. Peat water levels (monitoring locations GA101, GA102, and GA104) range from -0.2 to +0.45 m from the average water level. Most of the year, peat water levels are +/- 0.1 m from the average water level with only larger increases at the end of the winter season in response to snow depth.
 - b. Sediment groundwater levels (monitoring locations GA201, GA202, and GA300) range from -0.67 to +0.5 m from the average groundwater level.
2. The seasonal change in groundwater levels varies each year and is dependent on the quantity of precipitation.
3. For non-peat monitoring locations (GA201, GA202, and GA300), groundwater levels increase during the spring melt then slowly decline from the end of the spring melt through the winter. In some years, there are increases in groundwater levels during the summer/autumn precipitation events.
4. At peat monitoring locations (GA101, GA102, and GA104), measured changes in groundwater levels are a pressure response to increasing snow depth.
5. Simulated changes in groundwater levels are well matched to the measured changes in groundwater levels at monitoring wells within the sediment (GA201, GA202, and GA300).
6. As discussed in Section 4.0, the groundwater flow model is well calibrated to water-level magnitudes at monitoring locations within the peat (Appendix A). The groundwater flow model does not reflect the measured seasonal changes (GA 101, GA102, and GA104; Figure 5-6) in the peat, as measured seasonal peat groundwater levels are reflecting changes in pressure (increasing snowpack) and not actual water-level changes. The simulated groundwater-level variations at the peat monitoring locations during the calibration period

are +/- 0.1 m, which agrees reasonably well with a majority of the variation in the measured data.

Figure 5-7 shows the simulated change in groundwater levels for the predictive time period of Year 1 through Year 22 of mining for the 80% Success in Grouting Scenario with the NE Deposit. Also shown in the figure are the minimum and maximum measured groundwater levels from the 2012–2021 time period as defined in Figure 5-6, as well as the predicted drawdown at each monitoring location. The change in predicted groundwater levels from the average groundwater level is defined as the predicted groundwater level through time minus the average predicted water level. Predicted drawdown is determined by subtracting the predicted groundwater level under the mining condition from the predicted groundwater level without mining to estimate the change in groundwater level related to mining. Groundwater-level data are presented for the 80% Success in Grouting Scenario with the NE Deposit only, as the predictive drawdowns presented above demonstrate that there are limited differences between the predicted drawdowns in the mining area from the 80% and 65% Success in Grouting Scenarios with the NE Deposit.

The following can be observed with regard to future changes in groundwater levels:

1. At monitoring locations GA101, GA102, and GA201, the predicted change in groundwater levels and the predicted drawdown are within the range of historically measured seasonal change in groundwater levels.
2. At monitoring location GA300, the predicted drawdown is within the range of historically measured seasonal change in groundwater levels. The predicted change in groundwater level is up to 0.2 m below the minimum measured groundwater level in the winter season.
3. At monitoring location GA202, the predicted drawdown is greater than the historically measured seasonal change in groundwater levels by 0.15 m. The predicted change in groundwater level is up to 0.23 m below the minimum measured groundwater level in the winter season.
4. At monitoring location GA104, the predicted drawdown is greater than the historically measured seasonal change in water levels by 0.23 m. The predicted change in groundwater level is up to 0.23 m below the minimum measured groundwater level in the winter season.

5.2.3 Predicted Baseflow to the Kitinen River

Figure 5-8 shows the predicted baseflow (i.e., groundwater discharge into the river) to the Kitinen River over the LOM for the 80% and 65% Success in Grouting Scenarios and No-Mining Scenario. Due to mining, it is predicted that the groundwater discharge to the Kitinen River may decrease by up to 20 m³/hr. This flow rate decrease equates to approximately 4% to 6% of total simulated groundwater discharge to the Kitinen River (total simulated groundwater discharge ranges from 300 to 420 m³/hr). The total decrease in discharge is a negligible change in the total river flow rate (approximately a 0.01% change; SYKE 2022). The predicted decrease in the groundwater discharge to the Kitinen River does not incorporate the planned discharge of treated mine water to the Kitinen River. It is likely that, if treated water from the groundwater inflow from the Mine Workings and other site water is discharged to the Kitinen River, the amount of the treated water from the Mine Workings would be greater than the predicted reduction of the groundwater discharge of the Kitinen River.

5.3 PREDICTIVE RESULTS WITH ADDITIONAL MITIGATION FOR THE ENVIRONMENTAL ASSESSMENT

Drawdown predictions presented in Section 5.2 were used in preliminary analyses for the environmental and Natura 2000 assessment. The preliminary analyses indicated that there is potential for environmental effects in areas of the predicted drawdown of the Mire. Subsequently, AASM Oy plans to implement an additional mitigation strategy to minimize potential drawdown in the Mire area. This section of the report provides a summary of the additional mitigation strategy and the potential effects of this strategy on future drawdown and groundwater inflow rates. Comparisons will be made between the results within this section and the results from Section 5.2.

Drawdown in the Mire area was primarily due to the presence of the shallow underground workings associated with the NE deposit. To minimize the magnitude of drawdown in the Mire, AASM Oy plans to remove the NE deposit underground workings from the mine plan (areas of the NE deposit

are shown in Figure 3-30a). As such, the following two additional predictive groundwater flow model scenarios were simulated:

1. **80% Success in Grouting without the NE Deposit Scenario:** The 80% Success in Grouting without the NE Deposit Scenario assumes 80% effectiveness in grouting along fault structures and to a depth of 150 mbgs along the Declines, moderate- K -value backfill material (5.0×10^{-8} m/s), and free-draining stopes throughout the LOM. To simulate an 80% grouting efficiency, selected drain nodes (20% of nodes) are left open to drain in areas of grouting. This scenario assumes all underground workings associated with the NE deposit are not included in the simulated mine plan.
2. **65% Success in Grouting without the NE Deposit Scenario:** The 65% Success in Grouting without the NE Deposit Scenario assumes 65% effectiveness in grouting along fault structures and to a depth of 150 mbgs along the Declines, high- K -value backfill material (1.0×10^{-7} m/s), and free-draining stopes throughout the LOM. To simulate a 65% grouting efficiency, selected drain nodes (35% of nodes) are left open to drain in areas of grouting. This scenario assumes all underground workings associated with the NE deposit are not included in the simulated mine plan.

5.3.1 Predicted Groundwater Inflow Rates

Figure 5-9 shows the predicted groundwater inflow rates for the 80% and 65% Success in Grouting without the NE Deposit Scenarios. Table 5-3 provides a summary of the predicted groundwater inflow rates and cumulative volumes for the 80% and 65% Success in Grouting without the NE Deposit Scenarios over time. The following observations can be made regarding the future groundwater inflow rates for the 80% Success in Grouting without the NE Deposit Scenario:

1. The groundwater inflow rates begin to increase in Year 1 of mining as the four Declines are constructed. By mid-Year 2, the groundwater inflow rates reach a peak groundwater inflow rate of 118 m³/hr (2,830 m³/day) due to the presence of the permeable Basal Thrust. Peak groundwater inflow rates occur after the construction of the Declines and the shallow Mine Workings.
2. After reaching a peak groundwater inflow rate, the groundwater inflow rate decreases to approximately 100 m³/hr (2,400 m³/day) by Year 6 as mining is progressing in lower elevations that have lower bedrock K values. The groundwater inflow rate does not increase due to mining at the lower elevations where the bedrock has low K values.

3. Groundwater inflow rates slowly decrease through time after Year 6 of mining. Groundwater inflow rates remain between 95 and 100 m³/hr (2,280 to 2,400 m³/day) from Year 6 through Year 22.
4. The total cumulative volume of water extracted from the underground workings over the LOM is approximately 18.3 million m³. This is a reduction of 1.6 million m³ from the scenario with the NE deposit.

The following observations can be made regarding the future groundwater inflow rates for the 65% Success in Grouting without the NE Deposit Scenario (Figure 5-9 and Table 5-3):

1. The groundwater inflow rates begin to increase in Year 1 of mining as the four Declines are constructed. By mid-Year 2, the groundwater inflow rates reach a peak groundwater inflow rate of 122 m³/hr (2,930 m³/day) due to the presence of the permeable Basal Thrust. Peak groundwater inflow rates occur after the construction of the Declines and the shallow Mine Workings.
2. After reaching a peak groundwater inflow rate, the groundwater inflow rate decreases to approximately 107 m³/hr (2,570 m³/day) by Year 6 as mining is progressing in lower elevations that have lower bedrock *K* values. The groundwater inflow rate does not increase due to mining at the lower elevations where the bedrock has low *K* values.
3. Groundwater inflow rates slowly decrease through time after Year 6 of mining. Groundwater inflows rates remain between 100 and 105 m³/hr (2,400 to 2,520 m³/day) from Year 6 through Year 22.
4. The total cumulative volume of water extracted from the underground workings over the LOM is approximately 19.5 million m³. This is a reduction of 1.5 million m³ from the scenario with the NE deposit.

The predicted groundwater inflow rates for the 80% and 65% Success in Grouting without the NE Deposit Scenarios follow the same magnitude and timing patterns as the model scenarios with the NE Deposit described in Section 5.2 except groundwater inflow rates decrease over the LOM instead of increasing in Year 10 of mining.

5.3.2 Predicted Drawdown

Figure 5-10a and Figure 5-10b show drawdown hydrographs of 11 different hypothetical monitoring locations across the Project Site for the 80% and 65% Success in Grouting without the NE Deposit Scenarios, respectively. The locations of these hypothetical monitoring locations are also shown in Figure 5-10a and Figure 5-10b. It is assumed that the hypothetical monitoring locations are screened within the Shallow Groundwater System (from 0 to 10 mbgs). For each hypothetical monitoring location, the predicted drawdown is shown over the LOM. The predicted drawdown associated with mining was estimated by comparing the model-predicted drawdown in the 80% and 65% Success in Grouting without the NE Deposit Scenarios with the No-Mining Scenario. The following can be observed regarding the predicted drawdown across the Project Site for the 80% Success in Grouting without the NE Deposit Scenario (Figure 5-10a):

1. Predicted drawdown varies seasonally due to the simulated seasonal recharge from snowmelt. Seasonal peak drawdown rates are predicted to occur prior to snowmelt in the spring. Seasonal variations in drawdown range from 0.01 to 0.4 m.
2. Larger seasonal variations in drawdown occur at Monitoring Location 1 due to the smaller thickness of shallow sediments and the effects of recharge on lower *K*-value bedrock.
3. Drawdown begins to occur at Monitoring Locations 1 through 5 as the Declines are constructed during the initial part of mining development (Year 1 through Year 2).
4. Drawdowns at Monitoring Locations 3, 4, and 5 are larger than those at other locations due to the presence of the permeable Basal Thrust along the Declines. Peak drawdown rates along the Declines are approximately 0.93 and 0.75 m in the winter and summer seasons, respectively.
5. Drawdown at monitoring locations over the main deposit area slowly increase through time as underground mining progresses. Peak drawdown over the primary mining area is approximately 0.3 m in Year 22. In comparison with the drawdown for the mine plan with the NE deposit, there is a reduction in drawdown in the primary mining area due to removing the NE deposit underground workings from the mine plan.
6. There is little drawdown at Monitoring Locations 8, 9, and 10 in Year 10 as the shallow Mine Workings are developed at the main deposit. In comparison with the drawdown for the mine plan with the NE deposit, there is less drawdown at these locations due to removing the NE deposit underground workings from the mine plan.

7. Predicted drawdown of 0.3 m or less at the end of mining is less than the seasonal variation of 0.5 to 2 m in measured groundwater levels over the primary mining area.

The following can be observed regarding the predicted drawdown across the Project Site for the 65% Success in Grouting without the NE Deposit Scenario (Figure 5-10b):

1. Predicted drawdown patterns and timing are the same as in the 80% Success in Grouting Scenario without the NE deposit.
2. Seasonal variations in drawdown range from 0.01 to 0.8 m at the hypothetical monitoring locations.
3. Drawdowns at Monitoring Locations 1, 3, 4, and 5 are larger than those at other locations due to the presence of the permeable Basal Thrust along the Declines and the shallow Declines. Peak drawdown rates along the Declines are approximately 1.0 and 0.8 m in the winter and summer seasons, respectively.
4. Drawdown at monitoring locations over the main deposit area slowly increases through time as underground mining progresses. Peak drawdown over the primary mining area is approximately 0.3 m in Year 22. In comparison with the drawdown for the mine plan with the NE deposit, there is a reduction in drawdown in the primary mining area due to removing the NE deposit underground workings from the mine plan.
5. There is little drawdown at Monitoring Locations 8, 9, and 10 in Year 10 as the shallow Mine Workings are developed at the main deposit. In comparison with the drawdown for the mine plan with the NE deposit, there is less drawdown at these locations due to removing the NE deposit underground workings from the mine plan.
6. Predicted drawdown of 0.3 m or less at the end of mining is less than the seasonal variation of 0.5 to 2 m in measured groundwater levels over the primary mining area.

Figure 5-11a and Figure 5-11b show the predicted drawdown contours associated with mining within the HSA at the end of mining in Year 22 for the 80% and 65% Success in Grouting without the NE Deposit Scenarios, respectively. The predicted drawdown is greater along the Declines and in the area of the shallow Declines. The peak drawdown at the end of mining is centered around the shallow Decline and portal area. The peak drawdown at the end of mining is 2.8 m and 4.0 m for the 80% and 65% Success in Grouting without the NE Deposit Scenarios, respectively. There is less drawdown in the mining and NE deposit areas in these scenarios as compared to the simulated

scenarios with the NE deposit described in Section 5.2 due to removal of the NE deposit workings from the mine plan.

Similar to scenarios described in Section 5.2, it is likely that, as drawdown begins to occur within the Shallow Groundwater System, recharge to the groundwater system will increase. This increased recharge is not simulated in the groundwater flow model. An increase in recharge to the groundwater system would result in less drawdown in the Shallow Groundwater System than is currently predicted by the groundwater flow model.

Figure 5-10a and Figure 5-10b show predicted drawdown within the footprint of the Mire. This drawdown is predicted based on the assumption that the peat is hydraulically connected to the Shallow Groundwater System and behaves as porous media. Based on the available data, it is reasonable to assume that the peat within the Mire system is only partially hydraulically connected to the Shallow Groundwater System. Consequently, the predicted drawdown from the groundwater flow model is likely to be higher than the actual field-observed drawdown in the peat based on Itasca's experience at other mines with similar overburden hydrogeologic settings.

Figure 5-12 shows the simulated change in groundwater levels for the predictive time period of Year 1 through Year 22 of mining for the 80% Success in Grouting without the NE Deposit Scenario. Also shown in the figure are the minimum and maximum measured groundwater levels from the 2012–2021 time period as defined in Figure 5-6, as well as the predicted drawdown at each monitoring location. The change in predicted groundwater levels from the average groundwater level is defined as the predicted groundwater level through time minus the average predicted water level. Predicted drawdown is determined by subtracting the predicted groundwater level under the mining condition from the predicted groundwater level without mining to estimate the change in groundwater level related to mining. Groundwater-level data are presented for the 80% Success in Grouting Scenarios only, as predictive drawdown data demonstrate that there are minimal differences in predicted drawdown in the mining area between the 80% and 65% Success in

Grouting without the NE Deposit Scenarios. The following can be observed regarding the predicted groundwater-level change at monitoring locations in the Mire for the predictive groundwater flow model simulations without the NE deposit:

1. At monitoring locations GA101, GA102, GA201, GA200, and GA300, the predicted change in groundwater levels and the predicted drawdown are within the range of historically measured seasonal change in groundwater levels.
2. At monitoring location GA104, the predicted drawdown is greater than the historically measured seasonal change by 0.23 m. The predicted change in groundwater level is up to 0.23 m below the minimum measured groundwater level in the winter season.
3. Predicted changes in groundwater levels without the NE deposit show less drawdown and change in groundwater levels in comparison to those presented in Section 5.2 for the with the NE deposit scenarios.

5.3.3 Predicted Baseflow to the Kitinen River

Figure 5-13 shows the predicted baseflow (i.e., groundwater discharge into the river) to the Kitinen River over the LOM for the 80% and 65% Success in Grouting Scenarios without the NE Deposit and the No-Mining Scenario. Due to mining, it is predicted that the groundwater discharge to the Kitinen River may decrease by up to 20 m³/hr. This flow rate decrease equates to approximately 4% to 6% of total simulated groundwater discharge to the Kitinen River. The total decrease in discharge is a negligible change in the total river flow rate (approximately a 0.01% change; SYKE 2022). There are little to no differences in the predicted Kitinen River baseflow in the model scenarios with and without the NE deposit.

5.4 PREDICTIVE RESULTS OF GROUNDWATER RECOVERY AFTER MINING

After mining ends, it is expected that the Shallow and Deep Groundwater Systems will begin to recover. The groundwater flow model was used to estimate the time for the groundwater recovery in the Shallow and Deep Groundwater Systems for the mine plan with and without the NE deposit scenarios described in Sections 5.2 and 5.3, respectively.

5.4.1 Predicted Groundwater Recovery for Mine Plan with the NE Deposit

Two model scenarios were conducted to predict the future groundwater recovery based on the simulated LOM scenarios with the NE deposit. The setup and assumptions for these two groundwater recovery model scenarios are as follows:

1. **80% Success in Grouting Groundwater Recovery Scenario:** The 80% Success in Grouting Groundwater Recovery Scenario used the same assumptions described in Section 5.2 during the mining operation. After mining, the groundwater system is allowed to naturally recover. The future recharge rates are based on the estimated average recharge shown in Figure 5-1. The average monthly recharge rate is repeated annually over the entire model simulation.
2. **65% Success in Grouting Groundwater Recovery Scenario:** The 65% Success in Grouting Groundwater Recovery Scenario used the same assumptions described in Section 5.2 during the mining operation. After mining, the groundwater system is allowed to naturally recover. The future recharge rates are based on the estimated average recharge shown in Figure 5-1. The average monthly recharge rate is repeated annually over the entire model simulation.

Based on the above assumptions, the groundwater flow model was simulated for 400 years after mining. A 400-yr time period for groundwater recovery is simulated due to the low K value of the Unfractured Bedrock.

Groundwater recovery in the groundwater system is demonstrated by showing drawdown at the key monitoring locations over time. In order to assess the groundwater recovery over time, the following hypothetical piezometers as shown in Figure 5-14 were used:

1. Eleven shallow piezometers were populated in the areas of predicted drawdown. These piezometers monitor the groundwater levels in the first saturated model layer.
2. One piezometer was populated from the ground surface to the deep mining zone. This piezometer was assumed to be equipped with multiple transducers at eight different elevations.

The groundwater system is considered to be recovered as drawdown at each monitoring location approaches 0 m of drawdown. Figure 5-14a shows drawdown hydrographs for the 80% Success in

Grouting Groundwater Recovery Scenario at 11 different hypothetical monitoring wells and one piezometer at the Project Site during groundwater recovery. The predicted drawdown associated with groundwater recovery was estimated by comparing the model-predicted drawdown in the 80% Success in Grouting Groundwater Recovery Scenario with the No-Mining Scenario. The following can be observed regarding the groundwater recovery for the 80% Success in Grouting Groundwater Recovery Scenario across the Project Site:

1. Groundwater levels within the Shallow Groundwater System begin to recover after mining ends. Groundwater recovery begins to occur as the Mine Workings stop draining groundwater.
2. Within the Shallow Groundwater System monitoring locations, predicted recovered groundwater levels vary seasonally due to the simulated seasonal recharge from snowmelt. Seasonal variations range from 0.01 to 0.15 m.
3. Within 5 years, groundwater levels within the Shallow Groundwater System have recovered to within 0.1 m in comparison to the pre-mining condition.
4. Monitoring locations within the Shallow Groundwater System indicate that the groundwater system has recovered to drawdown with less than 0.01 m difference (greater than 99% recovery) from the No-Mining Scenario at all monitoring locations 75 years after mining ends.
5. At piezometer locations within the Unfractured Bedrock, there is increasing drawdown in the shallow elevations of the Unfractured Bedrock for the first 20 years of recovery after mining ends as the Deep Groundwater System begins to recover.
6. Due to the low K values of the Unfractured Bedrock, deeper monitoring locations require a longer time to recover than shallower monitoring locations. By 400 years after mining, all monitoring locations within the Unfractured Bedrock have drawdown less than 1 m.

Figure 5-14b shows drawdown hydrographs for the 65% Success in Grouting Groundwater Recovery Scenario at 11 different hypothetical monitoring wells and one piezometer at the Project Site during groundwater recovery. The following can be observed regarding the groundwater recovery for the 65% Success in Grouting Groundwater Recovery Scenario across the Project Site:

1. Groundwater levels within the Shallow Groundwater System begin to recover after mining ends. Groundwater recovery begins to occur as the Mine Workings stop draining groundwater.
2. Within the Shallow Groundwater System monitoring locations, predicted recovered groundwater levels vary seasonally due to the simulated seasonal recharge from snowmelt. Seasonal variations range from 0.01 to 0.15 m.
3. Within 10 years, groundwater levels within the Shallow Groundwater System have recovered to within 0.1 m in comparison to the pre-mining condition.
4. Monitoring locations within the Shallow Groundwater System indicate that the groundwater system has recovered to drawdown with less than 0.01 m difference (greater than 99% recovery) from the No-Mining Scenario at all monitoring locations 75 years after mining ends.
5. At piezometer locations within the Unfractured Bedrock, there is increasing drawdown in the shallow elevations of the Unfractured Bedrock for the first 20 years of recovery after mining ends as the Deep Groundwater System begins to recover.
6. Due to the low K values of the Unfractured Bedrock, deeper monitoring locations require a longer time to recover than shallower monitoring locations. By 400 years after mining, all monitoring locations within the Unfractured Bedrock have drawdown less than 2.5 m.

5.4.2 Predicted Groundwater Recovery for Mine Plan without the NE Deposit

Two model scenarios were conducted to predict the future groundwater recovery based on the simulated LOM scenarios without the NE deposit. The setup and assumptions for these two groundwater recovery model scenarios are as follows:

1. **80% Success in Grouting without the NE Deposit Groundwater Recovery Scenario:** The 80% Success in Grouting Groundwater Recovery Scenario used the same assumptions described in Section 5.3 during the mining operation. After mining, the groundwater system is allowed to naturally recover. The future recharge rates are based on the estimated average recharge shown in Figure 5-1. The average monthly recharge rate is repeated annually over the entire model simulation.
2. **65% Success in Grouting without the NE Deposit Groundwater Recovery Scenario:** The 65% Success in Grouting Groundwater Recovery Scenario used the same assumptions described in Section 5.3 during the mining operation. After mining, the groundwater system is allowed to naturally recover. The future recharge rates are based on the estimated average recharge

shown in Figure 5-1. The average monthly recharge rate is repeated annually over the entire model simulation.

Based on the above assumptions, the groundwater flow model was simulated for 400 years after mining. A 400-yr time period for groundwater recovery is simulated due to the low K value of the Unfractured Bedrock.

Groundwater recovery in the groundwater system is demonstrated by showing drawdown at the key monitoring locations over time. In order to assess the groundwater recovery over time, the following hypothetical piezometers, as shown in Figure 5-15, were used:

1. Eleven shallow piezometers were populated in the areas of predicted drawdown. These piezometers monitor the groundwater levels in the first saturated model layer.
2. One piezometer was populated from the ground surface to the deep mining zone. This piezometer was assumed to be equipped with multiple transducers at eight different elevations.

The groundwater system is considered to be recovered as drawdown at each monitoring location approaches 0 m of drawdown. Figure 5-15a shows drawdown hydrographs for the 80% Success in Grouting Groundwater Recovery Scenario at 11 different hypothetical monitoring wells and one piezometer at the Project Site during groundwater recovery. The predicted drawdown associated with groundwater recovery was estimated by comparing the model-predicted drawdown in the 80% Success in Grouting Groundwater Recovery Scenario with the No-Mining Scenario. The following can be observed regarding the groundwater recovery for the 80% Success in Grouting Groundwater Recovery Scenario across the Project Site:

1. Groundwater levels within the Shallow Groundwater System begin to recover after mining ends. Groundwater recovery begins to occur as the Mine Workings stop draining groundwater.

2. Within the Shallow Groundwater System monitoring locations, predicted recovered groundwater levels vary seasonally due to the simulated seasonal recharge from snowmelt. Seasonal variations range from 0.01 to 0.15 m.
3. Within 5 years, groundwater levels within the Shallow Groundwater System have recovered to within 0.1 m in comparison to the pre-mining condition.
4. Monitoring locations within the Shallow Groundwater System indicate that the groundwater system has recovered to drawdown with less than 0.01 m difference (greater than 99% recovery) from the No-Mining Scenario at all monitoring locations 75 years after mining ends.
5. At piezometer locations within the Unfractured Bedrock, there is increasing drawdown in the shallow elevations of the Unfractured Bedrock for the first 20 years of recovery after mining ends as the Deep Groundwater System begins to recover.
6. Due to the low K values of the Unfractured Bedrock, deeper monitoring locations require a longer time to recover than shallower monitoring locations. By 400 years after mining, all monitoring locations within the Unfractured Bedrock have drawdown less than 1 m.

Figure 5-15b shows drawdown hydrographs for the 65% Success in Grouting Groundwater Recovery Scenario at 11 different hypothetical monitoring wells and one piezometer at the Project Site during groundwater recovery. The following can be observed regarding the groundwater recovery for the 65% Success in Grouting Groundwater Recovery Scenario across the Project Site:

1. Groundwater levels within the Shallow Groundwater System begin to recover after mining ends. Groundwater recovery begins to occur as the Mine Workings stop draining groundwater.
2. Within the Shallow Groundwater System monitoring locations, predicted recovered groundwater levels vary seasonally due to the simulated seasonal recharge from snowmelt. Seasonal variations range from 0.01 to 0.15 m.
3. Within 10 years, groundwater levels within the Shallow Groundwater System have recovered to within 0.1 m in comparison to the pre-mining condition.
4. Monitoring locations within the Shallow Groundwater System indicate that the groundwater system has recovered to drawdown with less than 0.01 m difference (greater than 99% recovery) from the No-Mining Scenario at all monitoring locations 75 years after mining ends.

5. At piezometer locations within the Unfractured Bedrock, there is increasing drawdown in the shallow elevations of the Unfractured Bedrock for the first 20 years of recovery after mining ends as the Deep Groundwater System begins to recover.
6. Due to the low K values of the Unfractured Bedrock, deeper monitoring locations require a longer time to recover than shallower monitoring locations. By 400 years after mining, all monitoring locations within the Unfractured Bedrock have drawdown less than 2.5 m.

Observations of groundwater recovery are the same for the mining plans with and without the NE Deposit groundwater recovery scenarios. This is because for the Shallow and Deep Groundwater Systems, the drawdown from mining occurs over the main deposit and along the Decline, which remains unchanged between the two mining plans. Consequently, the groundwater recovery times remain unchanged between the mine plans with and without the NE deposit.

6.0 SUMMARY OF KEY MODEL UNCERTAINTIES

As a part of the project, Itasca assessed each of the key data that were used in the conceptual hydrogeologic model and groundwater flow model. Based on the industrial practice, AASM Oy has conducted sufficient investigations at this project stage in comparison to the data requirements presented in Figure 6-1. There is always uncertainty related to the groundwater model. However, the confidence level of the model increases as the project advances. Therefore, for reducing the uncertainty there is a need for monitoring data and periodic update of the conceptual model and numerical groundwater flow model.

The evolution of a groundwater flow model is presented in Figure 6-2. The model requires periodic validation and update based on the monitoring data. This process will continuously improve the confidence level of the groundwater flow model by reducing the data uncertainty.

Table 6-1 provides a summary of the key data used and their respective uncertainties. The following is a summary of the key uncertainties associated with the groundwater flow model predictions:

1. Site-specific hydraulic parameters were available over the primary area of the Mine Workings. Based on these data, the following assumptions were made in the conceptual and numerical models:
 - a. The bedrock along the Decline and Kitinen River area was assigned to be more permeable than the bedrock in the mining area based on *K*-value data. However, there are less measured *K*-value data in this area when compared to the extensive *K*-value dataset in the mining area.
 - b. Packer-testing data indicate that *K* values of structures in the mining area have similar *K* values to the bedrock around the faults. As such, it is assumed in the model that the faults/fractures in the mining area have the same *K* values as the bedrock.
 - c. The peat is simulated as one hydrogeologic unit with no spatial variation in *K* values. The simulated *K* values of the peat are in the middle to upper portion of the range of measured peat *K* values. The simulated approach of higher *K* values and no variation in *K* values of the peat in the groundwater flow model is a conservative approach to predict the potential drawdown in the peat area. Studies of the peat indicate that there is a distribution of *K* values within the peat, with a lower *K* value at the base of

the peat. This low- K -value zone can impede water seepage to underlying units and separate the peat from the underlying glacial and fluvial sediments in many areas. A reduction in peat K values with depth may limit hydraulic connection with the underlying hydrogeologic units and lower the predicted drawdown in the peat area.

- d. The K values of all bedrock units were assumed to decrease with depth based on measured K -value data. This assumption is reasonable based on the available data and can be further validated as more monitoring data become available during the mining operation.
2. The groundwater flow model is well calibrated to the available transient groundwater-level data based on calculated model statistics (Spitz and Moreno 1996; Anderson and Woessner 1992; Barnett et al 2012). The groundwater flow model is calibrated primarily to monitoring locations within the fluvial and glacial deposits, Fractured Bedrock, and shallow Unfractured Bedrock. Few data are available about groundwater levels in the Deep Groundwater System (greater than 200 mbgs).
 3. Recharge to the Shallow Groundwater System is the key component of the water balance and results in the seasonal fluctuations of the groundwater levels. A *MIKE SHE* model was used to estimate the recharge rate to the Shallow Groundwater System based on measured meteorological variables and calibration to the measured groundwater levels. The groundwater flow model presented in this report incorporated the *MIKE SHE* estimated recharge rates for the model calibration time period and used average recharge rates for predictive model simulations. The following are uncertainties in the simulated recharge rates:
 - a. Recharge was estimated by using a *MIKE SHE* model for the three hydrogeologic units that are the most relevant across the Project Site (tills, sorted sediments, and peat). These three hydrogeologic units have been extensively studied and are well understood. Recharge may vary at a more complex local scale than the assumed three hydrogeologic units for the HSA; however, the recharge to the HSA is well represented based on the overall model calibration to seasonal changes in water levels.
 - b. No data are available on future recharge rates for the HSA. Average recharge rates and estimates of recharge for a future climate were used in the groundwater flow model predictions. The estimated recharge rates are sensitive to the assigned meteorological parameters.
 4. The predicted drawdown does not consider the effects of dense vegetation, the suction effect of roots, and the large storage of the shallow surficial composed materials. These effects will reduce the predicted drawdown of the groundwater table.
 5. The peat drawdown is predicted based on the assumption that the peat is hydraulically connected to the Shallow Groundwater System and behaves as porous media. Based on the

available data, it is reasonable to assume that the peat within the Mire system has a low-*K*-value zone in many areas and is only partially hydraulically connected to the Shallow Groundwater System. Consequently, the predicted drawdown from the groundwater flow model is likely to be higher than the actual field-observed drawdown in the peat.

6. The predicted drawdown does not consider the increased recharge that will occur as the result of lowering of the water table induced by the mining operation. The increased recharge will reduce the predicted drawdown of the groundwater table.

As described in Figures 6-1 and 6-2, data collection is a long-term process. This process should be ongoing prior to, during, and after mining. Continued data collection is needed to validate and update the conceptual and numerical groundwater flow models. It is expected that over the LOM, the conceptual and numerical models are continually updated.

The geological and hydrogeological conditions in the vicinity of the Mine Workings and surrounding area have been extensively studied by AASM Oy. The developed conceptual hydrogeological model and groundwater flow model presented in this report were updated based on the most recent studies conducted by AASM Oy. The groundwater flow model code *MINEDW* has several attributes that were specifically developed to address mining environments, and the code has been applied in numerous projects for mines in different hydrogeological and meteorological conditions. The groundwater flow model described in this report has been significantly updated since the previously developed groundwater flow model. The following is an overview of the key strengths of the updated groundwater flow model:

1. The groundwater flow model domain boundary (the HSA) was chosen to represent a groundwater system area that is much larger than the Sakatti Project Site. The boundary is a significant distance away from the potential mining-induced hydraulic stresses to minimize any potential boundary effects. The model incorporates all Mine Workings. In addition, the model includes the entire environmentally sensitive area of the Viiankiaapa Mire. The predicted drawdown is located entirely within the model domain, and the model domain is not affecting the predicted results.
2. The model uses a considerable and reasonable amount of model layers and active elements to accurately represent the geological data and the Mine Workings.

3. The model simulates the effects of key surface-water bodies on the groundwater system and the effects of mining on the baseflow of the key surface-water bodies.
4. The description and application of groundwater recharge in the groundwater flow model is more precise and robust. Groundwater recharge was modeled with *MIKE SHE* to predict time-variable groundwater recharge rates for different hydrogeological units. These time-variable groundwater recharge rates are used directly in the groundwater flow model.
5. The groundwater flow model directly uses the most recent geologic and structure models that have been developed for the Sakatti Project Site for the Shallow and Deep Groundwater Systems. The calibrated *K* values of the geologic units are within the measured and literature ranges of *K* values.
6. The groundwater flow model was calibrated to 9 years of measured groundwater-level data from the Shallow and Deep Groundwater Systems. The groundwater flow model was well calibrated in all hydrogeologic units in the Main and NE deposit areas as well as the Kuusivaara area. The groundwater flow model is well calibrated to seasonal water-level changes in all hydrogeologic units. The differences between the measured and simulated groundwater levels were examined with well-known and used statistical indicators to assess the quality of the groundwater flow model calibration. Based on the key statistics, both steady-state and transient situation models are well calibrated.

The groundwater flow model can be used to accurately predict the location and magnitude of drawdown for the Sakatti Project. Predictive model results always have some level of uncertainty, as described above. However, the magnitude of the uncertainty depends on an understanding of local conditions. As described in Section 3 of the report, there have been extensive studies conducted at the Project Site in relation to the phase of the project (Figure 6-1), and as such, there is a high level of understanding of the Sakatti Project Site conditions. As a result, the uncertainties have been minimized based on the available data. Overall, the groundwater flow model predictions are considered conservative for the following reasons:

1. The simulated *K* values of the hydrogeologic units are at the middle or higher end of *K*-value ranges when compared with the measured *K*-value ranges. *K* values at the lower end of the measurement range were not applied.
2. The peat has been conservatively simulated as more water conducting than available measured data suggest. Based on previous studies and measurements, there exist compacted well-decomposed layers that result in low *K* values, which likely limit drawdown.

3. The assigned hydraulic properties of the faults were conservative and are simulated as more continuous zones in the groundwater model than available data suggest. The measured data suggest that the faults are not continuous, with varying hydraulic properties. Model representation of hydraulically interconnected faults led to overprediction of the inflow rate and groundwater-level drawdown.
4. The Basal Thrust is the most significant fault of deep bedrock that has measured higher K values when compared to surrounding deep bedrock. However, based on drilling, it is known that the Basal Thrust has areas that are clay filled where groundwater flow is limited. Therefore, the model predictions associated with the assumption of the Basal Thrust being hydraulically conductive led to overprediction of the inflow rate and groundwater-level drawdown.
5. The groundwater flow model does not account for the effects of lowering the groundwater level on groundwater recharge. When the groundwater level in the Shallow Groundwater System decreases, there will be a corresponding increase in the amount of water recharging the groundwater system. This will occur in the Sakatti Project area due to the abundance of available water (i.e., excess surface-water runoff) during the spring melt season.
6. The groundwater flow model does not incorporate the presence of saprolite at the bedrock depressions and along fault intersections, which restricts the propagation of drawdown to the Shallow Groundwater System.

7.0 CONCLUSIONS

A groundwater flow model was developed by Itasca based on the conceptual hydrogeologic model. The groundwater flow model was calibrated to the available groundwater-level data at the Project Site. Itasca considers the groundwater flow model to be reasonably constructed and calibrated to the available groundwater-level data. Based on the conceptual hydrogeologic model and numerical model development, the following are the conclusions regarding the predictions of future groundwater inflow and drawdown for the 80% Success in Grouting Scenario:

1. The predicted peak groundwater inflow rate to the Mine Workings occurs by mid-Year 2 of mining. The peak groundwater inflow rate is approximately 118 m³/hr. After reaching a peak groundwater inflow rate, the groundwater inflow rate gradually decreases to a range between 100 m³/hr and 110 m³/hr over the LOM.
2. Shallow Groundwater System drawdown along the Declines is predicted to be larger than at other locations due to the presence of the permeable Basal Thrust. Peak drawdown values along the Declines are approximately 0.93 and 0.75 m in the winter and summer seasons, respectively, at the end of mining operations (Year 22).
3. Peak drawdown over the primary mining area is approximately 0.6 m.
4. The largest drawdown is associated with the shallow Decline and portal area (where Mine Workings are less than 150 mbgs). Along this section of the Decline, peak drawdown at the end of mining is 2.8 m.
5. Predicted drawdown varies seasonally due to the simulated seasonal recharge from snowmelt. Seasonal peak drawdown rates are predicted to occur prior to snowmelt in the spring.
6. Predicted drawdown of 0.6 m or less at the end of mining is within the seasonal variation of 0.5 to 2 m in measured groundwater levels over the primary mining area.
7. Predicted drawdown of 2.8 m or less at the end of mining is within the seasonal variation of 1 to 20 m in measured groundwater levels in the Kuusivaara area.
8. It is predicted that the groundwater discharge to the Kitinen River may decrease by up to 20 m³/hr, which equates to approximately 4% to 6% of total groundwater discharge to the Kitinen River. The total decrease in discharge is a negligible change (approximately a 0.01% change) in the total river flow rate (SYKE 2022). The predicted decrease in the groundwater discharge to the Kitinen River does not incorporate the planned discharge of treated mine water to the Kitinen River. It is likely that, if treated water from the groundwater inflow from the Mine Workings and other site water is discharged to the Kitinen River, the amount of

the treated water from the Mine Workings would be greater than the predicted reduction of the baseflow of the Kitinen River.

9. Groundwater levels within the Shallow Groundwater System immediately begin to recover after mining ends. Within 5 years, groundwater levels within the Shallow Groundwater System have recovered to within 0.1 m of the pre-mining water level. The Shallow Groundwater System is predicted to recover 75 years after mining ends (within 0.01 m of the pre-mining water level).
10. Due to the low K values of the Unfractured Bedrock, deeper monitoring locations require a longer time to recover than shallower monitoring locations. By 400 years after mining, all monitoring locations within the Unfractured Bedrock have drawdown less than 1 m.

The following are the conclusions regarding the predictions of future groundwater inflow and drawdown for the 65% Success in Grouting Scenario:

1. The predicted peak groundwater inflow rate to the Mine Workings occurs by mid-Year 2 of mining. The peak groundwater inflow rate is approximately 122 m³/hr. After reaching a peak groundwater inflow rate, the groundwater inflow rate gradually decreases to a range between 107 m³/hr and 118 m³/hr over the LOM.
2. Shallow Groundwater System drawdown along the Declines is predicted to be larger than at other locations due to the presence of the permeable Basal Thrust. Peak drawdown values along the Declines are approximately 1.0 and 0.8 m in the winter and summer seasons, respectively, at the end of mining operations (Year 22).
3. Peak drawdown over the primary mining area is approximately 0.6 m.
4. The largest drawdown is associated with the shallow Decline and portal area (where Mine Workings are less than 150 mbgs). Along this section of the Declines, peak drawdown at the end of mining is 4.0 m.
5. Predicted drawdown varies seasonally due to the simulated seasonal recharge from snowmelt. Seasonal peak drawdown rates are predicted to occur prior to snowmelt in the spring.
6. Predicted drawdown of 0.6 m or less at the end of mining is within the seasonal variation of 0.5 to 2 m in measured groundwater levels over the primary mining area.
7. Predicted drawdown of 4.0 m or less at the end of mining is within the seasonal variation of 1 to 20 m in measured groundwater levels in the Kuusivaara area.
8. It is predicted that the groundwater discharge to the Kitinen River may decrease by up to 20 m³/hr, which equates to approximately 4% to 6% of total groundwater discharge to the Kitinen River. The total decrease in discharge is a negligible change (approximately a 0.01%

change) in the total river flow rate (SYKE 2022). The predicted decrease in the groundwater discharge to the Kitinen River does not incorporate the planned discharge of treated mine water to the Kitinen River. It is likely that, if treated water from the groundwater inflow from the Mine Workings and other site water is discharged to the Kitinen River, the amount of the treated water from the Mine Workings would be greater than the predicted reduction of the baseflow of the Kitinen River.

9. Groundwater levels within the Shallow Groundwater System immediately begin to recover after mining ends. Within 10 years, groundwater levels within the Shallow Groundwater System have recovered to within 0.1 m of the pre-mining water level. The Shallow Groundwater System is predicted to recover 75 years after mining ends (within 0.01 m of the pre-mining water level).
10. Due to the low K values of the Unfractured Bedrock, deeper monitoring locations require a longer time to recover than shallower monitoring locations. By 400 years after mining, all monitoring locations within the Unfractured Bedrock have drawdown less than 2.5 m.

The following are conclusions regarding the potential effects on the model predictions of future groundwater inflow and drawdown and groundwater recovery with the removal of the NE deposit from the mine plan:

1. There is a long-term reduction in groundwater inflow as compared to the model scenarios with the NE deposit. After Year 6 of mining, groundwater inflows reduce to 95 to 100 m³/hr and 100 to 105 m³/hr for the 80% and 65% Success in Grouting without the NE Deposit Scenarios, respectively. This is a reduction of approximately 5 to 10 m³/hr for each model scenario.
2. The peak drawdown over the primary mining area is approximately 0.2 m. This is a reduction of up to 0.4 m from the mine plan including the NE deposit.
3. Predicted drawdown of 0.3 m or less at the end of mining is less than the seasonal variation of 0.5 to 2 m in measured groundwater levels over the primary mining area.
4. There are limited to no effects on the predicted reduction in baseflow to the Kitinen River.
5. There are limited to no effects on the predicted groundwater recovery with the removal of the NE deposit from the mine plan. This is because for the Shallow and Deep Groundwater Systems, the drawdown from mining occurs over the main deposit and along the decline, which remains unchanged between the two mining plans. Consequently, the groundwater recovery times remain unchanged between the mine plans with and without NE deposit.

It should be noted that these conclusions do not include the following effects, as discussed in Section 6.0:

1. The predicted drawdown does not consider the effects of dense vegetation, the suction effect of roots, and the large storage of the shallow surficial composed materials. These effects will reduce the predicted drawdown of the groundwater table.
2. The peat drawdown is predicted based on the assumption that the peat is hydraulically connected to the Shallow Groundwater System and behaves as porous media. Based on the available data, it is reasonable to assume that the peat within the Mire system is only partially hydraulically connected to the Shallow Groundwater System. Consequently, the predicted drawdown from the groundwater flow model is likely to be higher than the actual field-observed drawdown in the peat.
3. The predicted drawdown does not consider the increased recharge that will occur as the result of lowering of the water table induced by the mining operation. The increased recharge will reduce the predicted drawdown of the groundwater table.

8.0 REFERENCES

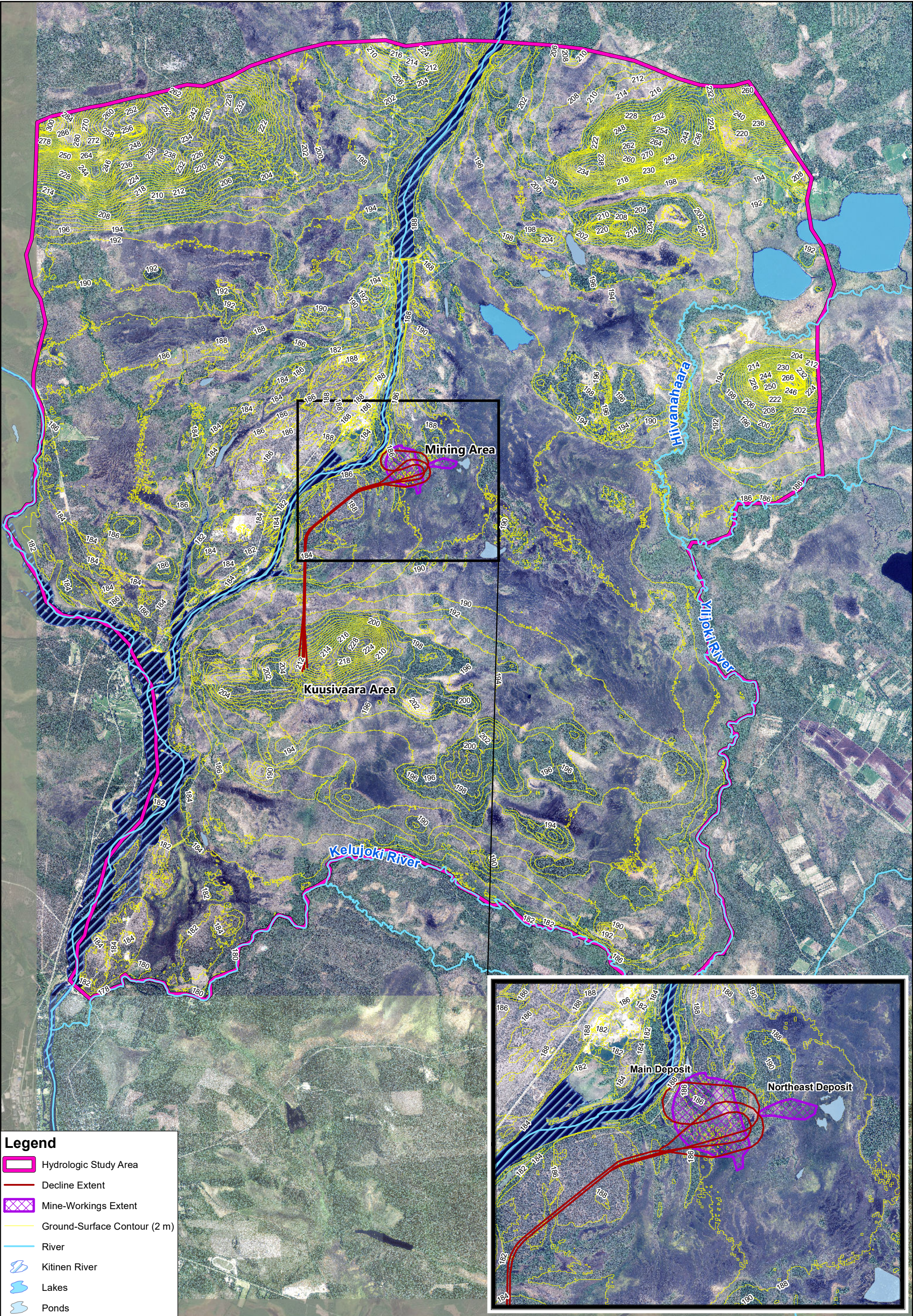
- AASM Oy. 2021. Review report 2021: Review of Sakatti project bedrock hydrogeological testing data from 2016–2021. Internal report prepared by Eero Heikkinen for Anglo American Sakatti Mining Oy, October.
- Åberg, S.C., A.K. Åberg, and K. Korkka-Niemi. 2021. Three-dimensional hydrostratigraphy and groundwater flow models in complex Quaternary deposits and weathered/fractured bedrock: evaluating increasing model complexity. *Hydrogeology Journal* 29: 1043–74.
- Åberg, S.C., A.K. Åberg, K. Korkka-Niemi, and V.-P. Salonen. 2017. Hydrostratigraphy and 3D modelling of a bank storage affected aquifer in a mineral exploration area in Sodankylä, northern Finland. In *Mine Water and Circular Economy*, vol. 1, edited by C. Wolkersdorfer, L. Sartz, M. Sillanpää, and A. Häkkinen, 237–44. Lappeenranta, Finland: Lappeenranta University of Technology.
- Åberg, S.C., K. Korkka-Niemi, A. Rautio, and A.K. Åberg. 2022. The effect of river regulation on groundwater flow patterns and the hydrological conditions of an aapa mire in northern Finland. *Journal of Hydrology: Regional Studies* 40 (April): 101044.
- Åberg, S.C., K. Korkka-Niemi, A. Rautio, V.-P. Salonen, and A.K. Åberg. 2019. Groundwater recharge/discharge patterns and groundwater-surface water interactions in a sedimentary aquifer along River Kitinen near Sodankylä, Northern Finland. *Boreal Environment Research* 24: 155–87.
- Åberg, A.K., S. Kultti, A. Kaakinen, K.O. Eskola, and V.-P. Salonen. 2020. Weichselian sedimentary record and ice-flow patterns in the Sodankylä area, central Finnish Lapland. *Bulletin of the Geological Society of Finland* 92 (2020): 77–98. <https://doi.org/10.17741/bgsf/92.2.001>.
- Anderson, M.P., and W.W. Woessner. 1992. *Applied groundwater modeling— Simulation of flow and advective transport*. San Diego: Academic Press, Inc.
- ASTM. 2008. ASTM Standard D5981-96(2008): Standard guide for calibrating a groundwater flow model application. West Conshohocken, PA: ASTM International.
- Barnett, B., L.R. Townley, V. Post, R.E. Evans, R.J. Hunt, L. Peeters, S. Richardson, A.D. Werner, A. Knapton, and A. Boronkay. 2012. Australian groundwater modelling guidelines. Waterlines Report Series No. 82. Canberra: National Water Commission.
- Bigler, P. 2019. Hydrogeology and hydrogeochemistry of the western margin of the Viiankiaapa mire in Sodankylä: Factors affecting the distribution of endangered species. Department of Geosciences and Geography, University of Helsinki, Helsinki.
- BLM. 2008. Groundwater modeling guidance for mining activities. United States Bureau of Land Management, Reno, NV, Instructional Memorandum NV-2008-035.
- Brutsaert, W. 1982. *Evaporation into the atmosphere: Theory, history, and applications*. Dordrecht, Netherlands: Springer.

- Copernicus Climate Store. 2022. Data for RCP4.5 climate case. Accessed April 2022. <https://cds.climate.copernicus.eu/cdsapp#!/dataset/sis-ecv-cmip5-bias-corrected?tab=overview>.
- Davis, J. 1986. *Statistics and data analysis in geology*. Toronto: John Wiley and Sons.
- DHI. 2017. *MIKE SHE user manual. Volume 2: Reference guide*. Hørsholm, Denmark: DHI.
- Eilu, P. 2012. Mineral deposits and metallogeny of Fennoscandia. Special Paper 53, Geological Survey of Finland, Espoo, Finland.
- ESI. 2017. Guide to using *Groundwater Vistas*, version 7, code documentation report. Reinholds, PA: Environmental Simulations, Inc.
- Freeze, R.A., and J.A. Cherry. 1979. *Groundwater*. Englewood Cliffs, NJ: Prentice-Hall.
- Geological Survey of Finland. 2022. Mineral deposits and exploration. Accessed February, March, and May 2022. <https://gtkdata.gtk.fi/mdae/index.html>.
- Golder. 2015. Viiankiaapa – pinta- ja pohjavesi- olosuhteiden selvitys. Report prepared for Anglo American Sakatti Mining Oy.
- Hall, A.M., S. Sarala, and K. Ebert. 2015. Late Cenozoic deep weathering patterns on the Fennoscandian shield in northern Finland: A window on ice sheet bed conditions at the onset of Northern Hemisphere glaciation. *Geomorphology* 246 (October): 472–88.
- Hättestrand, C., and A.P. Stroeven. 2002. A relict landscape in the centre of Fennoscandian glaciation: Geomorphological evidence of minimal Quaternary glacial erosion. *Geomorphology* 44 (April): 127–43.
- Helmens, K.F., M.E. Räsänen, P. Johansson, H. Jungner, and K. Korjonen. 2000. The Last interglacial-glacial cycle in NE Fennoscandia: A nearly continuous record from Sokli (Finnish Lapland) *Quaternary Science Reviews* 19, no. 16 (November): 1605–23.
- Helmens, K.F., J.A.A. Bos, S. Engels, C.J. van Meerbeeck, S.J.P. Bohncke, H. Renssen, O. Heiri, S.J. Brooks, H. Seppä, H.J.B. Birks, and B. Wohlfarth. 2007. Present-day temperatures in northern Scandinavia during the last glaciation. *Geology* 35 (11): 987–90.
- Hill, M.C. 1998. Methods and guidelines for effective model calibration, with application to UCODE, a computer code for universal inverse modeling, and MODFLOW, a computer code for inverse modeling with MODFLOW. USGS Water-Resources Investigations Report 98-4005. Accessed 28 October 2019. <http://pubs.er.usgs.gov/publication/wri984005>.
- Itasca. 2012. *MINEDW user manual*. Denver, CO: Itasca Denver, Inc.
- Korkka-Niemi, K., K. Koskimaa, and J. Karhu. 2020. Hydrogeology of the Sakatti exploration target area: Dating of groundwater. Report prepared by the University of Helsinki for Anglo American Sakatti Mining Oy.

- Korkka-Niemi, K. (ed.), A. Rautio, S. Åberg, A. Åberg, P. Bigler, and V.-P. Salonen. 2017. Hydro and environment geological studies during the years 2016-2017 around Sakatti exploration target. Final report (Draft 1): Characterization of geo-hydro-ecological factors possibly controlling the distribution of endangered species of Viiankiaapa Mire. Report prepared by the University of Helsinki for Anglo American Sakatti Mining Oy.
- Korkka-Niemi, K., and H. Turtiainen, H. 2020. Hydraulic properties of peat and hydrogeochemical characteristics of groundwater and porewater in Viiankiaapa Mire. Report prepared by the University of Helsinki for Anglo American Sakatti Mining Oy, 20 August.
- Lahtinen T. 2017. Hydrogeochemical characterization of the Sakatti mine prospecting area, Sodankylä, Finnish Lapland. MSc, Department of Geosciences and Geography, University of Helsinki.
- Lappalainen, E., and H. Pajunen. 1982. Lapin turvevarat. Geologinen tutkimuslaitos maaperäosasto, raportti P 13.6/80/20.
- Luoma, S., Klein, J., Backman, B. 2013. Climate change and groundwater: Impacts and adaptation in shallow coastal aquifer in Hanko, South Finland. In *Climate Change Adaptation in Practice: From Strategy Development to Implementation*, 137–55. Chichester, England: John Wiley & Sons.
- Luukas, J. 2017. Updates of the Sakatti deposit fault and lithological 3D models in May 2017. Report conducted by the Geological Survey of Finland for Anglo American Sakatti Mining Oy.
- Mikkonen, S., M. Laine, H. Mäkelä, H. Gregow, H. Tuomenvirta, M. Lahtinen, and A. Laaksonen, 2015. Trends in the average temperature in Finland, 1847–2013. *Stochastic Environmental Research and Risk Assessment* 29: 1521–29.
- MODIS. 2022. Data for *MIKE SHE* model including plant cover and evaporation. Accessed 2021. <https://modis.gsfc.nasa.gov/>.
- Moroizumi, T., N. Ito, J. Koskiahio, and S. Tattari. 2014. Long-term trends of pan evaporation and an analysis of its causes in Finland. Research prepared by Okayama University.
- Morris, P.J., J.M. Waddington, B.W. Benscoter, and M.R. Turetsky. 2011. Conceptual frameworks in peatland ecohydrology: Looking beyond the two-layered (acrotelm-catotelm) model. *Ecohydrology* 4 (1): 1–11.
- National Parks. 2022. Accessed May 2022. <https://www.nationalparks.fi/viiankiaapa>.
- NDEP. 2018a. Listing of accepted codes for groundwater and geochemical modeling at mine sites. Nevada Division of Environmental Protection, Bureau of Mining Regulation and Reclamation, 3 April.
- NDEP. 2018b. Guidance for hydrogeologic groundwater flow modeling at mine sites. Nevada Division of Environmental Protection, Bureau of Mining Regulation and Reclamation.

- Okkonen J., M. Jyrkama, and B. Klove. 2010. A conceptual approach for assessing the impact of climate change on groundwater and related surface waters in cold regions (Finland). *Hydrogeology Journal* 18: 429–39.
- Päivänen, J. 1973. Hydraulic conductivity and water retention in peat soils. *Acta Forestalia Fennica* 129: 1–70.
- Pulkkinen, E. 1983. Sattasen karttalehtialueen geokemiallisen kartoituksen tulokset. Geological Survey of Finland. Accessed 20 November 2019. http://tupa.gtk.fi/kartta/geokemiallinen_karttaselitys/gks_3714_s.pdf.
- Puumalainen, T. 2021. A 3D geological model and geochemical and hydrogeological properties of sediments in Kuusivaara, Sodankylä, Finland. Master's thesis. Department of Geosciences, University of Oulu.
- Read, J., and P. Stacy. 2009. *Guidelines for open pit slope design*. Boca Raton, FL: CRC Press.
- Reilly, T.E., and A.W. Harbaugh. 2004. Guidelines for evaluating groundwater flow models. U.S. Geological Survey Scientific Investigations Report No. 2004-5038.
- Ruosteenoja, K., K. Jylhä, and M. Kämäräinen. 2016. Climate projections for Finland under RCP forcing scenarios. *Geophysica* 51(1): 17–50.
- Salonen, V.P., K. Korkka-Niemi, A. Rautio, A. Åberg, and S. Åberg. 2014. Recent geological history of the Sakatti area, Sodankylä and its hydro-environmental implications – A baseline study on existing surveys. Report prepared by the University of Helsinki for Anglo American Sakatti Mining Oy.
- Salonen, V.-P., K. Korkka-Niemi, A. Rautio, E. Koivisto, A. Åberg, S. Åberg, J. Laakso, T. Lahtinen, and E. Suonperä. 2016. Sakatti geoenvironments: A baseline study on quaternary sediments, hydrogeological conditions, and groundwater-surface water interactions in Kersilö area, Sodankylä. Report prepared by the University of Helsinki for Anglo American Sakatti Mining Oy.
- Sarala, P., J. Räisänen, P. Johansson, and K.O. Eskola. 2015. Aerial LiDAR analysis in geomorphological mapping and geochronological determination of surficial deposits in the Sodankylä region, northern Finland. *GFF Journal of the Geological Society of Sweden* 137 (4): 293–303.
- Spitz, K., and J. Moreno. 1996. *A practical guide to groundwater and solute transport modeling*. New York: John Wiley and Sons.
- SRK. 2019. A hydrological impact assessment for the Sakatti Cu-Ni-PGE-Au deposit, Northern Finland. Report prepared by SRK Consulting for Anglo American Sakatti Mining Oy, June.
- Stantec. 2020. Groundwater modeling assessment of the proposed underground mine at the Sakatti Cu-Ni-PGE-Au Deposit. Report prepared by Stantec for Anglo American Sakatti Mining Oy, June.

- Suonperä, E. 2016. Holocene paleohydrology of Viiankiaapa mire, Sodankylä, Finnish Lapland. MSc, Department of Geosciences and Geography, University of Helsinki, Helsinki.
- Turtiainen, H. 2020. Hydraulic properties of peat and hydrogeochemical characteristics of groundwater and porewater in Viiankiaapa mire. Master's thesis. Department of Geosciences and Geography, University of Helsinki.
- Tyrväinen, A. 1983. Suomen geologinen kartta 1:100 000: Lehdet 3713 ja 3714: odankylän ja sattsasen kartta-alueiden kallioperä [Geological map of Finland 1:100,000, sheets 3713–3714: explanation to the bed rock maps of pre-Quaternary rocks]. Geological Survey of Finland, Espoo, Finland.



Legend

Hydrologic Study Area

Decline Extent

Mine-Workings Extent

Ground-Surface Contour (2 m)

River

Kitinen River

Lakes

Ponds

N

0

1,300

2,600

Meters

PROJECT NO.	4064
BY	SBM
CHECKED	HL
DRAWN	NP
DRAWING NAME	HSA
DRAWING DATE	Apr. 25, 2022
REVISION DATE	Jun. 16, 2022

ITASCA™

Denver, Inc.

Hydrologic Study Area of the Sakatti Project

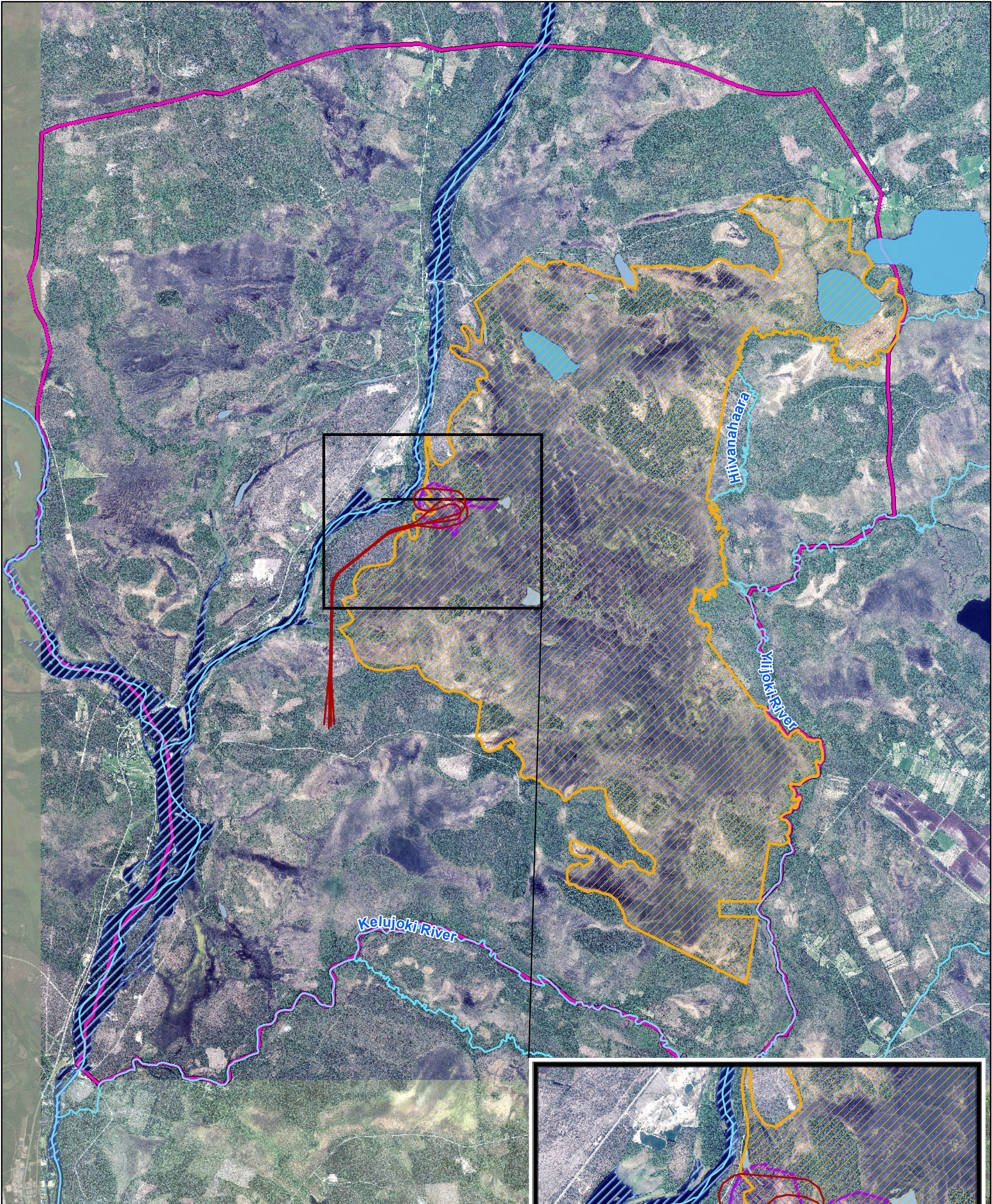
CLIENT:

Sakatti Mine

FIGURE NO.

2-1

C:\ARC\GIS\4064_Sakatti\MXD\Working\HSA.mxd



Legend

Hydrologic Study Area

Cross Section Line

Decline Extent

Viiankiaapa Extent (Natura 2000)

Mine-Workings Extent

River

Kitinen River

Lakes

Ponds

N

0

1,250

2,500

Meters

PROJECT NO.	4064
BY	SBM
CHECKED	HL
DRAWN	NP
DRAWING NAME	V_HSA
DRAWING DATE	Apr. 25, 2022
REVISION DATE	Jun. 16, 2022

ITASCATM

Denver, Inc.

Viiankiaapa Mire Area in the Hydrologic Study Area

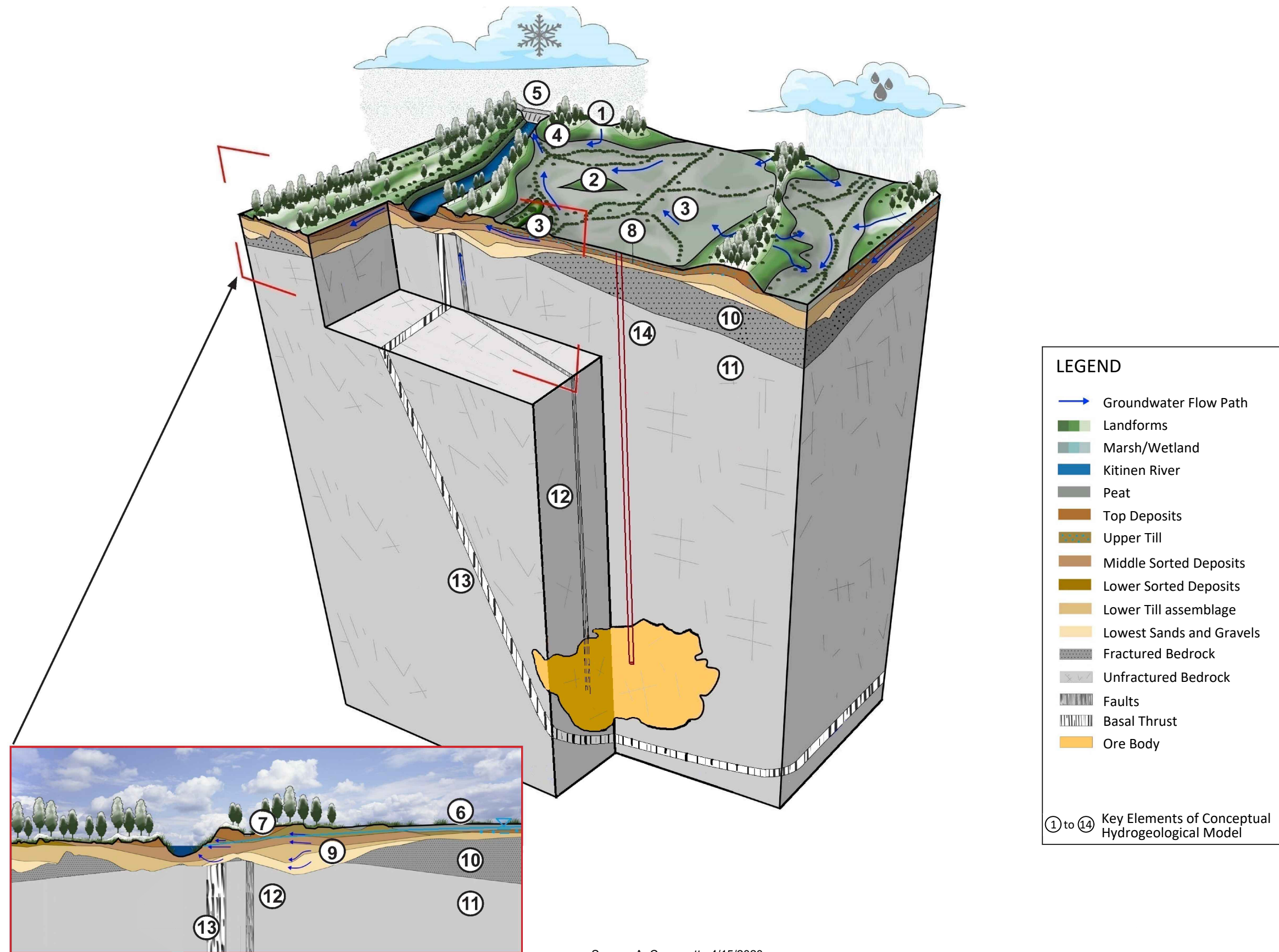
CLIENT:

Sakatti Mine

FIGURE NO.

2-2

G:\ARCGIS\4064_Sakatti\MXDs\Working\V_HSA.mxd



Source: A. Campgotto 4/15/2020

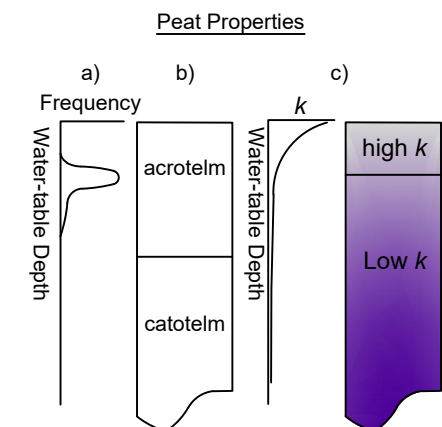
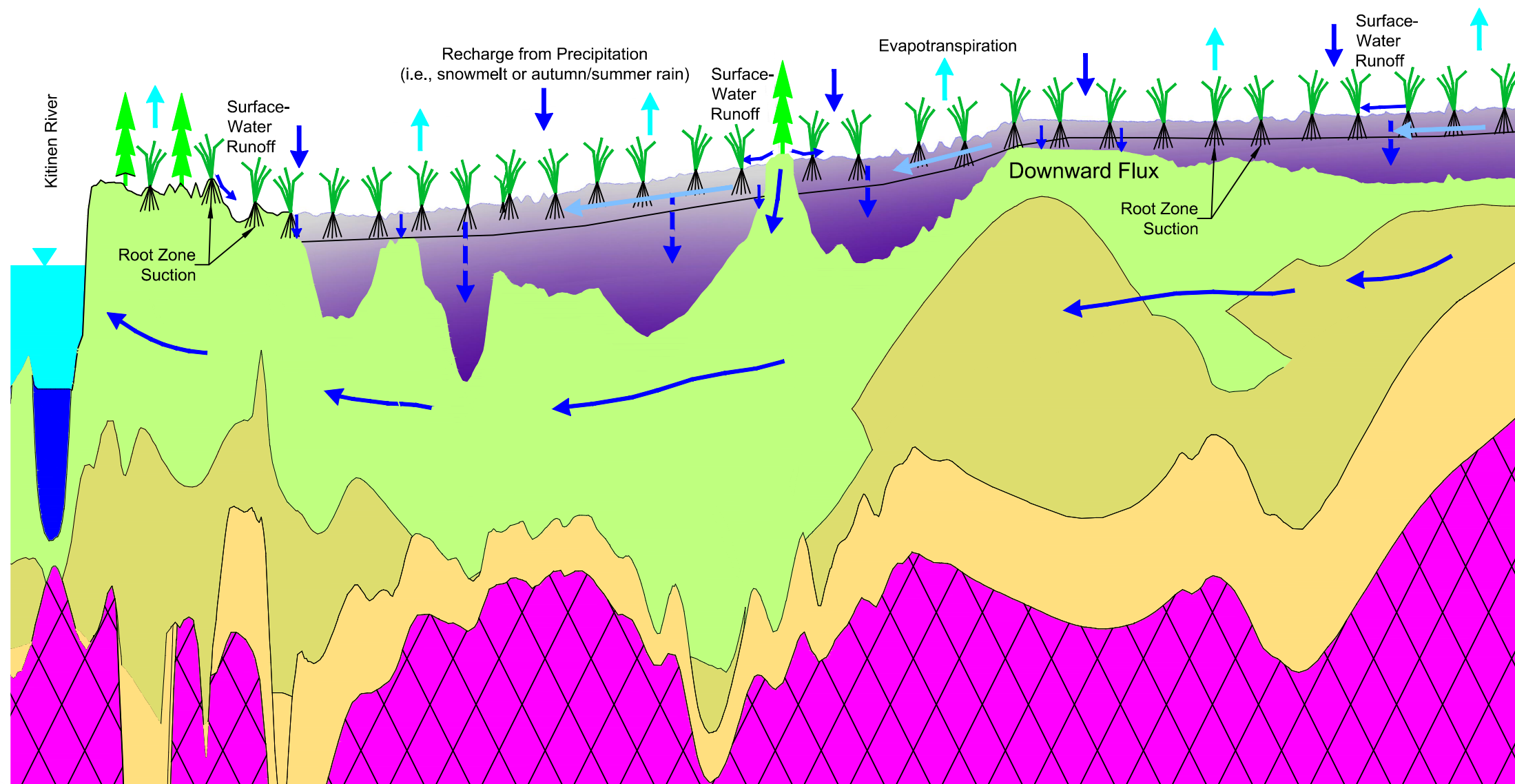
PROJECT NO.	4064
BY	SBM
CHECKED	HL
DRAWN	RJN
DRAWING NAME	CONCEPT
DRAWING DATE	25 OCT 2022
REVISION DATE	



Conceptual Hydrogeologic Model

CLIENT:
Sakatti Mine

FIGURE NO.
2-3



- Explanation**
- Peat
 - Glacial/Fluvial Deposits
 - Tills
 - Weathered Bedrock
 - Fractured Bedrock
 - Bedrock
 - River Sediments
 - Horizontal Peat Flow
 - Groundwater Flow
 - Downward Peat Flow from Acrotelm to Catotelm

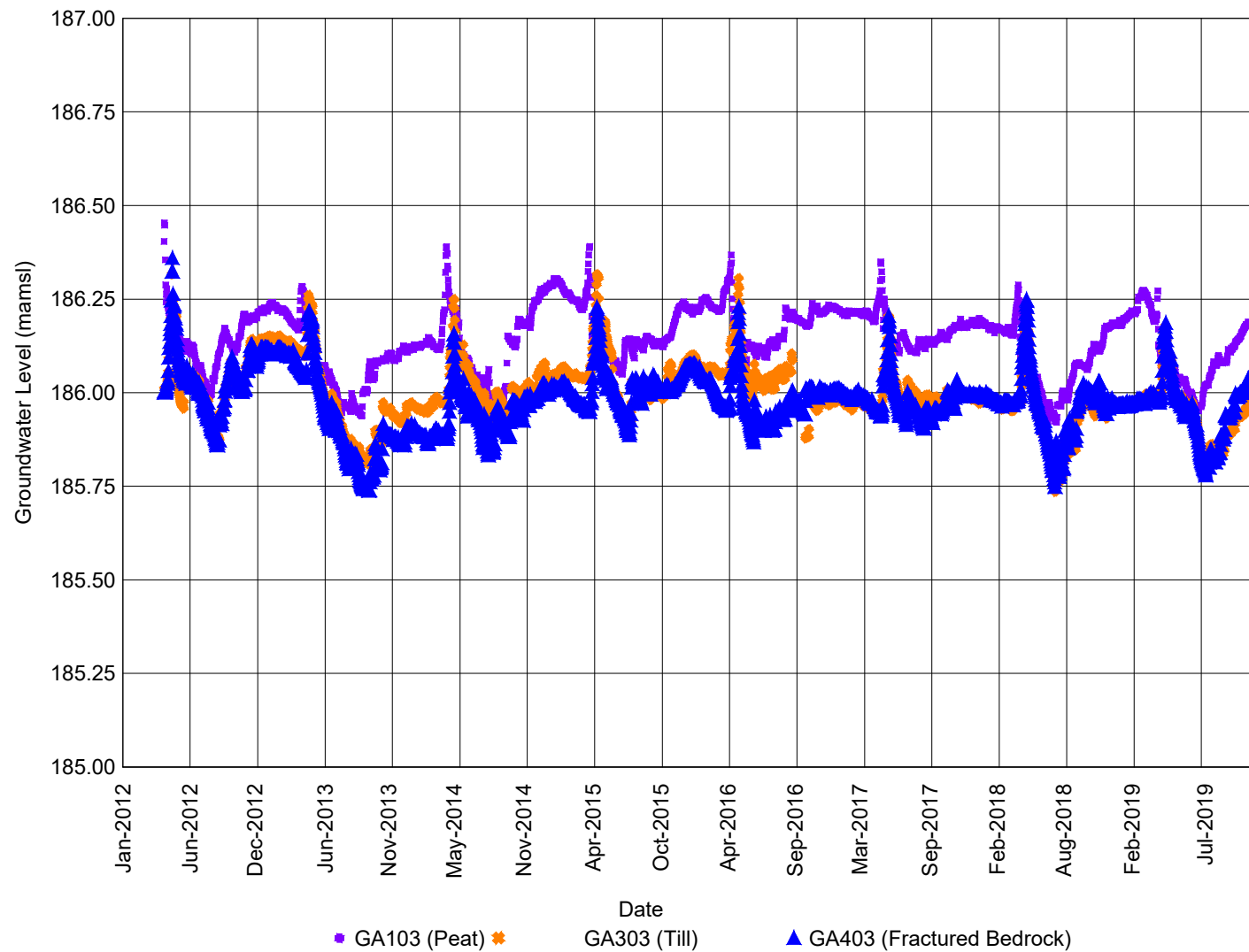
PROJECT NO.	4064
BY	SBM
CHECKED	HL
DRAWN	RJN
DRAWING NAME	XSEC100
DRAWING DATE	13 MAR 2023
REVISION DATE	



Conceptual Hydrogeologic Model of the Mire

CLIENT:
Sakatti Mine

FIGURE NO.
2-4a



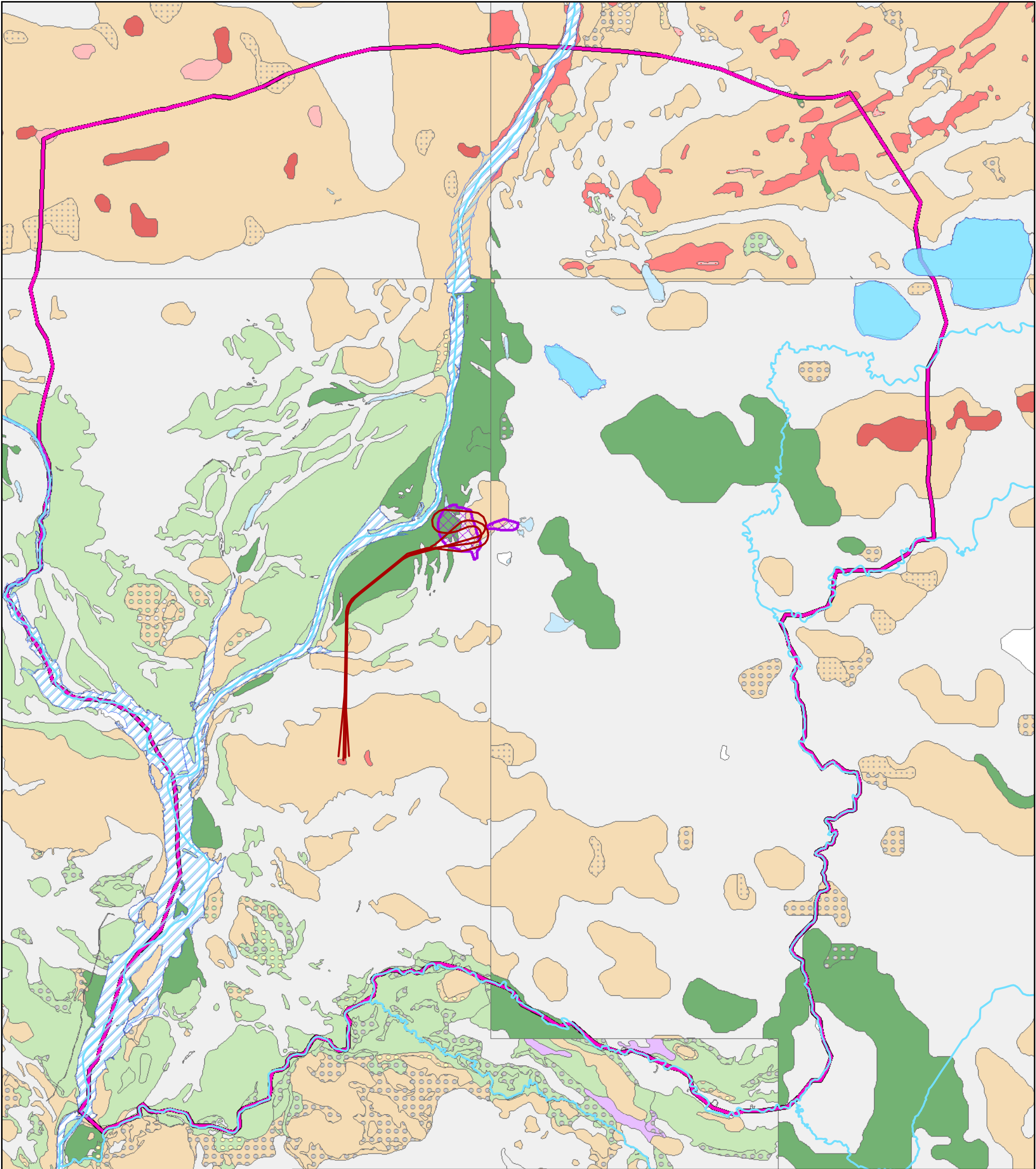
PROJECT NO.	4064
BY	SBM
CHECKED	HL
DRAWN	RJN
DRAWING NAME	EW
DRAWING DATE	13 MAR 2023
REVISION DATE	



Conceptual Hydrogeologic Model of the Mire

CLIENT:
Sakatti Mine

FIGURE NO.
2-4b



Legend

- River
- Decline Extent
- Kitinen River
- Lakes
- Ponds
- Mine-Workings Extent
- Hydrologic Study Area

Superficial deposits

- Bedrock outcrop (near surface and the outcrop)
- Weathered bedrock (RpKa)
- Gravel (Sr)
- Tills (sandy till, diamiction)
- Sand (Hk)
- Silt (Hs)
- Peat (sphagnum, carex, thick peat)

Surface sediment

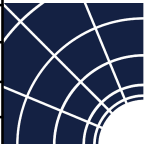
- Thinly peat-covered area (< 0.3 m)
- Thin peat deposit (0.3-0.6 m)

Note: Surficial deposit map was based on the 20:000, 50:000, 200:000 data from Geological Survey of Finland (2022)



0 1,250 2,500 Meters

PROJECT NO.	4064
BY	SBM
CHECKED	HL
DRAWN	NP
DRAWING NAME	SurfGeology
DRAWING DATE	Apr. 25, 2022
REVISION DATE	May. 26, 2022

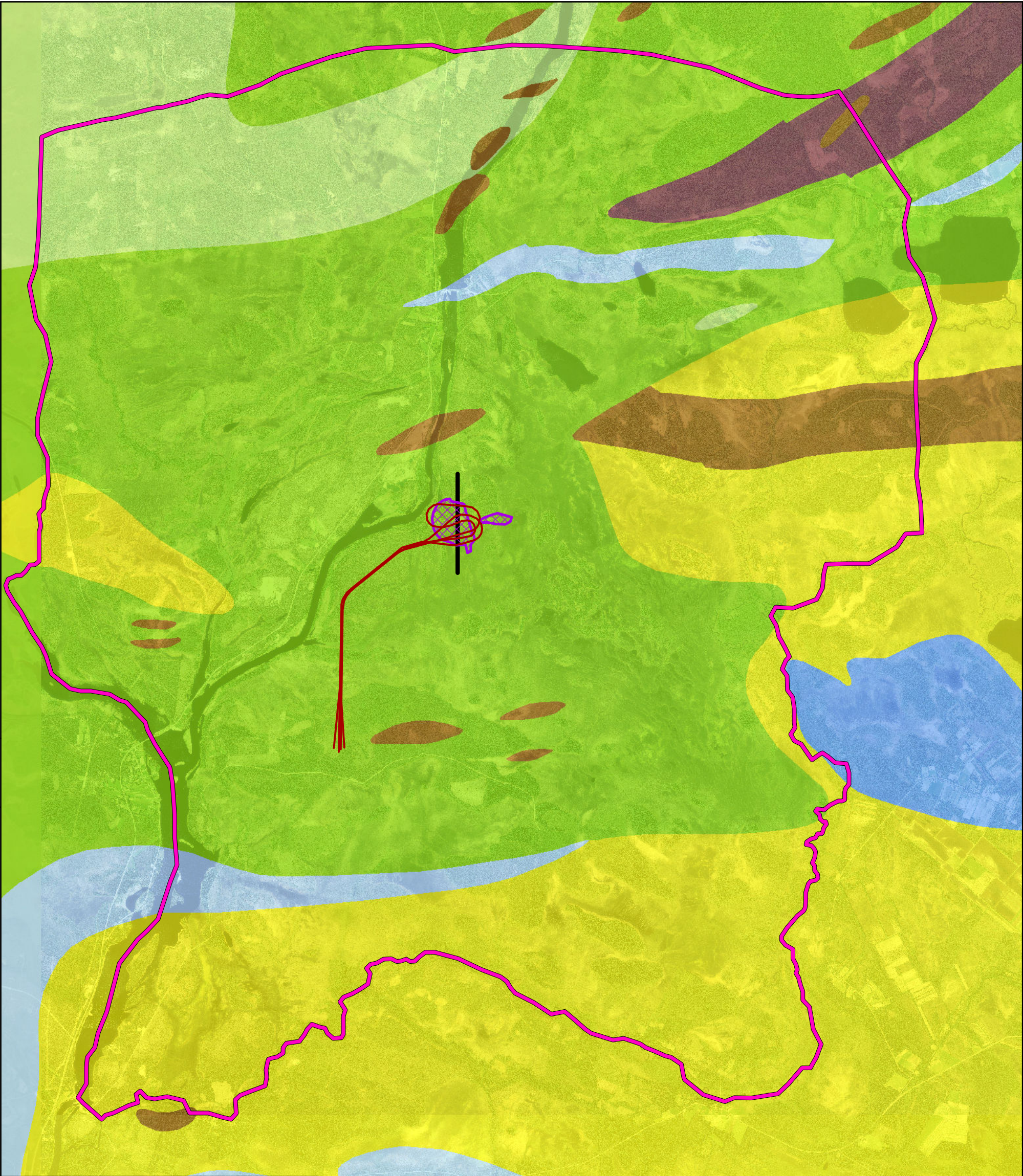


ITASCA
Denver, Inc.

Surficial Deposits within the Hydrologic Study Area

CLIENT:
Sakatti Mine

FIGURE NO.
3-1



Legend

Hydrologic Study Area

Decline Extent

Mine-Workings Extent

Geologic Section Line

Bedrock Units

Quartzite

Phyllite

Gneiss

}

Lower Sodankylä Group

Ultramafic Volcanics

Mafic Volcanic Tuff

Peridotites

Gabro

}

Upper Savukoski Group

N

0

1,250

2,500

Meters

PROJECT NO.	4064
BY	SBM
CHECKED	HL
DRAWN	NP
DRAWING NAME	Geology
DRAWING DATE	Apr. 25, 2022
REVISION DATE	Oct. 17, 2022

ITASCA[™]

Denver, Inc.

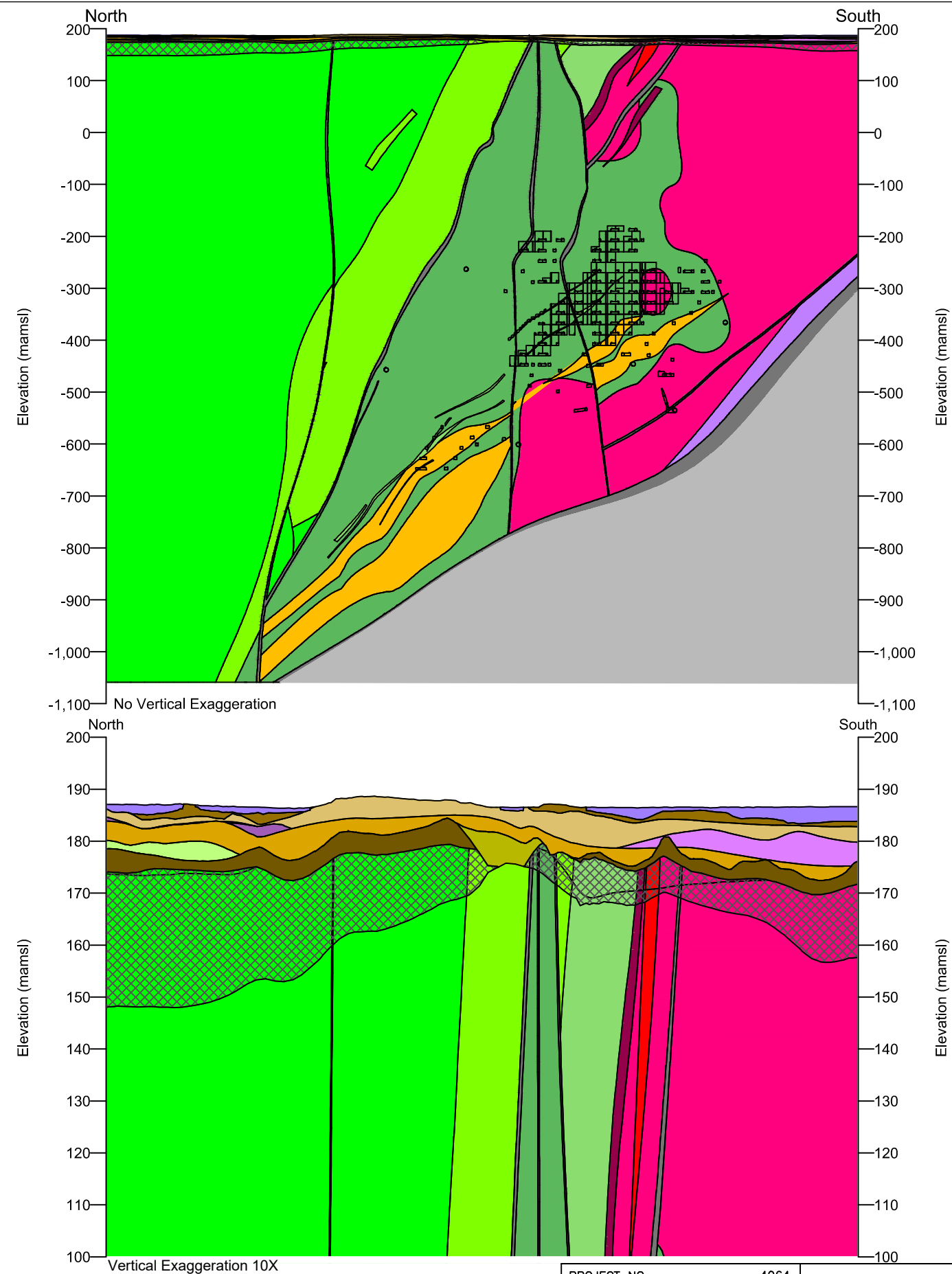
CLIENT:

Sakatti Mine

FIGURE NO.

3-2

G:\ARCGIS\4064_Sakatti\MXD\Working\Geology.mxd



- Explanation**
- Aphanite
 - Breccia
 - Dunite
 - Fault
 - Mafic Rock
 - Hanging Wall Volcaniclastics
 - Mafic Volcanic Rock
 - Peridotite
 - Serpentine
 - Shear Zone
 - Basement Rock
 - Fractured Bedrock Zone
 - Grus
 - Lower Till
 - Upper Till
 - Lower Sand and Gravel
 - Middle Sorted
 - Lower Sorted
 - Peat
 - Clay Weathering
 - Mine Working
- Bedrock Geology
- Shallow Sediments

Note: See Figure 3-2 for Location of Cross Section

0 200
SCALE (m)

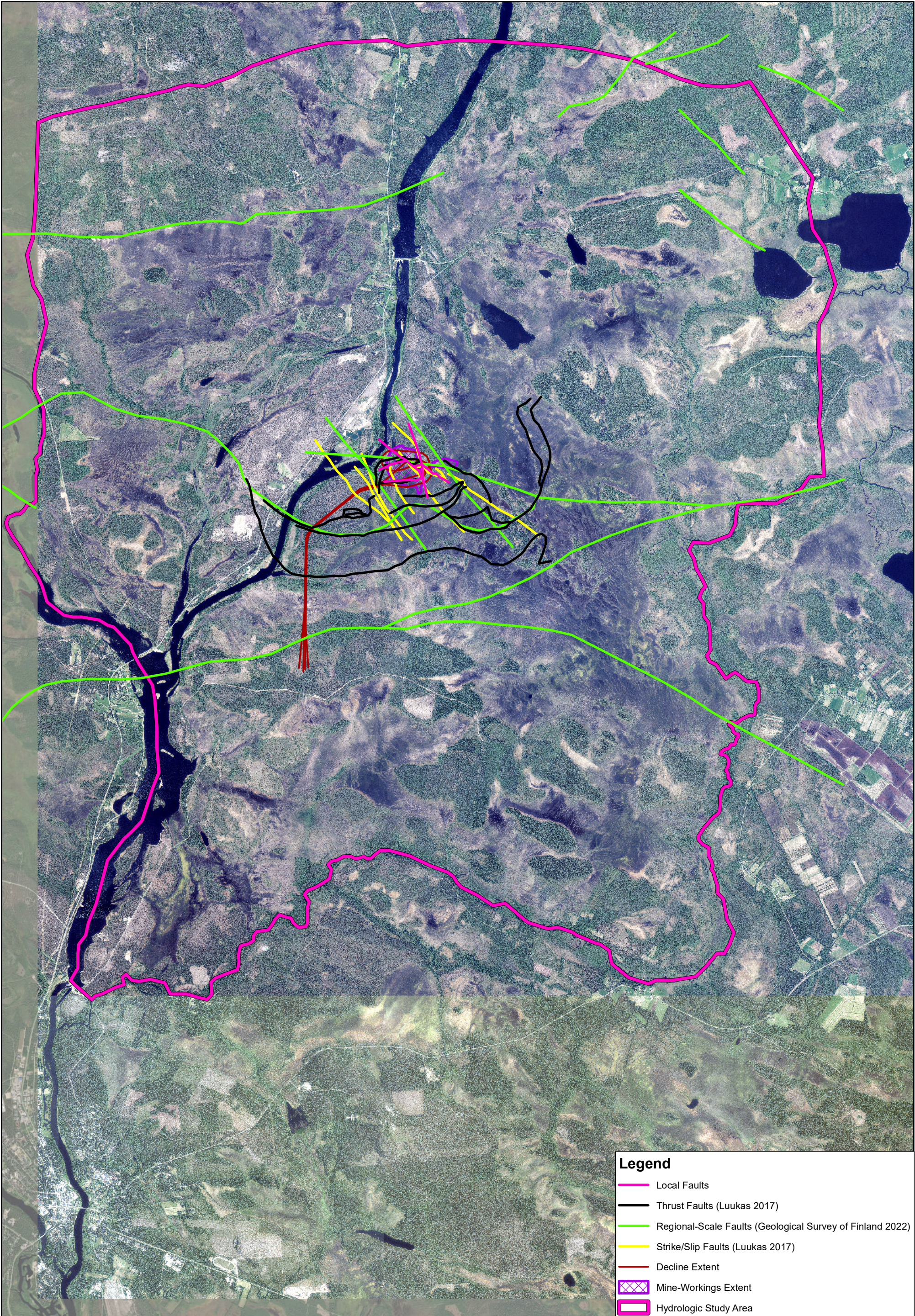
PROJECT NO.	4064
BY	SBM
CHECKED	HL
DRAWN	RJN
DRAWING NAME	NS
DRAWING DATE	25 OCT 2022
REVISION DATE	19 OCT 2022



North-South Cross Section of Geologic Units across the Mining Area

CLIENT:
Sakatti Mine

FIGURE NO.
3-3



Legend

Local Faults

Thrust Faults (Luukas 2017)

Regional-Scale Faults (Geological Survey of Finland 2022)

Strike/Slip Faults (Luukas 2017)

Decline Extent

Mine-Workings Extent

Hydrologic Study Area

N

0

1,250

2,500

Meters

PROJECT NO.	4064
BY	SBM
CHECKED	HL
DRAWN	NP
DRAWING NAME	FaultStr
DRAWING DATE	Apr. 25, 2022
REVISION DATE	Oct. 17, 2022

ITASCA™

Denver, Inc.

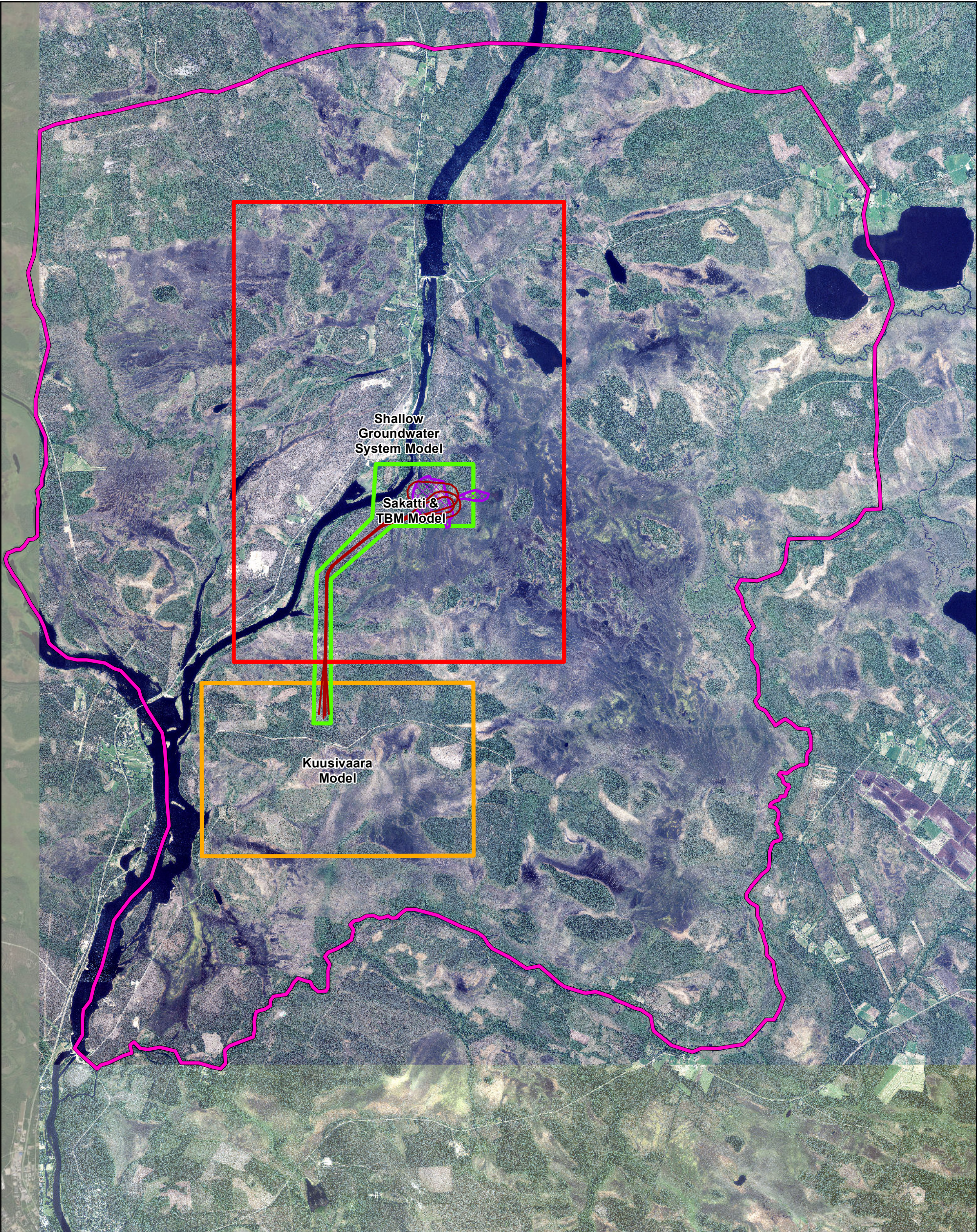
Local and Regional-Scale Faults
in the Hydrologic Study Area

CLIENT:

Sakatti Mine

FIGURE NO.

3-4



Legend

Hydrologic Study Area

Decline Extent

Mine-Workings Extent

Geologic Model Extent

Shallow Groundwater System Model

Sakatti & TBM Model

Kuusivaara Model

01,2502,500
Meters

PROJECT NO.	4064
BY	SBM
CHECKED	HL
DRAWN	NP
DRAWING NAME	GeoModels
DRAWING DATE	Apr. 25, 2022
REVISION DATE	May. 24, 2022

ITASCATM
Denver, Inc.

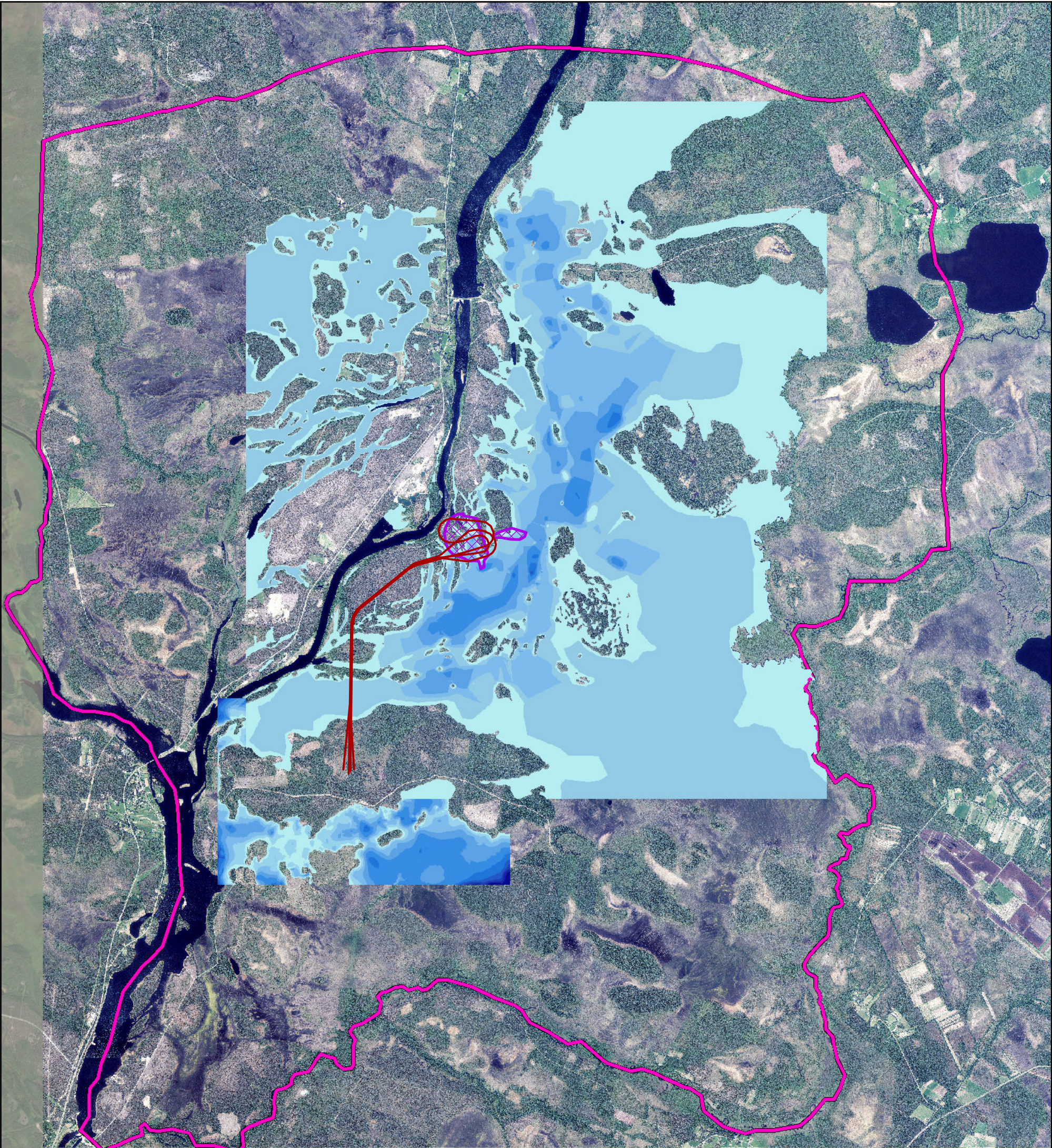
Extent of the Geologic Block Models
within the Hydrologic Study Area

CLIENT:




Sakatti Mine

FIGURE NO.










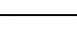
3-5



Legend

-  Hydrologic Study Area
-  Decline Extent
-  Mine-Workings Extent

Peat Thickness (m)

-  <0.1 - 1
-  1.01 - 2
-  2.01 - 3
-  3.01 - 4
-  4.01 - 5
-  5.01 - 6
-  6.01 - 7
-  7.01 - 8
-  8.01 - 9
-  9.01 - 11.1



0 1,250 2,500
Meters

PROJECT NO.	4064
BY	SBM
CHECKED	HL
DRAWN	NP
DRAWING NAME	Peat
DRAWING DATE	Apr. 25, 2022
REVISION DATE	Aug. 24, 2022

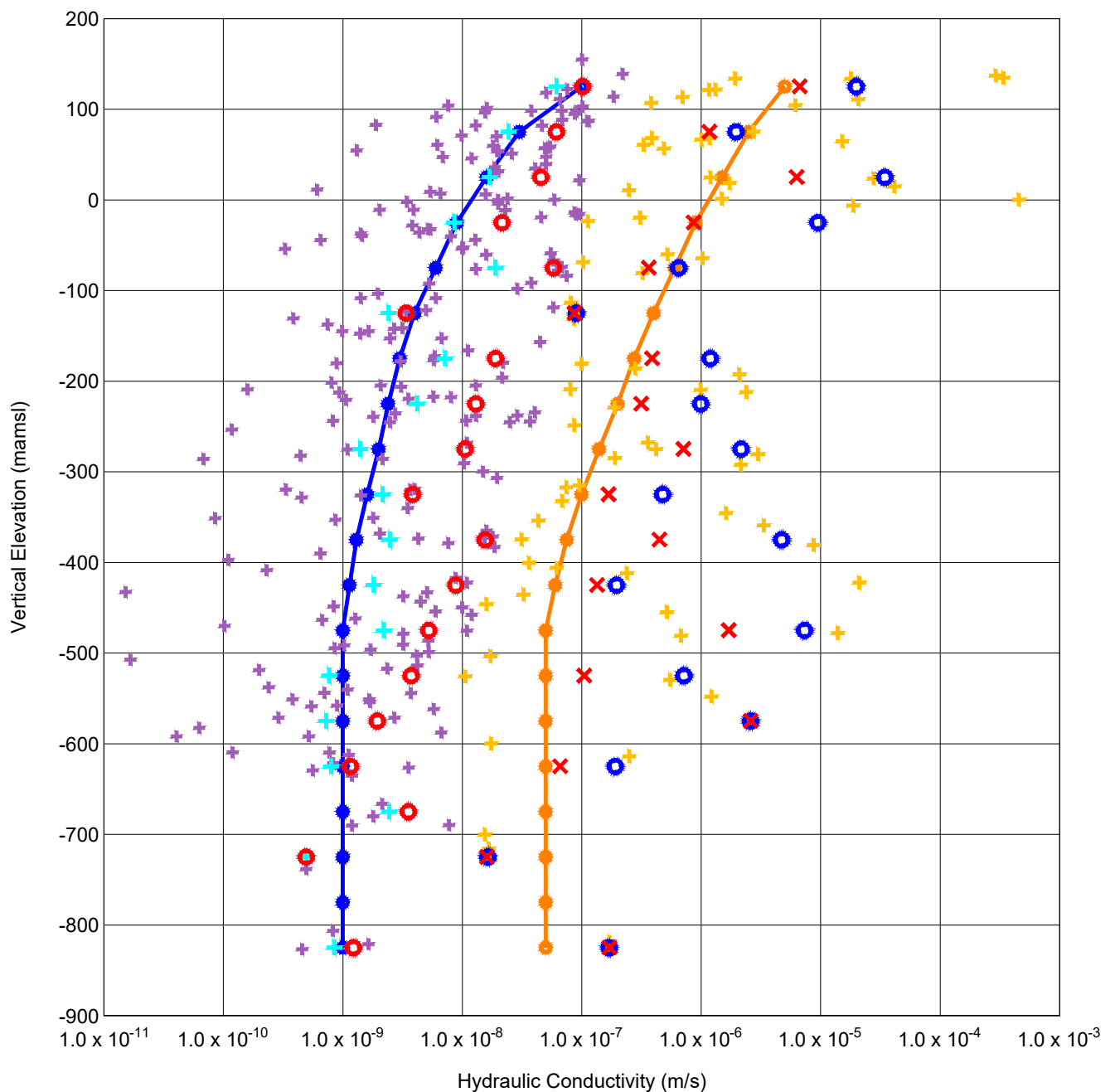


ITASCA
Denver, Inc.

**Estimated Thickness of the Peat Layer
at the Project Site**

CLIENT:
Sakatti Mine

FIGURE NO.
3-6



K Values from Packer Testing

- ✱ Bedrock
- ✚ Fracture

Statistics of Packer Testing Data

- 75th Percentile Every 50 m for Fractures
- 75th Percentile Every 50 m for Bedrock
- ✕ Geometric Mean Every 50 m for Fractures
- ✕ Geometric Mean Every 50 m for Bedrock
- Representative Trend Line of Geometric Mean of Bedrock
- Representative Trend Line of Geometric Mean of Fractures

Note: One packer test data point below 1×10^{-11} is not shown.

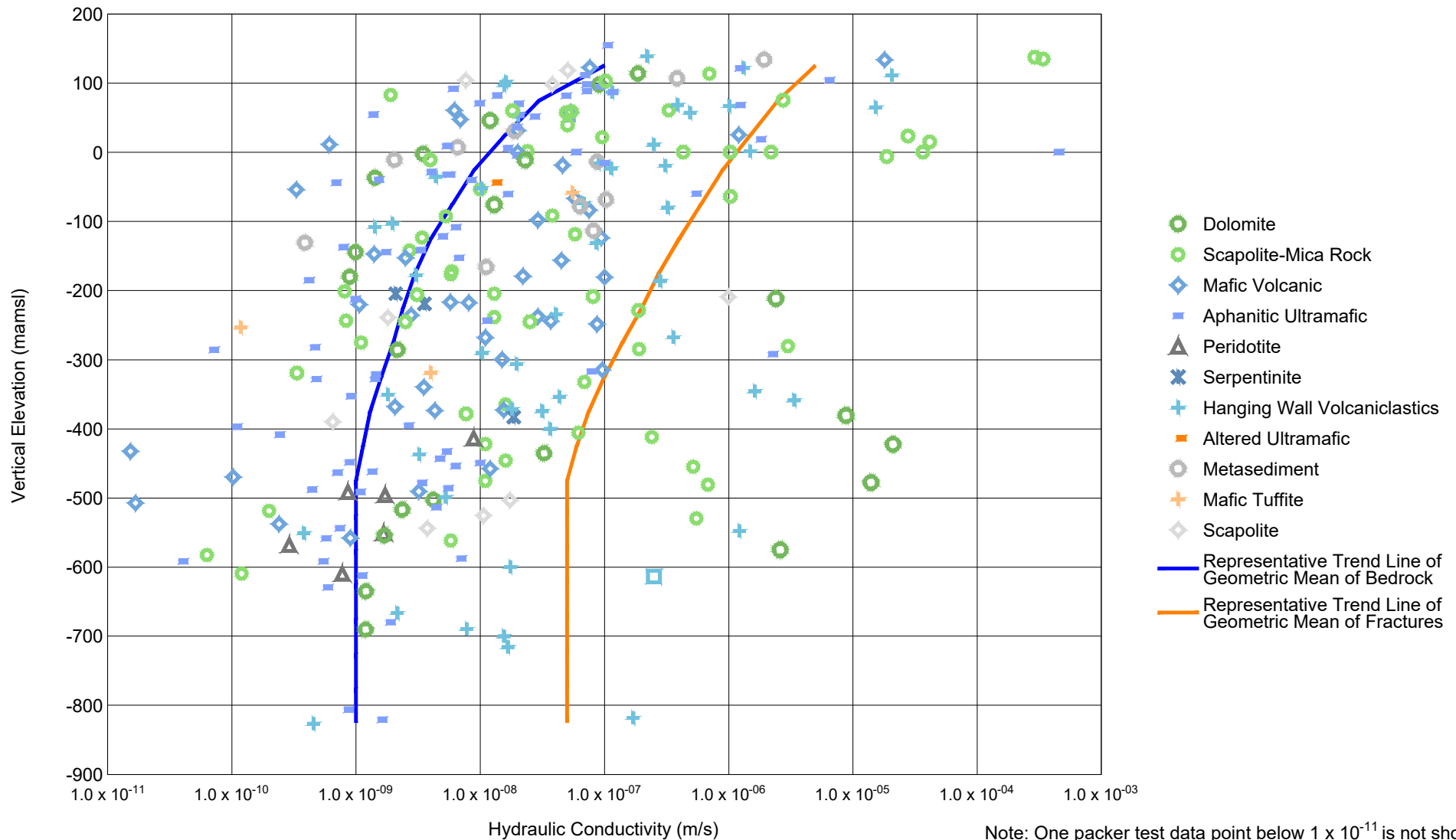
PROJECT NO.	4064
BY	SBM
CHECKED	HL
DRAWN	RJN
DRAWING NAME	PACKER
DRAWING DATE	24 MAY 2022
REVISION DATE	19 OCT 2022



Measured Hydraulic Conductivities from Packer Tests

CLIENT:
Sakatti Mine

FIGURE NO.
3-7



PROJECT NO.	4064
BY	SBM
CHECKED	HL
DRAWN	RJN
DRAWING NAME	GEO
DRAWING DATE	24 MAY 2022
REVISION DATE	19 OCT 2022

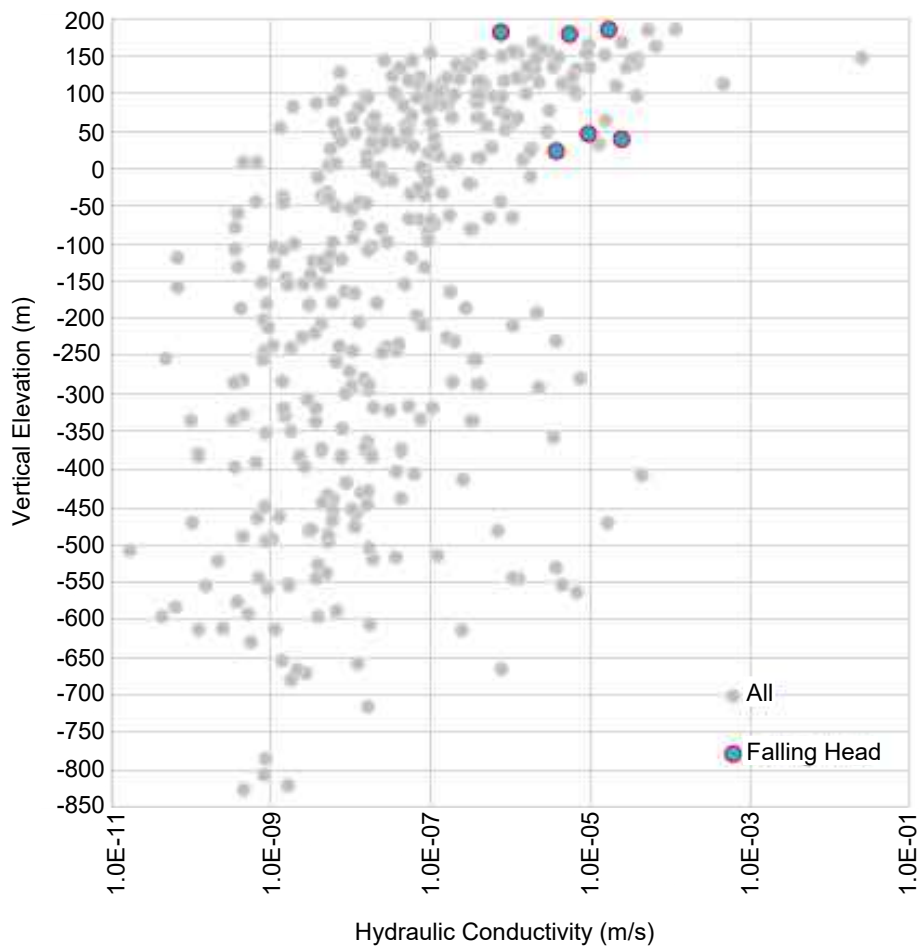


Measured Hydraulic Conductivities from
Packer Testing by Rock Type

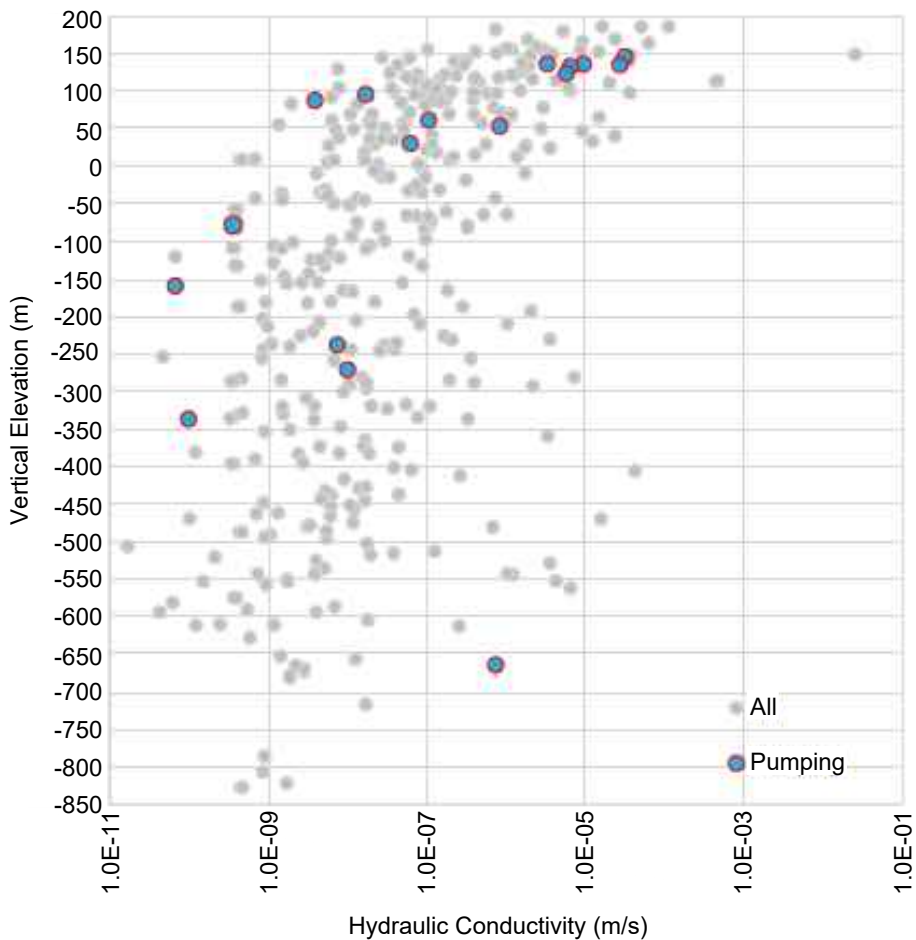
CLIENT:
Sakatti Mine

FIGURE NO.
3-8

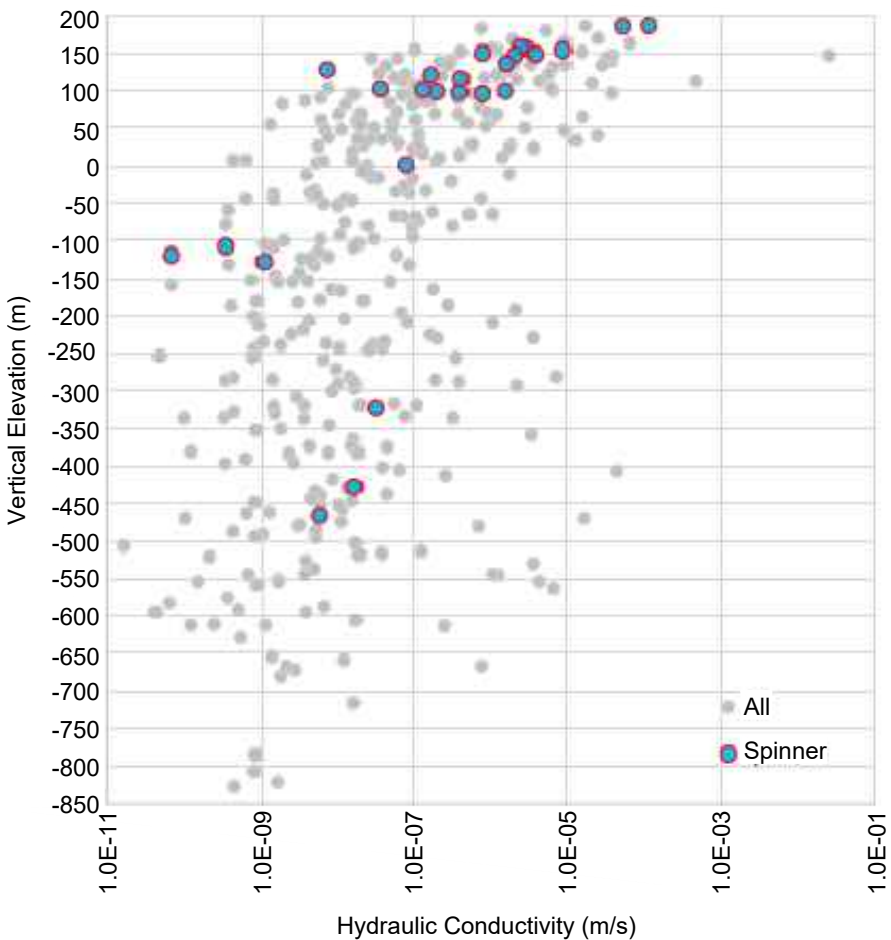
a) Measured Hydraulic Conductivities from Falling Head Tests



b) Measured Hydraulic Conductivities from Pump Tests



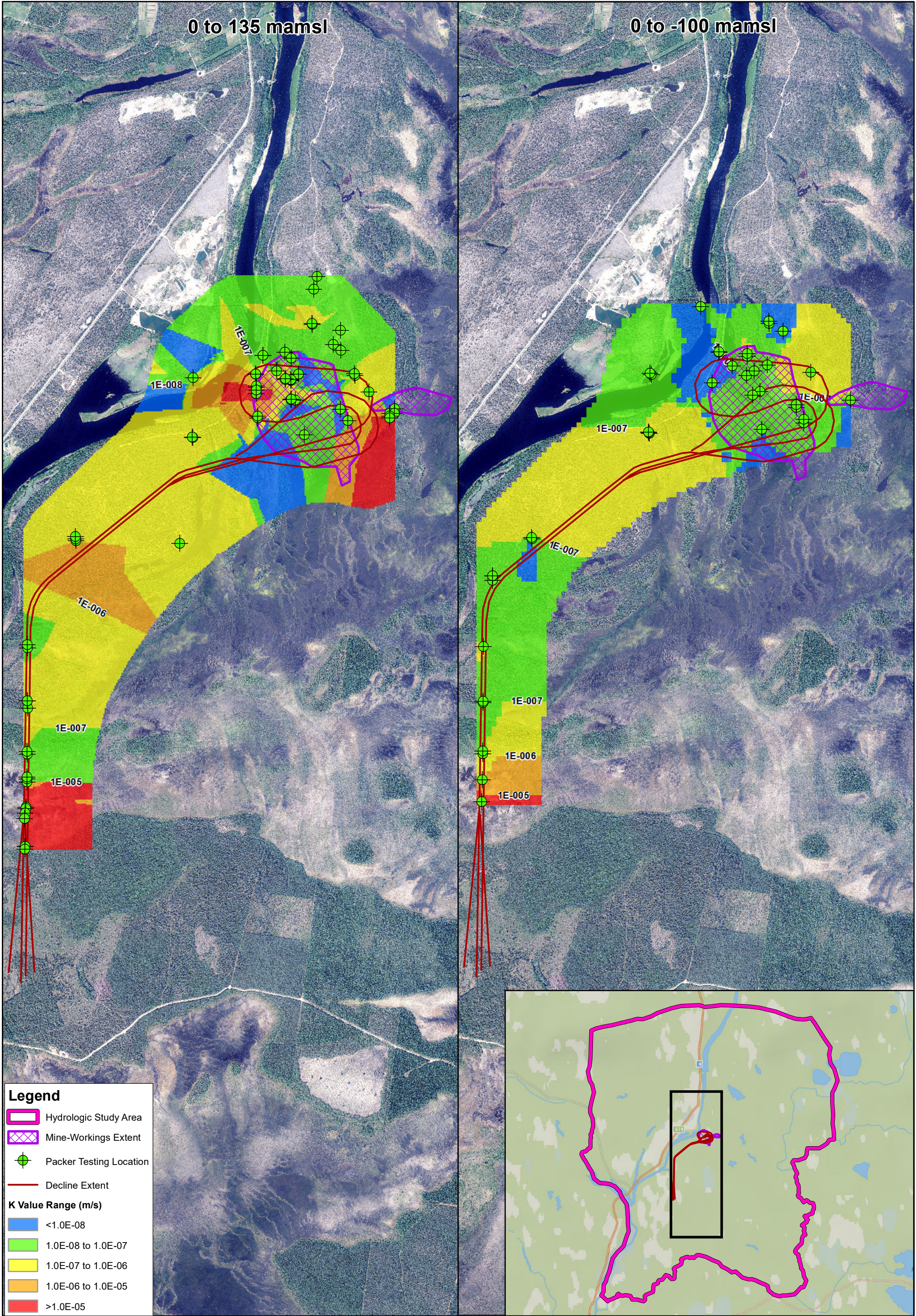
c) Measured Hydraulic Conductivities from Spinner Log Tests



PROJECT NO.	4064
BY	SBM
CHECKED	HL
DRAWN	RJN
DRAWING NAME	TESTS
DRAWING DATE	24 MAY 2022
REVISION DATE	19 OCT 2022

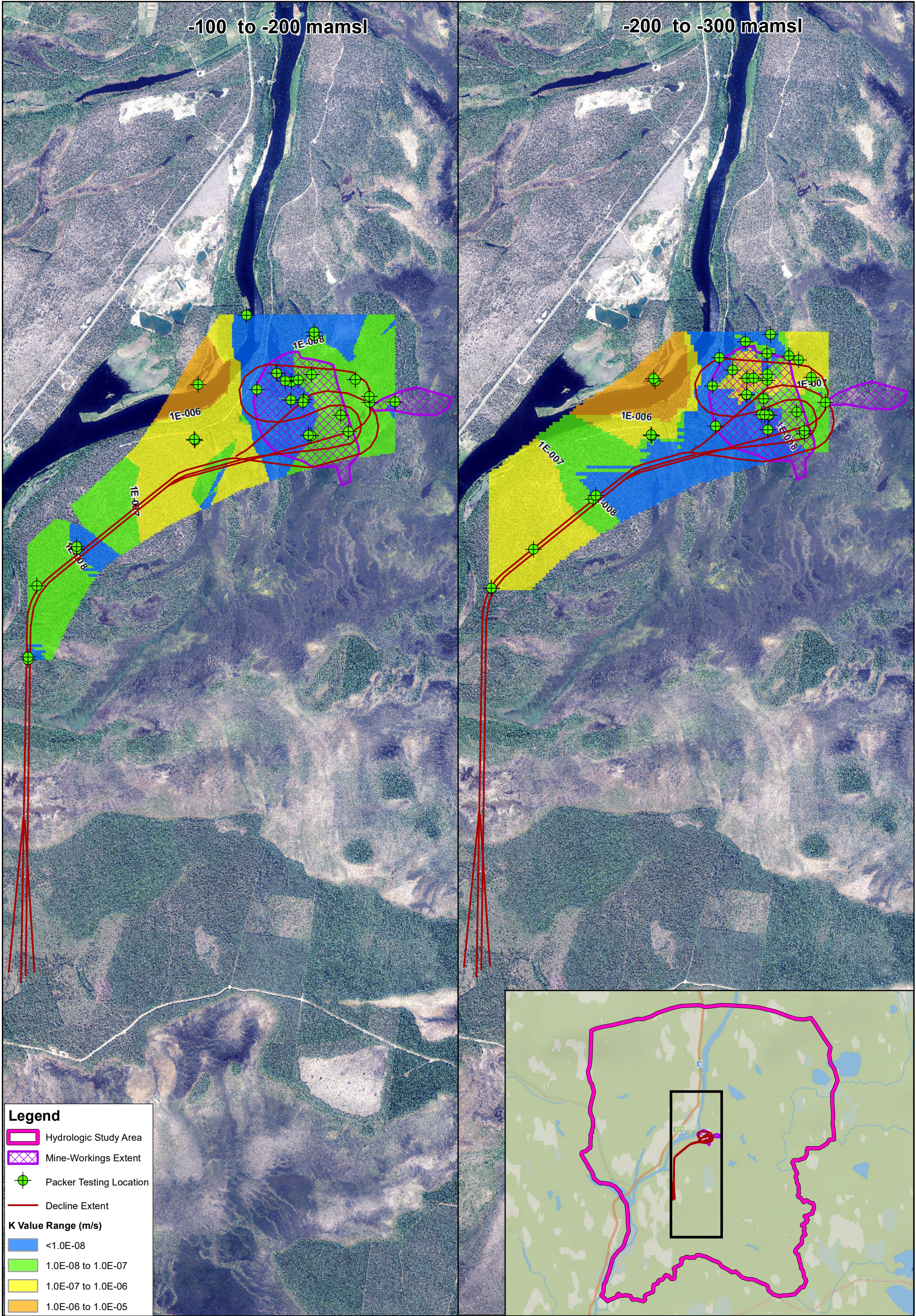


Measured Hydraulic Conductivities from Pumping, Spinner Log, and Falling Head Tests versus Packer Tests	
CLIENT: Sakatti Mine	FIGURE NO. 3-9

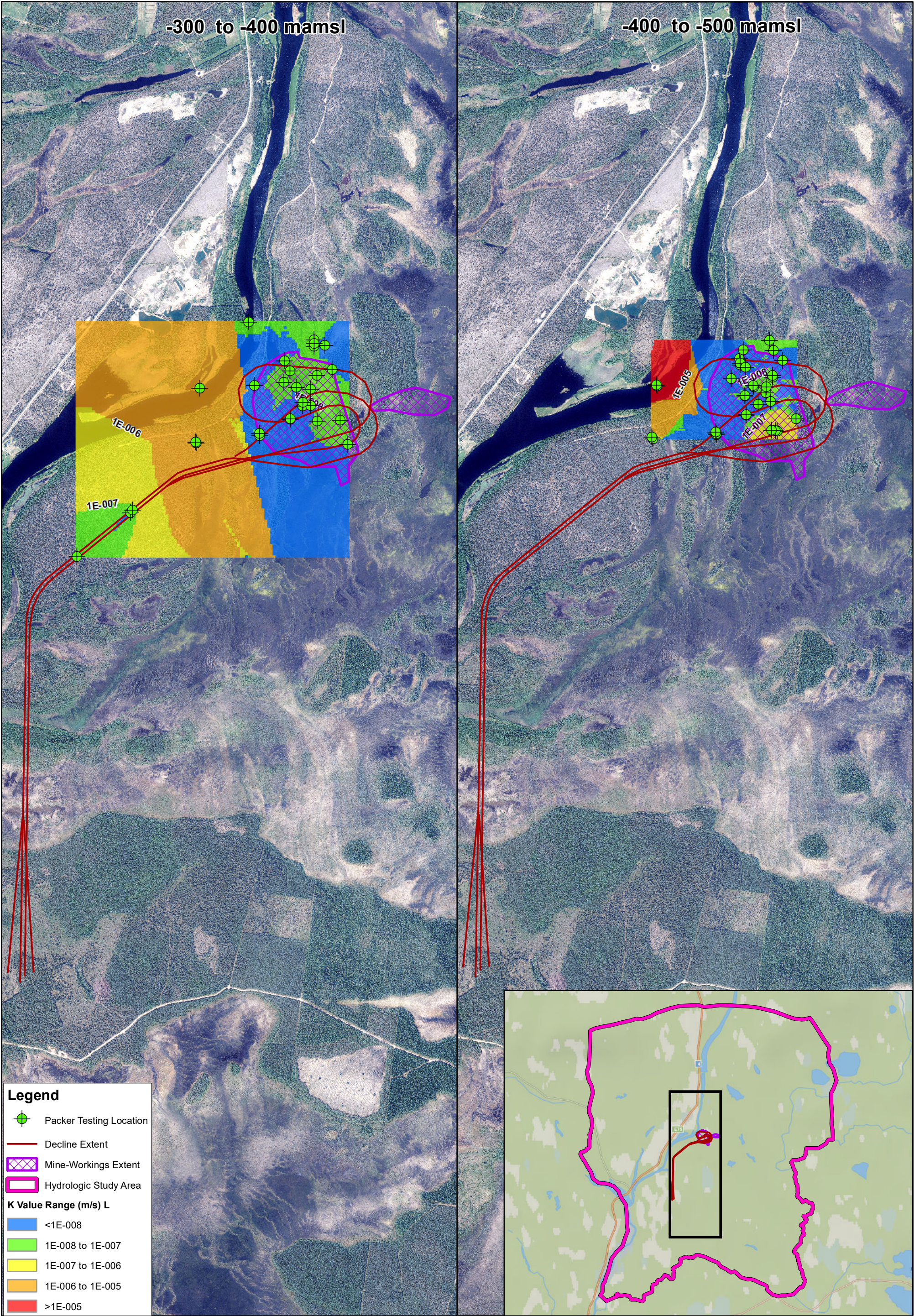


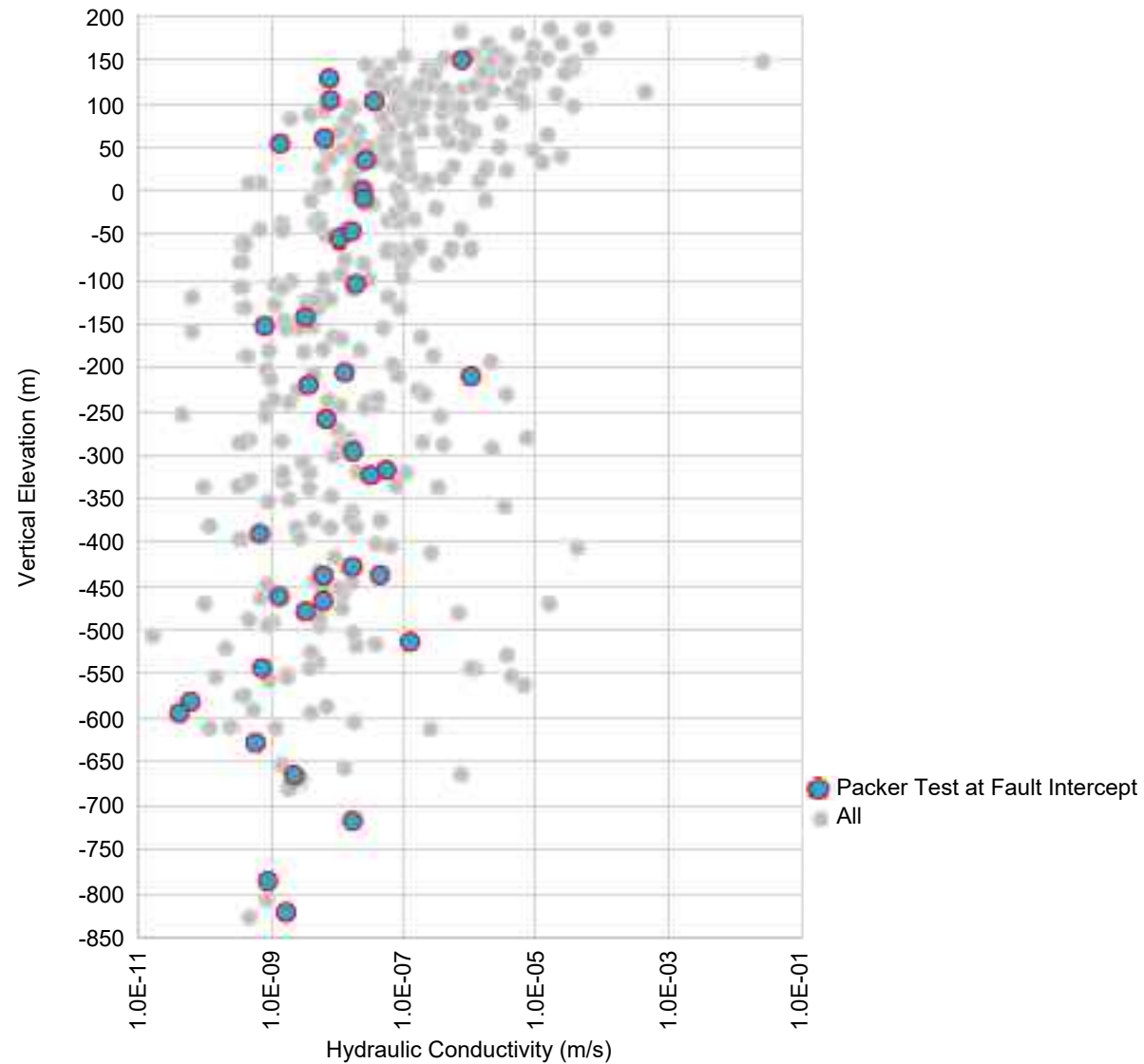
-100 to -200 mamsl

-200 to -300 mamsl



<div><div></div><div>N</div><div>0490980</div><div>Meters</div></div>	PROJECT NO.	4064	<div><div></div><div>ITASCA</div><div>Denver, Inc.</div></div>	Interpolated Hydraulic Conductivities from Packer Tests at Elevation Ranges of -100 to -200 mamsl and -200 to -300 mamsl	
	BY	SBM			
	CHECKED	HL			
	DRAWN	NP			
	DRAWING NAME	EHC_2			
	DRAWING DATE	Apr. 25, 2022			
	REVISION DATE	Feb. 10, 2023	CLIENT:	Sakatti Mine	FIGURE NO. 3-11





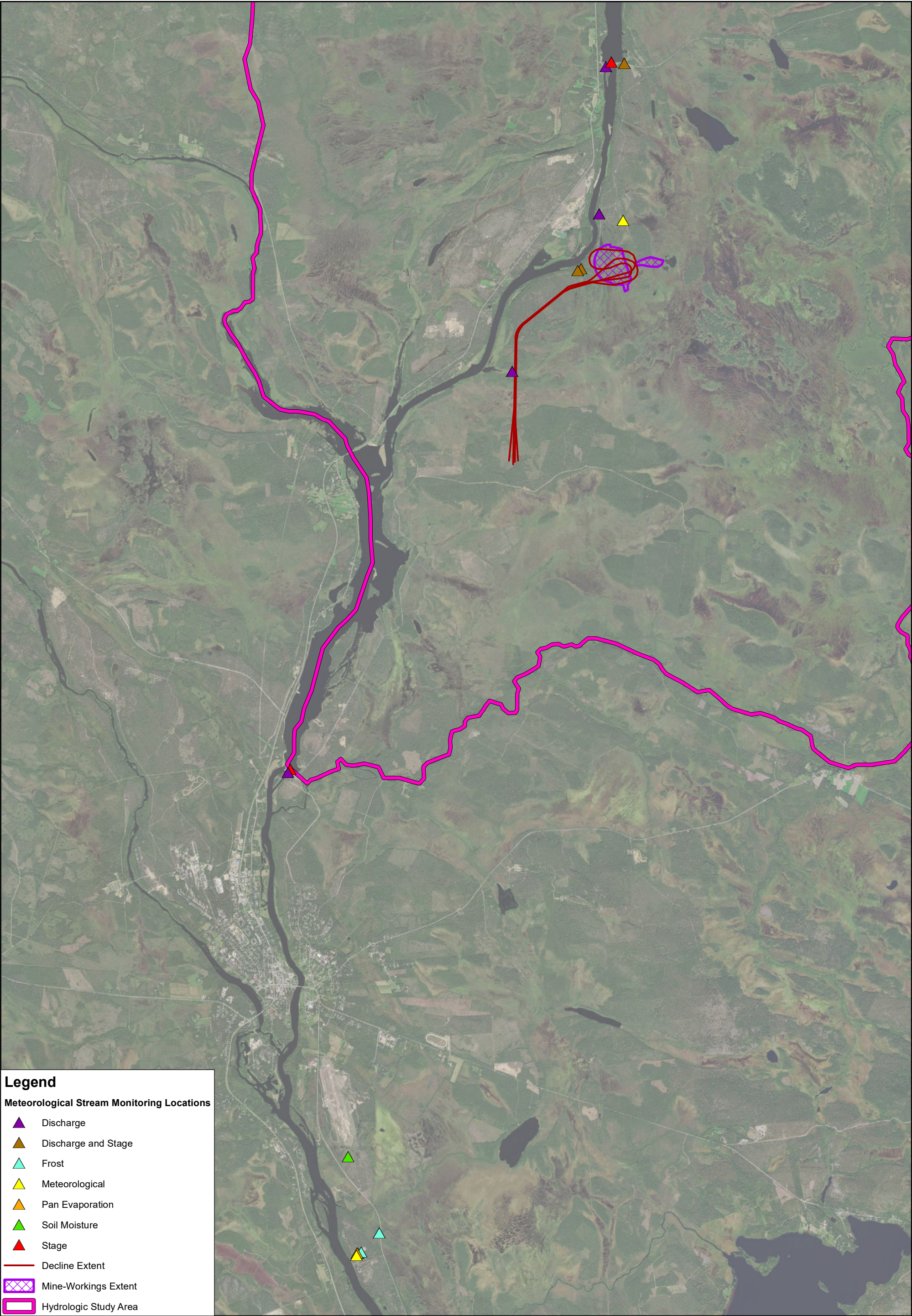
PROJECT NO.	4064
BY	SBM
CHECKED	HL
DRAWN	RJN
DRAWING NAME	FAULT
DRAWING DATE	24 MAY 2022
REVISION DATE	19 OCT 2022



Measured Hydraulic Conductivities of Faults from Packer Tests

CLIENT:
Sakatti Mine

FIGURE NO.
3-13



Legend

Meteorological Stream Monitoring Locations

Discharge

Discharge and Stage

Frost

Meteorological

Pan Evaporation

Soil Moisture

Stage

Decline Extent

Mine-Workings Extent

Hydrologic Study Area

N

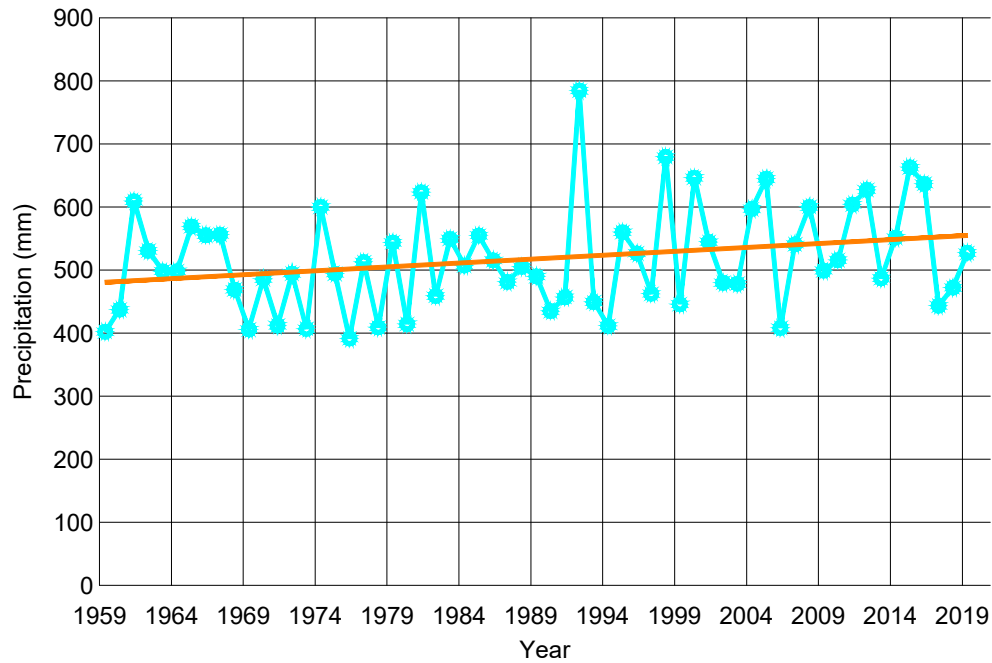
01,2502,500Meters

PROJECT NO.	4064
BY	SBM
CHECKED	HL
DRAWN	NP
DRAWING NAME	MetLocs
DRAWING DATE	Apr. 25, 2022
REVISION DATE	Jun. 16, 2022

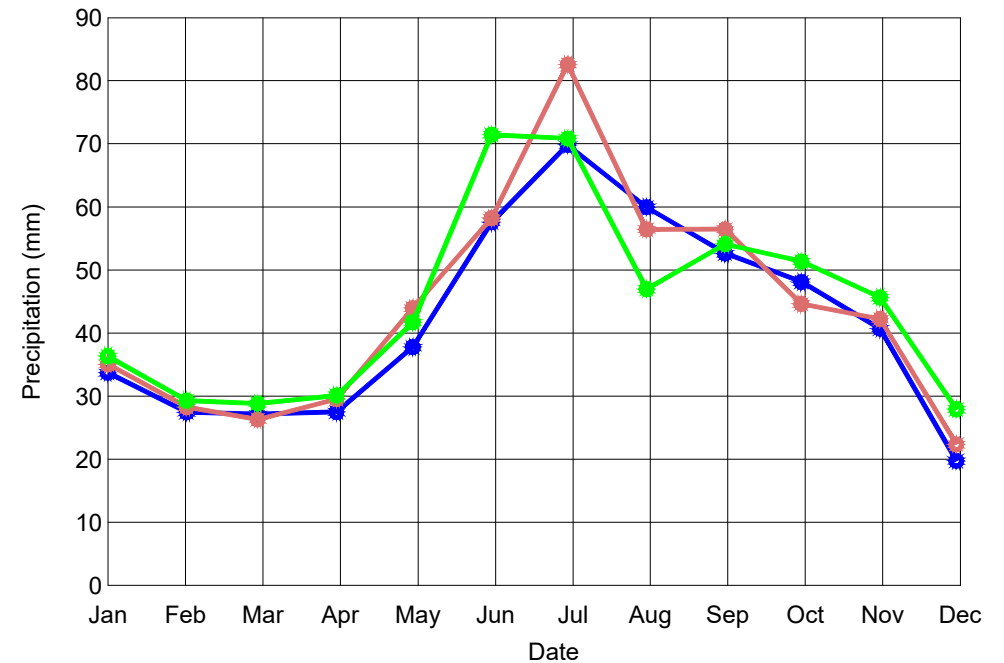
ITASCA[™]
Denver, Inc.

Meteorological Monitoring Locations Used by the Project Site	
CLIENT: Sakatti Mine	FIGURE NO. 3-14

a) Measured Annual Precipitation



b) Average Monthly Precipitation



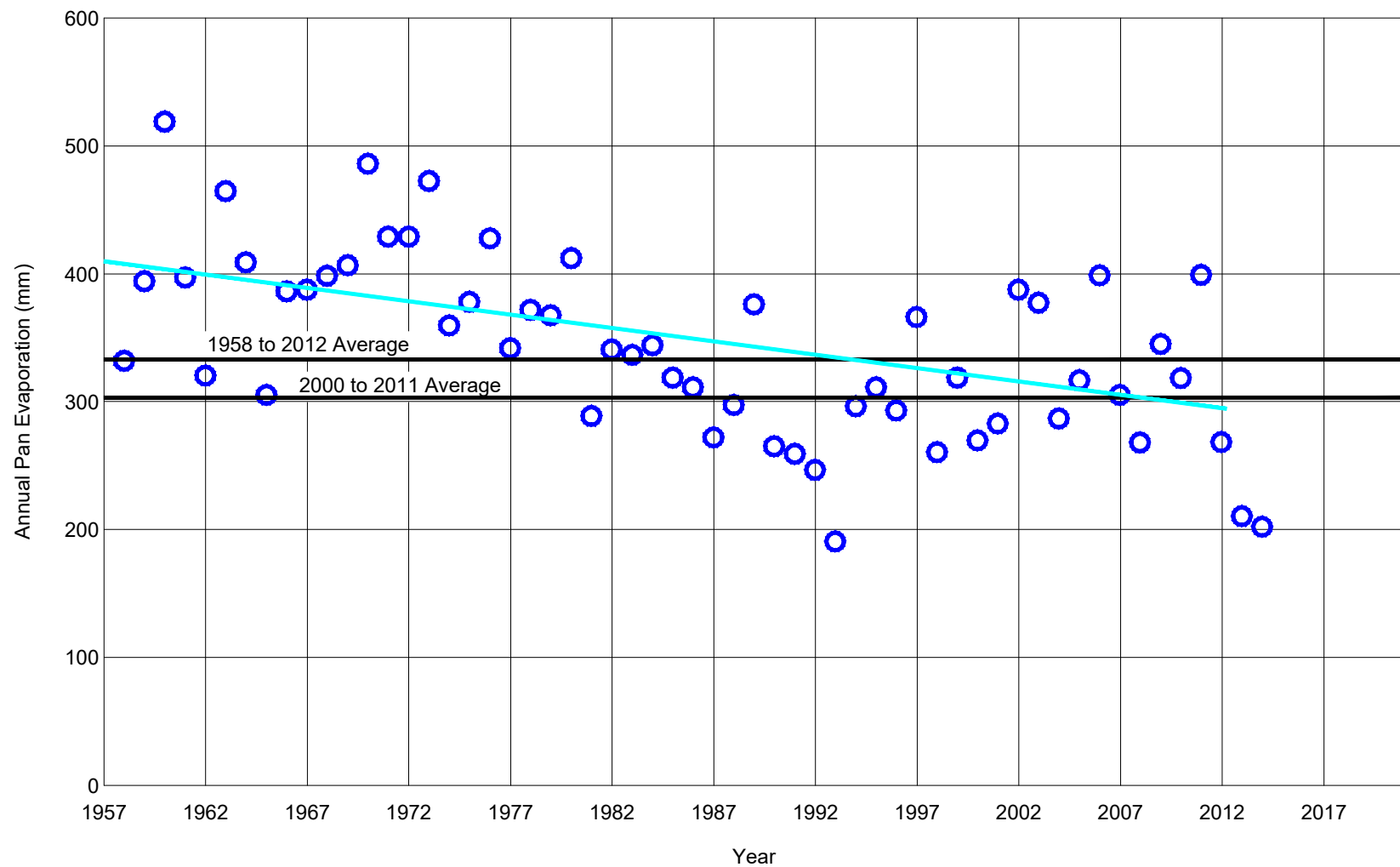
PROJECT NO.	4064
BY	SBM
CHECKED	HL
DRAWN	RJN
DRAWING NAME	PRECIP
DRAWING DATE	24 MAY 2022
REVISION DATE	



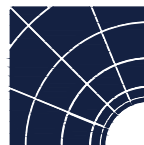
Measured Annual and Monthly Precipitation
at the Sodankylä Tähtelä Station

CLIENT:
Sakatti Mine

FIGURE NO.
3-15



PROJECT NO.	4064
BY	SBM
CHECKED	HL
DRAWN	RJN
DRAWING NAME	PAN
DRAWING DATE	13 JUN 2022
REVISION DATE	5 AUG 2022

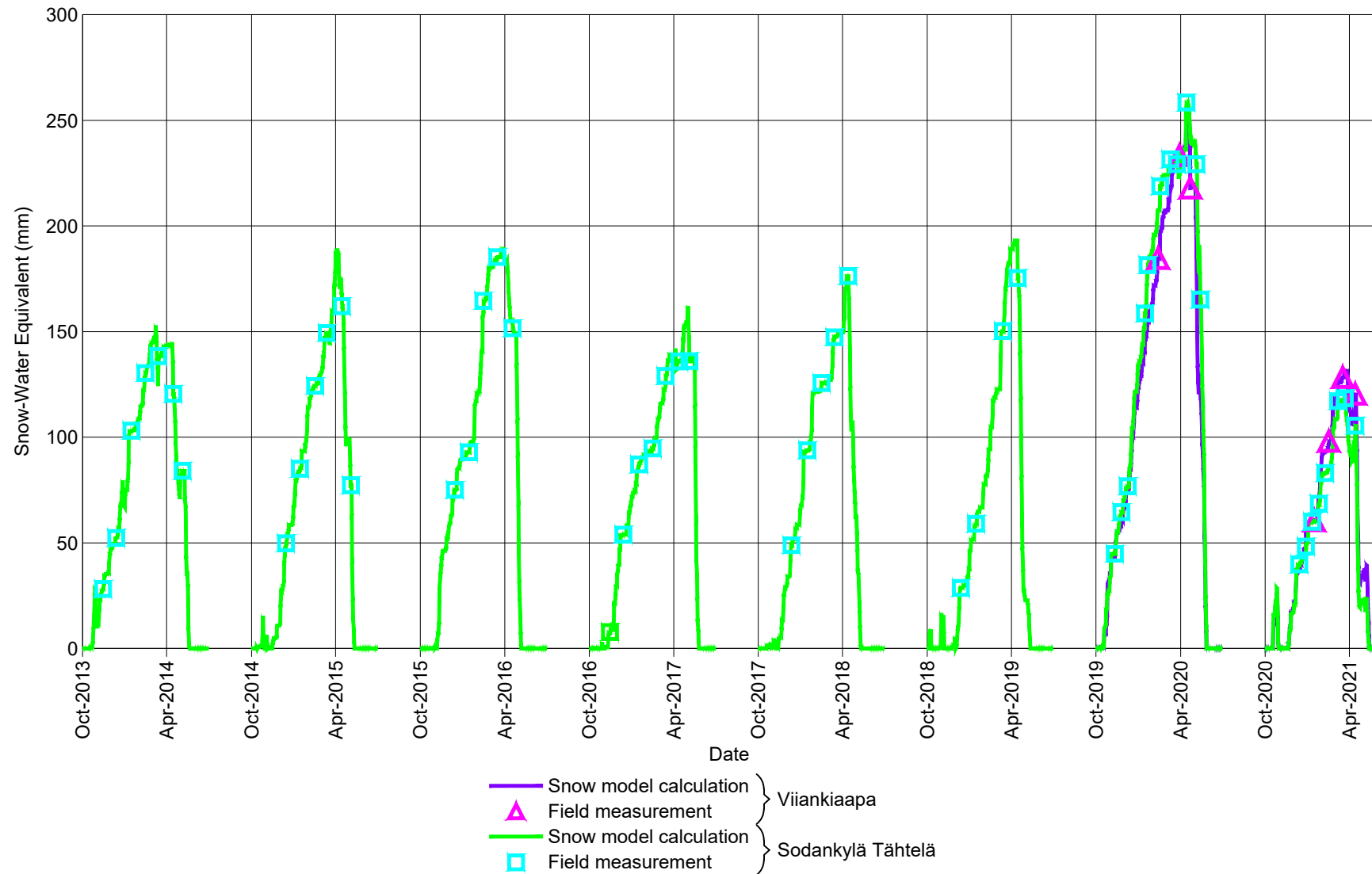


ITASCA[™]
Denver, Inc.

Measured Pan Evaporation Rate at the
Sodankylä Tähtelä Station

CLIENT:
Sakatti Mine

FIGURE NO.
3-16



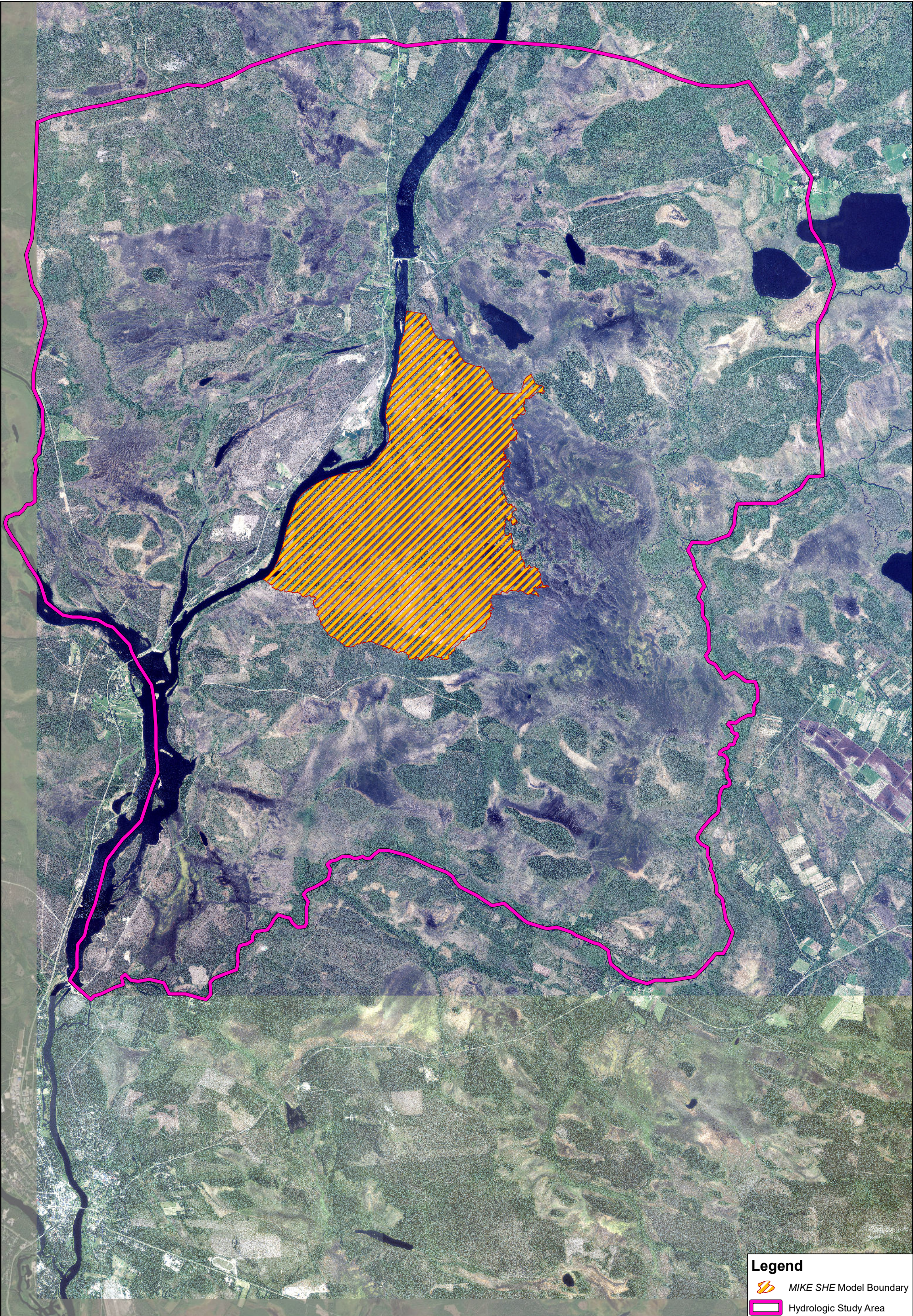
PROJECT NO.	4064
BY	SBM
CHECKED	HL
DRAWN	RJN
DRAWING NAME	SNOW
DRAWING DATE	15 JUN 2022
REVISION DATE	5 AUG 2022




Measured and Calculated Snow Water-Equivalent Depths


CLIENT:
Sakatti Mine


FIGURE NO.
3-17



Legend

 MIKE SHE Model Boundary

 Hydrologic Study Area


0 1,250 2,500
Meters

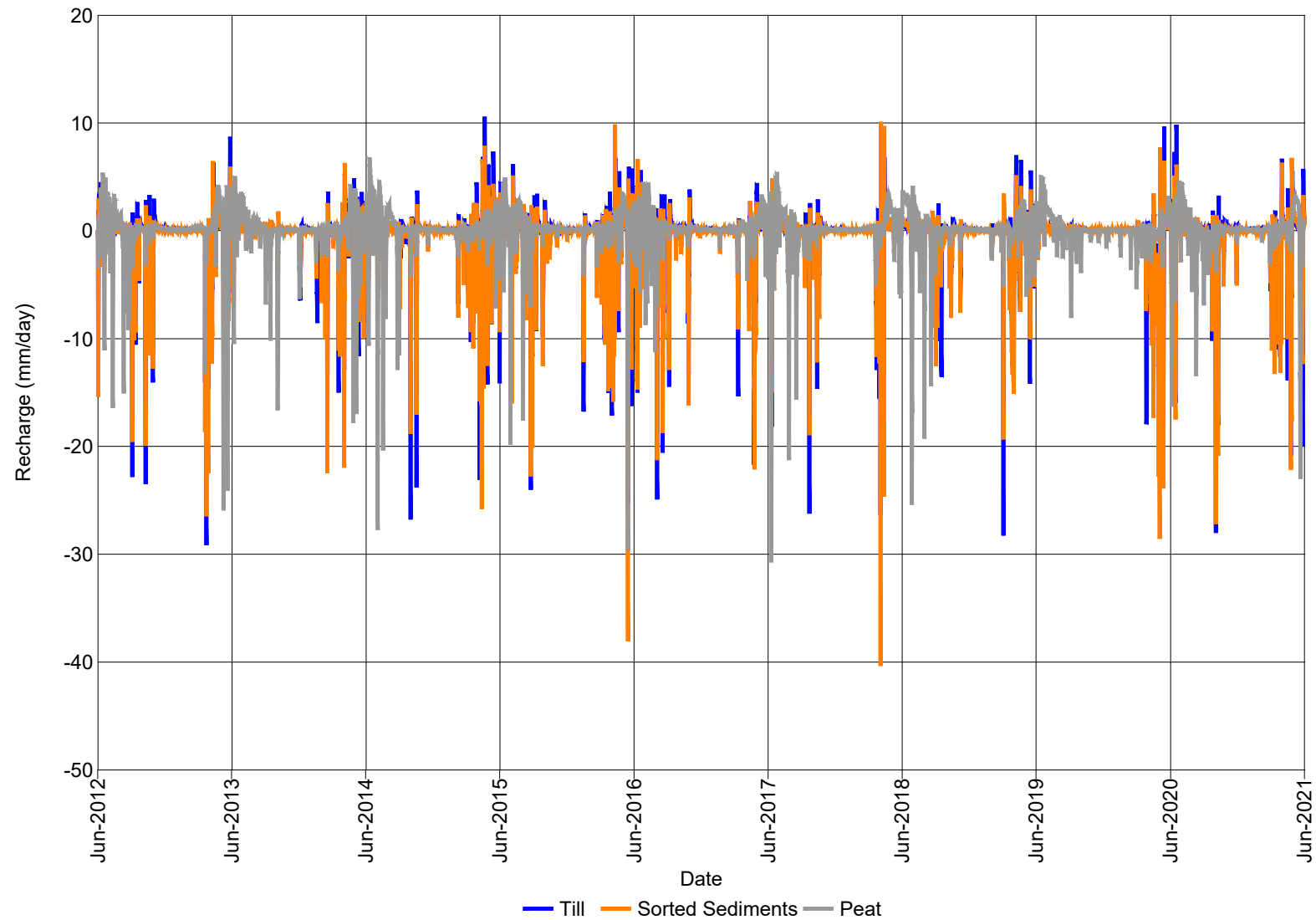
PROJECT NO.	4064
BY	SBM
CHECKED	HL
DRAWN	NP
DRAWING NAME	MIKESHE
DRAWING DATE	Apr. 25, 2022
REVISION DATE	May. 27, 2022


ITASCATM
Denver, Inc.

MIKE SHE and Hydrologic Study Area Boundaries

CLIENT: Sakatti Mine

FIGURE NO. 3-18



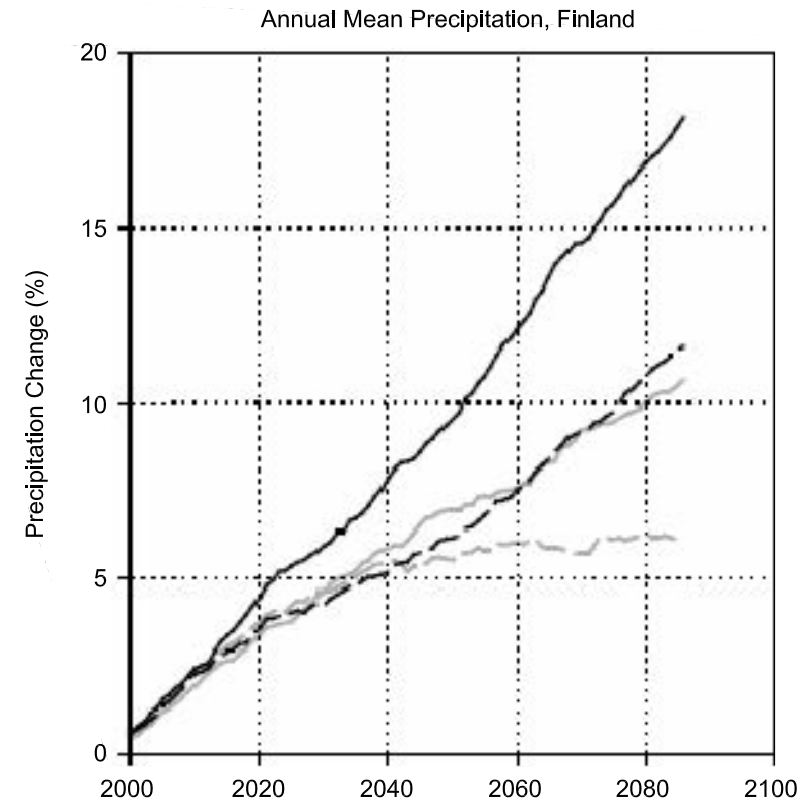
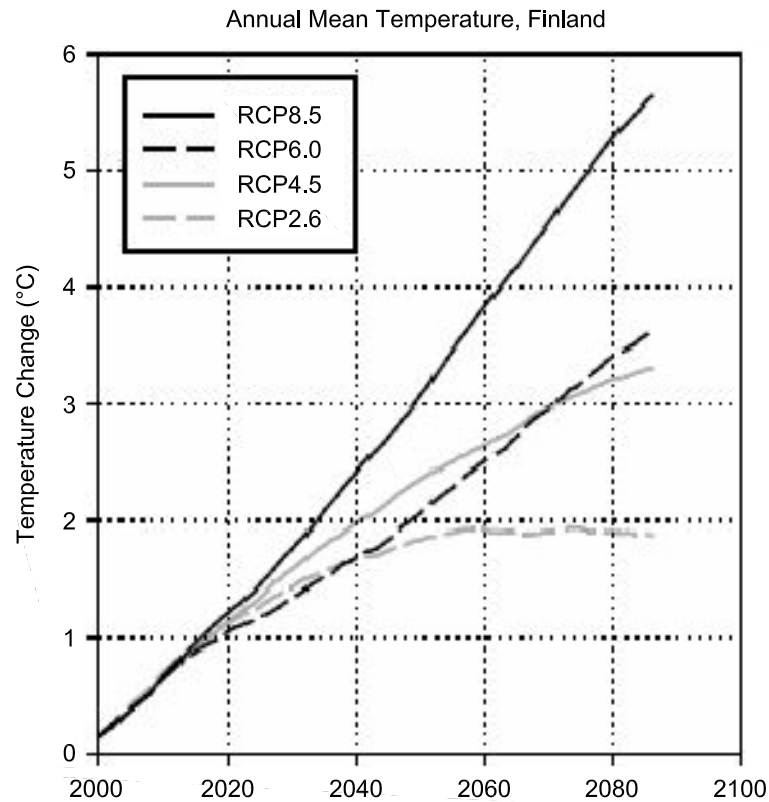
PROJECT NO.	4064
BY	SBM
CHECKED	HL
DRAWN	RJN
DRAWING NAME	RECHARGE
DRAWING DATE	13 JUN 2022
REVISION DATE	5 AUG 2022



Estimated Recharge Rates from the
MIKE SHE Model

CLIENT:
Sakatti Mine

FIGURE NO.
3-19



PROJECT NO.	4064
BY	SBM
CHECKED	HL
DRAWN	RJN
DRAWING NAME	FUTURE
DRAWING DATE	24 MAY 2022
REVISION DATE	

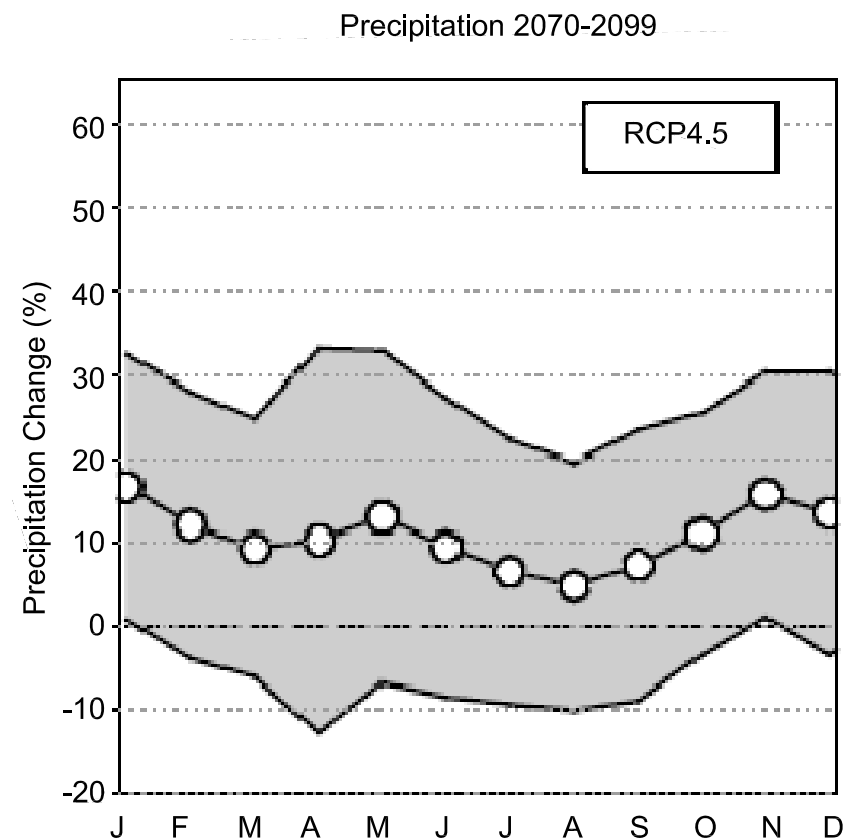
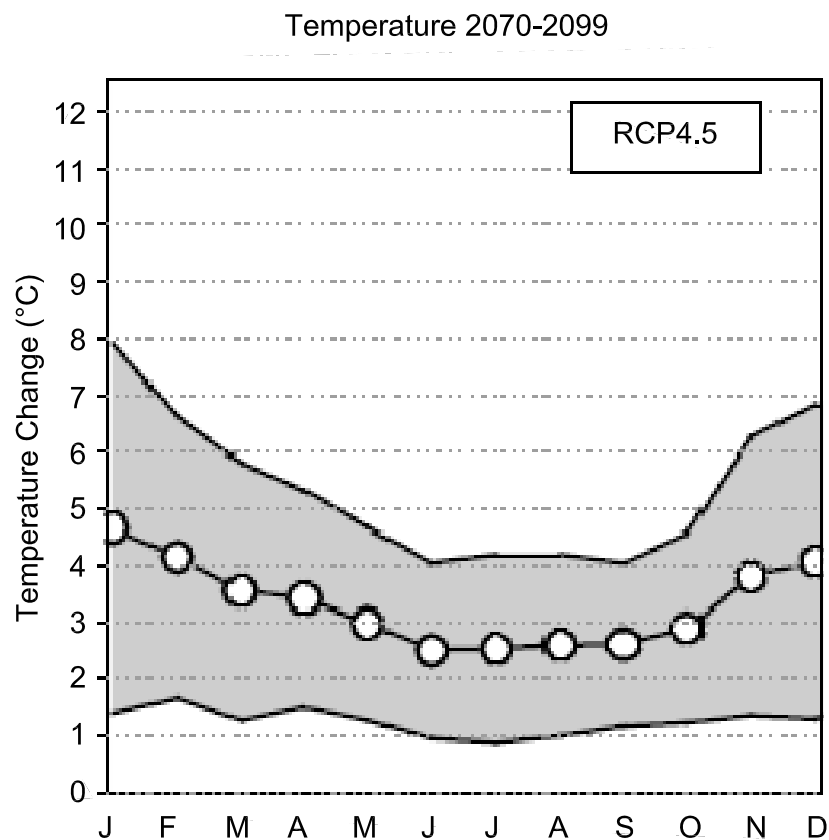


ITASCATM
Denver, Inc.

Future Temperature and Precipitation
in Finland under Various
Greenhouse Gas Scenarios

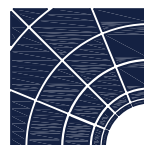
CLIENT:
Sakatti Mine

FIGURE NO.
3-20



Source: Ruosteenoja et al. 2016

PROJECT NO.	4064
BY	SBM
CHECKED	HL
DRAWN	RJN
DRAWING NAME	FUTURE
DRAWING DATE	15 JUN 2022
REVISION DATE	



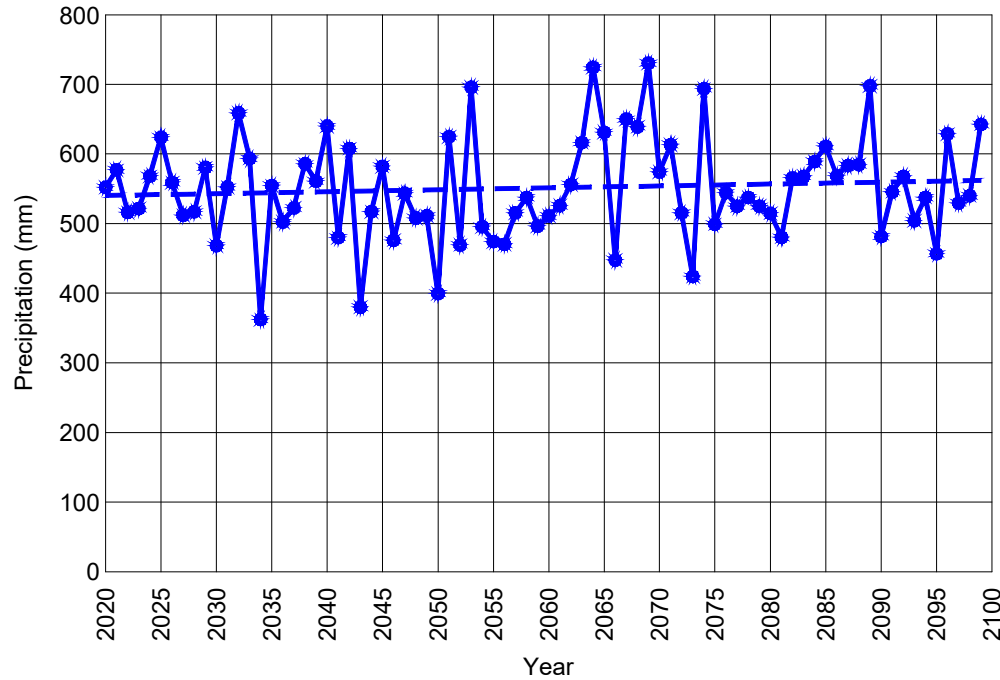
ITASCATM
Denver, Inc.

Future Average Monthly Temperature and
Precipitation for the Greenhouse Gas Case
RCP4.5 for 2070 to 2099

CLIENT:
Sakatti Mine

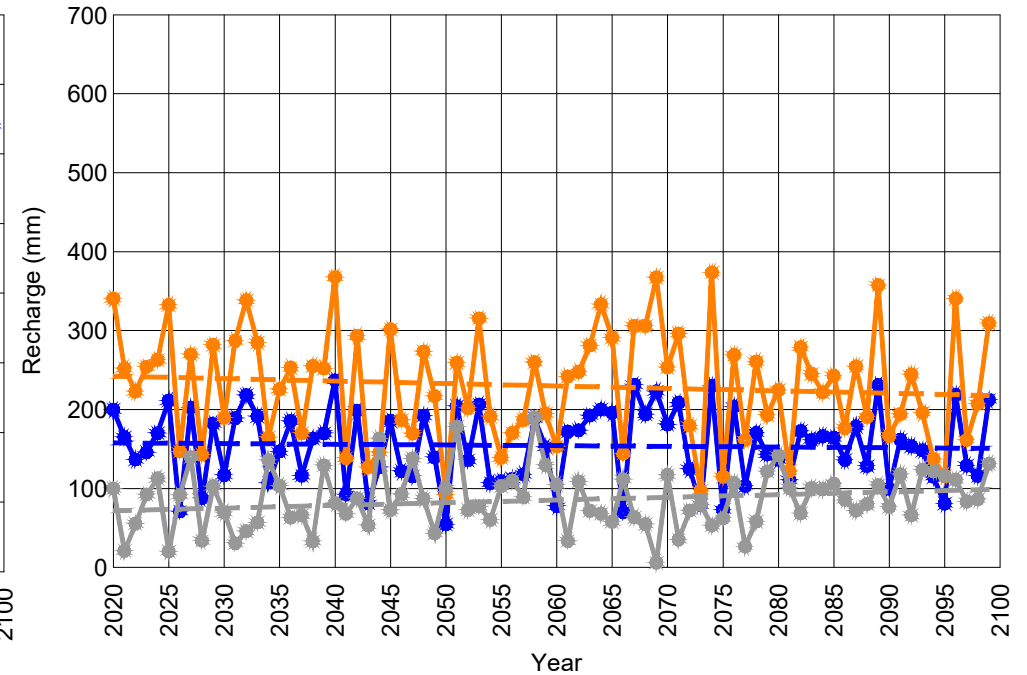
FIGURE NO.
3-21

a) Estimated Future Annual Precipitation Rates



● Precipitation Rate - - Trend Line of Precipitation Rate

b) Future Applied Annual Recharge Rates



Annual Recharge Rate
 ● Till ● Sorted Sediments ● Peat
 Linear Trend Line of Recharge Rate
 - - Till - - Sorted Sediments - - Peat

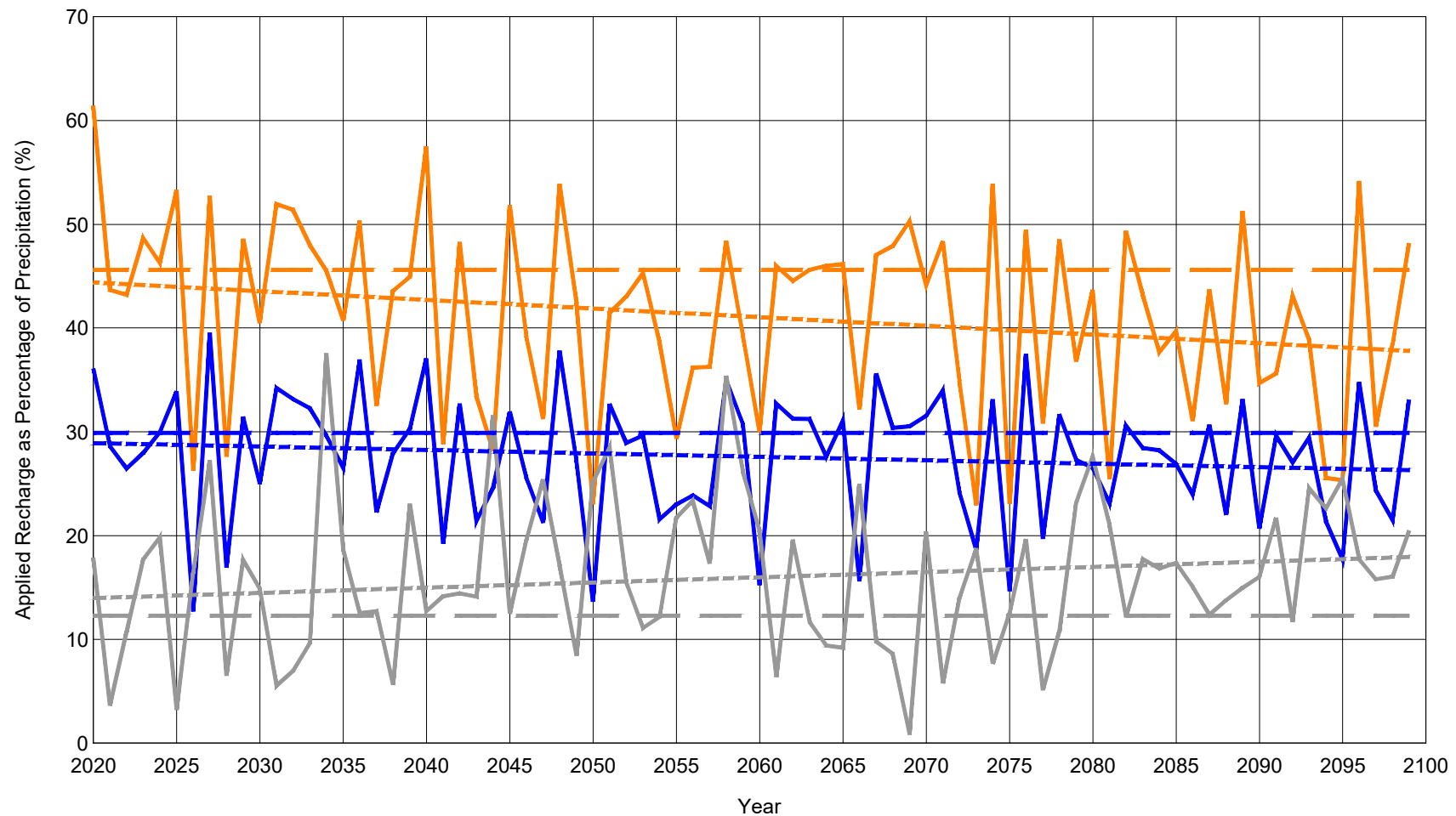
PROJECT NO.	4064
BY	SBM
CHECKED	HL
DRAWN	RJN
DRAWING NAME	ANNUAL
DRAWING DATE	13 JUN 2022
REVISION DATE	5 AUG 2022



Estimated Future Annual Precipitation and Recharge Rates

CLIENT:
Sakatti Mine

FIGURE NO.
3-22



Future Recharge Rate
 — Till — Sorted Sediments — Peat

Current Average Recharge Rate (2012 through 2021)
 — Till — Sorted Sediments — Peat

Linear Trend Line of Future Recharge Rate
 - - - Till - - - Sorted Sediments - - - Peat

PROJECT NO.	4064
BY	SBM
CHECKED	HL
DRAWN	RJN
DRAWING NAME	ANNUAL
DRAWING DATE	16 JUN 2022
REVISION DATE	5 AUG 2022



Future Applied Recharge Rates as a
Percentage of Annual Precipitation

CLIENT:
Sakatti Mine

FIGURE NO.
3-23



Hydrologic Study Area

Mine-Workings Extent

Decline Extent

Viiankiaapa Extent (Natura 2000)

River

Kitinen River

Lakes

Ponds

Surface-water Flow Directions

Ground-Surface Contour (2 m)

Springs

Discharge

Discharge and Stage

Stage

Meteorological Stream Monitoring Locations

Kitinen River

Lakes

Ponds

N

0

1,250

2,500

Meters

PROJECT NO.	4064
BY	SBM
CHECKED	HL
DRAWN	NP
DRAWING NAME	SurfaceWater
DRAWING DATE	Apr. 25, 2022
REVISION DATE	Mar. 08, 2023

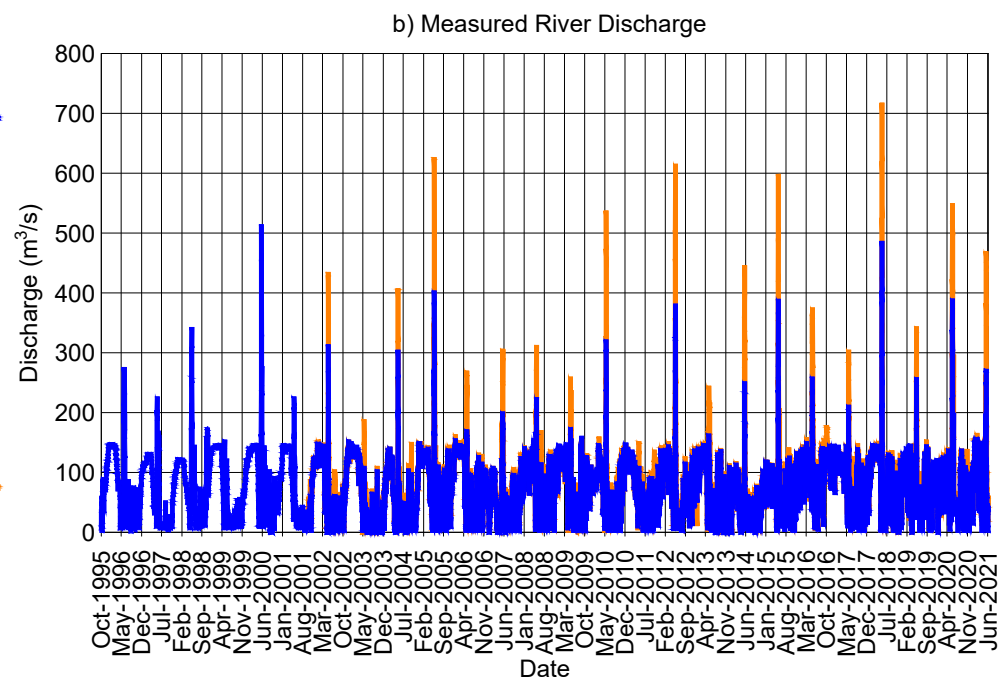
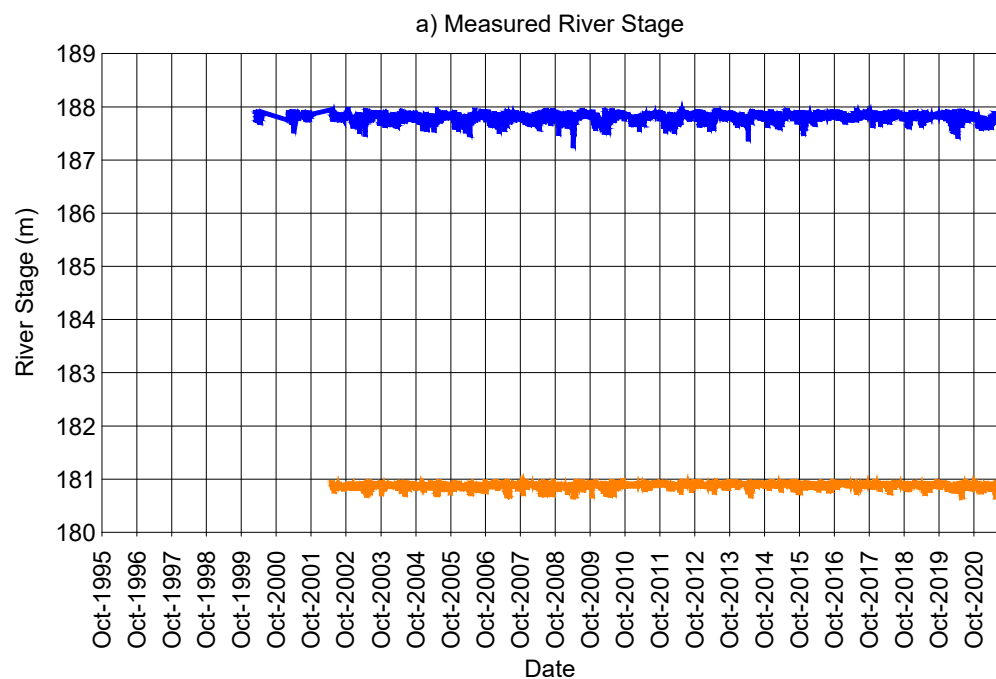
ITASCATM
Denver, Inc.

Surface-Water Bodies in the Hydrologic Study Area

CLIENT:
Sakatti Mine

FIGURE NO.
3-24

G:\ARCGIS\4064_Sakatti\MXD\Working\SurfaceWater.mxd



— Matarakoski (#6500435) — Kelukoski (#6500445)

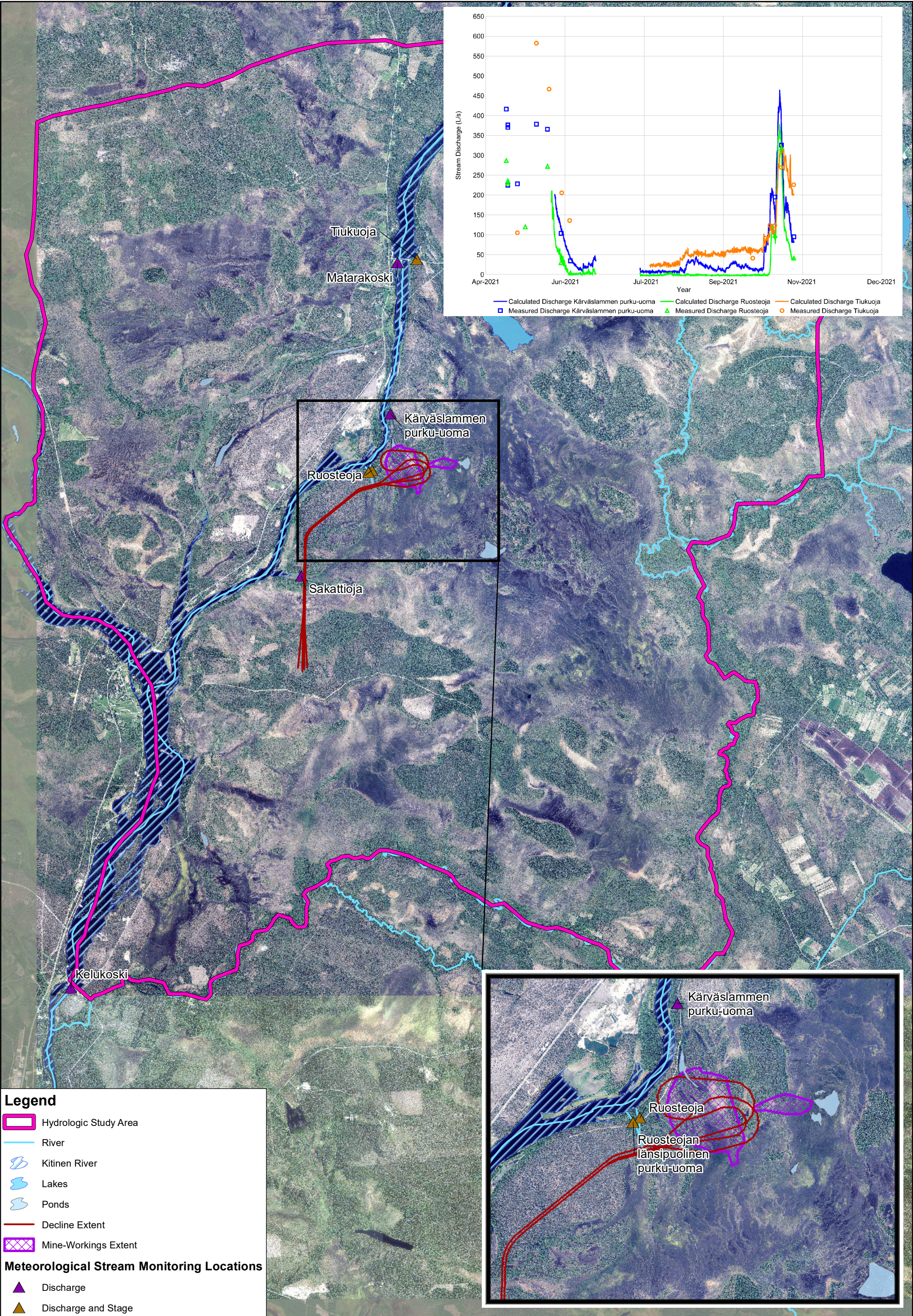
PROJECT NO.	4064
BY	SBM
CHECKED	HL
DRAWN	RJN
DRAWING NAME	RIVER
DRAWING DATE	13 JUN 2022
REVISION DATE	



Measured River Stages and Discharge
Rates from Dams along the Kitinen River

CLIENT:
Sakatti Mine

FIGURE NO.
3-25



Legend

- Hydrologic Study Area
- River
- Kitinen River
- Lakes
- Ponds
- Decline Extent
- Mine-Workings Extent

Meteorological Stream Monitoring Locations

- Discharge
- Discharge and Stage

N

01,2502,500

Meters

PROJECT NO.	4064
BY	SBM
CHECKED	HL
DRAWN	NP
DRAWING NAME	Streamflow
DRAWING DATE	Apr. 25, 2022
REVISION DATE	Feb. 10, 2023

ITASCA

Denver, Inc.

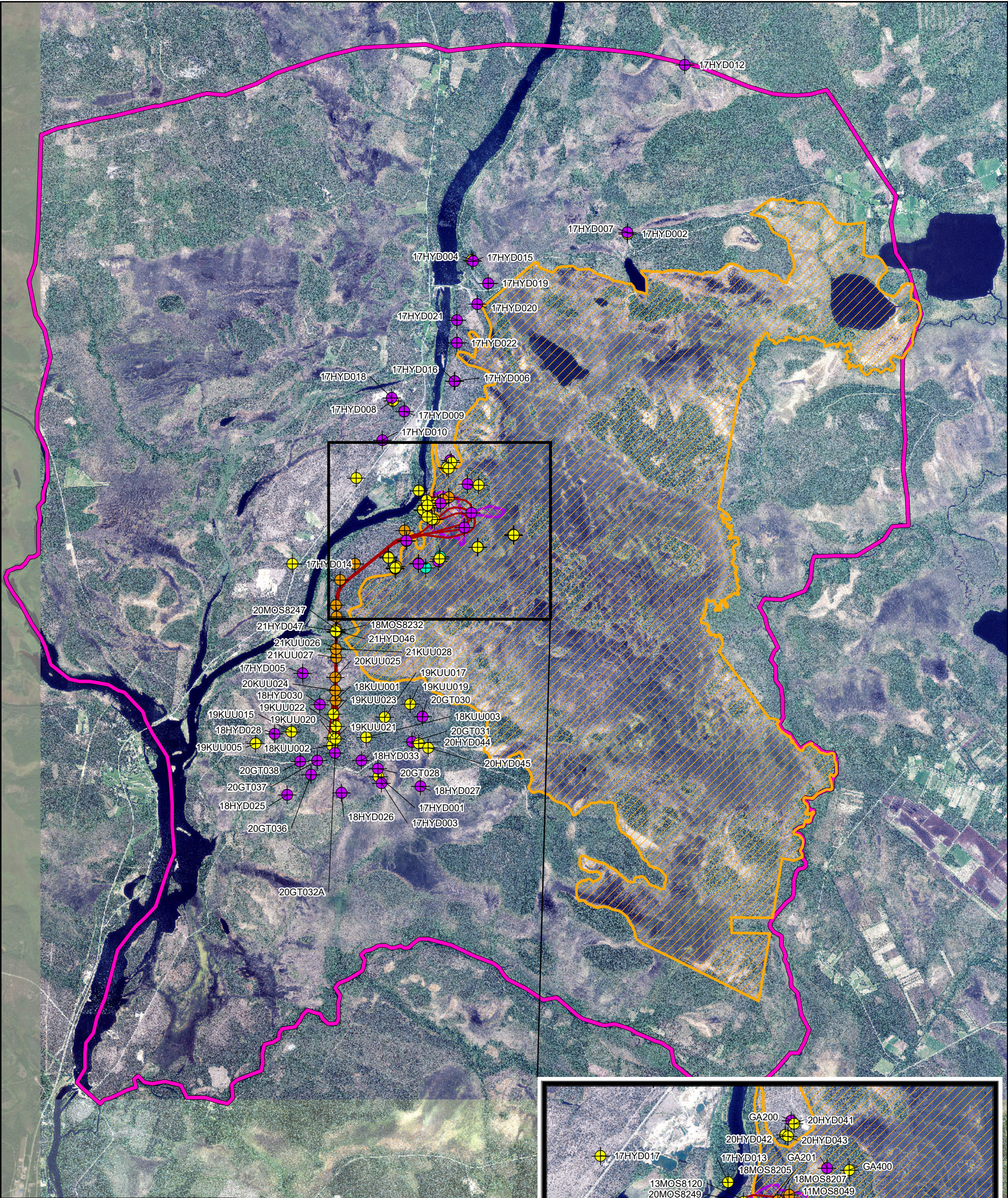
Measured and Calculated Streamflow Discharge Rates from the Mine Area

CLIENT:

Sakatti Mine

FIGURE NO.

3-26



Legend

Hydrologic Study Area

Decline Extent

Viiankiaapa Extent (Natura 2000)

Mine-Workings Extent

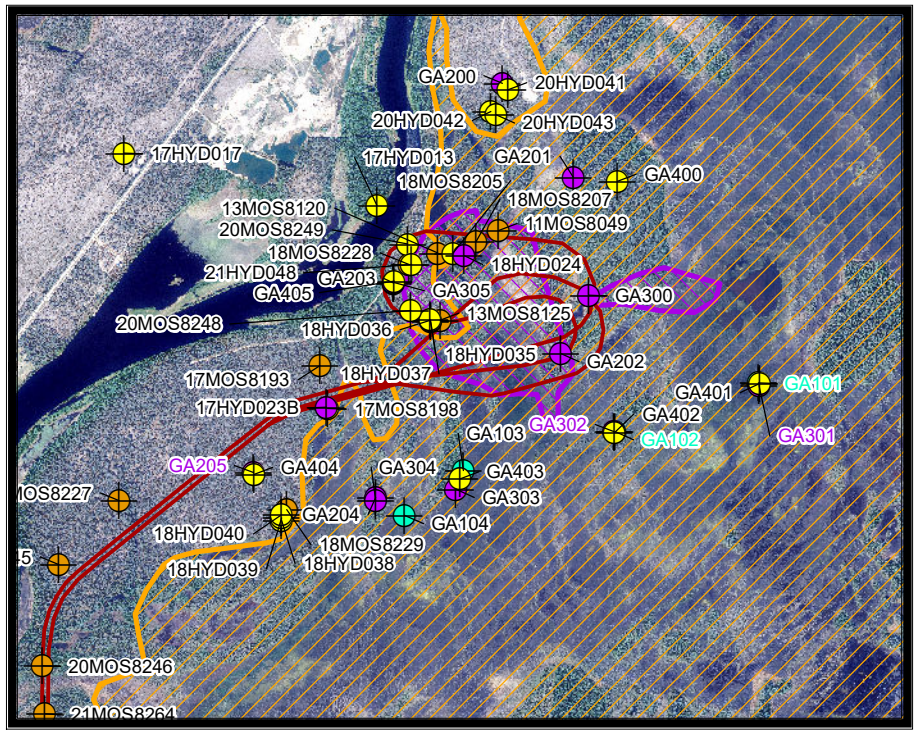
Monitoring Locations by Hydrogeologic Unit

Deep Bedrock

Peat

Shallow Sediment

Shallow Bedrock



N

0

1,250

2,500

Meters

PROJECT NO.	4064
BY	SBM
CHECKED	HL
DRAWN	NP
DRAWING NAME	MonLoc_Geo
DRAWING DATE	Apr. 25, 2022
REVISION DATE	Aug. 19, 2022

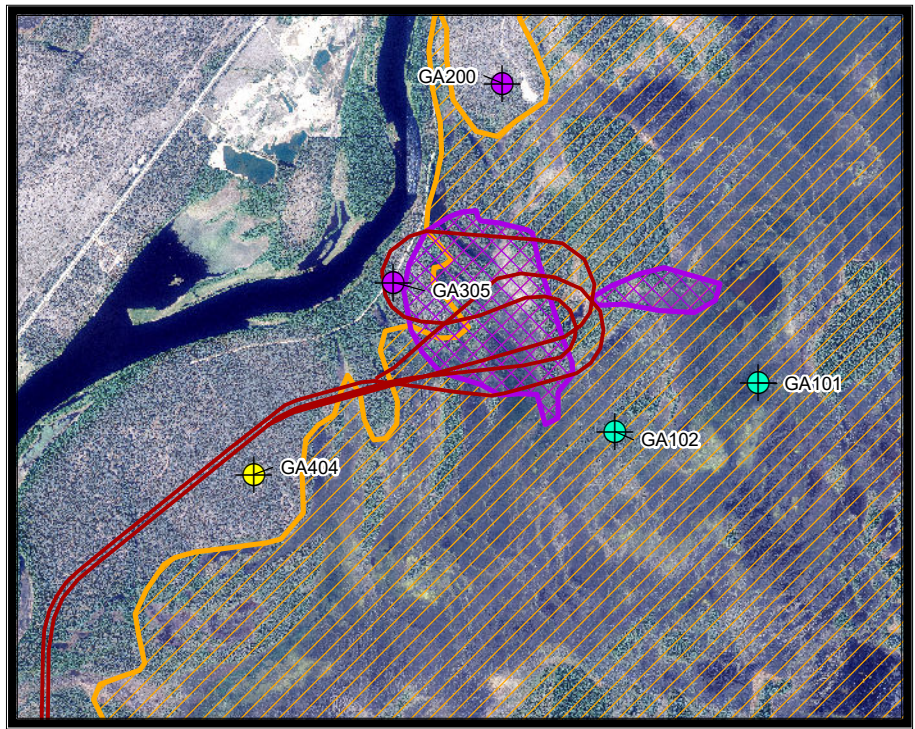
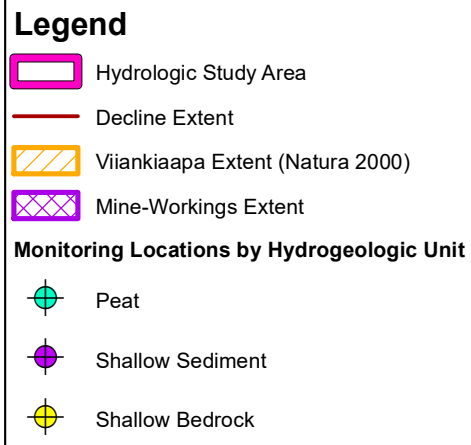
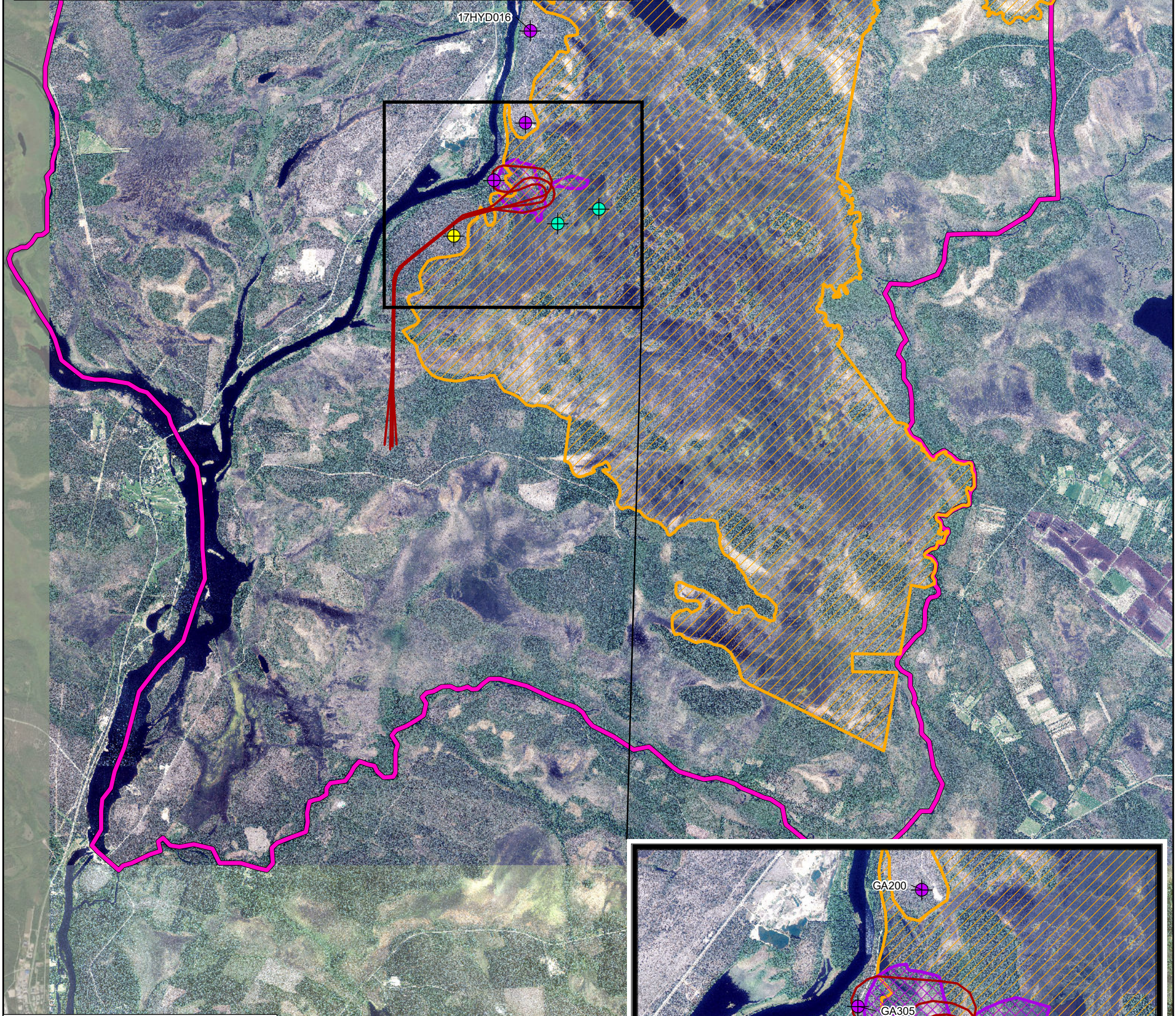
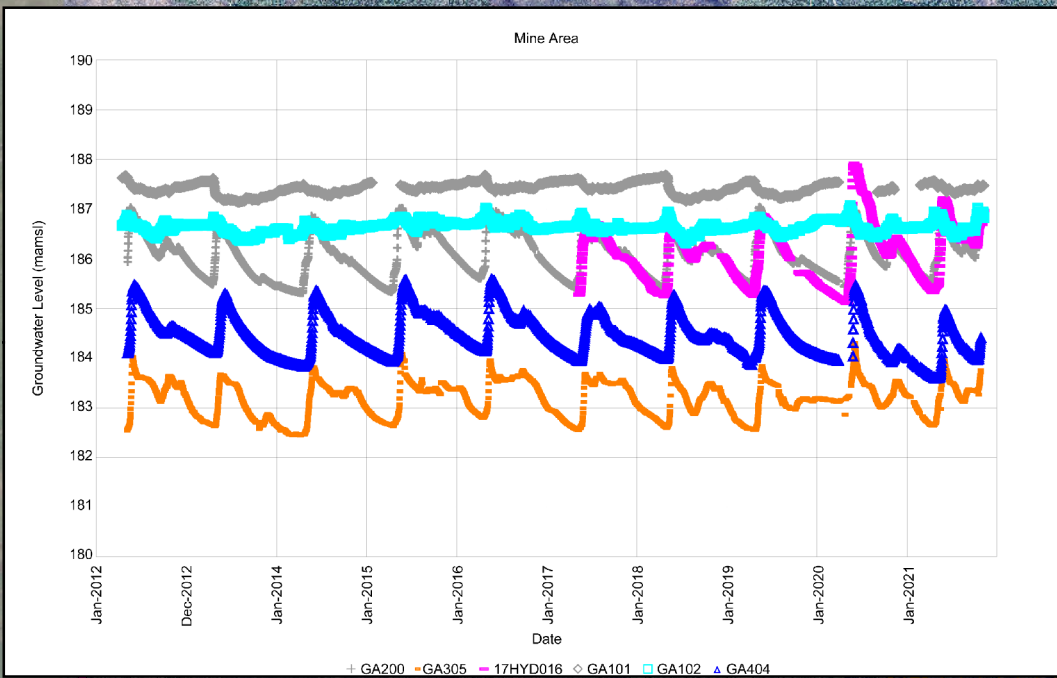
ITASCA
Denver, Inc.

Monitoring Locations by Hydrogeologic Unit
in the Hydrologic Study Area

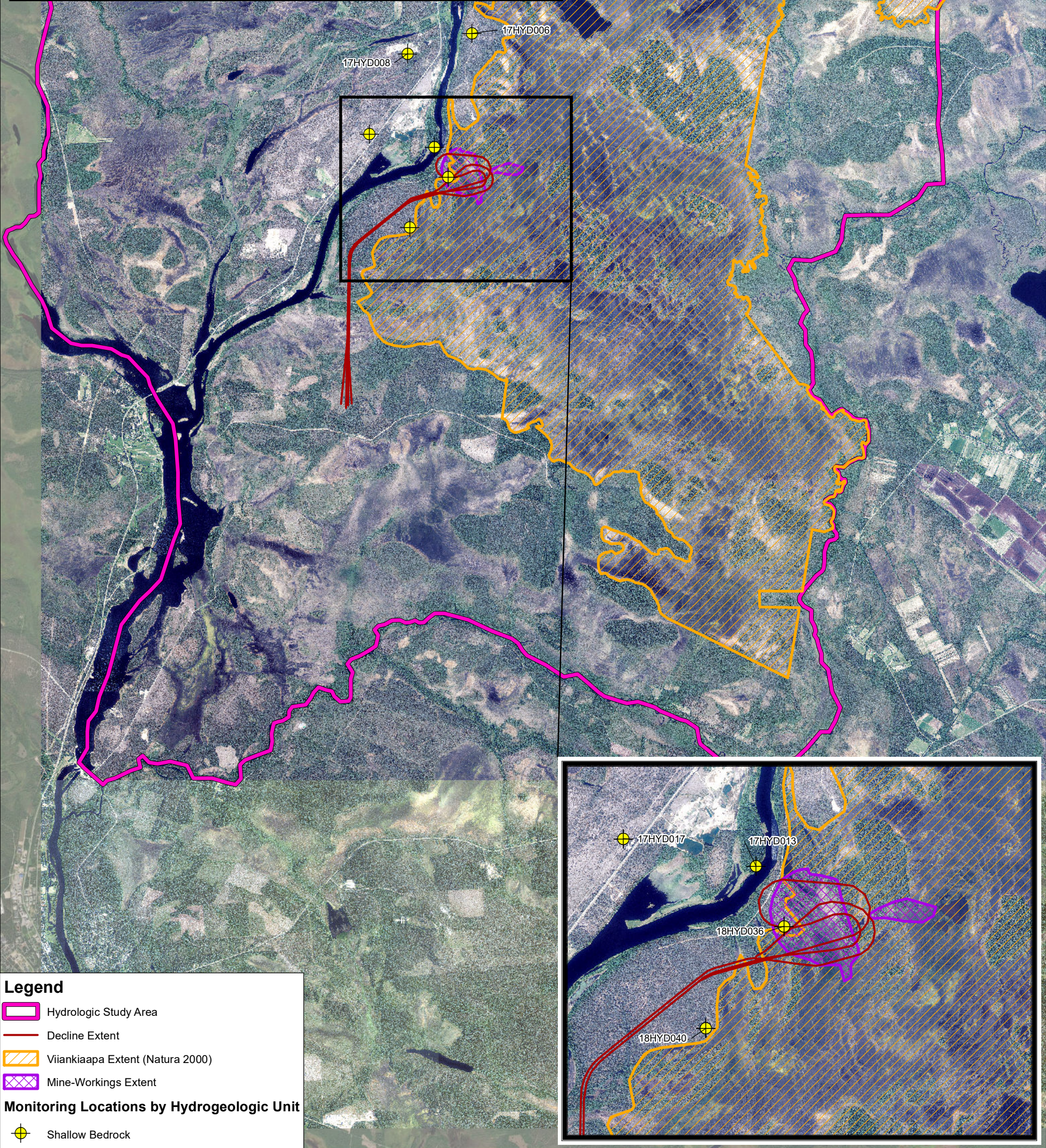
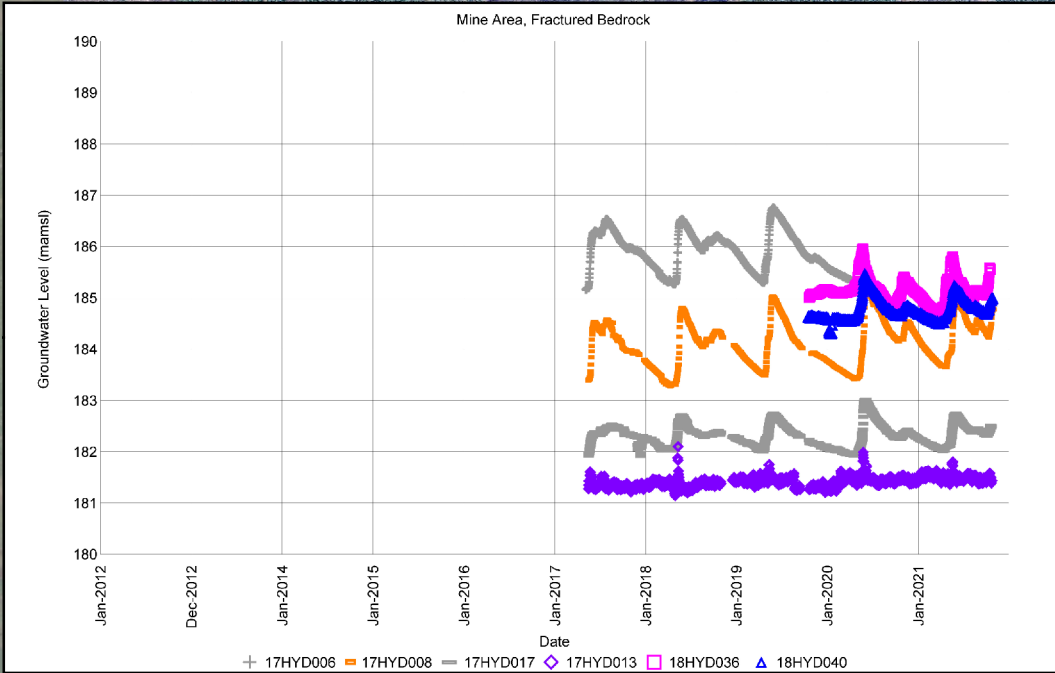
CLIENT:
Sakatti Mine

FIGURE NO.
3-28

G:\ARC\GIS\4064_Sakatti\MXDs\Working\MonLoc_Geo.mxd



 0 1,250 2,500 Meters	PROJECT NO.	4064	 ITASCA Denver, Inc.	Measured Groundwater Levels across the Project Site	
	BY	SBM			
	CHECKED	HL			
	DRAWN	NP			
	DRAWING NAME	GW_Sitea			
DRAWING DATE	Apr. 25, 2022	CLIENT:	Sakatti Mine	FIGURE NO.	3-29a
REVISION DATE	Oct. 24, 2022				



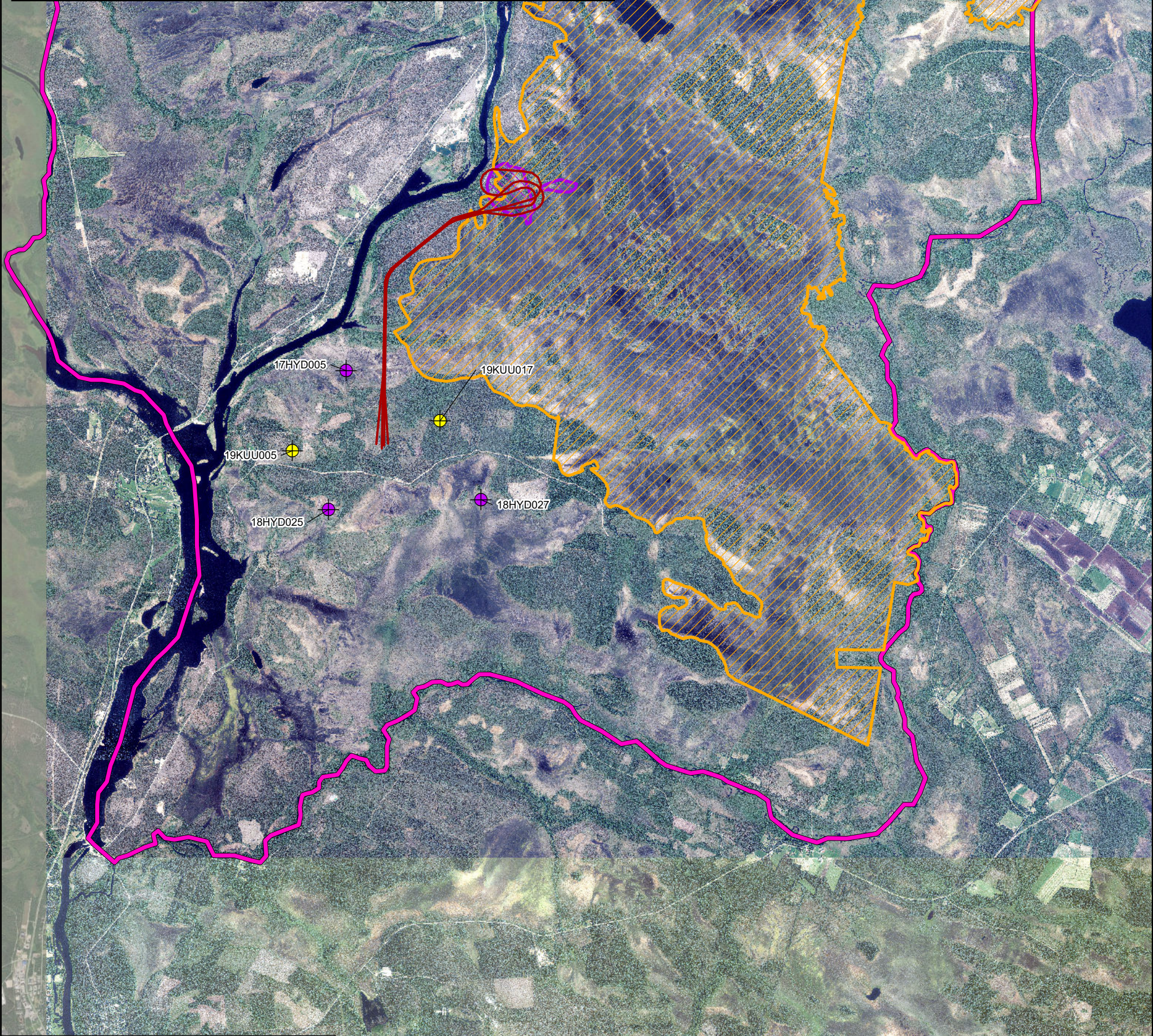
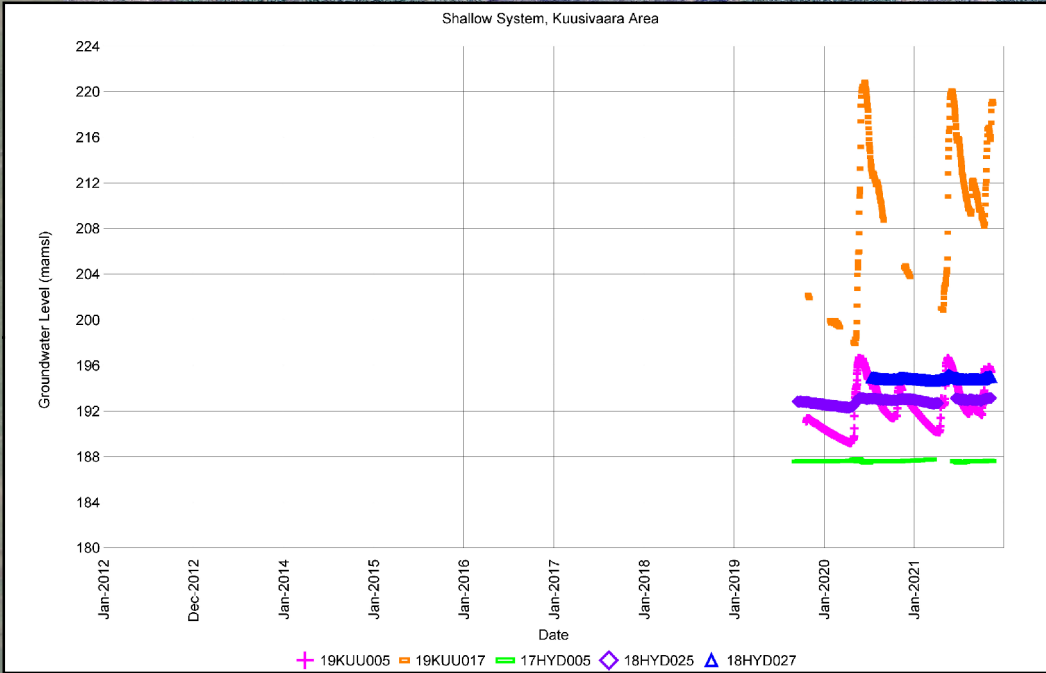
Legend

- Hydrologic Study Area
- Decline Extent
- Viiankiaapa Extent (Natura 2000)
- Mine-Workings Extent

Monitoring Locations by Hydrogeologic Unit

- Shallow Bedrock

 0 1,250 2,500 Meters	PROJECT NO.	4064	 ITASCA Denver, Inc.	Measured Groundwater Levels across the Project Site	
	BY	SBM			
	CHECKED	HL			
	DRAWN	NP			
	DRAWING NAME	GW_Siteb			
DRAWING DATE	Apr. 25, 2022	CLIENT:	Sakatti Mine	FIGURE NO.	3-29b
REVISION DATE	Aug. 19, 2022				



Legend

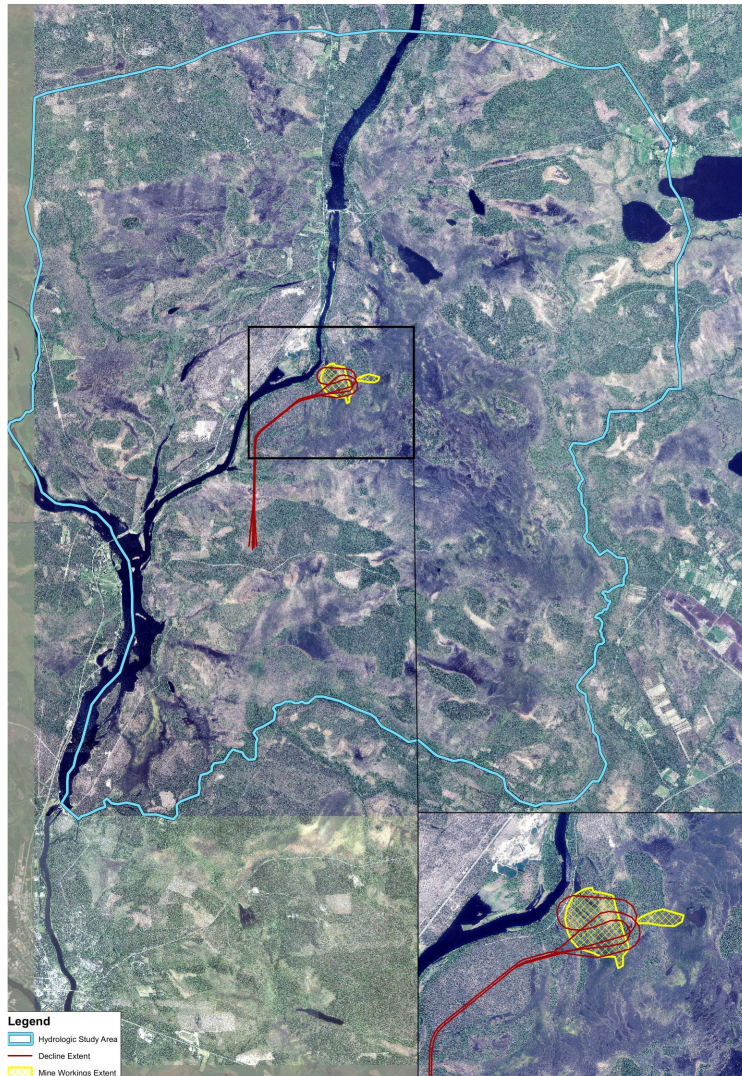
- Hydrologic Study Area
- Decline Extent
- Viiankiaapa Extent (Natura 2000)
- Mine-Workings Extent

Monitoring Locations by Hydrogeologic Unit

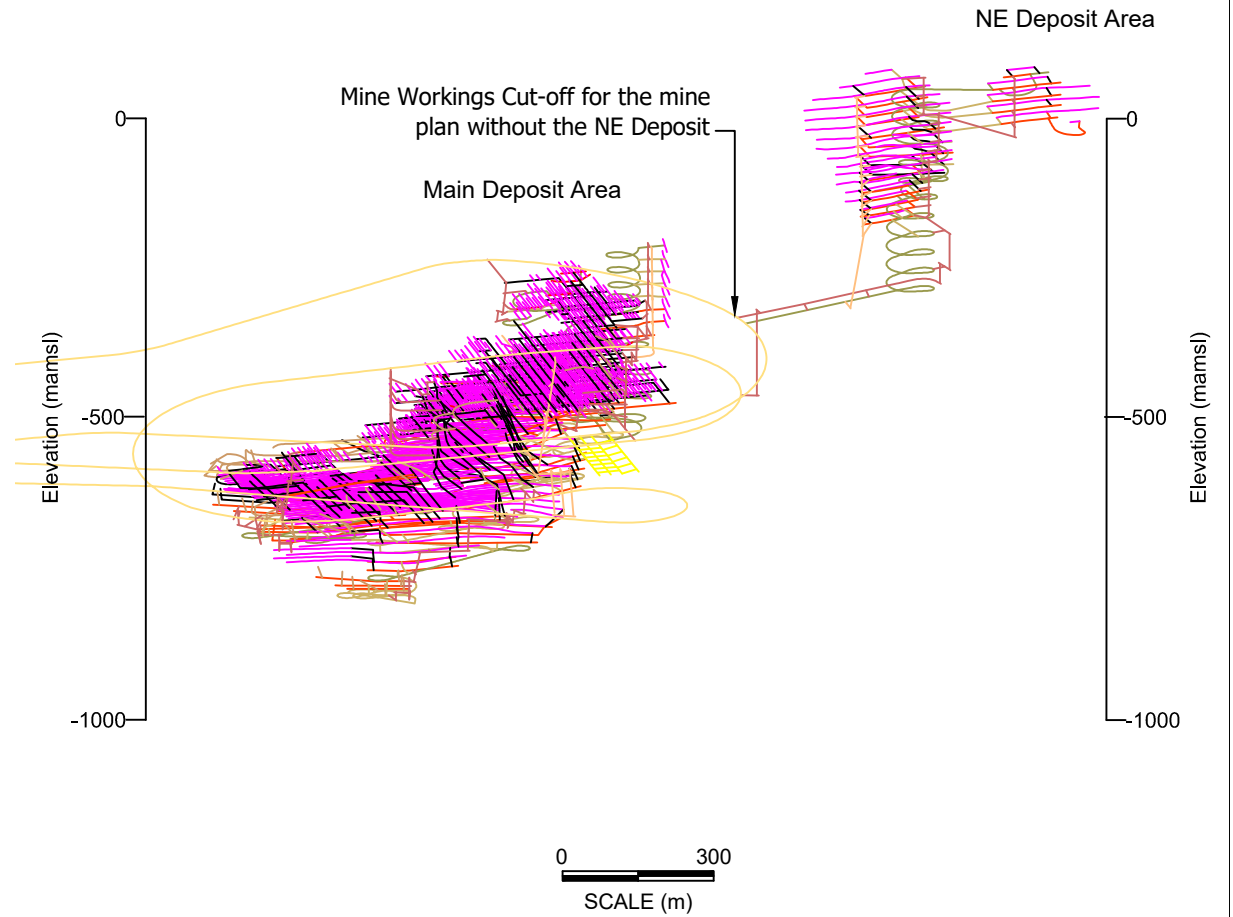
- Shallow Sediment
- Shallow Bedrock

	PROJECT NO.	4064		Measured Groundwater Levels across the Project Site	
	BY	SBM			
	CHECKED	HL			
	DRAWN	NP		CLIENT:	Sakatti Mine
	DRAWING NAME	GW_Sitec		FIGURE NO.	3-29c
	DRAWING DATE	Apr. 25, 2022			
REVISION DATE	Oct. 17, 2022				

a) Plan View



b) Access Drift and Mining Zones



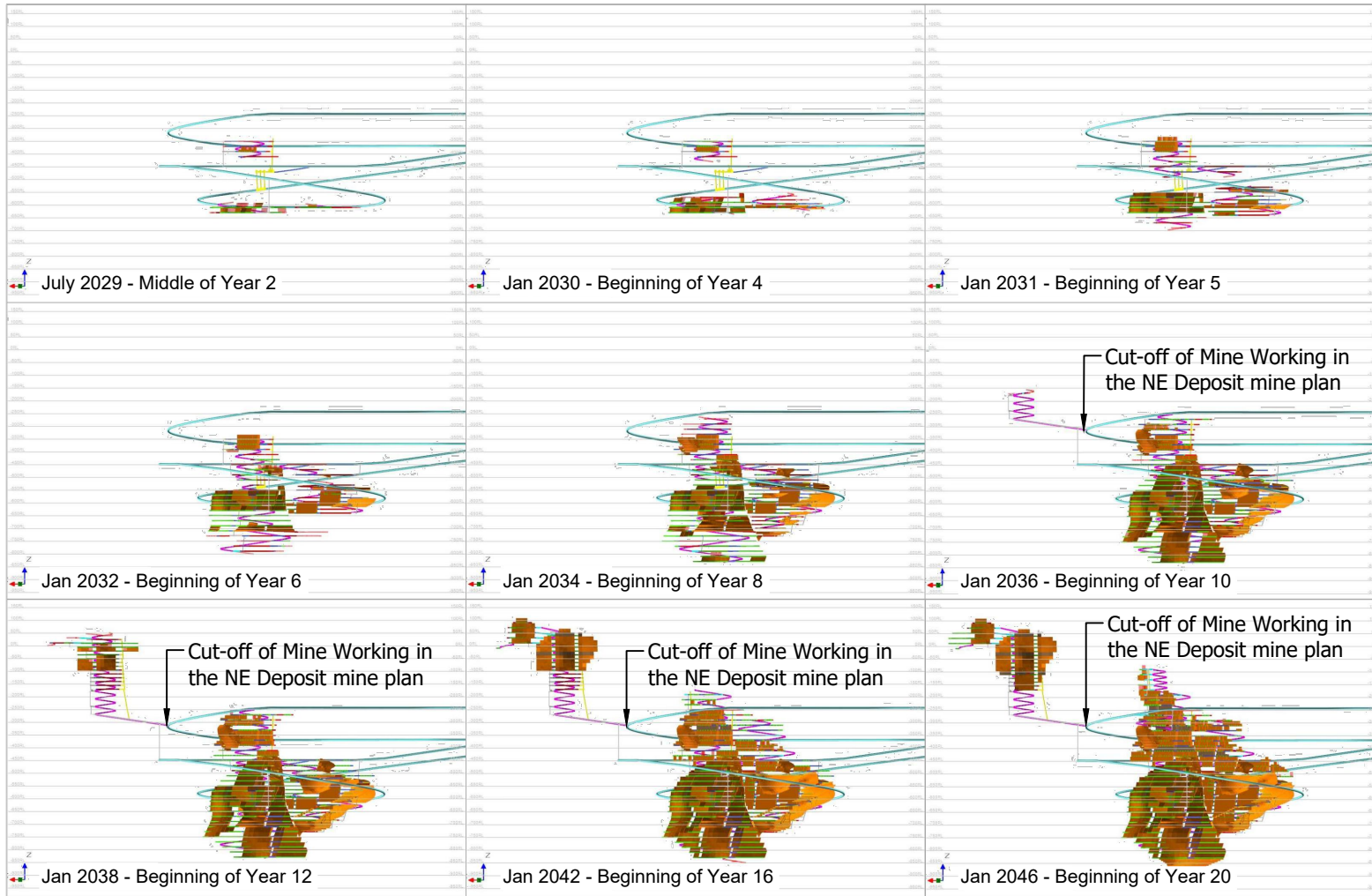
PROJECT NO.	4064
BY	SBM
CHECKED	HL
DRAWN	RJN
DRAWING NAME	MINEPLAN
DRAWING DATE	15 FEB 2023
REVISION DATE	



Future Spatial and Vertical Extent
of Decline and Mine Workings

CLIENT:
Sakatti Mine

FIGURE NO.
3-30a



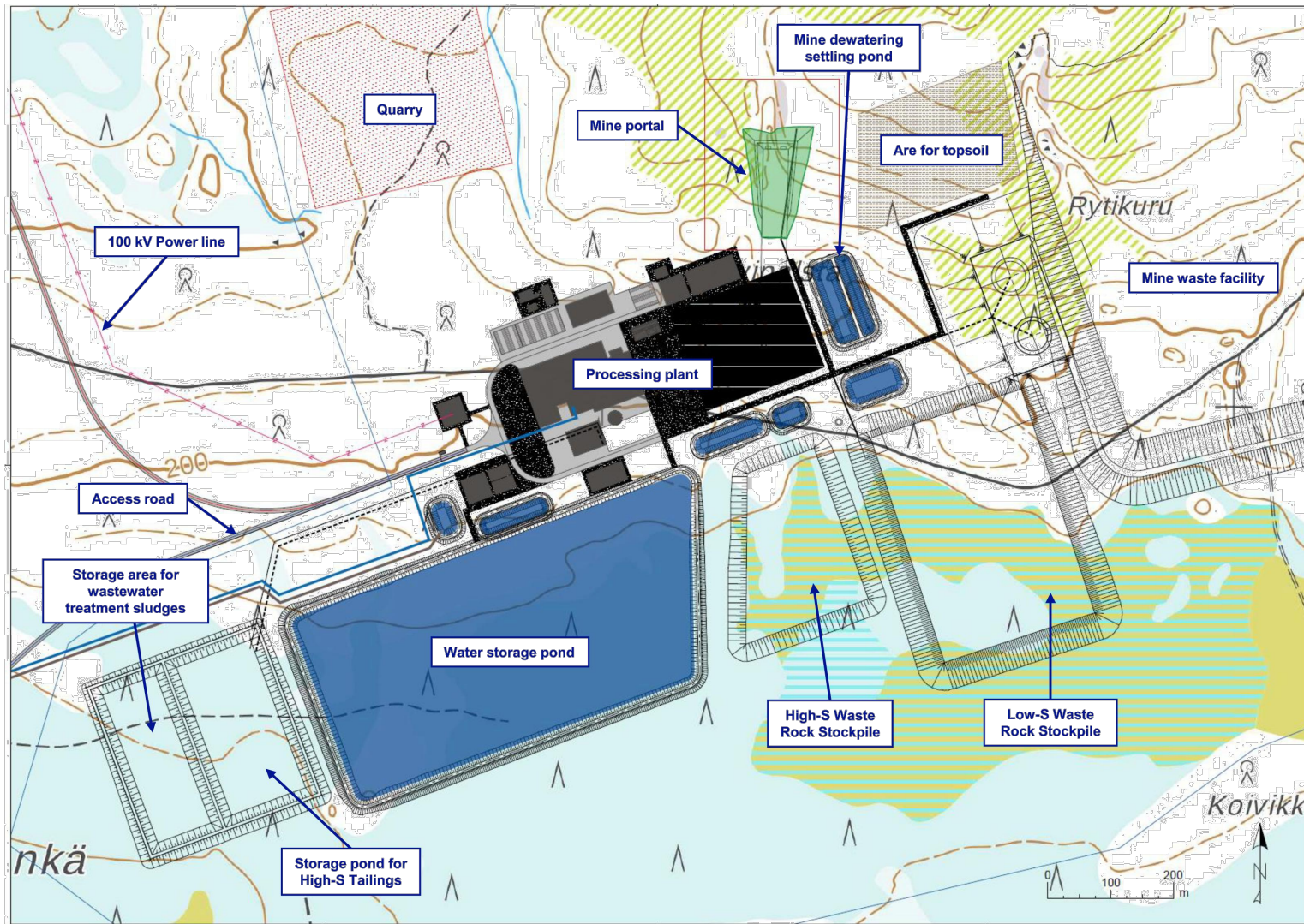
PROJECT NO.	4064
BY	SBM
CHECKED	HL
DRAWN	RJN
DRAWING NAME	MINEPLAN
DRAWING DATE	27 OCT 2022
REVISION DATE	



Progression of Mine Plan over Time

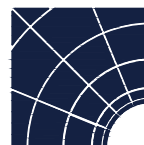
CLIENT:
Sakatti Mine

FIGURE NO.
3-30b



SOURCE: SRK

PROJECT NO.	4064
BY	SBM
CHECKED	HL
DRAWN	RJN
DRAWING NAME	SURFACE
DRAWING DATE	17 JUN 2022
REVISION DATE	



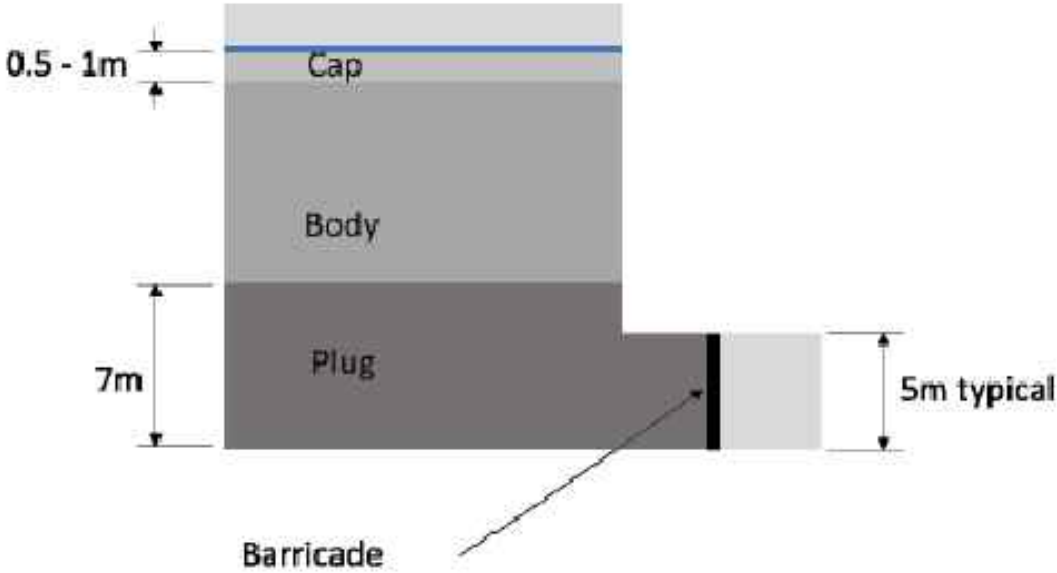
ITASCATM
Denver, Inc.

Surface Locations of Future Mine Infrastructure

CLIENT:
Sakatti Mine

FIGURE NO.
3-31

a) Illustration of Backfill Designs by Patterson Cooke (2021)



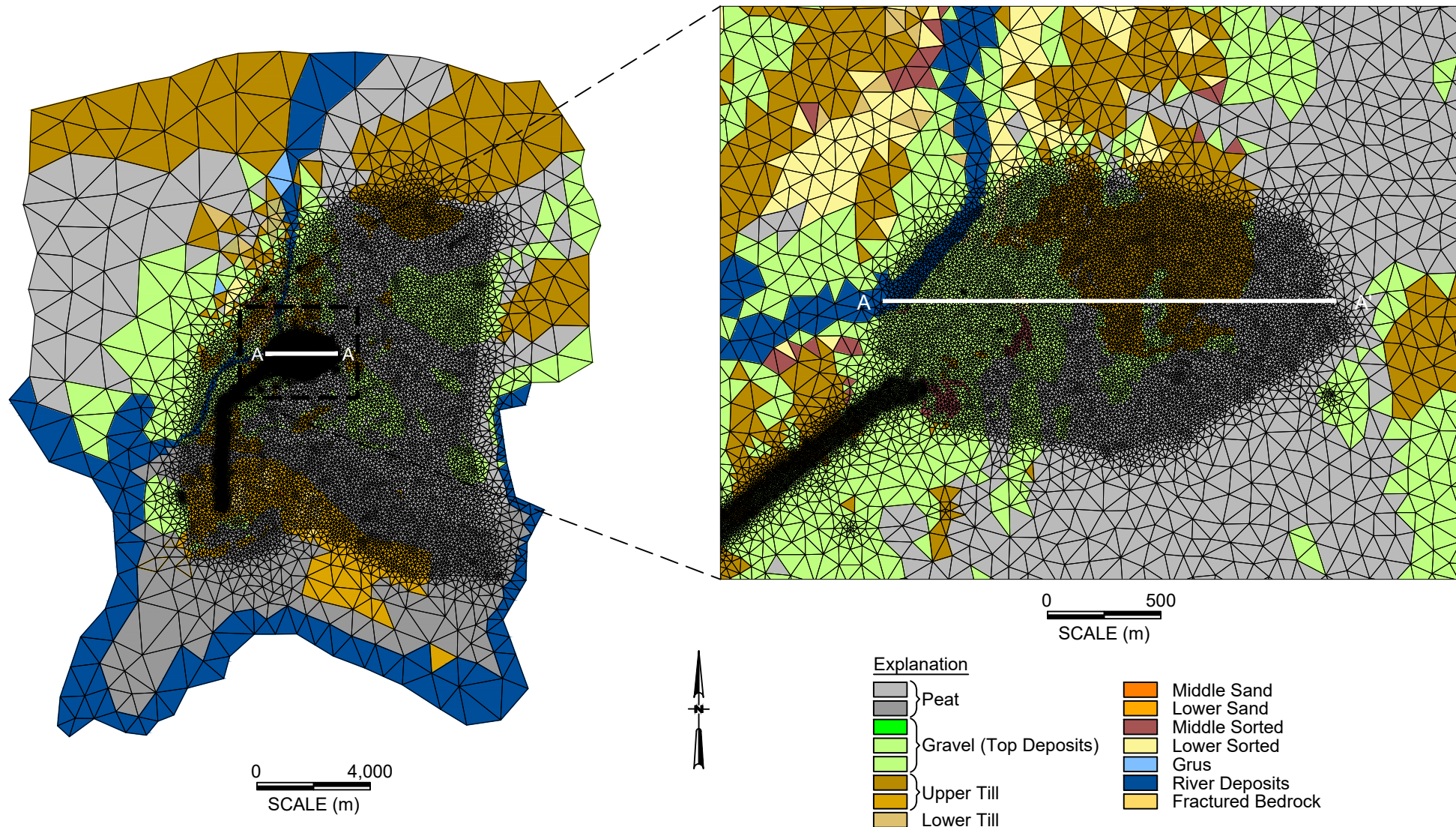
b) Estimated Hydraulic Conductivities of Backfill

Backfilling Hydraulic Properties	K Value (m/s)	S _y
High	1.00E-07	Not Available
Nominal	5.00E-08	
Low	2.00E-08	

PROJECT NO.	4064
BY	SBM
CHECKED	HL
DRAWN	RJN
DRAWING NAME	BACKFILL
DRAWING DATE	17 JUN 2022
REVISION DATE	



Backfilling Plans and Estimated Hydraulic Conductivities	
CLIENT: Sakatti Mine	FIGURE NO. 3-32



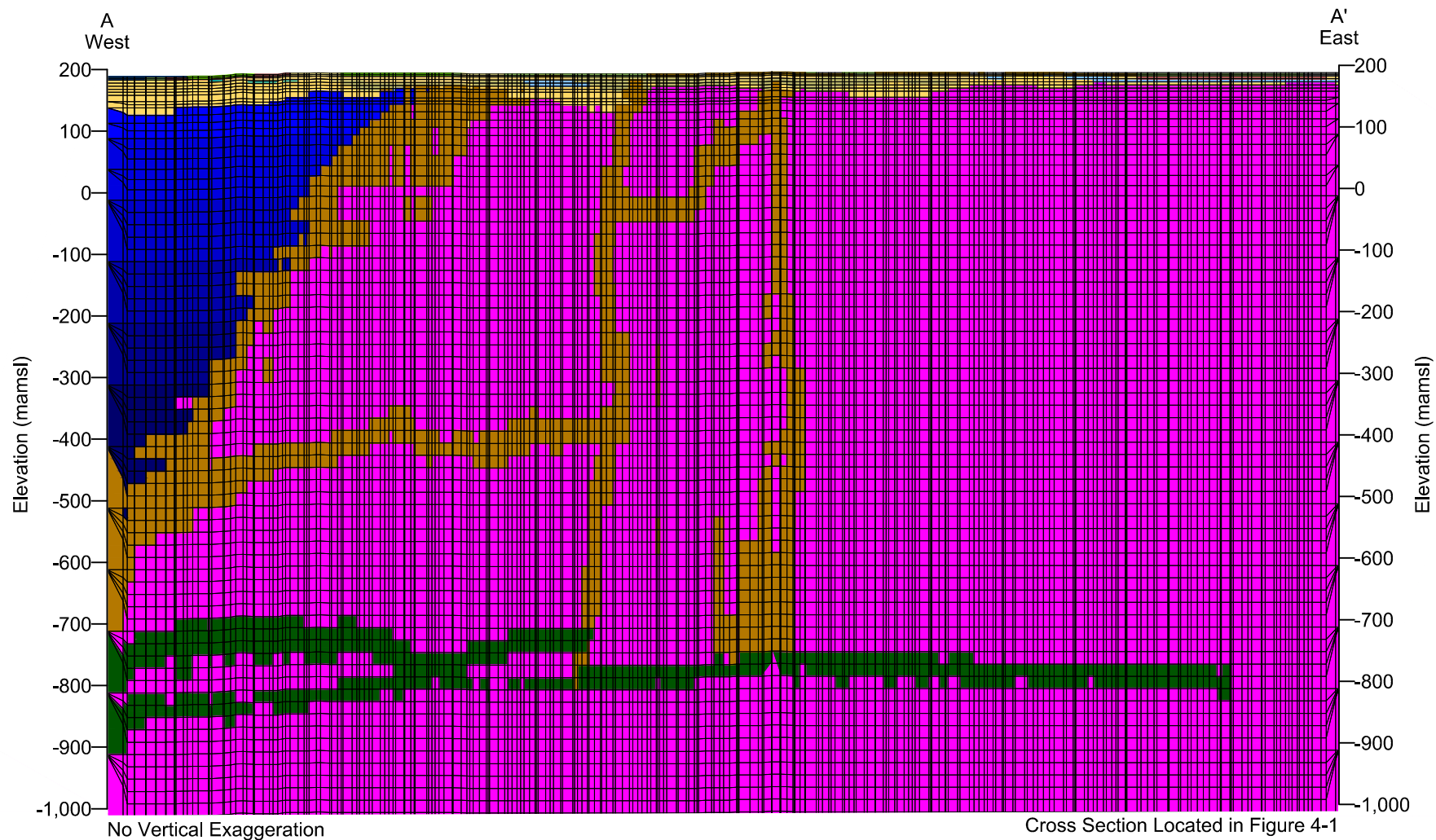
PROJECT NO.	4064
BY	SBM
CHECKED	HL
DRAWN	RJN
DRAWING NAME	MODEL
DRAWING DATE	13 JUN 2022
REVISION DATE	19 OCT 2022



Plan View of Simulated Hydrogeologic Units in Model Layer 1

CLIENT:
Sakatti Mine

FIGURE NO.
4-1



Explanation

Peat	Weathered Clay
Gravel (Top Deposits)	Fractured Bedrock
Upper Till	More Permeable Bedrock
Lower Till	Less Permeable Bedrock
Middle Sorted	Fault
Lower Sorted	Basal Thrust Fault
Grus	
River Deposits	
Basal Sediment	

0 4,000
SCALE (m)

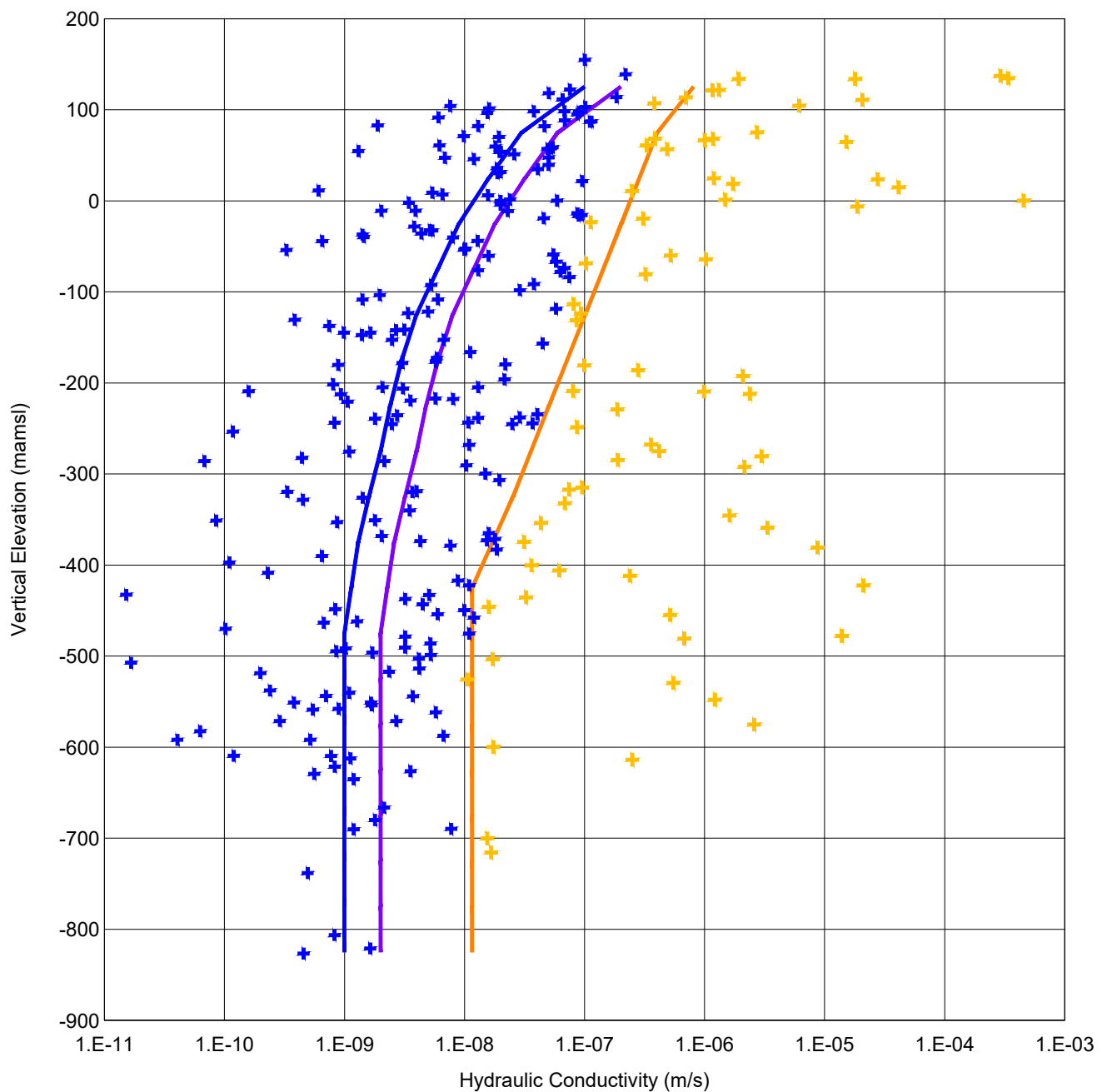
PROJECT NO.	4064
BY	SBM
CHECKED	HL
DRAWN	RJN
DRAWING NAME	XSEC
DRAWING DATE	24 MAY 2022
REVISION DATE	19 OCT 2022



West-East Cross Section of Simulated Hydrogeologic Units in the Mine Area

CLIENT:
Sakatti Mine

FIGURE NO.
4-2



- ★ K Values from Packer Tests of Bedrock
- ✚ K Values from Packer Tests of Fractures
- Simulated More Permeable Bedrock
- Simulated Less Permeable Bedrock and Faults
- Simulated Basal Thrust Fault

PROJECT NO.	4064
BY	SBM
CHECKED	HL
DRAWN	RJN
DRAWING NAME	SIM
DRAWING DATE	24 MAY 2022
REVISION DATE	19 OCT 2022



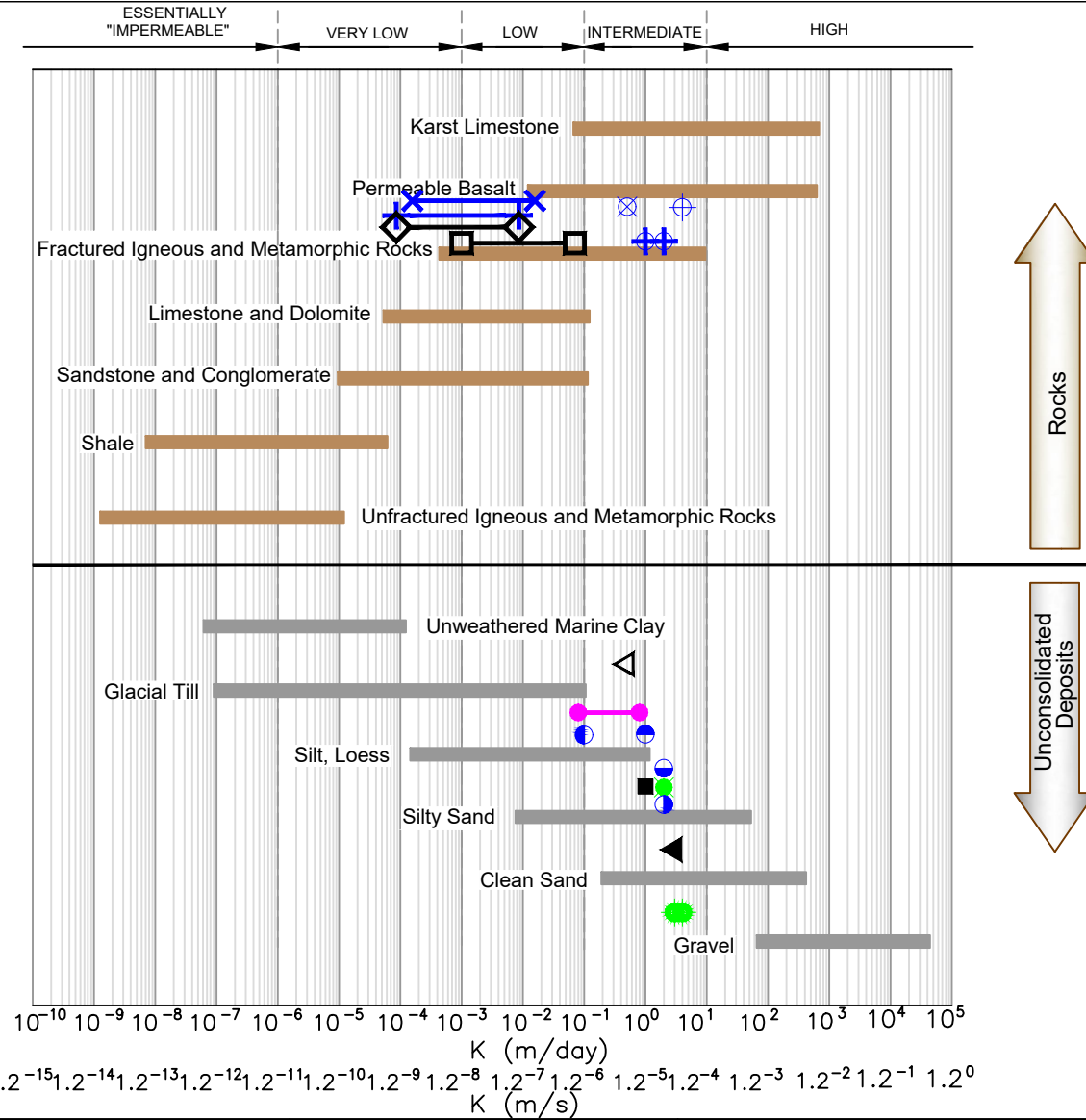
Simulated Hydraulic Conductivities in Groundwater Flow Model versus Measured Hydraulic Conductivities from Packer Tests

CLIENT:
Sakatti Mine

FIGURE NO.
4-3

EXPLANATION

- ◀ Upper Kuusivaara (Sorted Sediments)
- ◁ Till
- ⊕ Top Deposits (Sorted Sediments)
- Middle and Lower Sorted
- Sand
- Clay
- Grus
- Basal Sediment
- Kitinen River Deposits
- Peat
- ⊕ Fractured Bedrock along River
- ⊗ Fractured Bedrock over Mining Area
- ⊕ Fractured Bedrock near Decline
- ⊕ Bedrock along River
- ⊗ Bedrock over Mining Area
- ◻ Basal Thrust Fault
- ◊ Faults in Mining Area



BASED ON FREEZE AND CHERRY, 1979

NOTE: THESE REPRESENT THE K VALUES

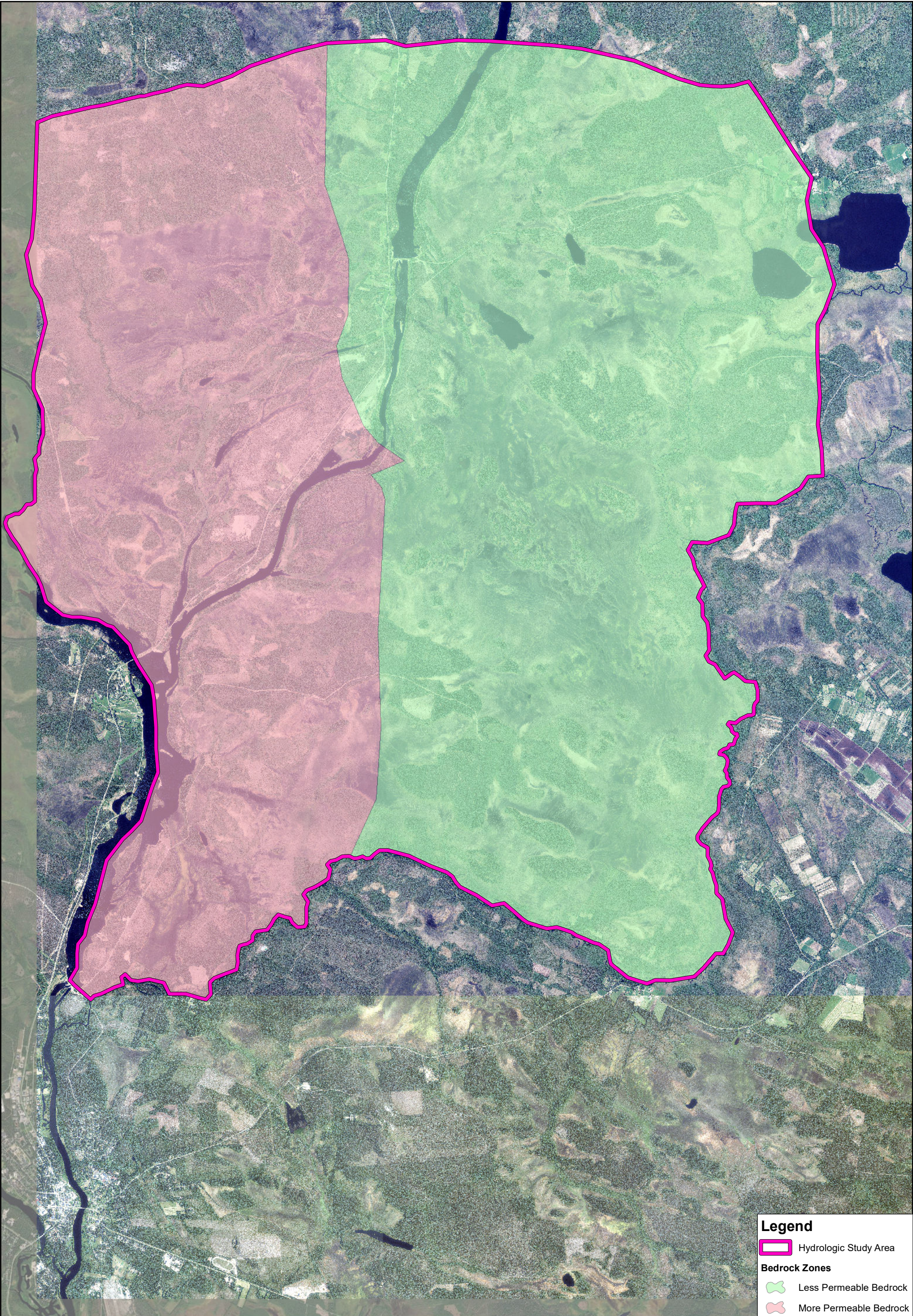
PROJECT NO.	1999
BY	SBM
CHECKED	HL
DRAWN	RJN
DRAWING NAME	KVALUES
DRAWING DATE	13 JUN 2022
REVISION DATE	5 AUG 2022



Values of Hydraulic Conductivity Used
in the 2022 Sakatti Mine Groundwater
Flow Model

CLIENT:
Sakatti Mine

FIGURE NO.
4-4



Legend

Hydrologic Study Area

Bedrock Zones

Less Permeable Bedrock

More Permeable Bedrock

N

0

1,250

2,500

Meters

PROJECT NO.	4064
BY	SBM
CHECKED	HL
DRAWN	NP
DRAWING NAME	PermBR
DRAWING DATE	Apr. 25, 2022
REVISION DATE	May. 24, 2022

ITASCA

Denver, Inc.

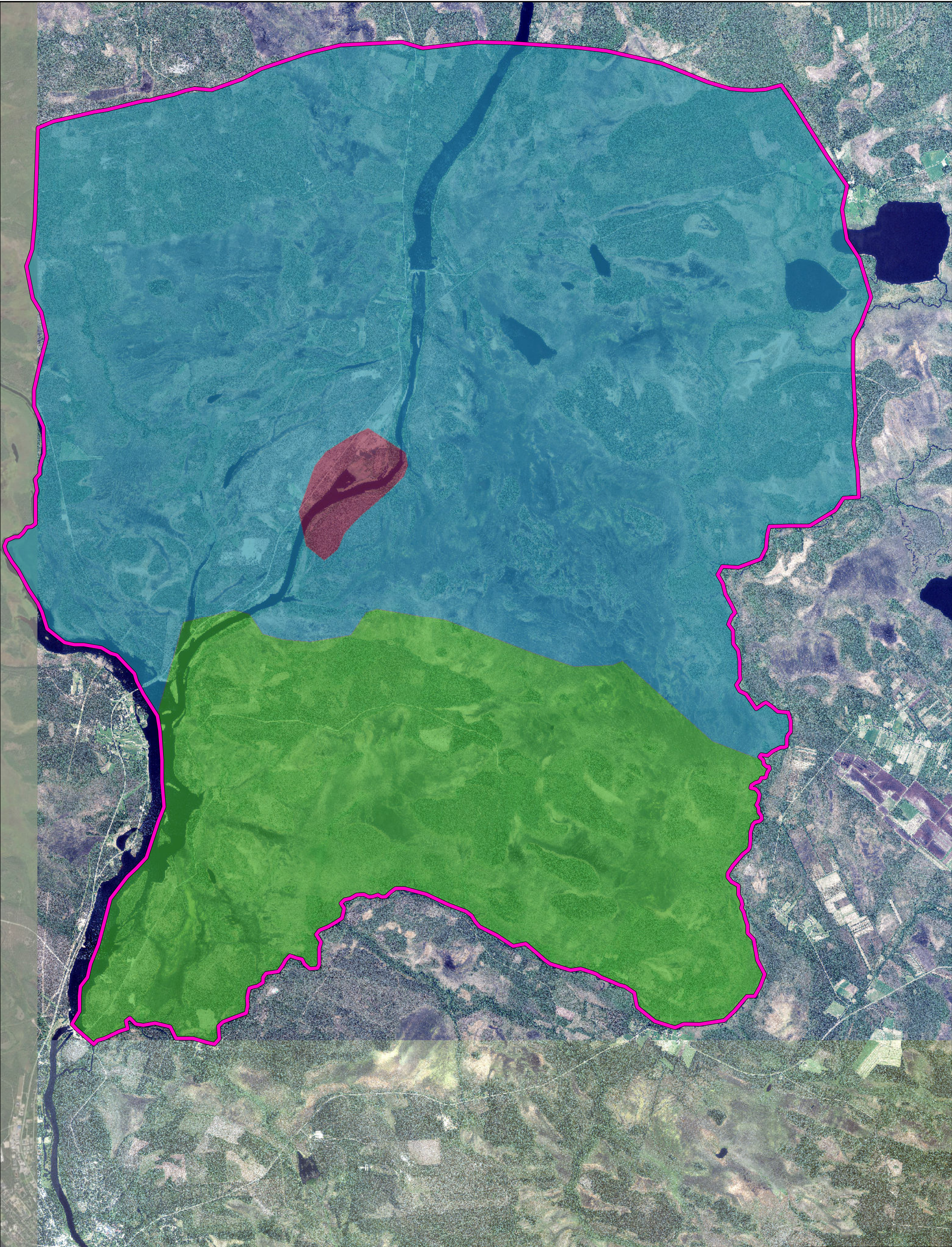
CLIENT:

Sakatti Mine

FIGURE NO.

4-5

G:\ARCGIS\4064_Sakatti\MXDs\Working\PermBR.mxd



Legend

Hydrologic Study Area

Fractured Bedrock Zones

Along Kitinen River

Kuusivaara Area

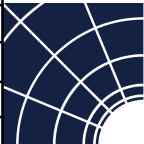
Main Area

N

01,3002,600

Meters

PROJECT NO.	4064
BY	SBM
CHECKED	HL
DRAWN	NP
DRAWING NAME	FracBR
DRAWING DATE	Apr. 25, 2022
REVISION DATE	Feb. 10, 2023

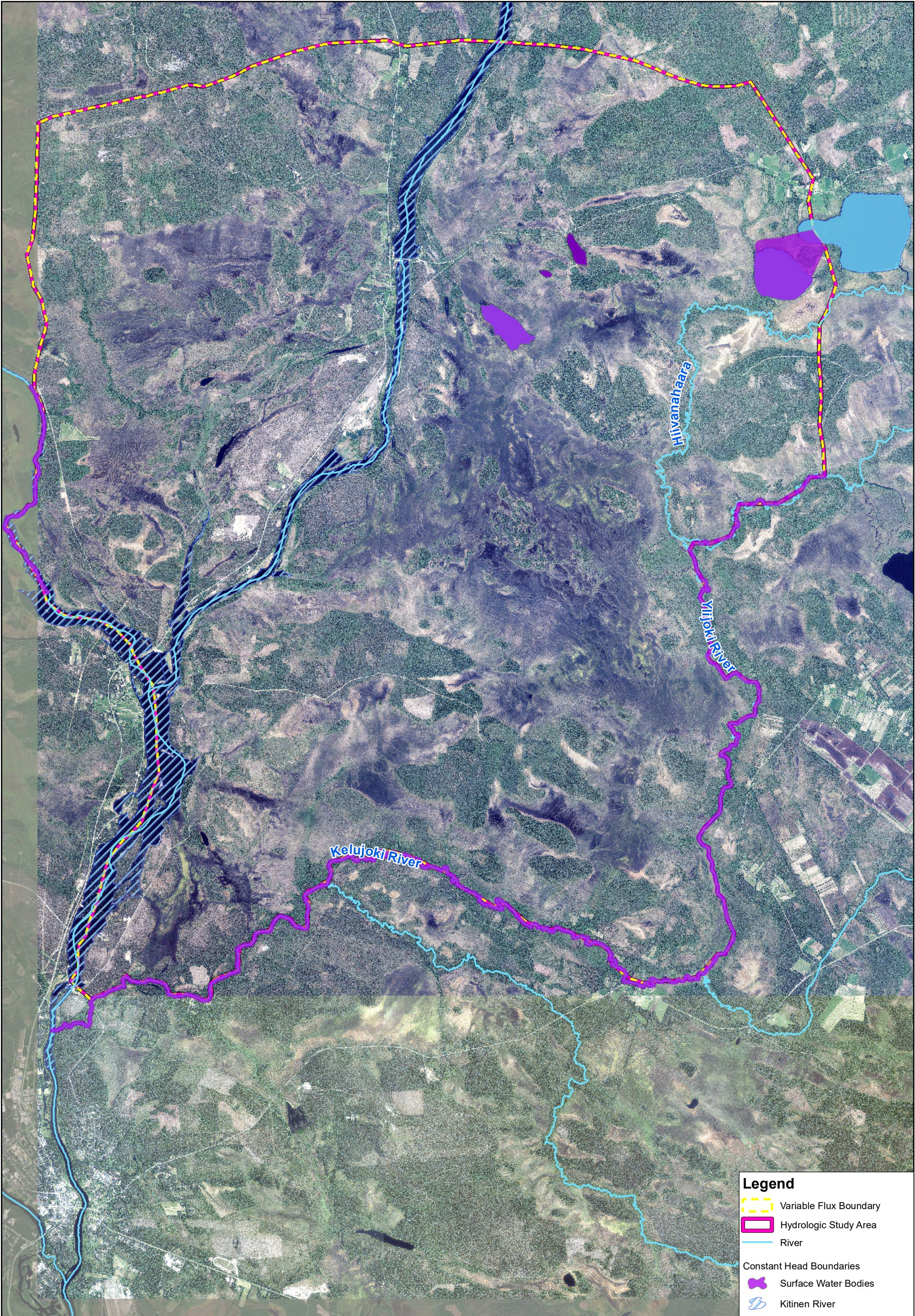


ITASCA
Denver, Inc.

Simulated Spatial Extents of the
Fractured Bedrock Units

CLIENT:
Sakatti Mine

FIGURE NO.
4-6



Legend

Variable Flux Boundary

Hydrologic Study Area

River

Constant Head Boundaries

Surface Water Bodies

Kitinen River

01,2502,500

Meters

PROJECT NO.	4064
BY	SBM
CHECKED	HL
DRAWN	NP
DRAWING NAME	SimBoundCon
DRAWING DATE	Apr. 25, 2022
REVISION DATE	Jun. 14, 2022

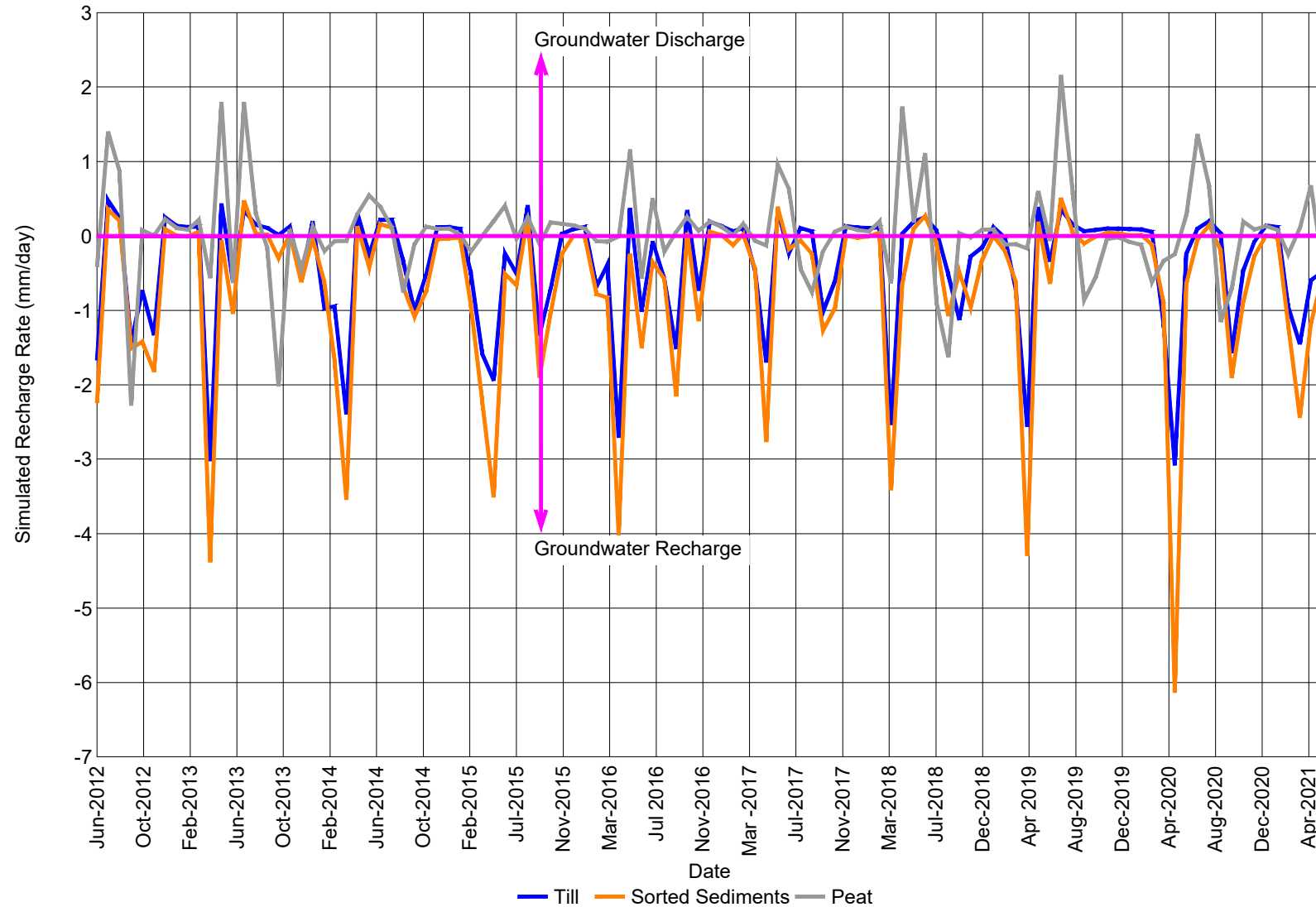


ITASCA
Denver, Inc.

Simulated Boundary Conditions
in the Groundwater Flow Model

CLIENT:
Sakatti Mine

FIGURE NO.
4-7



PROJECT NO.	4064
BY	SBM
CHECKED	HL
DRAWN	RJN
DRAWING NAME	RECHARGE
DRAWING DATE	13 JUN 2022
REVISION DATE	5 AUG 2022

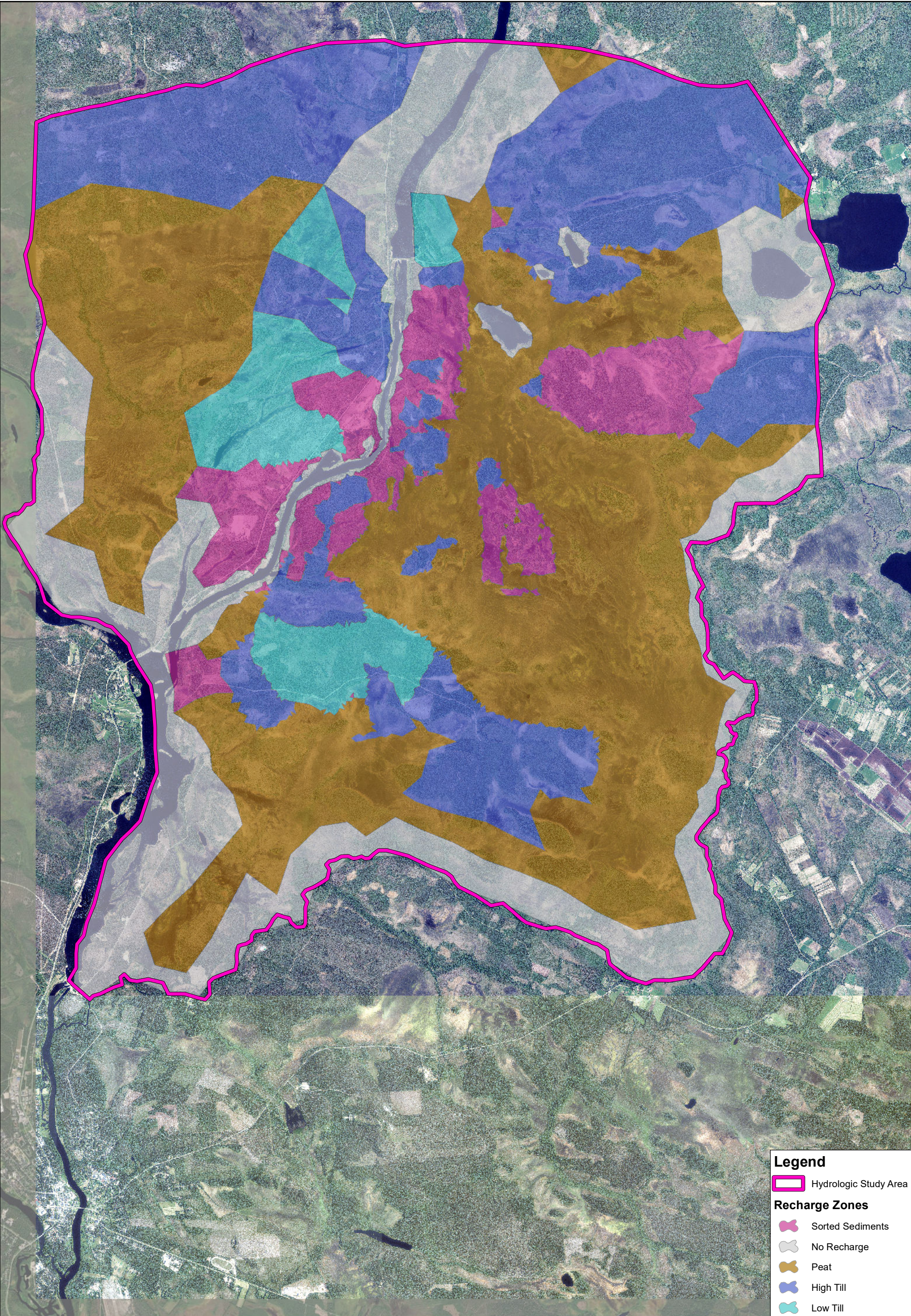


ITASCA[™]
Denver, Inc.

Simulated Recharge Rates in the
Groundwater Flow Model Based on the
MIKE SHE Model

CLIENT:
Sakatti Mine

FIGURE NO.
4-8



Legend

Hydrologic Study Area

Recharge Zones

Sorted Sediments

No Recharge

Peat

High Till

Low Till

N

01,2502,500

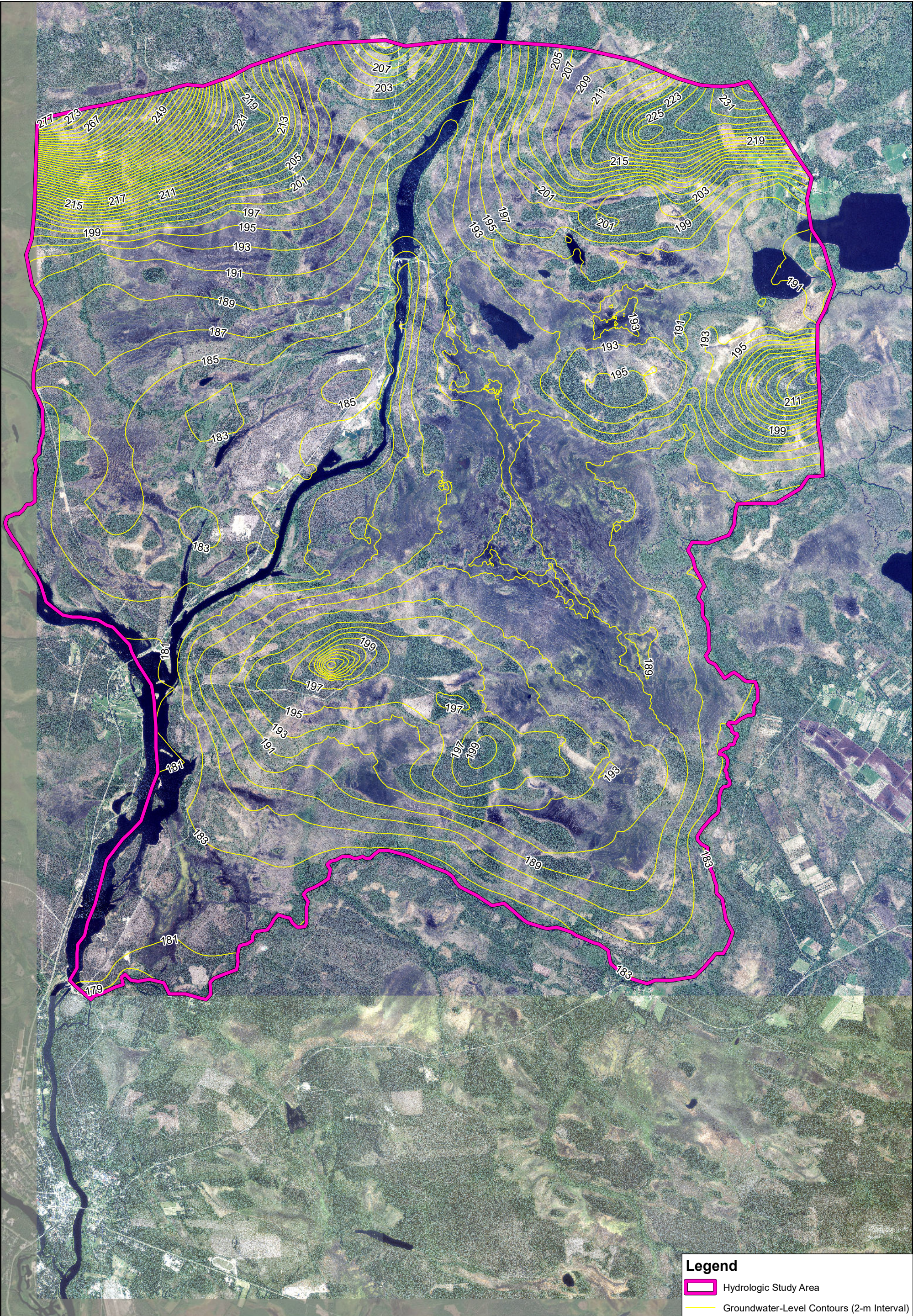
Meters

PROJECT NO.	4064
BY	SBM
CHECKED	HL
DRAWN	NP
DRAWING NAME	SimRecharge
DRAWING DATE	Apr. 25, 2022
REVISION DATE	Aug. 31, 2022


ITASCATM

Denver, Inc.


Simulated Spatial Extent of Recharge Zones in the Groundwater Flow Model	
CLIENT:	FIGURE NO.
Sakatti Mine	4-9



Legend



Hydrologic Study Area



Groundwater-Level Contours (2-m Interval)

N



0

1,250

2,500



Meters

PROJECT NO.	4064
BY	SBM
CHECKED	HL
DRAWN	NP
DRAWING NAME	SS_GW
DRAWING DATE	Apr. 25, 2022
REVISION DATE	Jun. 16, 2022



ITASCA™

Denver, Inc.

Simulated Steady-State Groundwater Levels
within the Hydrologic Study Area

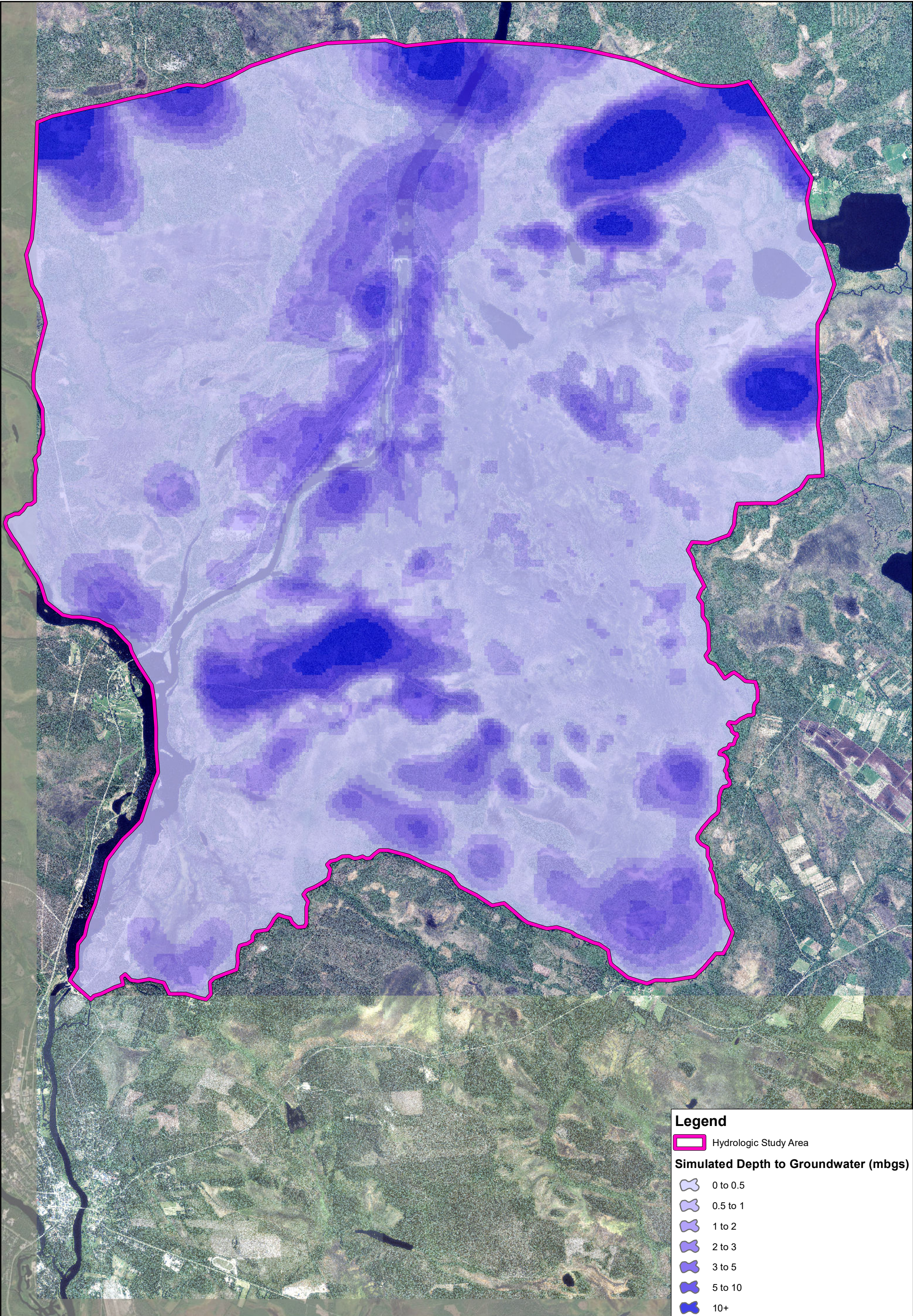
CLIENT:

Sakatti Mine


FIGURE NO.

4-10


G:\ARCGIS\4064_Sakatti\MXD\Working\SS_GW.mxd





Legend


 Hydrologic Study Area


Simulated Depth to Groundwater (mbgs)


 0 to 0.5


 0.5 to 1

 1 to 2

 2 to 3

 3 to 5

 5 to 10

 10+

N



0

1,300

2,600

Meters

PROJECT NO.	4064
BY	SBM
CHECKED	HL
DRAWN	NP
DRAWING NAME	SimDepth
DRAWING DATE	Apr. 25, 2022
REVISION DATE	May. 24, 2022



ITASCA

Denver, Inc.

Simulated Depth to Groundwater
under Steady-State Conditions

CLIENT:

Sakatti Mine

FIGURE NO.

4-11

G:\ARC\GIS\4064_Sakatti\MXDs\Working\SimDepth.mxd



Legend

Hydrologic Study Area

River

Kitinen River

Lakes

Ponds

Simulated Areas of Discharge

Areas of Discharge

Areas of Recharge

01,3002,600

Meters

PROJECT NO.	4064
BY	SBM
CHECKED	HL
DRAWN	NP
DRAWING NAME	Discharge
DRAWING DATE	Apr. 25, 2022
REVISION DATE	May. 24, 2022

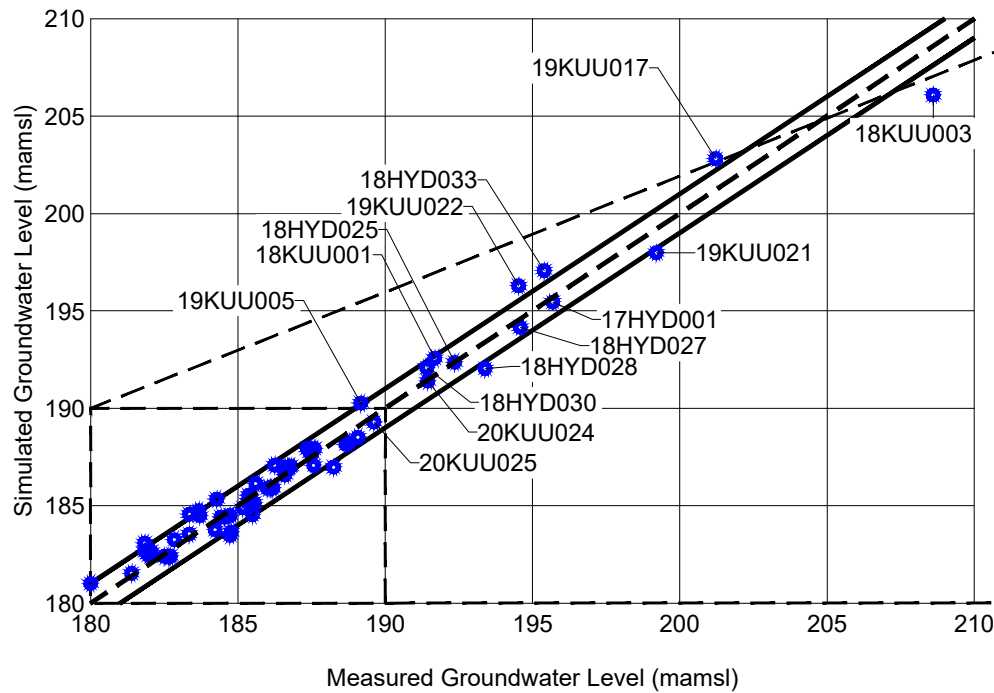
ITASCA
Denver, Inc.

Simulated Areas of Discharge and Recharge
under Steady-State Conditions

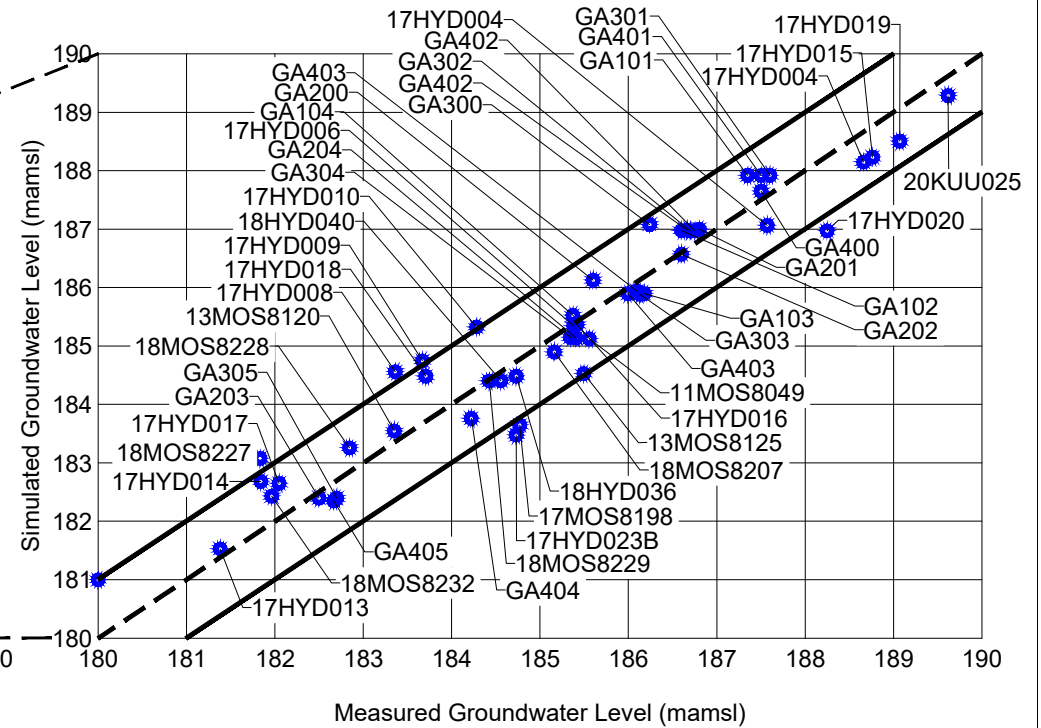
CLIENT:
Sakatti Mine

FIGURE NO.
4-12

a) Overall Model Calibration



b) Model Calibration from Range of 180 to 190 mamsl



Note: Measurement time of each data point is shown in Table 4-3.

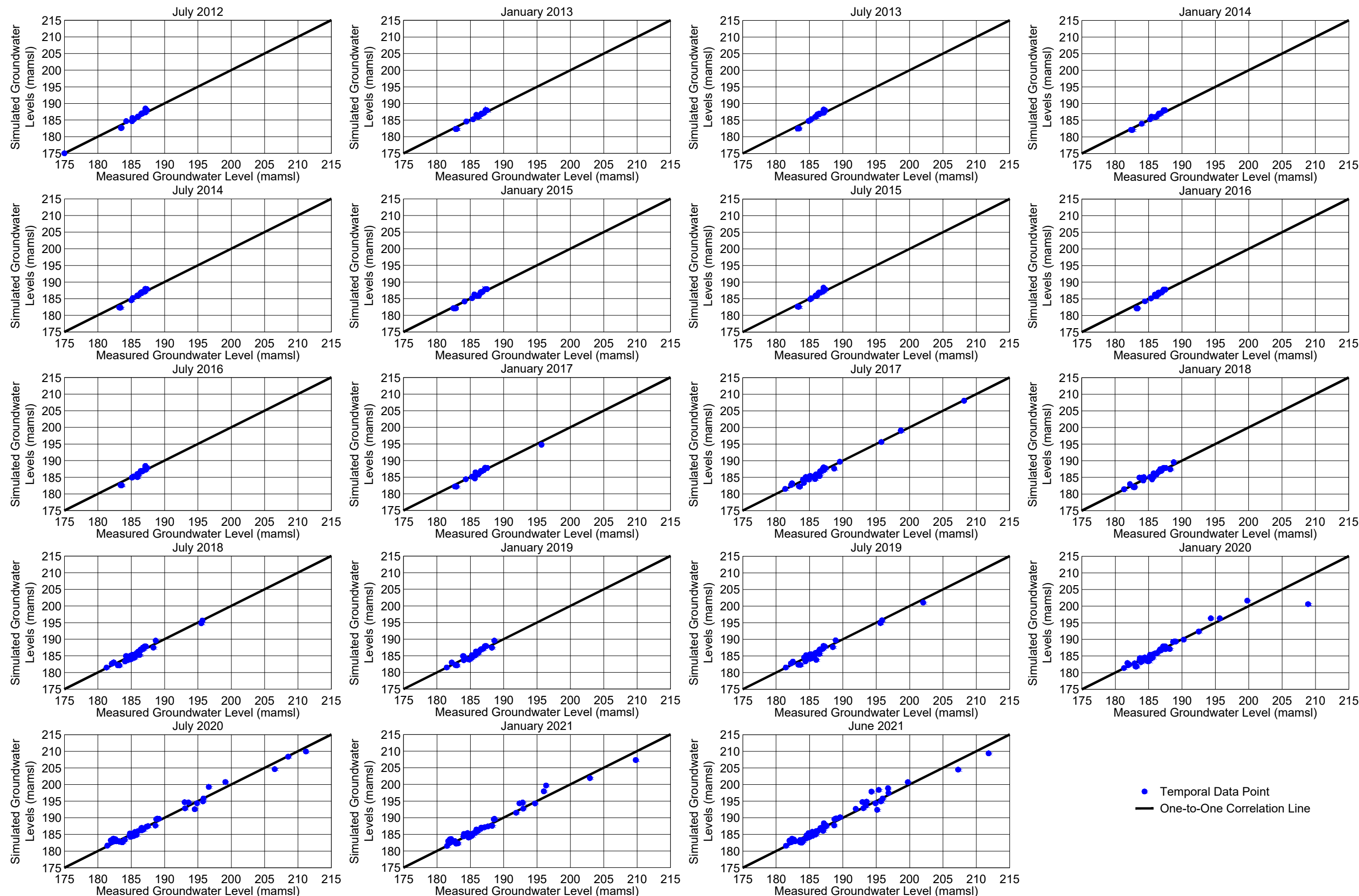
PROJECT NO.	4064
BY	SBM
CHECKED	HL
DRAWN	RJN
DRAWING NAME	SS
DRAWING DATE	25 OCT 2022
REVISION DATE	



Quality Line of Steady-State Model Calibration

CLIENT:
Sakatti Mine

FIGURE NO.
4-13



• Temporal Data Point
— One-to-One Correlation Line

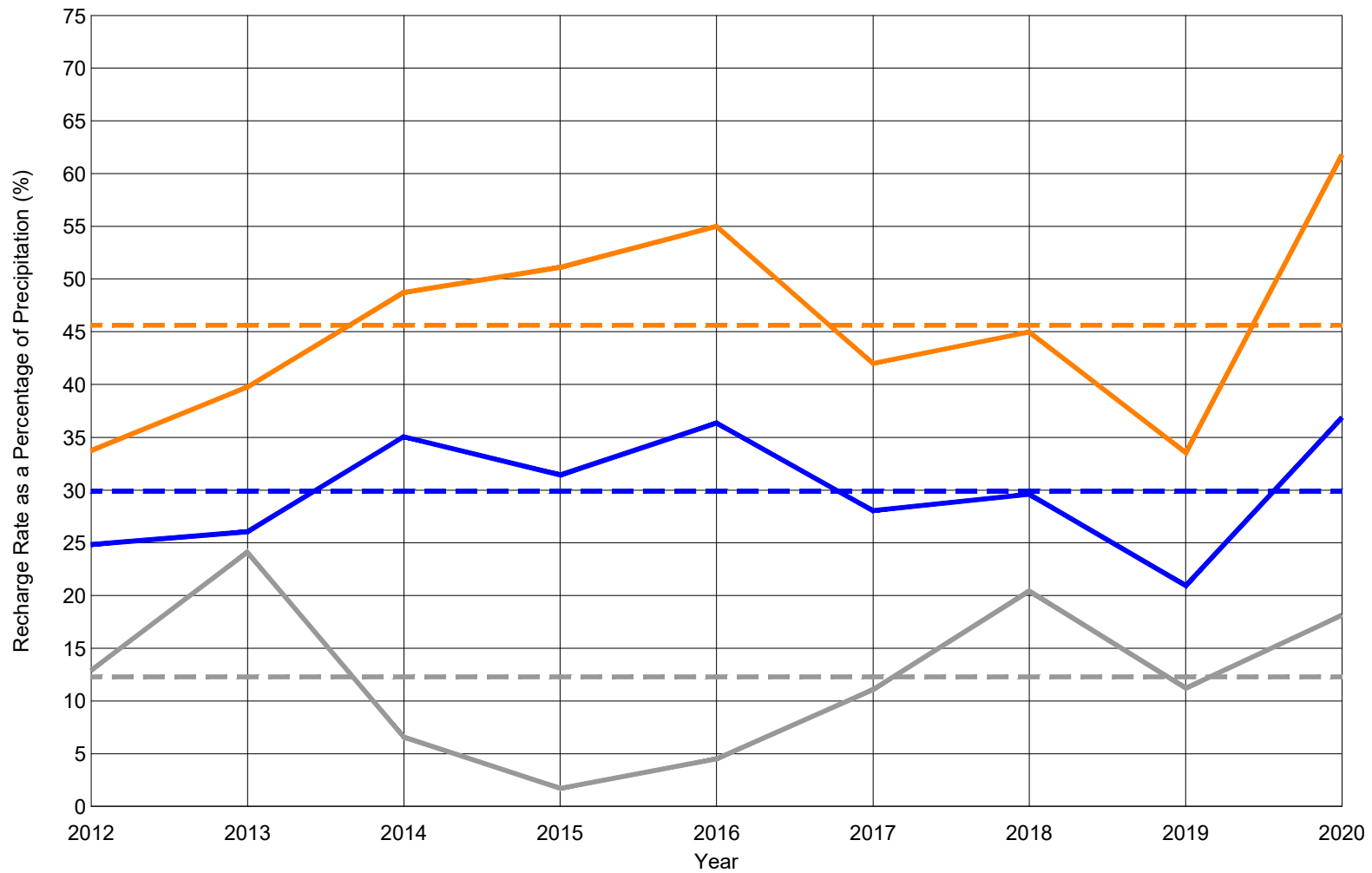
PROJECT NO.	4064
BY	SBM
CHECKED	HL
DRAWN	RJN
DRAWING NAME	TEMP
DRAWING DATE	16 JUN 2022
REVISION DATE	



Temporal Groundwater Flow Model Quality Lines of Measured versus Simulated Groundwater Levels

CLIENT:
Sakatti Mine

APPENDIX NO.
4-14



Till Sediments Peat
 — Annual — Annual — Annual
 - - Average - - Average - - Average

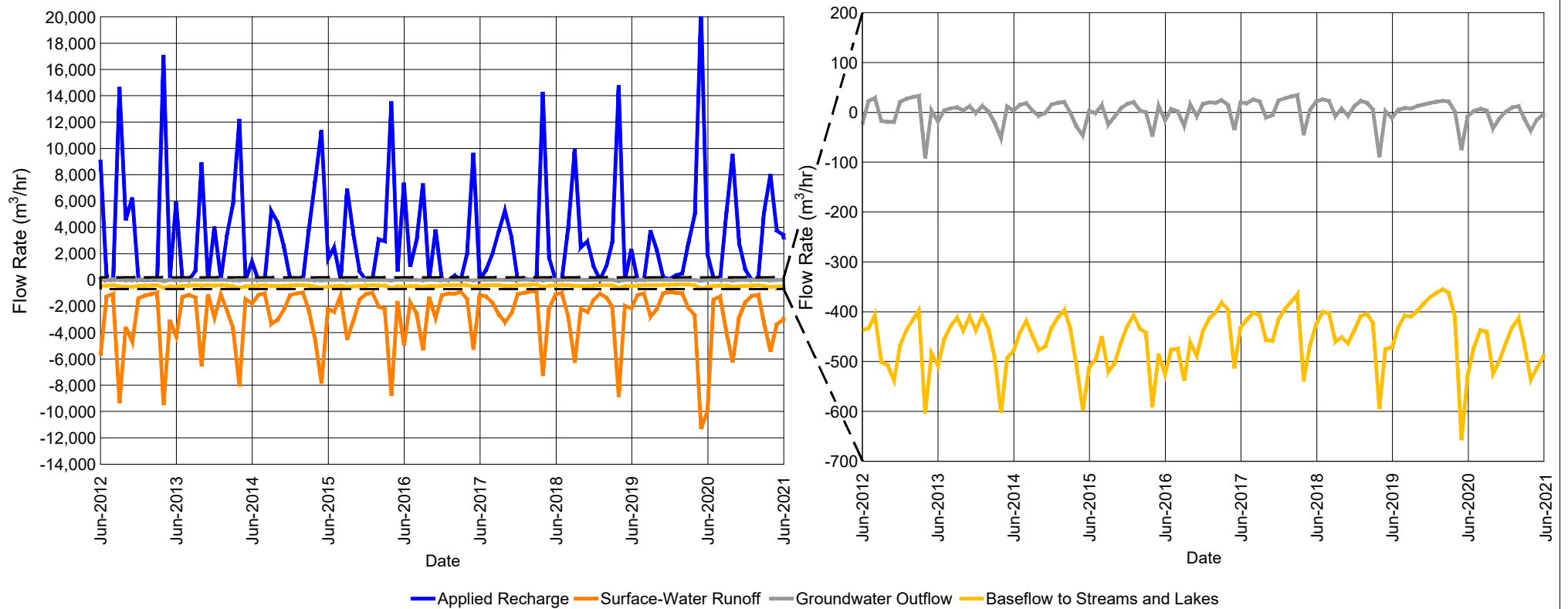
PROJECT NO.	4064
BY	SBM
CHECKED	HL
DRAWN	RJN
DRAWING NAME	CAL
DRAWING DATE	16 JUN 2022
REVISION DATE	



Simulated Annual Recharge Rates as a Percentage of Precipitation

CLIENT: Sakatti Mine

FIGURE NO.
4-15



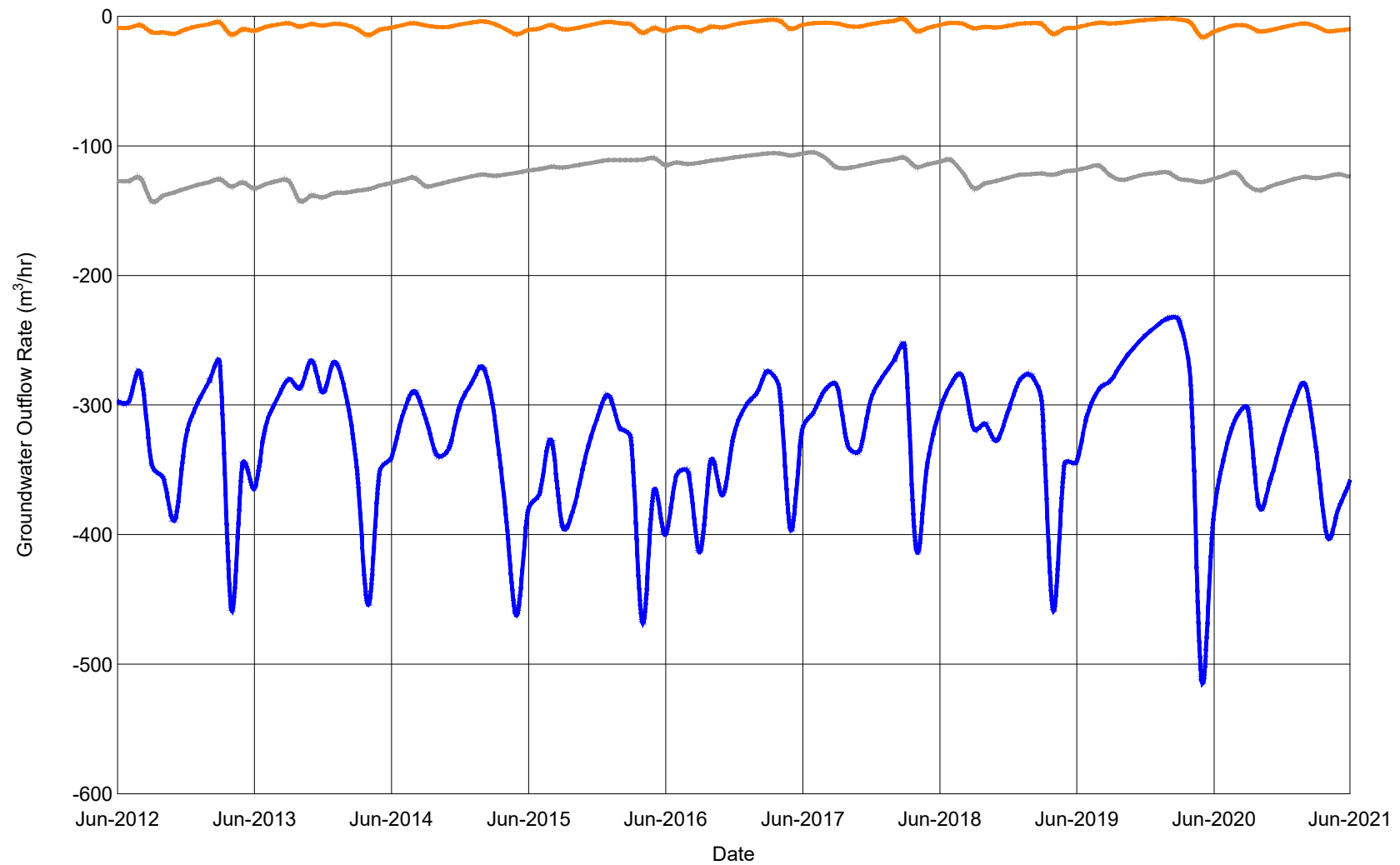
PROJECT NO.	4064
BY	SBM
CHECKED	HL
DRAWN	RJN
DRAWING NAME	CAL
DRAWING DATE	14 JUN 2022
REVISION DATE	



Calibrated Water Budget for the Groundwater Flow Model

CLIENT:
Sakatti Mine

FIGURE NO.
4-16



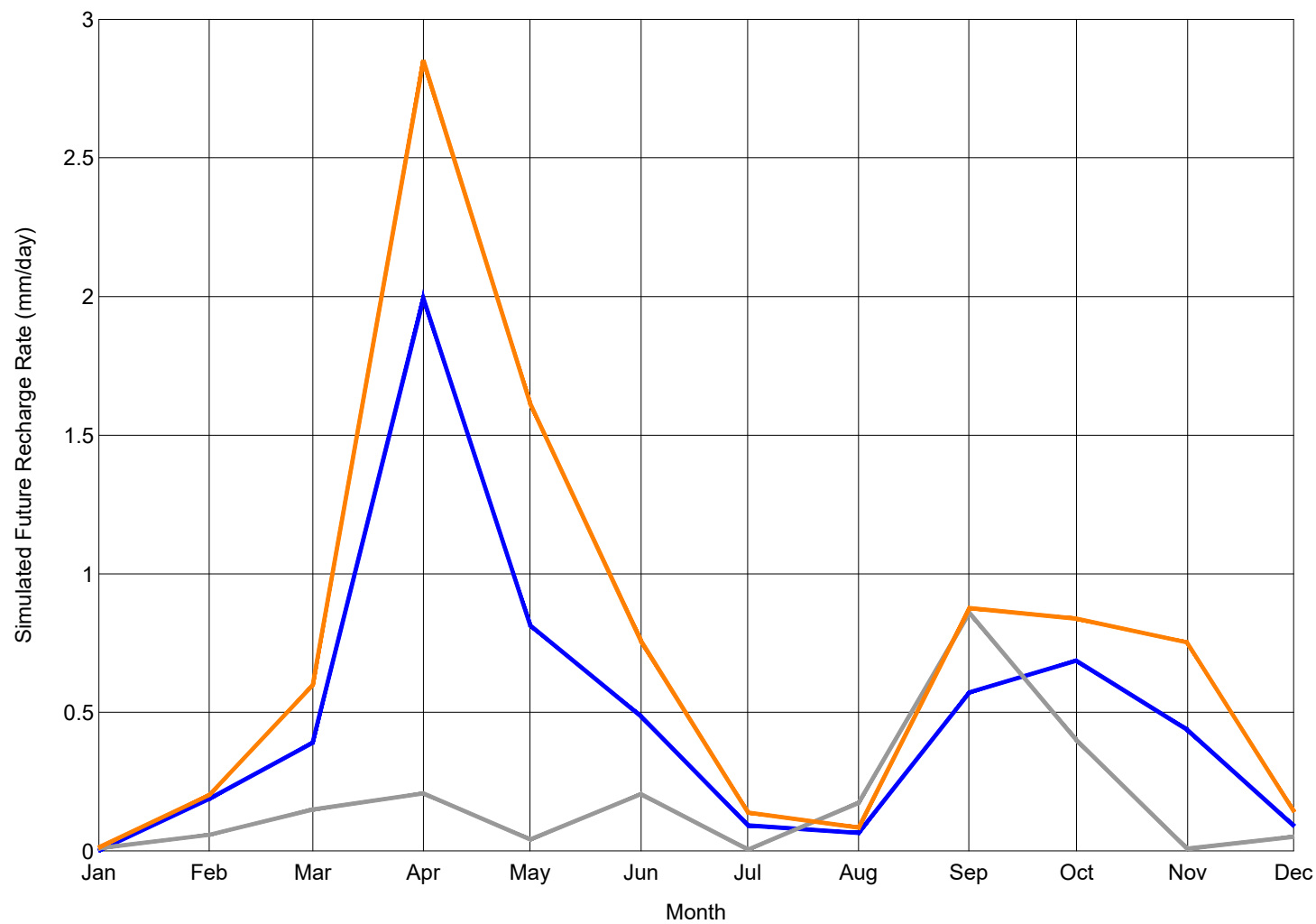
PROJECT NO.	4064
BY	SBM
CHECKED	HL
DRAWN	RJN
DRAWING NAME	CAL
DRAWING DATE	14 JUN 2022
REVISION DATE	



Calibrated Groundwater Outflow Rate
to Key Streams and Lakes

CLIENT:
Sakatti Mine

FIGURE NO.
4-17



— Till — Sorted Sediments — Peat

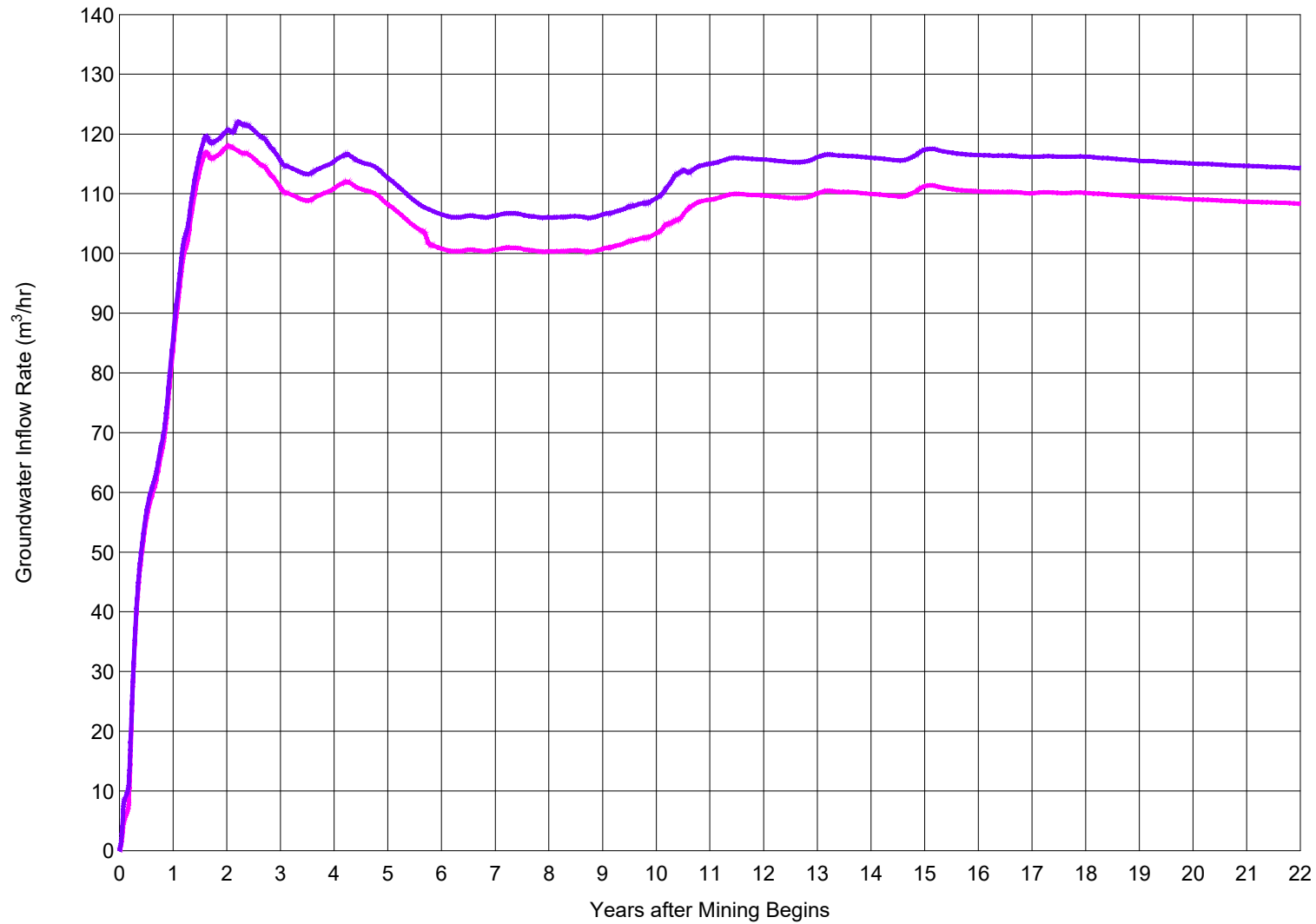
PROJECT NO.	4064
BY	SBM
CHECKED	HL
DRAWN	RJN
DRAWING NAME	RECHARGE
DRAWING DATE	13 JUN 2022
REVISION DATE	



Simulated Future Recharge Rates

CLIENT:
Sakatti Mine

FIGURE NO.
5-1



— 65% Success in Grouting — 80% Success in Grouting

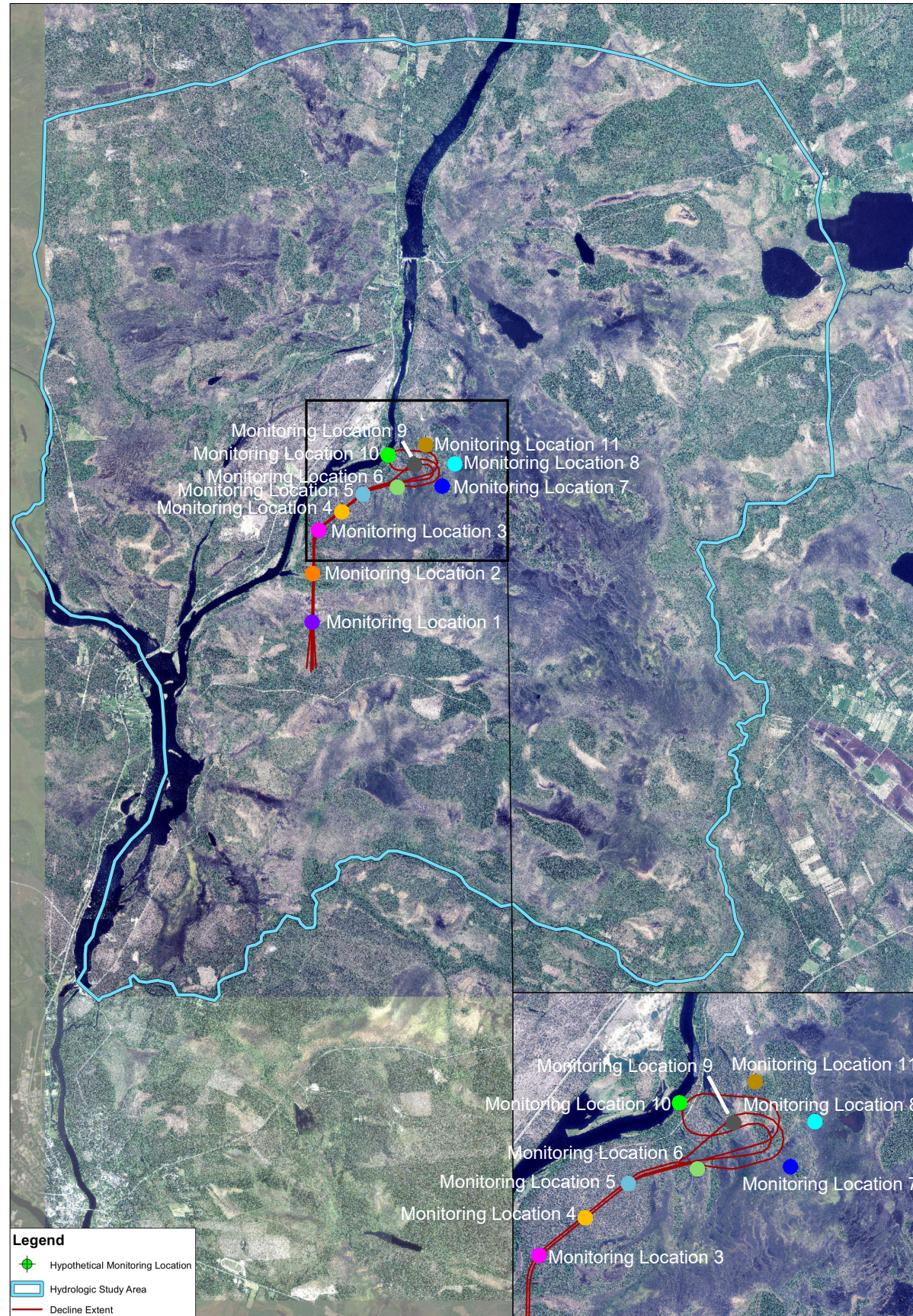
PROJECT NO.	4064
BY	SBM
CHECKED	HL
DRAWN	RJN
DRAWING NAME	PRED
DRAWING DATE	9 JAN 2023
REVISION DATE	



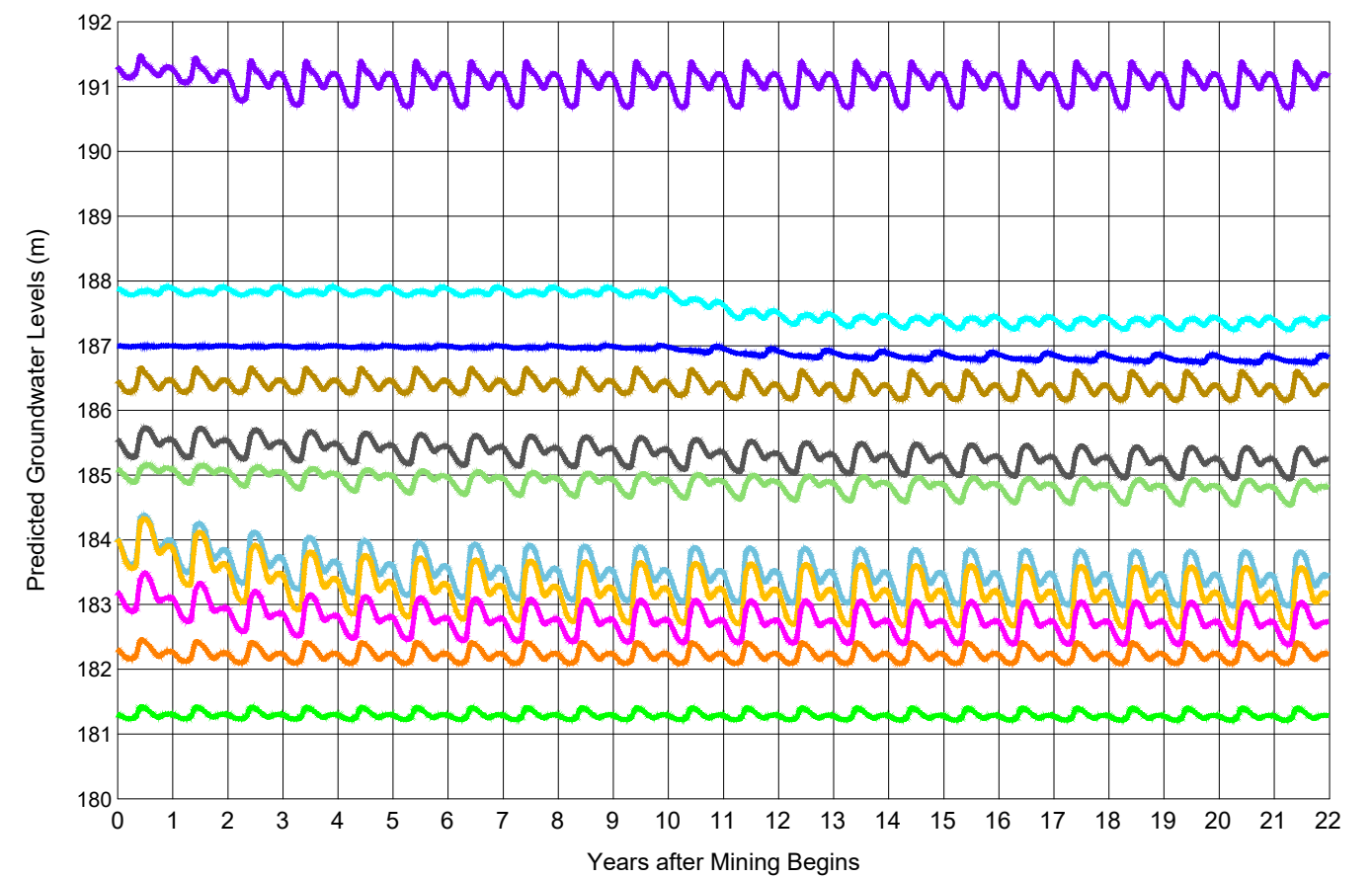
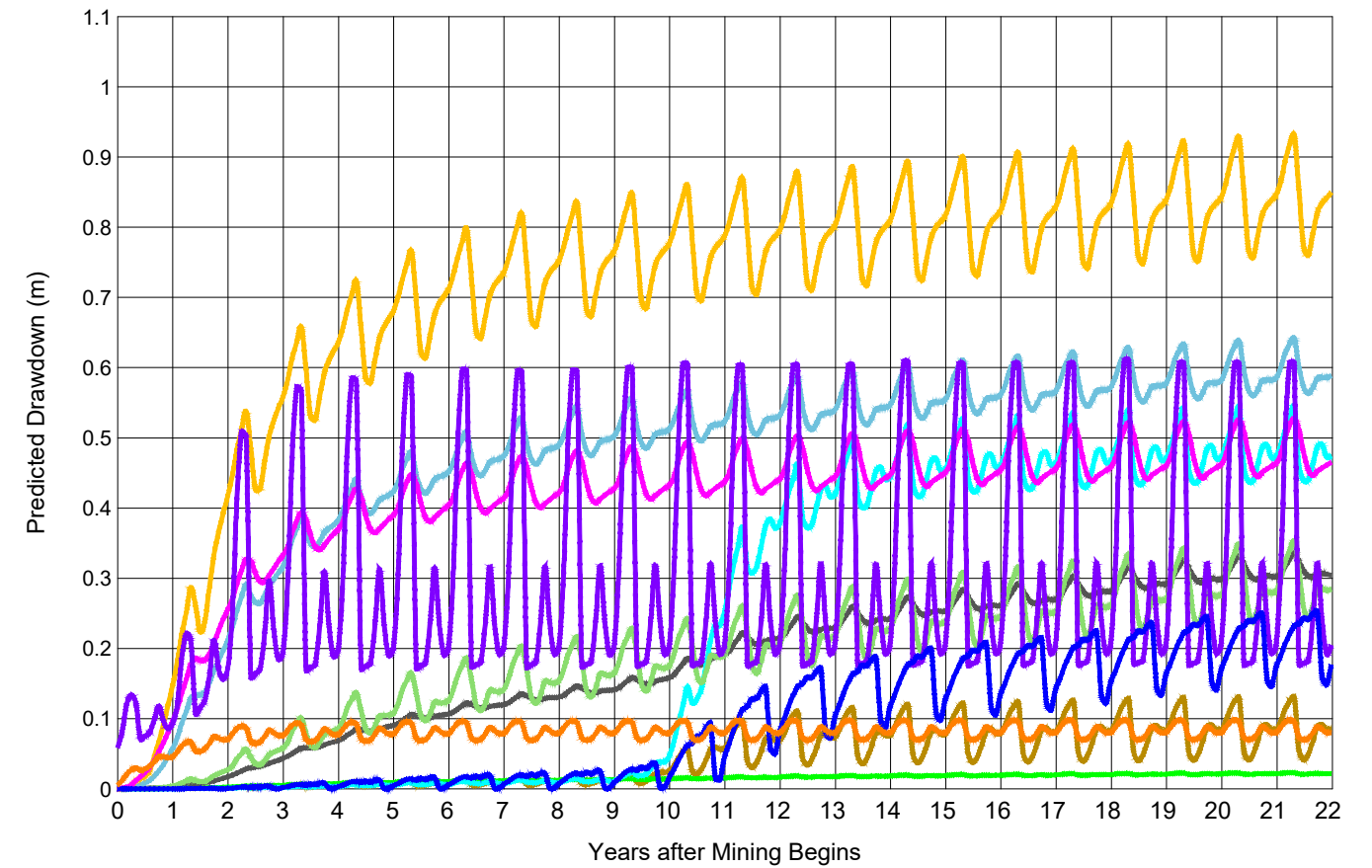
Predicted Groundwater Inflow for the
65% and 80% Success in Grouting Scenarios

CLIENT:
Sakatti Mine

FIGURE NO.
5-2



Monitoring Location 1 Monitoring Location 2 Monitoring Location 3 Monitoring Location 4
 Monitoring Location 5 Monitoring Location 6 Monitoring Location 7 Monitoring Location 8
 Monitoring Location 9 Monitoring Location 10 Monitoring Location 11



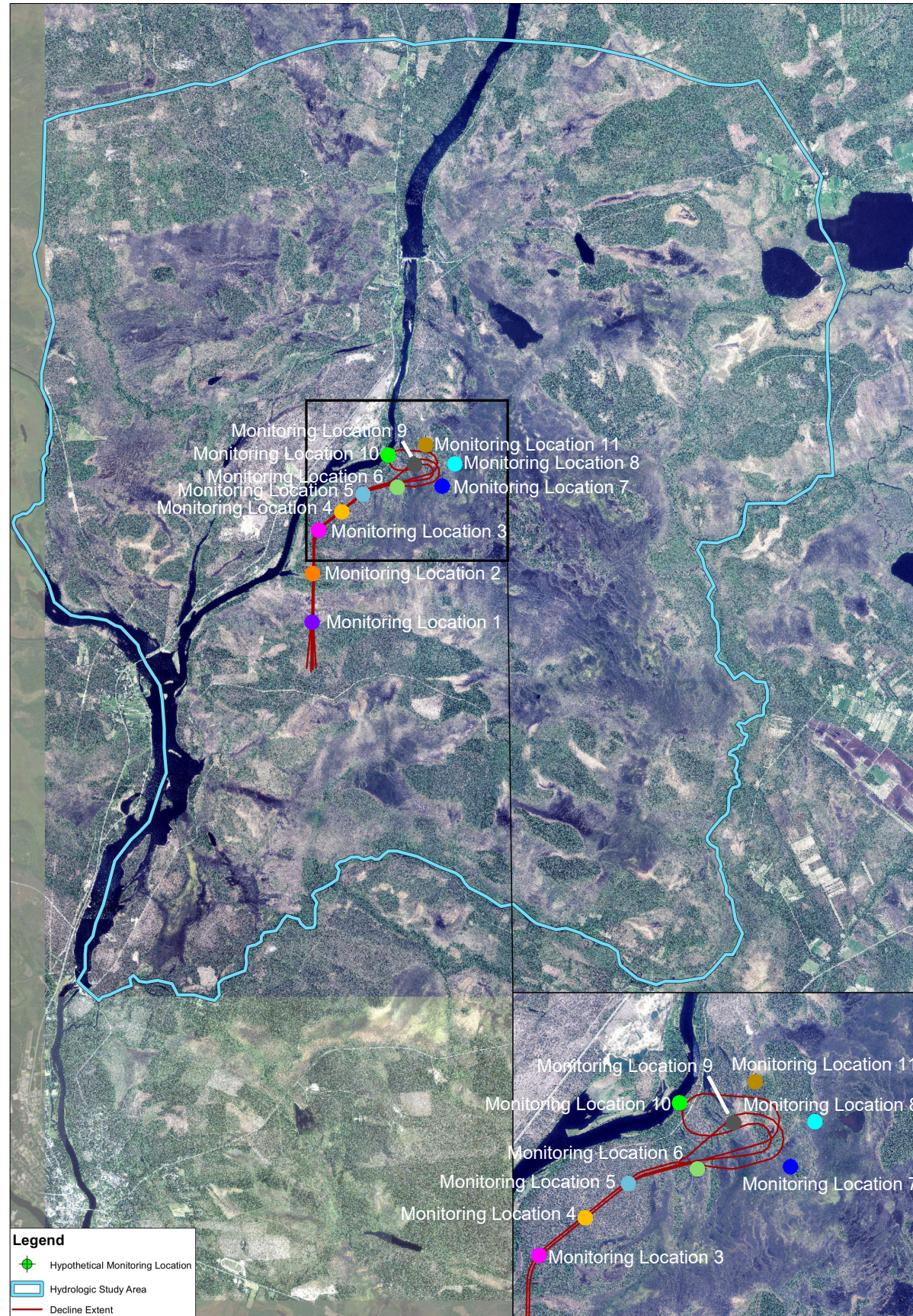
PROJECT NO.	4064
BY	SBM
CHECKED	HL
DRAWN	RJN
DRAWING NAME	DD
DRAWING DATE	25 OCT 2022
REVISION DATE	



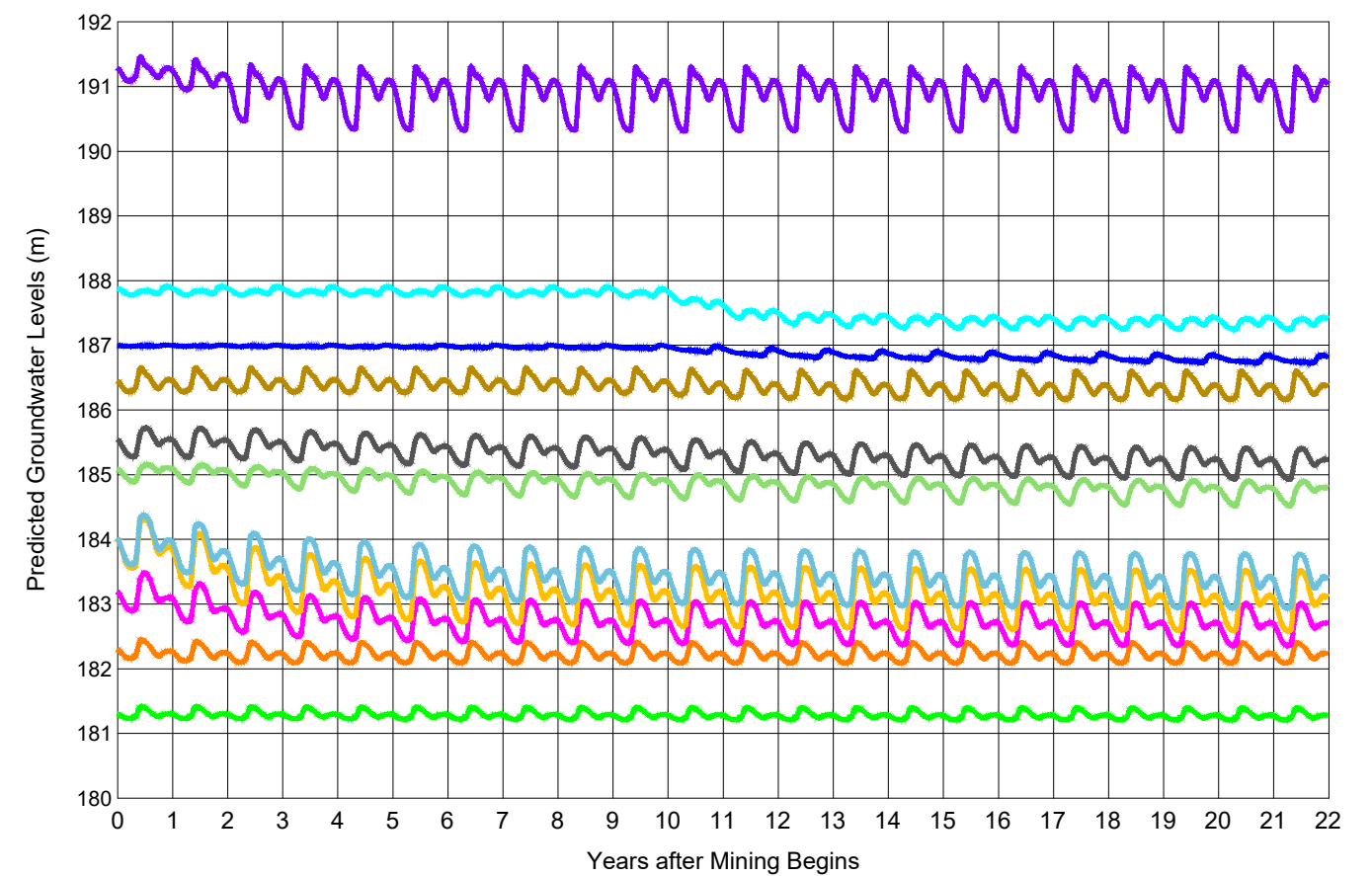
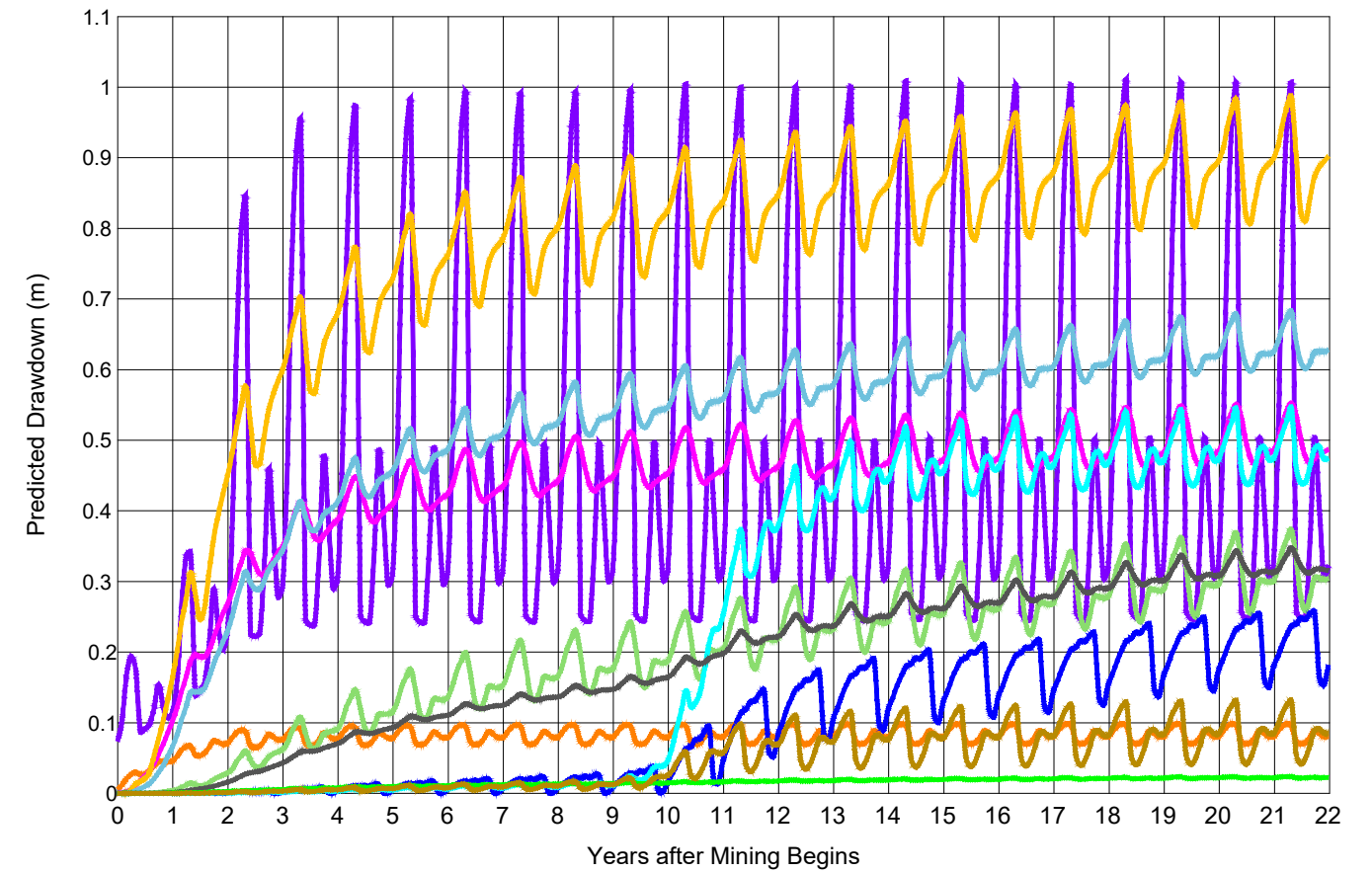
Predicted Drawdown over the LOM at Key Locations around the Mine Area for the 80% Success in Grouting Scenario

CLIENT:
Sakatti Mine

FIGURE NO.
5-3a



Monitoring Location 1 Monitoring Location 2 Monitoring Location 3 Monitoring Location 4
 Monitoring Location 5 Monitoring Location 6 Monitoring Location 7 Monitoring Location 8
 Monitoring Location 9 Monitoring Location 10 Monitoring Location 11



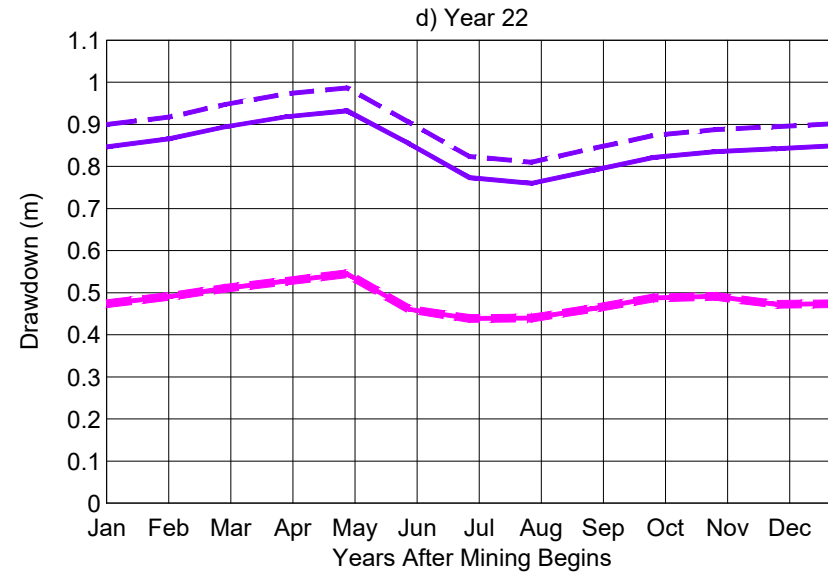
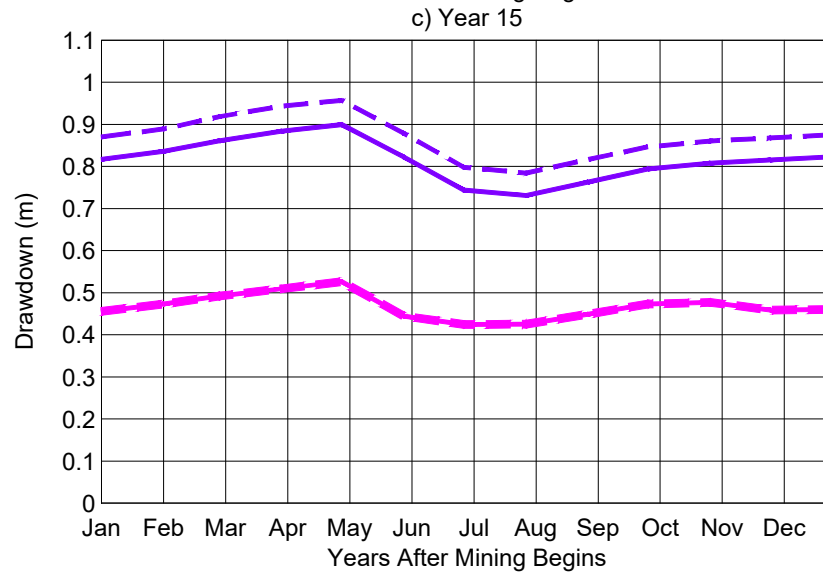
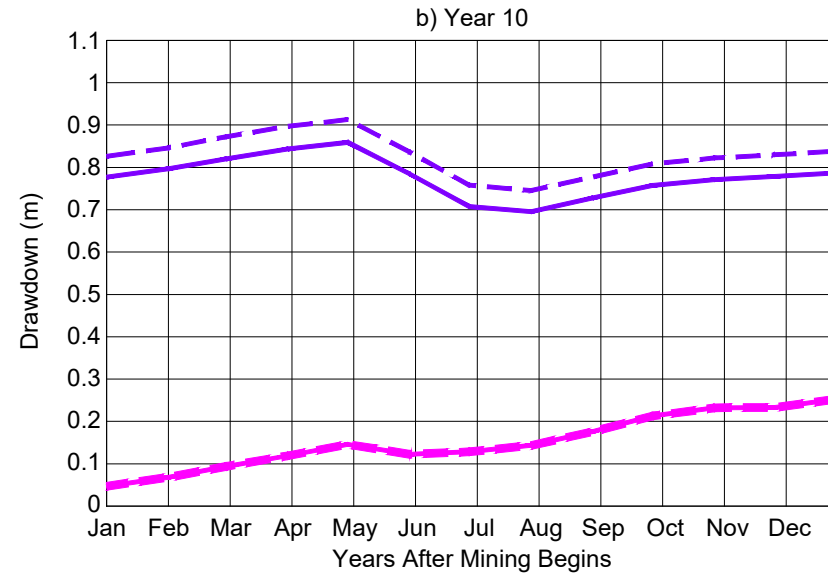
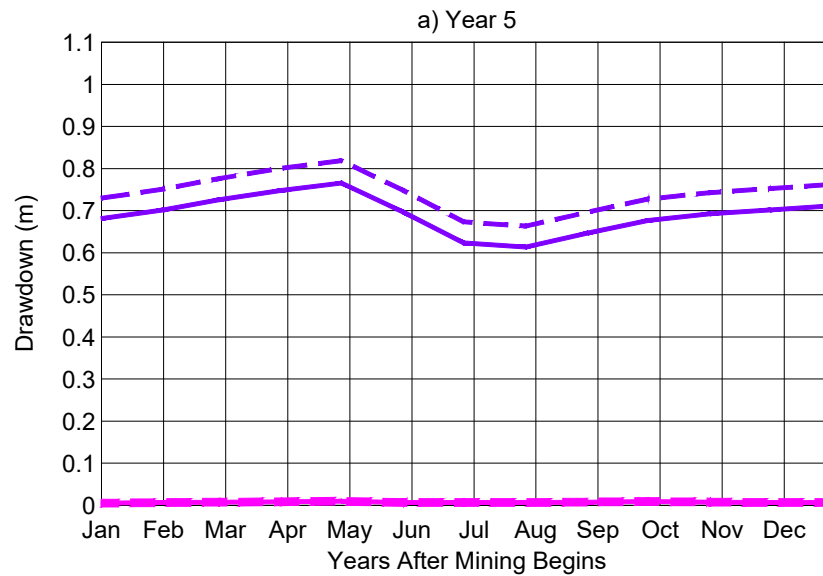
PROJECT NO.	4064
BY	SBM
CHECKED	HL
DRAWN	RJN
DRAWING NAME	DD
DRAWING DATE	25 OCT 2022
REVISION DATE	



Predicted Drawdown over the LOM at Key Locations around the Mine Area for the 65% Success in Grouting Scenario

CLIENT:
Sakatti Mine

FIGURE NO.
5-3b



Monitoring Location 4

- 65% Success in Grouting
- 80% Success in Grouting

Monitoring Location 8

- 65% Success in Grouting
- 80% Success in Grouting

PROJECT NO.	4064
BY	SBM
CHECKED	HL
DRAWN	RJN
DRAWING NAME	YEAR
DRAWING DATE	25 OCT 2022
REVISION DATE	

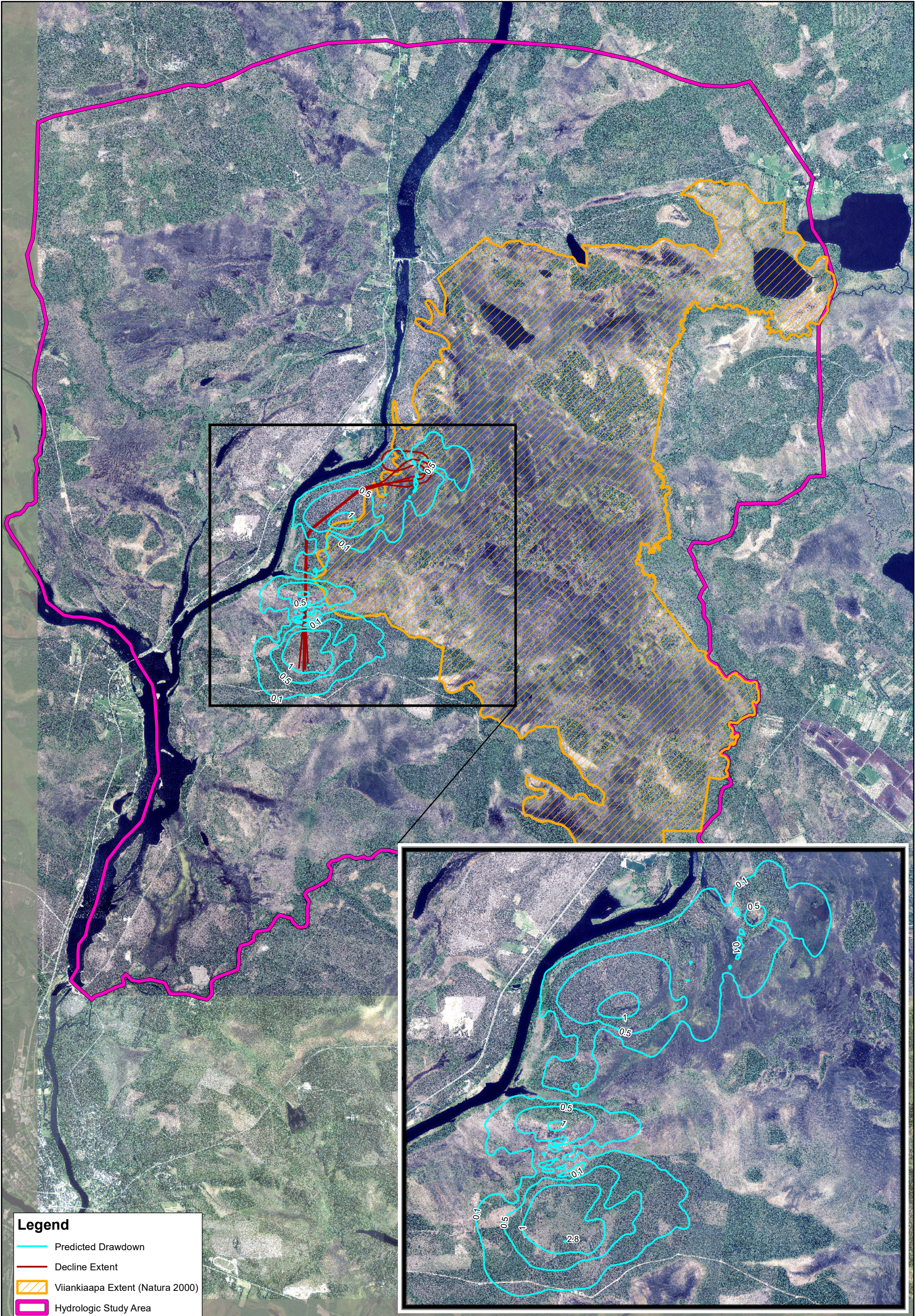


ITASCATM
Denver, Inc.

Monitoring Location Drawdown for
Selected Years over the Life of Mine

CLIENT:
Sakatti Mine

FIGURE NO.
5-4



Legend

Predicted Drawdown

Decline Extent

Viankiaapa Extent (Natura 2000)

Hydrologic Study Area

N

0

1,250

2,500

Meters

PROJECT NO.	4064
BY	SBM
CHECKED	HL
DRAWN	NP
DRAWING NAME	Draw_Prac
DRAWING DATE	Apr. 25, 2022
REVISION DATE	Jan. 12, 2023

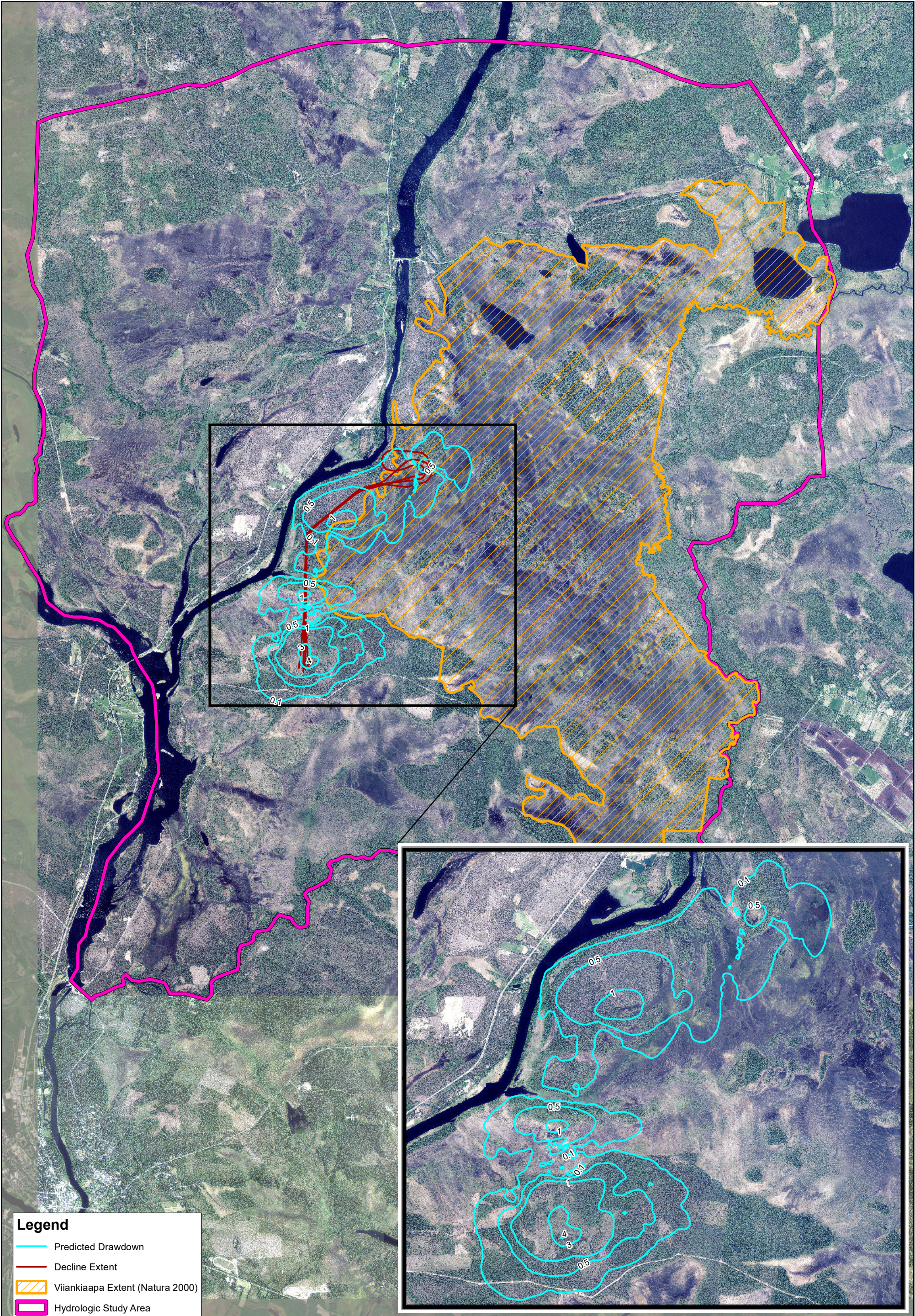
ITASCA
Denver, Inc.

Predicted Drawdown at the End of Mining
for the 80% Success in Grouting Scenario

CLIENT:
Sakatti Mine

FIGURE NO.
5-5a

G:\ARCGIS\4064_Sakatti\MXD\Working\Draw_Prac.mxd



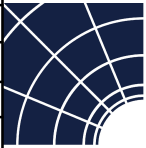
Legend

- Predicted Drawdown
- Decline Extent
- Viankiaapa Extent (Natura 2000)
- Hydrologic Study Area

N

0 1,250 2,500 Meters

PROJECT NO.	4064
BY	SBM
CHECKED	HL
DRAWN	NP
DRAWING NAME	Draw_Challenge
DRAWING DATE	Apr. 25, 2022
REVISION DATE	Jan. 13, 2023

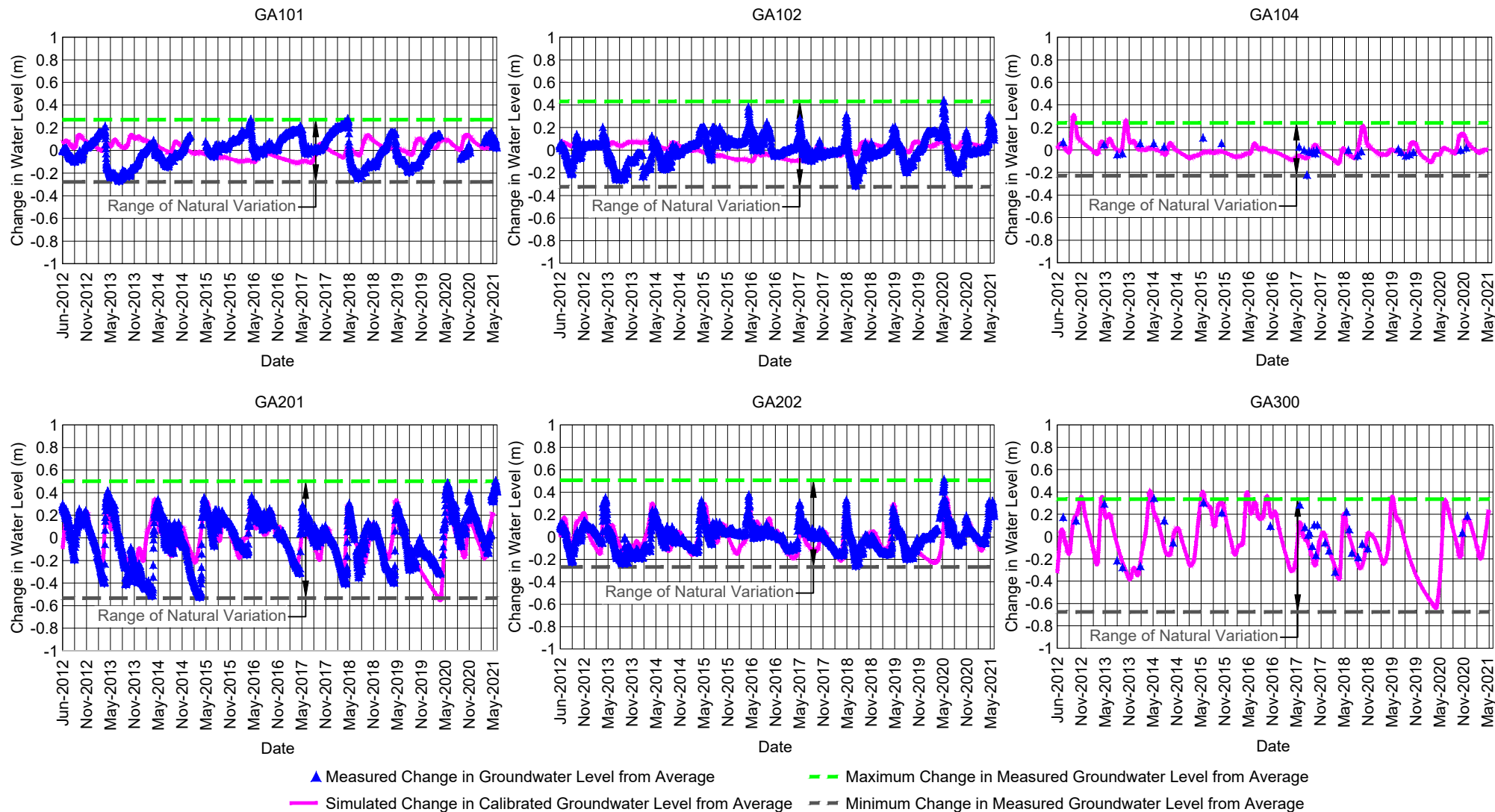


ITASCA
Denver, Inc.

Predicted Drawdown at the End of Mining
for the 65% Success in Grouting Scenario

CLIENT:
Sakatti Mine

FIGURE NO.
5-5b



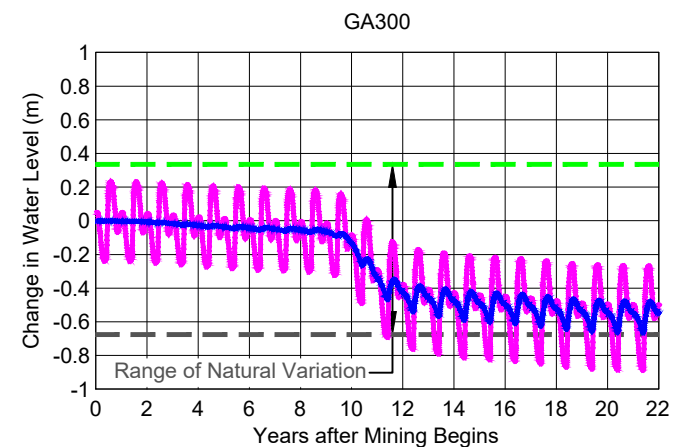
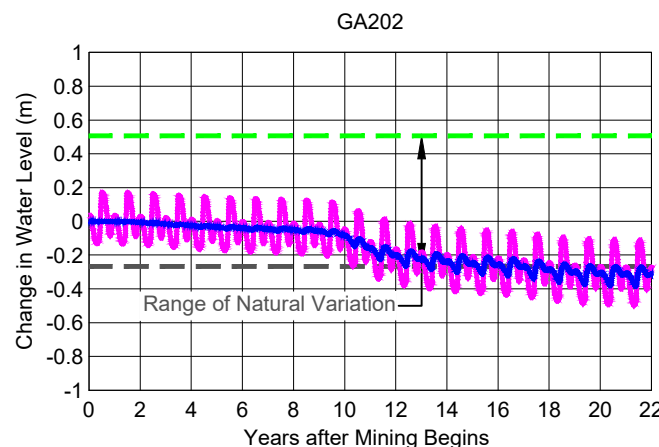
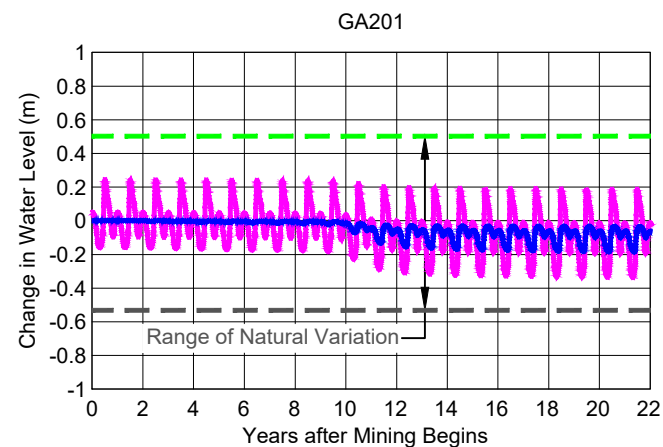
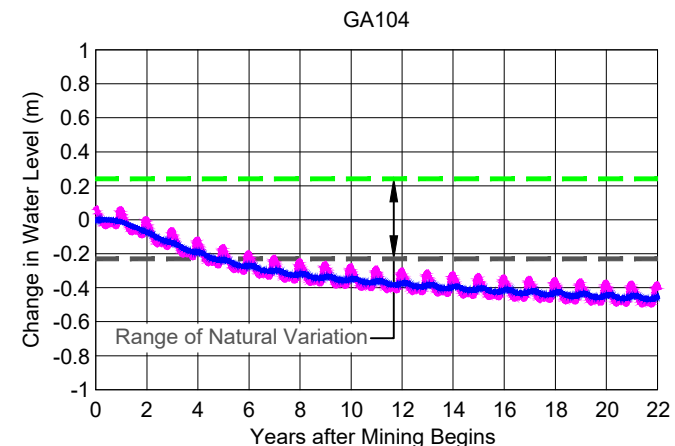
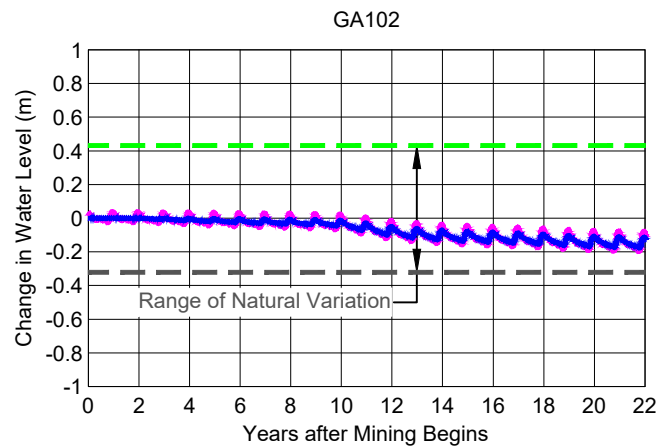
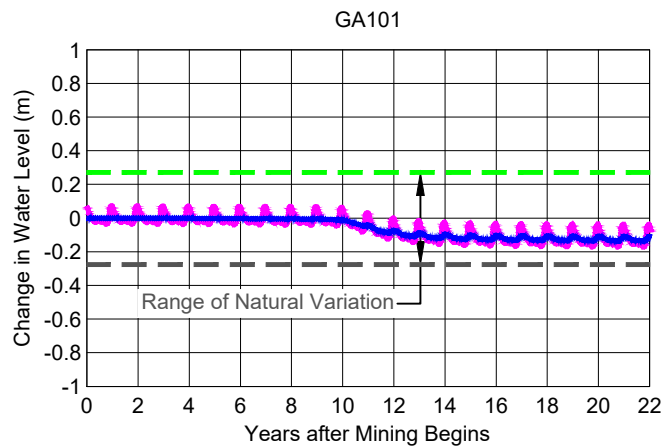
PROJECT NO.	4064
BY	SBM
CHECKED	HL
DRAWN	RJN
DRAWING NAME	WLC
DRAWING DATE	9 JAN 2023
REVISION DATE	



Comparison of Measured versus Simulated Seasonal Groundwater-Level Changes

CLIENT:
Sakatti Mine

FIGURE NO.
5-6



— Predicted Drawdown
 — Predicted Change in Groundwater Level from Average
 — Maximum Change in Measured Groundwater Level from Average from 2012-2021
 — Minimum Change in Measured Groundwater Level from Average from 2012-2021

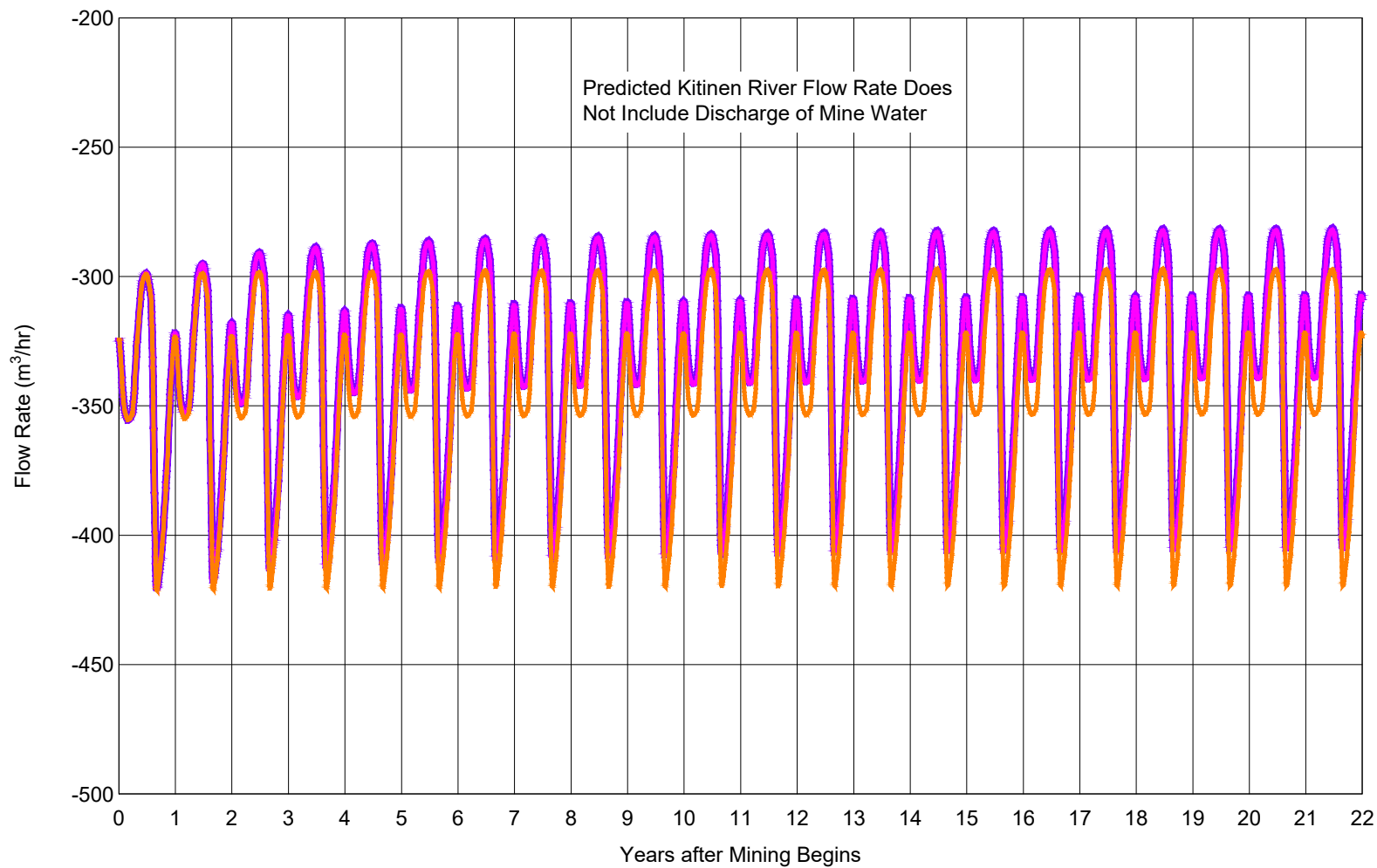
PROJECT NO.	4064
BY	SBM
CHECKED	HL
DRAWN	RJN
DRAWING NAME	WLC
DRAWING DATE	9 JAN 2023
REVISION DATE	



Predictions of Seasonal Groundwater-Level Changes for the 80% Success in Grouting with the NE Deposit Scenario

CLIENT:
Sakatti Mine

FIGURE NO.
5-7



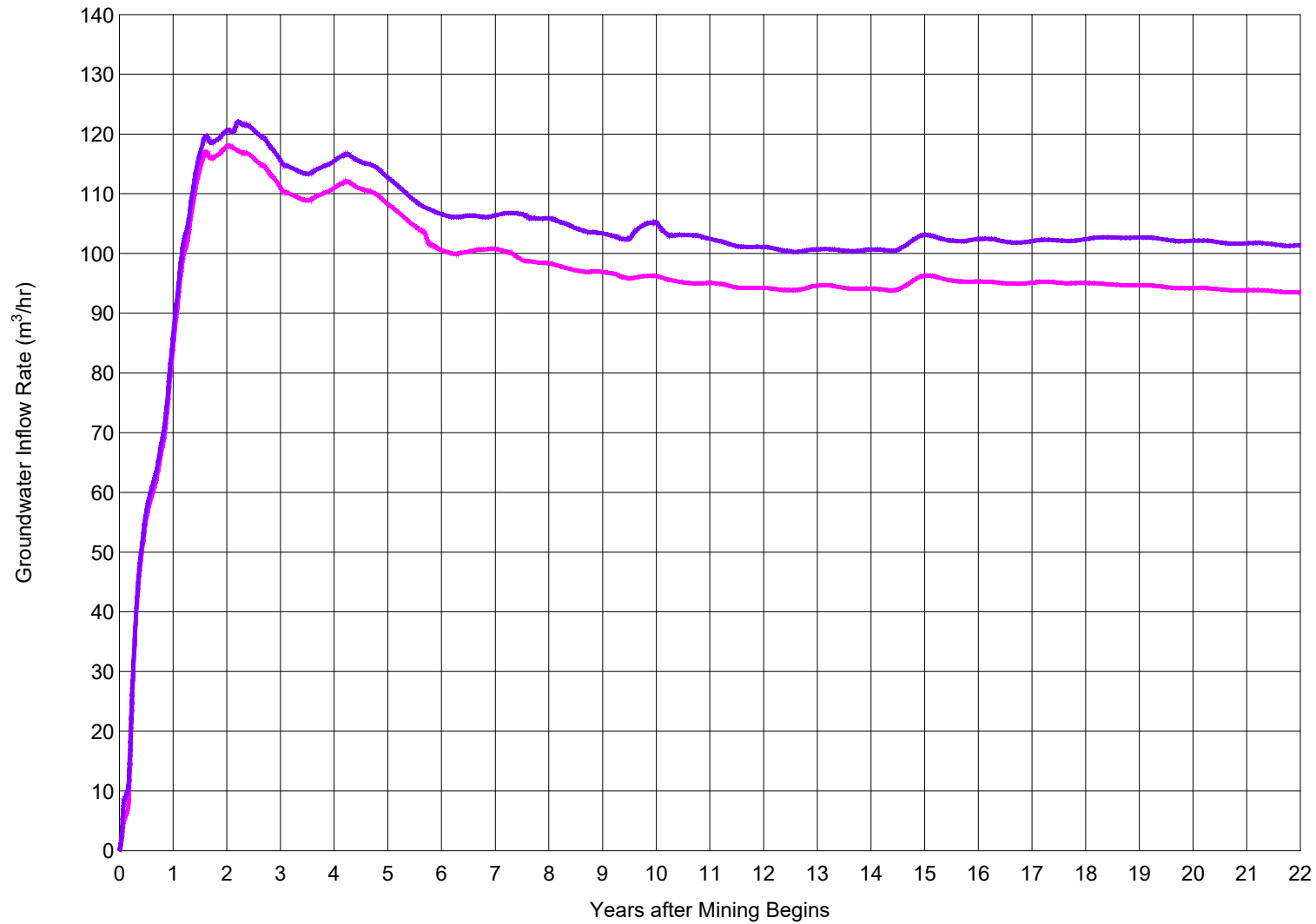
PROJECT NO.	4064
BY	SBM
CHECKED	HL
DRAWN	RJN
DRAWING NAME	PRED
DRAWING DATE	9 JAN 2023
REVISION DATE	



Predicted Baseflow to the Kitinen River
for the 65% and 80% Success in Grouting
with NE Deposit Scenarios

CLIENT:
Sakatti Mine

FIGURE NO.
5-8



— 65% Success in Grouting without the NE Deposit
 — 80% Success in Grouting without the NE Deposit

PROJECT NO.	4064
BY	SBM
CHECKED	HL
DRAWN	RJN
DRAWING NAME	PRED
DRAWING DATE	9 JAN 2023
REVISION DATE	

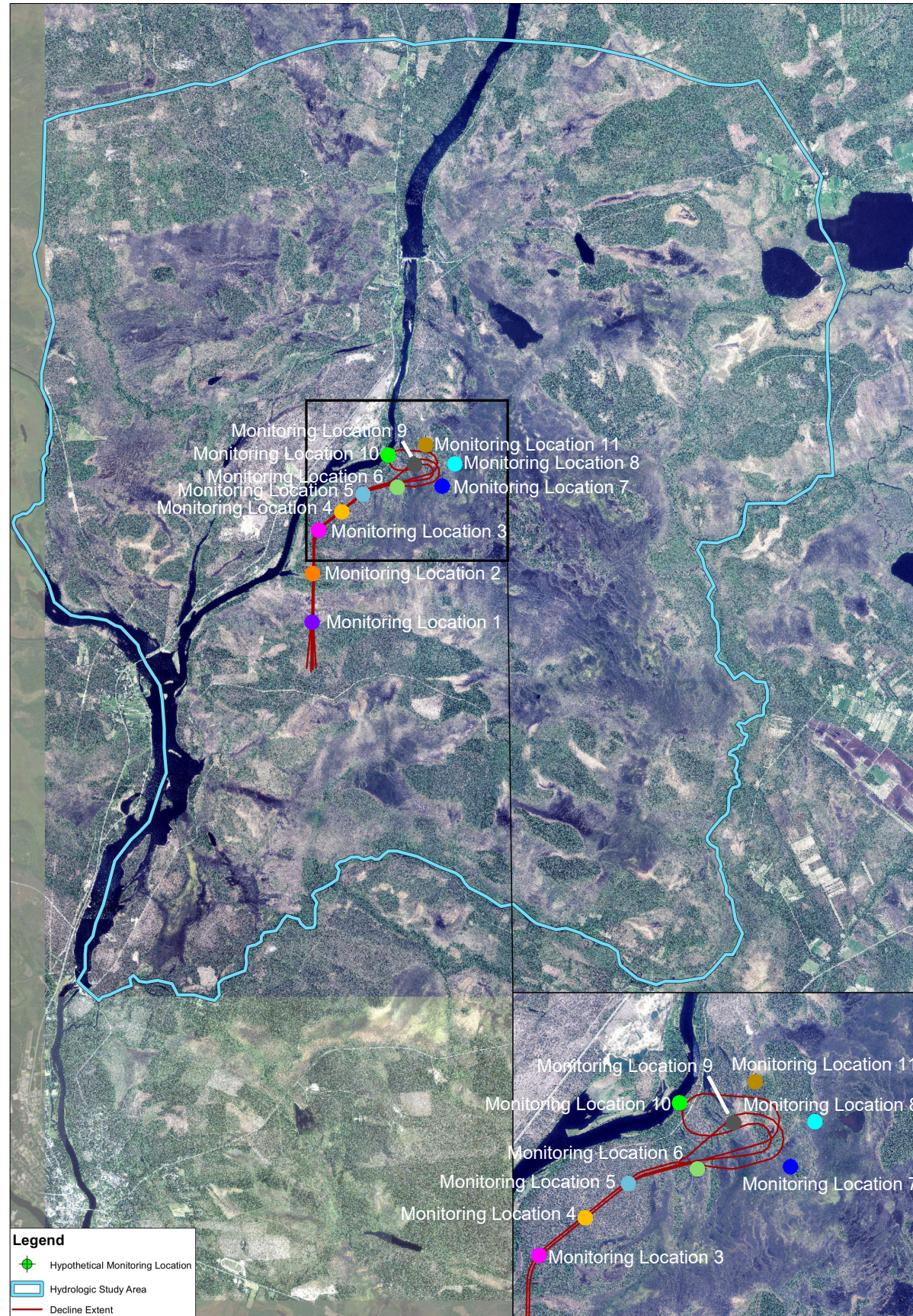


ITASCA[™]
Denver, Inc.

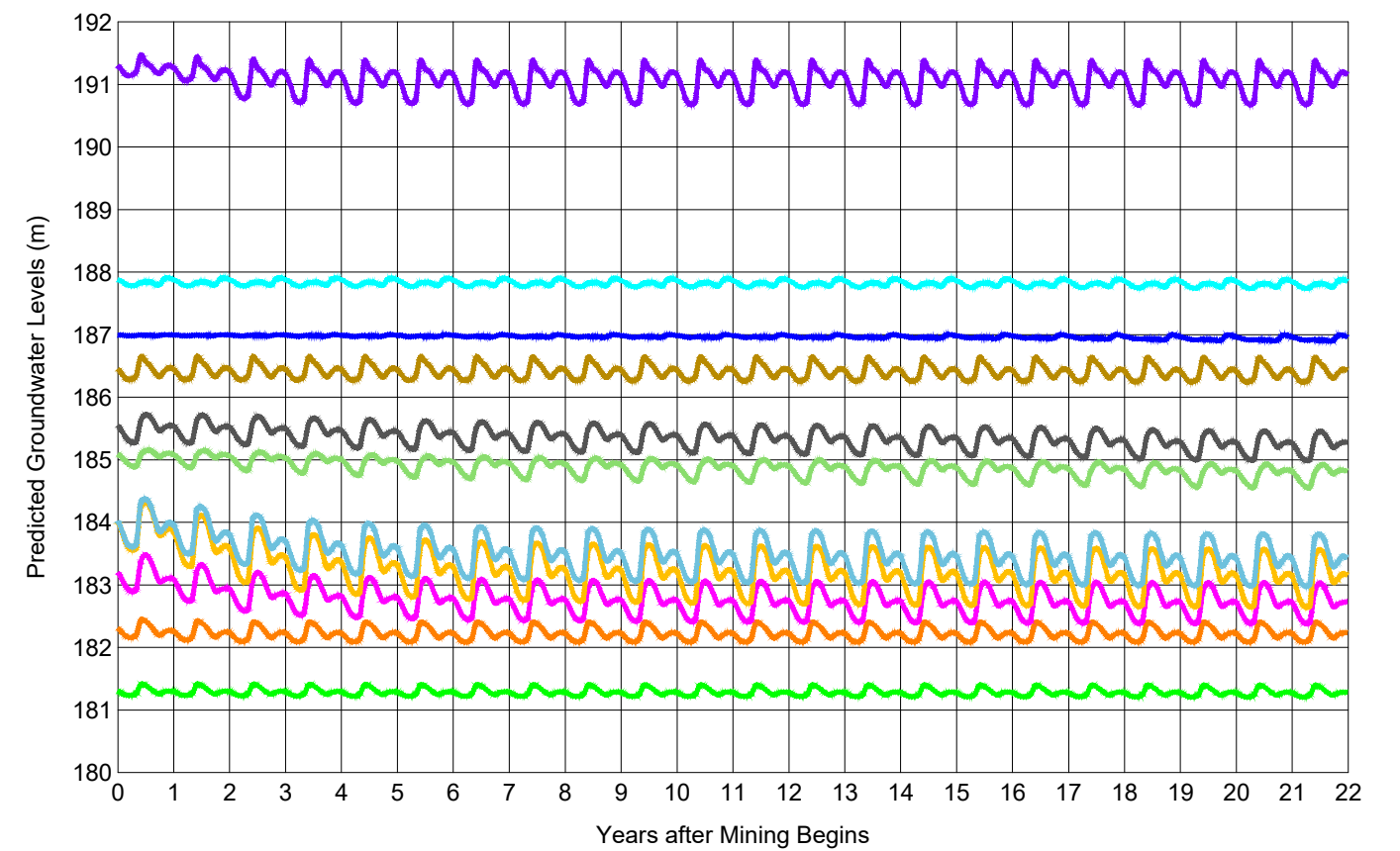
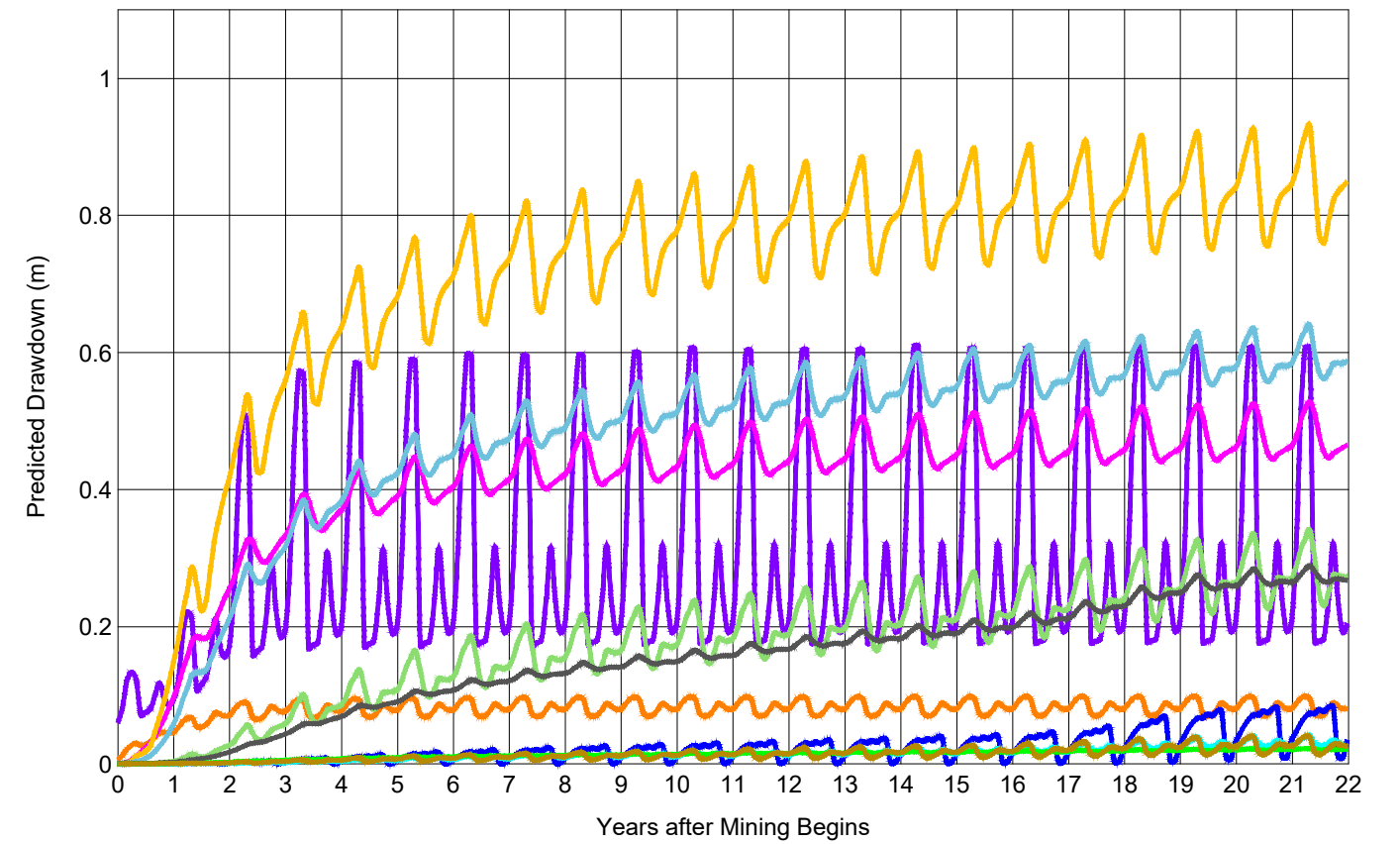
Predicted Groundwater Inflow for the
65% and 80% Success in Grouting without
the NE Deposit Scenarios

CLIENT:
Sakatti Mine

FIGURE NO.
5-9



Monitoring Location 1 Monitoring Location 2 Monitoring Location 3 Monitoring Location 4
Monitoring Location 5 Monitoring Location 6 Monitoring Location 7 Monitoring Location 8
Monitoring Location 9 Monitoring Location 10 Monitoring Location 11



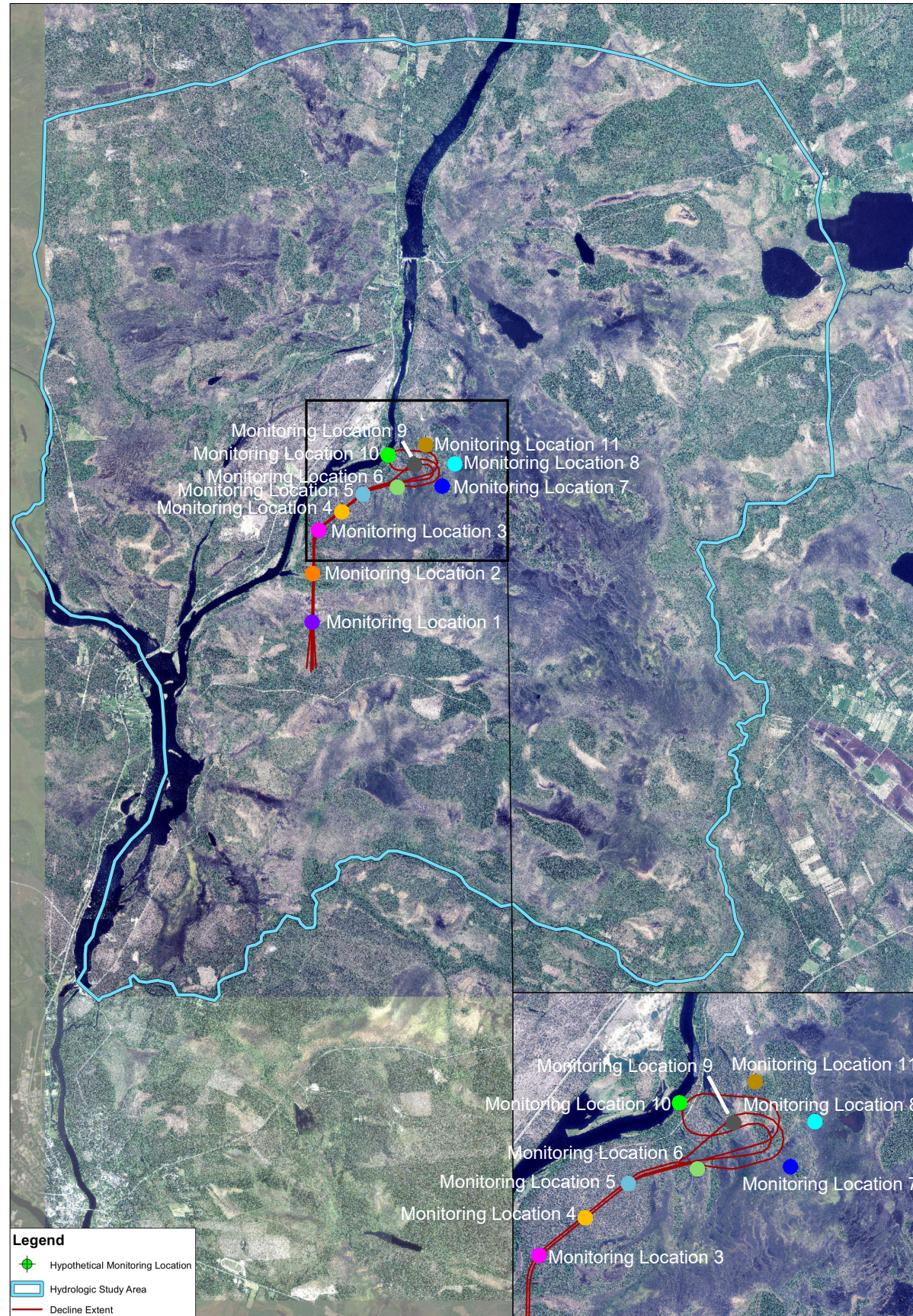
PROJECT NO.	4064
BY	SBM
CHECKED	HL
DRAWN	RJN
DRAWING NAME	DD
DRAWING DATE	9 JAN 2023
REVISION DATE	



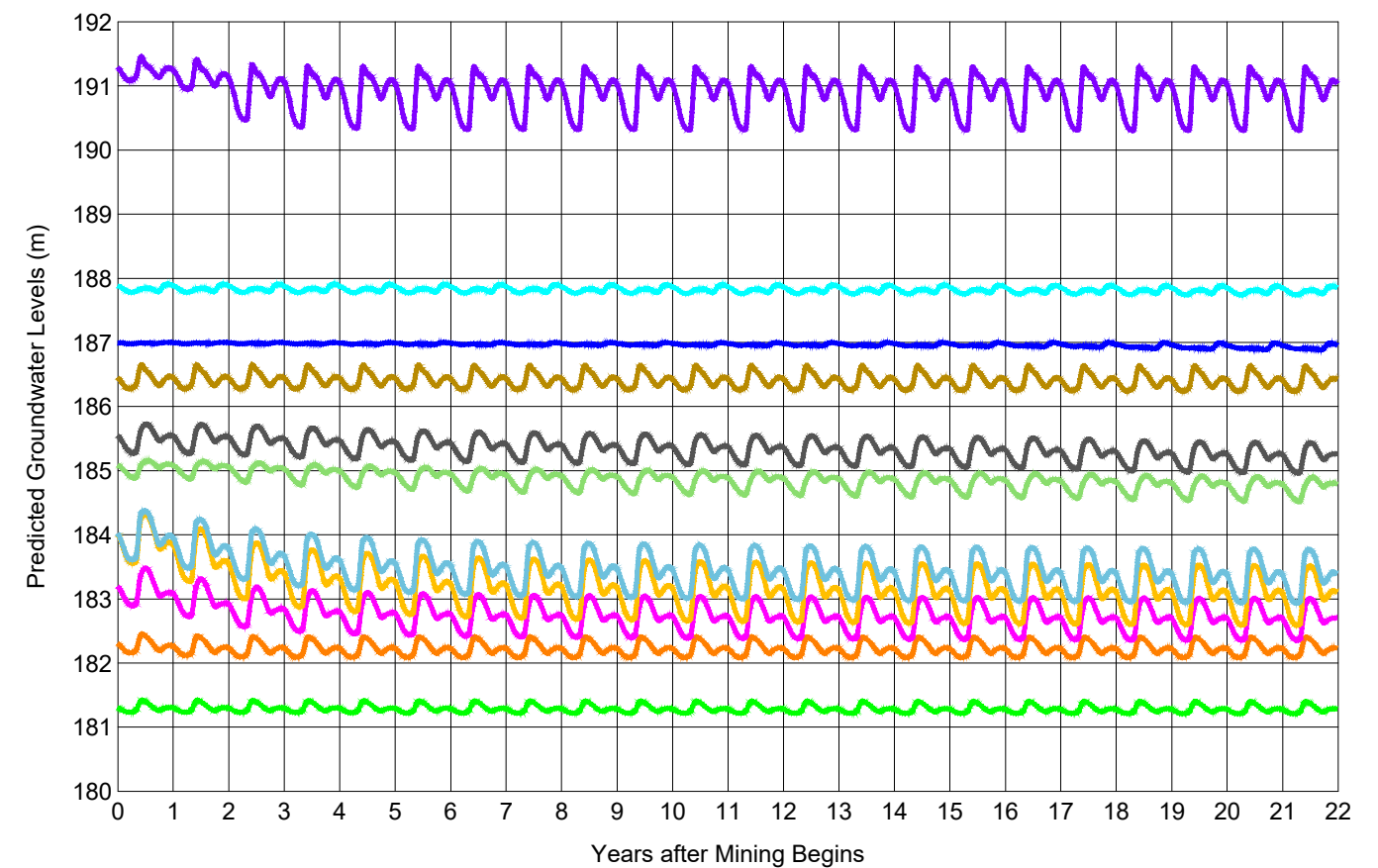
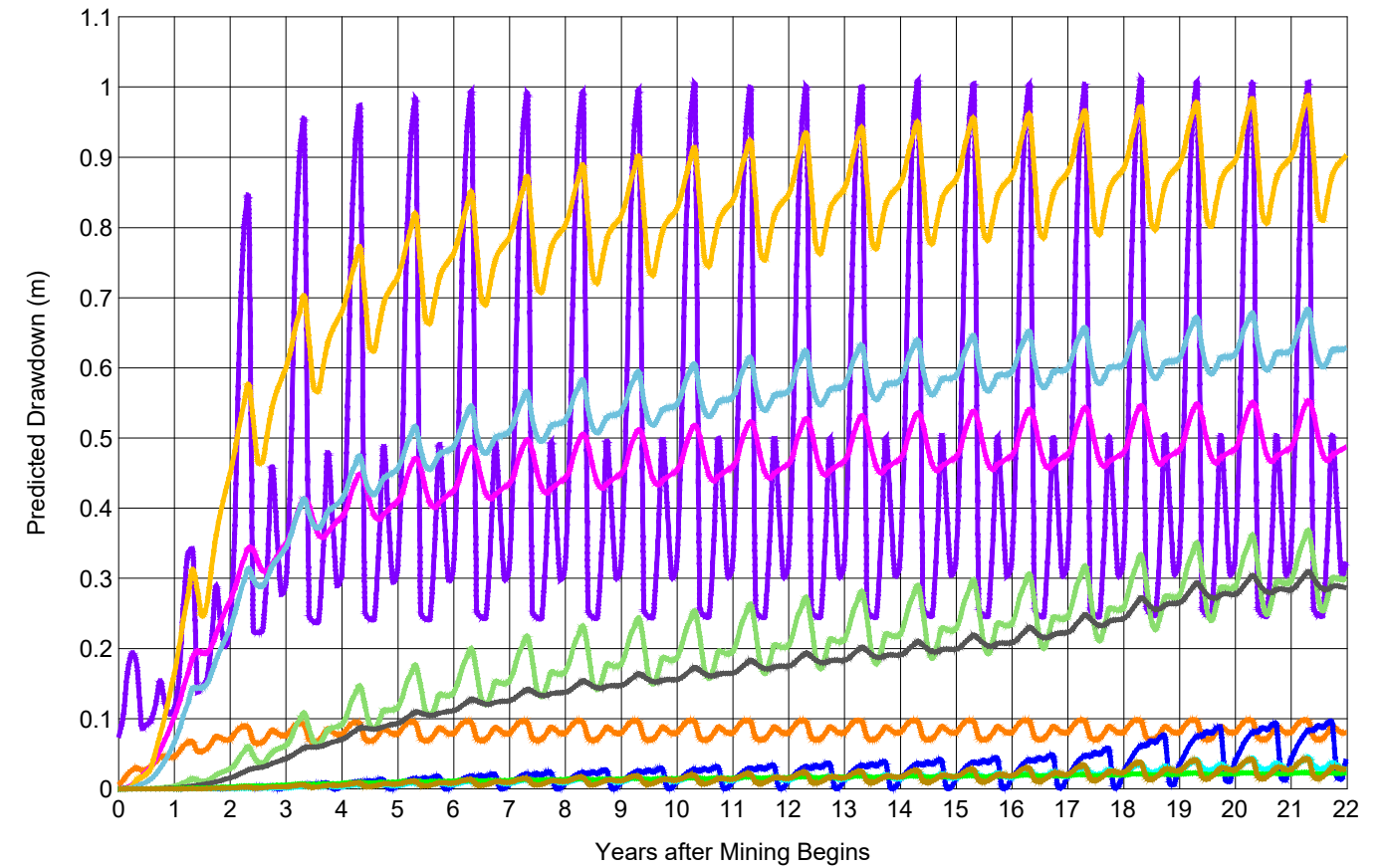
Predicted Drawdown over the LOM at Key Locations around the Mine Area for the 80% Success in Grouting without the NE Deposit Scenario

CLIENT: Sakatti Mine

FIGURE NO. 5-10a



Monitoring Location 1 Monitoring Location 2 Monitoring Location 3 Monitoring Location 4
Monitoring Location 5 Monitoring Location 6 Monitoring Location 7 Monitoring Location 8
Monitoring Location 9 Monitoring Location 10 Monitoring Location 11



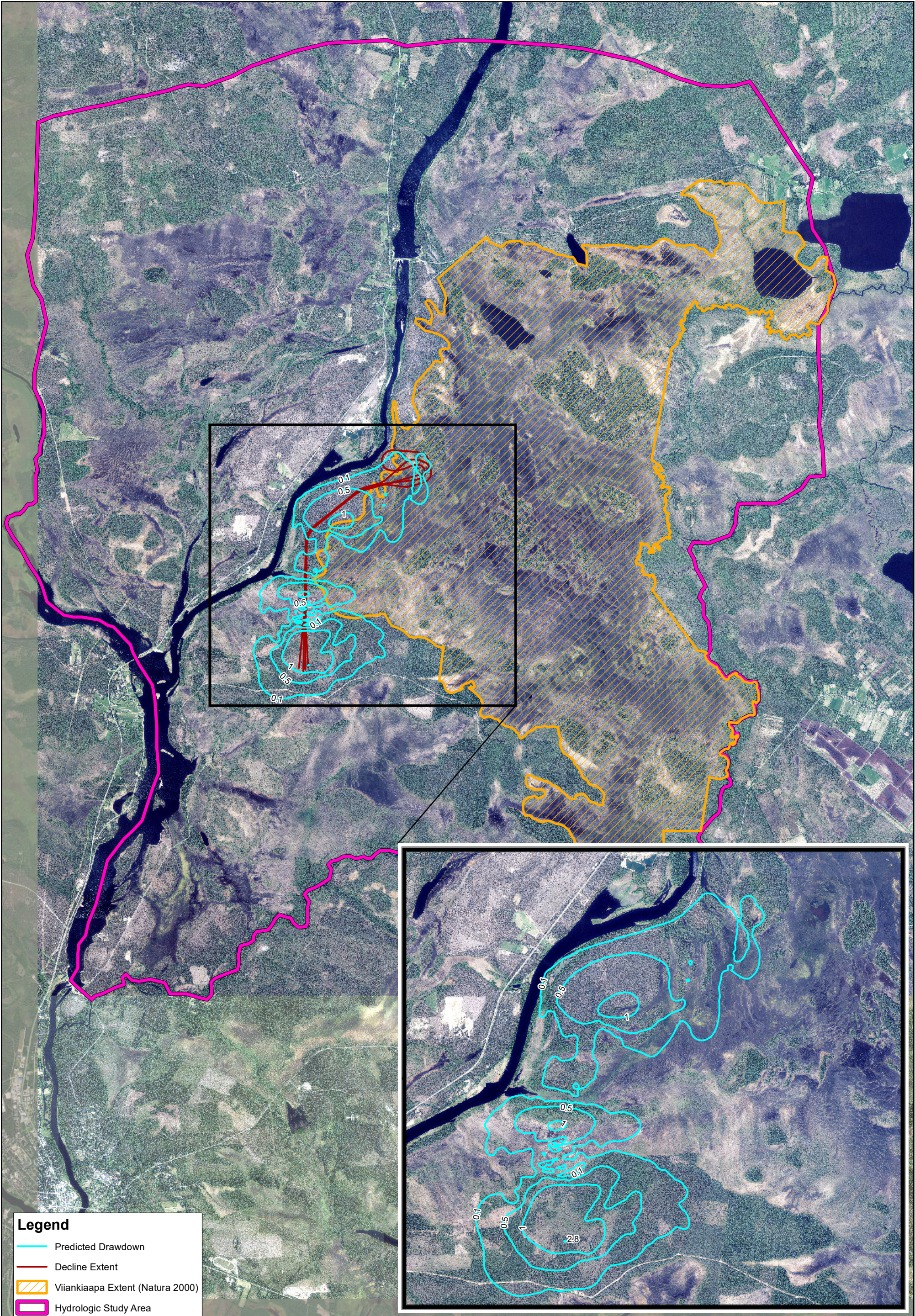
PROJECT NO.	4064
BY	SBM
CHECKED	HL
DRAWN	RJN
DRAWING NAME	DD
DRAWING DATE	9 JAN 2023
REVISION DATE	



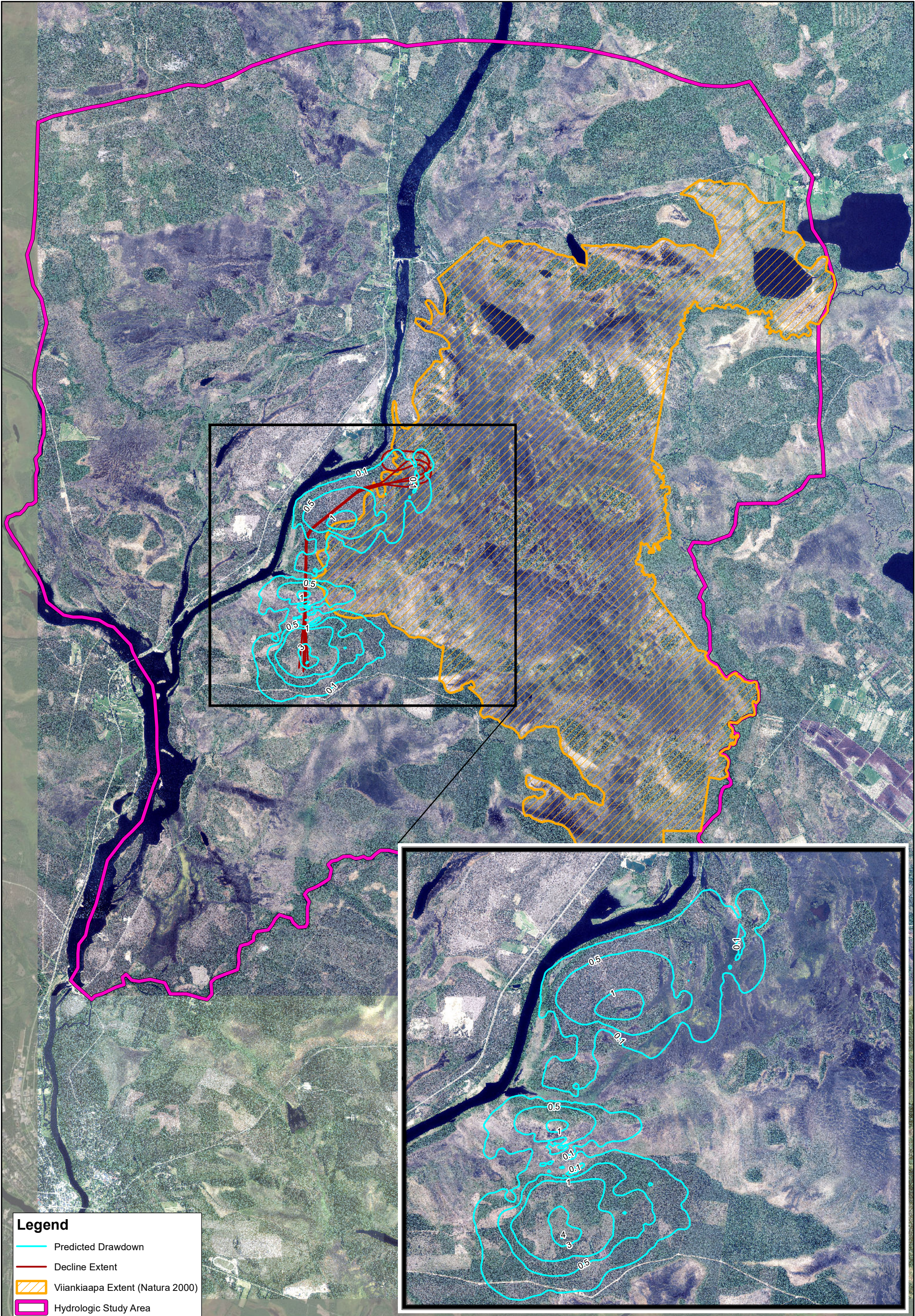
Predicted Drawdown over the LOM at Key Locations around the Mine Area for the 65% Success in Grouting without the NE Deposit Scenario

CLIENT: Sakatti Mine

FIGURE NO. 5-10b



 0 1,250 2,500 Meters	PROJECT NO.	4064	 ITASCA Denver, Inc.	Predicted Drawdown at the End of Mining for the 80% Success in Grouting without the NE Deposit Scenario	
	BY	SBM			
	CHECKED	HL			
	DRAWN	NP			
	DRAWING NAME	Draw_Prac_woNE			
DRAWING DATE	Apr. 25, 2022	CLIENT:	Sakatti Mine	FIGURE NO.	5-11a
REVISION DATE	Jan. 12, 2023				



Legend

Predicted Drawdown

Decline Extent

Viankiaapa Extent (Natura 2000)

Hydrologic Study Area

N

0

1,250

2,500

Meters

PROJECT NO.	4064
BY	SBM
CHECKED	HL
DRAWN	NP
DRAWING NAME	Draw_Challenge_woNE
DRAWING DATE	Apr. 25, 2022
REVISION DATE	Jan. 12, 2023

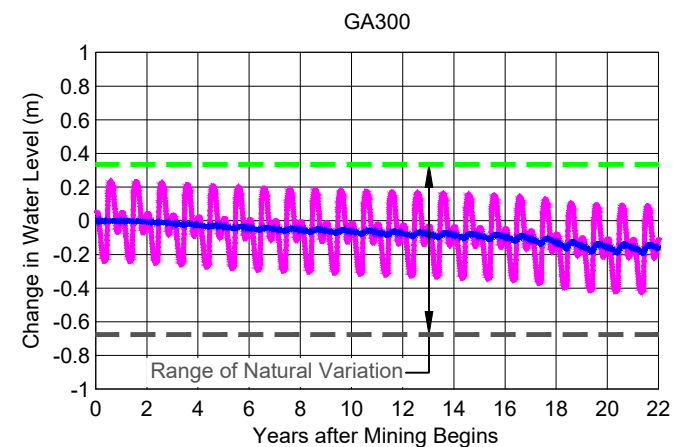
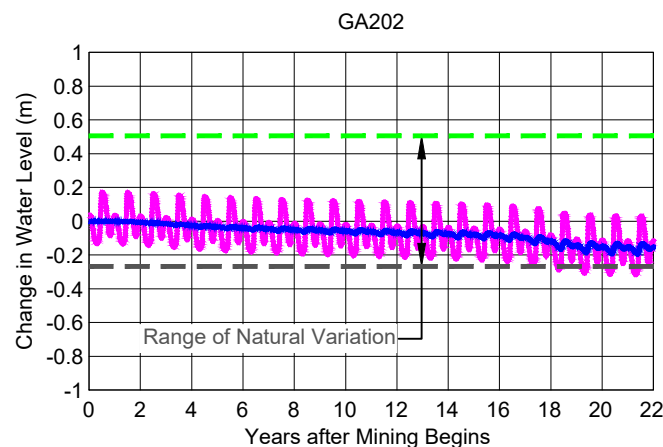
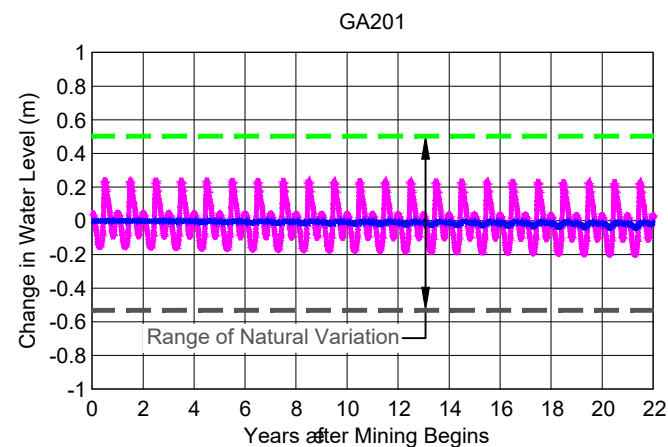
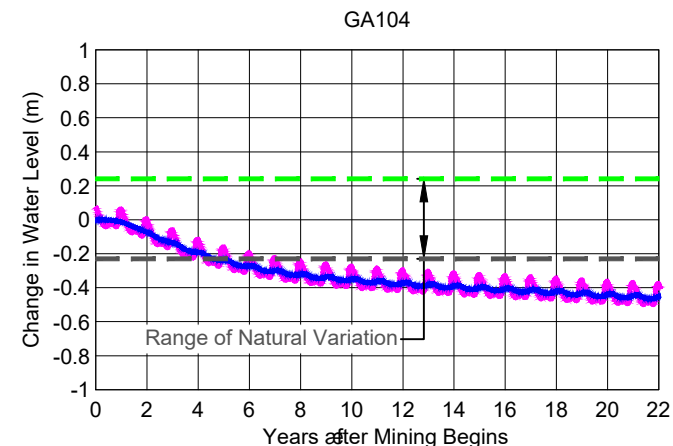
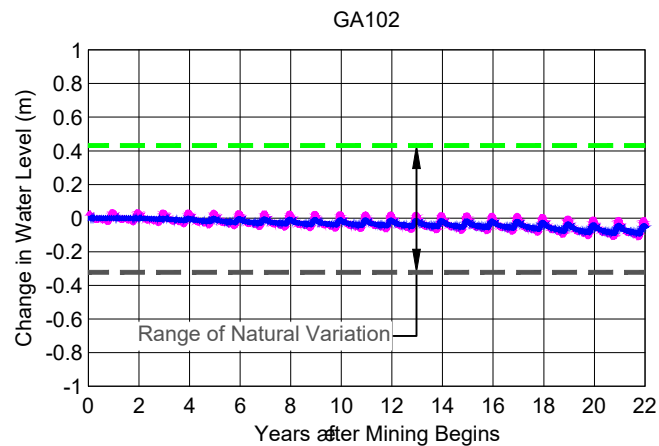
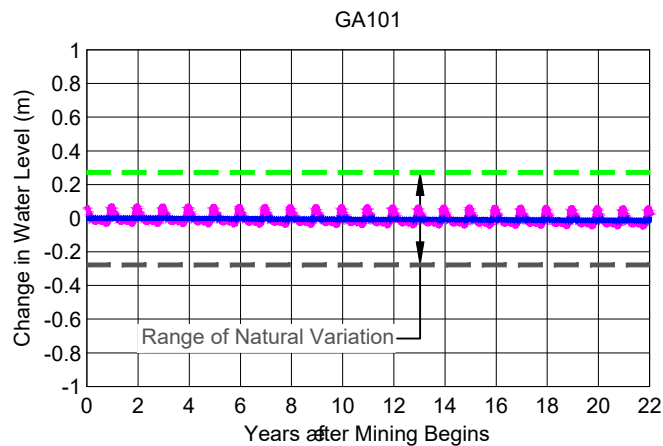
ITASCA

Denver, Inc.

Predicted Drawdown at the End of Mining
for the 65% Success in Grouting without
the NE Deposit Scenario

CLIENT:	FIGURE NO.
Sakatti Mine	5-11b

G:\ARC\GIS\4064_Sakatti\MXDs\Working\Draw_Challenge_woNE.mxd



— Predicted Drawdown
 — Predicted Change in Groundwater Level from Average
 - - - Maximum Change in Measured Groundwater Level from Average from 2012-2021
 - - - Minimum Change in Measured Groundwater Level from Average from 2012-2021

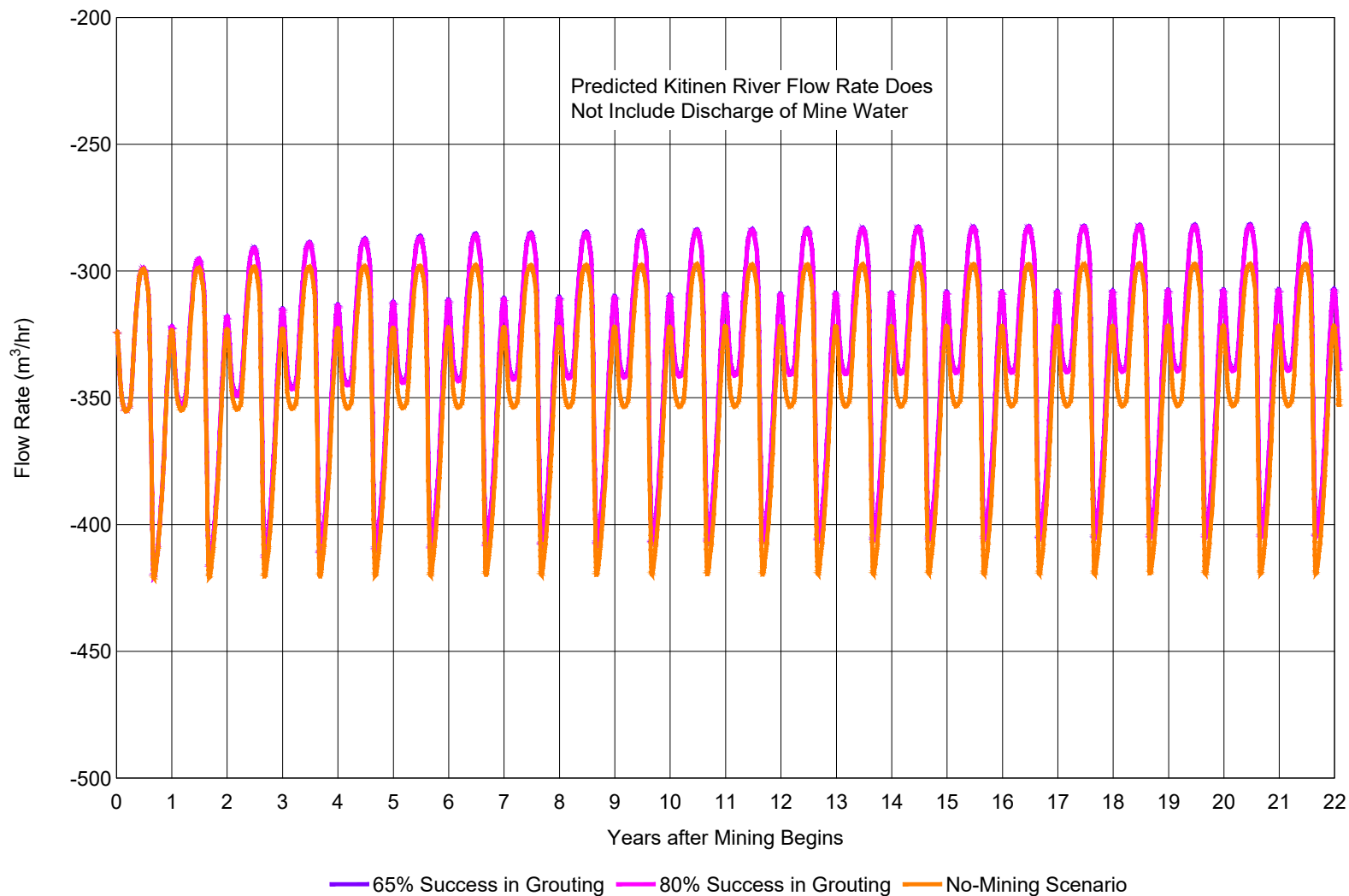
PROJECT NO.	4064
BY	SBM
CHECKED	HL
DRAWN	RJN
DRAWING NAME	WLC
DRAWING DATE	9 JAN 2023
REVISION DATE	



Predictions of Seasonal Groundwater Level Changes for the 80% Success in Grouting without the NE Deposit Scenario

CLIENT:
Sakatti Mine

FIGURE NO.
5-12



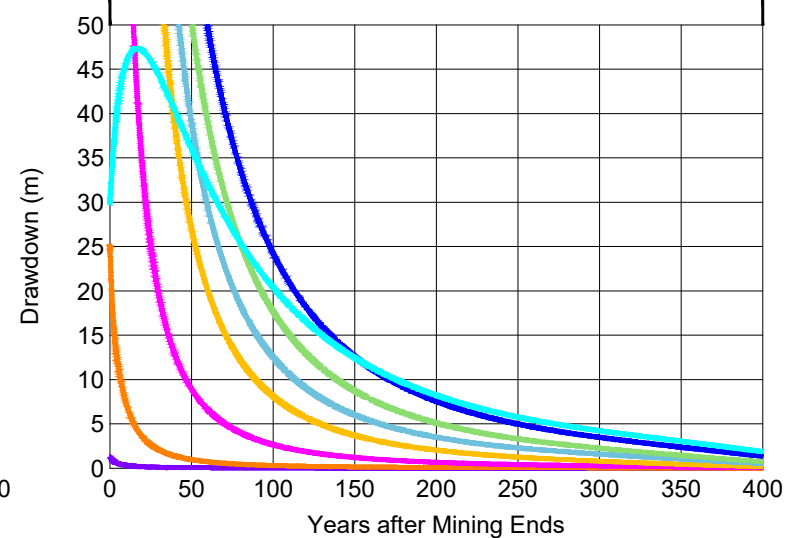
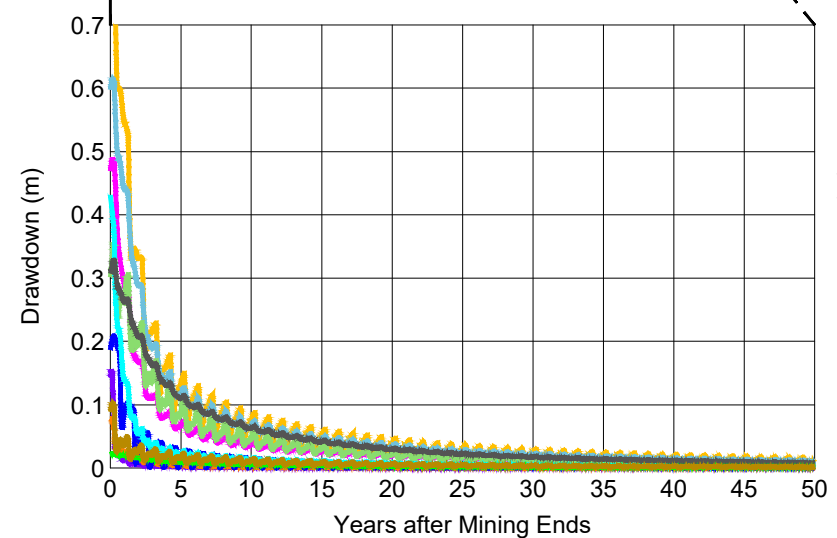
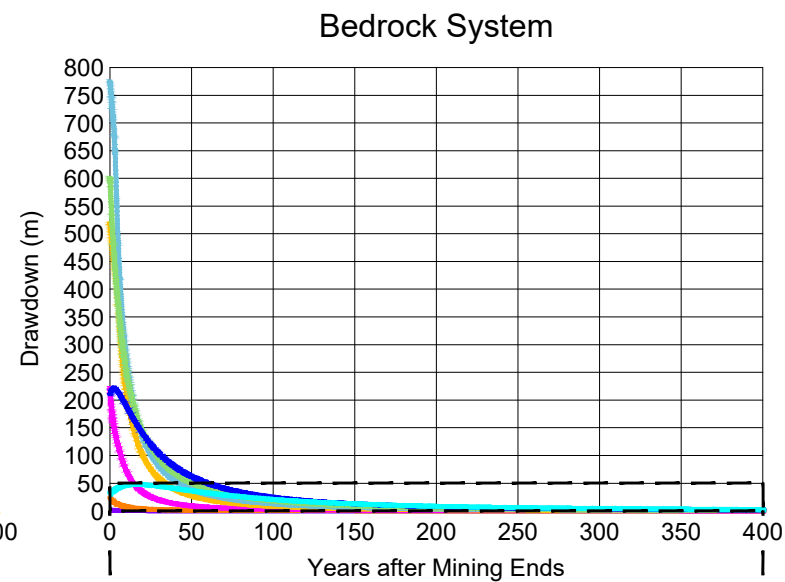
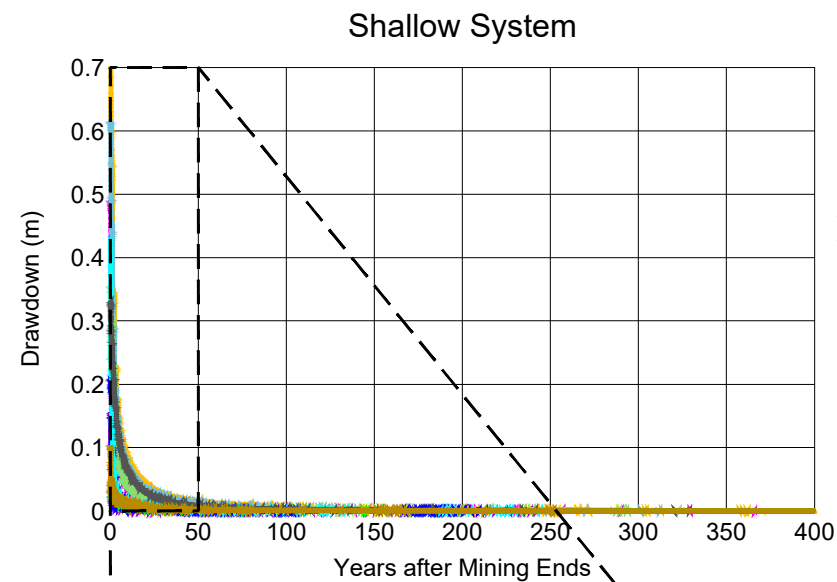
PROJECT NO.	4064
BY	SBM
CHECKED	HL
DRAWN	RJN
DRAWING NAME	PRED
DRAWING DATE	9 JAN 2023
REVISION DATE	



Predicted Baseflow to the Kitinen River
for the 65% and 80% Success in Grouting
without the NE Deposit Scenarios

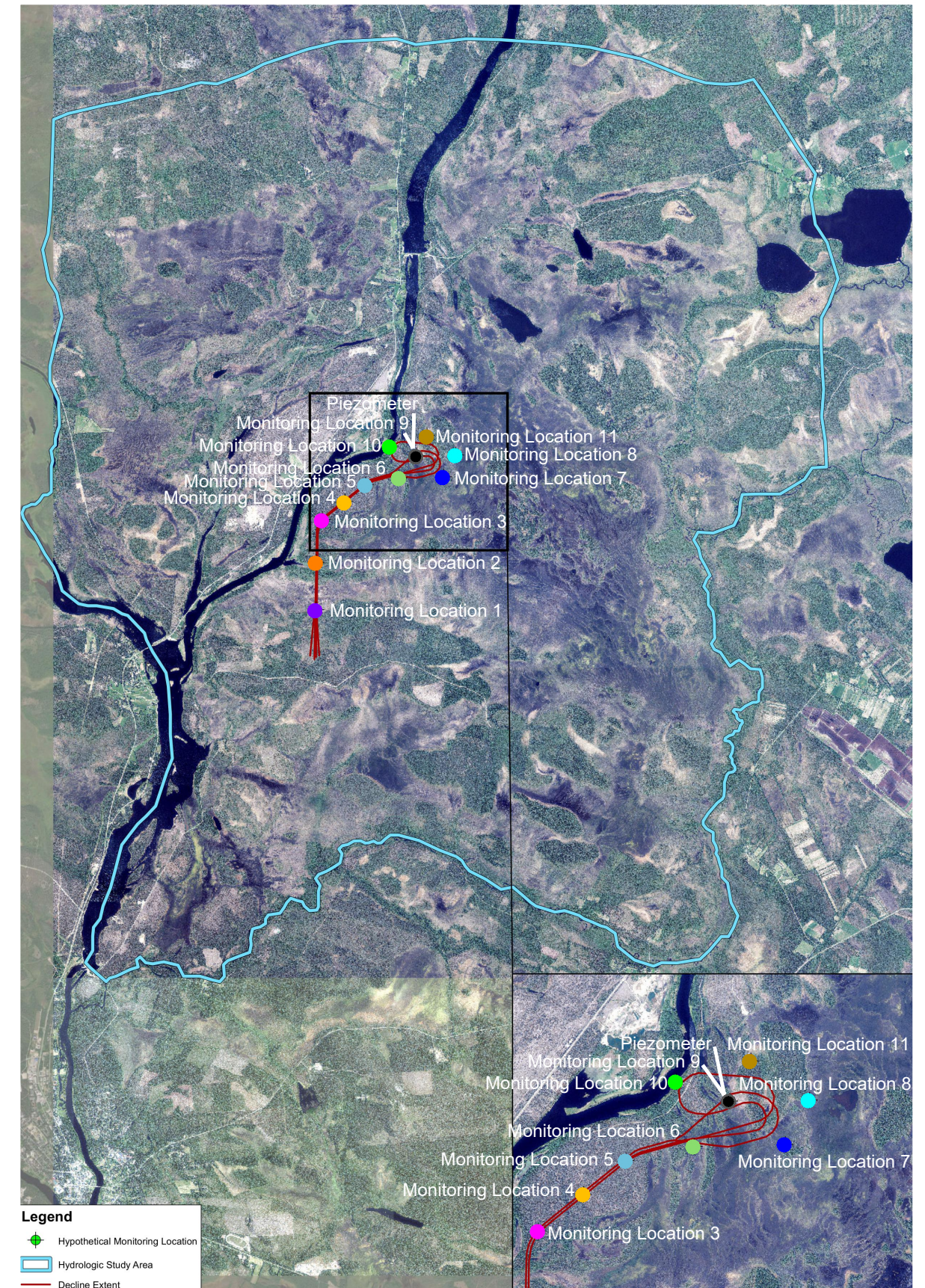
CLIENT:
Sakatti Mine

FIGURE NO.
5-13



- Monitoring Location 1 Monitoring Location 2 Monitoring Location 3
- Monitoring Location 4 Monitoring Location 5 Monitoring Location 6
- Monitoring Location 7 Monitoring Location 8 Monitoring Location 9
- Monitoring Location 10 Monitoring Location 11

- Piezometer - 100 mamsl Piezometer - 0 mamsl
- Piezometer - -200 mamsl Piezometer - -400 mamsl
- Piezometer - -600 mamsl Piezometer - -800 mamsl
- Piezometer - -1000 mamsl Piezometer - -1200 mamsl



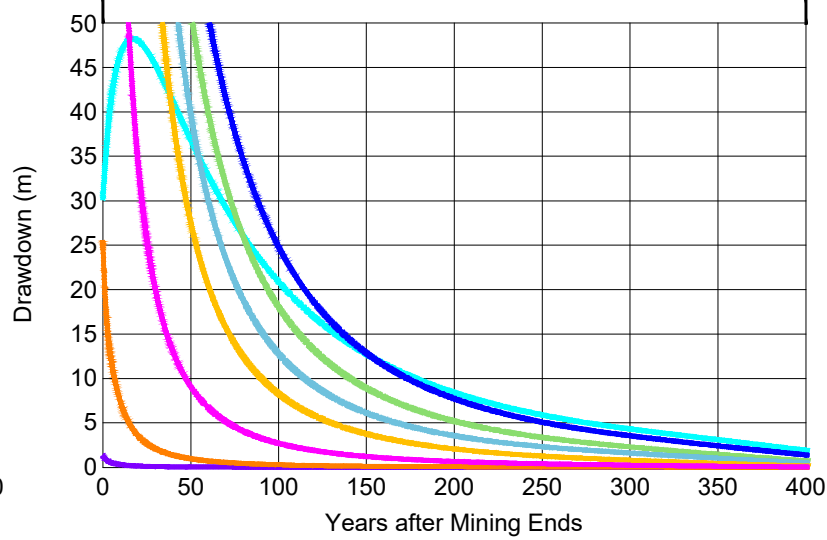
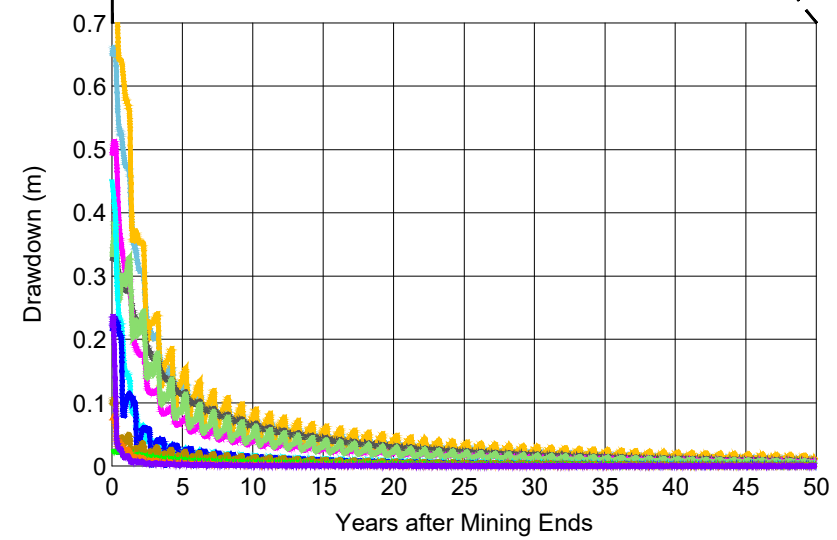
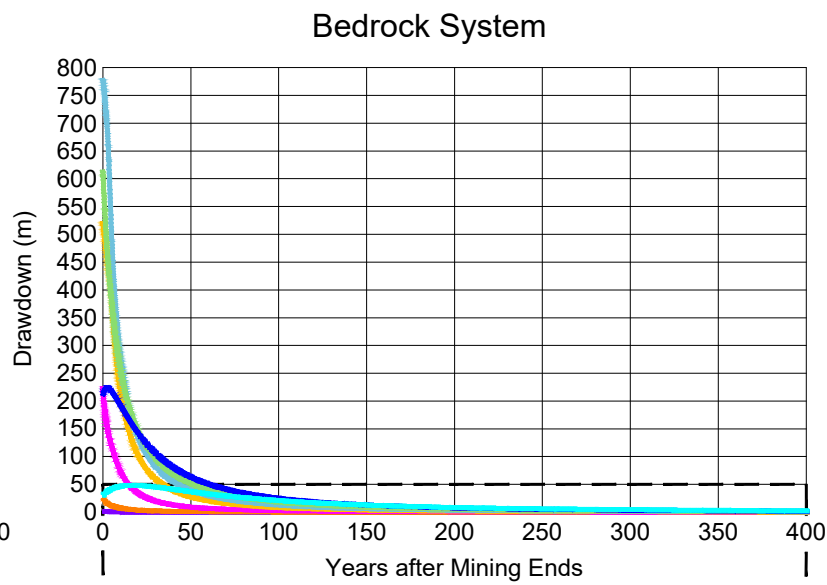
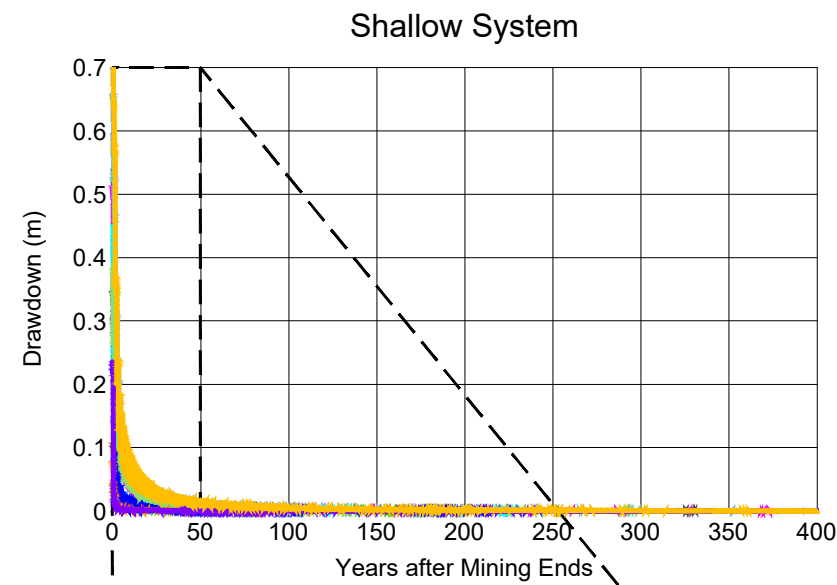
PROJECT NO.	4064
BY	SBM
CHECKED	HL
DRAWN	RJN
DRAWING NAME	RECOVER
DRAWING DATE	14 FEB 2023
REVISION DATE	



Predicted Groundwater Recovery After Mining at Key Locations around the Mine Area for the 80% Success in Grouting with the NE Deposit Scenario

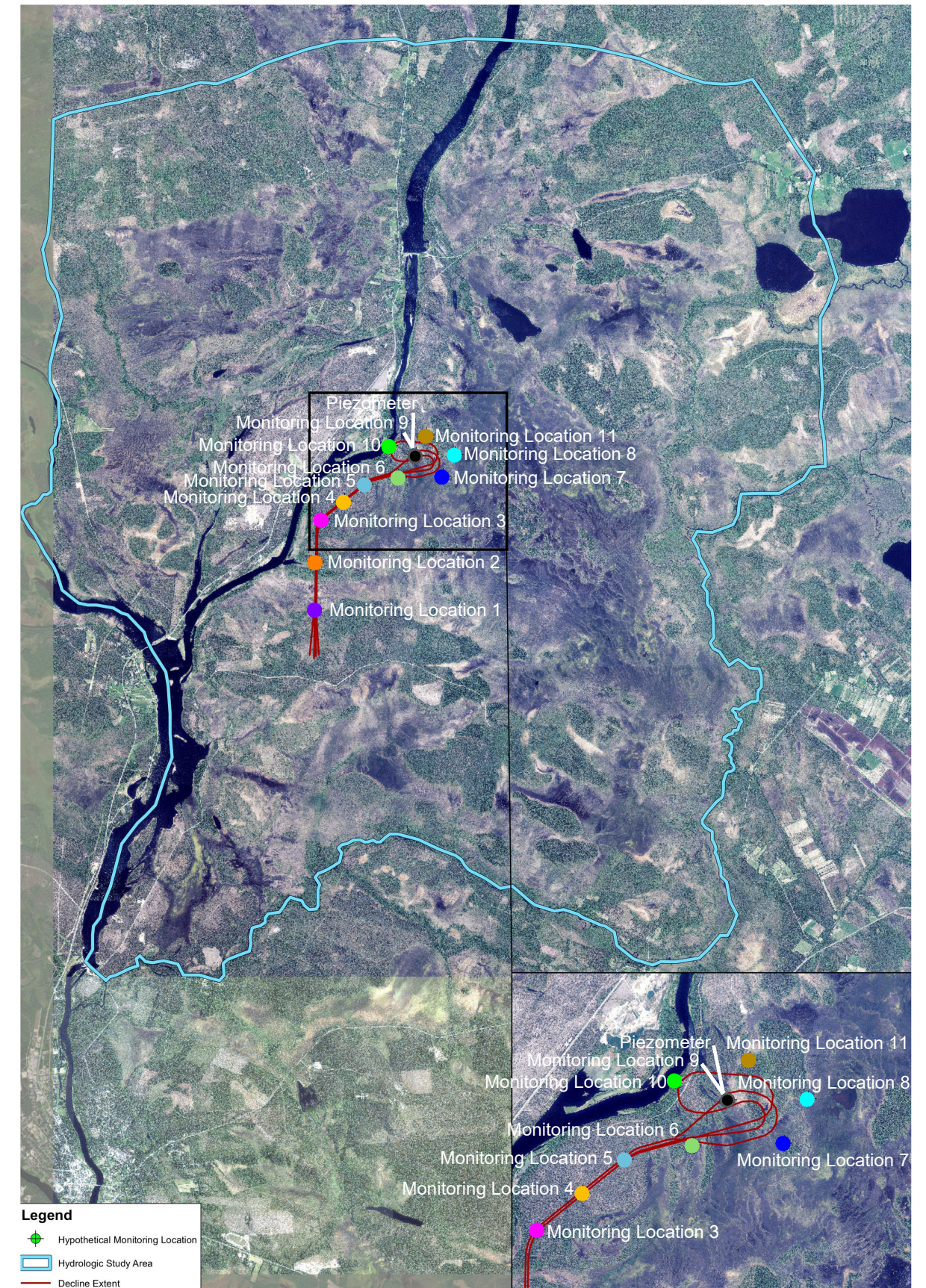
CLIENT:
Sakatti Mine

FIGURE NO.
5-14a



Monitoring Location 1
 Monitoring Location 4
 Monitoring Location 7
 Monitoring Location 10
 Monitoring Location 2
 Monitoring Location 5
 Monitoring Location 8
 Monitoring Location 11
 Monitoring Location 3
 Monitoring Location 6
 Monitoring Location 9

Piezometer - 100 mamsl
 Piezometer - -200 mamsl
 Piezometer - -600 mamsl
 Piezometer - -1000 mamsl
 Piezometer - 0 mamsl
 Piezometer - -400 mamsl
 Piezometer - -800 mamsl
 Piezometer - -1200 mamsl



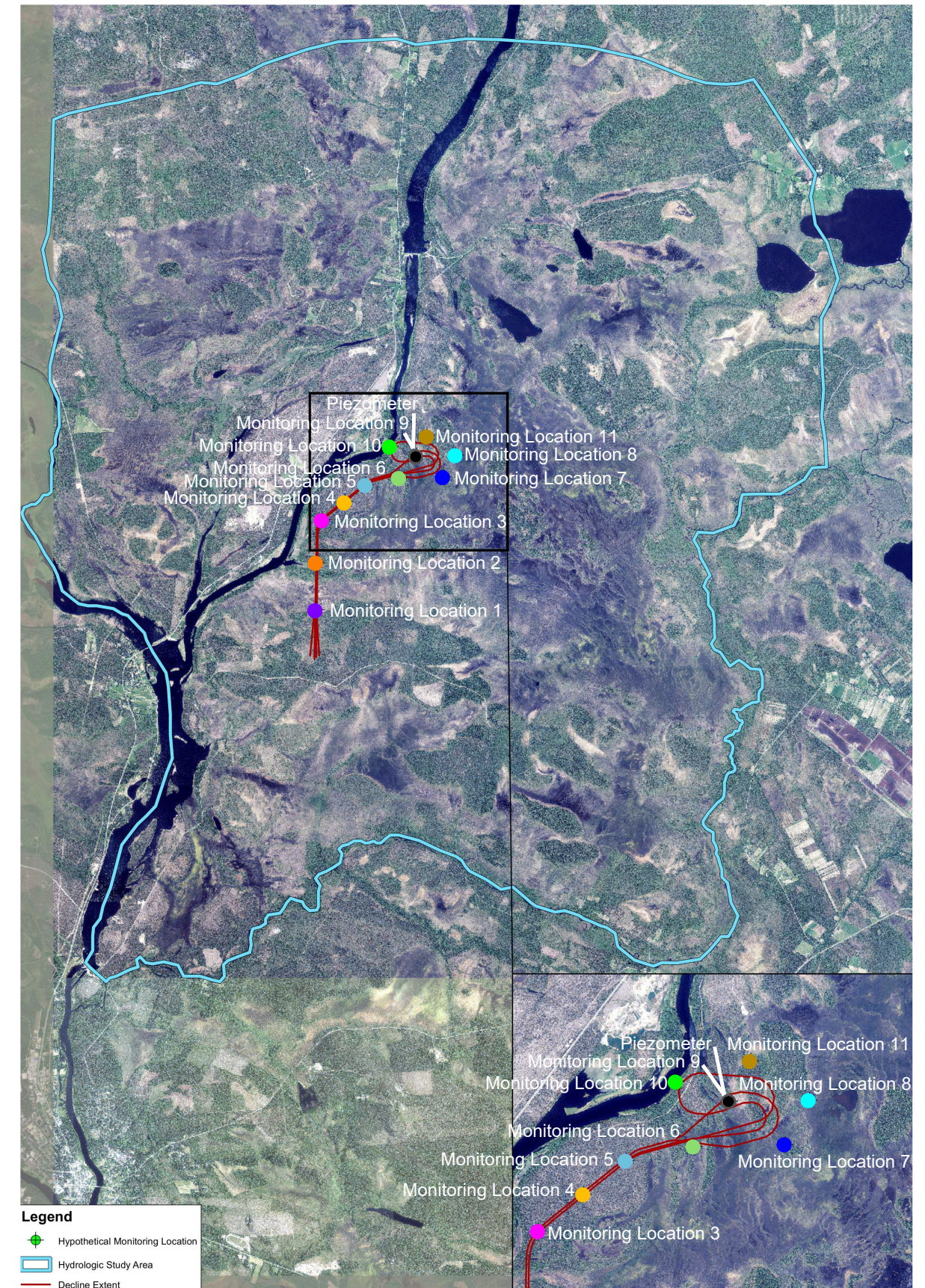
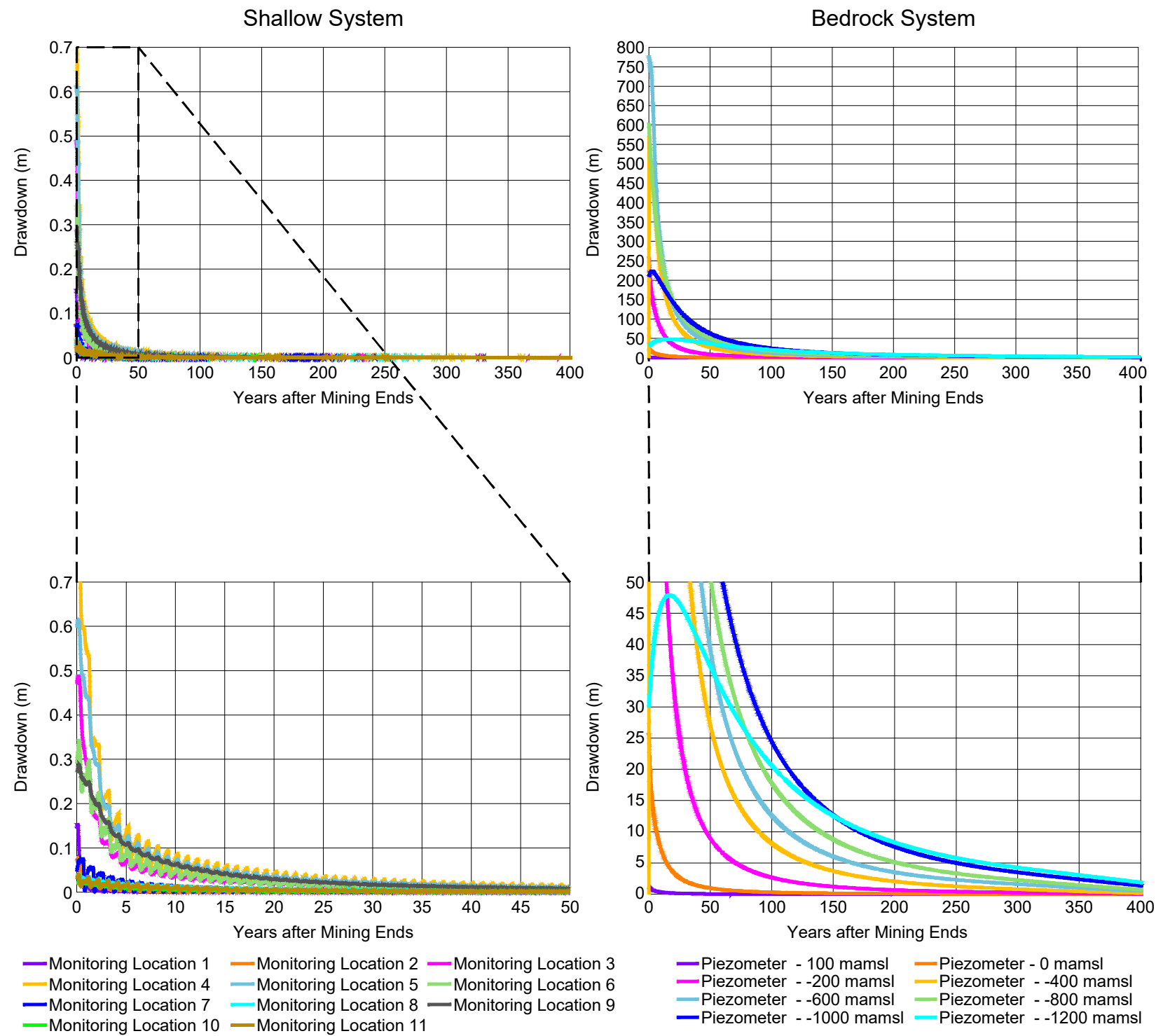
PROJECT NO.	4064
BY	SBM
CHECKED	HL
DRAWN	RJN
DRAWING NAME	RECOVER
DRAWING DATE	14 FEB 2023
REVISION DATE	



Predicted Groundwater Recovery After
 Mining at Key Locations around the Mine
 Area for the 65% Success in Grouting
 with the NE Deposit Scenario

CLIENT:
 Sakatti Mine

FIGURE NO.
 5-14b



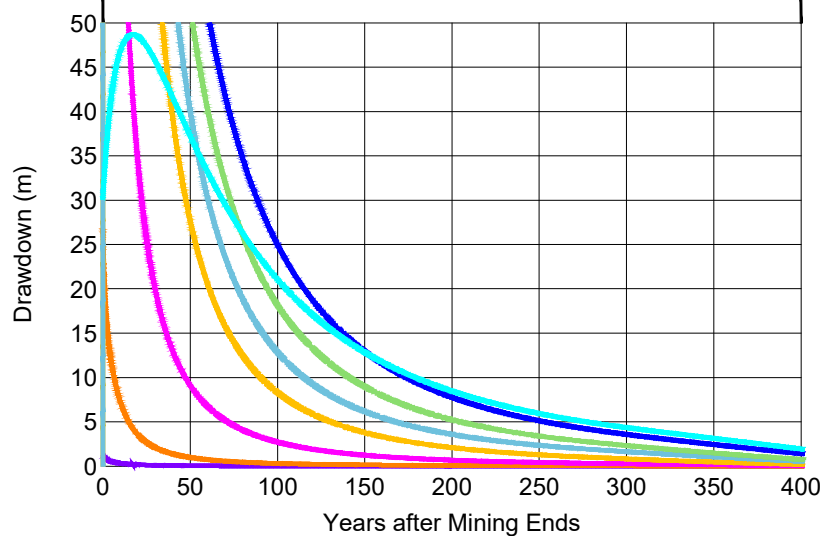
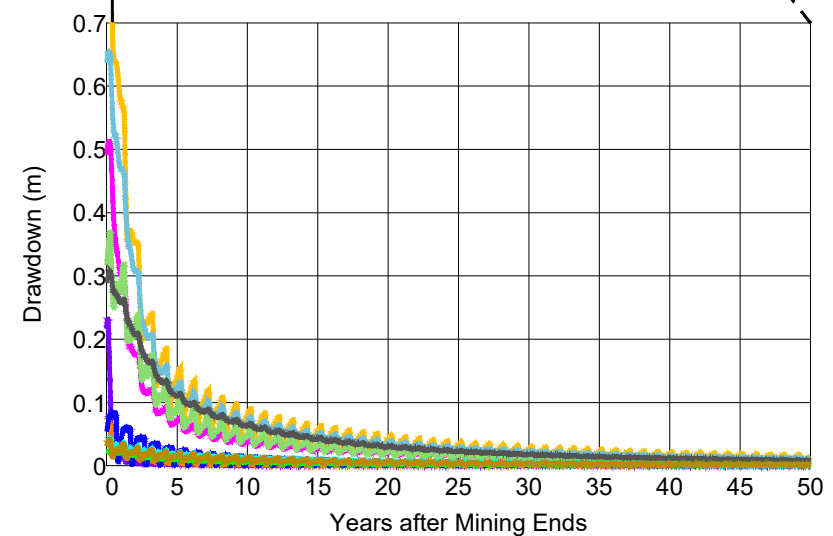
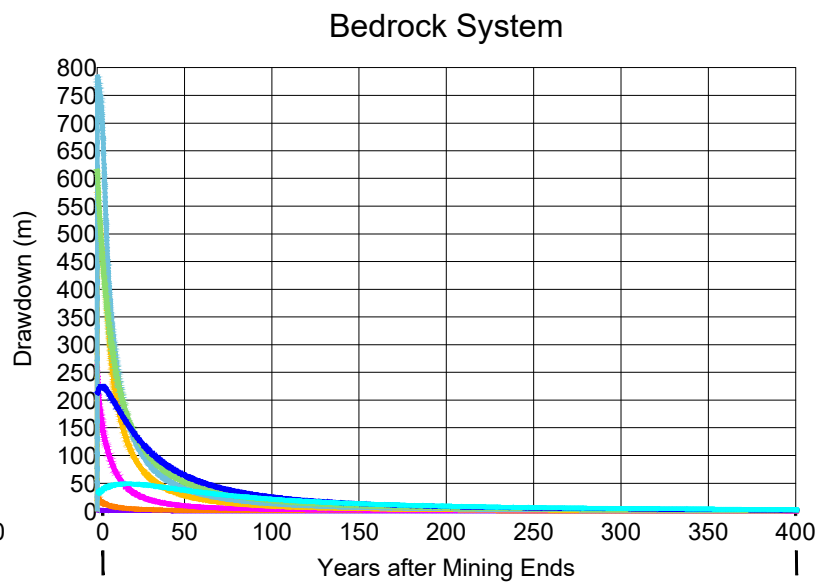
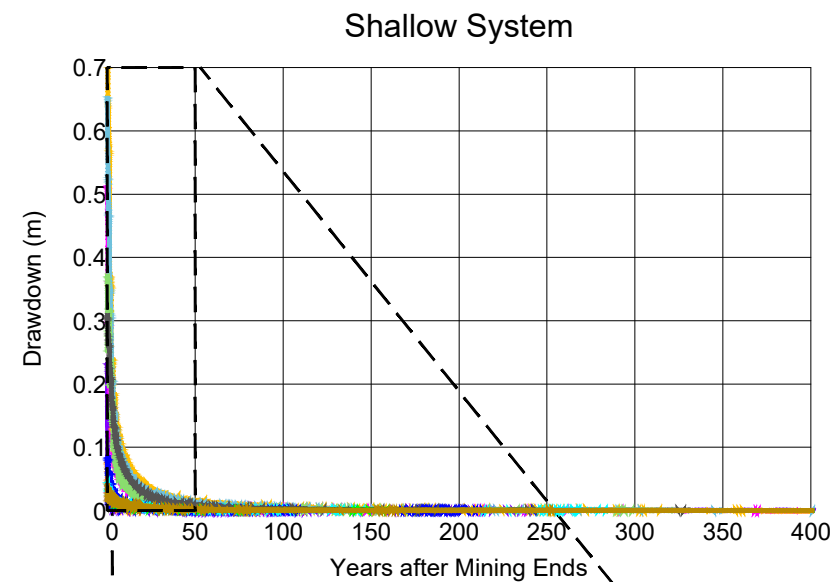
PROJECT NO.	4064
BY	SBM
CHECKED	HL
DRAWN	RJN
DRAWING NAME	RECOVER
DRAWING DATE	14 FEB 2023
REVISION DATE	



Predicted Groundwater Recovery After Mining at Key Locations around the Mine Area for the 80% Success in Grouting with the NE Deposit Scenario

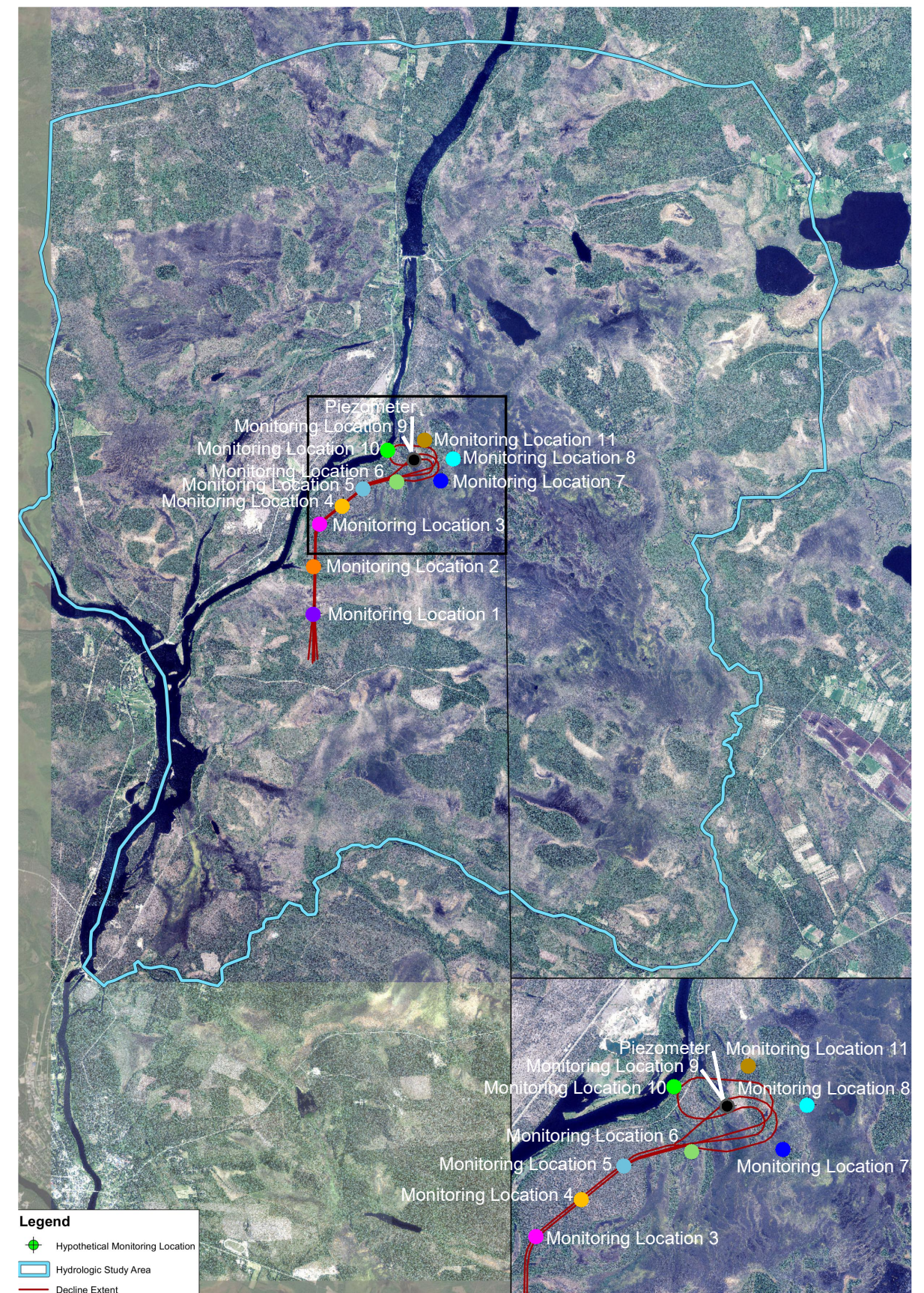
CLIENT:
Sakatti Mine

FIGURE NO.
5-15a



Monitoring Location 1
Monitoring Location 2
Monitoring Location 3
Monitoring Location 4
Monitoring Location 5
Monitoring Location 6
Monitoring Location 7
Monitoring Location 8
Monitoring Location 9
Monitoring Location 10
Monitoring Location 11

Piezometer - 100 mamsl
Piezometer - -200 mamsl
Piezometer - -600 mamsl
Piezometer - -1000 mamsl
Piezometer - 0 mamsl
Piezometer - -400 mamsl
Piezometer - -800 mamsl
Piezometer - -1200 mamsl



PROJECT NO.	4064
BY	SBM
CHECKED	HL
DRAWN	RJN
DRAWING NAME	RECOVER
DRAWING DATE	14 FEB 2023
REVISION DATE	



Predicted Groundwater Recovery After Mining at Key Locations around the Mine Area for the 65% Success in Grouting with the NE Deposit Scenario

CLIENT:
Sakatti Mine

FIGURE NO.
5-15b

PROJECT STAGE					
Project Level Status	Conceptual	Pre-Feasibility	Feasibility	Design and Construction	Operations
Geotechnical Level Status	Level 0	Level 1	Level 2	Level 3	Level 4
Hydrogeologic Model	Regional groundwater survey	Mine scale airlift, pumping and packer testing to establish initial hydrogeological parameters; initial hydrogeological database and model established	Targeted pumping and airlift testing; enhancement of hydrogeological database and 3D model; initial assessment of depressurization and dewatering requirements; injection/recovery rates	Installation of piezometers and dewatering or injection/recovery wells; refinement of hydrological database, 3D model, depressurization and dewatering requirements, recovery/injection requirements	Ongoing management of piezometer and dewatering well network; optimization of injection recovery rates and spacings; continued refinement of hydrogeological database and 3D model

Source: Read and Stacey, 2009

PROJECT NO.	4064
BY	SBM
CHECKED	HL
DRAWN	RJN
DRAWING NAME	STAGES
DRAWING DATE	25 MAY 2022
REVISION DATE	19 OCT 2022

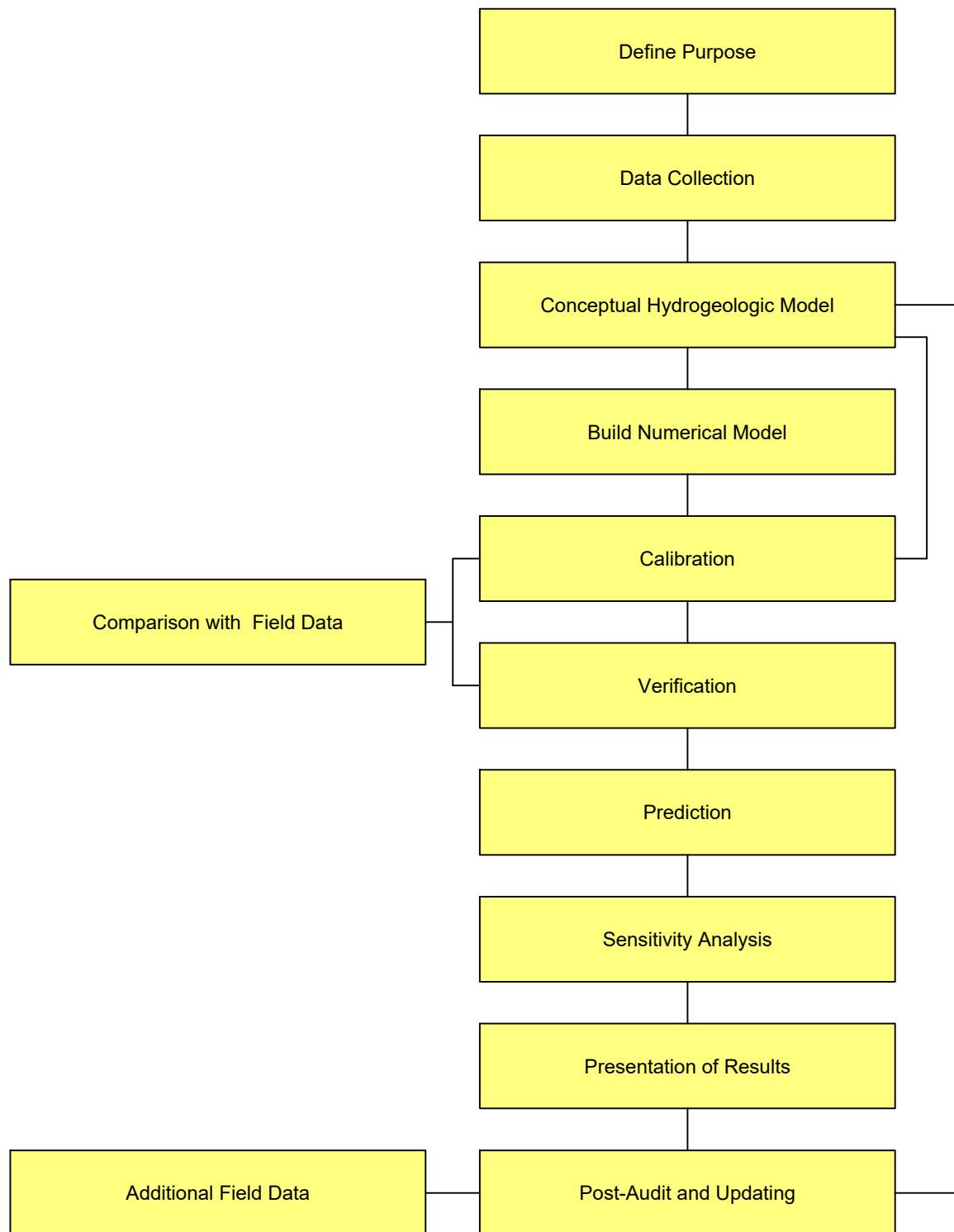


Levels of Hydrogeologic Effort at Different Project Stages

CLIENT:
Sakatti Mine

FIGURE NO.
6-1

Groundwater Flow Modeling Procedure



PROJECT NO.	4064
BY	SBM
CHECKED	HL
DRAWN	RJN
DRAWING NAME	FLOW
DRAWING DATE	25 MAY 2022
REVISION DATE	



Evolution of a Groundwater Flow Model

CLIENT:
Sakatti Mine

FIGURE NO.
6-2

TABLE 3-1

**Summary of Measured Hydraulic Conductivity Values of the
Primary Hydrogeologic Units within the Hydrologic Study Area**

Hydrogeologic Unit	Measured Range of Horizontal Hydraulic Conductivities (m/s)	Source(s)
Peat	1.0×10^{-7} to 1.0×10^{-5}	Golder 2015; Korkka-Niemi and Turtiainen 2020
Till	5.0×10^{-8} to 4.3×10^{-3}	Åberg et al. 2019; Åberg et al. 2021; Puumalainen 2021; Turtiainen 2020; SRK 2019
Sands / Gravels		
Fluvial and Glacial Sediments		
Fractured Bedrock	8.1×10^{-8} to 1.4×10^{-4}	AASM Oy 2021
Unfractured Bedrock	1.0×10^{-12} to 1.0×10^{-5}	AASM Oy 2021
Basal Thrust	5.9×10^{-7} to 9.6×10^{-7}	AASM Oy 2021
Other Faults	4.3×10^{-11} to 1.0×10^{-6}	AASM Oy 2021

TABLE 3-2

Summary of Measured Hydraulic Conductivity Values from Packer Tests
(Page 1 of 7)

Well ID	Test ID	Easting (m) ¹	Northing (m) ¹	Midpoint of Measurement (mamsl)	Hydraulic Conductivity (m/s)
20MOS8248	Test 1	3,489,112	7,495,581	121	1.17E-06
	Test 10	3,489,142	7,495,405	-464	6.74E-10
	Test 11	3,489,147	7,495,382	-544	7.04E-10
	Test 12	3,489,147	7,495,382	-559	5.46E-10
	Test 2	3,489,113	7,495,570	70	1.94E-08
	Test 5	3,489,129	7,495,470	-254	1.18E-10
	Test 6	3,489,131	7,495,456	-319	4.00E-09
	Test 7	3,489,134	7,495,442	-344	1.00E-12
	Test 8	3,489,137	7,495,427	-409	2.31E-10
	Test 9	3,489,141	7,495,413	-433	5.11E-09
16MOS8160	Test 1	3,489,495	7,495,878	-119	5.80E-08
	Test 10	3,489,493	7,495,688	-562	5.80E-09
	Test 11	3,489,494	7,495,983	-239	1.30E-08
	Test 2	3,489,495	7,495,904	-92	3.80E-08
	Test 3	3,489,496	7,495,840	-205	1.30E-08
	Test 4	3,489,496	7,495,794	-285	1.90E-07
	Test 5	3,489,495	7,495,772	-333	6.90E-08
	Test 6	3,489,495	7,495,750	-406	6.20E-08
	Test 7	3,489,494	7,495,708	-475	1.10E-08
	Test 8	3,489,493	7,495,688	-530	5.50E-07
	Test 9	3,489,492	7,495,670	-583	6.30E-11
16MOS8163	Test 1	3,489,444	7,495,448	1	2.40E-08
	Test 2	3,489,456	7,495,447	-54	1.00E-08
	Test 3	3,489,473	7,495,445	-142	2.70E-09
	Test 4	3,489,490	7,495,443	-173	5.90E-09
	Test 5	3,489,500	7,495,442	-244	8.30E-10
	Test 6	3,489,575	7,495,433	-481	6.80E-07
	Test 7	3,489,560	7,495,435	-455	5.20E-07
	Test 8	3,489,534	7,495,439	-412	2.40E-07
17MOS8158	Test 10	3,488,720	7,495,755	-478	1.40E-05
	Test 11	3,488,732	7,495,734	-575	2.60E-06
	Test 12	3,488,740	7,495,720	-614	2.50E-07
	Test 2	3,488,653	7,495,855	46	1.20E-08
	Test 3	3,488,663	7,495,845	-11	2.30E-08
	Test 4	3,488,672	7,495,834	-76	1.30E-08
	Test 5	3,488,689	7,495,807	-193	2.10E-06
	Test 6	3,488,689	7,495,807	-212	2.40E-06
	Test 7	3,488,699	7,495,791	-281	3.00E-06
	Test 8	3,488,707	7,495,779	-381	8.80E-06
	Test 9	3,488,717	7,495,761	-423	2.10E-05

TABLE 3-2

Summary of Measured Hydraulic Conductivity Values from Packer Tests
(Page 2 of 7)

Well ID	Test ID	Easting (m) ¹	Northing (m) ¹	Midpoint of Measurement (mamsl)	Hydraulic Conductivity (m/s)
17MOS8159	Test 3	3,489,024	7,496,317	-93	5.30E-09
	Test 4	3,489,034	7,496,299	-177	5.80E-09
	Test 5	3,489,055	7,496,251	-365	1.60E-08
17MOS8169	Test 1	3,489,350	7,495,702	113	7.00E-07
	Test 10	3,489,346	7,495,683	-519	2.00E-10
	Test 11	3,489,346	7,495,681	-610	1.20E-10
	Test 2	3,489,349	7,495,700	60	3.30E-07
	Test 3	3,489,349	7,495,699	21	9.60E-08
	Test 4	3,489,349	7,495,695	-124	3.40E-09
	Test 5	3,489,349	7,495,693	-202	8.10E-10
	Test 6	3,489,349	7,495,692	-276	1.10E-09
	Test 8	3,489,345	7,495,686	-422	1.10E-08
	Test 9	3,489,345	7,495,685	-446	1.60E-08
17MOS8170	Test 1	3,490,083	7,495,602	83	1.90E-09
	Test 2	3,490,085	7,495,632	11	6.10E-10
	Test3	3,490,086	7,495,653	-54	3.30E-10
	Test 4	3,490,087	7,495,683	-153	2.50E-09
17MOS8174	Test 2	3,489,700	7,495,630	60	6.20E-09
	Test 3	3,489,701	7,495,621	0	2.00E-08
	Test 4	3,489,703	7,495,602	-84	7.50E-08
	Test 5	3,489,704	7,495,586	-157	4.50E-08
	Test 6	3,489,705	7,495,571	-238	2.90E-08
	Test 7	3,489,706	7,495,553	-315	9.60E-08
	Test 8	3,489,707	7,495,521	-458	1.20E-08
17MOS8178	Test 10	3,489,565	7,495,625	-558	9.00E-10
	Test 2	3,489,380	7,495,694	57	5.30E-08
	Test 3	3,489,392	7,495,690	-19	4.60E-08
	Test 4	3,489,434	7,495,677	-147	1.40E-09
	Test 5	3,489,469	7,495,664	-245	3.70E-08
	Test 6	3,489,495	7,495,655	-340	3.50E-09
	Test 8	3,489,527	7,495,643	-491	3.20E-09
	Test 9	3,489,554	7,495,631	-538	2.40E-10
17MOS8180	Test 2	3,490,049	7,495,568	134	1.80E-05
	Test 3	3,490,049	7,495,582	122	7.60E-08
	Test 4	3,490,049	7,495,602	47	6.90E-09
17MOS8183	Test 3	3,489,903	7,495,752	25	1.20E-06
	Test 4	3,489,904	7,495,721	-124	9.40E-08
	Test 5	3,489,906	7,495,678	-180	2.20E-08
	Test 6	3,489,908	7,495,640	-268	1.10E-08

TABLE 3-2

Summary of Measured Hydraulic Conductivity Values from Packer Tests
(Page 3 of 7)

Well ID	Test ID	Easting (m) ¹	Northing (m) ¹	Midpoint of Measurement (mamsl)	Hydraulic Conductivity (m/s)
17MOS8184	Test 2	3,489,753	7,495,550	31	2.00E-08
	Test 3	3,489,755	7,495,519	-67	5.80E-08
	Test 4	3,489,756	7,495,493	-98	2.90E-08
	Test 5	3,489,757	7,495,472	-181	1.00E-07
	Test 6	3,489,759	7,495,437	-249	8.70E-08
	Test 8	3,489,759	7,495,415	-300	1.50E-08
	Test 9	3,489,760	7,495,378	-374	4.30E-09
17MOS8199	Test 3	3,489,502	7,495,548	-221	1.06E-09
	Test 4	3,489,511	7,495,548	-236	2.76E-09
	Test 7	3,489,477	7,495,550	-217	5.75E-09
	Test 8	3,489,541	7,495,547	-373	1.55E-08
	Test 9	3,489,454	7,495,551	-218	8.10E-09
17MOS8200	Test 10	3,489,353	7,495,546	-508	1.68E-11
	Test 11	3,489,354	7,495,544	-592	4.07E-11
	Test 6	3,489,352	7,495,553	-433	1.53E-11
	Test 7	3,489,353	7,495,548	-470	1.03E-10
	Test 8	3,489,351	7,495,557	-397	1.10E-10
	Test 9	3,489,350	7,495,564	-368	2.05E-09
17MOS8201	Test 1	3,489,531	7,495,790	-821	1.63E-09
18MOS8207	Test 7	3,489,395	7,495,786	-326	1.43E-09
	Test 10	3,489,410	7,495,740	-551	1.67E-09
	Test 11	3,489,413	7,495,731	-612	1.13E-09
	Test 12	3,489,410	7,495,740	-610	7.75E-10
	Test 2	3,489,402	7,495,881	71	9.90E-09
	Test 3	3,489,402	7,495,861	-4	2.00E-08
	Test 4	3,489,401	7,495,838	-122	5.00E-09
	Test 5	3,489,399	7,495,810	-205	2.09E-09
	Test 8	3,489,403	7,495,760	-450	9.99E-09
	Test 9	3,489,406	7,495,750	-496	1.71E-09
18MOS8208	Test 1	3,489,499	7,496,239	114	1.85E-07
	Test 10	3,489,519	7,496,122	-372	1.80E-08
	Test 11	3,489,519	7,496,078	-436	3.27E-08
	Test 12	3,489,518	7,496,057	-503	4.19E-09
	Test 13	3,489,517	7,496,048	-517	2.36E-09
	Test 14	3,489,515	7,496,024	-554	1.69E-09
	Test 15	3,489,513	7,496,007	-635	1.20E-09
	Test 16	3,489,512	7,495,987	-667	2.14E-09
	Test 17	3,489,516	7,496,026	-691	1.20E-09
	Test 2	3,489,501	7,496,232	98	9.01E-08
	Test 3	3,489,506	7,496,214	-2	3.46E-09

TABLE 3-2

Summary of Measured Hydraulic Conductivity Values from Packer Tests
(Page 4 of 7)

Well ID	Test ID	Easting (m) ¹	Northing (m) ¹	Midpoint of Measurement (mamsl)	Hydraulic Conductivity (m/s)
18MOS8208 (continued)	Test 4	3,489,509	7,496,196	-37	1.42E-09
	Test 5	3,489,512	7,496,177	-145	9.92E-10
	Test 6	3,489,515	7,496,152	-180	8.90E-10
	Test 7	3,489,519	7,496,122	-286	2.16E-09
	Test 8	3,489,520	7,496,097	-320	3.69E-09
	Test 9	3,489,519	7,496,078	-383	1.86E-08
18MOS8226	Test 1	3,488,648	7,495,431	57	4.88E-07
	Test 10	3,488,679	7,495,394	-346	1.62E-06
	Test 11	3,488,682	7,495,391	-359	3.36E-06
	Test 12	3,488,683	7,495,389	-401	3.64E-08
	Test 13	3,488,691	7,495,380	-499	5.26E-09
	Test 14	3,488,695	7,495,374	-548	1.22E-06
	Test 15	3,488,697	7,495,371	-600	1.75E-08
	Test 16	3,488,704	7,495,362	-700	1.55E-08
	Test 17	3,488,706	7,495,359	-716	1.67E-08
	Test 2	3,488,652	7,495,427	11	2.49E-07
	Test 3	3,488,652	7,495,426	-17	8.99E-08
	Test 4	3,488,655	7,495,423	-36	4.39E-09
	Test 5	3,488,658	7,495,419	-81	3.23E-07
	Test 6	3,488,662	7,495,415	-131	8.64E-08
	Test 7	3,488,666	7,495,409	-186	2.81E-07
	Test 8	3,488,670	7,495,405	-235	4.07E-08
	Test 9	3,488,674	7,495,400	-291	1.04E-08
18MOS8227	Test 1	3,487,813	7,494,740	139	2.20E-07
	Test 10	3,487,834	7,494,582	-307	1.96E-08
	Test 2	3,487,816	7,494,724	96	1.56E-08
	Test 3	3,487,818	7,494,710	54	2.02E-08
	Test 4	3,487,820	7,494,695	1	1.49E-06
	Test 5	3,487,822	7,494,679	-20	3.09E-07
	Test 6	3,487,823	7,494,668	-53	1.02E-08
	Test 7	3,487,825	7,494,655	-104	1.97E-09
	Test 8	3,487,828	7,494,635	-178	3.04E-09
	Test 9	3,487,833	7,494,596	-268	3.60E-07
18MOS8228	Test 1	3,489,102	7,495,765	111	2.06E-05
	Test 2	3,489,101	7,495,740	64	1.52E-05
18MOS8229	Test 1	3,488,558	7,494,674	68	3.87E-07

TABLE 3-2

Summary of Measured Hydraulic Conductivity Values from Packer Tests
(Page 5 of 7)

Well ID	Test ID	Easting (m) ¹	Northing (m) ¹	Midpoint of Measurement (mamsl)	Hydraulic Conductivity (m/s)
18MOS8231	Test 1	3,487,479	7,493,505	87	1.15E-07
	Test 2	3,489,351	7,495,993	101	1.61E-08
	Test 3	3,489,352	7,495,984	-24	1.13E-07
	Test 4	3,489,352	7,495,967	-74	6.81E-08
	Test 8	3,489,349	7,495,905	-354	4.34E-08
	Test 9	3,489,349	7,495,889	-437	3.22E-09
18MOS8232	Test 1	3,489,342	7,495,816	-819	1.70E-07
19MOS8237	Test 1	3,489,309	7,495,845	121	1.32E-06
	Test 10	3,489,303	7,495,795	-551	3.81E-10
	Test 11	3,489,309	7,495,769	-690	7.78E-09
	Test 2	3,489,308	7,495,841	66	1.01E-06
	Test 5	3,489,307	7,495,831	-108	1.42E-09
	Test 7	3,489,305	7,495,822	-375	3.15E-08
19MOS82329	Test 3	3,489,595	7,496,083	-351	1.80E-09
	Test 5	3,489,600	7,495,989	-827	4.55E-10
19MOS8240	Test 1	3,489,444	7,495,717	-44	1.29E-08
	Test 3	3,489,441	7,495,699	-186	4.20E-10
	Test 4	3,489,439	7,495,678	-320	1.45E-09
	Test 5	3,489,438	7,495,652	-394	2.66E-09
	Test 6	3,489,437	7,495,625	-488	4.44E-10
19MOS8242	Test 1	3,489,799	7,495,883	91	6.09E-09
	Test 2	3,489,802	7,495,869	9	5.42E-09
	Test 3	3,489,805	7,495,852	-64	1.03E-06
	Test 4	3,489,807	7,495,839	-153	6.75E-09
	Test 5	3,489,809	7,495,815	-245	2.51E-08
20HYD041	test 1	3,489,533	7,496,574	39	5.03E-08
20HYD043	test 1	3,489,510	7,496,483	60	1.82E-08
20KUU024	Test 1	3,487,458	7,492,505	103	1.02E-07
	Test 2	3,487,460	7,492,525	59	5.45E-08
	Test 3	3,487,460	7,492,526	57	4.92E-08
20KUU025	Test 1	3,487,456	7,492,720	137	2.91E-04
	Test 2	3,487,456	7,492,723	134	3.38E-04
	Test 3	3,487,460	7,492,760	75	2.74E-06
	Test 4	3,487,465	7,492,792	23	2.77E-05
	Test 5	3,487,467	7,492,803	15	4.14E-05
	Test 6	3,487,467	7,492,803	-7	1.87E-05
20MOS8244	Test 1	3,488,278	7,494,976	-206	3.09E-09
	Test 2	3,488,260	7,494,951	-245	2.49E-09
	Test 3	3,488,229	7,494,912	-320	3.35E-10
	Test 4	3,488,216	7,494,895	-379	7.68E-09

TABLE 3-2

Summary of Measured Hydraulic Conductivity Values from Packer Tests
(Page 6 of 7)

Well ID	Test ID	Easting (m) ¹	Northing (m) ¹	Midpoint of Measurement (mamsl)	Hydraulic Conductivity (m/s)
20MOS8245	Test 1	3,487,544	7,494,406	-11	3.94E-09
	Test 2	3,487,544	7,494,406	-11	2.04E-09
	Test 3	3,487,543	7,494,374	-78	6.34E-08
	Test 4	3,487,543	7,494,374	-114	8.14E-08
	Test 5	3,487,537	7,494,319	-209	8.07E-08
	Test 6	3,487,536	7,494,315	-229	1.88E-07
20MOS8246	Test 1	3,487,475	7,493,958	30	1.89E-08
	Test 2	3,487,478	7,493,935	7	6.59E-09
	Test 3	3,487,480	7,493,903	-69	1.03E-07
	Test 4	3,487,481	7,493,868	-131	3.88E-10
	Test 5	3,487,481	7,493,852	-166	1.12E-08
20MOS8247	Test 1	3,487,476	7,493,558	134	1.93E-06
	Test 2	3,487,476	7,493,560	107	3.83E-07
	Test 3	3,487,477	7,493,514	-14	8.74E-08
	Test 4	3,487,478	7,493,504	-59	5.52E-08
20MOS8249	test 1	3,489,098	7,495,881	87	1.11E-07
	test 2	3,489,098	7,495,879	68	1.18E-06
	test 1	3,489,095	7,495,798	-329	4.54E-10
20MOS8250	test 1	3,489,102	7,495,796	104	6.16E-06
	test 2	3,489,104	7,495,785	18	1.73E-06
	test 3	3,489,105	7,495,778	-40	1.45E-09
	test 4	3,489,106	7,495,769	-142	3.16E-09
	test 5	3,489,106	7,495,754	-213	9.37E-10
20MOS8253	test 1	3,489,150	7,496,014	95	8.77E-08
	test 2	3,489,150	7,496,011	82	1.30E-08
	test 3	3,489,151	7,495,998	-29	3.84E-09
	test 4	3,489,151	7,495,994	-40	8.04E-09
	test 5	3,489,155	7,495,954	-282	4.44E-10
	test 6	3,489,150	7,495,876	-514	4.21E-09
	test 7	3,489,145	7,495,828	-680	1.80E-09
20MOS8254	test 1	3,489,247	7,495,901	54	1.31E-09
	test 2	3,489,248	7,495,896	-32	5.16E-09
	test 3	3,489,248	7,495,887	-109	6.03E-09
	test 4	3,489,249	7,495,885	-145	1.65E-09
	test 5	3,489,250	7,495,870	-286	6.83E-11
20MOS8255	test 1	3,489,349	7,495,839	111	6.60E-08
	test 2	3,489,349	7,495,838	98	6.84E-08
	test 3	3,489,349	7,495,836	51	2.61E-08
	test 4	3,489,349	7,495,830	-61	1.59E-08
	test 5	3,489,350	7,495,824	-138	7.51E-10
	test 6	3,489,351	7,495,811	-292	2.16E-06

TABLE 3-2

Summary of Measured Hydraulic Conductivity Values from Packer Tests
(Page 7 of 7)

Well ID	Test ID	Easting (m) ¹	Northing (m) ¹	Midpoint of Measurement (mamsl)	Hydraulic Conductivity (m/s)
20MOS8258	test 1	3,489,340	7,496,070	-244	1.08E-08
21KUU026	test 1	3,487,472	7,493,215	155	1.01E-07
	test 2	3,487,472	7,493,198	88	6.88E-08
	test 3	3,487,474	7,493,178	36	1.87E-08
	test 4	3,487,475	7,493,162	-16	9.49E-08
	test 5	3,487,475	7,493,143	-60	5.23E-07
21KUU027	test 1	3,487,473	7,493,016	82	4.66E-08
	test 2	3,487,473	7,493,002	48	5.05E-08
	test 3	3,487,473	7,492,981	6	1.58E-08
	test 4	3,487,472	7,492,958	-33	5.42E-09
21MOS8245B	test 1	3,489,248	7,495,806	-443	4.50E-09
21MOS8256	test 1	3,489,306	7,496,035	54	1.97E-08
	test 2	3,489,312	7,495,917	-448	8.41E-10
	test 3	3,489,311	7,495,904	-479	3.22E-09
21MOS8256B	test 1	3,489,310	7,495,972	-353	8.70E-10
	test 2	3,489,305	7,495,949	-492	1.03E-09
21MOS8257C	test 1	3,489,547	7,496,007	-454	6.00E-09
	test 2	3,489,547	7,495,958	-630	5.62E-10
21MOS8258B	test 1	3,489,333	7,496,011	-486	5.24E-09
	test 4	3,489,344	7,495,930	-806	8.28E-10
21MOS8259	test 1	3,489,608	7,496,144	-44	6.55E-10
	test 2	3,489,601	7,495,800	-592	5.19E-10
21MOS8259B	test 1	3,489,613	7,495,935	-462	1.28E-09
	test 2	3,489,609	7,495,895	-588	6.69E-09
21MOS8260	test 1	3,489,539	7,495,868	-317	7.47E-08
	test 2	3,489,553	7,495,719	-540	1.10E-09
	test 3	3,489,553	7,495,715	-571	2.90E-10
21MOS8260B	test 1	3,489,540	7,495,827	-417	8.83E-09
	test 2	3,489,542	7,495,815	-495	8.59E-10
21MOS8261	test 1	3,489,701	7,496,193	98	3.80E-08
	test 2	3,489,697	7,495,980	-544	3.74E-09
21MOS8262	test 1	3,489,704	7,496,047	118	5.05E-08
	test 3	3,489,718	7,495,937	-210	9.93E-07
	test 4	3,489,698	7,495,727	-526	1.06E-08
21MOS8263	test 1	3,489,650	7,496,090	104	7.63E-09
	test 2	3,489,649	7,495,969	-239	1.80E-09
	test 3	3,489,648	7,495,913	-390	6.51E-10
	test 4	3,489,647	7,495,871	-504	1.73E-08

Note:

1. Coordinate System is KKJ3.

TABLE 3-3

Summary of Measured Hydraulic Conductivity Values from Falling Head Tests

Well ID	Drilled Depth (mbgs)	Top	Bottom	Aquifer Thickness (m)	Tested Formation	Test Date	Pumping Test Analysis					
							Method	K (m/day)	K (m/s)	T (m ² /day)	T (m ² /s)	Comments
11MOS8049	914.01	159.00	177.00	18.00	Hanging Wall Volcaniclastics	2/5/2017	Bouwer Rice	3.15E-01	3.65E-06	5.67E+00	6.56E-05	Falling Head Test
13MOS8120	1060.90	140.00	171.00	31.00	Breccia	2/3/2017	Bouwer Rice	2.09E+00	2.42E-05	6.47E+01	7.49E-04	Falling Head Test. At contact of hanging wall volcaniclastics and breccia (146 m). Poor rock quality at 151 - 154 m.
13MOS8125	820.80	126.00	157.00	31.00	Breccia	2/3/2017	Bouwer Rice	7.94E-01	9.19E-06	2.46E+01	2.85E-04	Falling Head Test. At contact of altered ultramafic and breccia (137 m). Poor rock quality at narrow intervals 130.2 - 130.6 m and 150.6 - 151.7 m.

TABLE 3-4

Summary of Measured Hydraulic Conductivity Values from Pump Tests

Well ID	Tested Formation	Pumping Test Analysis		
		Analysis Method	T (m ² /d)	K (m/s)
17MOS8193	Bedrock - Basal Thrust	Theis recovery	2.36E+01	9.59E-07
		Cooper-Jacob	1.46E+01	5.93E-07
		Papadopoulos-Cooper	1.66E+01	6.74E-07
18MOS8207	Bedrock - SE-NW Fault	Theis recovery	4.06E-03	9.96E-11
18MOS8205	Bedrock	Cooper-Jacob	2.67E-01	1.67E-08
17HYD001	Shallow Bedrock	Cooper-Jacob	1.42E+02	3.25E-05
17HYD002	Shallow Bedrock	Theis	1.76E+02	2.79E-05
17HYD014	Shallow Bedrock	Neuman unconfined	1.05E-02	3.76E-09
17HYD004	Shallow Bedrock	MLU multilayered aquifer	7.43E+01	9.51E-06
17HYD006	Shallow Bedrock	MLU multilayered aquifer	2.62E+01	3.33E-06
17HYD008	Shallow Bedrock	MLU with leaky aquifer	5.20E+01	6.56E-06
17MOS8169	Shallow Bedrock	Cooper-Jacob (drawdown and recovery)	1.84E+00	8.06E-08
11MOS8054	See spinner test log	Bouwer-Rice	1.03E-01	1.11E-09
13MOS8123	See spinner test log	Theis Recovery	7.71E-01	9.74E-09
16MOS8161	See spinner test log	Cooper-Jacob (drawdown and recovery)	5.66E-01	7.40E-09
12MOS8096	See spinner test log	Cooper-Jacob (recovery only)	1.72E+00	6.11E-08
17HYD013	See spinner test log	Cooper-Jacob	1.72E+00	1.04E-07
17HYD017	See spinner test log	Cooper-Jacob (recovery only)	2.94E+01	5.81E-06
17MOS8174	See spinner test log	Cooper-Jacob (recovery only)	5.57E-01	9.32E-09
17HYD016	Glacial (gravelly clayey sand)	MLU multilayered aquifer	2.93E+01	1.16E-04
17HYD015	Glacial (gravelly clayey sand)	MLU multilayered aquifer	1.31E+01	5.21E-05

TABLE 3-5

Summary of Measured Hydraulic Conductivity Values from Air-Lift Tests

Well ID	Depth (mbgs)	Measured Water Level (mbgs)	Saturated Aquifer Thickness (m)	Test Date	Airlift Test Analysis			
					Method	T (m ² /d)	K (m/d)	K (m/s)
17HYD003	12.09	1.19	10.90	5/1/2017	Theis recovery	75.78	6.952	8.05E-05
17HYD005	9.55	0.05	9.50	5/2/2017	Theis recovery	57.33	6.035	6.98E-05
17HYD007	16.00	1.54	14.46	4/24/2017	Theis recovery	0.81	0.056	6.48E-07
17HYD009	8.60	4.68	3.92	4/21/2017	Theis recovery	0.017	0.004	5.02E-08
17HYD011	12.74	0.10	12.64	4/30/2017	Theis recovery	10.24	0.810	9.38E-06
17HYD012	8.40	0.09	8.31	4/22/2017	Theis recovery	30.43	3.662	4.24E-05
17HYD015	11.50	0.70	10.80	4/30/2017	Theis recovery	33	3.056	3.54E-05
17HYD018	9.51	5.94	2.09	3/8/2017	Cooper-Jacob unconfined	0.677	0.324	3.75E-06
17HYD016	10.75	5.53	2.49	3/7/2017	Bouwer-Rice unconfined	0.041085	0.0165	1.91E-07

TABLE 3-6
Measured Hydraulic Conductivity Values at Fault Structures

Well ID	Test Type	Meters below Ground Surface (m)		Fault Structure	Measured Hydraulic Conductivity (m/s)
		From	To		
16MOS8160	Packer	380.4	480.4	HW Shear Central	1.26E-08
16MOS8160	Packer	795.35	893.1	SENW1	6.31E-11
16MOS8163	Packer	167.4	215.4	EW	2.37E-08
16MOS8163	Packer	215.4	281.75	EW	1.05E-08
17MOS8174	Packer	100.95	158.4	EW Central	6.17E-09
17MOS8174	Packer	158.4	242.4	EW Central	2.44E-08
17MOS8178	Packer	606.65	705.45	SENW1	6.04E-09
17MOS8184	Packer	477.25	572.2	SENW1	1.69E-08
17MOS8199	Packer	209.1	391.2	EW	1.87E-08
17MOS8200	Packer	396.15	496.15	EW	6.58E-09
17MOS8200	Packer	716.4	851.1	Lower Thrust 1	4.26E-11
17MOS8201	Packer	1039.25	1042	Lower Thrust 2	1.63E-09
17MOS8207	Packer	382.25	455.5	HW Shear Central, SENW1	3.56E-09
18MOS8208	Packer	858.35	930.8	HW Shear Central	2.14E-09
18MOS8208	Packer	930.8	1105.5	Lower Thrust 2	8.58E-10
18MOS8226	Packer	865.2	950	Lower Thrust 2	1.67E-08
18MOS8231	Packer	588.35	683.5	HW Shear Central	4.34E-08
20MOS8248	Packer	744.9	780	Not yet in model 2020	7.04E-10
20MOS8250	Packer	271.9	389.6	Not yet in model 2020	3.15E-09
20MOS8253	Packer	708.9	730.9	Not yet in model 2020	1.24E-07
20MOS8254	Packer	115.1	148.4	Not yet in model 2020	1.31E-09
20MOS8255	Packer	122.5	182.8	Not yet in model 2020	2.61E-08
20MOS8255	Packer	186.2	282.9	Not yet in model 2020	1.59E-08
20MOS8255	Packer	311.8	368.8	Not yet in model 2020	7.69E-10
20MOS8256	Packer	671.55	703.8	Not yet in model 2020	3.22E-09
21MOS8257C	Packer	789.9	903	Not yet in model 2020	5.62E-10
21MOS8259B	Packer	684.6	734.8	Not yet in model 2020	1.28E-09
21MOS8260	Packer	486.5	593.4	Not yet in model 2020	5.41E-08
21MOS8262	Packer	363.9	485.4	Not yet in model 2020	1.04E-06
21MOS8263	Packer	30.4	139.5	Not yet in model 2020	7.63E-09
21MOS8263	Packer	573.2	647.2	Not yet in model 2020	6.51E-10
13MOS8123	Spinner	312.6	316.66	Mylonitic shear	3.54E-08
16MOS8161	Spinner	64.16	104.16	Mylonitic Shear	7.40E-09
17HYD013	Spinner	28.75	35.75	Broken core	7.59E-07
17MOS8174	Spinner	508.15	512.55	Broken core	3.11E-08
17MOS8174	Spinner	600.95	629.15	Very broken	1.67E-08
17MOS8174	Spinner	653.35	654.75	Strongly altered	5.90E-09

TABLE 3-7

Measured Annual Precipitation Data at Sodankylä Tähtelä Station
(Page 1 of 2)

Year	Measured Annual Precipitation (mm)
1959	402
1960	437.4
1961	609.3
1962	530.4
1963	497.9
1964	498.4
1965	569.2
1966	555.3
1967	556.1
1968	469.2
1969	405.9
1970	485.9
1971	412
1972	494.2
1973	406.8
1974	600.3
1975	494.1
1976	391.4
1977	512.4
1978	409
1979	543.7
1980	414.4
1981	623.3
1982	458.9
1983	549.2
1984	507.4
1985	554.8
1986	515.6
1987	480.9
1988	505.2
1989	490.2
1990	434.8
1991	457
1992	784.7
1993	449.3
1994	411.5
1995	560.1
1996	526.6

TABLE 3-7
**Measured Annual Precipitation Data at Sodankylä Tähtelä Station
 (Page 2 of 2)**

Year	Measured Annual Precipitation (mm)
1997	462.2
1998	679.6
1999	445.9
2000	646.4
2001	544.5
2002	480
2003	478.1
2004	596.9
2005	644.6
2006	408.4
2007	540.6
2008	600.2
2009	498.9
2010	515.8
2011	604
2012	627.3
2013	486.7
2014	551.5
2015	662.9
2016	636.6
2017	443.4
2018	472.2
2019	527.4
2020	552
2021 ¹	170.9
Arithmetic Mean (1959 to 2020)	518
Arithmetic Mean (2000 to 2020)	548
Arithmetic Mean (2010 to 2020)	553

Note:

1. Year 2021 was not included in the geometric mean due to an incomplete dataset.

TABLE 3-8
Average Monthly and Daily Precipitation Rates at the Sodankylä Tähtelä Station

Month	Entire Record (1959 to 2020)		Last 20 Years (2000 to 2020)		Last 10 Years (2011 to 2020)	
	Daily Precipitation Rate (mm/day)	Total Monthly Precipitation (mm)	Daily Precipitation Rate (mm/day)	Total Monthly Precipitation (mm)	Daily Precipitation Rate (mm/day)	Total Monthly Precipitation (mm)
January	1.1	33.7	1.2	36.3	1.1	35.0
February	1.0	27.4	1.0	29.3	1.0	28.2
March	0.9	27.1	0.9	28.8	0.8	26.3
April	0.9	27.4	1.0	30.1	1.0	29.5
May	1.2	37.7	1.3	41.7	1.4	43.9
June	1.9	57.5	2.4	71.4	1.9	58.2
July	2.3	69.8	2.3	70.8	2.7	82.6
August	1.9	59.9	1.5	47.0	1.8	56.4
September	1.8	52.6	1.8	54.1	1.9	56.4
October	1.6	48.1	1.7	51.4	1.4	44.6
November	1.4	40.7	1.5	45.6	1.4	42.2
December	1.2	19.7	1.6	27.9	1.3	22.3

TABLE 3-9

Measured Annual Pan Evaporation Data at the Sodankylä Tähtelä Station
(Page 1 of 2)

Year	Pan Evaporation Rate (mm)
1957	78.1
1958	331.9
1959	393.9
1960	518.6
1961	397.0
1962	320.4
1963	464.2
1964	408.8
1965	305.1
1966	385.9
1967	387.2
1968	398.3
1969	406.6
1970	485.6
1971	428.8
1972	428.7
1973	472.3
1974	359.5
1975	377.9
1976	427.5
1977	341.5
1978	371.6
1979	367.3
1980	411.9
1981	288.5
1982	340.5
1983	336.4
1984	343.8
1985	318.6
1986	310.9
1987	271.9
1988	297.3
1989	375.9
1990	264.8
1991	259.1
1992	246.6
1993	190.7
1994	296.2

TABLE 3-9

**Measured Annual Pan Evaporation Data at the Sodankylä Tähtelä Station
(Page 2 of 2)**

Year	Pan Evaporation Rate (mm)
1995	310.9
1996	293.0
1997	365.9
1998	260.2
1999	318.6
2000	269.5
2001	282.6
2002	387.4
2003	377.3
2004	286.5
2005	316.7
2006	398.6
2007	305.2
2008	267.9
2009	344.8
2010	318.4
2011	398.8
2012	268.1
2013	210.3
2014	202.0
2015	122.6
Arithmetic Mean (1958 to 2011)	349
Arithmetic Mean (2000 to 2011)	329

Note:

1. Data from 1957 and 2012 through 2015 are excluded from the datasets due to anomalously low measured data.

TABLE 3-10

**Estimated Future Recharge Rates to Hydrogeologic Units for the Climate Case RCP4.5
 (Page 1 of 10)**

Date	Estimated Future Recharge Rate for RCP4.5 Case (mm/day)		
	Till	Sediment	Peat
7/1/2021	0.4	0.5	0.4
8/1/2021	0.9	1.3	0.0
9/1/2021	0.4	0.8	0.0
10/1/2021	0.0	0.0	0.0
11/1/2021	0.5	0.6	0.0
12/1/2021	0.0	0.0	0.0
1/1/2022	0.0	0.0	0.0
2/1/2022	0.1	0.5	0.1
3/1/2022	0.0	0.0	0.0
4/1/2022	0.9	1.3	0.3
5/1/2022	1.4	2.5	0.0
6/1/2022	0.4	0.5	0.6
7/1/2022	0.0	0.0	0.0
8/1/2022	0.0	0.0	0.0
9/1/2022	0.0	0.3	0.8
10/1/2022	1.3	1.4	0.1
11/1/2022	0.3	0.6	0.0
12/1/2022	0.1	0.2	0.0
1/1/2023	0.0	0.0	0.0
2/1/2023	0.2	0.4	0.1
3/1/2023	0.0	0.1	0.0
4/1/2023	0.6	0.9	0.2
5/1/2023	2.4	5.0	0.0
6/1/2023	0.0	0.0	0.0
7/1/2023	0.0	0.1	0.4
8/1/2023	0.0	0.0	0.0
9/1/2023	0.0	0.0	0.0
10/1/2023	0.0	0.1	1.1
11/1/2023	0.0	0.0	0.0
12/1/2023	1.5	1.6	1.2
1/1/2024	0.0	0.0	0.0
2/1/2024	0.0	0.0	0.0
3/1/2024	0.3	0.8	0.2
4/1/2024	1.1	1.6	0.2
5/1/2024	0.8	1.4	0.0
6/1/2024	0.0	0.0	0.0
7/1/2024	0.0	0.0	0.0

TABLE 3-10

**Estimated Future Recharge Rates to Hydrogeologic Units for the Climate Case RCP4.5
 (Page 2 of 10)**

Date	Estimated Future Recharge Rate for RCP4.5 Case (mm/day)		
	Till	Sediment	Peat
8/1/2024	2.0	2.4	3.3
9/1/2024	0.0	0.2	0.0
10/1/2024	0.6	0.8	0.0
11/1/2024	0.6	1.0	0.0
12/1/2024	0.1	0.3	0.0
1/1/2025	0.4	0.7	0.0
2/1/2025	0.0	0.0	0.0
3/1/2025	0.0	0.2	0.0
4/1/2025	2.5	4.0	0.0
5/1/2025	0.4	0.5	0.0
6/1/2025	0.3	0.8	0.0
7/1/2025	0.0	0.0	0.0
8/1/2025	0.0	0.2	0.5
9/1/2025	0.5	0.5	0.0
10/1/2025	1.1	1.4	0.1
11/1/2025	0.9	1.4	0.0
12/1/2025	0.9	1.2	0.0
1/1/2026	0.0	0.0	0.0
2/1/2026	0.0	0.0	0.0
3/1/2026	0.0	0.2	0.0
4/1/2026	2.4	3.2	0.3
5/1/2026	0.0	1.1	0.0
6/1/2026	0.0	0.0	0.0
7/1/2026	0.0	0.0	0.0
8/1/2026	0.0	0.0	0.0
9/1/2026	0.0	0.2	1.7
10/1/2026	0.0	0.1	0.9
11/1/2026	0.0	0.0	0.1
12/1/2026	0.0	0.0	0.0
1/1/2027	0.1	0.2	0.3
2/1/2027	0.0	0.0	0.0
3/1/2027	1.6	1.2	0.4
4/1/2027	2.1	3.5	0.3
5/1/2027	0.3	1.0	0.0
6/1/2027	0.0	0.0	0.0
7/1/2027	0.0	0.1	0.5
8/1/2027	0.0	0.0	0.0

TABLE 3-10

Estimated Future Recharge Rates to Hydrogeologic Units for the Climate Case RCP4.5
(Page 3 of 10)

Date	Estimated Future Recharge Rate for RCP4.5 Case (mm/day)		
	Till	Sediment	Peat
9/1/2027	0.0	0.0	0.0
10/1/2027	0.0	0.1	1.3
11/1/2027	0.0	0.0	0.6
12/1/2027	2.5	2.8	1.1
1/1/2028	0.0	0.1	0.0
2/1/2028	0.0	0.0	0.0
3/1/2028	0.5	1.0	0.2
4/1/2028	2.2	3.3	0.1
5/1/2028	0.0	0.0	0.0
6/1/2028	0.0	0.1	0.0
7/1/2028	0.1	0.2	0.2
8/1/2028	0.0	0.0	0.0
9/1/2028	0.0	0.0	0.3
10/1/2028	0.0	0.0	0.0
11/1/2028	0.0	0.0	0.3
12/1/2028	0.0	0.0	0.0
1/1/2029	0.0	0.0	0.5
2/1/2029	0.0	0.0	0.0
3/1/2029	0.0	0.0	0.0
4/1/2029	3.3	5.5	1.0
5/1/2029	0.0	0.0	0.0
6/1/2029	0.0	0.0	0.0
7/1/2029	0.0	0.0	0.6
8/1/2029	0.1	0.2	1.0
9/1/2029	1.5	1.4	0.1
10/1/2029	0.1	0.3	0.0
11/1/2029	0.9	1.4	0.1
12/1/2029	0.2	0.5	0.0
1/1/2030	0.0	0.0	0.0
2/1/2030	0.4	0.5	0.0
3/1/2030	0.0	0.3	0.0
4/1/2030	0.1	0.2	0.0
5/1/2030	2.3	4.0	0.0
6/1/2030	0.0	0.0	0.0
7/1/2030	0.0	0.0	0.0
8/1/2030	0.0	0.2	1.8
9/1/2030	0.1	0.2	0.4

TABLE 3-10

**Estimated Future Recharge Rates to Hydrogeologic Units for the Climate Case RCP4.5
 (Page 4 of 10)**

Date	Estimated Future Recharge Rate for RCP4.5 Case (mm/day)		
	Till	Sediment	Peat
10/1/2030	0.4	0.4	0.1
11/1/2030	0.6	0.3	0.0
12/1/2030	0.0	0.0	0.0
1/1/2031	2.3	3.7	0.4
2/1/2031	0.0	0.0	0.0
3/1/2031	0.0	0.0	0.0
4/1/2031	1.7	2.7	0.0
5/1/2031	0.0	0.1	0.0
6/1/2031	0.0	0.0	0.0
7/1/2031	0.0	0.0	0.0
8/1/2031	0.0	0.0	0.1
9/1/2031	1.4	1.4	0.4
10/1/2031	0.1	0.3	0.0
11/1/2031	0.8	1.1	0.1
12/1/2031	0.0	0.0	0.0
1/1/2032	0.0	0.0	0.0
2/1/2032	0.0	0.1	0.1
3/1/2032	0.0	0.0	0.0
4/1/2032	3.1	4.6	0.4
5/1/2032	0.4	0.6	0.0
6/1/2032	0.0	0.1	0.0
7/1/2032	0.8	1.0	0.5
8/1/2032	0.0	0.0	0.0
9/1/2032	0.2	0.7	0.4
10/1/2032	1.1	1.5	0.1
11/1/2032	1.1	1.6	0.0
12/1/2032	0.5	0.9	0.0
1/1/2033	0.7	1.1	0.0
2/1/2033	0.0	0.0	0.0
3/1/2033	0.0	0.0	0.0
4/1/2033	0.0	0.0	0.0
5/1/2033	1.6	2.2	0.1
6/1/2033	0.0	0.0	0.0
7/1/2033	0.0	0.3	1.5
8/1/2033	2.1	2.6	0.3
9/1/2033	0.5	0.8	0.0
10/1/2033	1.0	1.5	0.0

TABLE 3-10

**Estimated Future Recharge Rates to Hydrogeologic Units for the Climate Case RCP4.5
 (Page 5 of 10)**

Date	Estimated Future Recharge Rate for RCP4.5 Case (mm/day)		
	Till	Sediment	Peat
11/1/2033	0.3	0.7	0.0
12/1/2033	0.0	0.0	0.0
1/1/2034	0.0	0.0	0.0
2/1/2034	0.2	0.4	0.0
3/1/2034	0.0	0.1	0.0
4/1/2034	0.0	0.0	0.0
5/1/2034	2.1	3.3	0.0
6/1/2034	0.0	0.0	0.0
7/1/2034	0.0	0.0	0.0
8/1/2034	0.0	0.0	0.0
9/1/2034	0.0	0.0	0.0
10/1/2034	0.0	0.1	2.1
11/1/2034	0.0	0.9	1.1
12/1/2034	1.1	0.7	1.2
1/1/2035	0.4	0.9	0.4
2/1/2035	0.8	1.4	0.1
3/1/2035	0.0	0.0	0.0
4/1/2035	1.6	2.3	0.2
5/1/2035	0.3	0.5	0.0
6/1/2035	0.0	0.0	0.0
7/1/2035	0.0	0.0	0.0
8/1/2035	0.0	0.2	1.9
9/1/2035	0.0	0.1	0.4
10/1/2035	1.5	1.2	0.3
11/1/2035	0.2	0.9	0.0
12/1/2035	0.0	0.0	0.0
1/1/2036	1.0	1.4	0.2
2/1/2036	0.0	0.0	0.0
3/1/2036	0.0	0.1	0.0
4/1/2036	0.0	0.0	0.0
5/1/2036	1.6	2.5	0.0
6/1/2036	0.0	0.0	0.0
7/1/2036	0.0	0.0	0.2
8/1/2036	0.6	0.6	1.2
9/1/2036	0.6	0.5	0.1
10/1/2036	1.5	2.1	0.2
11/1/2036	0.0	0.0	0.0

TABLE 3-10

**Estimated Future Recharge Rates to Hydrogeologic Units for the Climate Case RCP4.5
 (Page 6 of 10)**

Date	Estimated Future Recharge Rate for RCP4.5 Case (mm/day)		
	Till	Sediment	Peat
12/1/2036	0.9	1.0	0.1
1/1/2037	0.6	1.1	0.0
2/1/2037	0.1	0.8	0.0
3/1/2037	0.0	0.0	0.0
4/1/2037	1.2	1.8	0.0
5/1/2037	0.0	0.0	0.0
6/1/2037	0.0	0.0	0.0
7/1/2037	0.8	0.9	0.0
8/1/2037	0.0	0.0	0.0
9/1/2037	0.0	0.0	0.4
10/1/2037	0.0	0.0	0.2
11/1/2037	0.0	0.3	1.4
12/1/2037	1.0	0.7	0.2
1/1/2038	0.0	0.2	0.0
2/1/2038	1.3	2.2	0.3
3/1/2038	0.0	0.1	0.0
4/1/2038	1.5	2.0	0.0
5/1/2038	0.2	0.1	0.0
6/1/2038	0.0	0.0	0.0
7/1/2038	0.6	0.8	0.0
8/1/2038	0.5	0.9	0.7
9/1/2038	0.1	0.3	0.0
10/1/2038	0.6	0.8	0.0
11/1/2038	0.6	1.0	0.0
12/1/2038	0.0	0.1	0.0
1/1/2039	1.2	1.7	0.0
2/1/2039	0.0	0.0	0.0
3/1/2039	0.0	0.0	0.0
4/1/2039	1.5	2.0	0.3
5/1/2039	0.2	0.6	0.0
6/1/2039	0.0	0.0	0.0
7/1/2039	0.0	0.0	0.0
8/1/2039	0.0	0.3	2.8
9/1/2039	1.5	1.4	1.0
10/1/2039	0.5	0.8	0.0
11/1/2039	0.7	1.2	0.0
12/1/2039	0.0	0.3	0.0

TABLE 3-10

**Estimated Future Recharge Rates to Hydrogeologic Units for the Climate Case RCP4.5
 (Page 7 of 10)**

Date	Estimated Future Recharge Rate for RCP4.5 Case (mm/day)		
	Till	Sediment	Peat
1/1/2040	0.0	0.0	0.0
2/1/2040	0.0	0.0	0.0
3/1/2040	0.0	0.1	0.0
4/1/2040	1.1	1.3	0.3
5/1/2040	1.8	3.6	0.0
6/1/2040	0.0	0.0	0.0
7/1/2040	1.3	1.9	1.8
8/1/2040	0.0	0.0	0.0
9/1/2040	0.3	0.4	0.6
10/1/2040	1.7	2.4	0.0
11/1/2040	0.7	1.0	0.0
12/1/2040	0.9	1.2	0.0
1/1/2041	1.0	1.8	0.0
2/1/2041	0.3	0.7	0.0
3/1/2041	0.0	0.0	0.0
4/1/2041	1.4	1.6	0.1
5/1/2041	0.0	0.0	0.0
6/1/2041	0.4	0.4	0.0
7/1/2041	0.0	0.0	0.0
8/1/2041	0.0	0.0	0.1
9/1/2041	0.0	0.1	0.3
10/1/2041	0.0	0.0	0.8
11/1/2041	0.0	0.0	0.5
12/1/2041	0.0	0.0	0.4
1/1/2042	0.0	0.0	0.0
2/1/2042	0.0	0.0	0.0
3/1/2042	0.0	0.0	0.0
4/1/2042	1.5	2.5	1.0
5/1/2042	0.0	0.0	0.0
6/1/2042	0.0	0.0	0.2
7/1/2042	1.5	1.8	1.1
8/1/2042	0.6	1.4	0.0
9/1/2042	0.0	0.2	0.4
10/1/2042	1.0	1.3	0.2
11/1/2042	1.9	2.4	0.0
12/1/2042	0.0	0.1	0.0
1/1/2043	0.7	1.1	0.0

TABLE 3-10

**Estimated Future Recharge Rates to Hydrogeologic Units for the Climate Case RCP4.5
 (Page 8 of 10)**

Date	Estimated Future Recharge Rate for RCP4.5 Case (mm/day)		
	Till	Sediment	Peat
2/1/2043	0.0	0.0	0.0
3/1/2043	0.0	0.0	0.0
4/1/2043	2.0	3.1	0.3
5/1/2043	0.0	0.0	0.0
6/1/2043	0.0	0.0	0.0
7/1/2043	0.0	0.0	0.0
8/1/2043	0.0	0.0	0.0
9/1/2043	0.0	0.0	0.5
10/1/2043	0.0	0.0	0.9
11/1/2043	0.0	0.0	0.0
12/1/2043	0.0	0.0	0.0
1/1/2044	0.0	0.0	0.1
2/1/2044	0.0	0.1	0.4
3/1/2044	0.0	0.0	0.3
4/1/2044	2.9	3.7	1.6
5/1/2044	0.0	0.0	0.0
6/1/2044	0.0	0.0	0.0
7/1/2044	0.0	0.0	0.0
8/1/2044	0.0	0.0	0.1
9/1/2044	0.0	0.2	2.5
10/1/2044	0.2	0.6	0.4
11/1/2044	0.0	0.1	0.0
12/1/2044	1.0	0.2	0.1
1/1/2045	0.0	0.0	0.0
2/1/2045	0.0	0.0	0.0
3/1/2045	0.0	0.1	0.1
4/1/2045	1.2	1.6	0.5
5/1/2045	1.7	3.6	0.0
6/1/2045	0.0	0.0	0.0
7/1/2045	0.1	0.2	1.3
8/1/2045	0.0	0.0	0.1
9/1/2045	1.6	2.0	0.4
10/1/2045	1.2	1.8	0.0
11/1/2045	0.2	0.5	0.0
12/1/2045	0.0	0.0	0.0
1/1/2046	0.0	0.0	0.0
2/1/2046	1.3	1.8	0.3

TABLE 3-10

**Estimated Future Recharge Rates to Hydrogeologic Units for the Climate Case RCP4.5
 (Page 9 of 10)**

Date	Estimated Future Recharge Rate for RCP4.5 Case (mm/day)		
	Till	Sediment	Peat
3/1/2046	0.0	0.0	0.0
4/1/2046	2.9	4.3	0.0
5/1/2046	0.0	0.0	0.0
6/1/2046	0.0	0.0	0.0
7/1/2046	0.0	0.0	0.0
8/1/2046	0.0	0.0	0.0
9/1/2046	0.0	0.1	0.7
10/1/2046	0.0	0.0	0.0
11/1/2046	0.0	0.2	2.0
12/1/2046	0.0	0.0	0.2
1/1/2047	0.0	0.0	0.0
2/1/2047	0.0	0.0	0.0
3/1/2047	0.0	0.0	0.0
4/1/2047	3.3	4.3	1.3
5/1/2047	0.0	0.1	0.0
6/1/2047	0.5	0.6	1.0
7/1/2047	0.0	0.0	0.0
8/1/2047	0.0	0.0	0.0
9/1/2047	0.0	0.0	0.6
10/1/2047	0.0	0.2	1.4
11/1/2047	0.0	0.1	0.1
12/1/2047	0.0	0.2	0.1
1/1/2048	0.0	0.0	0.0
2/1/2048	0.0	0.0	0.0
3/1/2048	0.1	0.3	0.1
4/1/2048	4.1	5.8	0.7
5/1/2048	0.0	0.0	0.0
6/1/2048	0.0	0.0	0.0
7/1/2048	0.0	0.2	0.7
8/1/2048	0.4	0.4	0.4
9/1/2048	0.4	0.5	0.7
10/1/2048	1.1	1.5	0.2
11/1/2048	0.0	0.0	0.0
12/1/2048	0.3	0.5	0.0
1/1/2049	0.0	0.0	0.0
2/1/2049	0.0	0.0	0.0
3/1/2049	0.3	0.5	0.1

TABLE 3-10

**Estimated Future Recharge Rates to Hydrogeologic Units for the Climate Case RCP4.5
 (Page 10 of 10)**

Date	Estimated Future Recharge Rate for RCP4.5 Case (mm/day)		
	Till	Sediment	Peat
4/1/2049	0.7	1.0	0.2
5/1/2049	1.5	2.7	0.0
6/1/2049	0.0	0.0	0.0
7/1/2049	0.0	0.1	0.4
8/1/2049	0.4	0.5	0.5
9/1/2049	1.1	1.2	0.1
10/1/2049	0.1	0.5	0.0
11/1/2049	0.0	0.2	0.0
12/1/2049	0.5	0.4	0.0
1/1/2050	0.0	0.0	0.0
2/1/2050	0.0	0.0	0.0
3/1/2050	0.0	0.0	0.0
4/1/2050	1.2	2.1	0.3
5/1/2050	0.6	0.7	0.0
6/1/2050	0.0	0.0	0.0
7/1/2050	0.0	0.0	0.0
8/1/2050	0.0	0.0	0.4
9/1/2050	0.0	0.0	0.4
10/1/2050	0.0	0.0	0.5
11/1/2050	0.0	0.1	1.4
12/1/2050	0.0	0.0	0.3

TABLE 3-11

**Summary of Details on Groundwater Monitoring Network at the Project Site
(Page 1 of 4)**

Well ID	Easting (m) ¹	Northing (m) ¹	Ground Surface Elevation (mamsl)	Installation Years	Well Depth (m)	Slotted/Open Interval (mbgs)	Azimuth	Dip	Time Period of Measured Groundwater Levels	Data Collection Type	Well Type	Hydrogeologic Unit
11MOS8049	3,489,500	7,495,950	185.44	2016	200	180–195	175	75	2017–2021	Manual + Data Logger	Smartwell	Deep Bedrock
13MOS8120	3,489,230	7,495,850	185.6	2017	175	141–171	89	70	2017–2021	Manual + Data Logger	Smartwell	Deep Bedrock
13MOS8125	3,489,240	7,495,550	187.19	2017	160	127–157	93	85	2017–2021	Manual + Data Logger	Smartwell	Deep Bedrock
16MOS8158	3,488,634	7,495,872	182.49	2017	605	NA	132	75	2017–2021	Continuous/Sensors	VWP	Deep Bedrock
16MOS8160	3,489,493	7,495,998	186.15	2017	823	NA	178	68	2017–2021	Continuous/Sensors	VWP	Deep Bedrock
16MOS8163	3,489,401	7,495,450	186.33	2017	727	NA	87	75	2017–2021	Continuous/Sensors	VWP	Deep Bedrock
17MOS8178	3,489,350	7,495,703	185.95	2017	760	NA	108	72	2017–2021	Continuous/Sensors	VWP	Deep Bedrock
17MOS8183	3,489,900	7,495,796	188.14	2017	545	NA	177	69	2017–2021	Terminated	VWP	Deep Bedrock
17HYD001	3,488,233	7,490,930	195.66	2017	76	27.7–75.7	0	90	2017–2021	Manual	Bedrock Monitoring Well	Shallow Bedrock
17HYD002	3,492,710	7,500,683	198.43	2017	100	26–100	0	90	2017	Manual	Bedrock Monitoring Well	Shallow Bedrock
17HYD003	3,488,285	7,490,807	195.60	2017	11	2–8	0	90	2017–2021	Manual	Shallow Sediment Well	Sediment
17HYD004	3,489,912	7,500,204	190.12	2017	100	32.8–99.8	0	90	2017–2021	Manual + Data Logger	Bedrock Monitoring Well	Shallow Bedrock
17HYD005	3,486,872	7,492,778	187.46	2017	10	3–5	0	90	2017–2021	Manual + Data Logger	Shallow Sediment Well	Sediment
17HYD006	3,489,607	7,498,030	190.67	2017	100	30–99	0	90	2017–2021	Manual + Data Logger	Bedrock Monitoring Well	Shallow Bedrock
17HYD007	3,492,706	7,500,704	198.47	2017	16	2.8–12.8	0	90	2017	Manual	Shallow Sediment Well	Sediment
17HYD008	3,488,494	7,497,684	189.07	2017	102	30–102	0	90	2017–2021	Manual + Data Logger	Bedrock Monitoring Well	Shallow Bedrock
17HYD009	3,488,700	7,497,492	188.31	2017	7	2.6–6.6	0	90	2017–2021	Manual	Shallow Sediment Well	Sediment
17HYD010	3,488,301	7,496,974	188.39	2017	7	1.4–3.4	0	90	2017–2021	Manual	Shallow Sediment Well	Sediment
17HYD011	3,481,069	7,505,428	216.81	2017	12.8	2.7–4.7; 10.7–12.7	0	90	2017	Manual	Shallow Sediment Well	Sediment
17HYD012	3,493,737	7,503,711	208.07	2017	8.2	4.3–7.8	0	90	2017	Manual	Shallow Sediment Well	Sediment
17HYD013	3,488,959	7,496,061	182.72	2017	251	29–251	54	76	2017–2021	Manual + Data Logger	Bedrock Monitoring Well	Shallow Bedrock
17HYD014	3,486,683	7,494,747	183.20	2017	112	22–112	0	90	2017–2021	Manual	Bedrock Monitoring Well	Shallow Bedrock
17HYD015	3,489,934	7,500,186	190.17	2017	11	3–5; 7–9	0	90	2017–2021	Manual + Data Logger	Shallow Sediment Well	Sediment
17HYD016	3,489,597	7,498,032	190.75	2017	11	3–7	0	90	2017–2021	Manual + Data Logger	Shallow Sediment Well	Sediment
17HYD017	3,487,834	7,496,295	188.01	2017	94.4	36.3–94.3	0	90	2017–2021	Manual + Data Logger	Bedrock Monitoring Well	Shallow Bedrock
17HYD018	3,488,469	7,497,725	189.35	2017	10.6	4.35–8.35	0	90	2017–2021	Manual + Data Logger	Shallow Sediment Well	Sediment
17HYD019	3,490,206	7,499,792	189.73	2017	9	1.2–3.2; 5.2–7.2	0	90	2017–2021	Manual + Data Logger	Shallow Sediment Well	Sediment
17HYD020	3,490,009	7,499,416	191.29	2017	10	4–8	0	90	2017–2021	Manual + Data Logger	Shallow Sediment Well	Sediment
17HYD021	3,489,642	7,499,133	189.69	2017	13.7	8–12	0	90	2017–2021	Barometric Data Logger	Shallow Sediment Well	Sediment

TABLE 3-11

**Summary of Details on Groundwater Monitoring Network at the Project Site
(Page 2 of 4)**

Well ID	Easting (m) ¹	Northing (m) ¹	Ground Surface Elevation (mamsl)	Installation Years	Well Depth (m)	Slotted/Open Interval (mbgs)	Azimuth	Dip	Time Period of Measured Groundwater Levels	Data Collection Type	Well Type	Hydrogeologic Unit
17HYD022	3,489,644	7,498,721	190.20	2017	14.4	8.25–12.25	0	90	2017–2021	Manual	Shallow Sediment Well	Sediment
17MOS8193	3,488,704	7,495,348	185.41	2017	1032	721.9–1006.9	155	80	2018–2021	Manual + Data Logger	Bedrock Pumping Well	Deep Bedrock
17MOS8198	3,488,740	7,495,158	186.06	2017	125	32.5–122.5	164	62	2018–2021	Manual + Data Logger	Bedrock Monitoring Well	Shallow Bedrock
17HYD023B	3,488,733	7,495,163	186.20	2018	15	2–14	0	90	2018–2021	Manual + Data Logger	Shallow Sediment Well	Sediment
18MOS8207	3,489,400	7,495,902	185.36	2018	902.5	284–774	174	76	2018–2021	Manual + Data Logger	Bedrock Pumping Well	Deep Bedrock
18MOS8205	3,489,298	7,495,850	185.9	2018	185.3	12.9–182.9	86	79	2019	Manual	Bedrock Monitoring Well	Shallow Bedrock
18HYD024	3,489,347	7,495,838	187.93	2018	7.3	6–7	0	90	2018–2021	Manual + Data Logger	Shallow Sediment Well	Sediment
18HYD025	3,486,594	7,490,597	192.87	2018	6.5	2.45–4.45	0	90	2018–2021	Manual + Data Logger	Shallow Sediment Well	Sediment
18HYD026	3,487,568	7,490,638	195.73	2018	14.4	2.8–4.8	0	90	2018	Manual	Shallow Sediment Well	Sediment
18HYD027	3,488,989	7,490,751	194.29	2018	6.4	2.3–4.3	0	90	2018–2021	Manual + Data Logger	Shallow Sediment Well	Sediment
18HYD028	3,486,369	7,491,695	193.54	2018	5.5	3.75–5.75	0	90	2018–2021	Manual + Data Logger	Shallow Sediment Well	Sediment
18HYD030	3,487,176	7,492,225	195.65	2018	9.3	7.9–9.9	0	90	2018–2021	Manual + Data Logger	Shallow Sediment Well	Sediment
18HYD033	3,487,929	7,491,219	200.02	2018	8.3	5.15–7.15	0	90	2018–2021	Manual + Data Logger	Shallow Sediment Well	Sediment
GA101	3,490,657	7,495,272	187.15	2012	5.1	3–5	0	90	2012–2021	Manual + Data Logger	Shallow Sediment Well	Peat
GA102	3,490,019	7,495,056	186.67	2012	3.3	1–3	0	90	2012–2021	Manual + Data Logger	Shallow Sediment Well	Peat
GA103	3,489,344	7,494,882	185.032	2012	2	1–2	0	90	2012–2021	Manual + Data Logger	Shallow Sediment Well	Peat
GA104	3,489,083	7,494,682	185.47	2012	3.7	2–4	0	90	2012–2021	Manual	Shallow Sediment Well	Peat
GA200	3,489,519	7,496,606	186.98	2012	6.4	4.5–6.5	0	90	2012–2021	Manual + Data Logger	Shallow Sediment Well	Sediment
GA201	3,489,834	7,496,186	187.49	2012	5	3–5	0	90	2012–2021	Manual + Data Logger	Shallow Sediment Well	Sediment
GA202	3,489,776	7,495,403	186.64	2012	5	4–5	0	90	2012–2021	Manual + Data Logger	Shallow Sediment Well	Sediment
GA203	3,489,033	7,495,716	187.54	2012	5.4	3.5–5.5	0	90	2012–2021	Manual + Data Logger	Shallow Sediment Well	Sediment
GA204	3,488,953	7,494,762	186.51	2012	4	2–4.5	0	90	2012–2021	Manual	Shallow Sediment Well	Sediment
GA205	3,488,408	7,494,872	187.75	2012	4	2–4	0	90	2012–2021	Manual	Shallow Sediment Well	Sediment
GA300	3,489,902	7,495,662	187.51	2012	3.5	2.5–3.5	0	90	2012–2021	Manual	Shallow Sediment Well	Sediment
GA301	3,490,661	7,495,260	187.22	2012	9.7	7.5–9.5	0	90	2012–2021	Manual + Data Logger	Shallow Sediment Well	Sediment
GA302	3,490,014	7,495,054	186.58	2012	10	8–10	0	90	2012–2021	Manual + Data Logger	Shallow Sediment Well	Sediment
GA303	3,489,310	7,494,800	186.06	2012	12.3	10.5–12.5	0	90	2012–2021	Manual + Data Logger	Shallow Sediment Well	Sediment
GA304	3,488,954	7,494,748	186.53	2012	14.2	12–14	0	90	2012–2021	Manual + Data Logger	Shallow Sediment Well	Sediment

TABLE 3-11

**Summary of Details on Groundwater Monitoring Network at the Project Site
(Page 3 of 4)**

Well ID	Easting (m) ¹	Northing (m) ¹	Ground Surface Elevation (mamsl)	Installation Years	Well Depth (m)	Slotted/Open Interval (mbgs)	Azimuth	Dip	Time Period of Measured Groundwater Levels	Data Collection Type	Well Type	Hydrogeologic Unit
GA305	3,489,034	7,495,720	187.44	2012	10	8–10	0	90	2012–2021	Manual + Data Logger	Shallow Sediment Well	Sediment
GA400	3,490,031	7,496,168	190.54	2012	6.9	5–7	0	90	2012–2021	Manual + Data Logger	Shallow Bedrock Well	Shallow Bedrock
GA401	3,490,663	7,495,268	187.22	2012	12.5	9.5–12.5	0	90	2012–2021	Manual + Data Logger	Shallow Bedrock Well	Shallow Bedrock
GA402	3,490,016	7,495,050	186.65	2012	13	11–13	0	90	2012–2021	Manual + Data Logger	Shallow Bedrock Well	Shallow Bedrock
GA403	3,489,329	7,494,844	186.04	2012	16.8	15–17	0	90	2012–2021	Manual + Data Logger	Shallow Bedrock Well	Shallow Bedrock
GA404	3,488,412	7,494,864	188.39	2012	10.4	8.5–10.5	0	90	2012–2021	Manual + Data Logger	Shallow Bedrock Well	Shallow Bedrock
GA405	3,489,035	7,495,723	187.41	2012	13.4	11.5–13.5	0	90	2012–2021	Manual + Data Logger	Shallow Bedrock Well	Shallow Bedrock
18MOS8232	3,487,479	7,493,522	183.14	2018	158	20–65.5	180	69	2018–2021	Manual + Data Logger	Bedrock Monitoring Well	Shallow Bedrock
18KUU001	3,487,464	7,492,301	196.62	2018	150	72–150	180	70	2018–2021	Manual + Data Logger	Bedrock Monitoring Well	Deep Bedrock
18KUU002	3,487,398	7,491,488	205.62	2018	70	13–70	43	60	2019, 2021	Manual + Data Logger	Bedrock Monitoring Well	Shallow Bedrock
18KUU003	3,488,012	7,491,630	216.7	2018	60	23–60	65	60	2018–2021	Manual + Data Logger	Bedrock Monitoring Well	Shallow Bedrock
18MOS8228	3,489,102	7,495,800	186.66	2018	197	162–178	180	60	2018–2021	Manual + Data Logger	Bedrock Monitoring Well	Deep Bedrock
18HYD035	3,489,199	7,495,546	186.83	2018	10	4–8	0	90	2018–2021	Manual + Data Logger	Shallow Sediment Well	Shallow Bedrock
18HYD036	3,489,198	7,495,550	186.73	2018	22	15–21	0	90	2018–2021	Manual + Data Logger	Bedrock Monitoring Well	Shallow Bedrock
18HYD037	3,489,196	7,495,554	186.8	2018	57	13–57	0	76	2018–2021	Manual + Data Logger	Bedrock Pumping Well	Shallow Bedrock
18MOS8227	3,487,811	7,494,748	185.37	2018	250	50–250	171	71	2018–2021	Manual + Data Logger	Bedrock Pumping Well	Deep Bedrock
18MOS8229	3,488,557	7,494,708	186.66	2018	158	138–160	179	70	2018–2021	Manual + Data Logger	Bedrock Monitoring Well	Deep Bedrock
18HYD038	3,488,534	7,494,660	186.95	2018	57	18–54	0	90	2018–2021	Manual + Data Logger	Bedrock Pumping Well	Shallow Bedrock
18HYD039	3,488,534	7,494,670	186.67	2018	15	5–12.5	0	90	2018–2021	Manual + Data Logger	Shallow Sediment Well	Shallow Bedrock
18HYD040	3,488,534	7,494,684	186.73	2018	30	24–30	0	90	2018–2021	Manual + Data Logger	Bedrock Monitoring Well	Shallow Bedrock
19KUU005	3,486,022	7,491,524	197.00	2019	50	20–50	1	60	2019–2021	Manual + Data Logger	Bedrock Monitoring Well	Shallow Bedrock
19KUU015	3,486,669	7,491,734	201.15	2019	15	9–15	1	60	2019–2021	Manual + Data Logger	Bedrock Monitoring Well	Shallow Bedrock
19KUU017	3,488,342	7,491,994	226.67	2019	51	0–50	360	60	2019–2021	Manual + Data Logger	Bedrock Monitoring Well	Shallow Bedrock
19KUU019	3,488,803	7,492,230	226.23	2019	51	20–50	1	60	2019–2021	Manual	Bedrock Monitoring Well	Shallow Bedrock
19KUU020	3,487,418	7,491,640	211.73	2019	70	50–55	71	60	No	No	Bedrock Monitoring Well	Shallow Bedrock
19KUU021	3,487,462	7,491,606	214.79	2019	60	7–60	288	60	2019–2021	Manual + Data Logger	Bedrock Monitoring Well	Shallow Bedrock
19KUU022	3,487,468	7,491,834	210.75	2019	100	80–100	319	60	2019–2021	Manual + Data Logger	Bedrock Monitoring Well	Shallow Bedrock
19KUU023	3,487,425	7,492,047	200.53	2019	53	33–50	30	60	2019–2021	Manual + Data Logger	Bedrock Monitoring Well	Shallow Bedrock

TABLE 3-11

Summary of Details on Groundwater Monitoring Network at the Project Site
(Page 4 of 4)

Well ID	Easting (m) ¹	Northing (m) ¹	Ground Surface Elevation (mamsl)	Installation Years	Well Depth (m)	Slotted/Open Interval (mbgs)	Azimuth	Dip	Time Period of Measured Groundwater Levels	Data Collection Type	Well Type	Hydrogeologic Unit
20MOS8245	3,487,543	7,494,463	184.6	2020	291	25–270	179	69	2020–2021	Manual + Data Logger	Bedrock Monitoring Well	Deep Bedrock
20MOS8246	3,487,468	7,494,011	183.56	2020	403	30–350	172	65	2020–2021	Manual + Data Logger	Bedrock Monitoring Well	Deep Bedrock
20MOS8247	3,487,476	7,493,572	184.57	2020	283	80–260	179	70	2020–2021	Manual + Data Logger	Bedrock Monitoring Well	Deep Bedrock
20KUU025	3,487,455	7,492,708	190.24	2020	203	100–200	4	60	2020–2021	Manual + Data Logger	Bedrock Monitoring Well	Deep Bedrock
20KUU024	3,487,457	7,492,474	192.23	2020	200	20–190	1	65	2020–2021	Manual + Data Logger	Bedrock Monitoring Well	Deep Bedrock
20GT028	3,488,222	7,491,067	198.71	2020	4.6	2.5–4.5	0	90	2021	Manual + Data Logger	Shallow Sediment Well	Sediment
20GT030	3,489,021	7,492,001	210.98	2020	5.6	3.5–5.5	0	90	2021	Terminated	Shallow Sediment Well	Sediment
20GT031	3,488,837	7,491,551	199.44	2020	4.7	2.5–4.5	0	90	2021	Manual + Data Logger	Shallow Sediment Well	Sediment
20GT032A	3,487,451	7,491,353	203.08	2020	2.8	0.8–2.8	0	90	2021	Terminated	Shallow Sediment Well	Sediment
20GT036	3,487,024	7,490,962	197.84	2020	4.6	1.5–4.5	0	90	2021	Manual + Data Logger	Shallow Sediment Well	Sediment
20GT037	3,487,131	7,491,215	203.54	2020	4.0	3–5	0	90	2021	Terminated	Shallow Sediment Well	Sediment
20GT038	3,486,826	7,491,204	203.75	2020	2.6	0.5–2.5	0	90	2021	Terminated	Shallow Sediment Well	Sediment
20HYD041	3,489,543	7,496,576	186.95	2020	201	145–195	276	85	No	No	Bedrock Monitoring Well	Deep Bedrock
20HYD042	3,489,466	7,496,479	187.06	2020	50	38–50	55	60	2021	Manual + Data Logger	Bedrock Monitoring Well	Shallow Bedrock
20HYD043	3,489,490	7,496,466	187	2020	216	25–120	49	64	No	No	Bedrock Monitoring Well	Shallow Bedrock
20HYD044	3,488,961	7,491,529	197.33	2020	122	16–32; 60–76; 108–112	231	60	No	No	Bedrock Monitoring Well	Shallow Bedrock
20HYD045	3,489,130	7,491,445	196.52	2020	123	25–260	0	60	2021	Manual + Data Logger	Bedrock Monitoring Well	Deep Bedrock
20MOS8248	3,489,110	7,495,595	186.31	2020	156	25–140	174	73	2021	Manual + Data Logger	Bedrock Monitoring Well	Shallow Bedrock
20MOS8249	3,489,097	7,495,889	188.19	2020	120	80–110	177	86	No	No	Bedrock Monitoring Well	Shallow Bedrock
21KUU026	3,487,471	7,493,221	187.60	2021	285	20–282.5	178	70	2021	Manual + Data Logger	Bedrock Monitoring Well	Deep Bedrock
21KUU027	3,487,475	7,493,067	188.28	2021	280	20–280	183	59	2021	Manual + Data Logger	Bedrock Monitoring Well	Deep Bedrock
21HYD046	3,487,472	7,493,542	183.65	2021	9	4–8	0	90	2021	Manual + Data Logger	Shallow Sediment Well	Sediment
21HYD047	3,487,465	7,493,543	183.93	2021	51	12–48	0	90	2021	Manual + Data Logger	Bedrock Monitoring Well	Shallow Bedrock
21HYD048	3,489,113	7,495,800	186.7	2021	110	38–108	180	70	2021	Manual + Data Logger	Bedrock Monitoring Well	Shallow Bedrock
21KUU028	3,487,467	7,493,221	187.66	2021	455	20–440	0	60	2021	Manual + Data Logger	Bedrock Monitoring Well	Deep Bedrock
21MOS8264	3,487,479	7,493,797	185.15	2021	339	109–329	177	68	2021	Manual + Data Logger	Bedrock Monitoring Well	Deep Bedrock

Note:

1. Coordinate system is KKJ3.

TABLE 4-1

Simulated Hydraulic Properties of the Hydrogeologic Units in the Sakatti Mine Groundwater Flow Model

Hydrogeologic Unit		Measured Range of Hydraulic Conductivity (m/s)	Model-Calibrated Hydraulic Parameters					Comment
			K_h (m/s) ¹	K_v (m/s)	Anisotropy K_h/K_v ²	S_s (m ⁻¹)	S_y	
Till	Upper Kuusivaara	5.0 x 10 ⁻⁸ to 4.3 x 10 ⁻³	3.5 x 10 ⁻⁵	3.5 x 10 ⁻⁶	10	1.0 x 10 ⁻⁶	0.025	
	Upper		5.8 x 10 ⁻⁶	2.9 x 10 ⁻⁶	2	1.0 x 10 ⁻⁶	0.05	
	Middle							
	Intermediate							
Lower								
Top Deposits (gravels)			3.5 x 10 ⁻⁵ 4.6 x 10 ⁻⁵	3.5 x 10 ⁻⁶ 4.6 x 10 ⁻⁶	10	1.0 x 10 ⁻⁶	0.15	
Sorted	Middle		2.3 x 10 ⁻⁵	5.8 x 10 ⁻⁶	4	1.0 x 10 ⁻⁶	0.05	
	Lower							
Sand	Upper		1.2 x 10 ⁻⁵	1.2 x 10 ⁻⁶	10	1.0 x 10 ⁻⁶	0.05	
	Middle							
	Lower							
Clay			1.2 x 10 ⁻⁶	1.2 x 10 ⁻⁷	10	1.0 x 10 ⁻⁶	0.05	
Grus			2.3 x 10 ⁻⁵	2.3 x 10 ⁻⁶	10	1.0 x 10 ⁻⁶	0.05	
Basal Sediment			1.2 x 10 ⁻⁵	1.2 x 10 ⁻⁶	10	1.0 x 10 ⁻⁶	0.05	
Kitinen River Deposits			2.3 x 10 ⁻⁵	2.3 x 10 ⁻⁶	10	1.0 x 10 ⁻⁶	0.25	
Peat		1.0 x 10 ⁻⁷ to 1.0 x 10 ⁻⁵	9.3 x 10 ⁻⁷ to 9.3 x 10 ⁻⁶	9.3 x 10 ⁻⁸ to 9.3 x 10 ⁻⁷	10	1.0 x 10 ⁻⁶	0.1 to 0.25	
Fractured Bedrock	Along River	8.1 x 10 ⁻⁸ to 1.4 x 10 ⁻⁴	2.3 x 10 ⁻⁵	2.3 x 10 ⁻⁶	10	5.0 x 10 ⁻⁶	0.01	
	Main Area		5.8 x 10 ⁻⁶	5.8 x 10 ⁻⁷	10	5.0 x 10 ⁻⁶	0.01	
	Kuusivaara Area		1.0 x 10 ⁻⁵ to 4.7 x 10 ⁻⁵	1.0 x 10 ⁻⁶ to 4.7 x 10 ⁻⁶	10	5.0 x 10 ⁻⁶	0.01	
Unfractured Bedrock	Along River	1.0 x 10 ⁻¹² to 3.4 x 10 ⁻⁵	2.0 x 10 ⁻⁹ to 2.0 x 10 ⁻⁷	2.0 x 10 ⁻¹⁰ to 2.0 x 10 ⁻⁸	10	5.0 x 10 ⁻⁶	0.005	K values decrease with depth based on the packer-testing data; see Figure 4-3.
	Over Mining Area		1.0 x 10 ⁻⁹ to 1.0 x 10 ⁻⁷	1.0 x 10 ⁻¹⁰ to 1.0 x 10 ⁻⁸	10	5.0 x 10 ⁻⁶	0.005	
Basal Thrust Fault		5.9 x 10 ⁻⁷ to 9.6 x 10 ⁻⁷	1.2 x 10 ⁻⁸ to 8.1 x 10 ⁻⁷	1.2 x 10 ⁻⁸ to 8.1 x 10 ⁻⁷	1	5.0 x 10 ⁻⁶	0.005	
Other Faults		4.3 x 10 ⁻¹¹ to 1.0 x 10 ⁻⁶	1.0 x 10 ⁻⁹ to 1.0 x 10 ⁻⁷	1.0 x 10 ⁻⁹ to 1.0 x 10 ⁻⁷	1	5.0 x 10 ⁻⁶	0.005	

Notes:

1. Assuming horizontal hydraulic conductivity in the x-direction (K_x) is equal to horizontal hydraulic conductivity in the y-direction (K_y).
2. Anisotropy between K_h and K_v was defined by the groundwater flow model calibration.

TABLE 4-2

Simulated Recharge Rates for the Hydrogeologic Units in the Groundwater Flow Model
(Page 1 of 3)

Date	Estimated Recharge Rate (mm/day)		
	Till	Sediment	Peat
6/1/2012	1.7	2.2	0.4
7/1/2012	0.0	0.0	0.0
8/1/2012	0.0	0.0	0.0
9/1/2012	1.4	1.5	2.3
10/1/2012	0.7	1.4	0.0
11/1/2012	1.3	1.8	0.0
12/1/2012	0.0	0.0	0.0
1/1/2013	0.0	0.0	0.0
2/1/2013	0.0	0.0	0.0
3/1/2013	0.0	0.0	0.0
4/1/2013	3.0	4.4	0.6
5/1/2013	0.0	0.1	0.0
6/1/2013	0.6	1.0	0.6
7/1/2013	0.0	0.0	0.0
8/1/2013	0.0	0.0	0.0
9/1/2013	0.0	0.0	0.2
10/1/2013	0.0	0.3	2.0
11/1/2013	0.0	0.0	0.0
12/1/2013	0.6	0.6	0.4
1/1/2014	0.0	0.0	0.0
2/1/2014	1.0	0.6	0.2
3/1/2014	0.9	1.7	0.1
4/1/2014	2.4	3.5	0.1
5/1/2014	0.0	0.0	0.0
6/1/2014	0.3	0.4	0.0
7/1/2014	0.0	0.0	0.0
8/1/2014	0.0	0.0	0.0
9/1/2014	0.3	0.7	0.8
10/1/2014	1.0	1.1	0.1
11/1/2014	0.5	0.7	0.0
12/1/2014	0.0	0.0	0.0
1/1/2015	0.0	0.0	0.0
2/1/2015	0.0	0.0	0.0
3/1/2015	0.5	0.9	0.2
4/1/2015	1.6	2.2	0.0
5/1/2015	1.9	3.5	0.0
6/1/2015	0.2	0.5	0.0

TABLE 4-2

Simulated Recharge Rates for the Hydrogeologic Units in the Groundwater Flow Model
(Page 2 of 3)

Date	Estimated Recharge Rate (mm/day)		
	Till	Sediment	Peat
7/1/2015	0.5	0.7	0.0
8/1/2015	0.0	0.0	0.0
9/1/2015	1.3	1.9	0.1
10/1/2015	0.7	1.0	0.0
11/1/2015	0.0	0.2	0.0
12/1/2015	0.0	0.0	0.0
1/1/2016	0.0	0.0	0.0
2/1/2016	0.7	0.8	0.1
3/1/2016	0.4	0.8	0.1
4/1/2016	2.7	4.0	0.0
5/1/2016	0.0	0.2	0.0
6/1/2016	1.0	1.5	0.6
7/1/2016	0.1	0.4	0.0
8/1/2016	0.6	0.6	0.2
9/1/2016	1.5	2.2	0.0
10/1/2016	0.0	0.0	0.0
11/1/2016	0.7	1.1	0.0
12/1/2016	0.0	0.0	0.0
1/1/2017	0.0	0.0	0.0
2/1/2017	0.0	0.1	0.0
3/1/2017	0.0	0.0	0.0
4/1/2017	0.5	0.4	0.1
5/1/2017	1.7	2.8	0.1
6/1/2017	0.0	0.0	0.0
7/1/2017	0.2	0.2	0.0
8/1/2017	0.0	0.1	0.4
9/1/2017	0.0	0.2	0.8
10/1/2017	1.0	1.3	0.2
11/1/2017	0.6	1.0	0.0
12/1/2017	0.0	0.0	0.0
1/1/2018	0.0	0.0	0.0
2/1/2018	0.0	0.0	0.0
3/1/2018	0.0	0.0	0.0
4/1/2018	2.5	3.4	0.6
5/1/2018	0.0	0.6	0.0
6/1/2018	0.0	0.0	0.0
7/1/2018	0.0	0.0	0.0

TABLE 4-2

Simulated Recharge Rates for the Hydrogeologic Units in the Groundwater Flow Model
(Page 3 of 3)

Date	Estimated Recharge Rate (mm/day)		
	Till	Sediment	Peat
8/1/2018	0.0	0.1	0.9
9/1/2018	0.5	1.1	1.6
10/1/2018	1.1	0.5	0.0
11/1/2018	0.3	1.0	0.0
12/1/2018	0.2	0.3	0.0
1/1/2019	0.0	0.0	0.0
2/1/2019	0.0	0.2	0.1
3/1/2019	0.7	0.6	0.1
4/1/2019	2.6	4.3	0.2
5/1/2019	0.0	0.0	0.0
6/1/2019	0.3	0.6	0.1
7/1/2019	0.0	0.0	0.0
8/1/2019	0.0	0.0	0.0
9/1/2019	0.0	0.1	0.9
10/1/2019	0.0	0.0	0.6
11/1/2019	0.0	0.0	0.0
12/1/2019	0.0	0.0	0.0
1/1/2020	0.0	0.0	0.1
2/1/2020	0.0	0.0	0.1
3/1/2020	0.0	0.1	0.6
4/1/2020	1.2	0.9	0.3
5/1/2020	3.1	6.1	0.2
6/1/2020	0.2	0.6	0.0
7/1/2020	0.0	0.0	0.0
8/1/2020	0.0	0.0	0.0
9/1/2020	0.0	0.2	1.2
10/1/2020	1.6	1.9	0.7
11/1/2020	0.5	0.9	0.0
12/1/2020	0.1	0.3	0.0
1/1/2021	0.0	0.0	0.0
2/1/2021	0.0	0.0	0.0
3/1/2021	1.0	1.2	0.2
4/1/2021	1.5	2.4	0.0
5/1/2021	0.6	1.2	0.0
6/1/2021	0.5	0.6	0.4

TABLE 4-3

Monitoring Locations Used in the Steady-State Groundwater Flow Model Calibration
(Page 1 of 3)

Well ID	Easting (m)	Northing (m)	Ground Surface Elevation (mamsl)	Screen Interval (mamsl)		Hydrogeologic Unit	Time of Sampled Measured Steady-State Groundwater Level	Measured Steady-State Groundwater Level (mamsl)	Simulated Steady-State Groundwater Level (mamsl)	Model Residual (m)
				Top	Bottom					
GA101	3,490,657	7,495,272	187.2	184.2	182.2	Peat	Mar-2013	187.6	187.9	0.32
GA102	3,490,019	7,495,056	186.7	185.7	183.7	Peat	Mar-2013	186.6	187.0	0.38
GA103	3,489,344	7,494,882	185.0	184.0	183.0	Peat	Mar-2013	186.2	185.9	-0.28
GA200	3,489,519	7,496,606	187.0	182.5	180.5	Sediment	Mar-2013	185.6	186.1	0.52
GA201	3,489,834	7,496,186	187.5	184.5	182.5	Sediment	Mar-2013	186.8	187.0	0.20
GA202	3,489,776	7,495,403	186.6	182.6	181.6	Sediment	Mar-2013	186.6	186.6	-0.03
GA203	3,489,033	7,495,716	187.5	184.0	182.0	Sediment	Mar-2013	182.5	182.4	-0.10
GA301	3,490,661	7,495,260	187.2	179.7	177.7	Sediment	Mar-2013	187.5	187.9	0.42
GA302	3,490,014	7,495,054	186.6	178.6	176.6	Sediment	Mar-2013	186.7	187.0	0.27
GA303	3,489,310	7,494,800	186.1	175.6	173.6	Sediment	Mar-2013	186.1	185.9	-0.24
GA304	3,488,954	7,494,748	186.5	174.5	172.5	Sediment	Mar-2013	185.3	185.1	-0.20
GA305	3,489,034	7,495,720	187.4	179.4	177.4	Sediment	Mar-2013	182.7	182.4	-0.31
GA401	3,490,663	7,495,268	187.2	177.7	174.7	Shallow Bedrock	Mar-2013	187.3	187.9	0.57
GA402	3,490,016	7,495,050	186.7	175.7	173.7	Shallow Bedrock	Mar-2014	186.7	187.0	0.32
GA403	3,489,329	7,494,844	186.0	171.0	169.0	Shallow Bedrock	Mar-2014	186.1	185.9	-0.15
GA404	3,488,412	7,494,864	188.4	179.9	177.9	Shallow Bedrock	Mar-2013	184.2	183.8	-0.46
GA405	3,489,035	7,495,723	187.4	175.9	173.9	Shallow Bedrock	Mar-2013	182.7	182.3	-0.32
11MOS8049	3,489,500	7,495,950	185.4	5.4	-9.6	Deep Bedrock	Mar-2017	185.6	185.1	-0.43
13MOS8120	3,489,230	7,495,850	185.6	44.6	14.6	Deep Bedrock	Mar-2017	183.4	183.5	0.19
13MOS8125	3,489,240	7,495,550	187.2	60.2	30.2	Deep Bedrock	Mar-2017	185.5	184.5	-0.96
17HYD004	3,489,912	7,500,204	190.1	157.3	90.3	Shallow Bedrock	Mar-2020	188.7	188.1	-0.52
17HYD006	3,489,607	7,498,030	190.7	160.7	91.6	Shallow Bedrock	Mar-2018	185.4	185.3	-0.03
17HYD008	3,488,494	7,497,684	189.1	158.6	86.9	Shallow Bedrock	Mar-2018	183.4	184.6	1.20
17HYD013	3,488,959	7,496,061	182.7	153.4	-68.7	Shallow Bedrock	Mar-2018	181.4	181.5	0.15

TABLE 4-3

Monitoring Locations Used in the Steady-State Groundwater Flow Model Calibration
(Page 2 of 3)

Well ID	Easting (m)	Northing (m)	Ground Surface Elevation (mamsl)	Screen Interval (mamsl)		Hydrogeologic Unit	Time of Sampled Measured Steady-State Groundwater Level	Measured Steady-State Groundwater Level (mamsl)	Simulated Steady-State Groundwater Level (mamsl)	Model Residual (m)
				Top	Bottom					
17HYD015	3,489,934	7,500,186	190.2	187.1	181.1	Sediment	Mar-2018	188.8	188.2	-0.53
17HYD016	3,489,597	7,498,032	190.7	187.7	183.7	Sediment	Mar-2018	185.4	185.4	-0.05
17HYD017	3,487,834	7,496,295	188.0	151.7	93.7	Shallow Bedrock	Mar-2018	182.0	182.7	0.60
17HYD018	3,488,469	7,497,725	189.3	185.0	181.0	Sediment	Mar-2018	183.7	184.5	0.78
17HYD020	3,490,009	7,499,416	191.3	187.3	183.3	Sediment	Mar-2018	188.2	187.0	-1.27
17HYD023B	3,488,733	7,495,163	186.2	184.2	172.2	Sediment	Mar-2019	184.7	183.5	-1.26
17MOS8198	3,488,740	7,495,158	186.1	153.6	63.6	Shallow Bedrock	Mar-2019	184.8	183.6	-1.13
18HYD036	3,489,198	7,495,550	186.7	171.7	165.7	Shallow Bedrock	Mar-2021	184.7	184.5	-0.25
18HYD040	3,488,534	7,494,684	186.7	162.7	156.7	Shallow Bedrock	Mar-2021	184.6	184.4	-0.15
18MOS8207	3,489,400	7,495,902	185.4	-98.6	-588.6	Deep Bedrock	Mar-2020	185.2	184.9	-0.26
18MOS8227	3,487,811	7,494,748	185.4	135.4	-64.6	Deep Bedrock	Mar-2021	181.8	183.1	1.25
18MOS8228	3,489,102	7,495,800	186.7	24.7	8.7	Deep Bedrock	Mar-2020	182.8	183.3	0.41
18MOS8229	3,488,557	7,494,708	186.7	48.7	26.7	Deep Bedrock	Mar-2020	184.4	184.4	-0.02
18MOS8232	3,487,479	7,493,522	183.1	163.1	117.6	Shallow Bedrock	Mar-2020	182.0	182.4	0.46
GA400	3,490,031	7,496,168	190.5	185.5	183.5	Shallow Bedrock	Mar-2020	187.5	187.7	0.15
GA402	3,490,016	7,495,050	186.7	175.7	173.7	Shallow Bedrock	Mar-2021	186.7	187.0	0.22
GA403	3,489,329	7,494,844	186.0	171.0	169.0	Shallow Bedrock	Mar-2021	186.0	185.9	-0.10
17HYD005	3,486,872	7,492,778	187.5	184.5	182.5	Sediment	Mar-2020	187.6	187.1	-0.50
18HYD025	3,486,594	7,490,597	192.9	190.4	188.4	Sediment	Mar-2020	192.4	192.4	0.01
18HYD027	3,488,989	7,490,751	194.3	192.0	190.0	Sediment	Mar-2021	194.6	194.2	-0.44
18HYD028	3,486,369	7,491,695	193.5	189.8	187.8	Sediment	Jun-2021	193.4	192.0	-1.35
18HYD030	3,487,176	7,492,225	195.6	187.7	185.7	Sediment	Apr-2020	191.4	192.1	0.68
18HYD033	3,487,929	7,491,219	200.0	194.9	192.9	Sediment	Apr-2020	195.4	197.1	1.67
18KUU001	3,487,464	7,492,301	196.6	124.6	46.6	Deep Bedrock	Apr-2020	191.7	192.6	0.89

TABLE 4-3

Monitoring Locations Used in the Steady-State Groundwater Flow Model Calibration
(Page 3 of 3)

Well ID	Easting (m)	Northing (m)	Ground Surface Elevation (mamsl)	Screen Interval (mamsl)		Hydrogeologic Unit	Time of Sampled Measured Steady-State Groundwater Level	Measured Steady-State Groundwater Level (mamsl)	Simulated Steady-State Groundwater Level (mamsl)	Model Residual (m)
				Top	Bottom					
18KUU003	3,488,012	7,491,630	216.7	193.7	156.7	Shallow Bedrock	Apr-2020	208.6	206.1	-2.53
19KUU005	3,486,022	7,491,524	197.0	177.0	147.0	Shallow Bedrock	Apr-2020	189.2	190.3	1.08
19KUU017	3,488,342	7,491,994	226.7	226.7	176.7	Shallow Bedrock	Apr-2021	201.2	202.8	1.59
19KUU021	3,487,462	7,491,606	214.8	207.8	154.8	Shallow Bedrock	Apr-2021	199.2	198.0	-1.22
19KUU022	3,487,468	7,491,834	210.7	130.7	110.7	Shallow Bedrock	Apr-2021	194.5	196.3	1.76
20KUU024	3,487,457	7,492,474	192.2	172.2	2.2	Deep Bedrock	Apr-2021	191.5	191.4	-0.06
20KUU025	3,487,455	7,492,709	190.2	90.2	-9.8	Deep Bedrock	Apr-2021	189.6	189.3	-0.33
17HYD001	3,487,467	7,493,221	195.7	168.0	120.0	Shallow Bedrock	May-2017	195.7	195.4	-0.24
17HYD009	3,488,700	7,497,492	188.3	185.7	181.7	Sediment	Apr-2020	183.7	184.7	1.07
17HYD010	3,488,301	7,496,974	188.4	187.0	185.0	Sediment	Apr-2020	184.3	185.3	1.04
17HYD014	3,486,683	7,494,747	183.2	161.2	70.9	Shallow Bedrock	Apr-2019	181.8	182.7	0.84
17HYD019	3,490,206	7,499,792	189.7	188.5	182.5	Sediment	Apr-2020	189.1	188.5	-0.56
GA104	3,489,083	7,494,682	185.5	183.5	181.5	Peat	Apr-2012	185.4	185.5	0.15
GA204	3,488,953	7,494,762	186.5	184.5	182.0	Sediment	Apr-2012	185.4	185.1	-0.27
GA300	3,489,902	7,495,662	187.5	185.0	184.0	Sediment	Apr-2012	186.2	187.1	0.84

Note:

1. Coordinate system is KKKJ3.

TABLE 4-4
Calculated Statistics of the Steady-State Groundwater Flow Model Calibration

Calculated Steady-State Groundwater Flow Model Statistics	
Mean Error (m)	0.1
Mean Absolute Error (m)	0.6
Root Mean Square Error (m)	0.8
Maximum Measured Water Level (mamsl)	208.6
Minimum Measured Water Level (mamsl)	181.4
Range of Measured Water Levels (m)	27.2
Normalized Root Mean Square Error (%)	3%
Coefficient of Determination (r^2)	0.99
Maximum Residual (m)	1.8
Minimum Residual (m)	-2.5
Number of Observations	69

TABLE 4-5

**Monitoring Locations Used in the Transient Groundwater Flow Model Calibration
(Page 1 of 4)**

Well ID	Easting (m)¹	Northing (m)¹	Groundwater Surface Elevation (mamsl)	Hydrogeologic Unit
11MOS8049	3,489,500	7,495,950	185.4	Deep Bedrock
13MOS8120	3,489,230	7,495,850	185.6	Deep Bedrock
13MOS8125	3,489,240	7,495,550	187.2	Deep Bedrock
16MOS8158	3,488,634	7,495,872	182.5	Deep Bedrock
16MOS8160	3,489,493	7,495,998	186.2	Deep Bedrock
16MOS8163	3,489,401	7,495,450	186.3	Deep Bedrock
17HYD001	3,488,233	7,490,930	195.7	Shallow Bedrock
17HYD002	3,492,710	7,500,683	198.4	Shallow Bedrock
17HYD003	3,488,285	7,490,807	195.6	Sediment
17HYD004	3,489,912	7,500,204	190.1	Shallow Bedrock
17HYD005	3,486,872	7,492,778	187.5	Sediment
17HYD006	3,489,607	7,498,030	190.7	Shallow Bedrock
17HYD007	3,492,706	7,500,704	198.5	Sediment
17HYD008	3,488,494	7,497,684	189.1	Shallow Bedrock
17HYD009	3,488,700	7,497,492	188.3	Sediment
17HYD010	3,488,301	7,496,974	188.4	Sediment
17HYD011	3,481,069	7,505,428	216.8	Sediment
17HYD012	3,493,737	7,503,711	208.1	Sediment
17HYD013	3,488,959	7,496,061	182.7	Shallow Bedrock
17HYD014	3,486,683	7,494,747	183.2	Shallow Bedrock
17HYD015	3,489,934	7,500,186	190.2	Sediment
17HYD016	3,489,597	7,498,032	190.7	Sediment
17HYD017	3,487,834	7,496,295	188.0	Shallow Bedrock
17HYD018	3,488,469	7,497,725	189.3	Sediment
17HYD019	3,490,206	7,499,792	189.7	Sediment

TABLE 4-5

Monitoring Locations Used in the Transient Groundwater Flow Model Calibration
(Page 2 of 4)

Well ID	Easting (m)¹	Northing (m)¹	Groundwater Surface Elevation (mamsl)	Hydrogeologic Unit
17HYD020	3,490,009	7,499,416	191.3	Sediment
17HYD021	3,489,642	7,499,133	189.7	Sediment
17HYD022	3,489,644	7,498,721	190.2	Sediment
17HYD023B	3,488,733	7,495,163	186.2	Sediment
17MOS8178	3,489,350	7,495,703	186.0	Deep Bedrock
17MOS8183	3,489,900	7,495,796	188.1	Deep Bedrock
17MOS8198	3,488,740	7,495,158	186.1	Shallow Bedrock
18HYD024	3,489,347	7,495,838	187.9	Sediment
18HYD025	3,486,594	7,490,597	192.9	Sediment
18HYD027	3,488,989	7,490,751	194.3	Sediment
18HYD028	3,486,369	7,491,695	193.5	Sediment
18HYD030	3,487,176	7,492,225	195.6	Sediment
18HYD033	3,487,929	7,491,219	200.0	Sediment
18HYD035	3,489,199	7,495,546	186.8	Shallow Bedrock
18HYD036	3,489,198	7,495,550	186.7	Shallow Bedrock
18HYD037	3,489,196	7,495,554	186.8	Shallow Bedrock
18HYD038	3,488,534	7,494,660	187.0	Shallow Bedrock
18HYD039	3,488,534	7,494,670	186.7	Shallow Bedrock
18HYD040	3,488,534	7,494,684	186.7	Shallow Bedrock
18KUU001	3,487,464	7,492,301	196.6	Deep Bedrock
18KUU002	3,487,398	7,491,488	205.6	Shallow Bedrock
18KUU003	3,488,012	7,491,630	216.7	Shallow Bedrock
18MOS8205	3,489,298	7,495,850	185.9	Shallow Bedrock
18MOS8207	3,489,400	7,495,902	185.4	Deep Bedrock
18MOS8227	3,487,811	7,494,748	185.4	Deep Bedrock

TABLE 4-5

Monitoring Locations Used in the Transient Groundwater Flow Model Calibration
(Page 3 of 4)

Well ID	Easting (m)¹	Northing (m)¹	Groundwater Surface Elevation (mamsl)	Hydrogeologic Unit
18MOS8228	3,489,102	7,495,800	186.7	Deep Bedrock
18MOS8229	3,488,557	7,494,708	186.7	Deep Bedrock
18MOS8232	3,487,479	7,493,522	183.1	Shallow Bedrock
19KUU005	3,486,022	7,491,524	197.0	Shallow Bedrock
19KUU015	3,486,669	7,491,734	201.2	Shallow Bedrock
19KUU017	3,488,342	7,491,994	226.7	Shallow Bedrock
19KUU019	3,488,803	7,492,230	226.2	Shallow Bedrock
19KUU021	3,487,462	7,491,606	214.8	Shallow Bedrock
19KUU022	3,487,468	7,491,834	210.7	Shallow Bedrock
19KUU023	3,487,425	7,492,047	200.5	Shallow Bedrock
20HYD045	3,489,130	7,491,445	196.5	Shallow Bedrock
20KUU024	3,487,457	7,492,474	192.2	Deep Bedrock
20KUU025	3,487,455	7,492,708	190.2	Deep Bedrock
20MOS8245	3,487,543	7,494,463	184.6	Deep Bedrock
20MOS8246	3,487,468	7,494,011	183.6	Deep Bedrock
20MOS8247	3,487,476	7,493,572	184.6	Deep Bedrock
21HYD046	3,487,472	7,493,542	183.7	Sediment
21HYD047	3,487,465	7,493,543	183.9	Shallow Bedrock
21KUU026	3,487,471	7,493,221	187.6	Deep Bedrock
21MOS8264	3,487,479	7,493,797	185.2	Deep Bedrock
GA101	3,490,657	7,495,272	187.2	Peat
GA102	3,490,019	7,495,056	186.7	Peat
GA103	3,489,344	7,494,882	185.0	Peat
GA104	3,489,083	7,494,682	185.5	Peat
GA200	3,489,519	7,496,606	187.0	Sediment

TABLE 4-5

**Monitoring Locations Used in the Transient Groundwater Flow Model Calibration
(Page 4 of 4)**

Well ID	Easting (m)¹	Northing (m)¹	Groundwater Surface Elevation (mamsl)	Hydrogeologic Unit
GA201	3,489,834	7,496,186	187.5	Sediment
GA202	3,489,776	7,495,403	186.6	Sediment
GA203	3,489,033	7,495,716	187.5	Sediment
GA204	3,488,953	7,494,762	186.5	Sediment
GA205	3,488,408	7,494,872	187.8	Sediment
GA300	3,489,902	7,495,662	187.5	Sediment
GA301	3,490,661	7,495,260	187.2	Sediment
GA302	3,490,014	7,495,054	186.6	Sediment
GA303	3,489,310	7,494,800	186.1	Sediment
GA304	3,488,954	7,494,748	186.5	Sediment
GA305	3,489,034	7,495,720	187.4	Sediment
GA400	3,490,031	7,496,168	190.5	Shallow Bedrock
GA401	3,490,663	7,495,268	187.2	Shallow Bedrock
GA402	3,490,016	7,495,050	186.7	Shallow Bedrock
GA403	3,489,329	7,494,844	186.0	Shallow Bedrock
GA404	3,488,412	7,494,864	188.4	Shallow Bedrock
GA405	3,489,035	7,495,723	187.4	Shallow Bedrock

Note:

1. Coordinate system is KKJ3.

TABLE 4-6

Summary of Calculated Statistics of the Transient Groundwater Flow Model Calibration
(Page 1 of 3)

Calculated Statistics	July 2012	January 2013	July 2013	January 2014	July 2014	January 2015	July 2015
Mean Error (m)	-0.14	-0.08	-0.18	-0.19	-0.04	-0.08	-0.11
Mean Absolute Error (m)	0.45	0.37	0.48	0.35	0.45	0.35	0.41
Root Mean Square Error (m)	0.56	0.42	0.58	0.42	0.57	0.41	0.51
Normalized Root Mean Square Error	14%	9%	14%	8%	14%	8%	12%
Coefficient of Determination (r^2)	97%	98%	99%	99%	99%	98%	98%
Maximum Measured Groundwater Level (mamsl)	183.5	182.8	183.2	182.4	183.2	182.5	183.2
Maximum Measured Groundwater Level (mamsl)	187.4	187.5	187.3	187.5	187.3	187.5	187.4
Range of Measured Water Levels	3.9	4.7	4.1	5.1	4.1	5.1	4.2
Count of Measured Groundwater Levels	22	17	18	18	18	18	18

TABLE 4-6

Summary of Calculated Statistics of the Transient Groundwater Flow Model Calibration
(Page 2 of 3)

Calculated Statistics	January 2016	July 2016	January 2017	July 2017	January 2018	July 2018	January 2019
Mean Error (m)	0.12	-0.03	0.07	0.09	-0.06	0.10	0.00
Mean Absolute Error (m)	0.41	0.44	0.39	0.46	0.51	0.57	0.52
Root Mean Square Error (m)	0.55	0.57	0.49	0.61	0.61	0.65	0.61
Normalized Root Mean Square Error	13%	14%	10%	2%	8%	5%	9%
Coefficient of Determination (r^2)	98%	97%	97%	96%	91%	95%	92%
Maximum Measured Groundwater Level (mamsl)	183.2	183.4	182.7	181.4	181.4	181.3	181.5
Maximum Measured Groundwater Level (mamsl)	187.5	187.4	187.5	216.7	188.8	195.7	188.6
Range of Measured Water Levels	4.3	4.0	4.8	35.3	7.4	14.4	7.1
Count of Measured Groundwater Levels	18	19	20	39	30	42	30

TABLE 4-6

Summary of Calculated Statistics of the Transient Groundwater Flow Model Calibration
(Page 3 of 3)

Calculated Statistics	July 2019	January 2020	July 2020	January 2021	July 2021
Mean Error (m)	0.16	0.31	-0.13	-0.31	-0.09
Mean Absolute Error (m)	0.54	0.75	0.69	0.77	0.77
Root Mean Square Error (m)	0.68	1.33	0.99	1.03	1.09
Normalized Root Mean Square Error	3%	5%	3%	4%	3%
Coefficient of Determination (r^2)	96%	91%	98%	97%	97%
Maximum Measured Groundwater Level (mamsl)	181.4	181.3	181.4	181.5	181.5
Maximum Measured Groundwater Level (mamsl)	202.0	208.9	212.7	209.8	217.1
Range of Measured Water Levels	20.6	27.6	31.2	28.3	35.7
Count of Measured Groundwater Levels	49	59	55	46	72

TABLE 5-1

Summary of Simulated Model Scenarios

Scenario Name	TBM Grouting Depth (mbgs)	TBM Grouting Efficiency (%)	Fault Grouting Efficiency (%)	<i>K</i> Value of Backfill (m/s)	Notes
80% Success in Grouting	150	80	80	5.0×10^{-8}	Most Likely
65% Success in Grouting	150	65	65	1.0×10^{-7}	

TABLE 5-2

**Summary of Predicted Groundwater Inflow Rates and Cumulative Volumes
for Model Scenarios with the NE Deposit
(Page 1 of 7)**

Years after Mining Begins	Groundwater Inflow Rate (m ³ /hr)		Cumulative Volume of Groundwater Inflow (m ³)	
	80% Success in Grouting	65% Success in Grouting	80% Success in Grouting	65% Success in Grouting
0.00	0.0	0.0	0	0
0.08	5.1	8.2	3,784	6,124
0.17	7.6	10.8	9,286	13,928
0.25	28.7	29.3	30,618	35,745
0.34	42.6	43.5	62,280	68,127
0.42	50.3	51.4	96,078	102,692
0.51	55.7	57.0	137,548	145,106
0.59	59.1	60.4	180,083	188,607
0.68	61.6	63.0	225,925	235,491
0.76	65.7	67.2	273,232	283,873
0.85	69.9	71.5	325,227	337,050
0.93	77.7	79.5	383,031	396,168
1.02	85.7	87.6	444,722	459,260
1.10	92.7	94.8	513,687	529,793
1.19	99.2	101.5	585,117	602,846
1.27	102.2	104.5	661,118	680,575
1.36	107.5	109.9	741,064	762,338
1.44	111.8	114.4	816,204	839,185
1.53	114.9	117.5	901,680	926,604
1.61	117.0	119.7	985,924	1,012,763
1.70	115.9	118.5	1,072,150	1,100,949
1.78	116.2	118.8	1,155,788	1,186,487
1.87	116.7	119.3	1,242,584	1,275,256
1.95	117.5	120.1	1,329,988	1,364,647
2.04	118.0	120.7	1,414,972	1,451,562
2.12	117.6	120.3	1,502,486	1,541,065
2.21	117.2	122.0	1,586,881	1,628,912
2.29	116.8	121.6	1,673,782	1,719,368
2.37	116.7	121.5	1,760,624	1,809,763
2.46	116.2	121.0	1,841,534	1,893,983
2.54	115.6	120.3	1,927,512	1,983,478
2.63	114.9	119.6	2,010,235	2,069,586
2.71	114.5	119.2	2,095,401	2,158,235
2.80	113.4	118.0	2,177,029	2,243,203
2.88	112.5	117.1	2,260,752	2,330,351
2.97	111.5	116.0	2,343,689	2,416,681
3.05	110.3	114.9	2,423,141	2,499,383
3.14	110.1	114.6	2,505,029	2,584,621

TABLE 5-2

**Summary of Predicted Groundwater Inflow Rates and Cumulative Volumes
for Model Scenarios with the NE Deposit
(Page 2 of 7)**

Years after Mining Begins	Groundwater Inflow Rate (m ³ /hr)		Cumulative Volume of Groundwater Inflow (m ³)	
	80% Success in Grouting	65% Success in Grouting	80% Success in Grouting	65% Success in Grouting
3.22	109.7	114.2	2,584,046	2,666,870
3.31	109.4	113.9	2,665,465	2,751,620
3.39	109.1	113.5	2,746,611	2,836,086
3.48	108.9	113.3	2,819,773	2,912,241
3.56	108.9	113.4	2,900,828	2,996,612
3.65	109.4	113.9	2,979,602	3,078,608
3.73	109.8	114.3	3,061,265	3,163,612
3.82	110.1	114.6	3,140,542	3,246,133
3.90	110.4	114.9	3,222,667	3,331,617
3.99	110.8	115.4	3,305,119	3,417,442
4.07	111.4	115.9	3,385,299	3,500,902
4.16	111.7	116.3	3,468,428	3,587,432
4.24	112.1	116.6	3,549,107	3,671,411
4.33	111.6	116.2	3,632,163	3,757,865
4.41	111.1	115.7	3,714,828	3,843,912
4.50	110.8	115.3	3,789,292	3,921,422
4.58	110.6	115.1	3,871,544	4,007,039
4.66	110.4	114.9	3,951,015	4,089,761
4.75	110.1	114.6	4,032,919	4,175,016
4.83	109.6	114.1	4,111,814	4,257,138
4.92	108.8	113.3	4,192,788	4,341,424
5.00	108.2	112.6	4,273,293	4,425,223
5.09	107.7	112.1	4,350,816	4,505,917
5.17	107.0	111.4	4,430,443	4,588,801
5.26	106.4	110.8	4,507,051	4,668,544
5.34	105.7	110.0	4,585,703	4,750,413
5.43	105.0	109.3	4,663,848	4,831,755
5.51	104.5	108.8	4,734,056	4,904,835
5.60	103.9	108.2	4,811,371	4,985,313
5.68	103.5	107.7	4,885,891	5,062,882
5.77	101.6	107.4	4,961,481	5,142,775
5.85	101.3	107.1	5,034,410	5,219,854
5.94	101.0	106.7	5,109,547	5,299,269
6.02	100.7	106.5	5,184,499	5,378,487
6.11	100.5	106.3	5,256,882	5,454,991
6.19	100.4	106.1	5,331,573	5,533,933
6.28	100.4	106.1	5,403,848	5,610,323
6.36	100.4	106.1	5,478,543	5,689,270

TABLE 5-2

**Summary of Predicted Groundwater Inflow Rates and Cumulative Volumes
for Model Scenarios with the NE Deposit
(Page 3 of 7)**

Years after Mining Begins	Groundwater Inflow Rate (m ³ /hr)		Cumulative Volume of Groundwater Inflow (m ³)	
	80% Success in Grouting	65% Success in Grouting	80% Success in Grouting	65% Success in Grouting
6.45	100.5	106.3	5,553,336	5,768,320
6.53	100.6	106.3	5,623,364	5,842,334
6.62	100.5	106.3	5,698,170	5,921,399
6.70	100.5	106.2	5,770,509	5,997,855
6.79	100.3	106.1	5,845,165	6,076,760
6.87	100.3	106.1	5,917,414	6,153,122
6.95	100.5	106.3	5,992,216	6,232,182
7.04	100.7	106.4	6,067,118	6,311,348
7.12	100.8	106.6	6,139,726	6,388,089
7.21	101.0	106.7	6,214,858	6,467,497
7.29	101.0	106.7	6,287,546	6,544,323
7.38	101.0	106.7	6,362,666	6,623,719
7.46	100.9	106.6	6,437,702	6,703,026
7.55	100.7	106.4	6,505,366	6,774,542
7.63	100.5	106.3	6,580,169	6,853,603
7.72	100.5	106.2	6,652,511	6,930,064
7.80	100.4	106.1	6,727,191	7,008,994
7.89	100.3	106.0	6,799,384	7,085,296
7.97	100.3	106.0	6,874,030	7,164,192
8.06	100.3	106.0	6,948,660	7,243,070
8.14	100.4	106.1	7,020,917	7,319,439
8.23	100.4	106.1	7,095,613	7,398,388
8.31	100.4	106.1	7,167,904	7,474,794
8.40	100.5	106.2	7,242,671	7,553,817
8.48	100.5	106.2	7,317,457	7,632,860
8.57	100.5	106.2	7,384,988	7,704,235
8.65	100.4	106.1	7,459,685	7,783,184
8.74	100.2	105.9	7,531,849	7,859,456
8.82	100.3	106.0	7,606,493	7,938,349
8.91	100.5	106.2	7,678,862	8,014,838
8.99	100.7	106.5	7,753,809	8,094,050
9.08	101.0	106.7	7,828,925	8,173,442
9.16	101.0	106.8	7,901,653	8,250,310
9.24	101.3	107.0	7,976,999	8,329,945
9.33	101.5	107.2	8,050,049	8,407,154
9.41	101.7	107.5	8,125,718	8,487,130
9.50	102.1	107.9	8,201,663	8,567,397
9.58	102.2	108.0	8,270,308	8,639,950

TABLE 5-2

**Summary of Predicted Groundwater Inflow Rates and Cumulative Volumes
for Model Scenarios with the NE Deposit
(Page 4 of 7)**

Years after Mining Begins	Groundwater Inflow Rate (m ³ /hr)		Cumulative Volume of Groundwater Inflow (m ³)	
	80% Success in Grouting	65% Success in Grouting	80% Success in Grouting	65% Success in Grouting
9.67	102.4	108.2	8,346,498	8,720,477
9.75	102.6	108.4	8,420,358	8,798,542
9.84	102.6	108.5	8,496,706	8,879,235
9.92	103.0	108.9	8,570,862	8,957,613
10.01	103.4	109.3	8,647,797	9,038,927
10.09	103.9	109.8	8,725,075	9,120,604
10.18	104.9	110.8	8,800,586	9,200,413
10.26	105.0	111.8	8,878,706	9,283,573
10.35	105.5	113.0	8,954,666	9,364,957
10.43	105.7	113.5	9,033,342	9,449,401
10.52	106.7	114.0	9,112,731	9,534,217
10.60	107.6	113.5	9,187,613	9,613,226
10.69	108.1	114.0	9,268,024	9,698,069
10.77	108.5	114.5	9,346,172	9,780,524
10.86	108.8	114.8	9,427,094	9,865,906
10.94	109.0	115.0	9,505,540	9,948,676
11.03	109.1	115.1	9,586,675	10,034,283
11.11	109.2	115.2	9,667,910	10,119,996
11.20	109.4	115.4	9,746,688	10,203,116
11.28	109.6	115.7	9,828,268	10,289,192
11.37	109.9	115.9	9,907,384	10,372,669
11.45	110.0	116.0	9,989,204	10,458,999
11.53	110.0	116.0	10,071,011	10,545,315
11.62	109.9	116.0	10,144,868	10,623,243
11.70	109.8	115.9	10,226,592	10,709,471
11.79	109.8	115.9	10,305,651	10,792,888
11.87	109.8	115.8	10,387,320	10,879,059
11.96	109.7	115.8	10,466,333	10,962,427
12.04	109.7	115.7	10,547,947	11,048,538
12.13	109.6	115.7	10,629,496	11,134,583
12.21	109.5	115.6	10,708,368	11,217,802
12.30	109.5	115.5	10,789,812	11,303,735
12.38	109.4	115.4	10,868,576	11,386,840
12.47	109.3	115.3	10,949,908	11,472,655
12.55	109.3	115.3	11,031,221	11,558,450
12.64	109.3	115.3	11,104,649	11,635,926
12.72	109.3	115.3	11,185,985	11,721,745
12.81	109.4	115.4	11,264,758	11,804,860

TABLE 5-2

**Summary of Predicted Groundwater Inflow Rates and Cumulative Volumes
for Model Scenarios with the NE Deposit
(Page 5 of 7)**

Years after Mining Begins	Groundwater Inflow Rate (m ³ /hr)		Cumulative Volume of Groundwater Inflow (m ³)	
	80% Success in Grouting	65% Success in Grouting	80% Success in Grouting	65% Success in Grouting
12.89	109.6	115.7	11,346,329	11,890,926
12.98	110.0	116.0	11,425,518	11,974,480
13.06	110.2	116.3	11,507,528	12,061,010
13.15	110.5	116.5	11,589,703	12,147,714
13.23	110.5	116.6	11,669,252	12,231,648
13.32	110.4	116.5	11,751,387	12,318,310
13.40	110.3	116.4	11,830,822	12,402,124
13.49	110.3	116.4	11,912,886	12,488,711
13.57	110.3	116.3	11,994,918	12,575,264
13.66	110.2	116.3	12,068,991	12,653,420
13.74	110.2	116.3	12,150,972	12,739,920
13.82	110.1	116.2	12,230,250	12,823,567
13.91	110.0	116.1	12,312,125	12,909,955
13.99	110.0	116.0	12,391,304	12,993,498
14.08	109.9	116.0	12,473,086	13,079,788
14.16	109.9	115.9	12,554,828	13,166,036
14.25	109.8	115.8	12,633,874	13,249,438
14.33	109.7	115.8	12,715,494	13,335,557
14.42	109.6	115.7	12,794,427	13,418,840
14.50	109.6	115.6	12,875,946	13,504,852
14.59	109.6	115.6	12,957,463	13,590,863
14.67	109.7	115.8	13,033,830	13,671,439
14.76	110.0	116.1	13,115,699	13,757,820
14.84	110.4	116.5	13,195,199	13,841,703
14.93	111.0	117.1	13,277,769	13,928,823
15.01	111.3	117.4	13,357,895	14,013,366
15.10	111.4	117.5	13,440,769	14,100,808
15.18	111.4	117.5	13,523,641	14,188,248
15.27	111.1	117.3	13,603,659	14,272,676
15.35	111.0	117.1	13,686,226	14,359,794
15.44	110.9	117.0	13,766,043	14,444,011
15.52	110.8	116.9	13,848,444	14,530,953
15.61	110.6	116.7	13,930,765	14,617,811
15.69	110.6	116.7	14,005,075	14,696,217
15.78	110.5	116.6	14,087,292	14,782,965
15.86	110.5	116.5	14,166,823	14,866,880
15.95	110.4	116.5	14,248,989	14,953,575
16.03	110.4	116.5	14,328,471	15,037,438

TABLE 5-2

**Summary of Predicted Groundwater Inflow Rates and Cumulative Volumes
for Model Scenarios with the NE Deposit
(Page 6 of 7)**

Years after Mining Begins	Groundwater Inflow Rate (m ³ /hr)		Cumulative Volume of Groundwater Inflow (m ³)	
	80% Success in Grouting	65% Success in Grouting	80% Success in Grouting	65% Success in Grouting
16.11	110.4	116.5	14,410,585	15,124,078
16.20	110.3	116.4	14,492,679	15,210,697
16.28	110.3	116.4	14,572,092	15,294,487
16.37	110.3	116.4	14,654,167	15,381,086
16.45	110.3	116.4	14,733,584	15,464,881
16.54	110.3	116.4	14,815,645	15,551,465
16.62	110.3	116.4	14,897,712	15,638,054
16.71	110.2	116.3	14,971,789	15,716,214
16.79	110.2	116.3	15,053,762	15,802,706
16.88	110.1	116.2	15,133,046	15,886,359
16.96	110.1	116.2	15,214,958	15,972,786
17.05	110.1	116.2	15,294,252	16,056,451
17.13	110.2	116.2	15,376,223	16,142,940
17.22	110.2	116.3	15,458,223	16,229,460
17.30	110.2	116.3	15,537,584	16,313,195
17.39	110.2	116.3	15,619,570	16,399,701
17.47	110.2	116.2	15,698,887	16,483,389
17.56	110.1	116.2	15,780,824	16,569,842
17.64	110.1	116.2	15,862,764	16,656,298
17.73	110.1	116.2	15,936,779	16,734,393
17.81	110.2	116.3	16,018,752	16,820,885
17.90	110.2	116.3	16,098,094	16,904,599
17.98	110.2	116.2	16,180,053	16,991,076
18.07	110.1	116.2	16,259,337	17,074,730
18.15	110.0	116.1	16,341,213	17,161,119
18.24	110.0	116.1	16,423,046	17,247,462
18.32	109.9	116.0	16,502,207	17,330,987
18.40	109.9	116.0	16,583,970	17,417,256
18.49	109.8	115.9	16,663,056	17,500,701
18.57	109.8	115.8	16,744,741	17,586,888
18.66	109.7	115.8	16,826,381	17,673,028
18.74	109.7	115.7	16,902,711	17,753,565
18.83	109.6	115.6	16,984,259	17,839,608
18.91	109.6	115.6	17,063,139	17,922,836
19.00	109.5	115.5	17,144,617	18,008,805
19.08	109.5	115.5	17,223,443	18,091,976
19.17	109.4	115.5	17,304,873	18,177,894
19.25	109.4	115.4	17,386,274	18,263,781

TABLE 5-2

**Summary of Predicted Groundwater Inflow Rates and Cumulative Volumes
for Model Scenarios with the NE Deposit
(Page 7 of 7)**

Years after Mining Begins	Groundwater Inflow Rate (m ³ /hr)		Cumulative Volume of Groundwater Inflow (m ³)	
	80% Success in Grouting	65% Success in Grouting	80% Success in Grouting	65% Success in Grouting
19.34	109.4	115.4	17,465,019	18,346,867
19.42	109.3	115.4	17,546,357	18,432,688
19.51	109.3	115.3	17,625,041	18,515,709
19.59	109.2	115.3	17,706,320	18,601,468
19.68	109.2	115.2	17,787,567	18,687,193
19.76	109.2	115.2	17,860,921	18,764,590
19.85	109.1	115.1	17,942,100	18,850,243
19.93	109.1	115.1	18,020,632	18,933,104
20.02	109.0	115.1	18,101,761	19,018,704
20.10	109.0	115.0	18,180,255	19,101,525
20.19	109.0	115.0	18,261,349	19,187,089
20.27	109.0	115.0	18,342,421	19,272,630
20.36	108.9	114.9	18,420,854	19,355,385
20.44	108.9	114.9	18,501,874	19,440,872
20.53	108.9	114.9	18,580,258	19,523,575
20.61	108.8	114.8	18,661,230	19,609,011
20.69	108.8	114.8	18,742,177	19,694,419
20.78	108.8	114.8	18,815,263	19,771,534
20.86	108.7	114.7	18,896,151	19,856,880
20.95	108.7	114.7	18,974,406	19,939,448
21.03	108.7	114.7	19,055,252	20,024,750
21.12	108.6	114.6	19,133,477	20,107,287
21.20	108.6	114.6	19,214,297	20,192,561
21.29	108.6	114.6	19,295,098	20,277,816
21.37	108.6	114.6	19,373,272	20,360,299
21.46	108.5	114.5	19,454,030	20,445,508
21.54	108.5	114.5	19,532,162	20,527,946
21.63	108.5	114.5	19,612,878	20,613,111
21.71	108.5	114.4	19,693,571	20,698,252
21.80	108.4	114.4	19,766,432	20,775,129
21.88	108.4	114.4	19,847,072	20,860,214
21.97	108.4	114.3	19,925,090	20,942,533
22.00	108.3	114.3	20,005,695	21,027,580

TABLE 5-3

**Summary of Predicted Groundwater Inflow Rates and Cumulative Volumes
for Model Scenarios without the NE Deposit
(Page 1 of 7)**

Years after Mining Begins	Groundwater Inflow Rate (m ³ /hr)		Cumulative Volume of Inflow (m ³)	
	80% Success in Grouting	65% Success in Grouting	80% Success in Grouting	65% Success in Grouting
0.00	0.0	0.0	0	0
0.08	5.1	8.2	3,784	6,124
0.17	7.6	10.8	9,286	13,928
0.25	28.7	29.3	30,618	35,745
0.34	42.6	43.5	62,280	68,127
0.42	50.3	51.4	96,077	102,692
0.51	55.7	57.0	137,548	145,106
0.59	59.1	60.4	180,083	188,607
0.68	61.6	63.0	225,925	235,491
0.76	65.7	67.2	273,232	283,873
0.85	69.9	71.5	325,227	337,050
0.93	77.7	79.5	383,031	396,168
1.02	85.7	87.6	444,722	459,260
1.10	92.7	94.8	513,687	529,793
1.19	99.2	101.5	585,117	602,846
1.27	102.2	104.5	661,118	680,575
1.36	107.5	109.9	741,064	762,338
1.44	111.8	114.4	816,204	839,185
1.53	114.9	117.5	901,680	926,604
1.61	117.0	119.7	985,924	1,012,763
1.70	115.9	118.5	1,072,150	1,100,949
1.78	116.2	118.8	1,155,788	1,186,487
1.87	116.7	119.3	1,242,584	1,275,256
1.95	117.5	120.1	1,329,988	1,364,647
2.04	118.0	120.7	1,414,972	1,451,562
2.12	117.6	120.3	1,502,486	1,541,065
2.21	117.2	122.0	1,586,881	1,628,912
2.29	116.8	121.6	1,673,782	1,719,368
2.37	116.7	121.5	1,760,624	1,809,763
2.46	116.2	121.0	1,841,534	1,893,983
2.54	115.6	120.3	1,927,512	1,983,478
2.63	114.9	119.6	2,010,235	2,069,586
2.71	114.5	119.2	2,095,401	2,158,235
2.80	113.4	118.0	2,177,029	2,243,203
2.88	112.5	117.1	2,260,752	2,330,351
2.97	111.5	116.0	2,343,689	2,416,681
3.05	110.3	114.9	2,423,141	2,499,383
3.14	110.1	114.6	2,505,029	2,584,621
3.22	109.7	114.2	2,584,046	2,666,870

TABLE 5-3

**Summary of Predicted Groundwater Inflow Rates and Cumulative Volumes
for Model Scenarios without the NE Deposit
(Page 2 of 7)**

Years after Mining Begins	Groundwater Inflow Rate (m ³ /hr)		Cumulative Volume of Inflow (m ³)	
	80% Success in Grouting	65% Success in Grouting	80% Success in Grouting	65% Success in Grouting
3.31	109.4	113.9	2,665,465	2,751,620
3.39	109.1	113.5	2,746,611	2,836,086
3.48	108.9	113.3	2,819,773	2,912,241
3.56	108.9	113.4	2,900,828	2,996,612
3.65	109.4	113.9	2,979,602	3,078,608
3.73	109.8	114.3	3,061,265	3,163,612
3.82	110.1	114.6	3,140,542	3,246,133
3.90	110.4	114.9	3,222,667	3,331,617
3.99	110.8	115.4	3,305,119	3,417,442
4.07	111.4	115.9	3,385,299	3,500,902
4.16	111.7	116.3	3,468,428	3,587,432
4.24	112.1	116.6	3,549,107	3,671,411
4.33	111.6	116.2	3,632,163	3,757,865
4.41	111.1	115.7	3,714,828	3,843,912
4.50	110.8	115.3	3,789,292	3,921,422
4.58	110.6	115.1	3,871,544	4,007,039
4.66	110.4	114.9	3,951,015	4,089,761
4.75	110.1	114.6	4,032,919	4,175,016
4.83	109.6	114.1	4,111,814	4,257,138
4.92	108.8	113.3	4,192,788	4,341,424
5.00	108.2	112.6	4,273,293	4,425,223
5.09	107.7	112.1	4,350,816	4,505,917
5.17	107.0	111.4	4,430,443	4,588,801
5.26	106.4	110.8	4,507,051	4,668,544
5.34	105.7	110.0	4,585,703	4,750,413
5.43	105.0	109.3	4,663,848	4,831,755
5.51	104.5	108.8	4,734,056	4,904,835
5.60	103.9	108.2	4,811,371	4,985,313
5.68	103.5	107.7	4,885,891	5,062,882
5.77	101.6	107.4	4,961,481	5,142,775
5.85	101.3	107.1	5,034,410	5,219,854
5.94	100.8	106.7	5,109,376	5,299,269
6.02	100.4	106.5	5,184,111	5,378,487
6.11	100.2	106.3	5,256,251	5,454,991
6.19	100.0	106.1	5,330,638	5,533,933
6.28	99.9	106.1	5,402,543	5,610,323
6.36	100.1	106.1	5,476,985	5,689,270
6.45	100.2	106.3	5,551,522	5,768,320
6.53	100.3	106.3	5,621,355	5,842,334

TABLE 5-3

**Summary of Predicted Groundwater Inflow Rates and Cumulative Volumes
for Model Scenarios without the NE Deposit
(Page 3 of 7)**

Years after Mining Begins	Groundwater Inflow Rate (m ³ /hr)		Cumulative Volume of Inflow (m ³)	
	80% Success in Grouting	65% Success in Grouting	80% Success in Grouting	65% Success in Grouting
6.62	100.5	106.3	5,696,116	5,921,399
6.70	100.6	106.2	5,768,556	5,997,855
6.79	100.6	106.1	5,843,429	6,076,760
6.87	100.7	106.1	5,915,938	6,153,122
6.95	100.8	106.3	5,990,904	6,232,182
7.04	100.7	106.4	6,065,810	6,311,348
7.12	100.5	106.6	6,138,164	6,388,089
7.21	100.3	106.7	6,212,754	6,467,497
7.29	100.1	106.7	6,284,798	6,544,323
7.38	99.5	106.7	6,358,858	6,623,719
7.46	99.1	106.6	6,432,561	6,703,026
7.55	98.7	106.4	6,498,911	6,774,542
7.63	98.6	105.9	6,572,292	6,853,352
7.72	98.5	105.9	6,643,246	6,929,584
7.80	98.5	105.8	6,716,500	7,008,292
7.89	98.4	105.8	6,787,330	7,084,457
7.97	98.3	105.8	6,860,484	7,163,195
8.06	98.2	105.8	6,933,573	7,241,892
8.14	98.0	105.5	7,004,128	7,317,816
8.23	97.8	105.2	7,076,871	7,396,082
8.31	97.6	104.9	7,147,113	7,471,643
8.40	97.4	104.6	7,219,548	7,549,483
8.48	97.2	104.3	7,291,837	7,627,052
8.57	97.0	104.0	7,357,041	7,696,956
8.65	96.9	103.7	7,429,149	7,774,145
8.74	96.8	103.5	7,498,867	7,848,681
8.82	96.9	103.5	7,570,991	7,925,719
8.91	96.9	103.4	7,640,778	8,000,185
8.99	96.9	103.4	7,712,857	8,077,082
9.08	96.8	103.2	7,784,853	8,153,862
9.16	96.6	103.0	7,854,428	8,228,033
9.24	96.5	102.8	7,926,200	8,304,540
9.33	96.1	102.5	7,995,419	8,378,313
9.41	95.9	102.4	8,066,785	8,454,473
9.50	95.8	102.4	8,138,038	8,530,631
9.58	95.9	103.5	8,202,469	8,600,165
9.67	96.0	104.2	8,273,898	8,677,671
9.75	96.1	104.7	8,343,108	8,753,026
9.84	96.2	105.0	8,414,665	8,831,165

TABLE 5-3

**Summary of Predicted Groundwater Inflow Rates and Cumulative Volumes
for Model Scenarios without the NE Deposit
(Page 4 of 7)**

Years after Mining Begins	Groundwater Inflow Rate (m ³ /hr)		Cumulative Volume of Inflow (m ³)	
	80% Success in Grouting	65% Success in Grouting	80% Success in Grouting	65% Success in Grouting
9.92	96.2	105.1	8,483,926	8,906,842
10.01	96.2	105.1	8,555,487	8,985,071
10.09	95.9	104.1	8,626,857	9,062,496
10.18	95.7	103.4	8,695,751	9,136,946
10.26	95.5	103.0	8,766,803	9,213,545
10.35	95.3	103.0	8,835,445	9,287,703
10.43	95.2	103.1	8,906,282	9,364,385
10.52	95.1	103.0	8,977,023	9,441,045
10.60	95.0	103.0	9,043,161	9,512,749
10.69	95.0	103.0	9,113,819	9,589,387
10.77	94.9	103.0	9,182,148	9,663,545
10.86	95.0	102.7	9,252,813	9,739,985
10.94	95.0	102.5	9,321,220	9,813,807
11.03	95.0	102.4	9,391,915	9,889,961
11.11	94.9	102.2	9,462,554	9,965,980
11.20	94.9	102.0	9,530,847	10,039,427
11.28	94.7	101.8	9,601,339	10,115,190
11.37	94.5	101.5	9,669,395	10,188,289
11.45	94.4	101.3	9,739,592	10,263,652
11.53	94.2	101.1	9,809,699	10,338,886
11.62	94.2	101.1	9,873,002	10,406,809
11.70	94.2	101.0	9,943,074	10,481,989
11.79	94.2	101.0	10,010,884	10,554,744
11.87	94.2	101.1	10,080,955	10,629,938
11.96	94.2	101.1	10,148,756	10,702,696
12.04	94.2	101.1	10,218,814	10,777,879
12.13	94.1	100.9	10,288,825	10,852,958
12.21	94.0	100.8	10,356,526	10,925,507
12.30	93.9	100.6	10,426,404	11,000,338
12.38	93.8	100.4	10,493,968	11,072,640
12.47	93.8	100.3	10,563,780	11,147,299
12.55	93.8	100.2	10,633,589	11,221,873
12.64	93.9	100.2	10,696,662	11,289,238
12.72	94.0	100.3	10,766,582	11,363,883
12.81	94.2	100.5	10,834,401	11,436,227
12.89	94.4	100.6	10,904,637	11,511,066
12.98	94.5	100.6	10,972,694	11,583,516
13.06	94.6	100.7	11,043,090	11,658,434
13.15	94.7	100.7	11,113,519	11,733,377

TABLE 5-3

**Summary of Predicted Groundwater Inflow Rates and Cumulative Volumes
for Model Scenarios without the NE Deposit
(Page 5 of 7)**

Years after Mining Begins	Groundwater Inflow Rate (m ³ /hr)		Cumulative Volume of Inflow (m ³)	
	80% Success in Grouting	65% Success in Grouting	80% Success in Grouting	65% Success in Grouting
13.23	94.6	100.7	11,181,640	11,805,884
13.32	94.5	100.6	11,251,935	11,880,734
13.40	94.3	100.5	11,319,857	11,953,104
13.49	94.2	100.4	11,389,958	12,027,829
13.57	94.1	100.4	11,459,977	12,102,508
13.66	94.1	100.3	11,523,186	12,169,939
13.74	94.1	100.4	11,593,164	12,244,607
13.82	94.1	100.4	11,660,897	12,316,919
13.91	94.1	100.6	11,730,899	12,391,738
13.99	94.1	100.6	11,798,628	12,464,173
14.08	94.1	100.6	11,868,607	12,539,032
14.16	94.0	100.6	11,938,540	12,613,882
14.25	93.9	100.5	12,006,144	12,686,270
14.33	93.8	100.5	12,075,916	12,761,019
14.42	93.8	100.4	12,143,429	12,833,299
14.50	93.9	100.6	12,213,327	12,908,156
14.59	94.3	101.0	12,283,482	12,983,330
14.67	94.7	101.5	12,349,399	13,053,963
14.76	95.3	102.1	12,420,274	13,129,901
14.84	95.7	102.5	12,489,209	13,203,734
14.93	96.1	102.9	12,560,701	13,280,326
15.01	96.3	103.1	12,630,007	13,354,542
15.10	96.2	103.0	12,701,606	13,431,175
15.18	96.1	102.8	12,773,128	13,507,688
15.27	95.9	102.5	12,842,167	13,581,517
15.35	95.7	102.3	12,913,365	13,657,662
15.44	95.5	102.2	12,982,142	13,731,235
15.52	95.4	102.1	13,053,122	13,807,200
15.61	95.3	102.0	13,124,020	13,883,090
15.69	95.3	102.0	13,188,034	13,951,646
15.78	95.2	102.1	13,258,889	14,027,586
15.86	95.2	102.2	13,327,467	14,101,179
15.95	95.3	102.3	13,398,352	14,177,315
16.03	95.3	102.4	13,466,936	14,251,034
16.11	95.2	102.5	13,537,797	14,327,257
16.20	95.2	102.4	13,608,630	14,403,463
16.28	95.1	102.4	13,677,136	14,477,172
16.37	95.1	102.2	13,747,878	14,553,194
16.45	95.0	102.0	13,816,290	14,626,646

TABLE 5-3

**Summary of Predicted Groundwater Inflow Rates and Cumulative Volumes
for Model Scenarios without the NE Deposit
(Page 6 of 7)**

Years after Mining Begins	Groundwater Inflow Rate (m ³ /hr)		Cumulative Volume of Inflow (m ³)	
	80% Success in Grouting	65% Success in Grouting	80% Success in Grouting	65% Success in Grouting
16.54	95.0	101.9	13,886,941	14,702,462
16.62	94.9	101.8	13,957,549	14,778,202
16.71	94.9	101.8	14,021,306	14,846,597
16.79	94.9	101.8	14,091,906	14,922,336
16.88	94.9	101.9	14,160,259	14,995,684
16.96	95.0	102.0	14,230,954	15,071,570
17.05	95.1	102.1	14,299,424	15,145,089
17.13	95.2	102.2	14,370,241	15,221,145
17.22	95.2	102.2	14,441,070	15,297,216
17.30	95.2	102.3	14,509,605	15,370,840
17.39	95.1	102.2	14,580,392	15,446,901
17.47	95.1	102.2	14,648,848	15,520,462
17.56	95.0	102.1	14,719,542	15,596,430
17.64	95.0	102.0	14,790,205	15,672,350
17.73	95.0	102.1	14,854,036	15,740,943
17.81	95.0	102.1	14,924,716	15,816,925
17.90	95.0	102.2	14,993,133	15,890,527
17.98	95.0	102.3	15,063,831	15,966,670
18.07	95.0	102.5	15,132,241	16,040,438
18.15	95.0	102.6	15,202,912	16,116,757
18.24	94.9	102.7	15,273,553	16,193,135
18.32	94.9	102.7	15,341,876	16,267,073
18.40	94.8	102.7	15,412,424	16,343,462
18.49	94.8	102.6	15,480,644	16,417,358
18.57	94.7	102.6	15,551,104	16,493,692
18.66	94.6	102.6	15,621,522	16,569,994
18.74	94.6	102.6	15,687,376	16,641,376
18.83	94.6	102.6	15,757,762	16,717,690
18.91	94.6	102.6	15,825,884	16,791,570
19.00	94.6	102.6	15,896,288	16,867,936
19.08	94.6	102.6	15,964,413	16,941,841
19.17	94.6	102.7	16,034,809	17,018,219
19.25	94.6	102.6	16,105,162	17,094,541
19.34	94.5	102.5	16,173,195	17,168,331
19.42	94.4	102.4	16,243,430	17,244,492
19.51	94.3	102.2	16,311,334	17,318,106
19.59	94.2	102.1	16,381,446	17,394,098
19.68	94.2	102.0	16,451,498	17,470,008
19.76	94.1	102.0	16,514,755	17,538,559

TABLE 5-3

**Summary of Predicted Groundwater Inflow Rates and Cumulative Volumes
for Model Scenarios without the NE Deposit
(Page 7 of 7)**

Years after Mining Begins	Groundwater Inflow Rate (m ³ /hr)		Cumulative Volume of Inflow (m ³)	
	80% Success in Grouting	65% Success in Grouting	80% Success in Grouting	65% Success in Grouting
19.85	94.1	102.0	16,584,783	17,614,457
19.93	94.1	102.0	16,652,562	17,687,931
20.02	94.2	102.1	16,722,615	17,763,885
20.10	94.2	102.1	16,790,411	17,837,403
20.19	94.2	102.1	16,860,477	17,913,395
20.27	94.1	102.1	16,930,512	17,989,344
20.36	94.1	102.0	16,998,248	18,062,787
20.44	94.0	101.9	17,068,185	18,138,598
20.53	93.9	101.8	17,135,808	18,211,883
20.61	93.9	101.7	17,205,637	18,287,544
20.69	93.8	101.6	17,275,412	18,363,132
20.78	93.8	101.6	17,338,423	18,431,398
20.86	93.8	101.6	17,408,185	18,506,989
20.95	93.8	101.6	17,475,710	18,580,172
21.03	93.8	101.7	17,545,504	18,655,832
21.12	93.8	101.7	17,613,054	18,729,071
21.20	93.8	101.8	17,682,868	18,804,779
21.29	93.8	101.7	17,752,655	18,880,450
21.37	93.7	101.6	17,820,153	18,953,628
21.46	93.7	101.5	17,889,848	19,029,171
21.54	93.6	101.4	17,957,240	19,102,200
21.63	93.5	101.3	18,026,832	19,177,602
21.71	93.5	101.3	18,096,375	19,252,934
21.80	93.5	101.2	18,159,178	19,320,972
21.88	93.5	101.3	18,228,713	19,396,314
21.97	93.5	101.3	18,296,021	19,469,259
22.00	93.5	101.4	18,365,594	19,544,675

TABLE 6-1

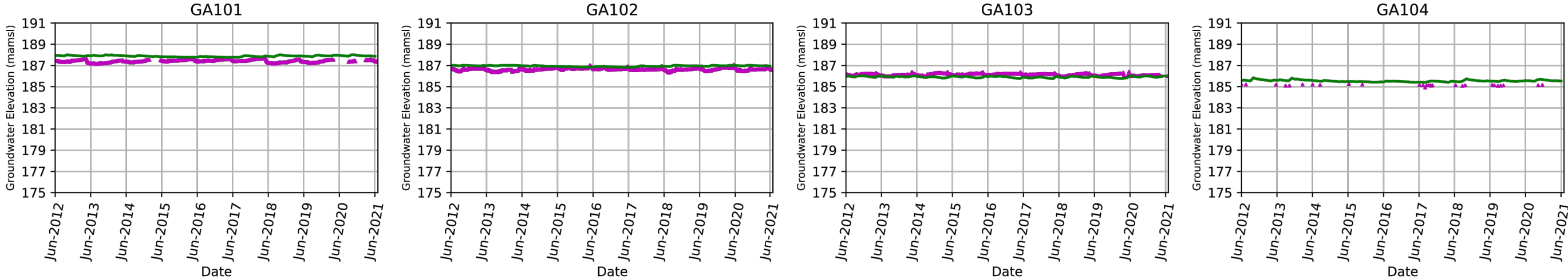
Summary of Key Model Parameters and Uncertainties

Item	Parameter/Factor	Effect/Influence	Source of Data	Data Status	Data Confidence	What Is Needed to Improve Confidence	Potential Uncertainty of Model Prediction
1	K_h and K_v of Geologic Units	1. Model calibration to groundwater levels 2. Predicted groundwater inflows 3. Predicted drawdown	The Mine provided K value data from an extensive hydraulic testing program.	1. The Mine has conducted a robust hydraulic testing program. This includes packer tests, pump tests, falling head, and air-lift test. 2. K value data are available for the bedrock geologic units at various depths. 3. K value data are primarily located around the future mine workings.	High	Installation of well-designed VWPS to collect groundwater levels in the bedrock.	+/- 25%
2	K_h and K_v of Faults	1. Model calibration to groundwater levels 2. Predicted groundwater inflows 3. Predicted drawdown	The Mine provided K value data for faults within the Mine area.	1. K value data are available for local fault structures. 2. K value data are unknown about regional structures.	Medium	1. Characterization of regional fault structures that intersect the Mine area or other local structures. 2. Installation of piezometers to monitor the water levels during the mining operation.	+/- 25%
3	Measured Groundwater Levels	Model calibration	The Mine provided groundwater levels at monitoring wells within the Shallow Groundwater System.	The Mine has been measuring groundwater levels at the Mine site since 2012. Data are collected to measure seasonal responses to recharge in various shallow system hydrogeologic units.	High	1. Continued water-level data collected. 2. Installation of a monitoring network within the peat.	+/- 10%
4	Measured Groundwater Levels in the Bedrock Groundwater System	Model calibration	The Mine provided groundwater levels at monitoring wells and VWPs.	1. The Mine has installed monitoring wells primarily within the fractured bedrock system and some monitoring wells within the unfractured bedrock. All data below 200 mbgs are questionable. 2. Data at VWPs are all questionable.	Medium	Installation of multi-level VWPs with grouted-in transducers near the future Mine Workings and Declines.	+/- 10%
5	Recharge and Climate	Model calibration of water levels	The Mine has provided estimates of recharge for the current and future time periods.	1. Recharge is estimated using a <i>MIKE SHE</i> model. 2. The model is sensitive to the applied recharge rates in the future.	Medium	1. Further work is needed to understand future effects to recharge due to a changing climate. 2. Further work is needed to understand how drawdown may affect recharge over the Mine area.	+/-20%

APPENDIX A

Measured versus Simulated Hydrographs of the Transient Groundwater Flow Model Calibration

Water Levels in the Peat

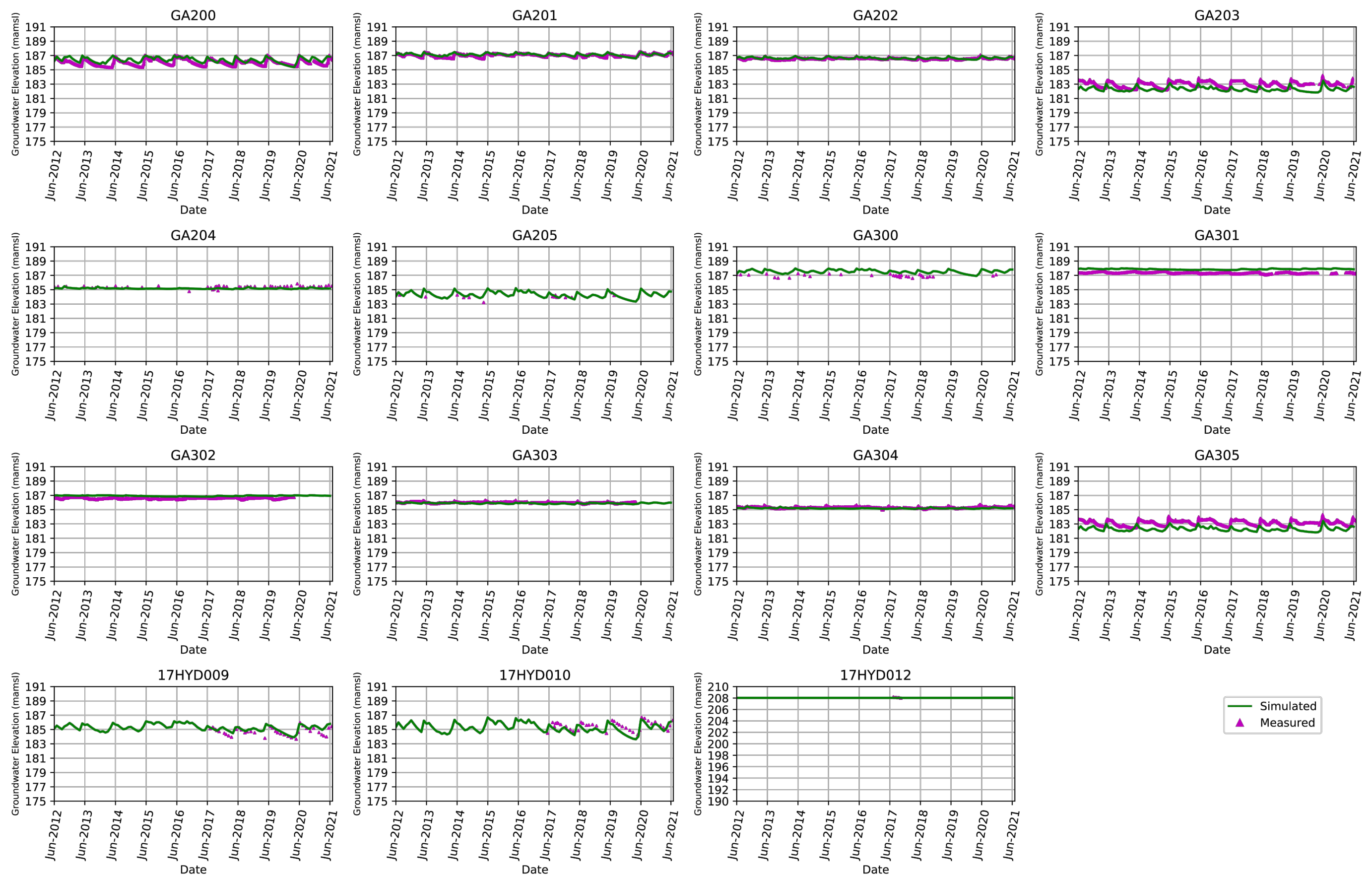


PROJECT NO.	4064
BY	SBM
CHECKED	HL
DRAWN	RJN
DRAWING NAME	APPENDIX
DRAWING DATE	27 Oct 2022
REVISION DATE	



Measured versus Simulated Hydrographs of the Transient Groundwater Flow Model Calibration	
CLIENT: Sakatti Mine	FIGURE NO. A1

Groundwater Levels in Sediment



PROJECT NO.	4064
BY	SBM
CHECKED	HL
DRAWN	RJN
DRAWING NAME	APPENDIX
DRAWING DATE	27 Oct 2022
REVISION DATE	

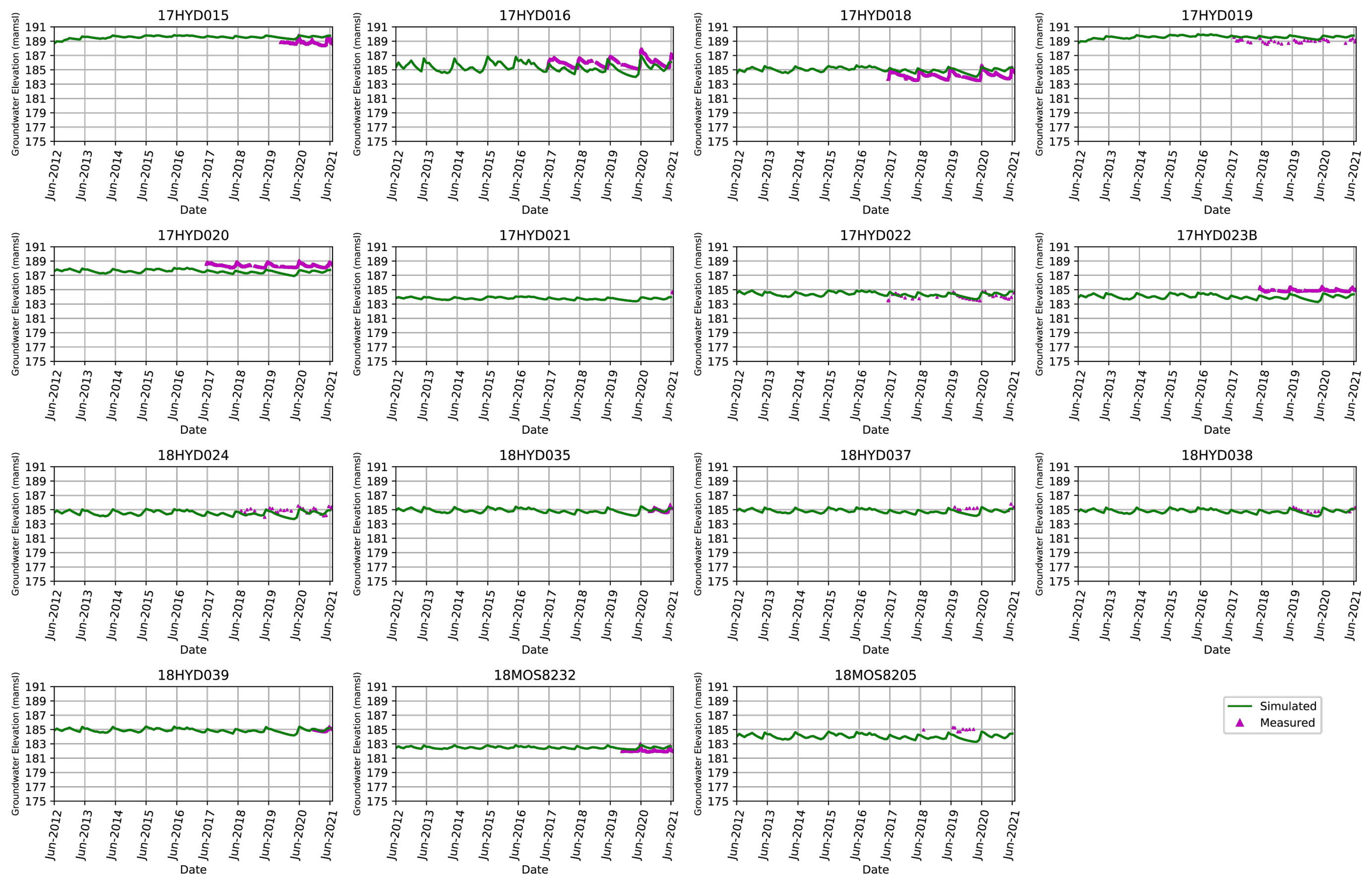


Measured versus Simulated Hydrographs
of the Transient Groundwater Flow
Model Calibration

CLIENT:
Sakatti Mine

FIGURE NO.
A2

Groundwater Levels in Sediment



PROJECT NO.	4064
BY	SBM
CHECKED	HL
DRAWN	RJN
DRAWING NAME	APPENDIX
DRAWING DATE	27 Oct 2022
REVISION DATE	

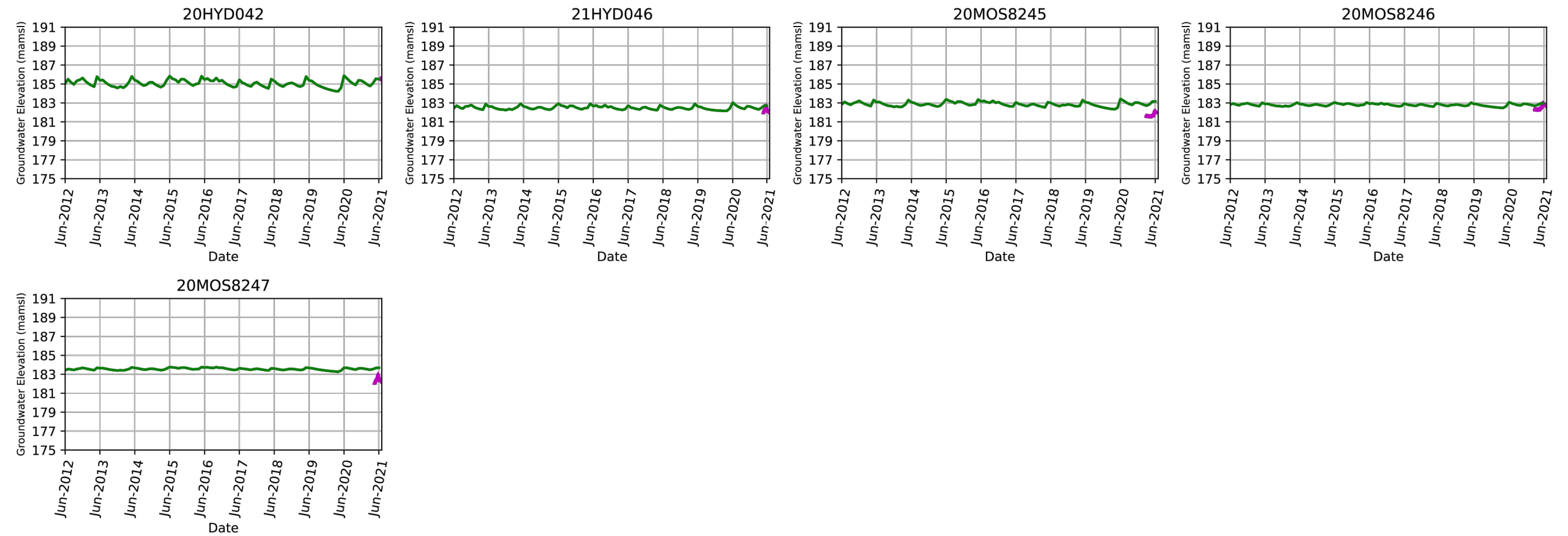


Measured versus Simulated Hydrographs
of the Transient Groundwater Flow
Model Calibration

CLIENT:
Sakatti Mine

FIGURE NO.
A3

Groundwater Levels in Sediment



— Simulated
▲ Measured

PROJECT NO.	4064
BY	SBM
CHECKED	HL
DRAWN	RJN
DRAWING NAME	APPENDIX
DRAWING DATE	27 Oct 2022
REVISION DATE	

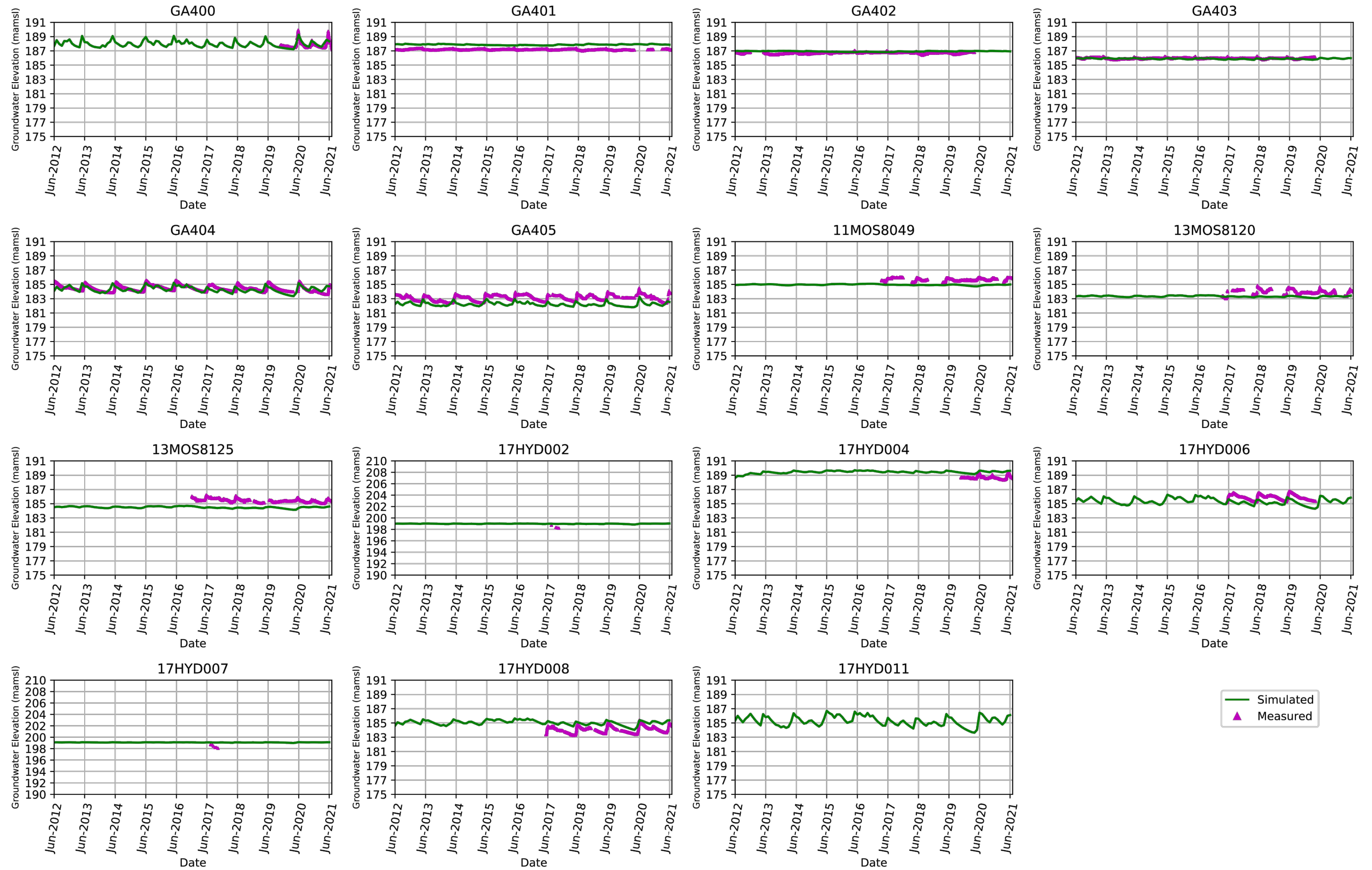


Measured versus Simulated Hydrographs
of the Transient Groundwater Flow
Model Calibration

CLIENT:
Sakatti Mine

FIGURE NO.
A4

Groundwater Levels in Bedrock



PROJECT NO.	4064
BY	SBM
CHECKED	HL
DRAWN	RJN
DRAWING NAME	APPENDIX
DRAWING DATE	27 Oct 2022
REVISION DATE	

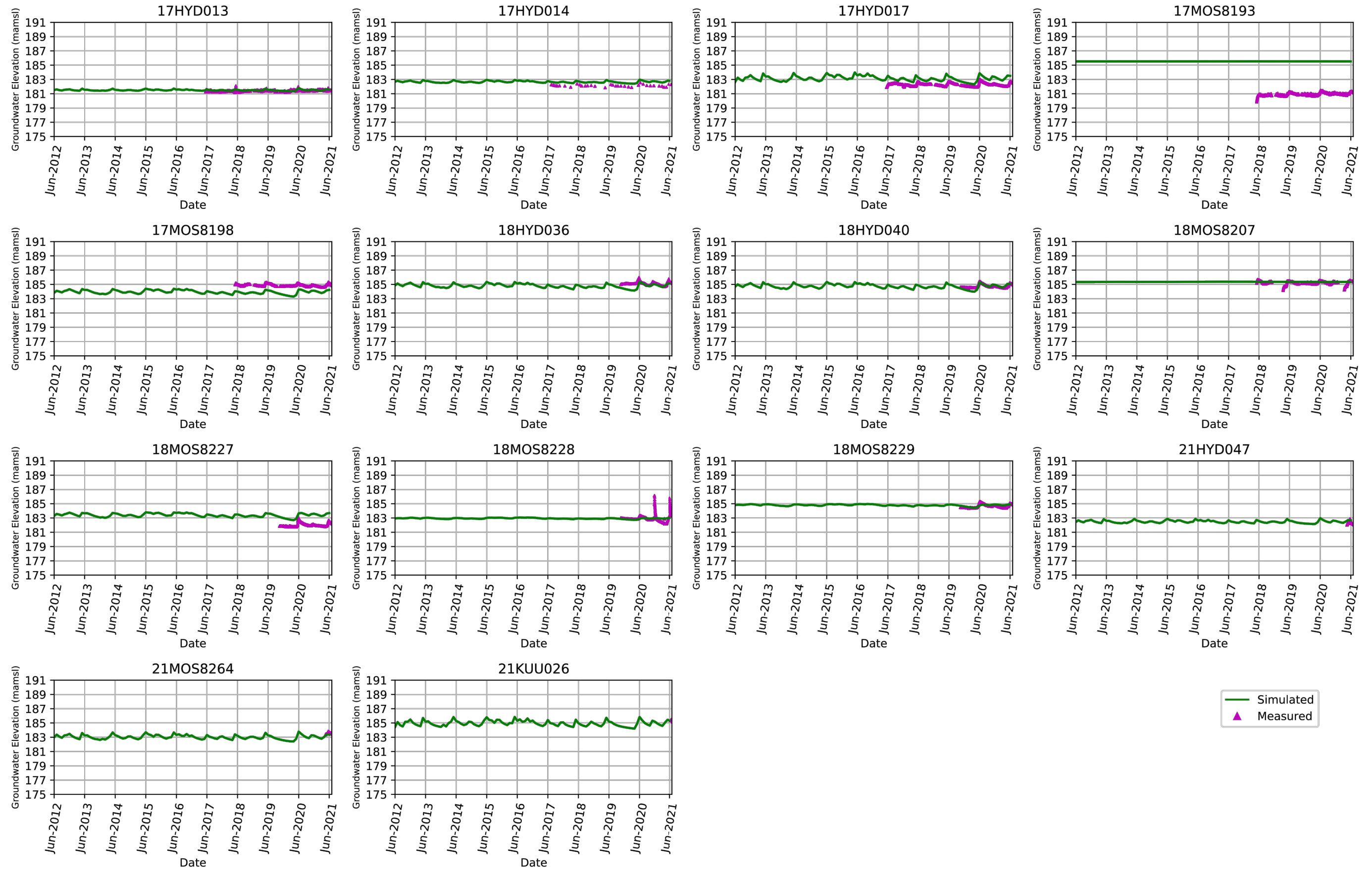


Measured versus Simulated Hydrographs
of the Transient Groundwater Flow
Model Calibration

CLIENT:
Sakatti Mine

FIGURE NO.
A5

Groundwater Levels in Bedrock



PROJECT NO.	4064
BY	SBM
CHECKED	HL
DRAWN	RJN
DRAWING NAME	APPENDIX
DRAWING DATE	27 Oct 2022
REVISION DATE	

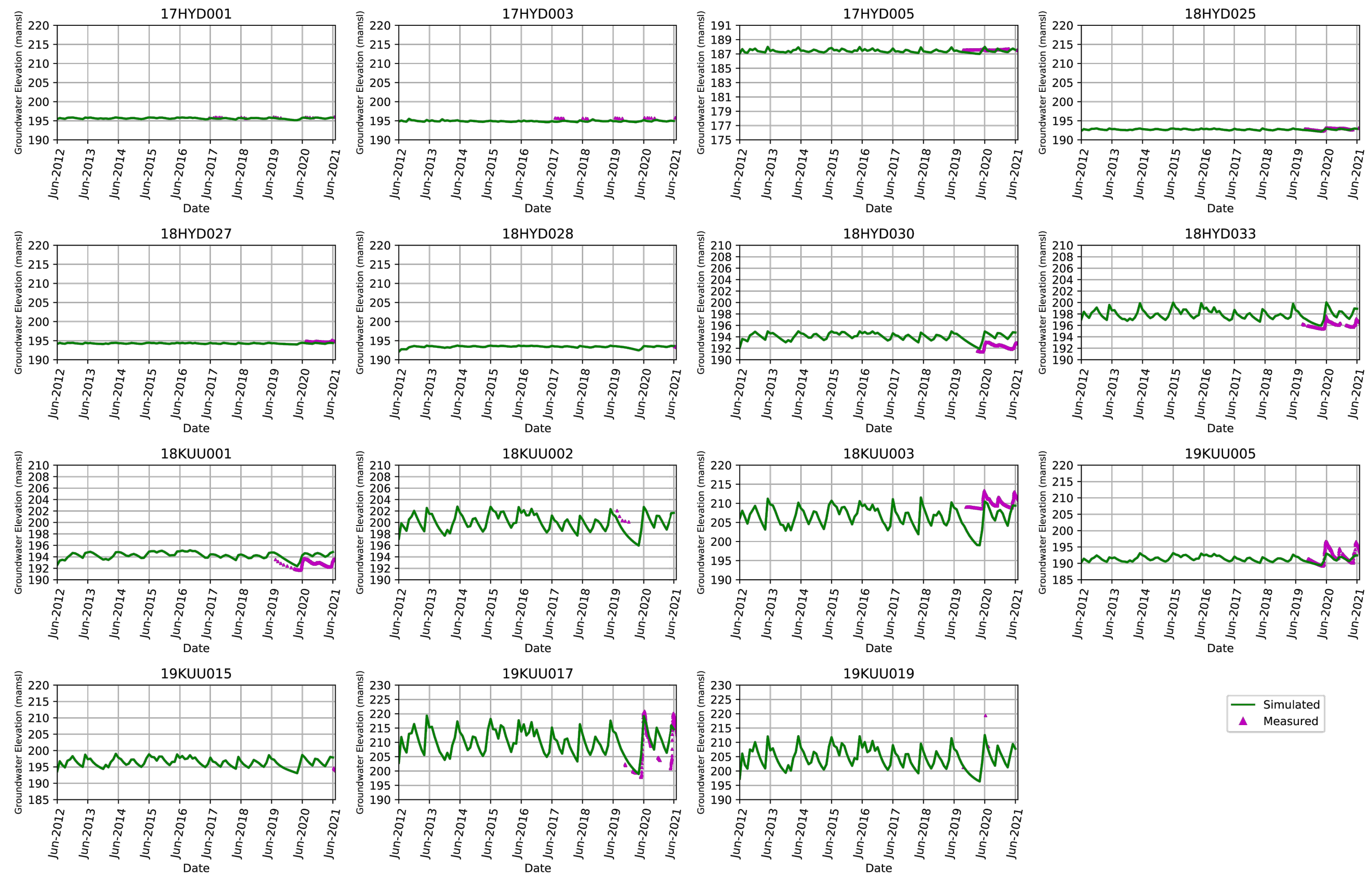


Measured versus Simulated Hydrographs
of the Transient Groundwater Flow
Model Calibration

CLIENT:
Sakatti Mine

FIGURE NO.
A6

Groundwater Levels in Kuusivaara Area



— Simulated
▲ Measured

PROJECT NO.	4064
BY	SBM
CHECKED	HL
DRAWN	RJN
DRAWING NAME	APPENDIX
DRAWING DATE	27 Oct 2022
REVISION DATE	

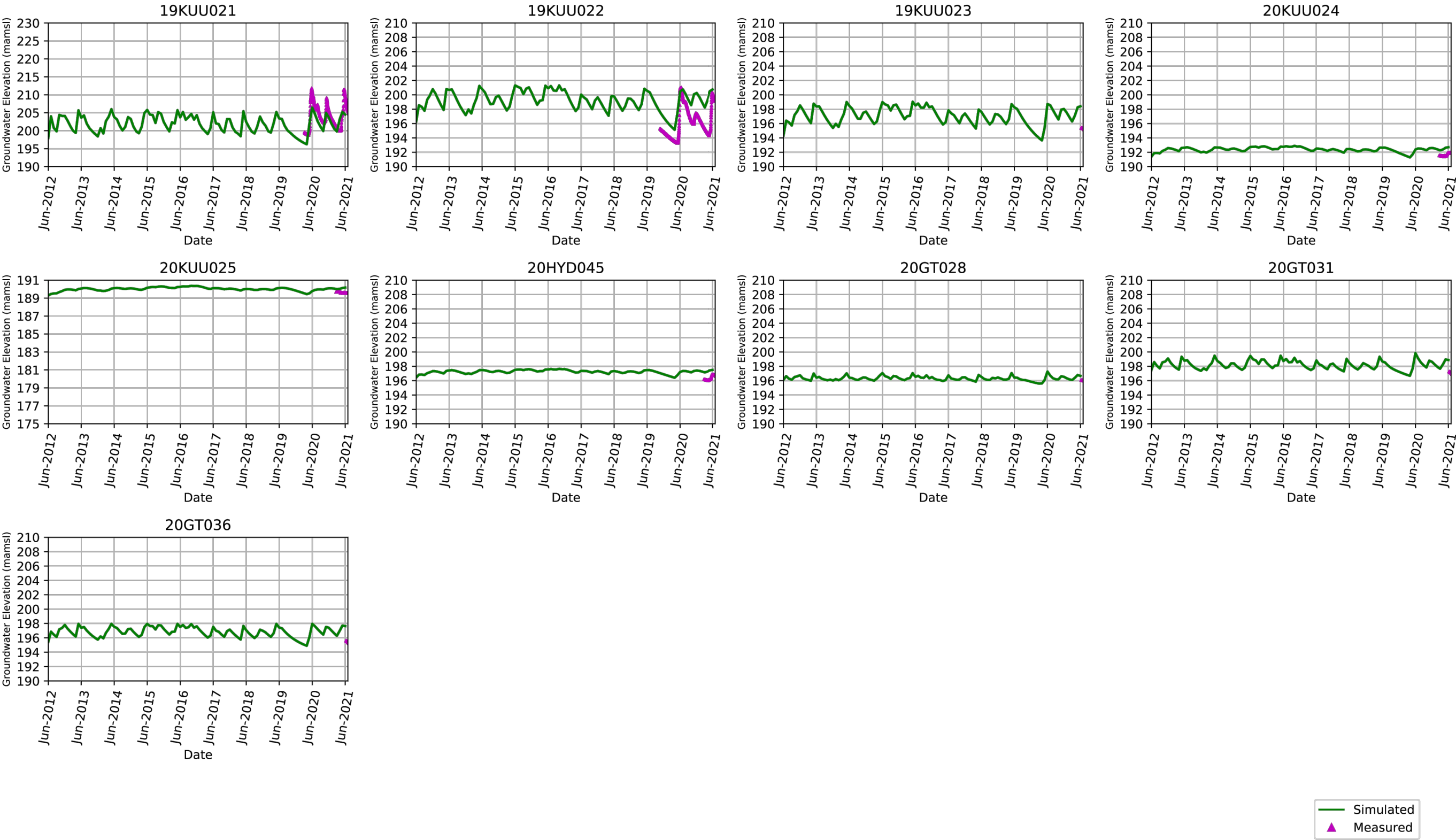


Measured versus Simulated Hydrographs
of the Transient Groundwater Flow
Model Calibration

CLIENT:
Sakatti Mine

FIGURE NO.
A7

Groundwater Levels in Kuusivaara Area



PROJECT NO.	4064
BY	SBM
CHECKED	HL
DRAWN	RJN
DRAWING NAME	APPENDIX
DRAWING DATE	27 Oct 2022
REVISION DATE	



Measured versus Simulated Hydrographs
of the Transient Groundwater Flow
Model Calibration

CLIENT:
Sakatti Mine

FIGURE NO.
A8

APPENDIX B

Predictive Results for Sensitivity Model Scenarios

APPENDIX B
PREDICTIVE RESULTS FOR SENSITIVITY MODEL SCENARIOS

PREDICTIVE MODEL SIMULATIONS FOR SENSITIVITY ANALYSIS

Additional predictive groundwater flow model simulations were conducted to estimate the sensitivity of the key simulated mining parameters. The predictive groundwater flow model simulations were based on the life of mine (LOM) model setup described in the report. The following is a summary of the predictive model scenarios simulated for the sensitivity analyses:

1. **100% Success in Grouting Scenario:** This scenario simulates all components from the 80 percent (%) Success in Grouting Scenario but assumes grouting effectiveness is 100% along fault structures and to a depth of 150 mbgs along the Declines. To simulate a 100% grouting efficiency, no drain nodes are left open to freely drain in the grouting areas. The purpose of this scenario is to demonstrate the effects of increased grouting efficiency.
2. **90% Success in Grouting Scenario:** This scenario simulates all components from the 80% Success in Grouting Scenario but assumes grouting effectiveness is 90% along fault structures and to a depth of 150 mbgs along the Declines. To simulate a 90% grouting efficiency, selected drain nodes (10% of nodes) are left open to drain in areas of grouting. The purpose of this scenario is to demonstrate the effects of increased grouting efficiency.
3. **Alternative Backfill Scenario A:** This scenario simulates all components from the 80% Success in Grouting Scenario but assumes a low- K -value backfill of 2.0×10^{-8} meters per second (m/s). The purpose of this scenario is to determine the effects of the backfill K values on the model predictions.
4. **Alternative Backfill Scenario B:** This scenario simulates all components from the 80% Success in Grouting Scenario but assumes a high- K -value backfill of 2.0×10^{-6} m/s. The purpose of this scenario is to determine the effects of backfill K values on the model predictions.
5. **Closed Stope Scenario:** This scenario simulates all components from the 80% Success in Grouting Scenario but assumes the mined stopes are sufficiently backfilled and groundwater inflow from the mined stopes is negligible. Drains are turned off in previously mined stopes one month after mining. The purpose of this scenario is to determine the effects of leakage around backfilled stopes on the model predictions.
6. **Alternative Mine Plan Scenario:** As discussed above, the mine plan includes the NE deposit area with the shallowest Mine Workings. An alternative mine plan was simulated with the

shallowest mining elevation of 52 meters above mean sea level (mamsl) instead of the primary mine plan of 112 mamsl in the NE deposit area. This would include the removal of the three upper stope levels in the NE deposit. The purpose of this scenario is to estimate the effects of shallow Mine Workings on the model predictions. All other components of the scenario are the same as in the 80% Success in Grouting Scenario.

In addition to sensitivity analyses related to mining parameters, a sensitivity analysis was also conducted for a varying climate (i.e., varying recharge) in the future. The future climate in Finland is predicted to change, with warmer temperatures and more precipitation. As such, additional model scenarios were simulated for both the 80% and 65% Success in Grouting Scenarios under a changing future climate. The simulated future climate variables were discussed in Section 3.2.5. Future recharge rates that were estimated under the RCP4.5 climate case were simulated directly in the groundwater flow model.

PREDICTIVE RESULTS DURING MINING FOR THE SENSITIVITY SCENARIO

Predicted Groundwater Inflow Rates

Figure B-1 shows the predicted groundwater inflow rates for the sensitivity model scenarios and the 80% and 65% Success in Grouting Scenarios. Scenarios presented on the graph include all mining-related model sensitivity scenarios. The climate variation scenario is presented in the next section of the appendix. The following can be concluded regarding the sensitivity of the future groundwater inflow rates relative to the results from the 80% Success in Grouting Scenario:

1. For the grout efficiency from 65% to 100%, an increase in grout efficiency decreases the groundwater inflow rate into the Mine Workings. Predictions of groundwater inflow decrease by 15% to 25% with increasing grout efficiency.
2. In the alternative backfill scenarios, a change in the K value of the backfill has minor effects on long-term groundwater inflow rates (less than 2 cubic meters per hour [m^3/hr]) because the K value of the backfill is higher than that of the in-situ rock mass. Most of the groundwater inflow occurs in the Mine Workings that surround the mining area.
3. In the Closed Stopes Scenario, backfilled stopes reduce peak groundwater inflow rates and have minor effects on long-term groundwater inflow rates (less than 2 m^3/hr). Most of the groundwater inflow occurs in the Mine Workings that surround the mining area.

4. The Alternative Mine Plan Scenario results in a reduction of long-term groundwater inflow rates by less than 5 m³/hr.

Predicted Drawdown

Figures B-2a and B-2b show drawdown hydrographs for each model scenario at 11 hypothetical locations across the Project Site. A spatial map of the hypothetical locations is shown in the figures. The predicted drawdown associated with mining was estimated by comparing the model-predicted drawdown in each specific sensitivity scenario with the No-Mining Scenario. The following can be observed regarding the predicted drawdown across the Project Site:

1. Predicted drawdown decreases as grout efficiency increases. The primary locations where drawdown decreases are near the Basal Thrust and the shallow decline. Drawdown decreases by 20% to 30% in the Basal Thrust area as grout efficiency is increased from 65% to 100%.
2. Over the mining area, in the Closed Stope Scenario (i.e., completely sealed stopes with backfill with no leakage), there is a small decrease in drawdown (less than 0.05 m at Monitoring location 8) in the NE deposit area because most of the groundwater inflow occurs in the Mine Workings that surround the mining area.
3. There is little difference in drawdown in the Alternative Backfill Scenarios. Because the backfill is more permeable than the surrounding bedrock, drainage through the backfill material to the Mine Workings still occurs.
4. The Alternative Mine Plan Scenario (i.e., removing shallow stopes from the NE deposit) results in a reduction in drawdown in the NE deposit area by 0.1 to 0.2 m.

Figure B-3a, Figure B-3b, and Figure B-3c show the predicted drawdown contours at the end of mining due to mining for selected sensitivity scenarios. Predicted drawdown is only shown for cases with significant variation from the 80% Success in Grouting Scenario (over 0.1 m change). As such, only the 100% and 90% Success in Grouting Scenarios and the Alternative Mine Plan Scenario are shown. The following is a summary of the predicted drawdown at the end of mining for the selected model scenarios:

1. The Grout Scenarios result in decreased drawdown along the Basal Thrust and the shallow decline area as grout efficiency increases.
2. The Alternative Mine Plan Scenario results in decreased drawdown in the NE deposit area.

Predicted Water Budget for the Kitinen River

Figure B-4 shows the predicted baseflow to the Kitinen River over the LOM for the sensitivity scenarios, 80% and 65% Success in Grouting Scenarios, and No-Mining Scenario. Similar to the 80% and 65% Success in Grouting Scenarios, all sensitivity scenarios predicted that the groundwater outflow to the Kitinen River may decrease by up to 20 m³/hr. The sensitivity analyses suggest that the reduction of the predicted baseflow is not sensitive to the parameters used in the sensitivity analyses.

PREDICTIVE RESULTS DURING MINING FOR THE CLIMATE SCENARIOS

A varying climate in the future is likely to affect the way precipitation occurs (either snow or rain), potential snow depths, and the timing of snowmelts. To assess the effect of the potential changes in a future climate on the predicted groundwater inflow rate and drawdown, AASM Oy conducted future simulations with the *MIKE SHE* model to estimate changes to monthly and annual recharge rates to the till, sorted sediments, and peat areas for the RCP4.5 climate case. Data from these model simulations were presented in Section 3.2.5 of the main report. The following is a summary of the high-level changes to the climate for the RCP4.5 case that were presented in the report:

1. Annual precipitation and recharge rates show more variability.
2. Recharge rates for the sorted sediments show a slight decrease through time. It is likely that decreases in recharge to the sorted sediments are due to decreases in snow depth and spring thaw recharge and an increase in evapotranspiration (ET).
3. Recharge rates for the till slightly decrease through time. It is likely that decreases in recharge to the till are due to the decreases in snow depth and spring thaw recharge and an increase in ET.
4. Recharge rates for the peat increase through time. The reason for increasing recharge in the peat is due to decreased surface-water runoff resulting in increased recharge into the peat.

Based on the *MIKE SHE* model from AASM Oy, the overall balance of water (recharge and discharge) from the peat is still a net gaining water from precipitation.

Predictive groundwater flow model simulations were simulated for the 80% and 65% Success in Grouting Scenarios with varying climate recharge rates. These will be referred to as the 80% and 65% Success in Grouting Climate Scenarios. Comparisons will be made between the 80% and 65% Success in Grouting Base Scenarios and the 80% and 65% Success in Grouting Climate Scenarios. The “Base Scenarios” are defined as predictive model scenarios with average future recharge rates. The Base Scenarios are described in the report.

Predicted Groundwater Inflow Rate for Climate Scenarios

Figure B-5 shows the predicted groundwater inflow rate over time for the Mine Workings for the Climate and Base Scenarios with 80% and 65% Success in Grouting. A varying climate does not affect the predicted groundwater inflow rate into the Mine Workings. This is because the Mine Workings are not directly connected to the Shallow Groundwater System. The predicted groundwater inflow rates into the Mine Workings are related to the removal of groundwater storage.

Predicted Drawdown for Climate Scenarios

Figure B-6a and Figure B-6b show drawdown hydrographs for the 80% Success in Grouting Base and Climate Scenarios at 11 hypothetical locations across the Project Site. Figure B-6c and Figure B-6d show drawdown hydrographs for the 65% Success in Grouting Base Scenario and Climate Scenarios at 11 hypothetical locations across the Project Site. The predicted drawdown associated with mining was estimated by comparing the model-predicted drawdown in the Base and Climate Scenarios with the No-Mining Scenarios. The following can be observed regarding the predicted drawdown across the Project Site:

1. Predicted drawdown in the Climate Scenarios is highly variable due to changes in annual precipitation and recharge rates. In drier years, the predicted drawdown rate is increased. In wetter years, the predicted drawdown rate is decreased.

2. Long-term trends indicate increased drawdown in the Climate Scenarios as compared to the Base Scenarios in monitoring locations that are near sorted sediments and tills, as the future predicted recharge rates are declining in these hydrogeologic units.
3. Long-term trends indicate decreased or similar drawdown in the Climate Scenarios as compared to the Base Scenarios in monitoring locations that are within or near peat, as the future predicted recharge rates are increasing in this hydrogeologic unit.
4. The seasonal signal of drawdown varies in the Climate Scenarios from the Base Scenarios. The seasonal signal and timing changes are related to changes when recharge occurs because precipitation is changing (either snow or rain) or the snowmelt is occurring sooner due to increasing temperature.

Figure B-7a and Figure B-7b show the predicted drawdown contours associated with mining within the HSA for the 80% Success in Grouting and 65% Success in Grouting Climate Scenarios, respectively. Similar to the Base Scenarios, the predicted drawdown is greater in the shallow deposit area and along the decline. The predicted peak drawdown in the 80% and 65% Success in Grouting Climate Scenarios is 4.9 and 8.0 meters (m) in the portal area, respectively. The Climate Scenarios indicate that there is likely to be less drawdown in areas of peat and more drawdown in areas dominated by till and sediments when compared with the Base Scenarios.

Predicted Water Budget for the Kitinen River

Figure B-8 shows the predicted baseflow to the Kitinen River over the LOM for the Climate Scenarios and No-Mining Scenario. Similar to the Base Scenarios, the Climate Scenarios indicate that the groundwater discharge to the Kitinen River may decrease by up to 20 m³/hr.

Predicted Groundwater Recovery for Climate Scenarios

After mining ends, it is expected that the Shallow and Deep Groundwater Systems will begin to recover. The groundwater flow model was used to estimate the time for the groundwater recovery in the Shallow and Deep Groundwater Systems. Two model scenarios were conducted to predict the future groundwater recovery. The setup and assumptions for these two groundwater recovery model scenarios are as follows:

1. **80% Success in Grouting Climate Groundwater Recovery Scenario:** This scenario assumes mining occurs under the 80% Success in Grouting Climate Scenario assumptions described above. After mining, the groundwater system is allowed to naturally recover. The future recharge rates are based on the climate scenario presented in Section 3.2.5. Future recharge rates for the varying climate were only available through Year 2100. After 2100, recharge rates from Year 2100 are repeated annually over the rest of the model simulation time period.
2. **65% Success in Grouting Climate Groundwater Recovery Scenario:** This scenario assumes mining occurs under the 65% Success in Grouting Climate Scenario assumptions described above. After mining, the groundwater system is allowed to naturally recover. The future recharge rates are based on the climate scenario presented in Section 3.2.5 of the main report. Future recharge rates for the varying climate were only available through Year 2100. After 2100, recharge rates from Year 2100 are repeated annually over the rest of the model simulation time period.

Based on the above assumptions, the groundwater flow model was simulated for 400 years after mining. A 400-year time period for groundwater recovery is simulated due to the low K value of the Unfractured Bedrock.

Groundwater recovery in the groundwater system is demonstrated by showing drawdown at the key monitoring locations over time. In order to assess the groundwater recovery over time, the following hypothetical piezometers, as shown in Figure B-9, were used:

1. Eleven shallow piezometers were populated in the areas of predicted drawdown. These piezometers monitor the groundwater levels in the first saturated model layer with elevations ranging from approximately 184 to 194 mamsl.
2. One virtual piezometer was populated from the ground surface to the deep mining zone. This piezometer was assumed to be equipped with virtual multiple-level transducers at eight different elevations.

Figure B-9a and Figure B-9b show drawdown hydrographs for the 80% Success in Grouting and 65% Success in Grouting Climate Groundwater Recovery Scenarios, respectively, at 11 different hypothetical monitoring wells and one piezometer at the Project Site during groundwater recovery. The following can be observed regarding the groundwater recovery for the 80% Success in Grouting Climate Scenario across the Project Site (B-9a):

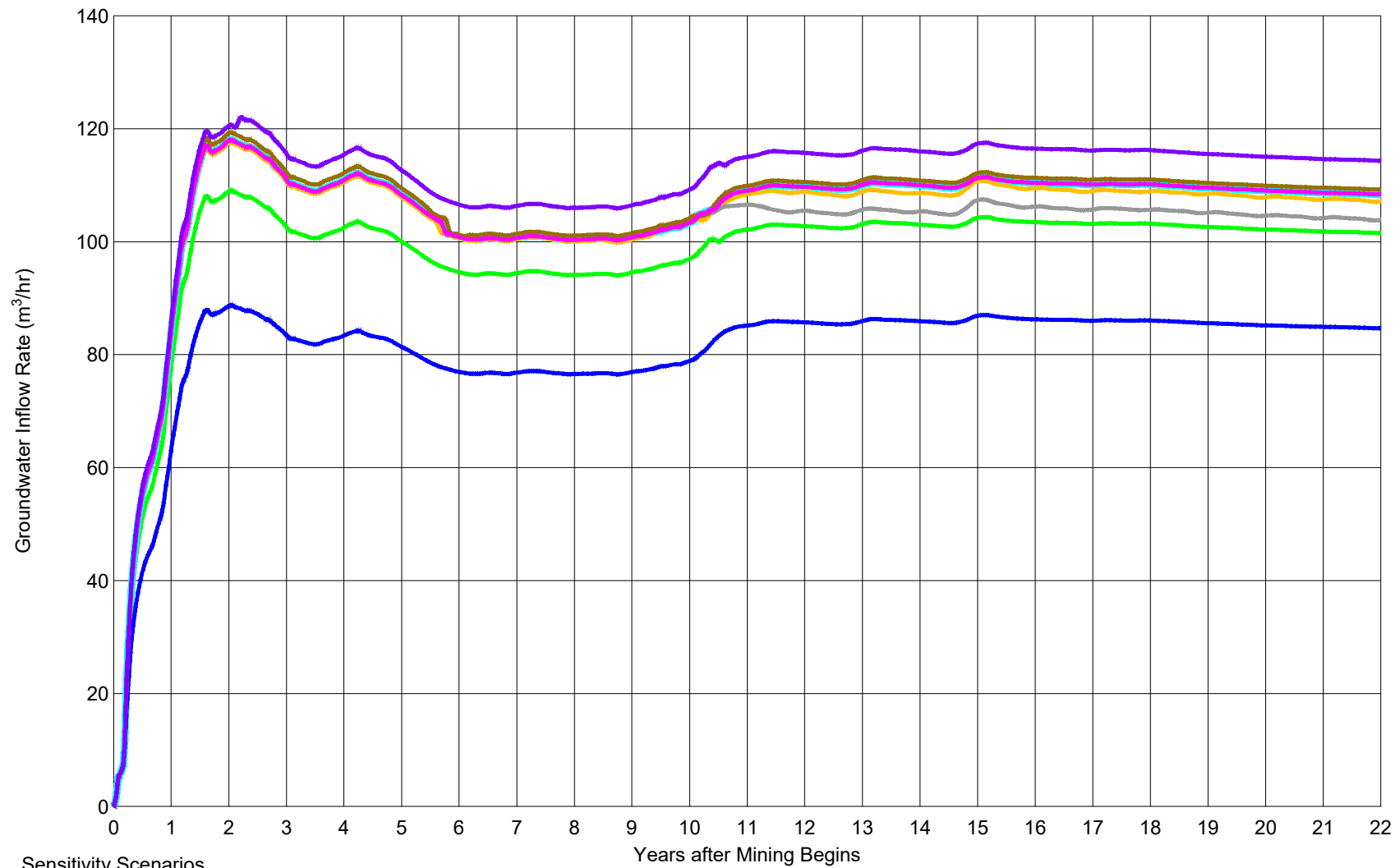
1. Groundwater levels within the Shallow Groundwater System begin to recover after mining ends. Groundwater recovery begins to occur as the Mine Workings stop draining.
2. Within 11 years, groundwater levels within the Shallow Groundwater System have recovered to within 0.1 m in comparison to the pre-mining condition.
3. Within the Shallow Groundwater System monitoring locations, predicted groundwater recovery varies seasonally due to the simulated seasonal recharge from snowmelt. Seasonal variations range from 0.01 to 0.15 m.
4. Shallow Groundwater System monitoring locations indicate more seasonal variation during groundwater recovery for the Climate Groundwater Recovery Scenario than in the Base Groundwater Recovery Scenario due to the simulated recharge rates for the Climate Scenario.
5. Monitoring locations within the Shallow Groundwater System indicate that the groundwater system has recovered to drawdown with less than 0.01 m difference (greater than 99% recovery) from the No-Mining Scenario at all monitoring locations 75 years after mining ends.
6. At piezometer locations within the Unfractured Bedrock, there is increasing drawdown in the shallow elevations of the Unfractured Bedrock for the first 20 years after mining ends as the Deep Groundwater System begins to recover.
7. Due to the low K values of the Unfractured Bedrock, deeper monitoring locations require a longer time to recover than shallower monitoring locations. By 400 years after mining, all monitoring locations within the Unfractured Bedrock have drawdown less than 2 m.

The following can be observed regarding the groundwater recovery for the 65% Success in Grouting Climate Scenarios (Figure B9-b) across the Project Site:

1. Groundwater levels within the Shallow Groundwater System begin to recover after mining ends. Groundwater recovery begins to occur as the Mine Workings stop draining.
2. Within 11 years, groundwater levels within the Shallow Groundwater System have recovered to within 0.1 m in comparison to the pre-mining condition.
3. Within the Shallow Groundwater System monitoring locations, predicted groundwater recovery varies seasonally due to the simulated seasonal recharge from snowmelt. Seasonal variations range from 0.01 to 0.15 m.
4. Shallow Groundwater System monitoring locations indicate more seasonal variation for the Climate Groundwater Recovery Scenario than in the Base Groundwater Recovery Scenario due to the simulated recharge rates for the Climate Scenario.

5. Monitoring locations within the Shallow Groundwater System indicate that the groundwater system has recovered to drawdown with less than 0.01 m difference (greater than 99% recovery) from the No-Mining Scenario at all monitoring locations 75 years after mining ends.
6. At piezometer locations within the Unfractured Bedrock, there is increasing drawdown in the shallow elevations of the Unfractured Bedrock for the first 20 years after mining ends as the Deep Groundwater System begins to recover.
7. Due to the low *K* values of the Unfractured Bedrock, deeper monitoring locations require a longer time to recover than shallower monitoring locations. By 400 years after mining, all monitoring locations within the Unfractured Bedrock have drawdown less than 2.5 m.

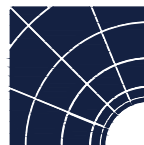
Attachments: Figure B-1 – Predicted Groundwater Inflows for the Sensitivity Scenarios
Figure B-2 – Predicted Drawdown over the LOM at Key Locations around the Mine Area for the Sensitivity Scenarios
Figure B-3 – Predicted Drawdown at the End of Mining for the Selected Sensitivity Scenarios
Figure B-4 – Predicted Baseflow to the Kitinen River for the Sensitivity Scenarios
Figure B-5 – Predicted Groundwater Inflows for the Climate Scenarios
Figure B-6 – Predicted Drawdown over the LOM at Key Locations around the Mine Area for the Climate Scenarios
Figure B-7 – Predicted Drawdown at the End of Mining for the Climate Scenarios
Figure B-8 – Predicted Baseflow to the Kitinen River for the Climate Scenarios
Figure B-9 – Predicted Groundwater Recovery after Mining at Key Locations around the Mine Area for the Climate Scenarios



Sensitivity Scenarios

- 65% Success in Grouting Scenario
- 80% Success in Grouting Scenario
- Alternative Backfill: High K
- Alternative Backfill: Low K
- Closed Stopes
- Alternative Mine Plan
- 90% Success in Grouting Scenario
- 100% Success in Grouting Scenario

PROJECT NO.	4064
BY	SBM
CHECKED	HL
DRAWN	RJN
DRAWING NAME	SENS
DRAWING DATE	9 JAN 2023
REVISION DATE	

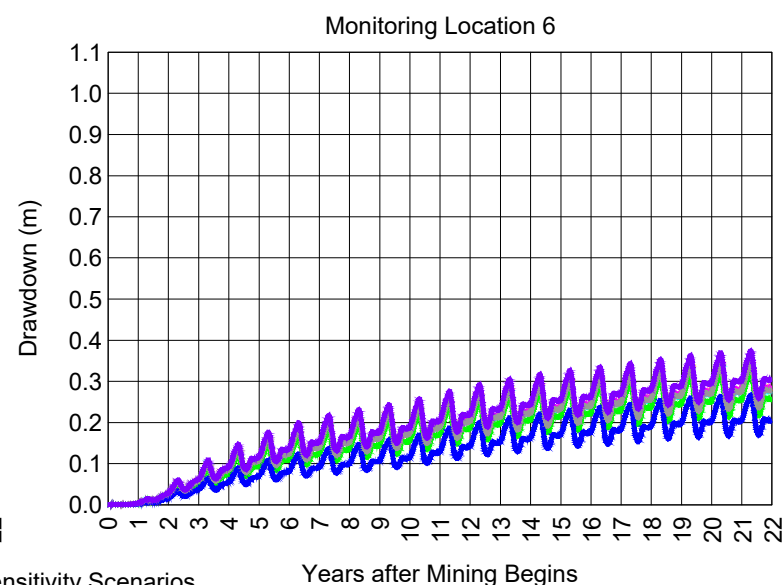
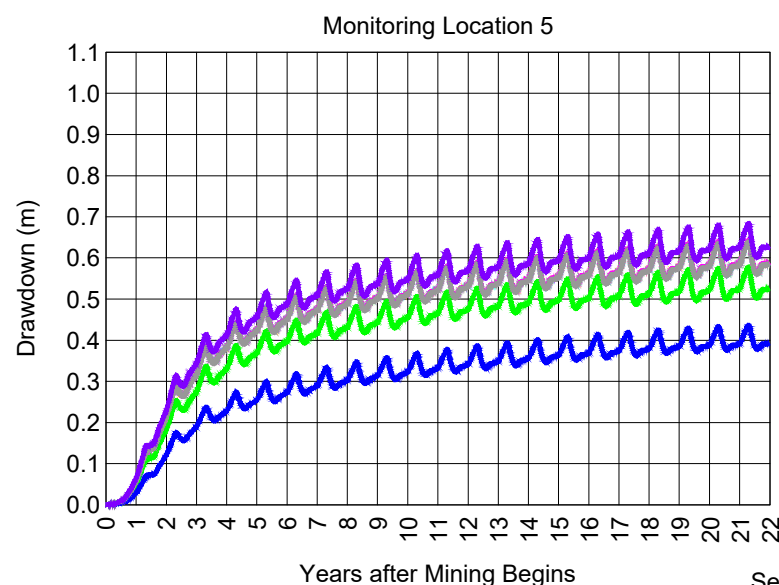
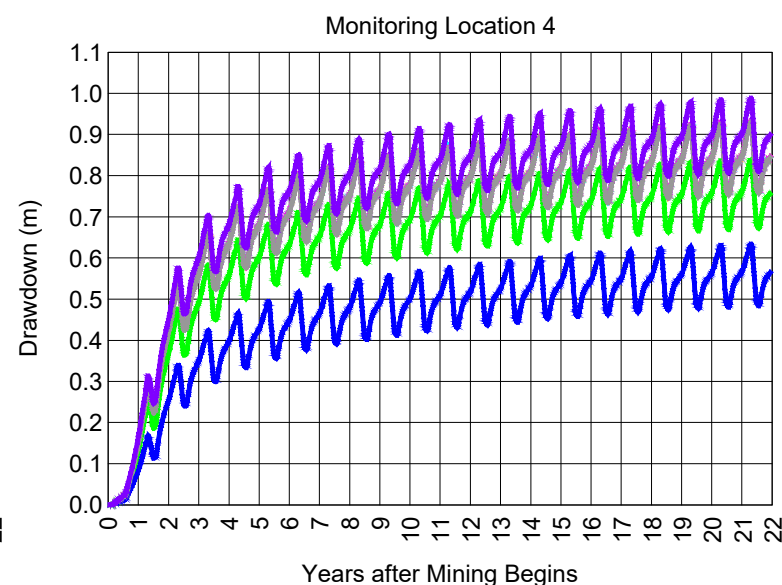
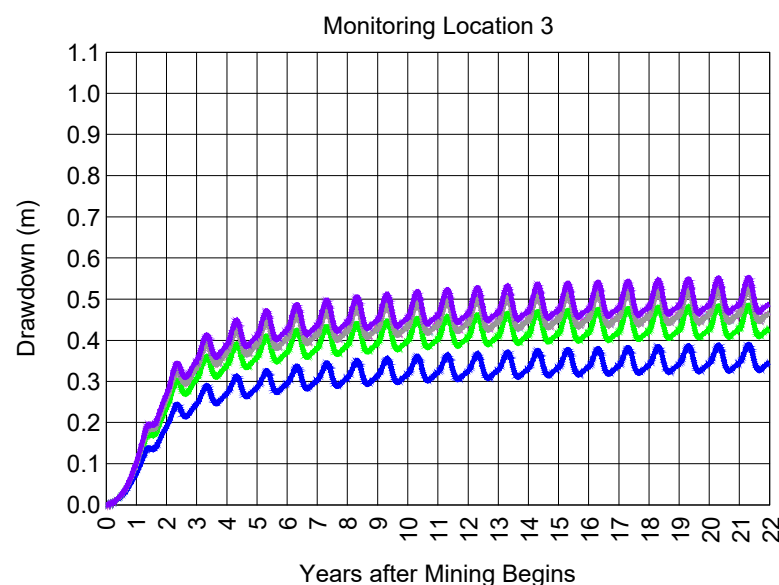
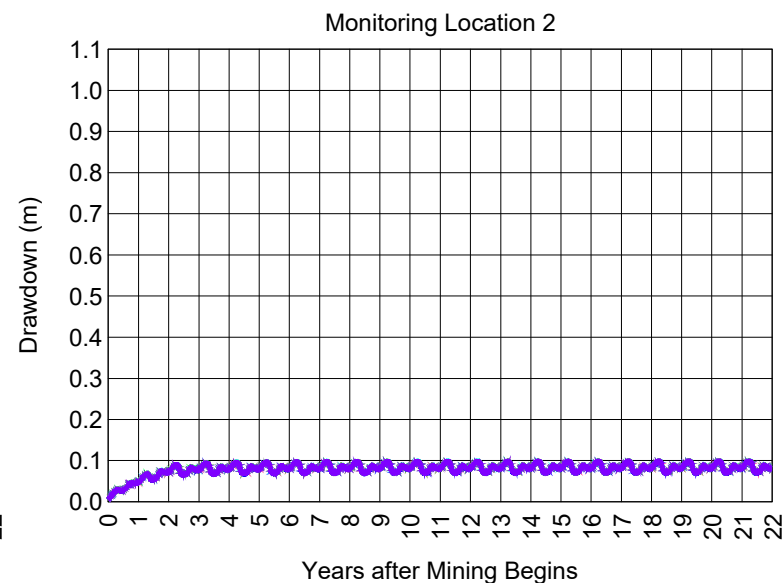
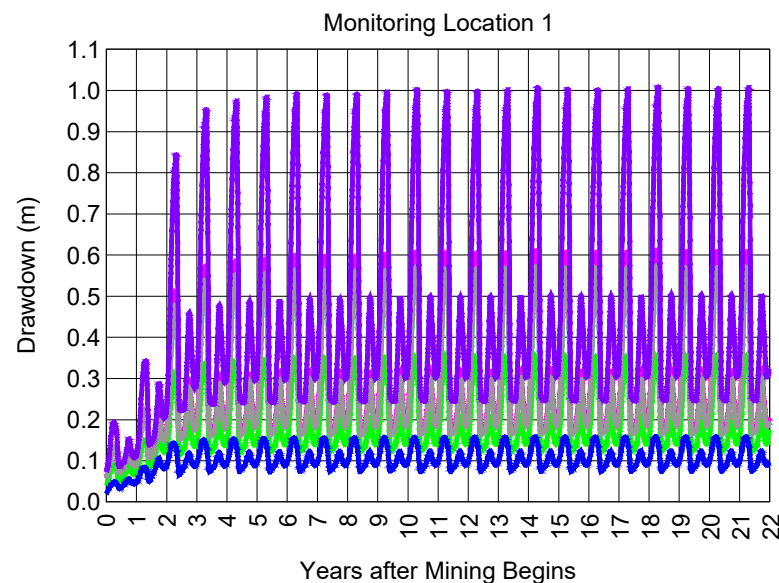


ITASCATM
Denver, Inc.

Predicted Groundwater Inflows for the Sensitivity Scenarios

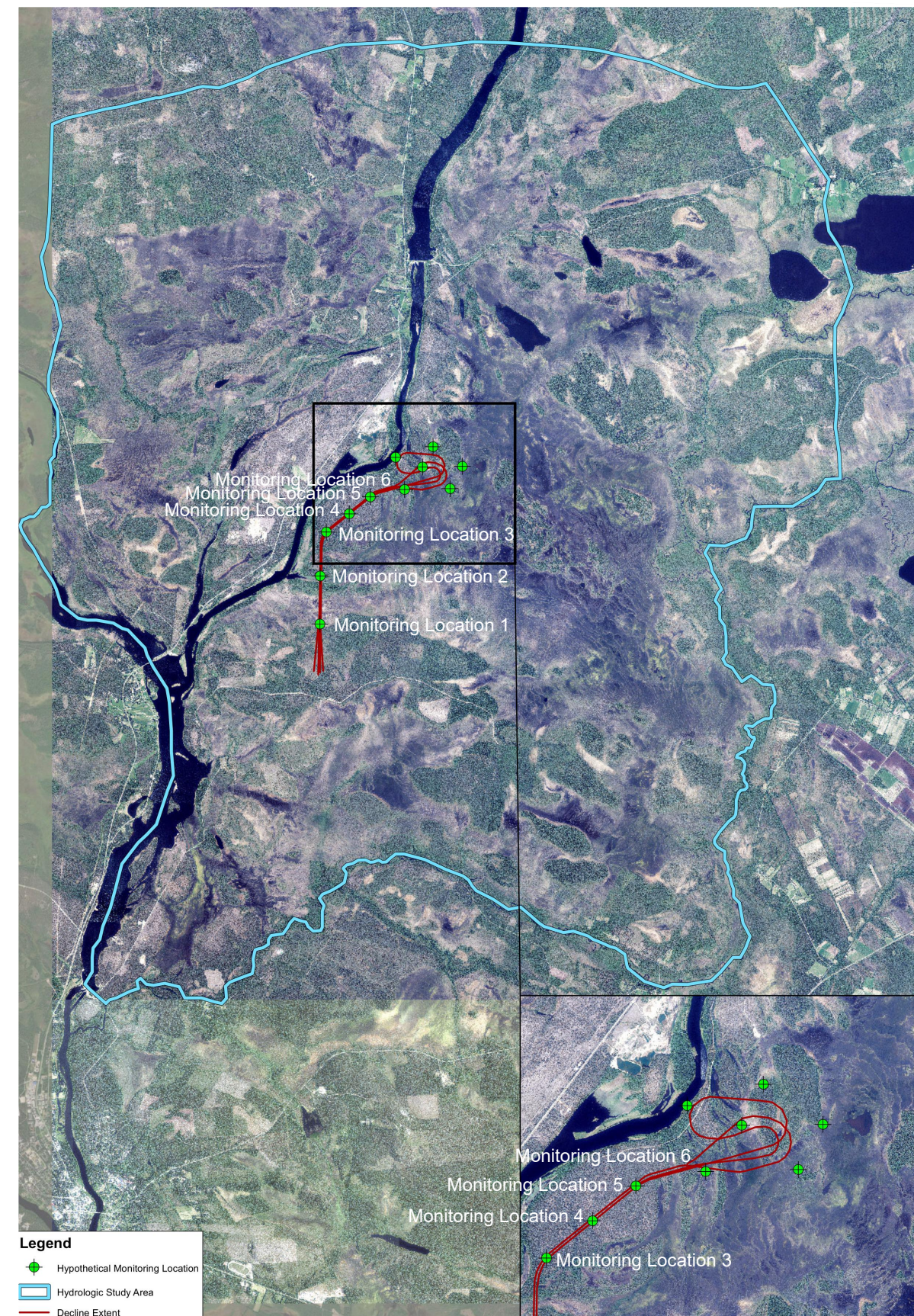
CLIENT:
Sakatti Mine

FIGURE NO.
B-1



- Sensitivity Scenarios**
- 65% Success in Grouting Scenario
 - 80% Success in Grouting Scenario
 - Alternative Backfill: High K
 - Alternative Backfill: Low K
 - Closed Stopes
 - Alternative Mine Plan
 - 90% Success in Grouting Scenario
 - 100% Success in Grouting Scenario

Note: Sensitivity Scenarios of Closed Stopes, Alternative Backfill, have negligible differences from 80% Success in Grouting Scenario



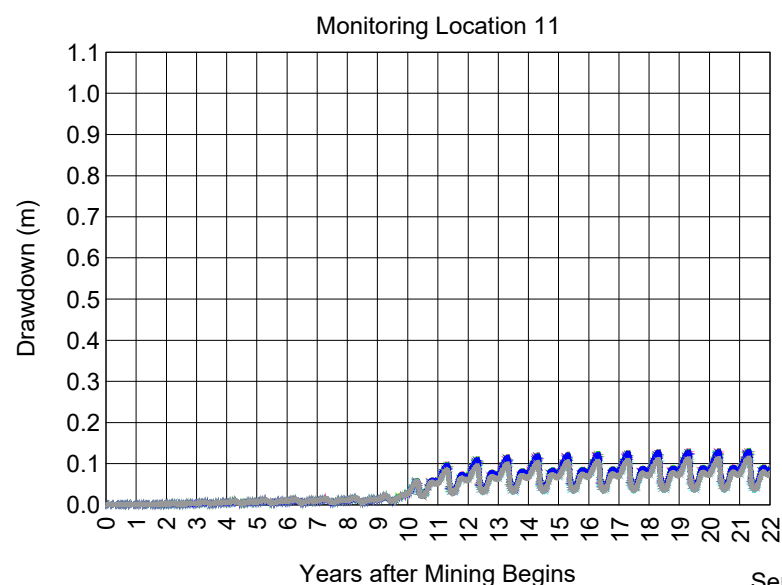
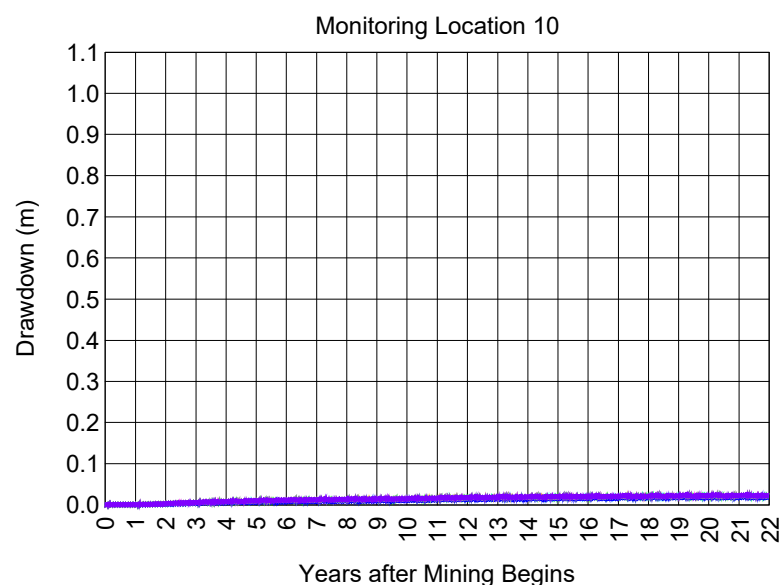
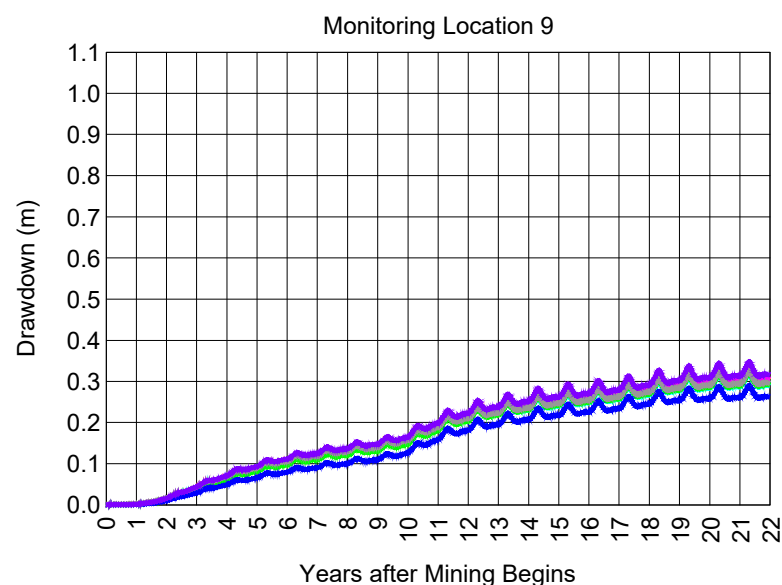
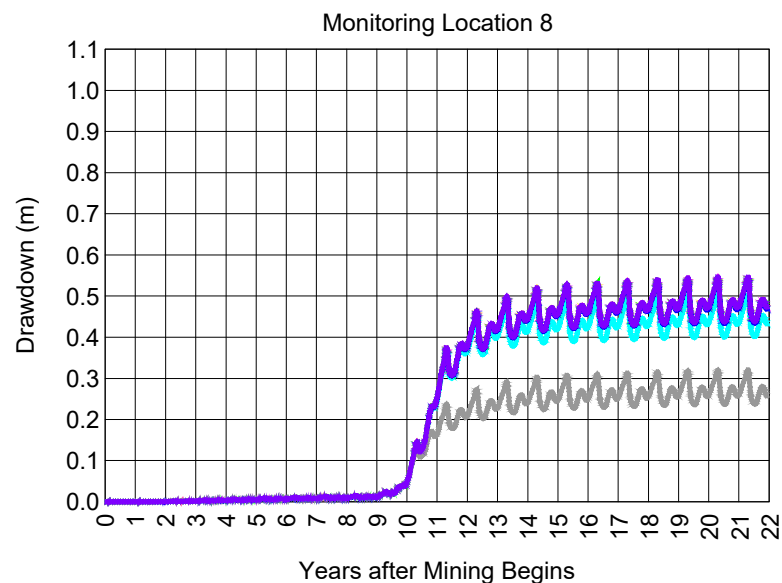
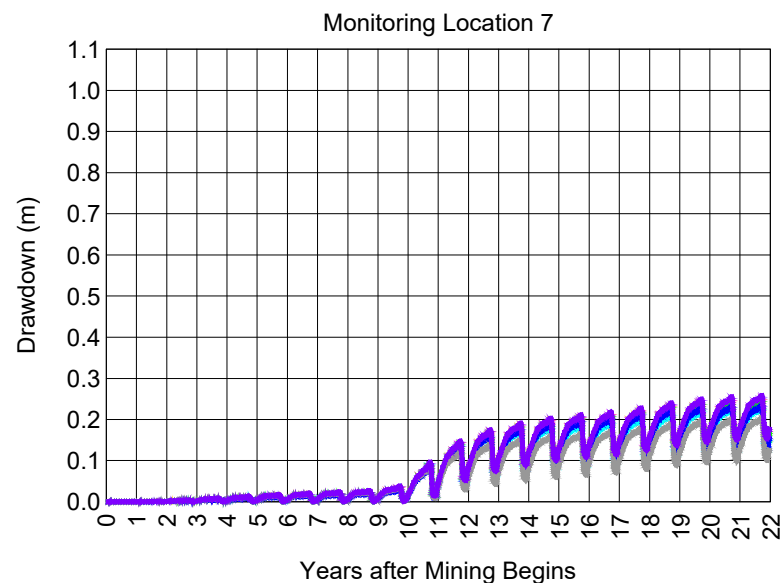
PROJECT NO.	4064
BY	SBM
CHECKED	HL
DRAWN	RJN
DRAWING NAME	KEY
DRAWING DATE	16 NOV 2022
REVISION DATE	



Predicted Drawdown over the LOM
at Key Locations around the
Mine Area for the Sensitivity Scenarios

CLIENT:
Sakatti Mine

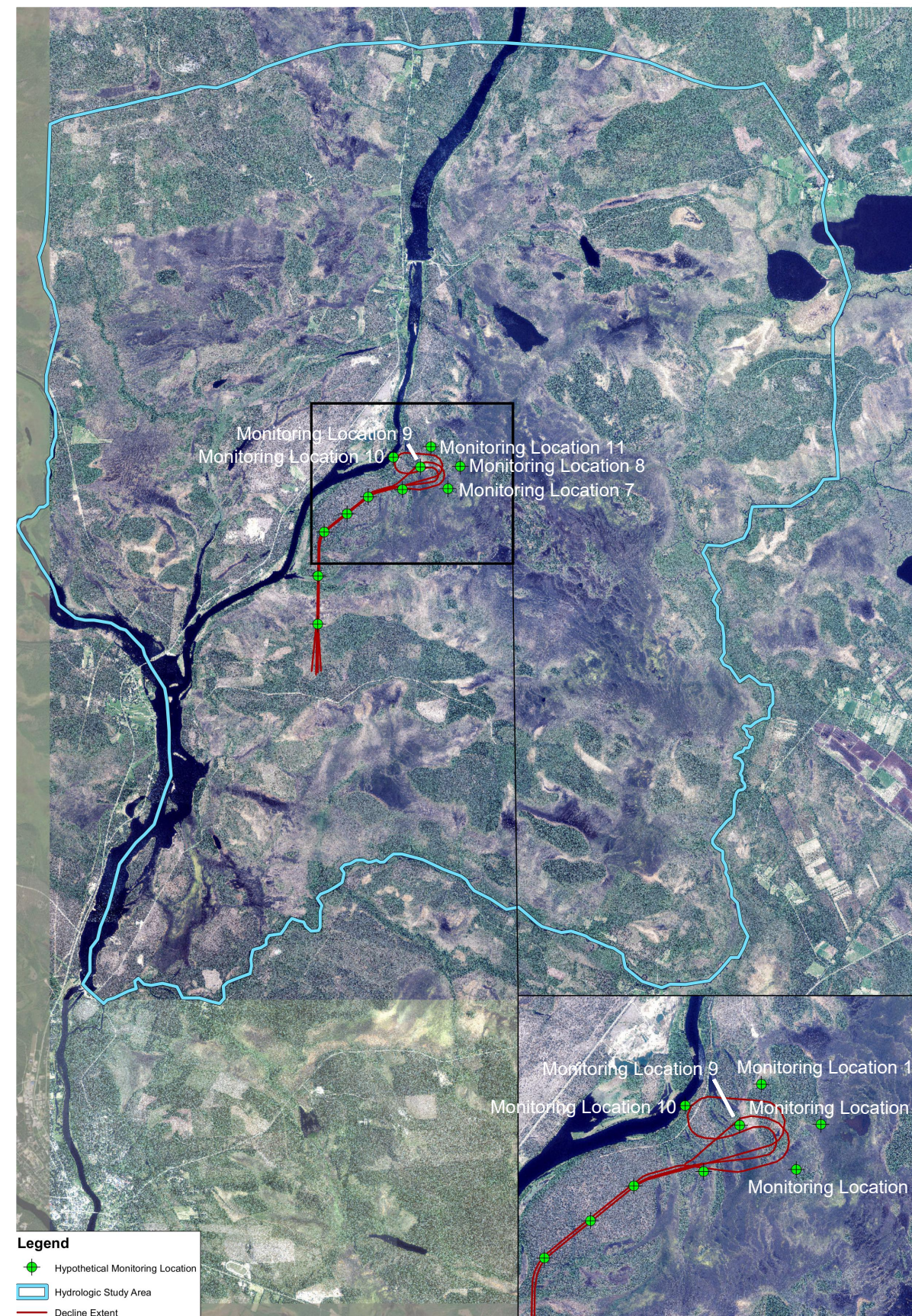
FIGURE NO.
B-2a



Sensitivity Scenarios

- 65% Success in Grouting Scenario
- 80% Success in Grouting Scenario
- Alternative Backfill: High *K*
- Alternative Backfill: Low *K*
- Closed Stopes
- Alternative Mine Plan
- 90% Success in Grouting Scenario
- 100% Success in Grouting Scenario

Note: Sensitivity Scenarios of Closed Stopes, Alternative Backfill, have negligible differences from 80% Success in Grouting Scenario



- Legend**
- Hypothetical Monitoring Location
 - Hydrologic Study Area
 - Decline Extent

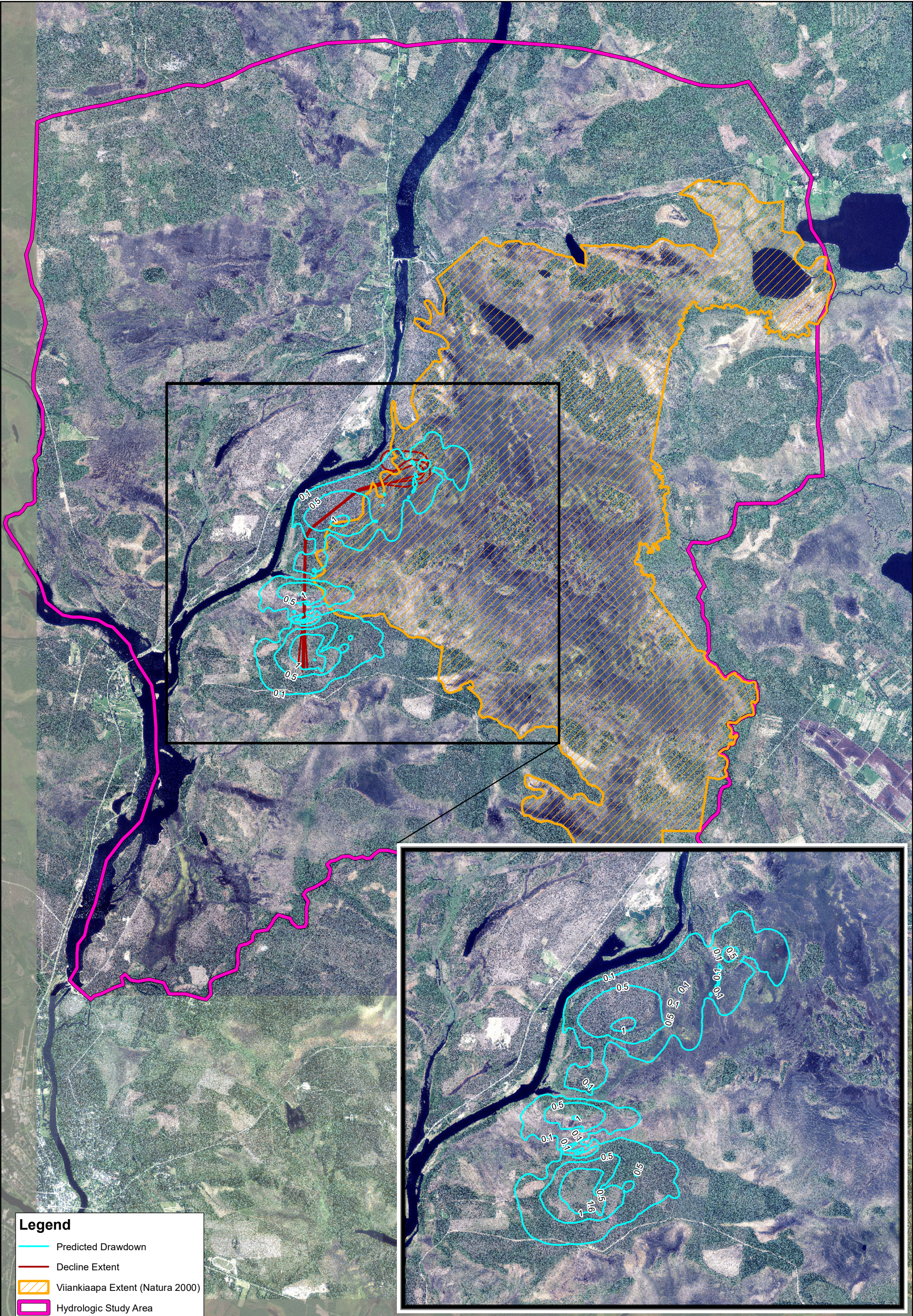
PROJECT NO.	4064
BY	SBM
CHECKED	HL
DRAWN	RJN
DRAWING NAME	KEY
DRAWING DATE	16 NOV 2022
REVISION DATE	



Predicted Drawdown over the LOM
at Key Locations around the
Mine Area for the Sensitivity Scenarios

CLIENT:
Sakatti Mine

FIGURE NO.
B-2b



Legend

- Predicted Drawdown
- Decline Extent
- Viiankiaapa Extent (Natura 2000)
- Hydrologic Study Area



0 1,250 2,500 Meters

PROJECT NO.	4064
BY	SBM
CHECKED	HL
DRAWN	NP
DRAWING NAME	Draw_SSS_Base
DRAWING DATE	Apr. 25, 2022
REVISION DATE	Jan. 12, 2023



ITASCA
Denver, Inc.

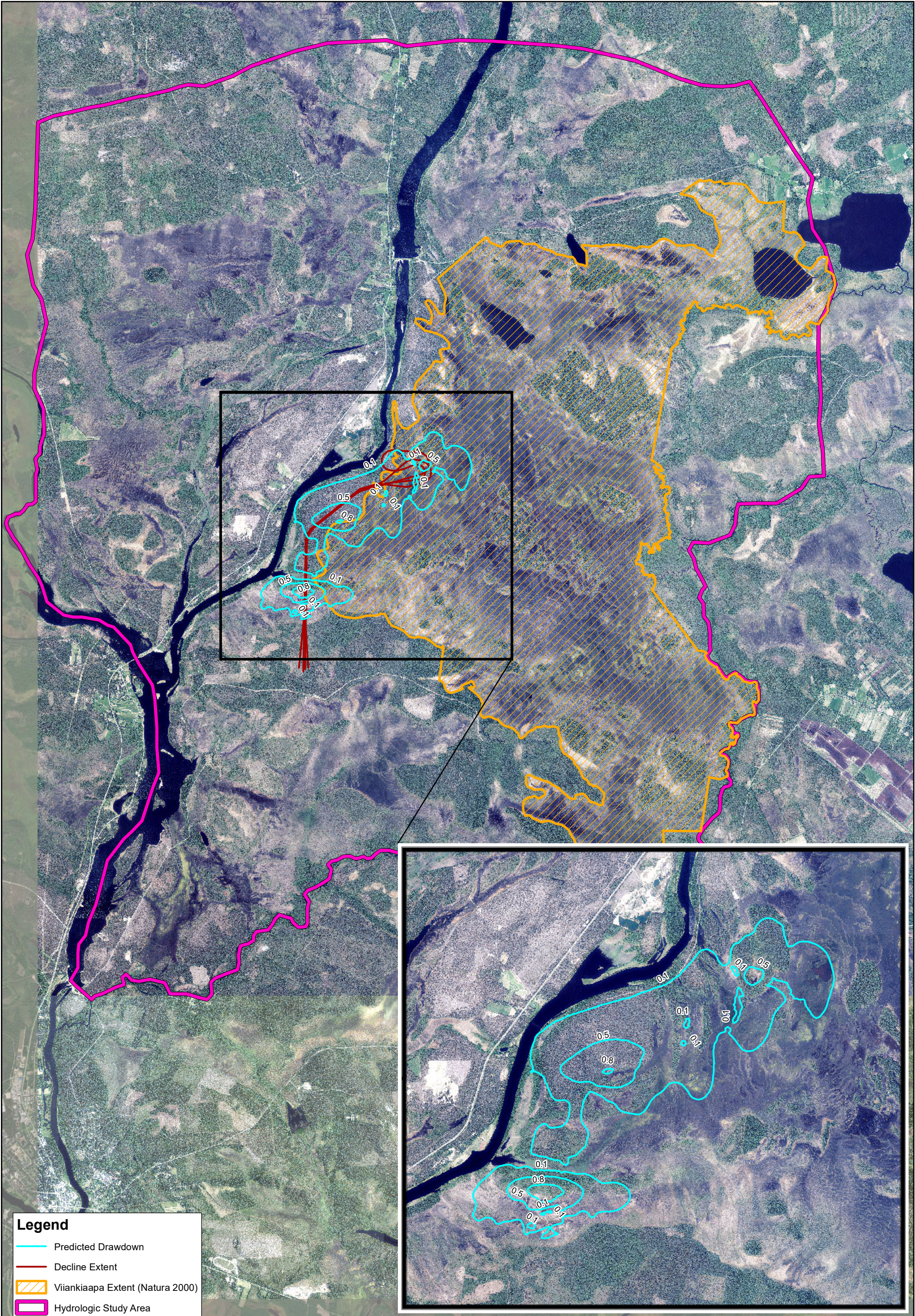
Predicted Drawdown at the End of Mining
for the Selected Sensitivity Scenarios:
90% Success in Grouting Scenario

CLIENT:

Sakatti Mine

FIGURE NO.

B-3a



Legend

Predicted Drawdown

Decline Extent

Viankiaapa Extent (Natura 2000)

Hydrologic Study Area

N

0

1,250

2,500

Meters

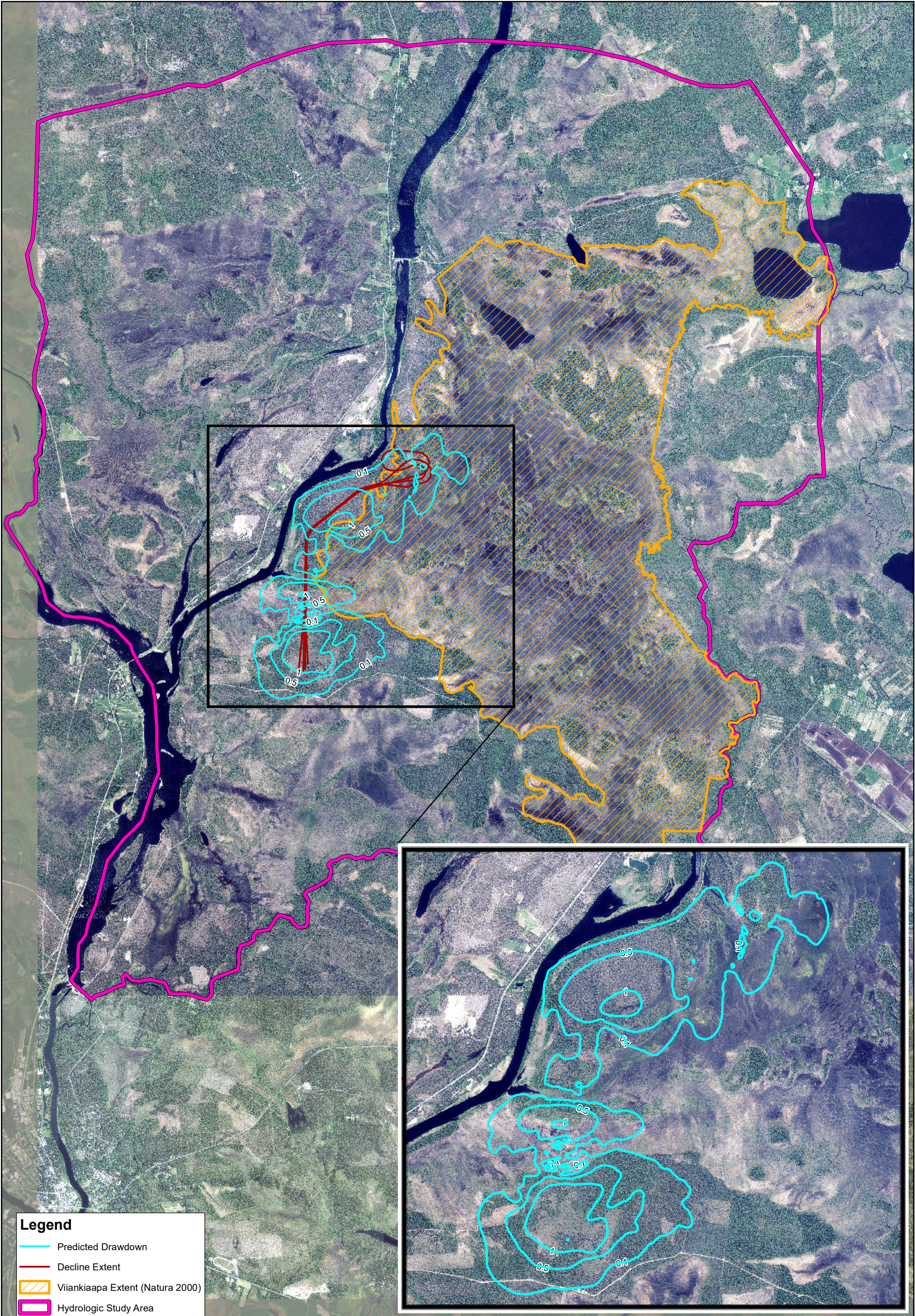
PROJECT NO.	4064
BY	SBM
CHECKED	HL
DRAWN	NP
DRAWING NAME	Draw_SSS_100b
DRAWING DATE	Apr. 25, 2022
REVISION DATE	Jan. 12, 2023

ITASCA
Denver, Inc.

Predicted Drawdown at the End of Mining
for the Selected Sensitivity Scenarios:
100% Success in Grouting Scenario

CLIENT:	FIGURE NO.
Sakatti Mine	B-3b

G:\ARCGIS\4064_Sakatti\MXDs\Working_Appendix\Draw_SSS_100b.mxd



Legend

- Predicted Drawdown
- Decline Extent
- Viiankiaapa Extent (Natura 2000)
- Hydrologic Study Area

PROJECT NO.	4064
BY	SBM
CHECKED	HL
DRAWN	NP
DRAWING NAME	Draw_SSSc_Alt
DRAWING DATE	Apr. 25, 2022
REVISION DATE	Jan. 12, 2023



ITASCA
Denver, Inc.

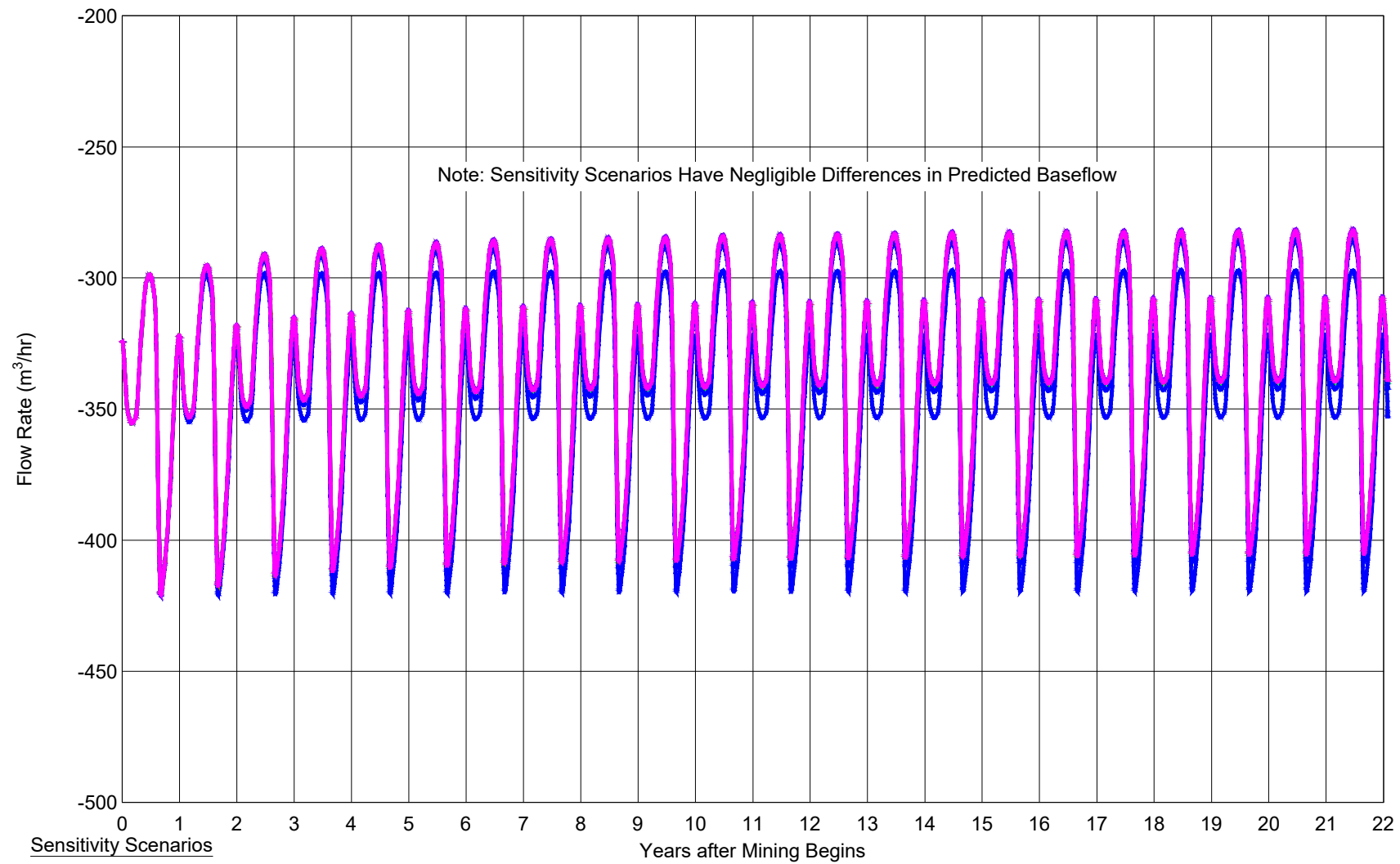
Predicted Drawdown at the End of Mining
for the Selected Sensitivity Scenarios:
Alternative Mine Plan Scenario

CLIENT:

Sakatti Mine

FIGURE NO.

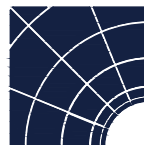
B-3c



Sensitivity Scenarios

- 65% Success in Grouting Scenario
- 80% Success in Grouting Scenario
- Alternative Backfill: High K
- Alternative Backfill: Low K
- Closed Stopes
- Alternative Mine Plan
- No-Mining
- 90% Success in Grouting Scenario
- 100% Success in Grouting Scenario

PROJECT NO.	4064
BY	SBM
CHECKED	HL
DRAWN	RJN
DRAWING NAME	SENS
DRAWING DATE	16 NOV 2022
REVISION DATE	

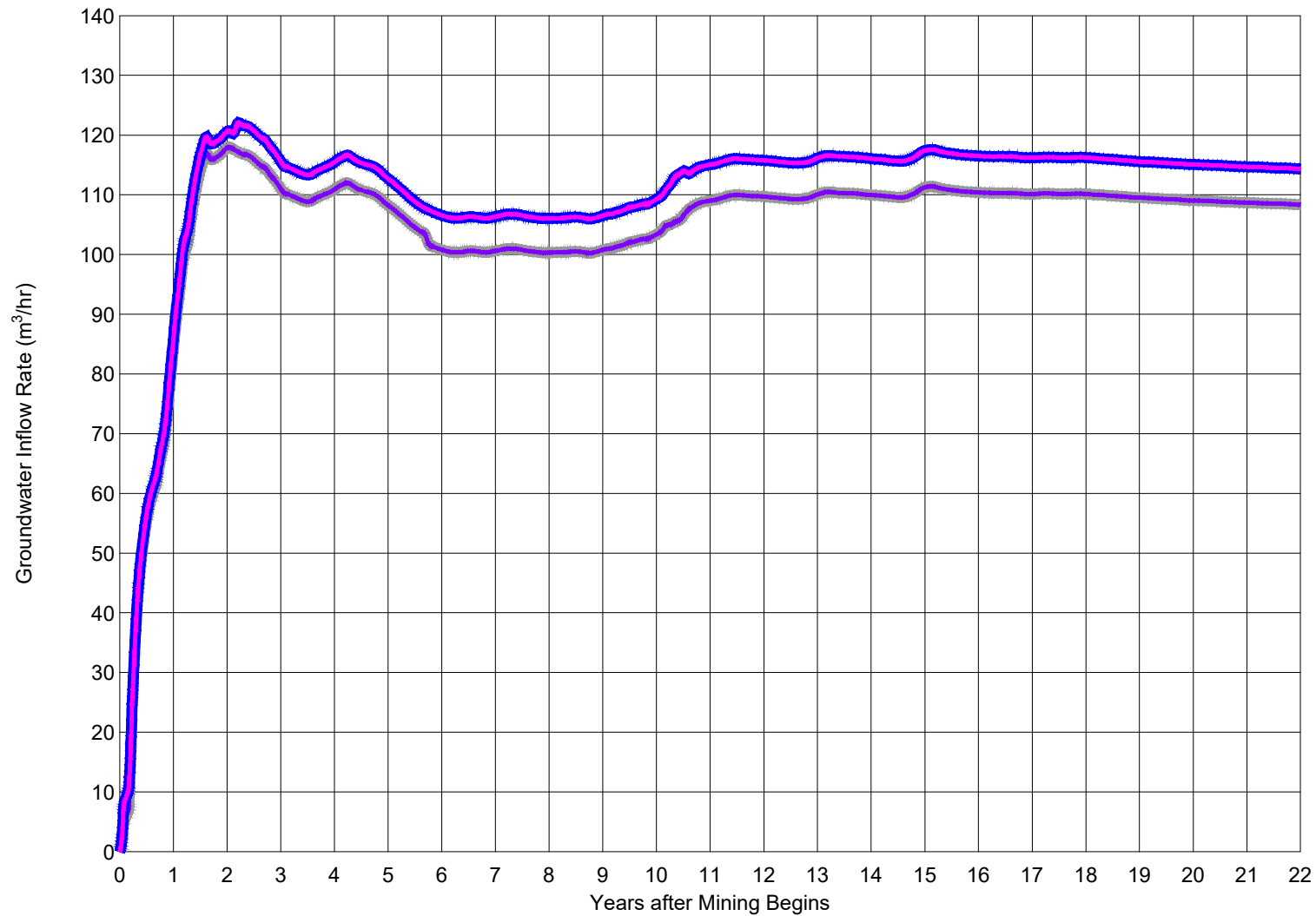


ITASCA
Denver, Inc.

Predicted Baseflow to the Kitinen River
for the Sensitivity Scenarios

CLIENT:
Sakatti Mine

FIGURE NO.
B-4



Base Scenarios

- 65% Success in Grouting
- 80% Success in Grouting

Climate Scenarios

- 65% Success in Grouting
- 80% Success in Grouting

Note: Climate and Base Scenarios are plotted on top of each other with negligible differences.

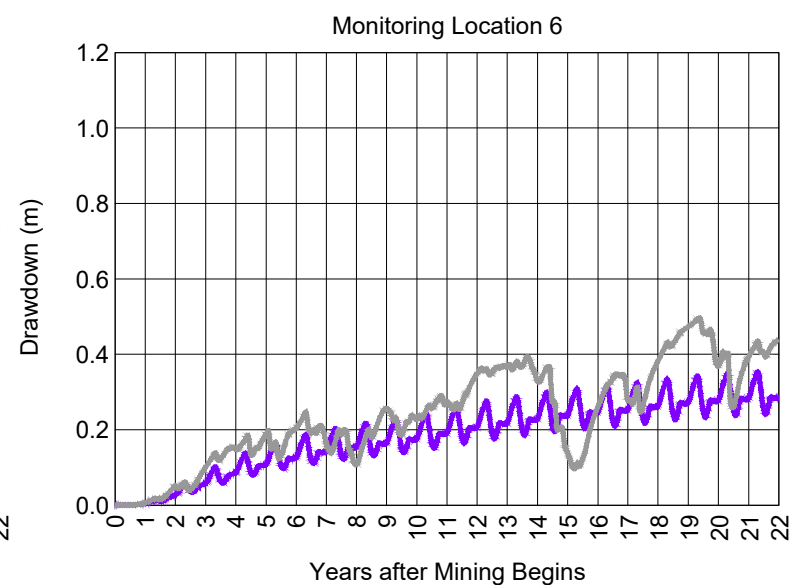
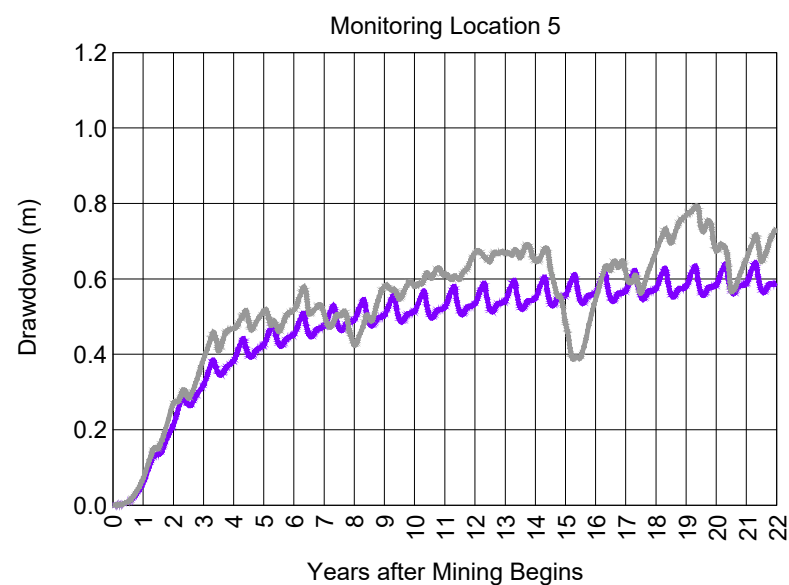
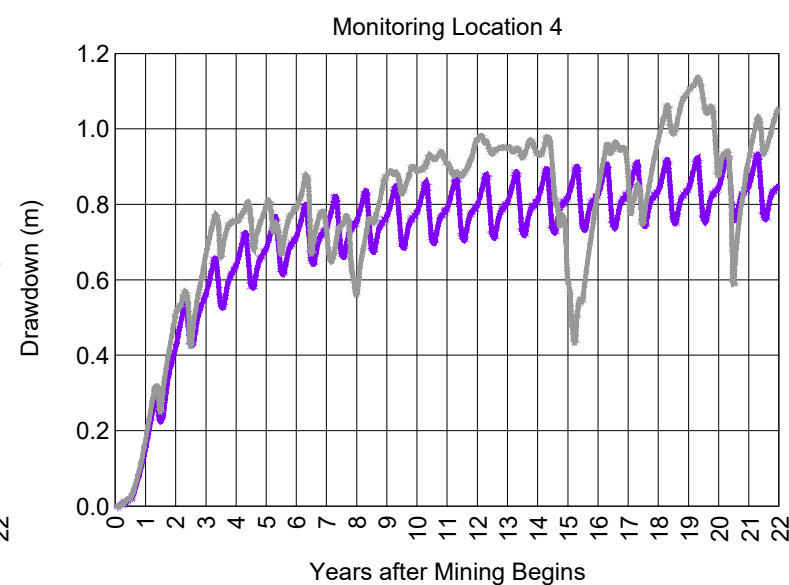
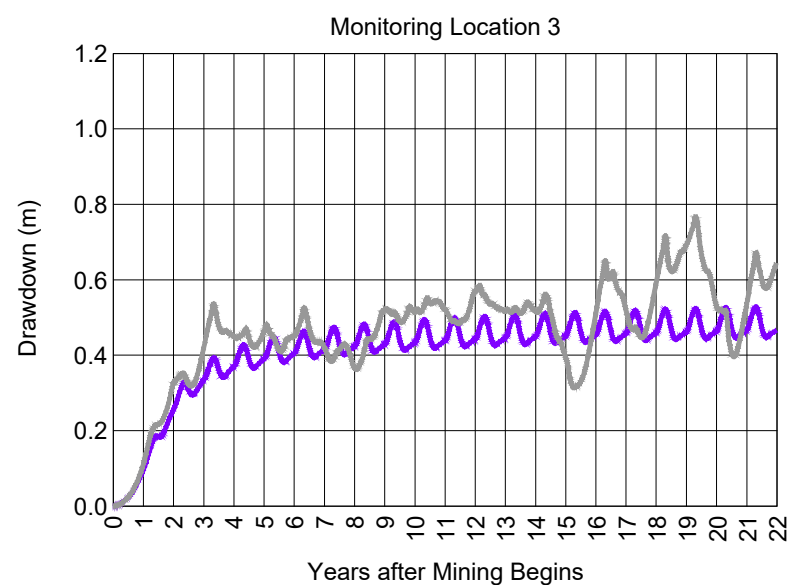
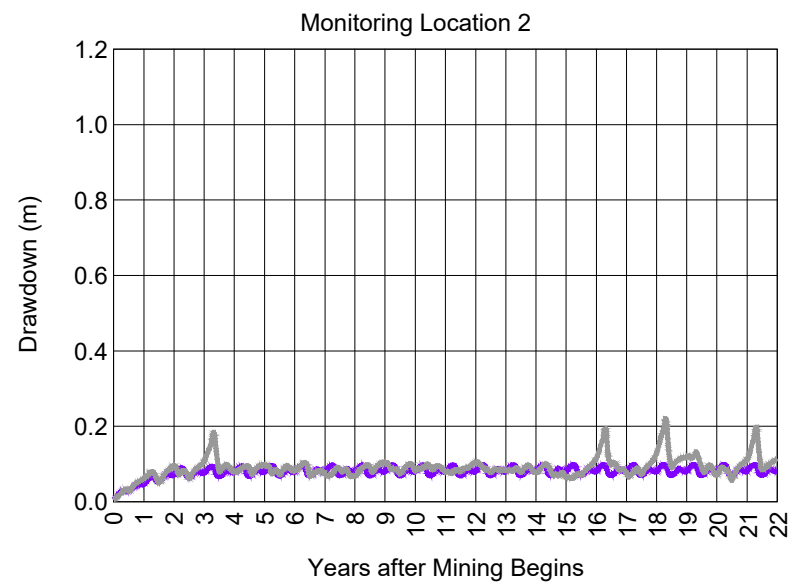
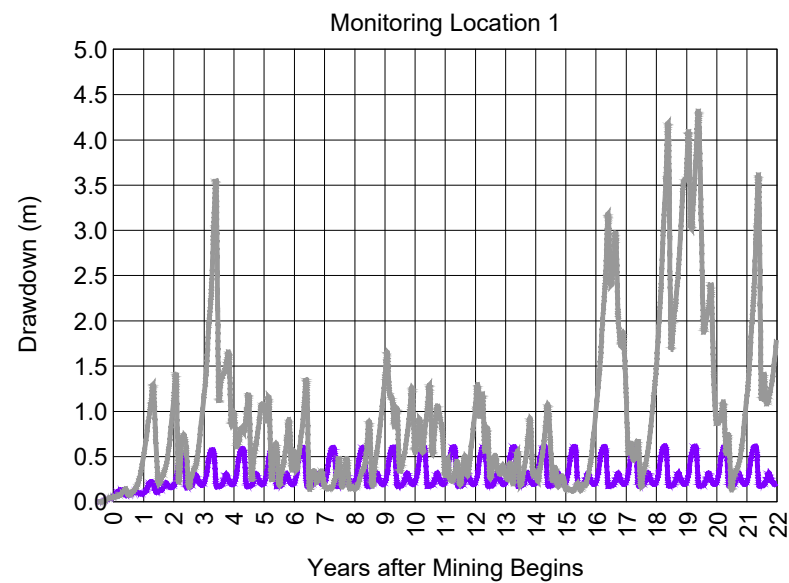
PROJECT NO.	4064
BY	SBM
CHECKED	HL
DRAWN	RJN
DRAWING NAME	CLIMATE
DRAWING DATE	16 NOV 2022
REVISION DATE	



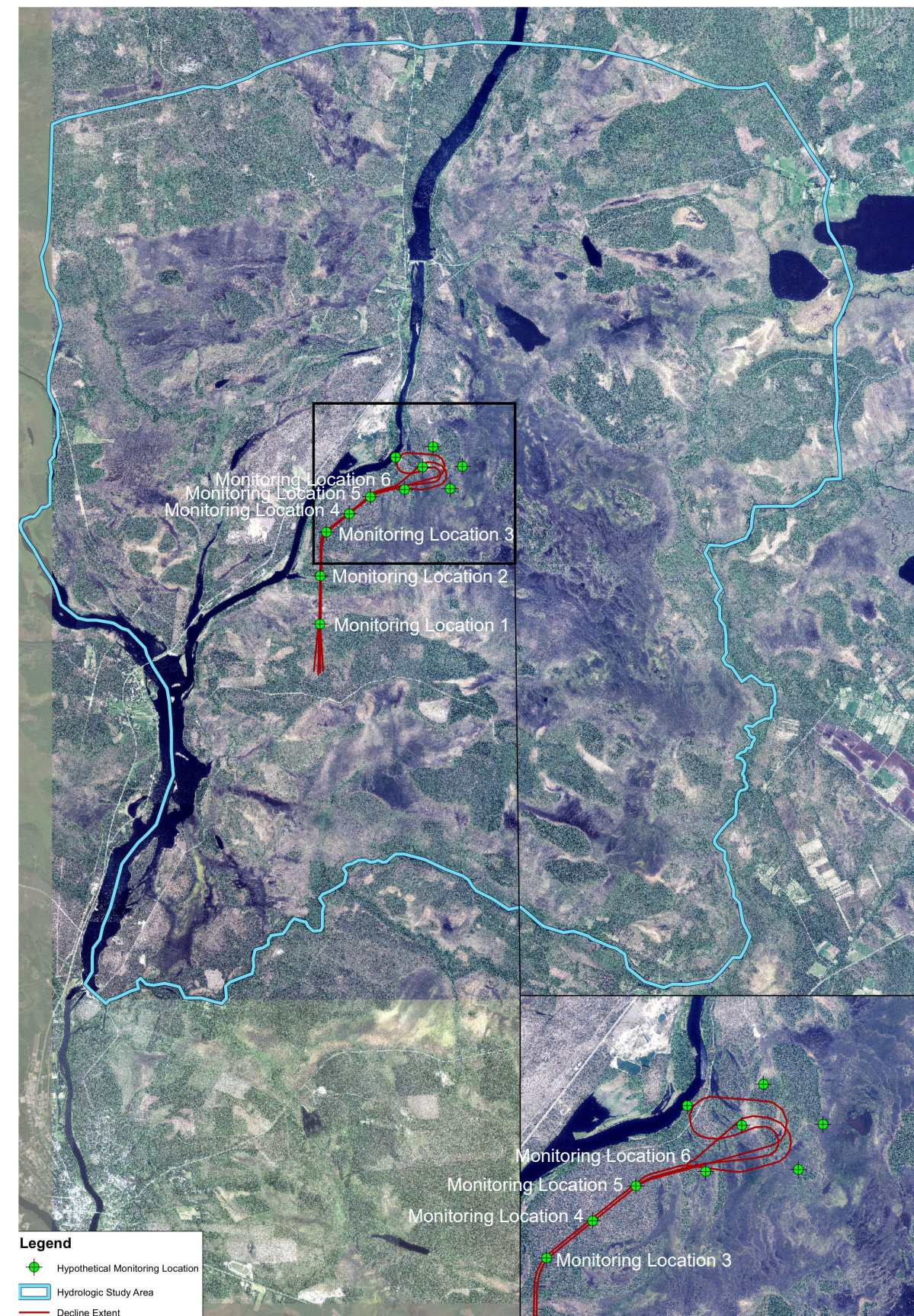
Predicted Groundwater Inflows for the Climate Scenarios

CLIENT:
Sakatti Mine

FIGURE NO.
B-5



— 80% Success in Grouting Scenario — 80% Success in Grouting Climate Scenario



Legend
 ● Hypothetical Monitoring Location
 □ Hydrologic Study Area
 — Decline Extent

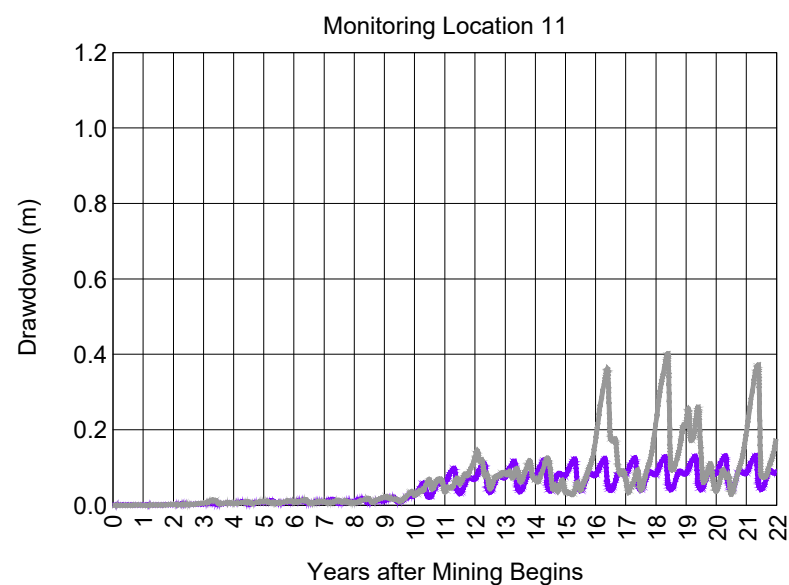
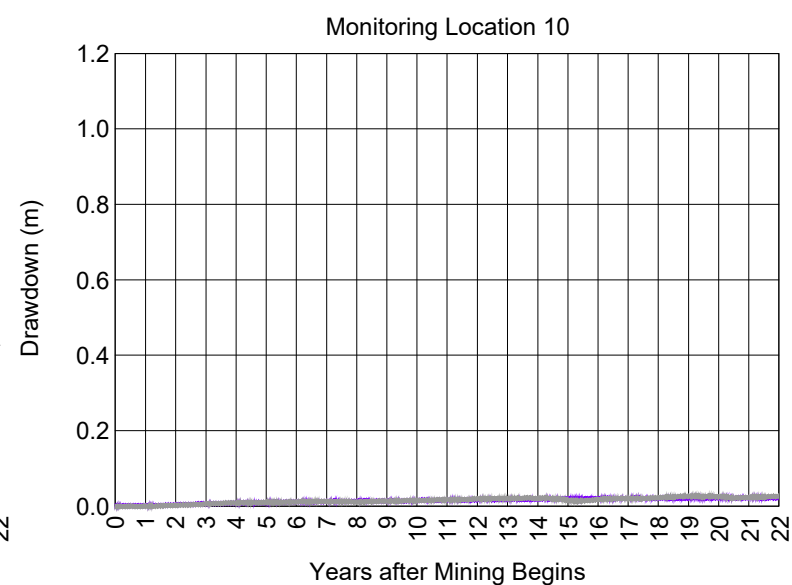
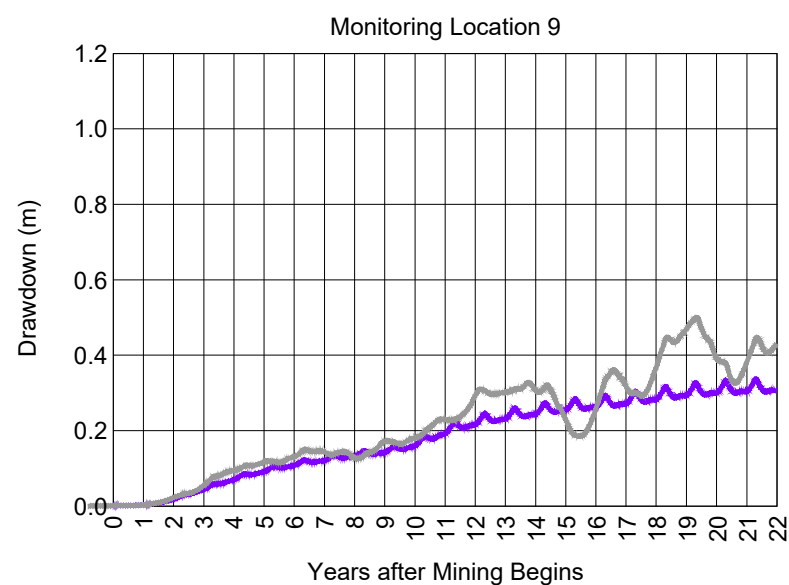
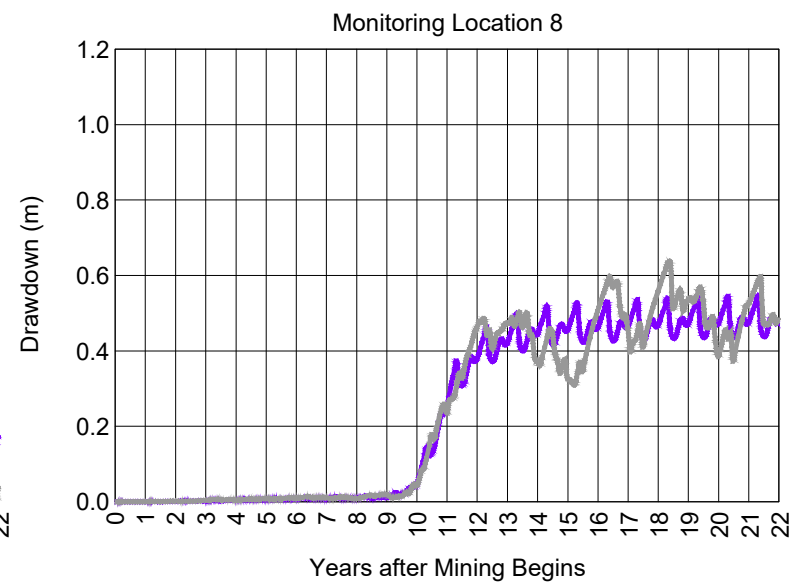
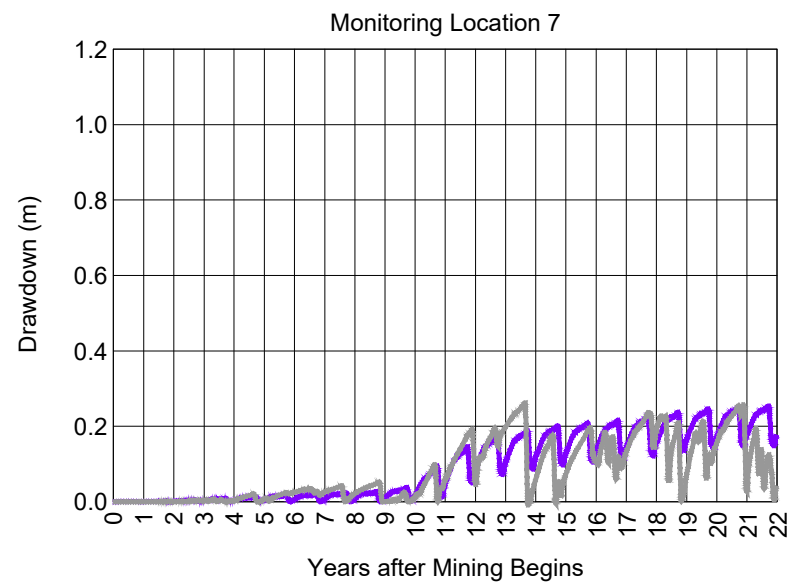
PROJECT NO.	4064
BY	SBM
CHECKED	HL
DRAWN	RJN
DRAWING NAME	KEY
DRAWING DATE	16 NOV 2022
REVISION DATE	



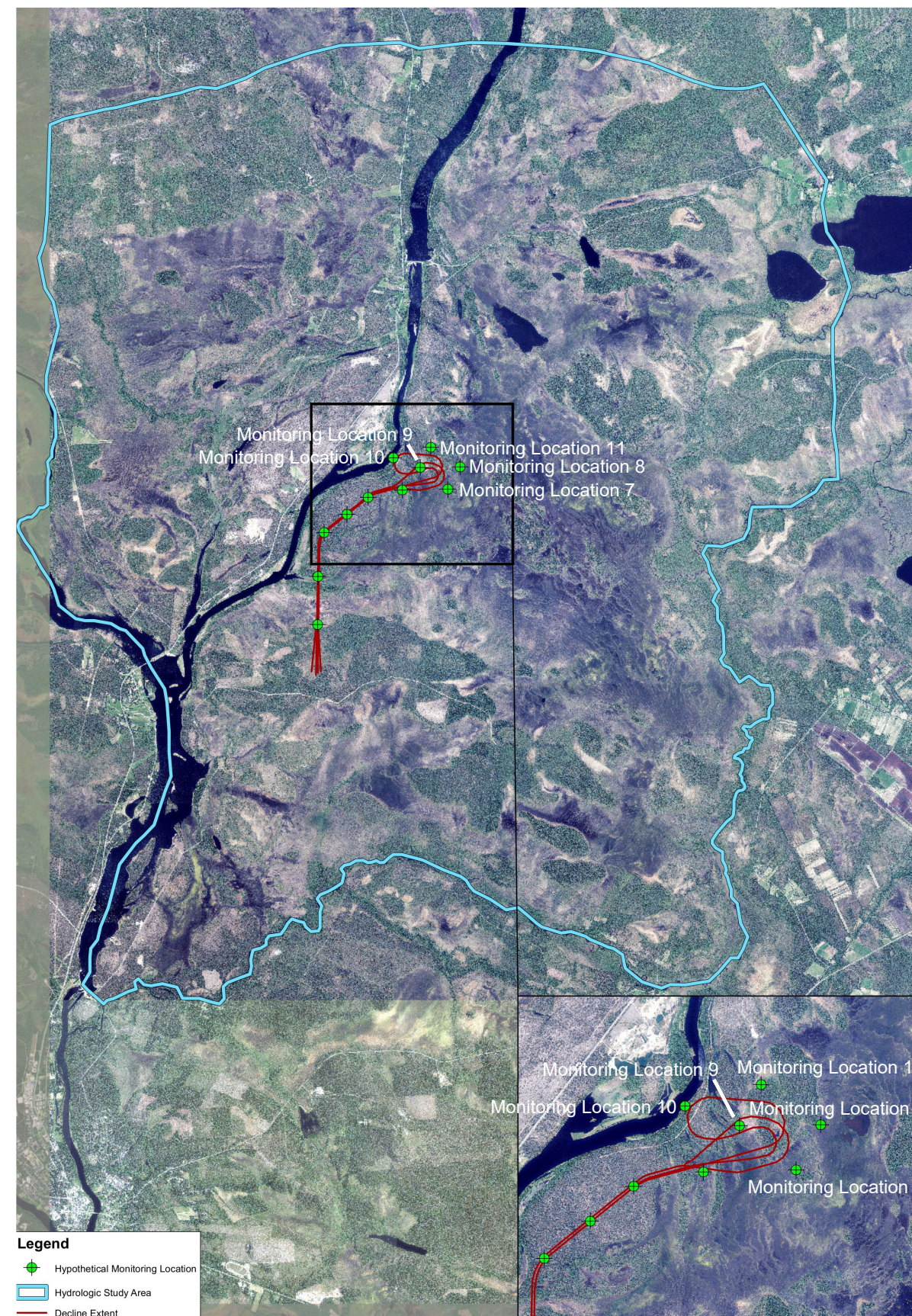
Predicted Drawdown over the LOM at Key Locations around the Mine Area for the 80% Success in Grouting Climate Scenario

CLIENT:
Sakatti Mine

FIGURE NO.
B-6a



— 80% Success in Grouting Scenario — 80% Success in Grouting Climate Scenario



Legend
 ● Hypothetical Monitoring Location
 □ Hydrologic Study Area
 — Decline Extent

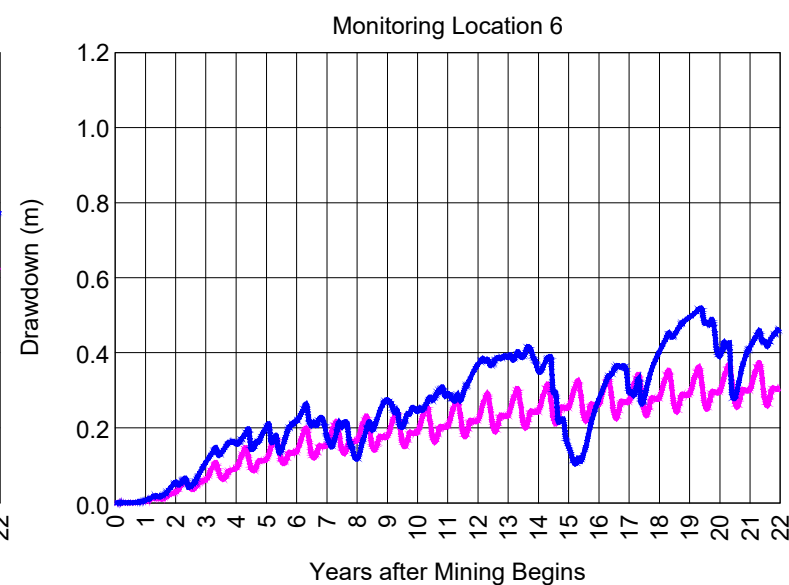
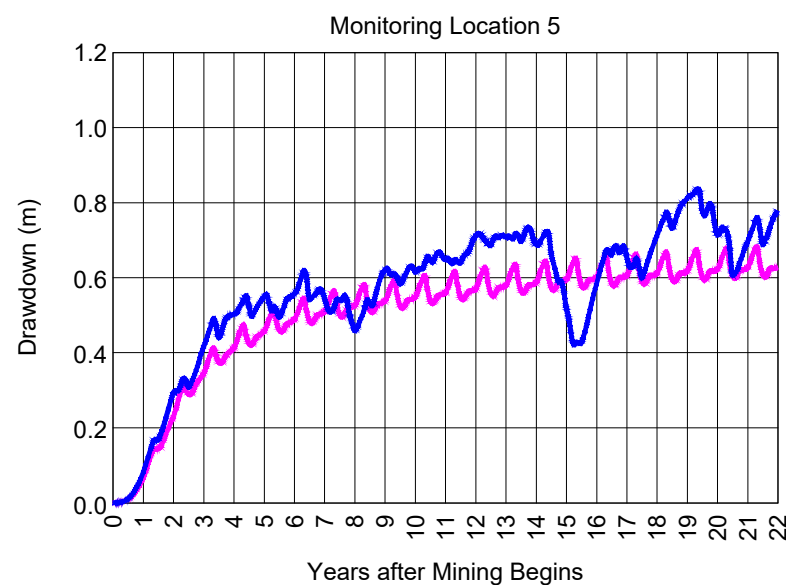
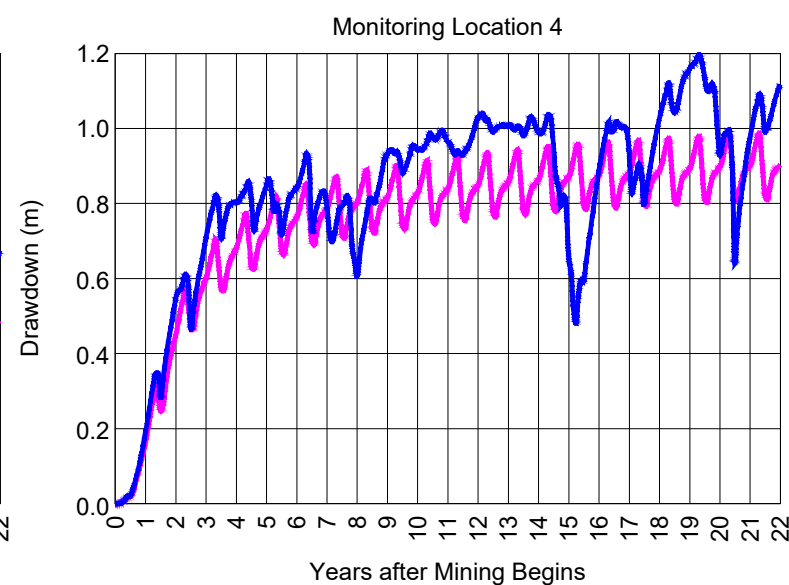
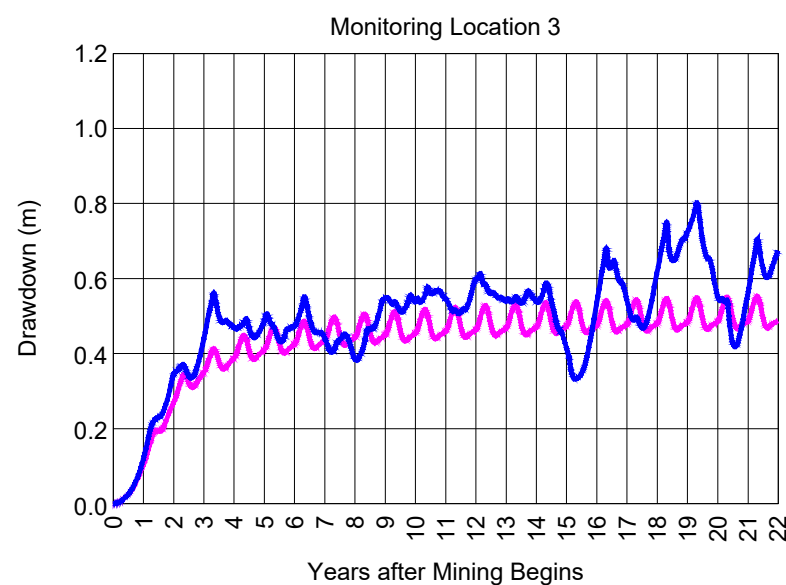
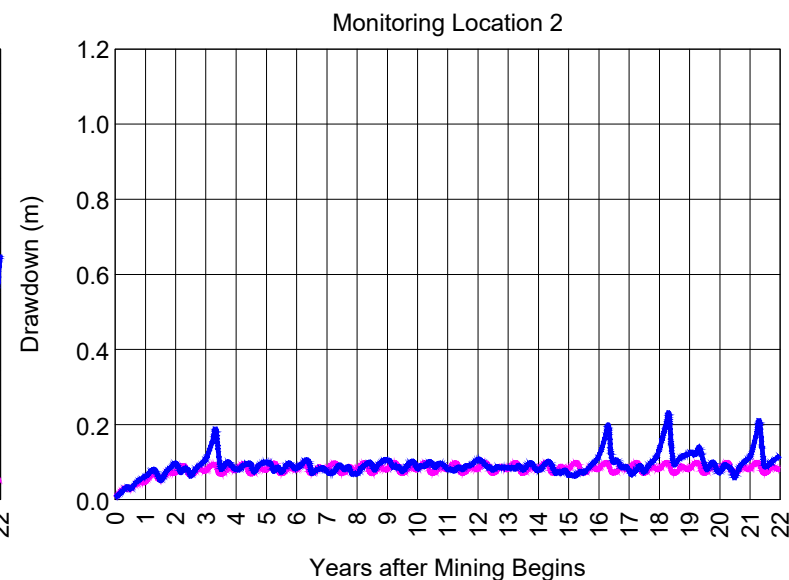
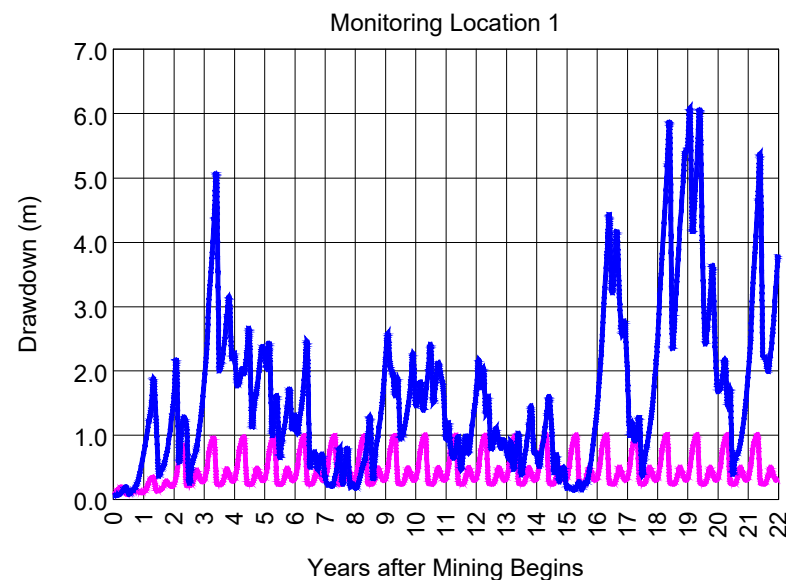
PROJECT NO.	4064
BY	SBM
CHECKED	HL
DRAWN	RJN
DRAWING NAME	KEY
DRAWING DATE	16 NOV 2022
REVISION DATE	



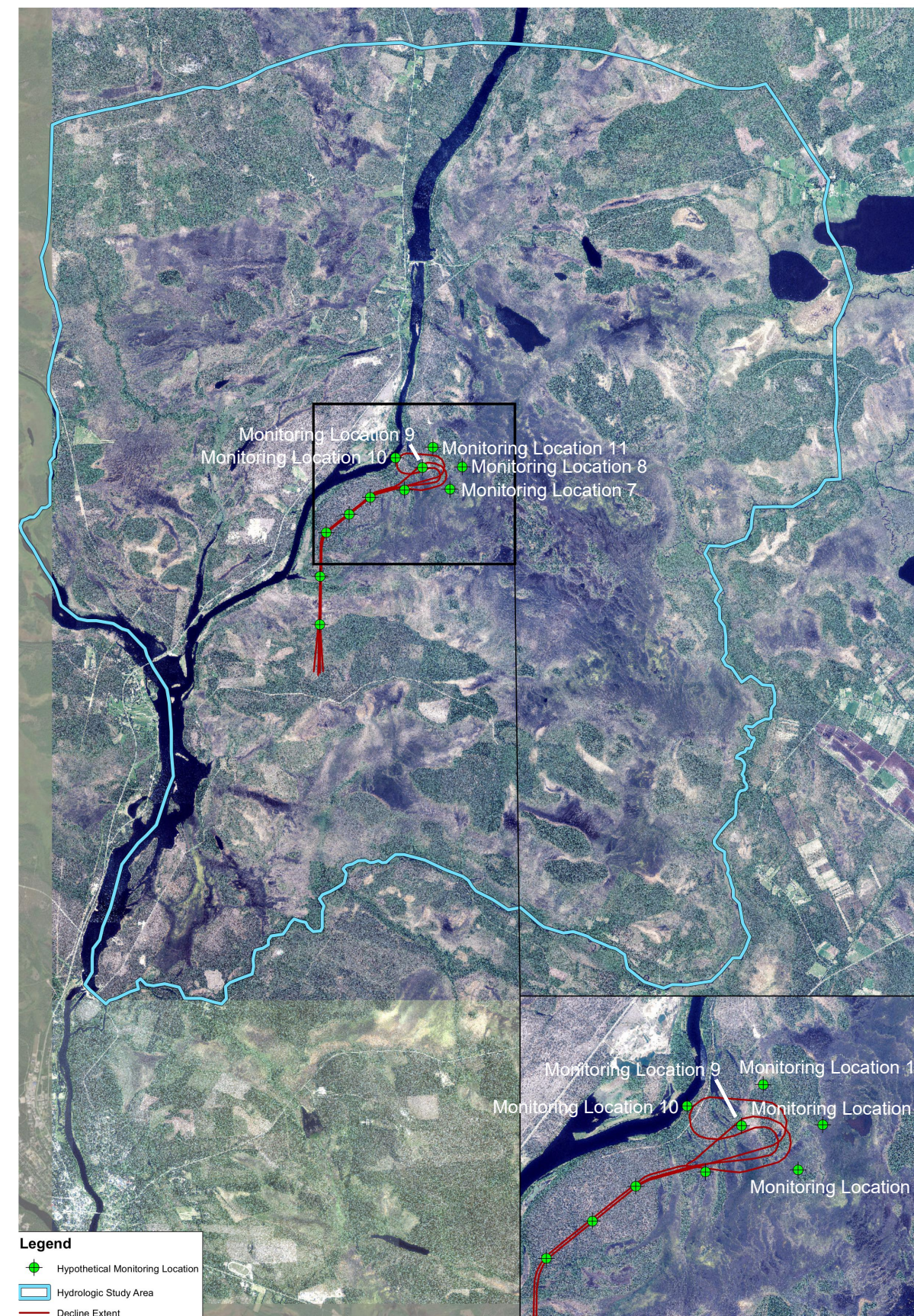
Predicted Drawdown over the LOM at Key Locations around the Mine Area for the 80% Success in Grouting Climate Scenario

CLIENT: Sakatti Mine

FIGURE NO. B-6b



— 65% Success in Grouting Scenario — 65% Success in Grouting Climate Scenario



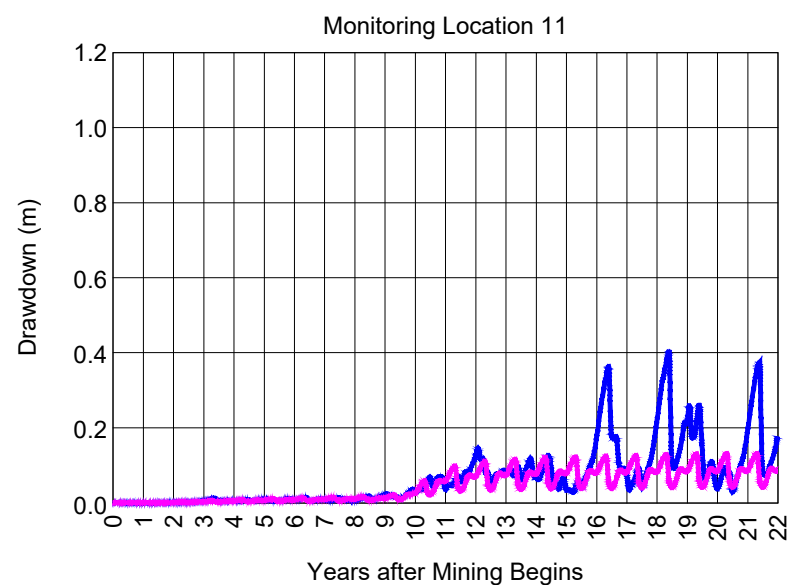
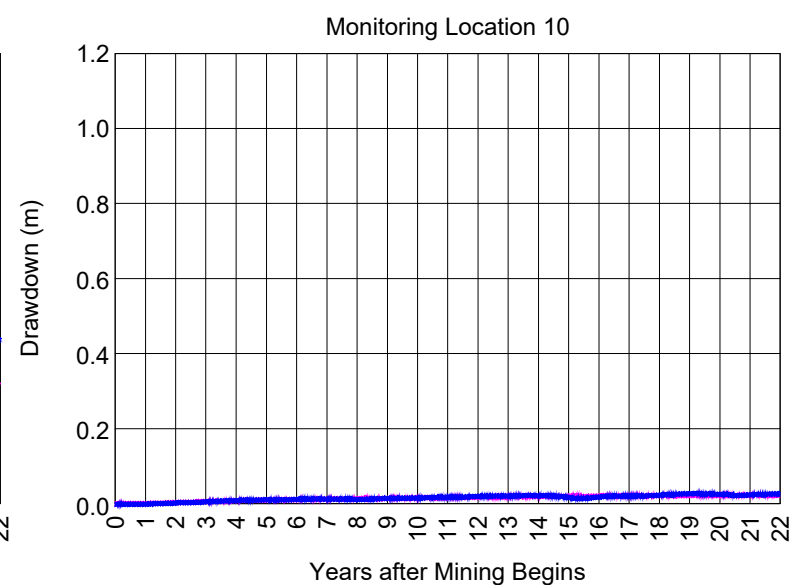
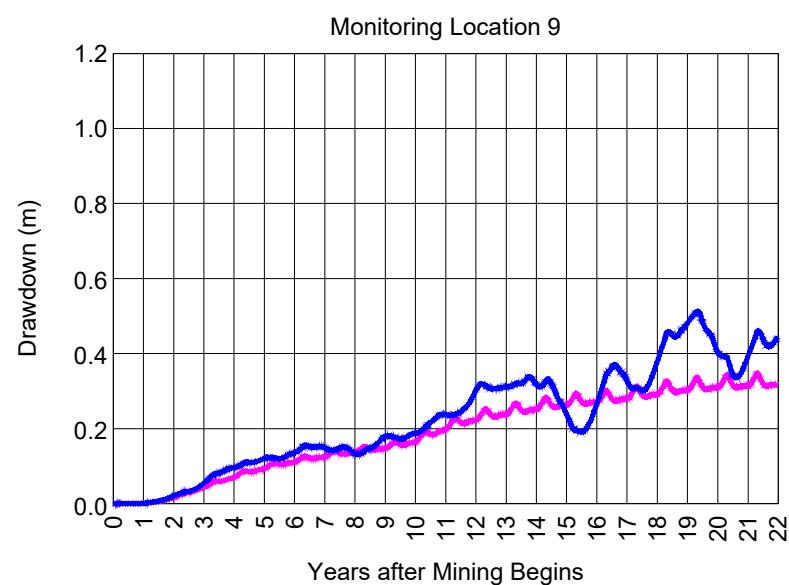
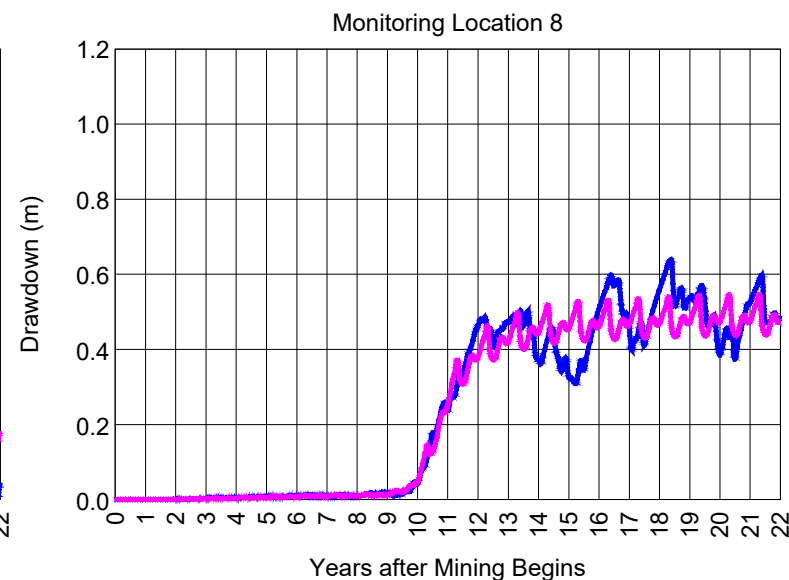
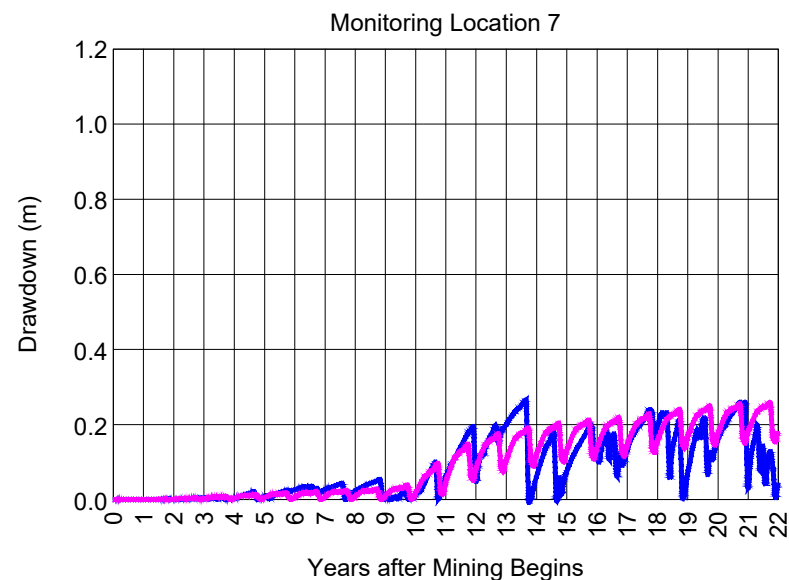
PROJECT NO.	4064
BY	SBM
CHECKED	HL
DRAWN	RJN
DRAWING NAME	KEY
DRAWING DATE	16 NOV 2022
REVISION DATE	



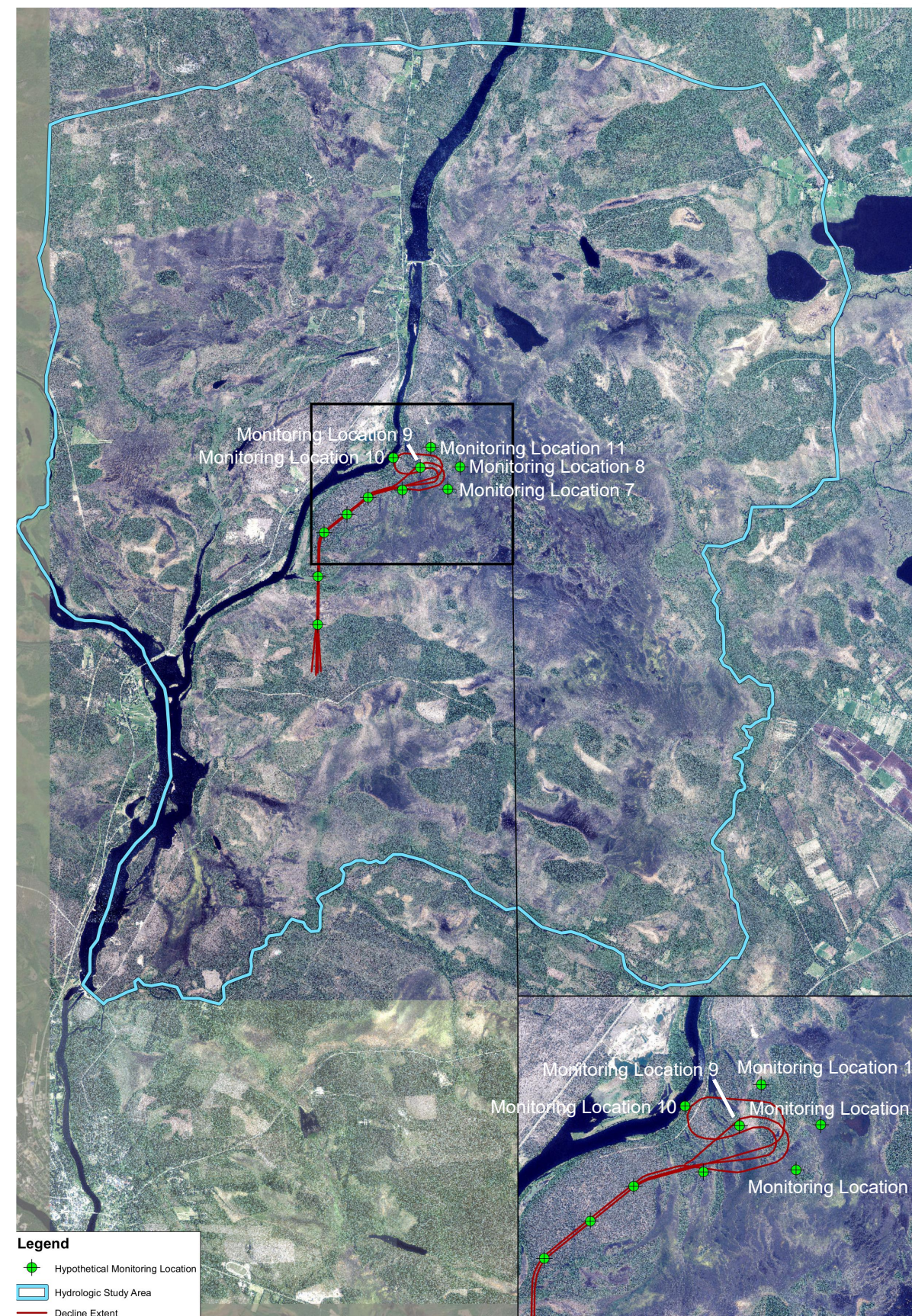
Predicted Drawdown over the LOM at Key Locations around the Mine Area for the 65% Success in Grouting Climate Scenario

CLIENT:
Sakatti Mine

FIGURE NO.
B-6c



— 65% Success in Grouting Scenario — 65% Success in Grouting Climate Scenario



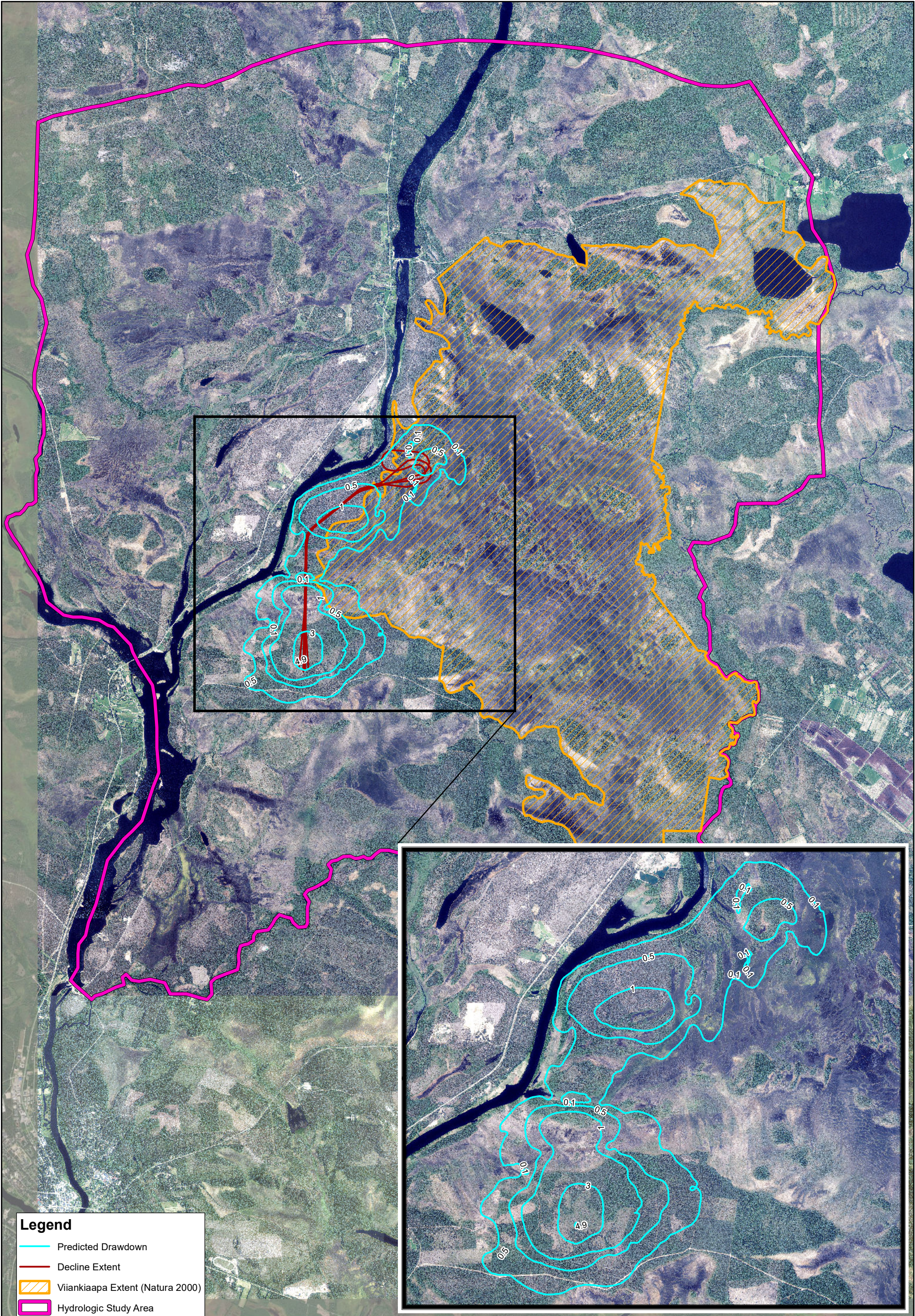
PROJECT NO.	4064
BY	SBM
CHECKED	HL
DRAWN	RJN
DRAWING NAME	KEY
DRAWING DATE	16 NOV 2022
REVISION DATE	



Predicted Drawdown over the LOM at Key Locations around the Mine Area for the 65% Success in Grouting Climate Scenario

CLIENT:
Sakatti Mine

FIGURE NO.
B-6d

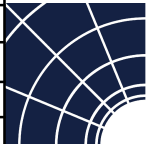


Legend

- Predicted Drawdown
- Decline Extent
- Viiankiaapa Extent (Natura 2000)
- Hydrologic Study Area

0 1,250 2,500 Meters

PROJECT NO.	4064
BY	SBM
CHECKED	HL
DRAWN	NP
DRAWING NAME	Draw_Climate80
DRAWING DATE	Apr. 25, 2022
REVISION DATE	Jan. 12, 2023

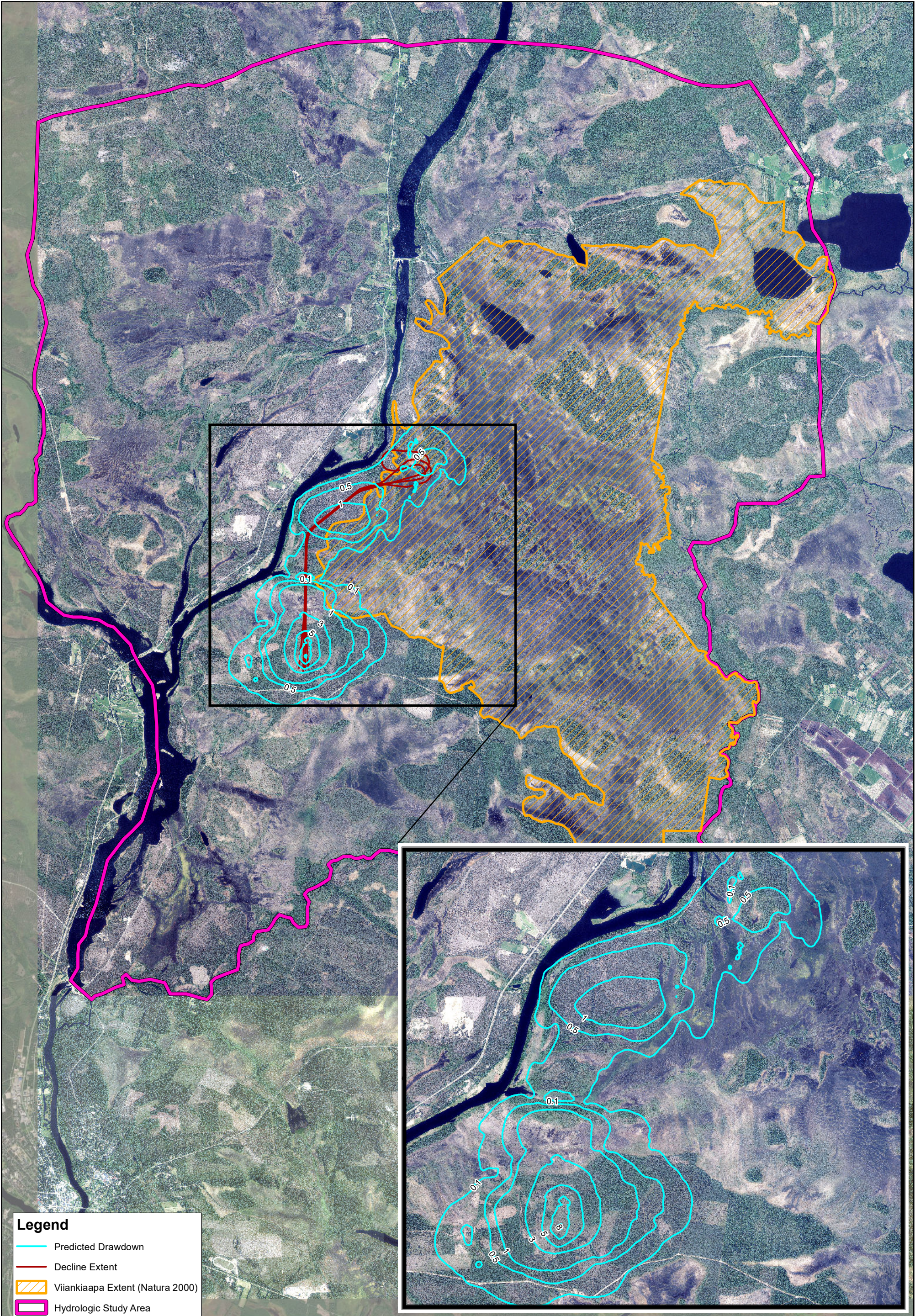


ITASCA
Denver, Inc.

Predicted Drawdown at the End of Mining
for the 80% Success in Grouting Climate Scenario

CLIENT:
Sakatti Mine

FIGURE NO.
B-7a



Legend

Predicted Drawdown

Decline Extent

Viankiaapa Extent (Natura 2000)

Hydrologic Study Area

N

0

1,250

2,500

Meters

PROJECT NO.	4064
BY	SBM
CHECKED	HL
DRAWN	NP
DRAWING NAME	Draw_Climate65
DRAWING DATE	Apr. 25, 2022
REVISION DATE	Jan. 12, 2023

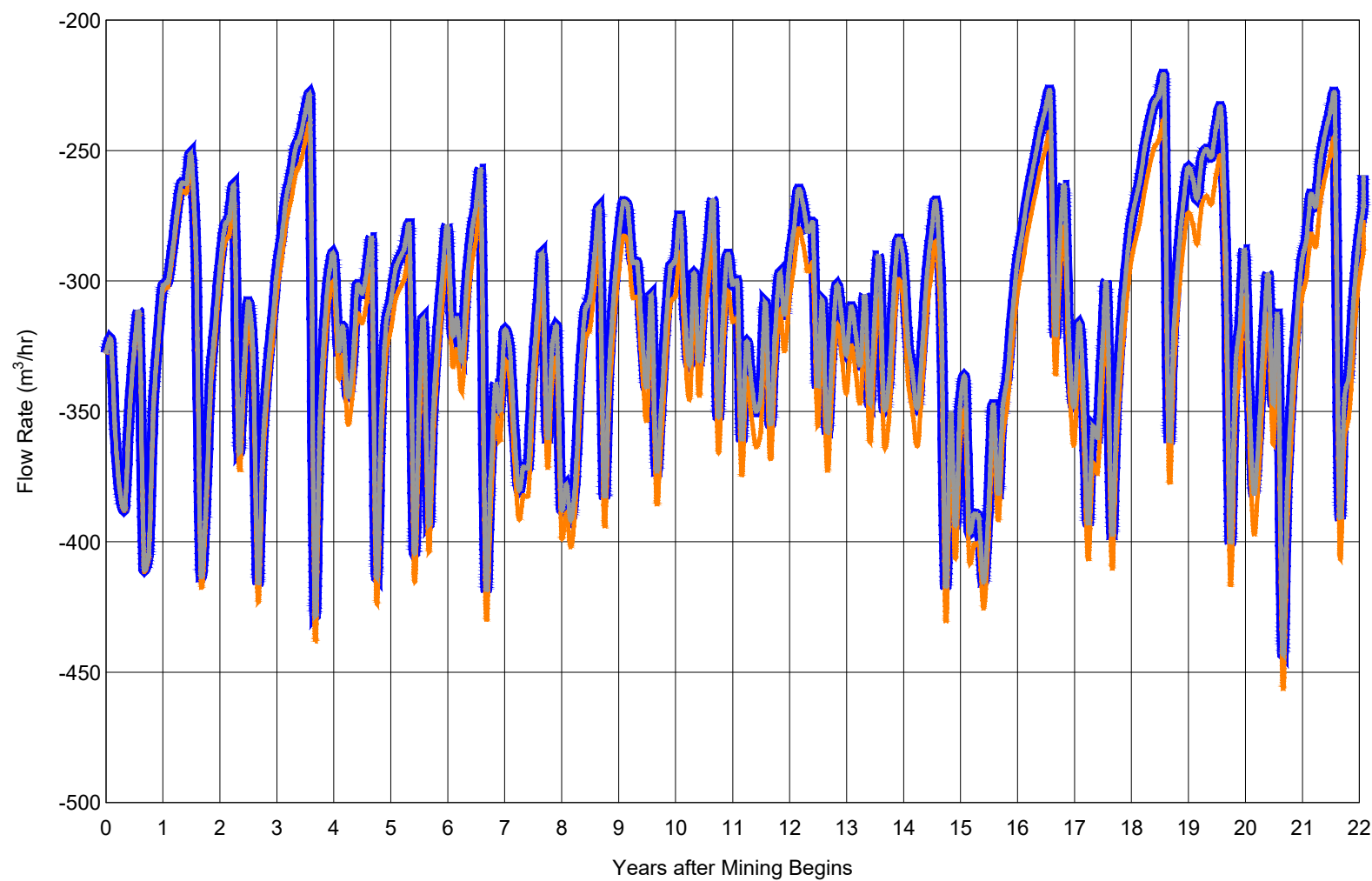
ITASCA
Denver, Inc.

Predicted Drawdown at the End of Mining
for the 65% Success in Grouting Climate Scenario

CLIENT:
Sakatti Mine

FIGURE NO.
B-7b

G:\ARC\GIS\4064_Sakatti\MXDs\Working\Appendix\Draw_Climate65.mxd



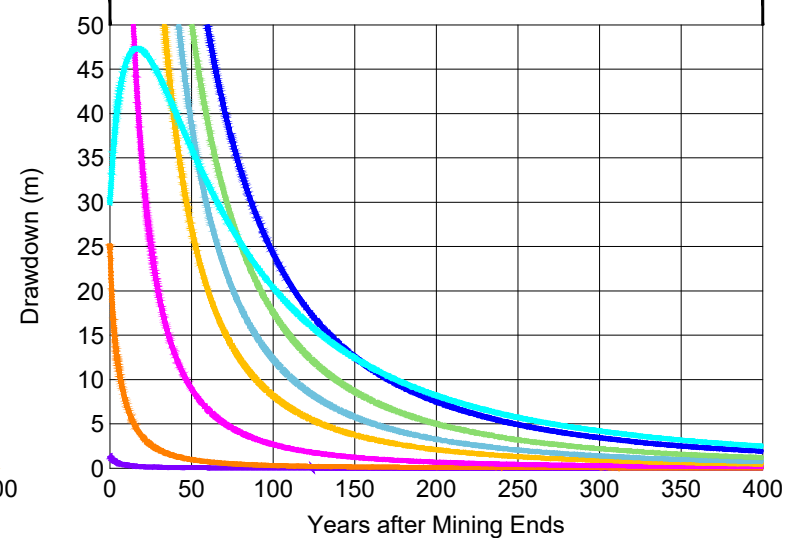
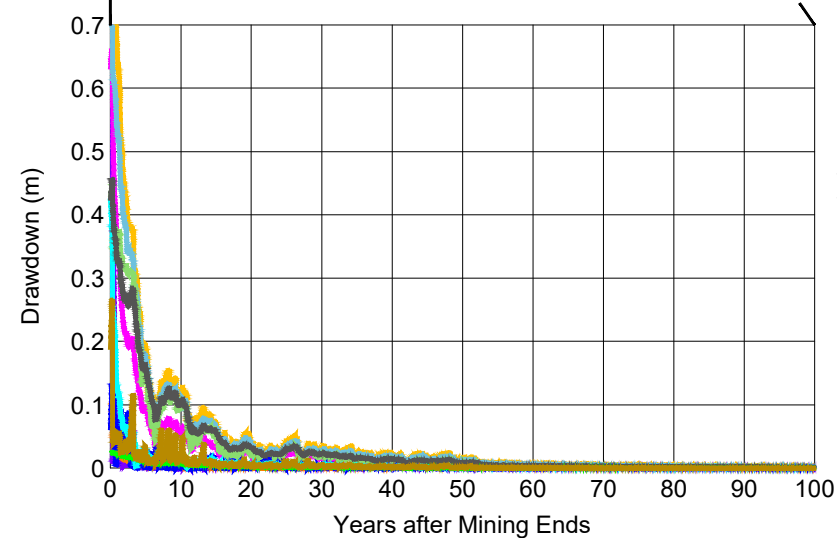
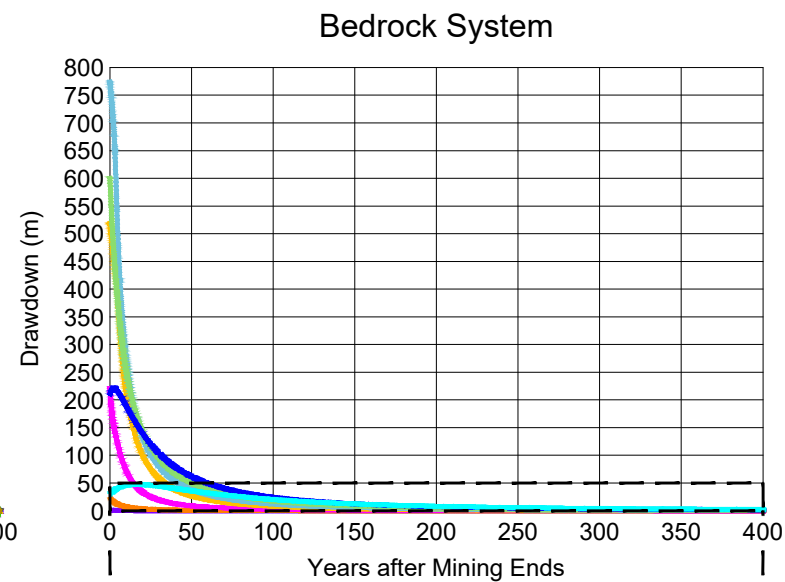
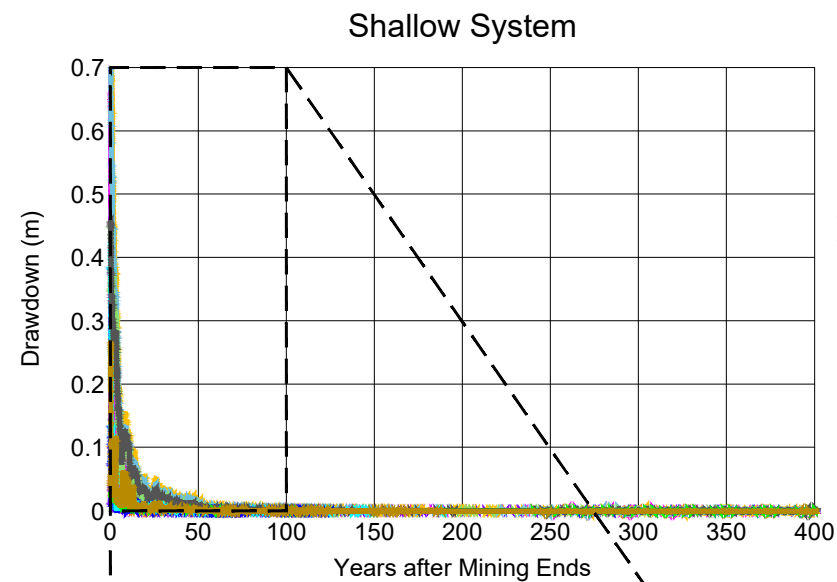
PROJECT NO.	4064
BY	SBM
CHECKED	HL
DRAWN	RJN
DRAWING NAME	CLIMATE
DRAWING DATE	16 NOV 2022
REVISION DATE	



Predicted Baseflow to the Kitinen River
for the Climate Scenarios

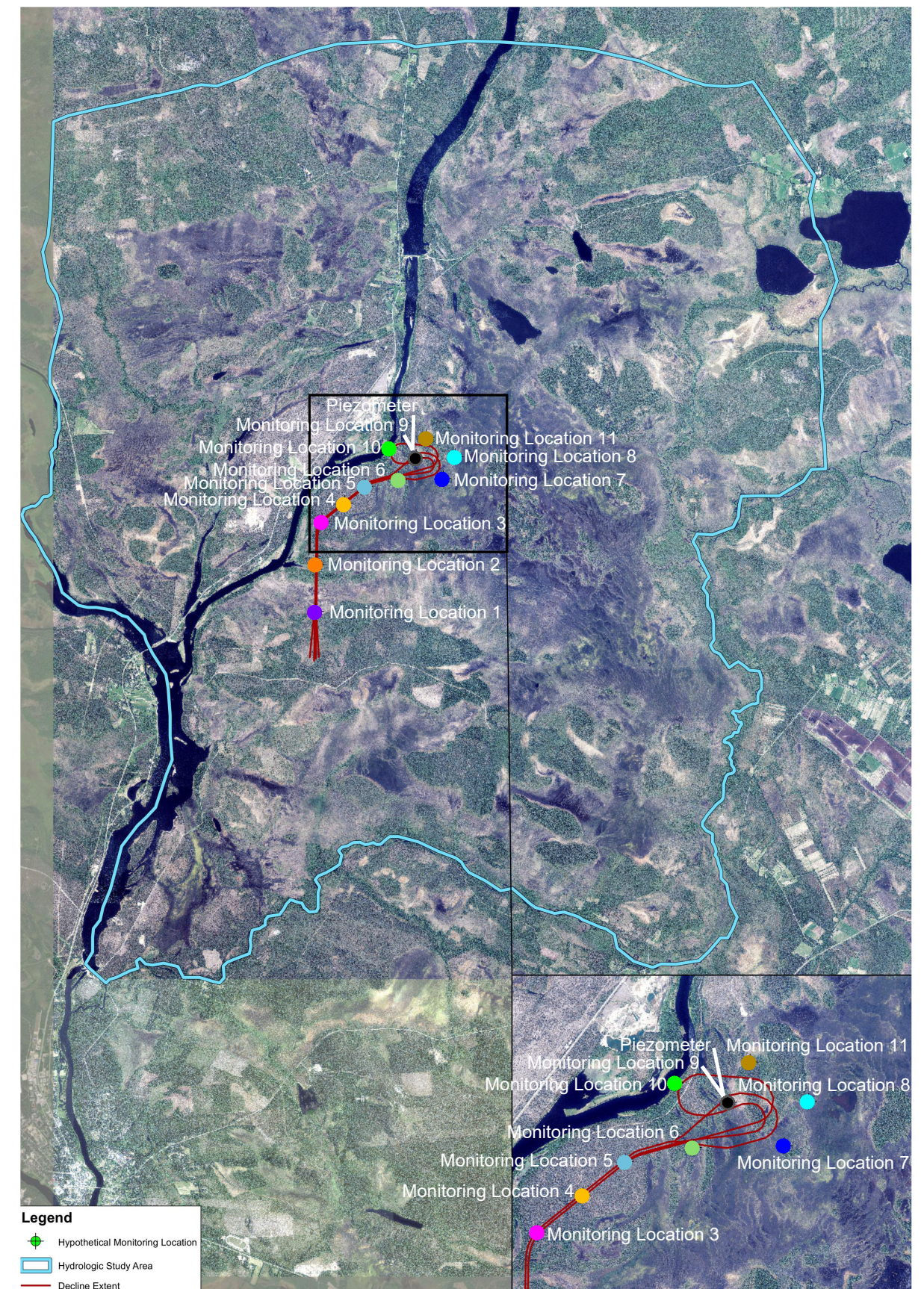
CLIENT:
Sakatti Mine

FIGURE NO.
B-8



Monitoring Location 1
 Monitoring Location 4
 Monitoring Location 7
 Monitoring Location 10
 Monitoring Location 2
 Monitoring Location 5
 Monitoring Location 8
 Monitoring Location 11
 Monitoring Location 3
 Monitoring Location 6
 Monitoring Location 9

Piezometer - 100 mamsl
 Piezometer - -200 mamsl
 Piezometer - -600 mamsl
 Piezometer - -1000 mamsl
 Piezometer - 0 mamsl
 Piezometer - -400 mamsl
 Piezometer - -800 mamsl
 Piezometer - -1200 mamsl



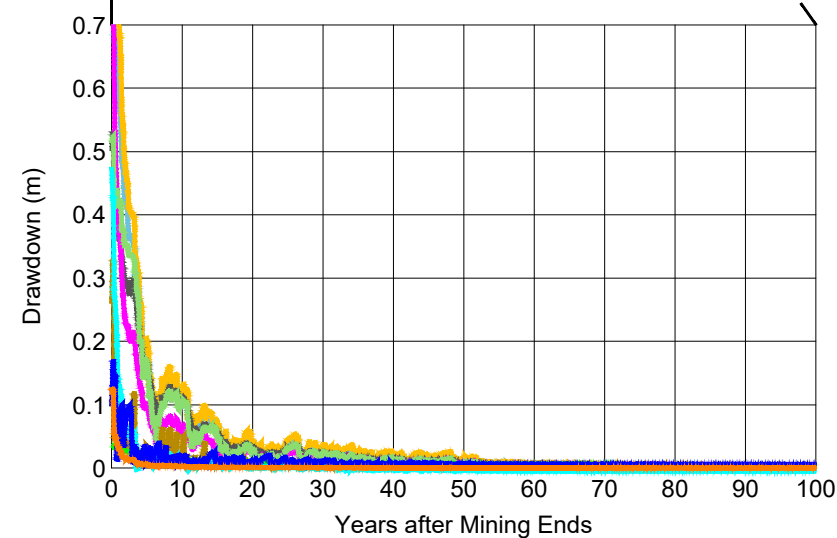
PROJECT NO.	4064
BY	SBM
CHECKED	HL
DRAWN	RJN
DRAWING NAME	RECOVER
DRAWING DATE	16 NOV 2022
REVISION DATE	



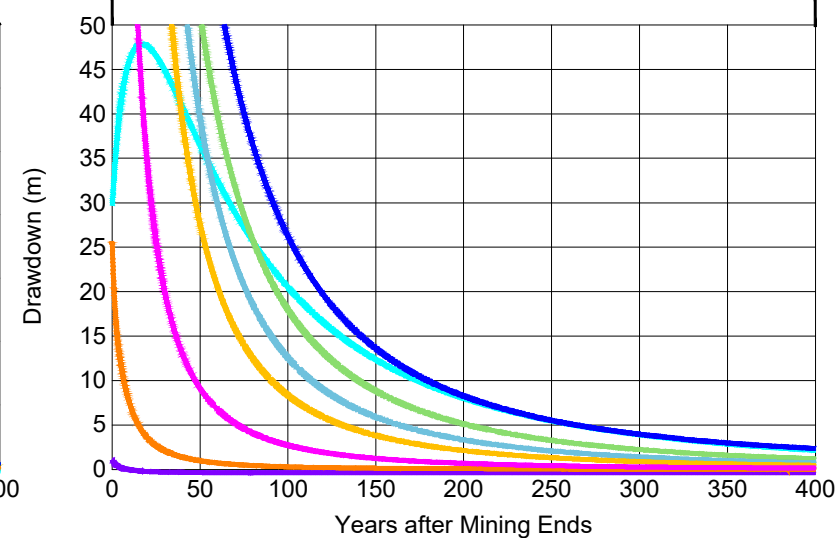
Predicted Groundwater Recovery After Mining at Key Locations around the Mine Area for the 80% Success in Grouting Climate Scenario

CLIENT: Sakatti Mine

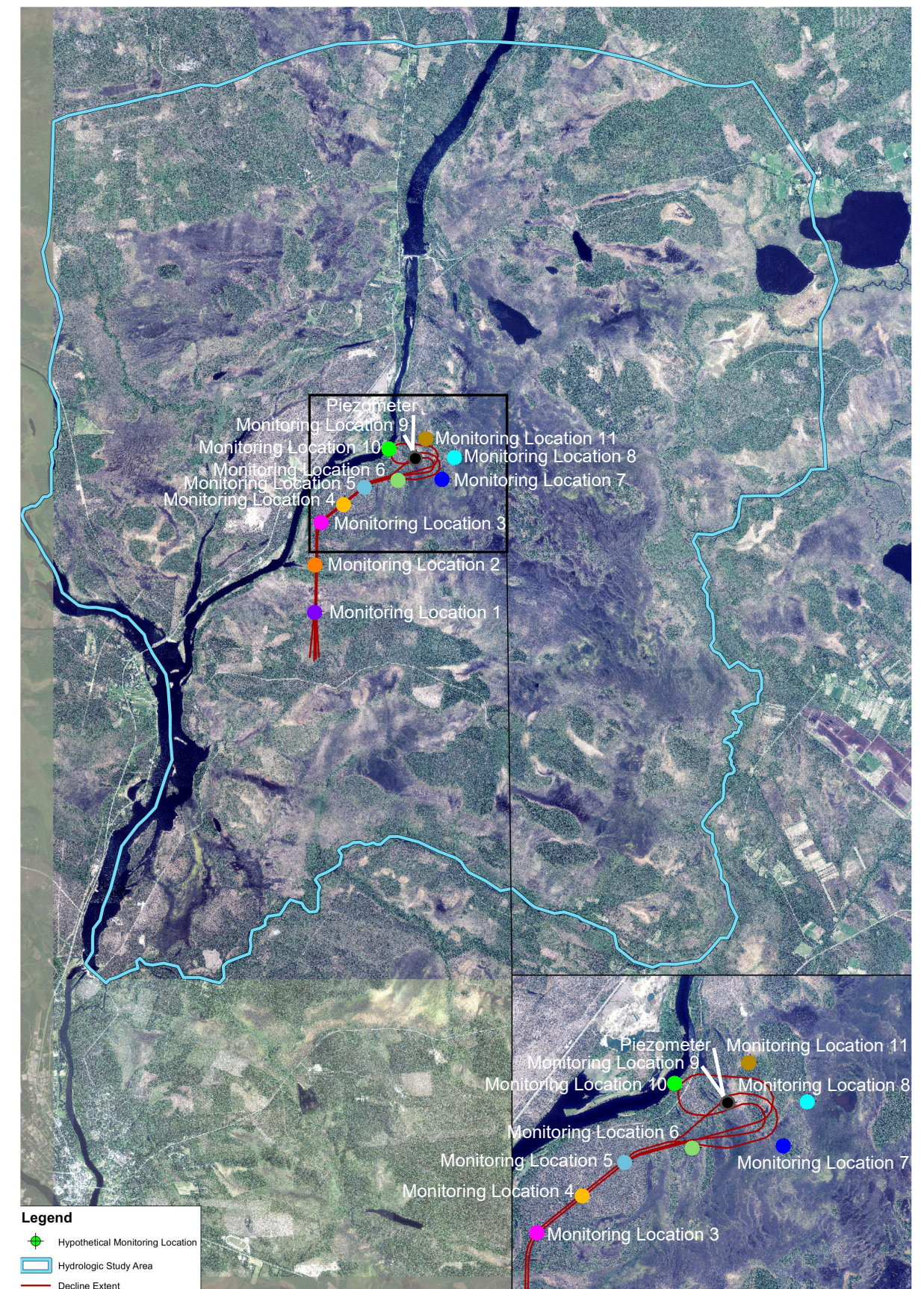
FIGURE NO. B-9a



■ Monitoring Location 1
 ■ Monitoring Location 2
 ■ Monitoring Location 3
■ Monitoring Location 4
 ■ Monitoring Location 5
 ■ Monitoring Location 6
■ Monitoring Location 7
 ■ Monitoring Location 8
 ■ Monitoring Location 9
■ Monitoring Location 10
 ■ Monitoring Location 11



- Piezometer - 100 mamsl
- Piezometer - -200 mamsl
- Piezometer - -600 mamsl
- Piezometer - -1000 mamsl
- Piezometer - 0 mamsl
- Piezometer - -400 mamsl
- Piezometer - -800 mamsl
- Piezometer - -1200 mamsl



PROJECT NO.	4064
BY	SBM
CHECKED	HL
DRAWN	RJM
DRAWING NAME	RECOVER
DRAWING DATE	16 NOV 2022
REVISION DATE	



Predicted Groundwater Recovery After Mining at Key Locations around the Mine Area for the 65% Success in Grouting Climate Scenario

CLIENT:
Sakatti Mine

FIGURE NO.
B-9b